ENANTIOSELECTIVE DESYMMETRIZATION OF CARBOXYLIC ACIDS BY BRØNSTED BASE CATALYSIS; PREPARATION OF ARYLGLYCINE PEPTIDES; PROGRESS TOWARD THE SYNTHESIS OF (+)-ZWITTERMICIN A

By

Matthew Knowe

Dissertation

Submitted to the Faculty of the
Graduate school of Vanderbilt University
in partial fulfillment of the requirements
for the degree of

DOCTOR OF PHILOSOPHY

in

Chemistry

May 11, 2018

Approved:
Jeffrey N. Johnston, Ph.D. (Advisor)
Gary A. Sulikowski, Ph.D.
Nathan D. Schley, Ph.D.
Lars Plate, Ph.D.

To my wife Madison and son JB.

ACKNOWLEDGEMENTS

I would like to express my gratitude to everyone that has helped me during and leading up to my graduate education. Although independent thinking and creativity is one of the chief goals of a graduate education, I believe all the more that collaboration and cooperation amongst coworkers plays a vital role in achieving success.

I want to specifically thank my advisor, Dr. Jeffrey N. Johnston, for all of his time and energy spent mentoring me throughout my years in his laboratory. I want to thank him for trusting me with ambitious projects, giving me opportunities to mentor and lecture, and encouraging me to solve problems in my research.

I have had professors and teachers throughout my education that have inspired and encouraged me to pursue this degree. My undergraduate research advisor, Dr. Marcello Forconi, was instrumental in helping me discover my love for research. My organic chemistry lecturers, Dr. Rich Heldrich and Dr. Neil Tonks, were responsible for first showing me the creativity and fun of organic chemistry. Dr. Heldrich was the one who all but forced me to register for undergraduate research and teaching organic chemistry recitation. The College of Charleston chemistry and biochemistry department was a wonderful and enjoyable place to learn. I am grateful for all of their continued support.

I would also like to thank my committeeDr. Sulikowski, Dr. Schley, Dr. Stauffer, and Dr. Plate for their commitment to my education and scientific development. Thank you for giving of your time, for giving me feedback on my projects and proposals, and for advising me.

I owe much of my growth to all of the post-docs that have come through our lab in my time here. Dr. Yasunori Toda invested so much time and energy into teaching me theory and technique. It was a blessing to be forced into sharing a single bench with him, due to lack of lab space. I'll never forget how he spent most of his day helping and talking to lab mates about their chemistry, before spending his evenings working on his own projects. It is rare to see someone invest so selflessly in the people around them. He always tried to make the projects around him succeed, and he would frequently turn down opportunities to be formally listed as a co-author. I am grateful for his early influence in my graduate career, and his continued friendship since. I am confident that he will be very successful as a professor. I'm happy that I get to be his English spellchecker and keep in touch with him.

Dr. Sergey Tsukanov and Dr. Roozbeh Yousefi were also active mentors in my first few years of graduate school. Sergey was one of the happiest chemists I ever had the privilege of working with. He was always so active in our problem set sessions, provoking deeper thought whenever he could. Roozbeh was a really good benchmate for a couple of years. His

expertise in halolactonizations was instrumental to my project. I loved getting to learn about Iran and Russia from these post-docs. Good luck in the World Cup! They have also kept in touch with me after moving on, for which I am grateful. Dr. Kazuyuki Tokumaru was a great mentor in our lab as well. He brought an industry perspective and expertise that had been lacking in our lab. His ability to consume beer was also remarkable. Current post-docs, Mahesh Vishe, Kali Bera, and Rashanique Quarels have become great friends already, and I want to thank them for the skills and experience that they have enriched our lab with.

I would like to also thank my former graduate studentsMike Danneman for his personality, impressions, hard work, and initiation of my main project; Ken Schweiter for his Microsoft Word skills, his UmAS skills, and his common love of soccer; Dan Sprague for his utter enthusiasm for learning and chemistry; and Brandon Vara for his mentorship during my rotation and early days in the lab.

Andrew Flach was a pleasure to work with, receive chemistry advice from, and discuss anything with, even though every discussion somehow ended up at economics and inflation. Michael Crocker has been a great friend and benchmate. I'd like to thank him for his discussions about chemistry, for his NMR skills, for always asking good questions, for his incredible ability to consume sugar. Jade Bing has been a great friend and coworker, and I appreciate her constant positive attitude in the lab. It has been a privilege to work with them, and they have made my graduate school experience better.

I want to salute the current graduate students and wish them all of the bestMichael Crocker, Jade Bing, Jenna Payne, Abby Smith, and Jade Izaguirre. They are already very good chemists and researchers, and I am thankful for their friendship.

Thank you to Wes Bauer, Katie Chong, and Robby Davis, who have been great friends outside of the Johnston lab. Going through graduate school together has been a blast.

Thank you to my friends that have supported me in my personal and spiritual life throughout graduate school: Nick Maples, Aaron Legg, Mason Prophator, Steven Maples, and Ben Chapman. They have all been like brothers to me. I don't have a clue where I would be without you all and our church, Immanuel Nashville. The good news of Jesus never ceases to amaze me. He is my deepest foundation.

My family has supported me throughout my entire life. My Mom and Dad always highly valued education and encouraged a curious attitude in me. I'm happy to follow in the footsteps of my Dad, Dr. Knowe. My sisters Laura and Becca have been so constant and supportive of me. I must also thank my new family, Jeff, Debbie, Lauren, and Didaddy Hohman. Thank you for welcoming me into your family and supporting our family in whatever way possible.

Second to last, I must thank Thomas Struble. He has been one of my best friends since we began research in Dr. Forconi's lab our junior year of undergrad. I feel that I have spent more time with him than anyone else over the past eight years. I have always been inspired by his creativity and willingness to take risks. He is an incredible coworker – always volunteering his time to help anyone in need, talk through a research problem, or to fix anything (even if he didn't know how to fix it… yet). So much of my work has been influenced by him that he could easily be a co-author on both papers that have been published. It has been a privilege to watch him grow as a scientist through graduate school, and I am confident that he will be successful in whatever he sets his mind to. More than all of this, he has been an incredible friend to my family. He was a hugely supportive groomsman in my wedding. He has cared for our pets and home many times when we are out of town. He loves our son, JB. He has helped me be a better husband to my wife, Madison. He left a major mark on my life, and I will always consider him one of my best friends.

Finally, I would like to thank and honor my immediate family. My son, JB, is a joy to our family. His sense of humor and resilience amazes me, and I am so proud to call him my son. Finally, I must attempt to thank my wife and best friend, Madison. Through many challenges, I am grateful to say that we have only grown closer. I am proud of her for her endurance she has shown over the past year, losing grandparents, parting with her longtime cat Johnnie (whom I still need to name a catalyst after), and dealing with the challenges of being diagnosed and treated for thyroid cancer. We moved to Nashville almost six year ago for us to begin our respective graduate programs. Since finishing her degree four years ago, she has been so patiently supportive of our family. Being far more academically inclined than me, I want to acknowledge her strength and selflessness in supporting our family financially before being able to pursue a doctoral degree for herself. She has sacrificed a lot to make graduate school possible for me. She has always kept me grounded, reminding me of what the most important things in life are. She has helped me to enjoy life so much more than I would have ever dared to on my own. I am inspired by how she approaches her work and research in the education field, and my teaching has been greatly helped by her! All that to say, I am so grateful for her love and support.

Table of Contents

LIST OF FIGURES

Figure Page

LIST OF TABLES

Table Page

1 Enantioselective desymmetrization of a carboxylic acid

1.1 Introduction

1.1.1 Organocatalysis

Organic chemists have employed small, organic molecules to facilitate enantioselective reactions since their advent in the 60s[1] and 70s,[2] and more so in their current renaissance beginning in the late 90s.[3] The development of these chiral catalysts (in addition to chiral, transition metal-based catalysts[4]) correlates with the demand for chiral, nonracemic molecules, and more efficient manners for their synthesis.[5] When contrasted with the enzymatic structures evolved by nature over the course of biological history, the transformations achieved by organocatalysts are truly remarkable. The advances in in oragnocatalysis have coincided with an ever-expanding catalog of small molecules at the disposal of the chemistry community. These can be roughly organized into four types: [6] Lewis acids,[7] Lewis bases,[8] Brønsted acids,[9] and Brønsted bases.[10] Organocatalysts have multiplied within these types based upon successful and well-established scaffolds: i.e. phosphoric acids,[11] thioureas,[12] cinchona alkaloids and quaternary ammonium salts,[13]

[1] a)Pracejus, H. *Ann.* **1960**, *634*, 23. b)Pracejus, H. *Ann.* **1960**, *634*, 9.

[2] a)Hajos, Z. G.; Parrish, D. R. *J. Org. Chem.* **1974**, *39*, 1615.b) Eder, U.; Sauer, G.; Wiechert, R. *Angew. Chem. Int. Ed.* **1971**, *10*, 496.

[3] Dalko, P. I.; Moisan, L. *Angew. Chem. Int. Ed.* **2004**, *43*, 5138.

[4] a) Knowles, W. S.; Sabacky, M. J.; Vineyard, B. D. *J. Chem. Soc., Chem. Commun.* **1972**, 10. b) Noyori, R.; Ohkuma, T.; Kitamura, M.; Takaya, H.; Sayo, N.; Kumobayashi, H.; Akutagawa, S. *J. Am. Chem. Soc.* **1987**, *109*, 5856. c) Katsuki, T.; Sharpless, K. B. *J. Am. Chem. Soc.* **1980**, *102*, 5974.

[5] a) Dalko, P. I.; Moisan, L. *Angew. Chem. Int. Ed.* **2001**, *40*, 3726. b) Dondoni, A.; Massi, A. *Angew Chem Int Ed Engl* **2008**, *47*, 4638.

[6] Seayad, J.; List, B. *Org. Biomol. Chem.* **2005**, *3*, 719.

[7] Denmark, S. E.; Beutner, G. L.; Wynn, T.; Eastgate, M. D. *J. Am. Chem. Soc.* **2005**, *127*, 3774.

[8] a) Denmark, S. E.; Beutner, G. L. *Angew Chem Int Ed Engl* **2008**, *47*, 1560. b) Sakakura, A.; Ukai, A.; Ishihara, K. *Nature* **2007**, *445*, 900.

[9] Kampen, D.; Reisinger, C. M.; List, B. In *Asymmetric Organocatalysis*; List, B., Ed.; Springer Berlin Heidelberg: Berlin, Heidelberg, 2009, p 1.

[10] a) Palomo, C.; Oiarbide, M.; Lopez, R. *Chem. Soc. Rev.* **2009**, *38*, 632. b) Zamfir, A.; Schenker, S.; Freund, M.; Tsogoeva, S. M. *Org. Biomol. Chem.* **2010**, *8*, 5262.

[11] Terada, M. *Chem Commun (Camb)* **2008**, 4097.

[12] Connon, S. J. *Chem Commun (Camb)* **2008**, 2499.

[13] Marcelli, T.; Hiemstra, H. *Synthesis* **2010**, *2010*, 1229.

phosphines,[14] N-heterocyclic carbenes,[15] strong acids,[16] and guanidines.[17] These scaffolds are being applied to a growing range of functions as: phase transfer catalysts,[18] nucleophilic catalysts,[19] covalent catalysts,[20] frustrated pair catalysts,[21] ion pairing catalysts,[22] anion binding catalysts,[23] hydrogen bonding catalysts,[24] and organocatalytic photoredox catalysts[25] to select a few examples.

1.1.2 Chiral Proton Catalysis

Within this realm of organocatalysis, a relatively simple bifunctional catalyst **1**, was discovered by coordination of a bis(amidine) (BAM) ligand to one equivalent of triflic acid (Figure 1).[26] This "chiral proton" was capable of activating aryl imine electrophiles **2** through hydrogen bonding, as well as activating acidic nitroalkanes **3** by the second aminoquinoline base through deprotonation, acting as a bifunctional catalyst. Control over these two reactive partners was key to achieving both high enantioselectivity and diastereoselectivity of **4**. However, due to the relatively low catalyst activity, only highly electron deficient aryl imines could be used, and solvent amounts of nitroalkane (~50 equivalents) were required to achieve acceptable results.

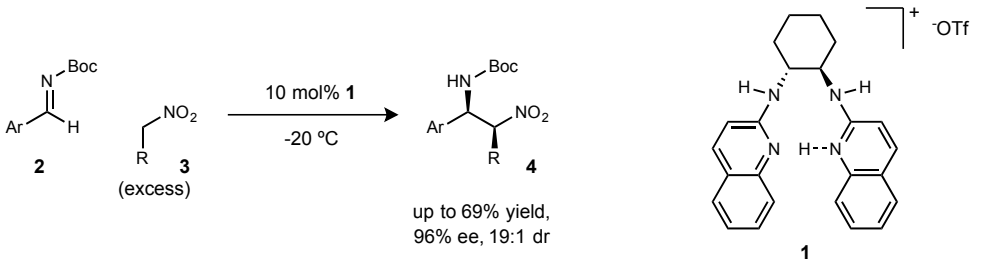

Figure 1: Early enantioselective aza-Henry reaction.[26]

---

[14] Methot, J. L.; Roush, W. R. *Adv. Synth. Catal.* **2004**, *346*, 1035.

[15] Enders, D.; Niemeier, O.; Henseler, A. *Chem. Rev.* **2007**, *107*, 5606.

[16] a) Akiyama, T.; Mori, K. *Chem Rev* **2015**, *115*, 9277. b) Rueping, M.; Nachtsheim, B. J.; Ieawsuwan, W.; Atodiresei, I. *Angew Chem Int Ed Engl* **2011**, *50*, 6706.

[17] a) Coles, M. P. *Chem Commun (Camb)* **2009**, 3659. b) Leow, D.; Tan, C. H. *Chem.--Asian J.* **2009**, *4*, 488.

[18] Shirakawa, S.; Maruoka, K. *Angew Chem Int Ed Engl* **2013**, *52*, 4312.

[19] a) Fu, G. C. *Acc. Chem. Res.* **2000**, *33*, 412. b) Taylor, J. E.; Bull, S. D.; Williams, J. M. *Chem. Soc. Rev.* **2012**, *41*, 2109.

[20] Bertelsen, S.; Jorgensen, K. A. *Chem. Soc. Rev.* **2009**, *38*, 2178.

[21] Stephan, D. W. *Science* **2016**, *354*.

[22] Mahlau, M.; List, B. *Angew Chem Int Ed Engl* **2013**, *52*, 518.

[23] Zhang, Z.; Schreiner, P. R. *Chem. Soc. Rev.* **2009**, *38*, 1187.

[24] Doyle, A. G.; Jacobsen, E. N. *Chem. Rev.* **2007**, *107*, 5713.

[25] Romero, N. A.; Nicewicz, D. A. *Chem. Rev.* **2016**, *116*, 10075.

[26] Nugent, B. M.; Yoder, R. A.; Johnston, J. N. *J. Am. Chem. Soc.* **2004**, *126*, 3418.

The ability to fine-tune this catalyst framework is exemplified by its catalysis of nitroacetate (**5**) additions into imines (**6**) (Figure 2a).[27] When the previously developed quinoline BAM **1** was employed, moderate yield and stereoselectivity was observed. Upon further exploration of the catalyst structure, non C_2 symmetric BAM **7** was discovered to deliver the product in excellent enantioselectivity and high yield of the *anti* diastereomer **8** (up to 12:1 dr in select examples). Replacing a quinoline with a 6-anthracenyl pyridine drastically altered the steric environment of the catalyst pocket. Combined with the impact of the large ester, these are believed to be responsible for the reversal of diastereoselectivity. In order to facilitate the addition of more highly substituted nitroacetates **9**, catalyst **10** was enlisted, bearing a 4-methoxy relative to the quinoline nitrogen (Figure 2b).[28] This more basic catalyst improved reactivity and selectivity significantly, yet the *syn*-diastereomer **11** was preferred. This difference has since been capitalized upon to produce the *anti*-diastereomer in high selectivity with another novel catalyst,[29] and the origins for the diastereodivergence has been illuminated by computational methods.[30]

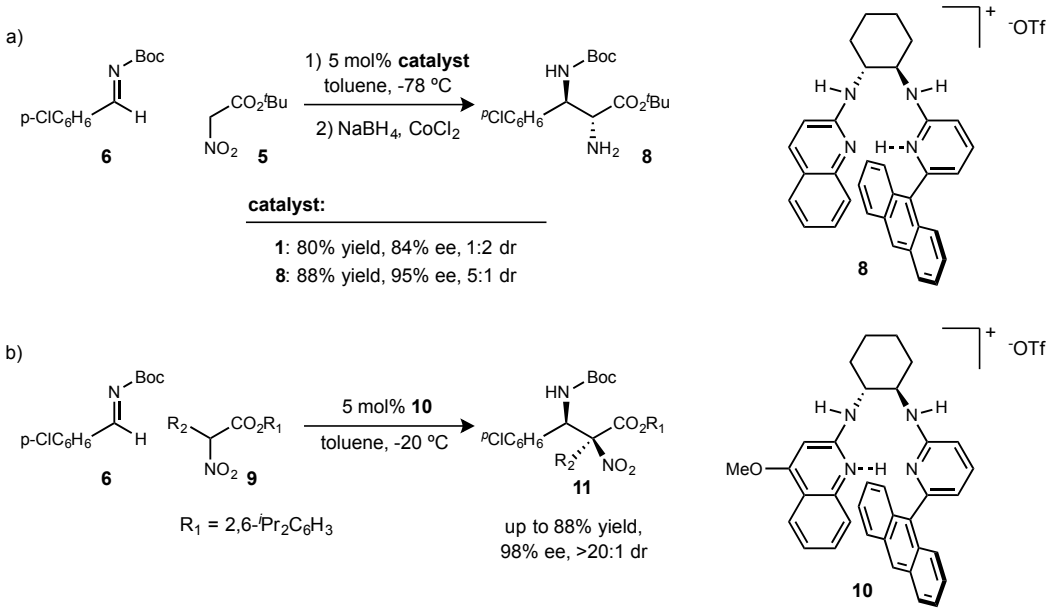

Figure 2: Enantioselective aza-Henry reactions catalyzed by electronically and sterically tuned BAM catalysts.

With this knowledge of catalyst modulation in hand, the prior limitations of the aza-Henry methodology of simple nitroalkanes was revisited (Figure 3, compare to Figure 1).[31]

[27] Singh, A.; Yoder, R. A.; Shen, B.; Johnston, J. N. *J. Am. Chem. Soc.* **2007**, *129*, 3466.

[28] Singh, A.; Johnston, J. N. *J. Am. Chem. Soc.* **2008**, *130*, 5866.

[29] Sprague, D. J.; Singh, A.; Johnston, J. N. *Chem. Sci.* **2018**, doi: 10.1039/C7SC05176J

[30] Struble, T. J.; Johnston, J. N. *Submitted.*

[31] Davis, T. A.; Wilt, J. C.; Johnston, J. N. *J. Am. Chem. Soc.* **2010**, *132*, 2880.

Several catalysts with higher basicity were screened under more practical reaction conditions (1.5 equivalents of nitroethane, a full range of electron rich and poor imines). It was observed that catalyst **1** performed poorly, with lowered enantioselectivity (87% ee) and poor yield (29%). More basic catalysts with methoxy (**12**) or pyrrolidyl (**13**) at the 4-quinoline position increased selectivity, but more importantly conversion, significantly. PBAM•HOTf (**13**) was hence discovered to benefit not only from utilizing a "chiral proton" to activate imine electrophiles, but also benefit from increased basicity for nucleophile activation. Optimization of the catalyst to acid ratio led to the conclusion that the $(PBAM)_2(HOTf)_3$ state was best, with yields up to 99% and selectivities up to 95% and >20:1 dr. This methodology and bifunctional catalyst have since enabled successful application to other aza-Henry variants, using aryl nitromethane pronucleophiles,[32] silyl imine electrophiles,[33] bromonitromethane pronucleophiles (for production of non-natural, alkyl amino amides),[34] and fluronitroalkane pronucleophiles.[35]

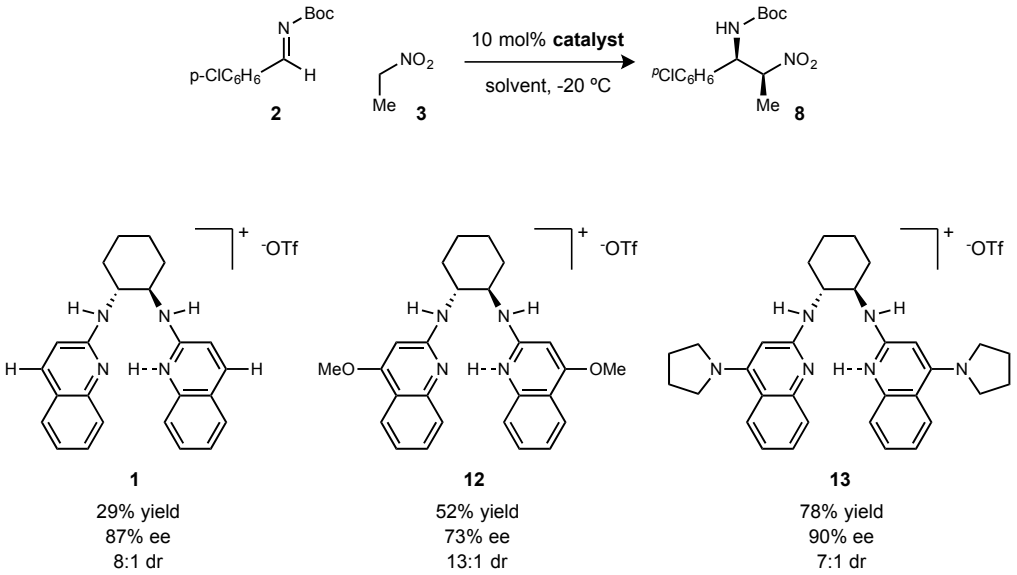

Figure 3: More Brønsted basic (acid) catalysts increase reactivity and selectivity.

1.1.3 Catalytic asymmetric halofunctionalizations of alkenes

[32] Davis, T. A.; Johnston, J. N. *Chem. Sci.* **2011**, *2*, 1076. Vara, B. A.; Mayasundari, A.; Tellis, J. C.; Danneman, M. W.; Arredondo, V.; Davis, T. A.; Min, J.; Finch, K.; Guy, R. K.; Johnston, J. N. *J. Org. Chem.* **2014**, *79*, 6913.

[33] Makley, D. M.; Johnston, J. N. *Org. Lett.* **2014**, *16*, 3146.

[34] a) Schwieter, K. E.; Johnston, J. N. *ACS Catalysis* **2015**, *5*, 6559. b) Lim, V.; Tsukanov, S. V.; Doody, A.; Johnston, J. N. *Org. Synth.* **2016**, *93*, 88.

[35] Vara, B. A.; Johnston, J. N. *J. Am. Chem. Soc.* **2016**, *138*, 13794.

While bifunctional BAM catalysis was being used to control azomethine functionalities, it was discovered to also have utility in alkene functionalizations: namely, halofunctionalizations. Using a newly developed catalyst, StilbPBAM•$HNTf_2$ (**14**), the intramolecular iodolactonization[36] of 1,1-disubstituted alkenes could be achieved in very good yield and enantioselectivity, and will be further discussed in the ensuing discussion.[37]

There have been a variety of strategies reported by the synthetic community to accomplish asymmetric halocyclizations.[38] Most of these methods could arguably be categorized under Lewis base, Lewis acid, Brønsted base, or Brønsted acid catalysis (or a multifunctional combination of these), along with more specific categories such as chiral anion binding and phase transfer catalysis. Some of the earliest examples of selective

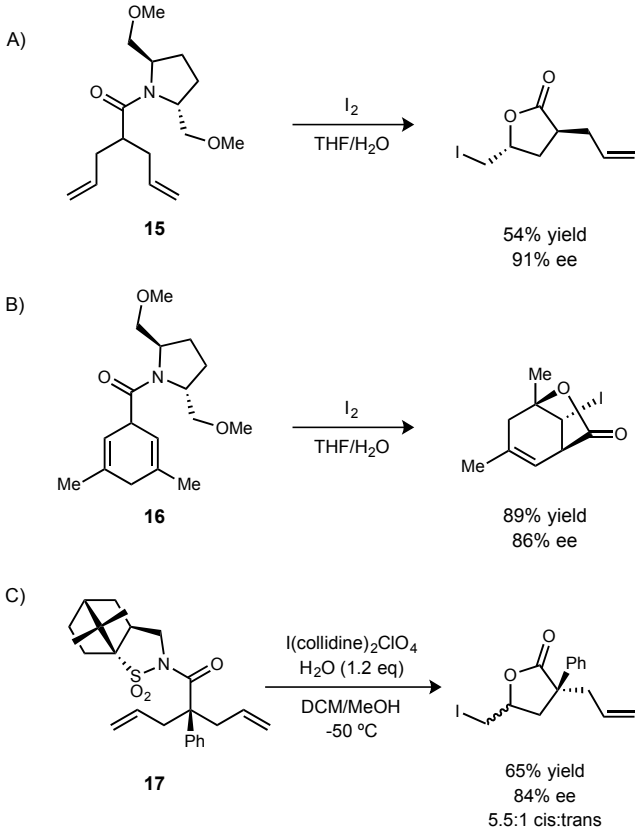

Figure 4: Iodolactionizations utilizing chiral auxiliaries.

[36] van Tamelen, E. E.; Shamma, M. *J. Am. Chem. Soc.* **1954**, *76*, 2315.

[37] Dobish, M. C.; Johnston, J. N. *J. Am. Chem. Soc.* **2012**, *134*, 6068.

[38] Enantioselective halocyclization reviews: a) Tan, C.; Zhou, L.; Yeung, Y.-Y. *Synlett* **2011**, 1335. b) Hennecke, U. *Chem. - Asian J.* **2012**, *7*, 456. c) Denmark, S. E.; Kuester, W. E.; Burk, M. T. *Angew. Chem. Int. Ed.* **2012**, *51*, 10938. d) Fujioka, H.; Murai, K. *Heterocycles* **2013**, *87*, 763. e) Cheng, Y.; Yu, W.; Yeung, Y.-Y. *Org. Biomol. Chem.* **2014**, *12*, 2333. f) Mukherjee, S. *Catalytic Enantioselective Halocyclizations beyond Lactones: Emerging Routes to Enantioenriched Nitrogenous Heterocycles.* g) Hennecke, U.; Wilking, M. *Synlett* **2014**, *25*, 1633.

halocyclizations required the use of chiral auxiliaries, as demonstrated by the Fuji group in 1990 (Figure 4A and B)[39] and the Shibuya group in 1992 (Figure 4C).[40] Fuji and coworkers employed a chiral amide substrate bearing a C_2-symmetric pyrrolidine auxiliary to accomplish diastereoselective iodolactonizations of simple dienes **15** and **16** in good yield and good enantioselectivity. Shibuya and coworkers used chiral camphor sultam-derived imide **17** to produce similar products in decent enantioselectivity and moderate diastereoselectivity.

Taguchi and coworkers reported the earliest example of catalytic enantioselective halocyclizations using chiral Lewis acid catalysts (Figure 5). A stoichiometric amount of chiral titanium complex **18** was used to first achieve a diastereo- and enantioselective iodolactonization of diene **19** (58:1 dr, 64% ee) (Figure 5A).[41] A 20 mol % loading of **18** was used for an iodocarbocyclization of alkene **20** in high enantioselectivity (94% ee). X-Ray crystallography of the titanium complex bound to acetylacetone enabled the development of a hypothesis for the origins of enantioselectivity.[42] Binding of the malonate moiety to titanium and deprotonation by the alkoxide ligand generates a chiral enolate complex. The alkene electrophile can be ordered by the chiral ligands into an energetically favored chair, leading to the major enantiomer.

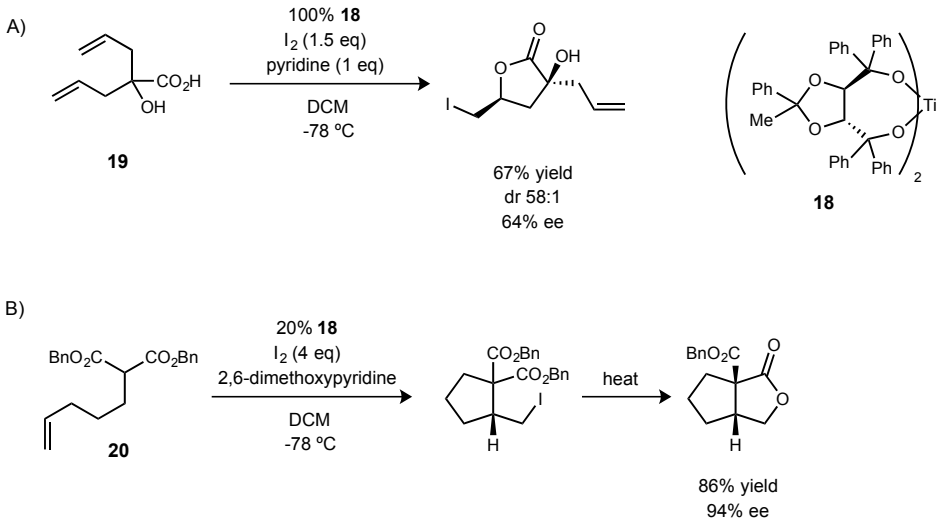

Figure 5: A) Enantioselective iodolactonization and B) iodocarbocyclization by a chiral titanium catalyst.

[39] Kaoru, F.; Manabu, N.; Yoshimitsu, N.; Takeo, K. *Tetrahedron Lett.* **1990**, *31*, 3175.

[40] Yokomatsu, T.; Iwasawa, H.; Shibuya, S. *Tetrahedron Lett.* **1992**, *33*, 6999.

[41] Kitagawa, O.; Hanano, T.; Tanabe, K.; Shiro, M.; Taguchi, T. *J. Chem. Soc., Chem. Commun.* **1992**, *0*, 1005.

[42] Inoue, T.; Kitagawa, O.; Ochiai, O.; Shiro, M.; Taguchi, T. *Tetrahedron Lett.* **1995**, *36*, 9333.

Following Taguchi's work, several groups made progress in establishing selectivity based on chiral Lewis base binding to halogen electrophiles. One of the earliest examples of chiral Lewis base catalysis was reported by the Grossman group, from the University of Kentucky, in 1998 (Figure 6A).[43] Based on the hypothesis that Taguchi's earlier work proceeds via a covalently bound, chiral titanium enolate, Grossman's work is the earliest example of enantioselectivity in a halocyclization by noncovalent, or reagent, control. Using two equivalents of dihydroquinidine **21** and one equivalent of iodine, a hypothesized chiral source of halonium is generated, delivering products **22** in 'promising' initial selectivities (15% ee). The Brown group applied a different Lewis base, 2-menthyl pyridine **23**, to generate a preformed, chiral bromonium source (Figure 6B).[44] Pentenoic acid **24** was converted to bromo lactone **25** in 5% enantiomeric excess. Soon after, the Wirth group reported a significant advance in this stragetgy (Figure 6C).[45] Chiral amines were screened as ligands for iodine, with the surprisingly simple **26** found to facilitate this lactonization in relatively high enantioselectivity (45%). However, this result only stands for 1,1

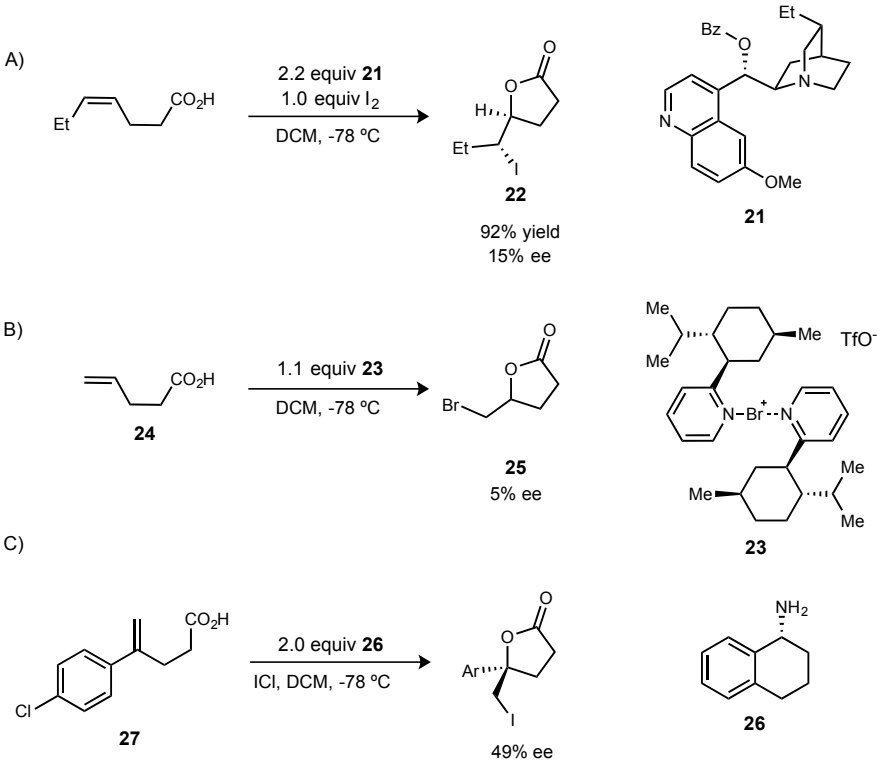

Figure 6: The earliest enantioselective catalyzed halolactonizations.

disubstituted aryl alkenes **27**. Alkyl substituted alkenes, similar to those used in Grossman's and Brown's work, produced racemic products. It should be that there is debate about the

[43] Grossman, R. B.; Trupp, R. J. *Can. J. Chem.* **1998**, *76*, 1233.

[44] Cui, X.-L.; Brown*, R. S. *J. Org. Chem.* **2000**, *65*, 5653.

[45] Haas, J.; Piguel, S.; Wirth, T. *Org. Lett.* **2002**, *4*, 297.

mechanism of this class of reaction, with recent findings providing evidence for Brønsted base mechanisms being operative instead of Lewis base.[46]

A remarkable extension of this Lewis base strategy was realized by Ishihara and coworkers in 2007 (Figure 7A).[47] Phosphoramidite **28** was used as a stoichiometric chiral promoter to facilitate an iodopolycyclization reminiscent of squalene synthase. Polycyclic iodides **29** are produced from polyenes **30** in modest yield and excellent selectivities (94:6 dr, 99% ee). Although substoichiometric Lewis base activation of halogens still remains a challenge, selenophosphoramide catalysts have been recently used to accomplish

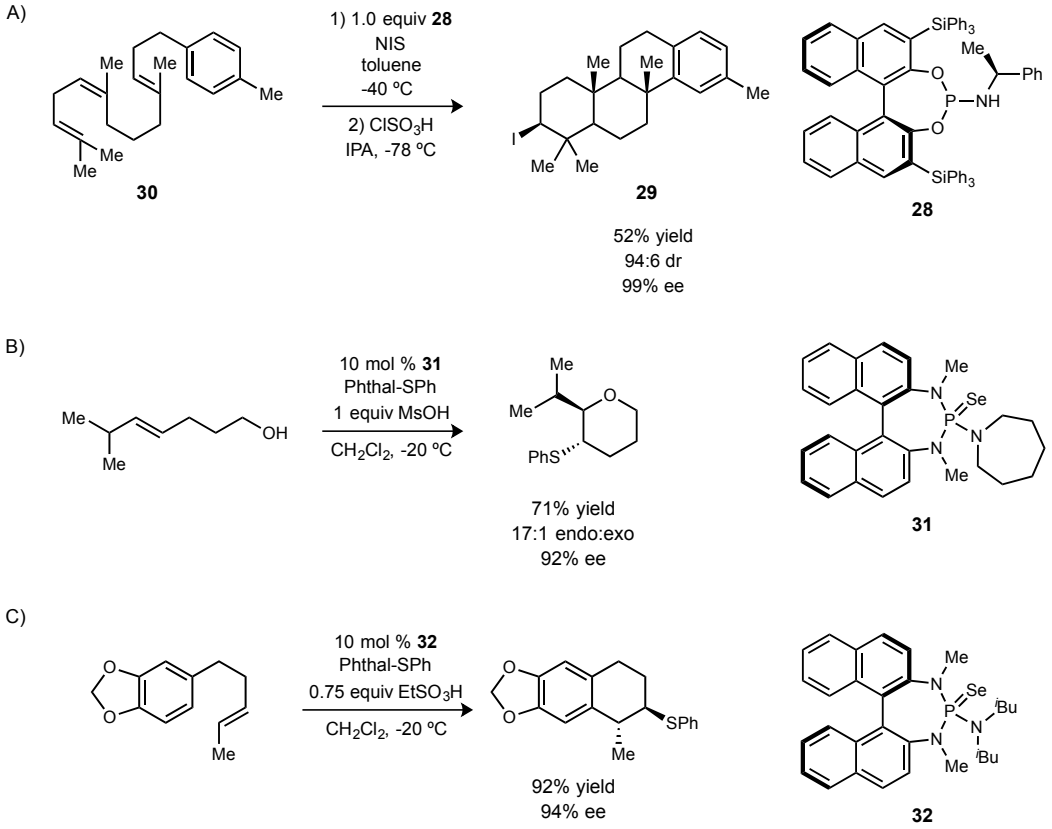

Figure 7: A) Enantioselective polycyclization, B) sulfenyletherification, and C) carbosulfenylation by chiral Lewis bases.

enantioselective sulfenylcyclizations of alkenes. Using selenophosphoramide **31**, Denmark and coworkers could achieve a selective sulfenyletherification with good selectivity (92% ee) (Figure 7B).[48] This work could be extended to the carbosulfenylation of alkenes with related catalyst **32** (Figure 7C).[49] These selenophosphoramides are proposed to bind to and deliver

[46] Denmark, S. E.; Ryabchuk, P.; Burk, M. T.; Gilbert, B. B. *J. Org. Chem.* **2016**, *81*, 10411.

[47] Sakakura, A.; Ukai, A.; Ishihara, K. *Nature* **2007**, *445*, 900.

[48] Denmark, S. E.; Kornfilt, D. J. P.; Vogler, T. *J. Am. Chem. Soc.* **2011**, *133*, 15308.

[49] Denmark, S. E.; Jaunet, A. *J. Am. Chem. Soc.* **2013**, *135*, 6419.

sulfenium to the alkene, selectively forming a thiiranium ion which is captured by the nucleophile intramolecularly.

Chiral ion pairing catalysis, also known as "asymmetric counteranion-directed catalysis" (ACDC[50]), has emerged as a powerful tool in asymmetric synthesis by Brønsted acids.[16,51] This catalysis frequently uses chiral phosphoric acids, chiral carboxylic acids, and chiral *N*-triflyl phosphoramides[52] to achieve a variety of enantioselective reactions, such as spiroacetalizations,[53] hydroaminations,[54] and halocyclizations. One of the earliest applications used a chiral BINOL-based phosphate salt **33** to catalyze an enantioselective iodoetherification (Figure 8).[55] Hennecke and coworkers propose the formation of an iodonium-chiral phosphate ion pair as the origin of enantioselectivity. By employing symmetric alkene substrate **34**, they were able to avoid the necessity of forming the iodonium enantioselectively, as other groups had been previously focused on. Rather, the phosphate counterion must control which alcohol cyclizes onto the *meso*-iodonium ion in order to succeed. Interestingly, the corresponding phosphoric acids were unable to achieve significant levels of enantioselectivity. Upon generation of the chiral ion pair, sodium pyrrolidinone is generated, and this is likely basic enough to activate the alcohol nucleophile for cyclization. However, a mechanism for how enantioselectivity is achieved is not addressed in detail. Interestingly, when **33** was applied to the bis(carboxylic acid) version of substrate **34**, only racemic iodolactone product was generated. Results from the phosphoric acid of **33** are not reported.

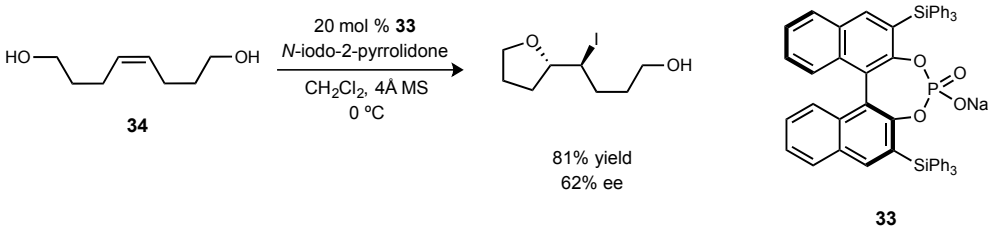

Figure 8: Chiral ion pairing applied to halocyclizations by enantioselective desymmetrization.

[50] Mahlau, M.; List, B. *Angew Chem Int Ed Engl* **2013**, *52*, 518.

[51] a) Parmar, D.; Sugiono, E.; Raja, S.; Rueping, M. *Chem. Rev.* **2014**, *114*, 9047. b) Min, C.; Seidel, D. *Chem. Soc. Rev.* **2017**, *5889*.

[52] Kampen, D.; Reisinger, C. M.; List, B. In *Asymmetric Organocatalysis*; List, B., Ed.; Springer Berlin Heidelberg: Berlin, Heidelberg, 2009, p 1.

[53] Coric, I.; List, B. *Nature* **2012**, *483*, 315.

[54] Ackermann, L.; Althammer, A. *Synlett* **2008**, *2008*, 995.

[55] Hennecke, U.; Müller, C. H.; Fröhlich, R. *Org. Lett.* **2011**, *13*, 860.

The Toste group also made significant advances in the area of chiral ion pairing catalysis (chiral anion phase-transfer catalysis) (Figure 9).[56] This work stands upon the realization that insoluble halogen sources can advantageously inhibit the racemic background reaction from occurring. Only when the tetrafluoroborate counterion is exchanged for a chiral phosphate counterion can reaction with the substrate occur. As such, this methodology has been successfully applied to the cyclization of amides with a range of halogen sources. The fluorocyclization of amides **35** is accomplished using highly insoluble Selectfluor as the halogen source, and a derivative of TRIP, **36**, as the catalyst (Figure 9A).[56a] **36** is deprotonated *in situ* and then can undergo salt metathesis with Selectfluor to generate a soluble halogen source possessing at least one phosphate counterion. A non-linear effect was observed, indicating that two phosphate counterions may be present in the enantiodetermining step. Fluorocyclizations were achieved in good yields and high selectivities (96% ee, >20:1 dr). This methodology significantly advanced the stereoselective construction of carbon-fluorine bonds, and it's utility was further demonstrated by extension to other halogen cyclizations. Using highly insoluble, tricationic halonium reagents **37** and **38**, the highly enantioselective bromo- and iodo- cyclizations of amides **39** could be performed under nearly identical conditions by phosphoric acid **40** (Figure 9B).[56b]

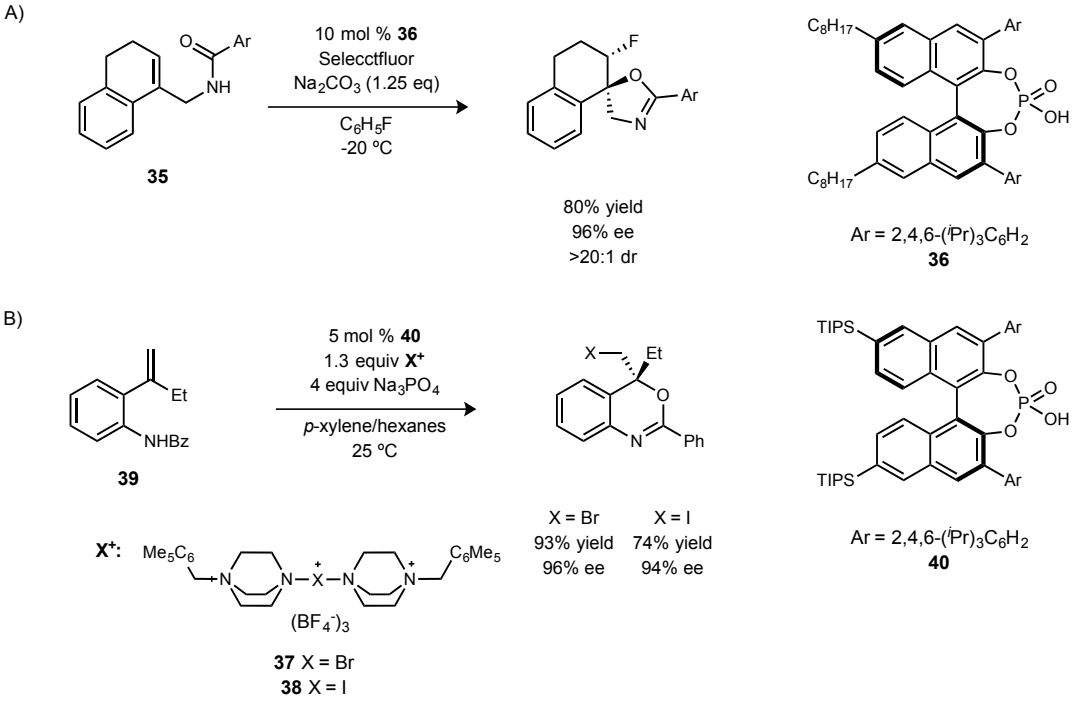

Figure 9: A) Fluoro-, B) bromo-, and iodocyclizations of amides by chiral ion pairing.

[56] a) Rauniyar, V.; Lackner, A. D.; Hamilton, G. L.; Toste, F. D. *Science* **2011**, *334*, 1681. b) Wang, Y.-M.; Wu, J.; Hoong, C.; Rauniyar, V.; Toste, D. F. *J. Am. Chem. Soc.* **2012**, *134*.

Haloaminations and haloetherification have also been achieved using chiral ion pairing catalysis. The Shi group and the Denmark group simultaneously reported bromocyclizations of similar alkenes (**41** and **42**) using similar methodology (Figure 10). The Shi group was able to achieve both bromo –aminations and –etherifications of unactivated alkenes in high enantioselectivity (products **43a** and **44b**, 90% ee and 81% ee, respectively) (Figure 10A).[57] However, styrenyl substrates gave poor exo:endo selectivity, and (*E*) alkenes reacted in lower enantioselectivities. This work is hypothesized to generate a halonium/phosphate ion pair, but phosphoric acid catalyst **45** is hypothesized to simultaneously activate nucleophile and electrophile (although the calcium salt has been mistakenly used in the past[58]). Denmark's work is remarkably similar, save for the addition of a catalytic Lewis base, triphenylphosphine sulfide, to facilitate bromonium transfer from succinimide to the alkene (Figure 10B).[59] Consequently, this methodology is capable of functionalizing styrenyl alkenes efficiently. When (*Z*)-**42** is used, bromofuran **46** is produced in high levels of *exo*- and enantioselectivity (95:5 *exo*:*endo*, and 82% ee). (*E*)-**42** also yields the *exo*-product **46** in good enantioselectivity, but an equal amount of *endo*-product is produced racemically.

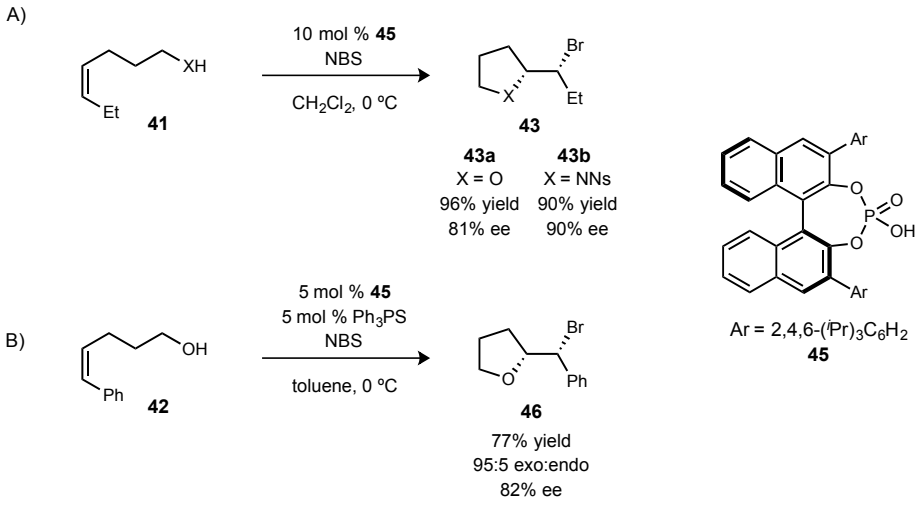

Figure 10: A) Haloamination and B) haloetherification of alkenes by chiral ion pairing.

Arguably the most common strategy for enantioselective halofunctionalizations of alkenes is bifunctional catalysis. Oftentimes these catalysts have an acidic, hydrogen bond donating functionality combined with basic functionality (acting as either a Brønsted base or Lewis base). Most proposed mechanisms focus overwhelmingly on catalyst activation and control of the halogen source, however several recent studies have brought renewed emphasis

[57] Huang, D.; Wang, H.; Xue, F.; Guan, H.; Li, L.; Peng, X.; Shi, Y. *Org. Lett.* **2011**, *13*, 6350.

[58] Hatano, M.; Moriyama, K.; Maki, T.; Ishihara, K. *Angew. Chem.* **2010**, *122*, 3911.

[59] Denmark, S. E.; Burk, M. T. *Org. Lett.* **2012**, *14*, 256.

on the role of catalyst nucleophile activation.[46,60] One of the earliest examples of an organocatalyst achieving high selectivity in a halofunctionalization was reported by the Jacobsen group in 2010 (Figure 11A).[61] Using bifunctional **47** as a catalyst, the iodolactonization of 1,1 disubstituted alkenes **48** to lactones **49** was performed in high yields and selectivities. A unique, phthalimide iodonium source **50** provided the highest enantioselectivity (94% ee), and a catalytic amount of iodine was mandatory for reactivity (3% yield without I_2). An extensive catalytic cycle is proposed in which a key catalytic intermediate (**51**, Figure 11B) serves to deliver iodine to the alkene in an enantioselective fashion, and the authors classify this mode as chiral ion pairing catalysis. They propose that urea **47** reacts with *N*-iodophthalimide to generate **51**. Then the hydrogen bonded phthalimide anion purportedly activates the carboxylic acid nucleophile as the tertiary amine moiety delivers iodine to the alkene. The main support for this proposal is based on the impact of different halogen-source structures on the stereoselectivity of the reaction, indicating its involvement in the enantiodetermining step. A simpler, and experimentally consistent, mechanistic proposal wherein the Brønsted base (tertiary amine) moiety activates the carboxylic acid nucleophile and the Brønsted acidic thiourea activates the phthalimide electrophile is not discussed as a possibility, however.

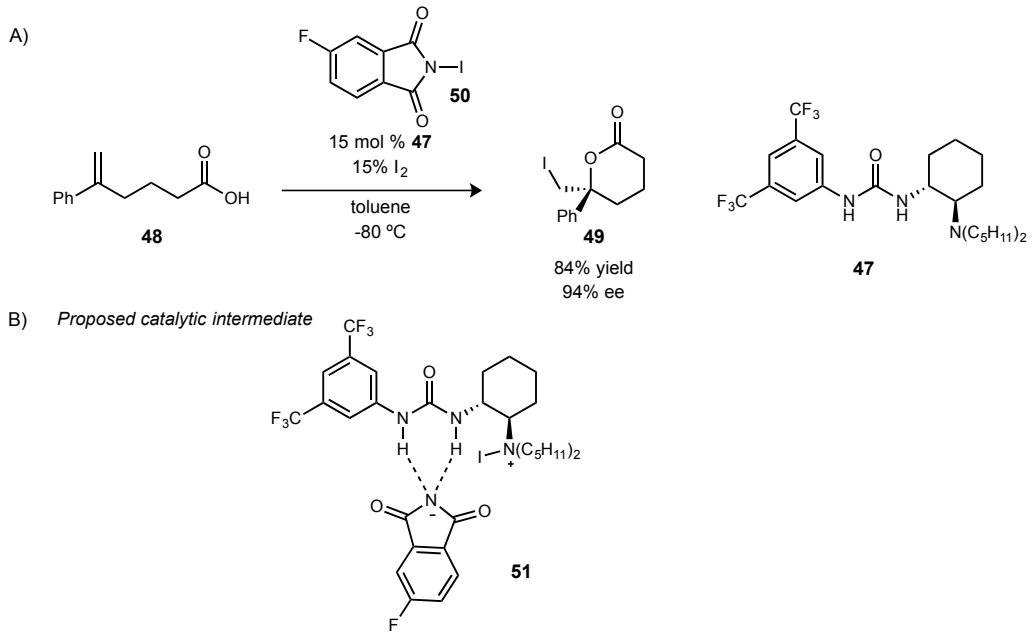

Figure 11: A) Jacobsen's enantioselective iodolactonization using a bifunctional catalyst; B) proposed ion binding activation mode.

[60] Ashtekar, K. D.; Vetticatt, M.; Yousefi, R.; Jackson, J. E.; Borhan, B. *J. Am. Chem. Soc.* **2016**, *138*, 8114.

[61] Veitch, G. E.; Jacobsen, E. N. *Angew. Chem. Int. Ed.* **2010**, *49*, 7332.

The Yeung group soon after reported an example of Lewis base/Brønsted base bifunctional catalysis for the enantioselective bromolactonization of pentenoic acids (Figure 12A).[62] Using a cinchonine scaffold with an appended thiocarbamate, bifunctional catalyst **53** was found to impact the reaction in good yield and selectivity (90% ee). Under the premise that an additional hydrogen bond donor may help, several weak acid additives were tested, and *p*-nitrobenzenesulfonamide was found to increase enantioselectivity from 87% to 90%. The authors also mention the possible formation of NsNHBr from *p*-nitrobenzenesulfonamide, which could serve as the active brominating agent. The catalyst thiocarbamate functionality is proposed to activate and position NBS through hydrogen bonding and sulfur-bromine coordination (**54**, Figure 12B). Simultaneous deprotonation of carboxylic acid **55** by the catalyst quinuclidine would position the substrate for enantioselective formation of bromolactone **56**.

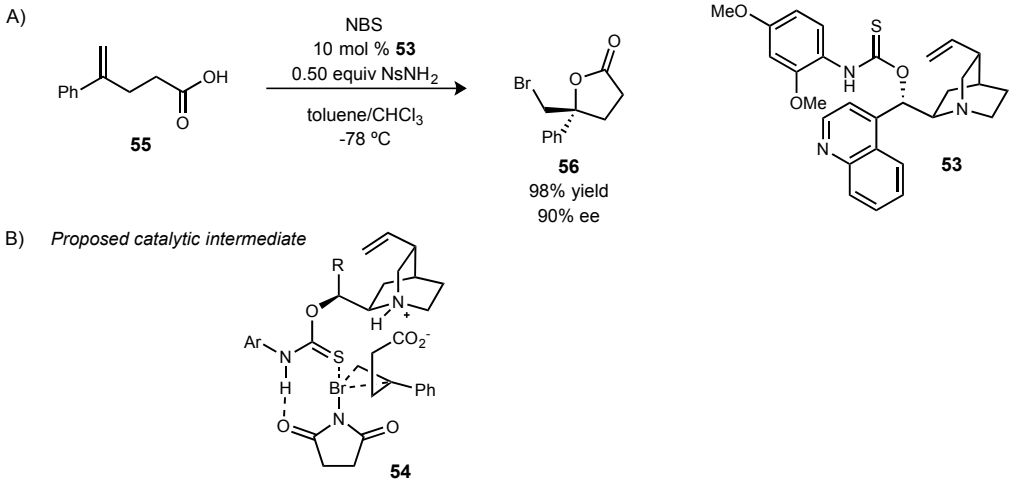

Figure 12: A) Yeung's Lewis base/Brønsted base catalyzed bromolactonization; B) proposed Lewis base/Brønsted base catalytic activation mode.

An organocatalyst (**57**) which partners an acidic phenol and a basic amidine was developed by Martin and coworkers for an enantioselective bromolactonization (Figure 13A).[63] As in previous methodologies, higher selectivity was observed for *Z*-olefins (**58)** versus *E*-olefins. This catalytic system could even desymmetrize prochiral substrate **59** to the 4-*exo* lactone **60**, albeit in low enantioselectivity (46%) (Figure 13B). These conditions were also amenable to iodolactonizations with only minor adjustments.[64] The authors propose that the amidine stabilizes a bromonium ion by Lewis base interaction and that the phenol hydrogen bonds to the carboxylic acid (or carboxylate) to orient the substrate (Figure 13C). This proposal must assume that the brominating agent, TBCO, reacts with

[62] Zhou, L.; Tan, C.; Jiang, X.; Chen, F.; Yeung, Y.-Y. *J. Am. Chem. Soc.* **2010**, *132*, 15474.

[63] Paull, D. H.; Fang, C.; Donald, J. R.; Pansick, A. D.; Martin, S. F. *J. Am. Chem. Soc.* **2012**, *134*, 11128.

[64] Fang, C.; Paull, D. H.; Hethcox, J. C.; Shugrue, C. R.; Martin, S. F. *Org. Lett.* **2012**, *14*, 6290.

the substrate initially to form zwitterionic bromonium-carboxylate species **61**, which then is coordinated by the catalyst. A plausible, yet unmentioned, alternative would involve amidine activation of the substrate carboxylic acid as a Brønsted base, and catalyst phenol activation of TBCO as a Brønsted acid. However, an early focus on Lewis base control of halogenation influenced the proposed mechanism.

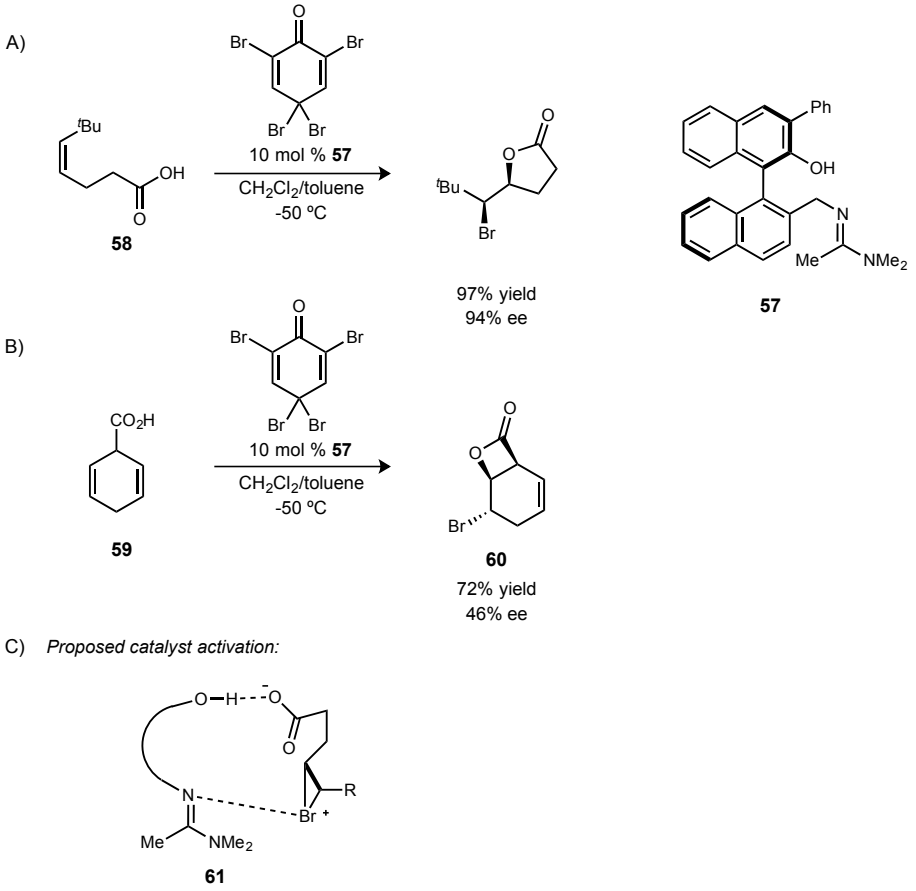

Figure 13: A) Martin's bifunctionally catalyzed bromolactonization, B) enantioselective desymmetrization, and C) proposed Lewis base/Brønsted acid catalytic activation mode.

Another example of bifunctional catalysis was developed by the Borhan group, and they reported the enantioselective chlorolactonization of 1,1-disubstituted pentenoic acids (**62**, Figure 14)[65] by the previously developed organocatalyst, $(DHQD)_2PHAL$.[66] Production of **63** was optimized to high yields and high enantioselectivities (81% and 89%, respectively), finding that one equivalent of benzoic acid was required to reach 89% ee. This additive is hypothesized to protonate a catalyst quinidine, forming a hydrogen bond donor to activate

[65] Whitehead, D. C.; Yousefi, R.; Jaganathan, A.; Borhan, B. *J. Am. Chem. Soc.* **2010**, *132*, 3298.

[66] a) Jacobsen, E. N.; Marko, I.; Mungall, W. S.; Schroeder, G.; Sharpless, K. B. *J. Am. Chem. Soc.* **1988**, *110*, 1968. b) Li, G.; Chang, H.-T.; Sharpless, K. B. *Angew. Chem. Int. Ed.* **1996**, *35*, 451. c) Becker, H.; Sharpless, K. B. *Angew. Chem. Int. Ed.* **1996**, *35*, 448.

the hydantoin chloronium source, and NMR studies revealed a binding interaction between catalyst and dichlorohydantoin. The remaining quinidine serves as a Brønsted base to deprotonate the carboxylic acid nucleophile. Interestingly, a screen of chloronium sources revealed the larger diphenylhydantoin (89% ee) to perform better than smaller halogen sources, such as dimethylhydantoin (84% ee). A matched/mismatched case was discovered between chiral chlorohydantoin structures and catalyst, as (*S*)-5-isopropyl-1,3-dichlorohydantoin was found to be more reactive and more selective (78% yield, 83% ee) than its (*R*) counterpart (44% yield, 69% ee). This further corroborated the hypothesized interaction between catalyst and oxidant in the enantiodetermining step. This work has been further developed to the asymmetric chlorocyclization of amides,[67] intermolecular haloetherifications,[68] and dihalogenation of alkenes.[69]

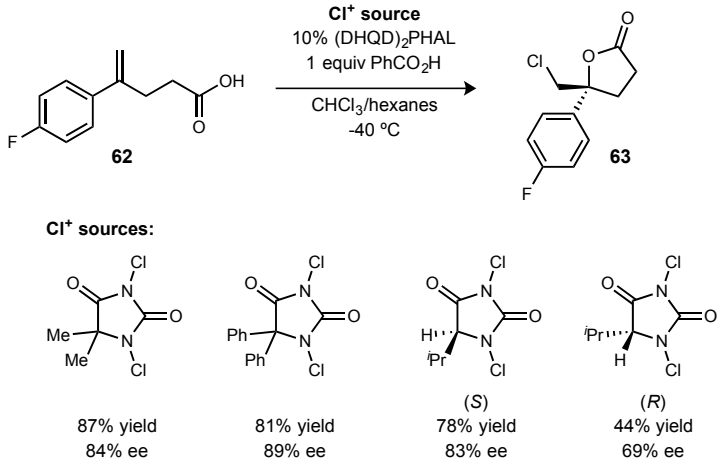

Figure 14: Enantioselective chlorolactonization using bifunctional catalysis.

A desire to further understand the origin of enantioselectivity in this methodology inspired a series of mechanistic investigations. The Borhan group sought to understand the nature of chloronium delivery in their prior work (Figure 15A): enantioselective formation of a bridged chloronium ion **64** followed by stereospecific (*anti*) nucleophilic addition, or formation of planar carbocation **65** followed by catalyst controlled addition of the carboxylate nucleophile. In order to provide a record of the path of attack without structurally altering the 1,1-disubstituted alkene substrates, *E*-deuterated alkene **66** was prepared (Figure 15B).[70] This enabled the observation of chlorine facial selectivity, bridged chloronium or carbocation formation, and relative stereochemical orientation between chlorine and carboxylate. Cyclization of **67** was highly diastereoselective, yielding 89% of

[67] Jaganathan, A.; Garzan, A.; Whitehead, D. C.; Staples, R. J.; Borhan, B. *Angew. Chem. Int. Ed.* **2011**, *50*, 2593.
[68] Soltanzadeh, B.; Jaganathan, A.; Staples, R. J.; Borhan, B. *Angew. Chem. Int. Ed.* **2015**, *54*, 9517.
[69] Soltanzadeh, B.; Jaganathan, A.; Yi, Y.; Yi, H.; Staples, R. J.; Borhan, B. *J. Am. Chem. Soc.* **2017**, *139*, 2132.
[70] Yousefi, R.; Ashtekar, K. D.; Whitehead, D. C.; Jackson, J. E.; Borhan, B. *J. Am. Chem. Soc.* **2013**, *135*, 14524.

5*R*,6*R*-**68**, which surprisingly arose from a net *syn* addition of chlorine and carboxylate across the alkene. This result eliminated the possibility of a bridged chloronium intermediate

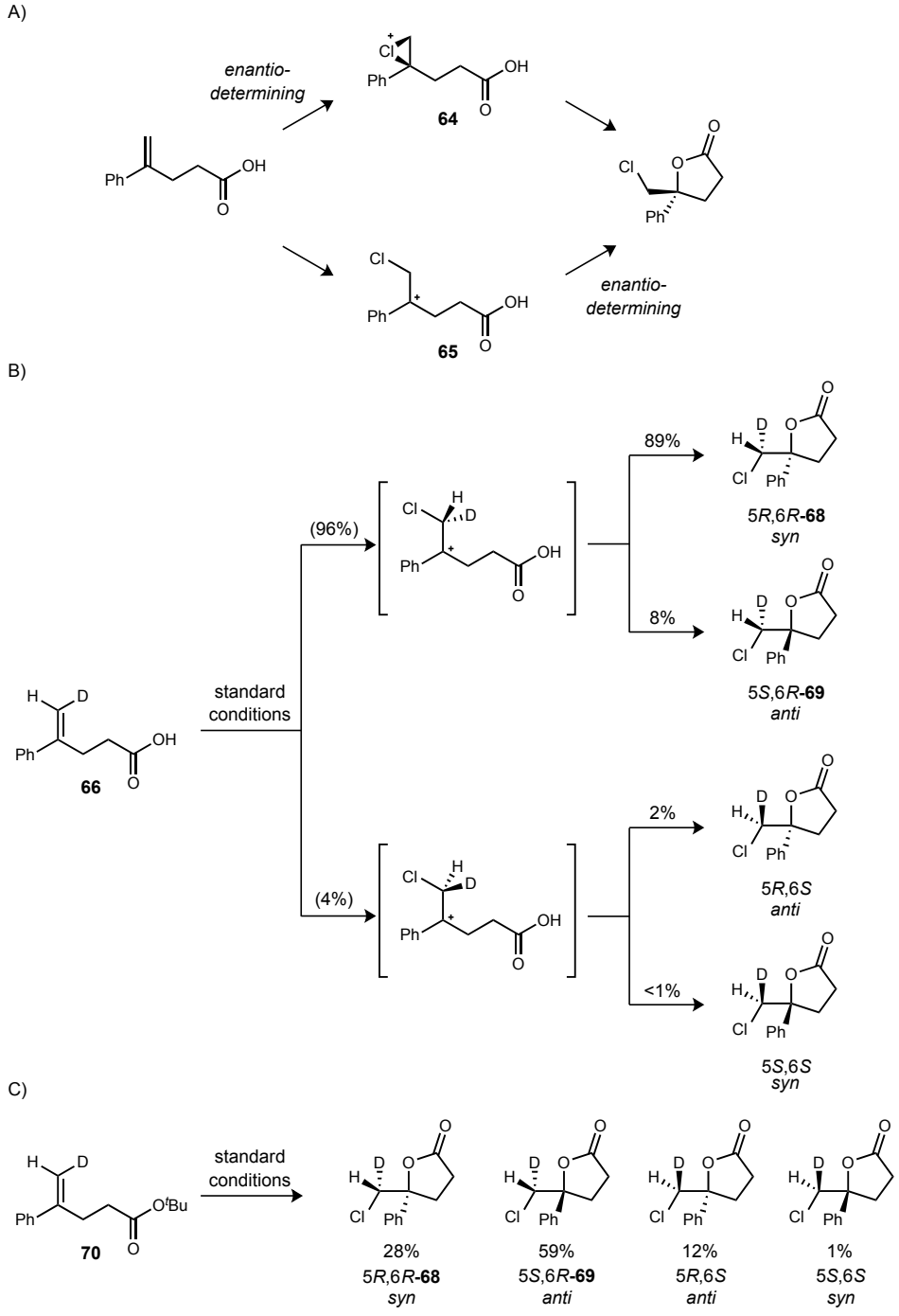

Figure 15: A) Two possible pathways for enantioselective chlorolactonizations; B) mechanistic investigations into alkene facial control and nucleophile addition in chlorolactonizations; C) segregating nucleophile and electrophile control.

and supported a carbocation intermediate.[71] The second most abundant diastereomer, 5*S*,6*R*-**69** (8%), has the same configuration at the chlorine center, indicating a total of 96% of the starting alkene was electrophilically attacked by chloronium at the pro-*R* face. The highly stereoselective delivery of chlorine linked the catalyst to this step. Additionally, the preference for the *syn* diastereomer implicated a second catalyst role in nucleophilic addition to the carbocation intermediate.

In order to individually investigate the two catalyst roles, a *tert*-butyl ester substrate analog was tested in the chlorolactonization reaction, to prevent catalyst binding to the nucleophile. The product was produced in 20% ee, indicating a catalyst influence over nucleophile addition in the typical lactonization. When deuterated *tert*-butyl ester **70** was subjected, a broader distribution of stereoisomers was obtained (Figure 15C). The preferred relative stereoselectivity was reversed, with the *anti* diastereomer now favored. Although enantioselectivity was low due to poor nucleophile control, high *R*-facial selectivity (87%) was still observed for chloronium delivery (28% 5*R*,6*R*-**68** plus 59% 5*S*,6*R*-**69**). Therefore, the authors concluded that both chlorination of the alkene and cyclization to the lactone product are both under distinct influences from $(DHQD)_2PHAL$. A quantitative study of the reactivity of halogenating agents with various Lewis bases was subsequently conducted, yielding the halenium affinity (*HalAI*) scale.[72] This report addresses the frequent invocation of bridged halonium species in mechanism proposals. Based upon calculations on styrenyl substrates for a variety of halonium sources (B3LYP/6-31g*/LanL2DZ), the open carbocation form was always found to be more stable and have a low barrier to rotation. This is consistent with previous findings of a highly selective, *syn* chlorolactonization (Figure 15A). The *HalA* method also claims that traditional imide-based halonium sources (NIS, DBDMH, etc) cannot effectively transfer halonium to an olefin, as the resultant imide anion is a better nucleophile than the olefin. Activation of the olefin and/or activation of the halonium source is required.

This led the Borhan group to investigate the nucleophilic addition portion of halocyclizations, arriving at the concept of Nucleophile Assisted Alkene Activation (NAAA) (Figure 16B).[60] The activation of olefins by neighboring nucleophiles has long been hypothesized as the cause for the ease of intramolecular halocyclizations relative to intermolecular halocyclizations.[73] Increasing electron density of the carboxylic acid functionality of **71** was observed to shift the alkene protons and carbons by NMR in a

[71] A prior study had found that bromonium and chloronium ions of 1,2 disubstituted alkenes were configurationally stable: Denmark, S. E.; Burk, M. T.; Hoover, A. J. *J. Am. Chem. Soc.* **2010**, *132*, 1232.

[72] Ashtekar, K. D.; Marzijarani, N. S.; Jaganathan, A.; Holmes, D.; Jackson, J. E.; Borhan, B. *J. Am. Chem. Soc.* **2014**, *136*, 13355.

[73] a) Staninets, V. I. S., E. A. *Russ. Chem. Rev.* **1971**, *40*. b) Williams, D. L. H.; Bienvenue-Goetz, E.; Dubois, J. E. *J. Chem. Soc. B* **1969**, 517.

manner consistent with a pre-polarized complex (Figure 16C). The authors find that addition of chloronium from chlorohydantoin (174 kcal/mol) to an olefin (165 kcal/mol) should be too endothermic to occur. The rate of chlorolactonization by an Ad_E2 mechanism depends on the electron-richness of the nucleophile,[46,73a] with ammonium salt **72** having an almost 20 kcal/mol lower barrier to reaction than the carboxylic acid **71** (B3LYP/6-31g*/SM8-$CHCl_3$) (Figure 16C). Calculated potential pathways found that carboxylic acid interaction with the olefin is the only substrate conformation capable of weakening the N-Cl bond toward chlorolactonization. Without NAAA, calculations minimize to a simple Van der Waals complex between substrate and halogen donor. Kinetic isotope effect studies on ^{18}O labeled carboxylic acid **71** revealed a significant effect (K $^{16}O/^{18}O$ = 1.026), implying involvement in the rate determining step. The authors conclude that conditions in which stabilized, bridging halonium ions are known to be generated do not translate to synthetically useful conditions, and that nucleophile interaction with an olefin enables reaction with commonly used halogen sources.

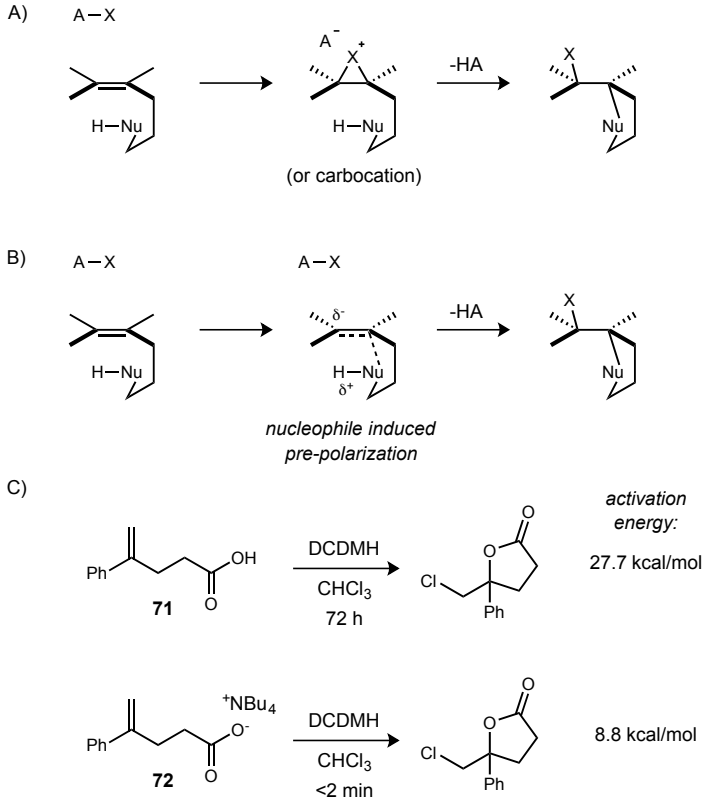

Figure 16: A) Traditional stepwise electrophilic addition to olefins; B) nucleophile assisted alkene activation in addition to olefins; C) base activation of the nucleophile lowers the activation energy for chlorolactonizations.

The eloquent and instructive mechanistic work by Borhan and coworkers leads one to wonder about the effectiveness of simple, chiral Brønsted bases.[74] Examples of solely Brønsted base catalysis in halocyclizations are perhaps the least common, however, this could be partially due to inadvertent categorization as Lewis base catalysis. This was recently investigated by Denmark and coworkers. Their attempt to use Lewis bases to catalyze the chlorolactonization of challenging 1,2-substituted alkenes eventually led to the conclusion that Brønsted base catalysis was actually operative.[46] The TBDMS ester of their

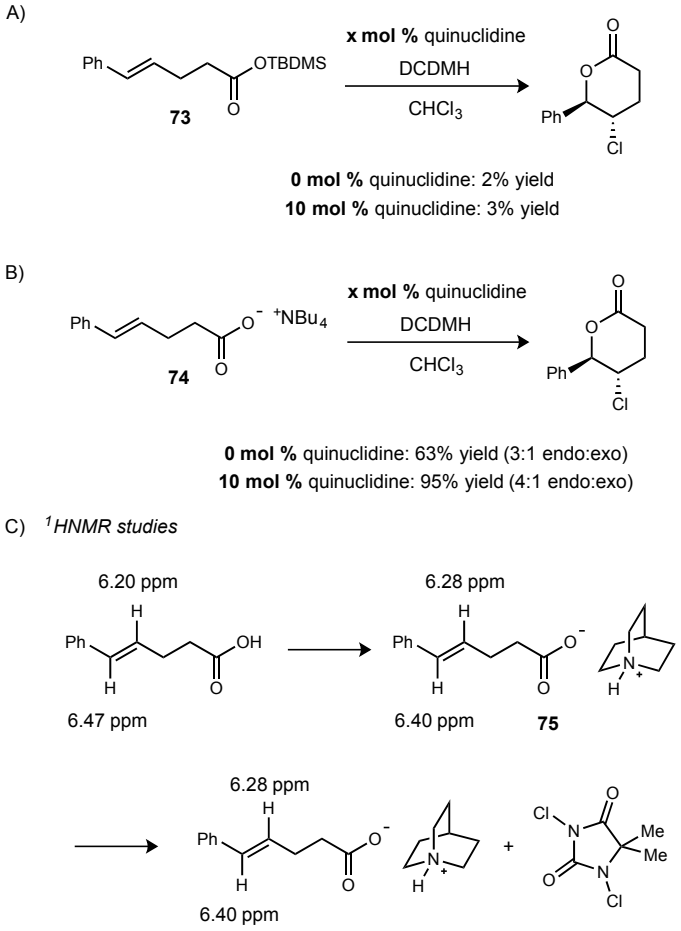

Figure 17: Mechanistic investigation into a previously proposed Lewis base catalyzed chlorolactonization: A) cyclization of a silyl ester, B) lactonization of an ammonium carboxylate, and C) ^{1}HNMR studies of the vinylic protons in various reaction conditions.

test substrate (**73**) could not undergo lactonization with or without quinuclidine present (Figure 17A). However, the ammonium carboxylate **74** easily reacted even without a catalyst present (Figure 17B), and the *N*-chloroquinuclidine was never observed by ^{1}HNMR when it was reacted with quinuclidine catalyst. In solution, quinuclidinium carboxylate **75** shows shifted alkene protons relative to its carboxylic acid counterpart (Figure 17C).

[74] Palomo, C.; Oiarbide, M.; Lopez, R. *Chem. Soc. Rev.* **2009**, *38*, 632.

Subsequent addition of DCDMH does not further alter the chemical shift of the alkene protons significantly. Brønsted acid activation of DCDMH by the conjugate acid of quinuclidine may be operative in addition to the nucleophilic alkene activation. The authors state that "what was initially interpreted as Lewis base catalysis is, in fact, Brønsted base/Brønsted acid catalysis." Experimental evidence was also found for the configurational instability of benzylic chloriranium ions, suggesting benzylic carbocation formation is favored.

The Hennecke group reported the first enantioselective halolactonization of alkynes in the desymmetrization of diynoic acids such as **76** (Figure 18).[7576] This substrate could undergo 5-*exo* bromolactonization to **77** by the dimeric Brønsted base, $(DHQD)_2PHAL$, in good yield and 72% ee. The authors hypothesize that the base catalyst is able to activate the carboxylic acid to cyclize onto one alkyne selectively. Binding to the carboxylic acid was tested by submitting the potassium carboxylate salt of **76** to the reaction, and only racemic product was generated. This indirectly indicates that deprotonation of the substrate by the catalyst is vital for binding and selectivity.

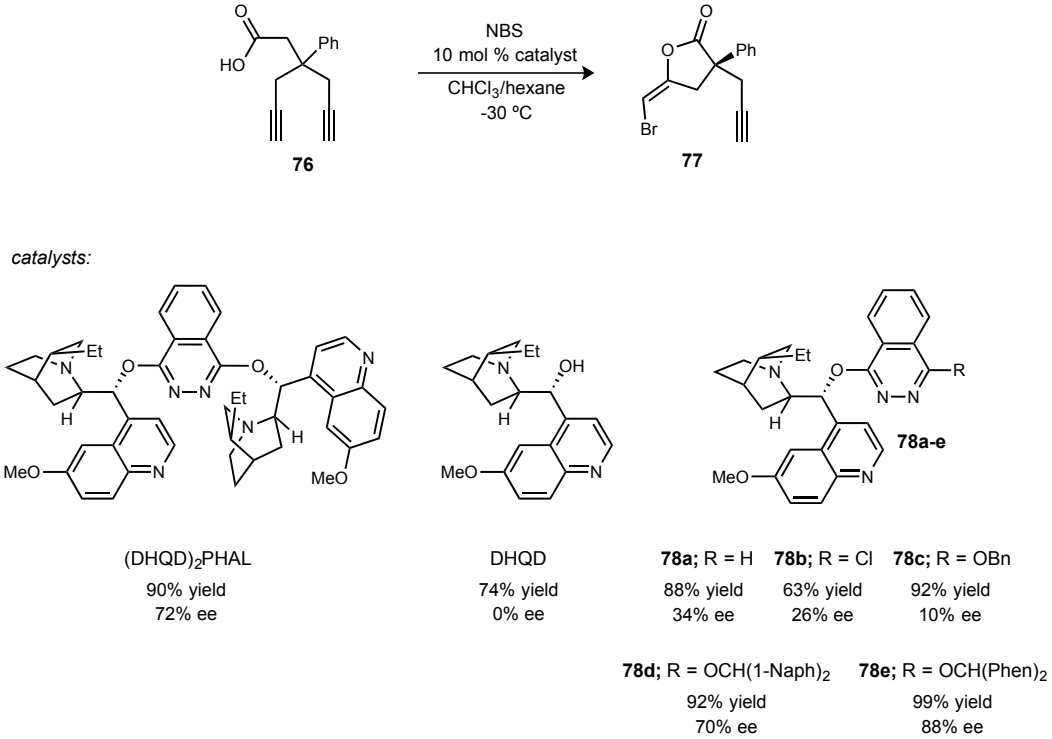

Figure 18: Bromolactonization of diynoic acids and catalyst screens based on dihydroquinidine.

[75] Wilking, M.; Mück-Lichtenfeld, C.; Daniliuc, C. G.; Hennecke, U. *J. Am. Chem. Soc.* **2013**, *135*, 8133.

[76] See also an earlier example of hydro-carboxylation of alkynes: Yoshida, S.; Fukui, K.; Kikuchi, S.; Yamada, T. *J. Am. Chem. Soc.* **2010**, *132*, 4072.

Additional catalyst screens were undertaken to better understand the roles this catalyst plays.[77] Dihydroquinidine itself could not induce enantioselectivity, indicating the phthalazine's importance. Monomeric dihydroquinidine alkaloids **78** were screened, with **78a** rescuing some enantioselectivity by inclusion of the phthalazine moiety. More electron donating substituents were found to be optimal (**78a** - **78c**), and bulky alkoxy substituents delivered the product in better yield (99%) and selectivity (88%) than $(DHQD)_2PHAL$ (**78d** and **78e**). Therefore, the second alkaloid may be mainly serving to help create a catalytic pocket around the pthalazine and first quinuclidine ring. NMR titration studies confirm that these catalysts bind tightly to carboxylic acid **76** in a one to one ratio. A similar proton shift of the alkynyl protons is observed by ^1H NMR due to nucleophile-assisted alkene activation. No evidence is presented for any Lewis base activation of bromine, but the authors do not rule that out as a possible second catalytic function.

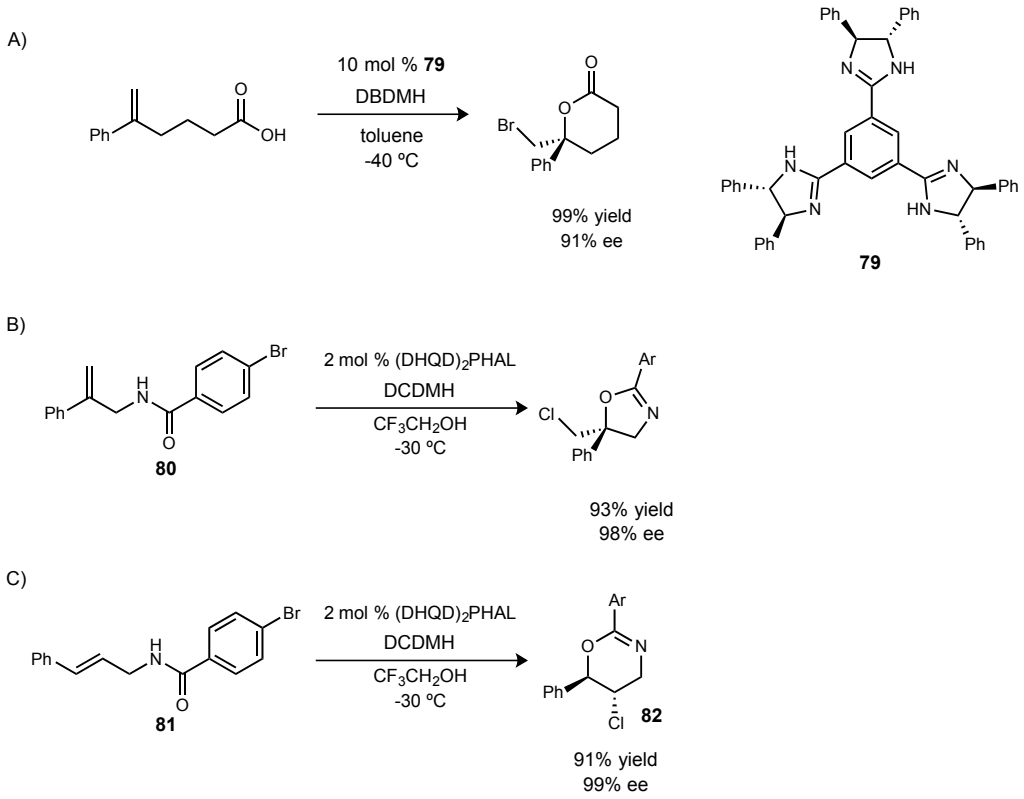

Figure 19: Brønsted base catalysis by: A) trisimidazolines in an enantioselective bromolactonization, B) $(DHQD)_2PHAL$ in the 5-*exo* chlorocyclization of amides, and C) the 6-*endo* chlorocyclization of amides.

[77] Wilking, M.; Daniliuc, C. G.; Hennecke, U. *Chem. Eur. J.* **2016**, *22*, 18601.

The Fujioka group has developed highly effective and unique tris(imidazoline) catalysts (**79**) for the Brønsted base catalyzed bromolactonization (Figure 19A).[78] Interestingly, the bis- and mono- imidazoline catalyst analogs demonstrated similar reactivity but much lower enantioselectivities (28% and 6%, respectively). This work was extended to cyclization of symmetric bis(carboxylic acids), as well.[79]

The Borhan group was able to apply prior methodology to the enantioselective chlorocyclization of allylic acylamides (**80**, Figure 19B).[80] The polar protic solvent, trifluoroethanol, was surprisingly found to be the optimal solvent for enantioselectivity, while chloroform only provided product in 57% ee. Additionally, no benzoic acid additive was required in this case, despite having a similar alkene and the same chlorine source. Granted, benzoic acid only had a minimal effect in the bromolactonization chemistry. The catalyst is likely acting as a Brønsted base for activation of the amide. These conditions were impressively amenable to *trans*-alkene **81**, providing 6-*endo* products **82** in good yield and excellent enantioselectivities (99%) (Figure 19C). Further still, this same methodology was used to effect an intramolecular, enantioselective haloetherification[81] and an enantioselective dichlorination.[82]

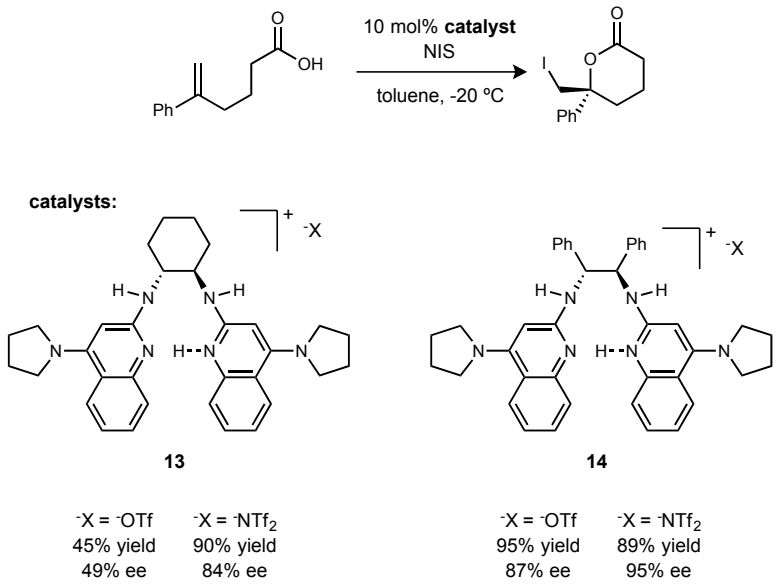

Figure 20: Application of bifunctional BAM catalysis to an iodocyclization.

[78] Murai, K.; Matsushita, T.; Nakamura, A.; Fukushima, S.; Shimura, M.; Fujioka, H. *Angew. Chem. Int. Ed.* **2010**, *49*, 9174.

[79] Murai, K.; Nakajima, J.; Nakamura, A.; Hyogo, N.; Fujioka, H. *Chem. - Asian J.* **2014**, *9*, 3511.

[80] Jaganathan, A.; Garzan, A.; Whitehead, D. C.; Staples, R. J.; Borhan, B. *Angew. Chem. Int. Ed.* **2011**, *50*, 2593.

[81] Soltanzadeh, B.; Jaganathan, A.; Staples, R. J.; Borhan, B. *Angew. Chem. Int. Ed.* **2015**, *54*, 9517.

[82] Soltanzadeh, B.; Jaganathan, A.; Yi, Y.; Yi, H.; Staples, R. J.; Borhan, B. *J. Am. Chem. Soc.* **2017**, *139*, 2132.

This overall journey by the synthetic community from a focus on catalytic control of the electrophile towards a greater understanding of nucleophilic control is also reflected in the development of halocyclizations in the Johnston group. Using the previously developed PBAM•HOTf (**13**, Figure 3), the intramolecular iodolactonization[36] of 1,1 disubstituted alkenes could be achieved in promising yield and enantioselectivity (Figure 20).[37] A range of sulfonic, triflamidic, and triflimidic acid salts of PBAM were screened, and triflimidic acid was found to give the best results (90% yield, 84% ee). In general, more acidic and sterically encumbered acids performed better. The free base of PBAM had comparable reactivity yet much lower enantioselectivity (19% ee), indicating that one protonated amidine was necessary for selectivity. At this point, other catalyst chiral backbones were tested. A stilbene diamine derived catalyst was found to provide better selectivity, with triflic acid salt of StilbPBAM (**14**) delivering the product in high yield and increased selectivity (95% yield, 87% ee). Again, changing to the larger and more acidic acid additive, $HNTf_2$, proved optimal. StilbPBAM•$HNTf_2$ facilitated the iodolactionization in 89% yield and 95% ee. This methodology could be applied to a range of aryl and alkyl 1,1-disubstituted alkenes, and found that lower selectivities were observed for alkyl, electron rich aryl, and unsubstituted alkene substrates.

The cause of StilbPBAM's greater selectivity relative to PBAM remains uncertain, although it is hypothesized that its smaller dihedral angle[83] and it's two phenyl groups may restrict substrate conformation to a greater extent than PBAM upon binding. The acidic additive $HNTf_2$, that increases the enantioselection relative to the free base, is hypothesized to orchestrate the reaction by hydrogen bond donation to the succinimide electrophile (Figure 21A). This bifunctional activation hypothesis builds on the paradigm developed during investigations of chiral proton catalysis in prior aza-Henry investigations. It implies a catalyst role in enantioselective delivery of iodine to the alkene, accompanied by a stereospecific lactonization step. Another important feature of this hypothesis is the strength of the triflimide/amidinium ion pair, which may be separated during binding to the carbonyl of *N*-iodosuccinimide. Alternatively, recent highly selective results with the free base of BAM catalysts (*vida infra*) in related systems indicate the amidinium/counterion moiety may modify the steric environment of the catalyst structure in a beneficial manner specific to certain cyclizations (Figure 21B). This alternative implies that amidine deprotonation and binding to the carboxylic acid positions the substrate in a chair-like conformation with one alkene face toward the carboxylate and one open to electrophilic activation. The amidinium/triflimide ion pair could be more tightly associated, serving as a steric "wall," and only allowing *N*-iodosuccinimide approach from one face. Each of these two hypotheses

[83] Kim, H.; Yen, C.; Preston, P.; Chin, J. *Org. Lett.* **2006**, *8*, 5239.

appear reasonable for BAM catalysis, and the hierarchy of these two functions will be the subject of further discussion in this chapter.

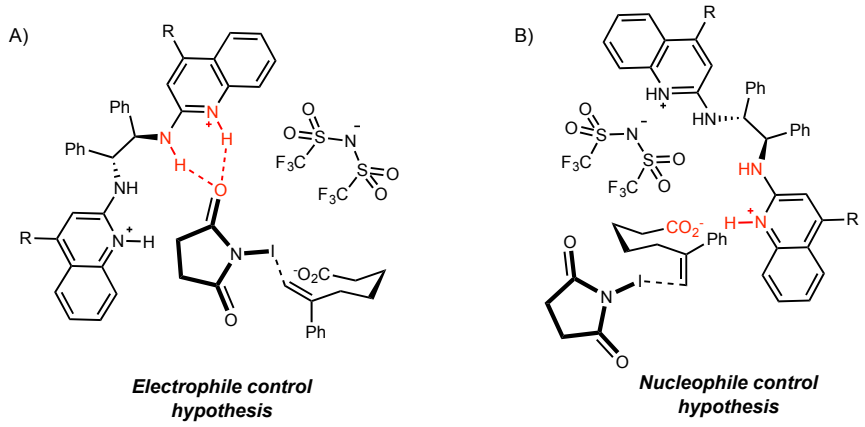

Figure 21: Two faces of bifunctional activation: electrophilic and nucleophilic control hypotheses based on counterion displacement, and counterion block, respectively.

Studies of halocyclizations led to the application of StilbPBAM•$HNTf_2$ to the first organocatalytic, enantioselective capture of CO_2 (Figure 22A).[84] Using homoallylic alcohols such as **83**, enriched iodocarbonates (**84**) could be produced in good yield (91%) and selectivity (95% ee). Catalyst-substrate complex **85** is believed to sufficiently stabilize the carbonic acid intermediate to enable the unfavorable addition of an alcohol into carbon dioxide.

A similar capture of CO_2 has been developed for homoallylic amines, **86** (Figure 22B).[85] Several challenges arise in this methodology. Upon addition of CO_2 to the reaction, fast reaction with amine substrate generates carbamic acid. Further reaction with another equivalent of amine substrate produces a stable ammonium/carbamate salt dimer. Additionally, amines are more basic than any substrate used previously with BAM catalysis. Being more basic than an amidine, the amine substrate likely deprotonates the acidic triflimidic acid from the catalyst. A more basic catalyst, ^{7}MeOStilbPBAM•$HNTf_2$ (**87**) was required to activate the ammonium substrate salt generated in the conditions, and successfully produced enantioenriched carbonates (86% yield, 92% ee). The ability of the catalyst to corral the variety of possible intermediates, adducts, and dimers into a major product and stereoisomer is notable.

The concept of intermolecular generation of a sufficiently acidic nucleophile by capture of CO_2 by alcohols and amines inspired the search for CO_2 surrogates. The capture of tosyl isocyanate by an allylic amine (**88**) would generate an acidic imide capable of *N*-

[84] Vara, B. A.; Struble, T. J.; Wang, W.; Dobish, M. C.; Johnston, J. N. *J. Am. Chem. Soc.* **2015**, *137*, 7302.
[85] Yousefi, R.; Struble, T. J.; Johnston, J. N. *Unpublished results.*

or *O*- cyclization, and stereoselectively forming a C-N bond was rare and attractive. Upon catalyst screening, the more basic ^{6,7}(MeO)$_2$StilbPBAM (**89**, Figure 22) was found to be most effective in the free base form, favoring *N*-cyclization to produce enantioenriched ureas (**90**, 91% ee, 82% yield, Figure 22C).[86] The reversal of previously observed alkene facial selectivity was notable as well. The same conditions were remarkably general, and they were applied to both *cis*- and *trans*- 1,2 disubstituted alkenes. *trans*-1,2-Disubstituted alkenes **91** underwent 6-*exo*, *N*-cyclization in good yield and excellent enantioselectivies (**92**, 60% and 94%, respectively, Figure 22D), and *cis*-1,2 disubstituted alkenes reverted back to a 5-*exo* cyclization (93% yield, 93% ee).

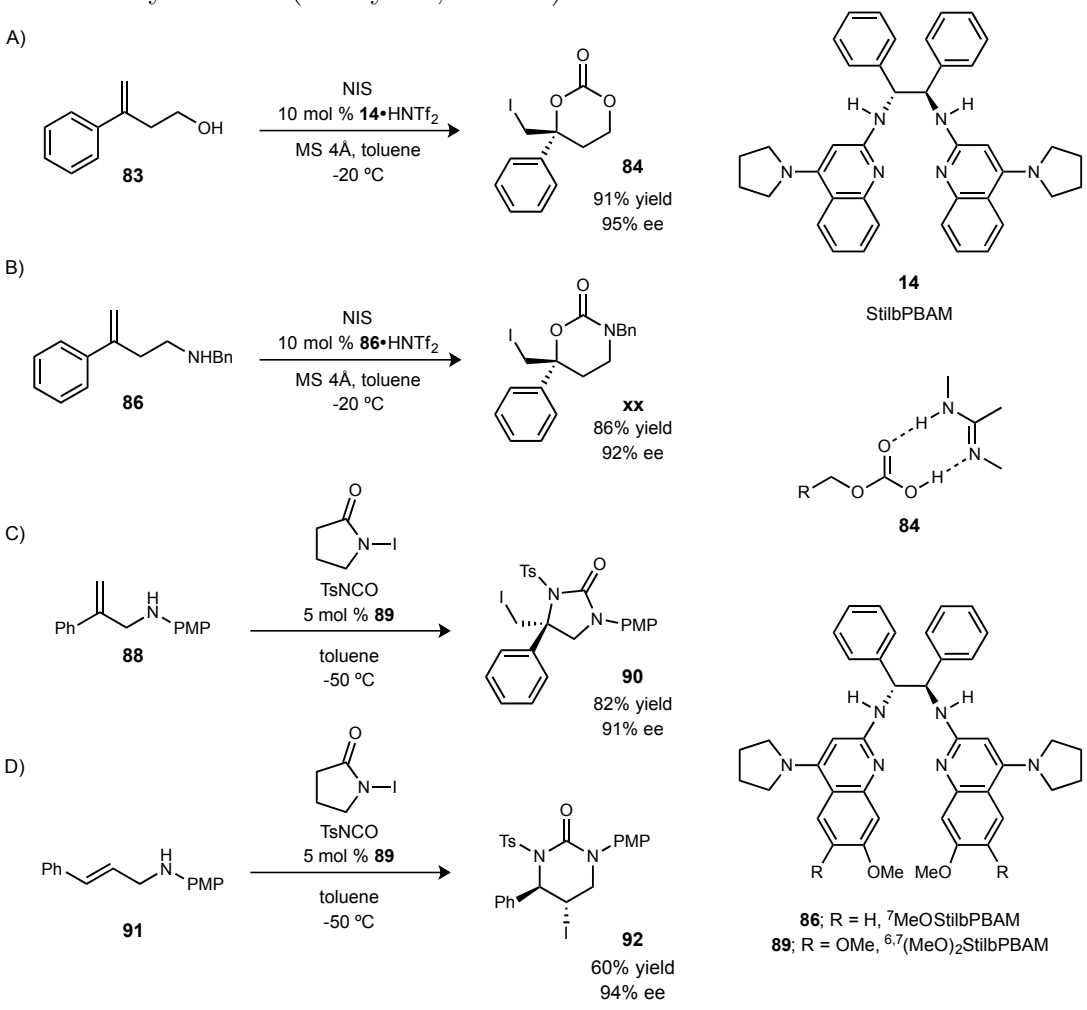

Figure 22: Enantioselective halocyclizations by the Johnston group.

The success of free base BAM catalysis in this methodology (Figure 22C and D) was surprising. It should be noted that both *N*-iodosuccinimide and *N*-iodopyrrolidinone performed well in this reaction, but *N*-iodopyrrolidinone was employed because it converted

[86] Struble, T. J.; Johnston, J. N. *Manuscript in preparation.*

the starting material more quickly. This amide iodine source is less electrophilic than the imide source, NIS. It would have been previously hypothesized that additional Brønsted acidic activation, not less, would be required for use of *N*-iodopyrrolidinone. Yet use of the triflimidic acid salt of $^{6,7}(OMe)_2$StilbPBAM•$HNTf_2$ was inferior to the freebase. It appears at this time that the acidic role of BAM salts may have been over-generalized, since predicting when it will be beneficial does not follow working hypotheses.

A significant, and somewhat fortuitous, advancement in the understanding of how the Brønsted basic function of BAM catalysts operate began with the discovery of the halocyclizations of phosphoramidic acids. An unanticipated benefit from the use of these unique substrates was the configurational stability of chiral phosphorous atoms. In the iodocyclization of phosphoramidic acids (**93**), StilbPBAM•$HNTf_2$ was found to be most effective for the 5-*exo* cyclization (Figure 23A), providing the products in good yield (**94**, 85%), excellent enantioselectivity (96%), and high diastereoselectivity (>20:1).[87] Essentially, the alkene facial selectivity (as is common with 1,1-disubstituted alkenes) *and* the selectivity at the phosphorous atom were both very high. When examining how this selectivity at phosphorous arises, it became apparent that upon deprotonation of the phosphoramidic acid, a prochiral anion (**95**) is generated. Which oxygen of the phosphoramidate cyclizes onto the alkene determines the configuration at phosphorous. Therefore, the catalyst could be selecting for one oxygen over the other. Alternatively, perhaps selective generation of a chiral iodonium provides the necessary conformation to get a highly diastereoselective cyclization.

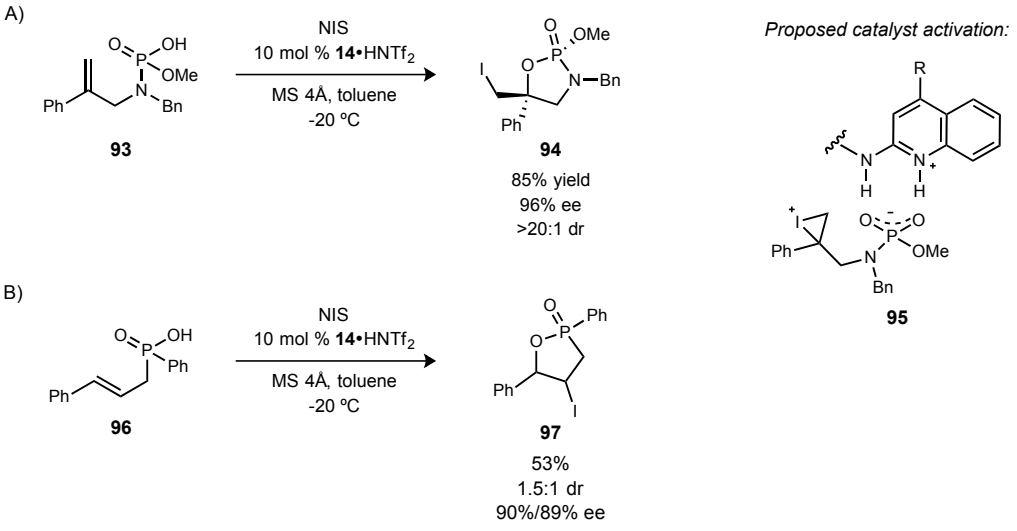

Figure 23: Enantioselective iodocyclization of phosphorous-based acids.

[87] Toda, Y.; Pink, M.; Johnston, J. N. *J. Am. Chem. Soc.* **2014**, *136*, 14734.

To further investigate, the cyclization of *trans*-alkene substrates **96** was undertaken (Figure 23B).[88] With six stereoisomers now possible, optimized conditions afforded the 5-*endo* cyclization product in decent yield but poor diastereoselectivity (**97**, 1.5:1), with each diastereomer having high enantioselectivity (90% and 89%). The absolute and relative stereochemistry of these two diastereomers was not known. Presuming that a *trans* relationship between the phenyl and iodine will exist, the source of the poor diastereoselectivity could either be poor alkene facial selectivity or poor nucleophile selectivity. To investigate, reductive deiodination was performed, and the diastereomers were separated into *trans* -d_1 and *cis* **98**-d_2 (Figure 24). Phenyl Grignard addition to each diastereomer ablated the phosphorous stereocenters, leaving only chiral alcohol **99** behind. Upon optical rotation analysis, it was determined that *trans* -d_1 produced (*S*)- **99** and *cis* **98**-d_2 produced (*R*)-**99**. Therefore, the alkene stereocenter was the source of poor selectivity. The major diastereomer had configurations of (2*S*,4*R*,5*R*) and the minor (2*S*,4*S*,5*S*), with the stereocenter at phosphorous being conserved. From these results, it appears that the priority of stereoselectivity by BAM catalysis relies first on nucleophile control before alkene facial selectivity.

These findings of high degrees of nucleophile control in BAM catalysis were quite surprising, and led to the investigation of nucleophile control in much more common substrates: carboxylic acids.

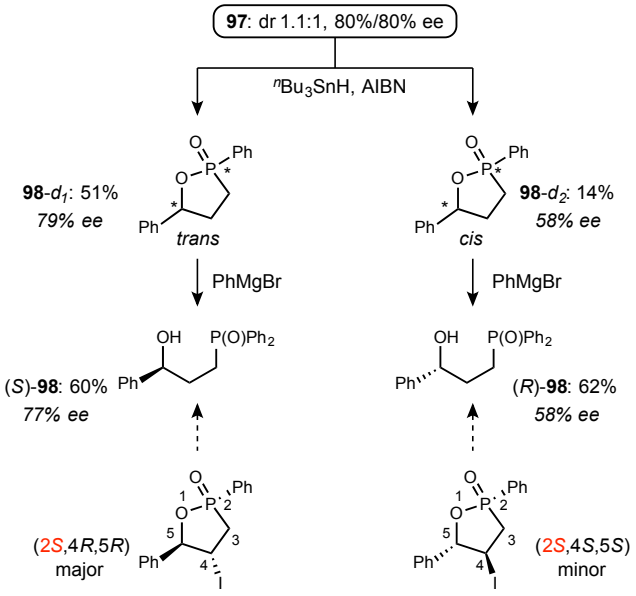

Figure 24: Derivatization of **97** diastereomers to find the source of poor diastereoselectivity.

[88] Toda, Y.; Johnston, J. N. *Manuscript in preparation.*

1.1.4 Activation of carboxylic acids in synthesis and nature

Studies of chiral phosphoric acid activation mechanisms[89] have resulted in a better understanding of their roles in both electrophile and nucleophile activation, and this knowledge has enabled their frequent use and derivatization in chemical synthesis.[10] Carboxylic acids are commonly used as catalysts[90,51b] and as substrates, however, studies on their mechanism have been relatively sparse.[91,92]

List and coworkers have begun developing a catalytic activation mode for carboxylic acids by chiral phosphoric acids. Recognizing that bulky BINOL based phosphoric acids (TRIP, **45**) cannot readily homodimerize, they hypothesized that small carboxylic acids could form heterodimers with them instead (Figure 25A).[91a] Their hypothesis was supported by the elucidation of a cocrystal structure of TRIP bound to acetic acid in the solid state. In solution, diffusion-ordered spectroscopy (DOSY) studies confirmed an increase in volume when the species were heterodimerized. A strong binding constant (K_a = 1948 M^{-1}) between acetic acid and TRIP (**100**) was revealed by NMR titration studies, which is close to the binding constant of a carboxylic acid and quinidine ($K_a = 1.9e^4$ M^{-1}).[93] The authors propose that this heterodimer could in fact raise the HOMO energy of the carboxylic acid by hydrogen bonding to the "basic" P=O functionality. However, an equally important interaction between the carboxyl C=O and the phosphoric acid OH could be argued to decrease the nucleophilicity of the carboxylic acid. The selectivity between carboxylate or phosphate addition to electrophiles is likely due to the greater steric hindrance about the phosphate. Ultimately, the fact that a stronger acid can activate a weaker acid towards nucleophilic addition is quite interesting. The asymmetric ring opening of *meso*-aziridines **101** was accomplished in excellent yields and selectivities (99% ee, Figure 25B). As is depicted in Figure 25A, the dimer is proposed to protonate the aziridine and add carboxylate in a concerted fashion. The thermodynamically favorable heterodimer also acts to protect

---

[89] a) Champagne, P. A.; Houk, K. N. *J. Am. Chem. Soc.* **2016**, *138*, 12356. b) Duarte, F.; Paton, R. S. *J. Am. Chem. Soc.* **2017**. c) Yang, C.; Xue, X. S.; Jin, J. L.; Li, X.; Cheng, J. P. *J. Org. Chem.* **2013**, *78*, 7076. d) Yang, C.; Xue, X. S.; Li, X.; Cheng, J. P. *J. Org. Chem.* **2014**, *79*, 4340. e) Simon, L.; Goodman, J. M. *J. Am. Chem. Soc.* **2008**, *130*, 8741. f) Simon, L.; Goodman, J. M. *J. Org. Chem.* **2011**, *76*, 1775.

[90] a) Hashimoto, T.; Maruoka, K. *J. Am. Chem. Soc.* **2007**, *129*, 10054. b) Hashimoto, T.; Hirose, M.; Maruoka, K. *J. Am. Chem. Soc.* **2008**, *130*, 7556. c) Hashimoto, T.; Maruoka, K. *Synthesis* **2008**, *2008*, 3703. d) Hashimoto, T.; Uchiyama, N.; Maruoka, K. *J. Am. Chem. Soc.* **2008**, *130*, 14380. e) Hashimoto, T.; Kimura, H.; Maruoka, K. *Angew. Chem., Int. Ed.* **2010**, *49*, 6844. f) Hashimoto, T.; Nakatsu, H.; Takiguchi, Y.; Maruoka, K. *J. Am. Chem. Soc.* **2013**, *135*, 16010. g) Hashimoto, T.; Gálvez, A. O.; Maruoka, K. *J. Am. Chem. Soc.* **2013**, *135*, 17667.

[91] a) Monaco, M. R.; Poladura, B.; Diaz de Los Bernardos, M.; Leutzsch, M.; Goddard, R.; List, B. *Angew. Chem. Int. Ed.* **2014**, *53*, 7063. b) Monaco, M. R.; Fazzi, D.; Tsuji, N.; Leutzsch, M.; Liao, S.; Thiel, W.; List, B. *J. Am. Chem. Soc.* **2016**, *138*, 14740.

[92] Hashimoto, T.; Kimura, H.; Nakatsu, H.; Maruoka, K. *J. Org. Chem.* **2011**, *76*, 6030.

[93] Lah, J.; Maier, N. M.; Lindner, W.; Vesnaver, G. *J. Phys. Chem. B* **2001**, *105*, 1670.

the catalyst from degradation, by preventing protonation and phosphate addition to electrophiles.

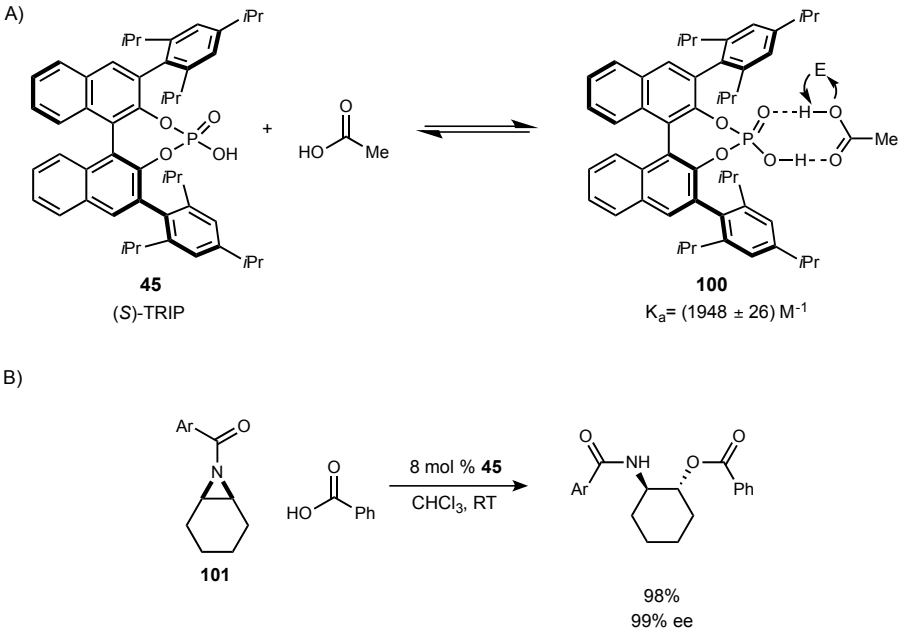

Figure 25: Brønsted acid activation of carboxylic acids.

Calculations of the stabilization free energies were performed on 1) a complex between TRIP and pyridine, and 2) a trimeric complex between TRIP, pyridine, and acetic acid (B3LYP/cc-pVTZ).[91b] The first complex was found to be 12 kcal/mol less stable than the second, trimeric complex. Within these computed structures, the heterodimer also displayed increased acidity compared to TRIP, as evidenced by the protonation of pyridine by the heterodimer, whereas full protonation of the pyridine is not observed by TRIP alone. The frontier molecular orbitals of the carboxylic acid were also found to be altered when heterodimerized with TRIP. The LUMO increased in energy by 0.08 eV, and the HOMO inceased by 0.25 eV, showing a greater increase in nucleophilicity than electrophilicity. Work conducted by a separate laboratory has found that an increase of negative charge on the phosphate oxygen has also been shown to stabilize transient positive charged intermediates in several transformations, and in ring openings of epoxides, this may contribute to the regioselectivity of nucleophilic attack.[91,94] They also were able to minimize transition state structures where TRIP was simultaneously activating a nucleophile and electrophile.[94a] The increased understanding of this activation mode has allowed the reaction to applied to the enantioselective opening of *meso*-epoxides and the kinetic resolution of aziridines, epoxides, and chiral carboxylic acids.[91]

[94] a) Seguin, T. J.; Wheeler, S. E. *ACS Catalysis* **2016**, *6*, 2681. b) Duarte, F.; Paton, R. S. *J. Am. Chem. Soc.* **2017**.

The carboxylic acid activation mode was used by the Tan group to achieve the first highly general three-component Passerini reaction (Figure 26A).[95] They sought to apply List's heterodimerization strategy between chiral phosphoric acid **102** and a carboxylic acid to simultaneously activate an aldehyde and isocyanide. The proposed mode of activation is depicted in Figure 26B, and is supported by studies of complexes in solution by ^{31}P NMR. When the aldehyde was added to just catalyst **102**, no significant shift of the phosphorous peak was observed. However, when either carboxylic acid or isocyanide was added, dramatic shifts were detected (0.85 and 1.03 ppm, respectively). When both acid and isocyanide were added to the catalyst, a larger shift of 1.54 ppm was observed. Ultimately, this carboxylic acid activation mode was able to control aldehyde facial selectivity as well as isocyanide addition. This reaction has a wide substrate scope, with aromatic and alkyl aldehydes, alkyl and aromatic carboxylic acids, and various isocyanides all providing products **103** in good yield and excellent enantioselectivities.

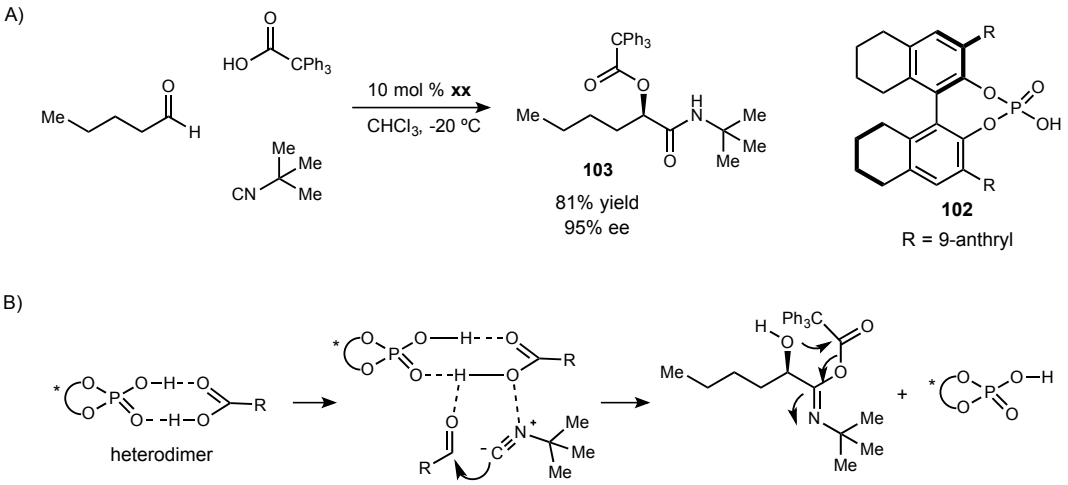

Figure 26: Enantioselective Passerini reaction enabled by carboxylic acid activation.

The Maruoka group has heavily investigated the applications of carboxylic acids as "Brønsted acid-assisted Brønsted acid" catalysts.[90] In one such investigation, an axially dicarboxylic acid catalyst, **104**, was found to facilitate a highly enantioselective Mannich reaction of an imine with diazoacetates (Figure 27).[92] Internal hydrogen bonding between the carboxylic acids serves two purposes: to generate a large dihedral angle of the binaphthyl junction by forming a 9-membered ring (93º versus 55º in TRIP), and to increase the acidity of one carboxylic acid by assistance from the second acid. These mechanistic characteristics as well as a proposed transition state are derived from a cocatalyst structure of **104** and pyridine.

[95] Zhang, J.; Lin, S.-X.; Cheng, D.-J.; Liu, X.-Y.; Tan, B. *J. Am. Chem. Soc.* **2015**, *137*, 14039.

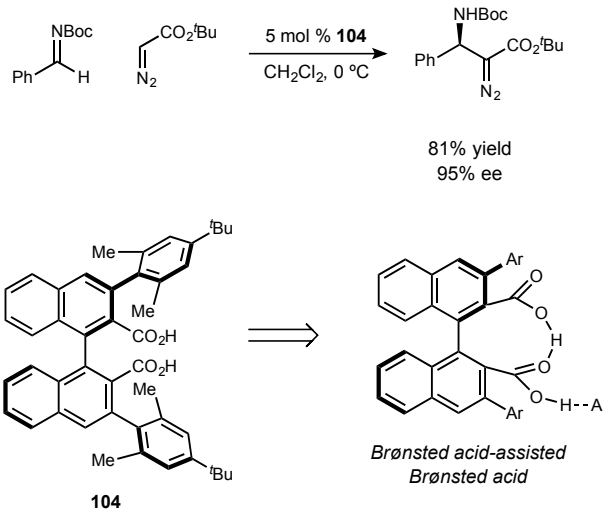

Figure 27: Mauroka's chiral dicarboxylic acid catalyst.

The use of carboxylic acids by enzymes is pervasive in nature, in large part due to the prevalence of amino acids in biological processes. In fact, a key step in the evolution of modern biology was the ability of ribozymes (RNA enzymes) to harness amino acids for peptide bond synthesis.[96] The majority of enzyme catalyzed transformations of carboxylates is their deprotonation and phosphorylation, generating an active ester primed for nucleophilic acyl substitution, an example is in the conversion of glutamic acid to glutamine by glutamine synthetase (Figure 28A).[97] Based on crystal structure data, multiple hydrogen bonds to nearby arginines and ionic bonding to magnesium position the substrate carboxylates and readies one for phosphorylation. An intriguing example, although not of carboxylate control but of carbamate control, is found in the enzyme dethiobiotin synthetase, which is the penultimate enzyme of the biotin biosynthetic pathway.[98] Diaminononanoic acid (**105**) is converted into dethiobiotin (**106**) by an ATP dependent carboxylase, dethiobiotin synthetase (Figure 28B). One of the amine substrates reacts with carbon dioxide to generate a carbamate intermediate, which is activated by ATP before subsequent cyclization. According to crystal structure data, this carbamate intermediate makes four hydrogen bonds. Significantly, one oxygen is accepting two neutral hydrogen bonds, and the other oxygen is accepting only one charge-assisted hydrogen bond. The authors note that the singly bound oxygen atom "is almost perfectly aligned for nucleophilic attack on the phosphorus atom." This unique oxygen atom selectivity, combined with

[96] Polacek, N.; Mankin, A. S. *Crit. Rev. Biochem. Mol. Biol.* **2005**, *40*, 285.

[97] a) Liaw, S. H.; Eisenberg, D. *Biochemistry* **1994**, *33*, 675. b) Eisenberg, D.; Gill, H. S.; Pfluegl, G. M. U.; Rotstein, S. H. *Biochimica et Biophysica Acta (BBA) - Protein Structure and Molecular Enzymology* **2000**, *1477*, 122.

[98] Huang, W.; Jia, J.; Gibson, K. J.; Taylor, W. S.; Rendina, A. R.; Schneider, G.; Lindqvist, Y. *Biochemistry* **1995**, *34*, 10985.

previous enantioselective cyclizations of phosphoric acids (Figure 23), led to the search for a system to challenge BAM catalysis to selectively react one oxygen of a carboxylic acid.

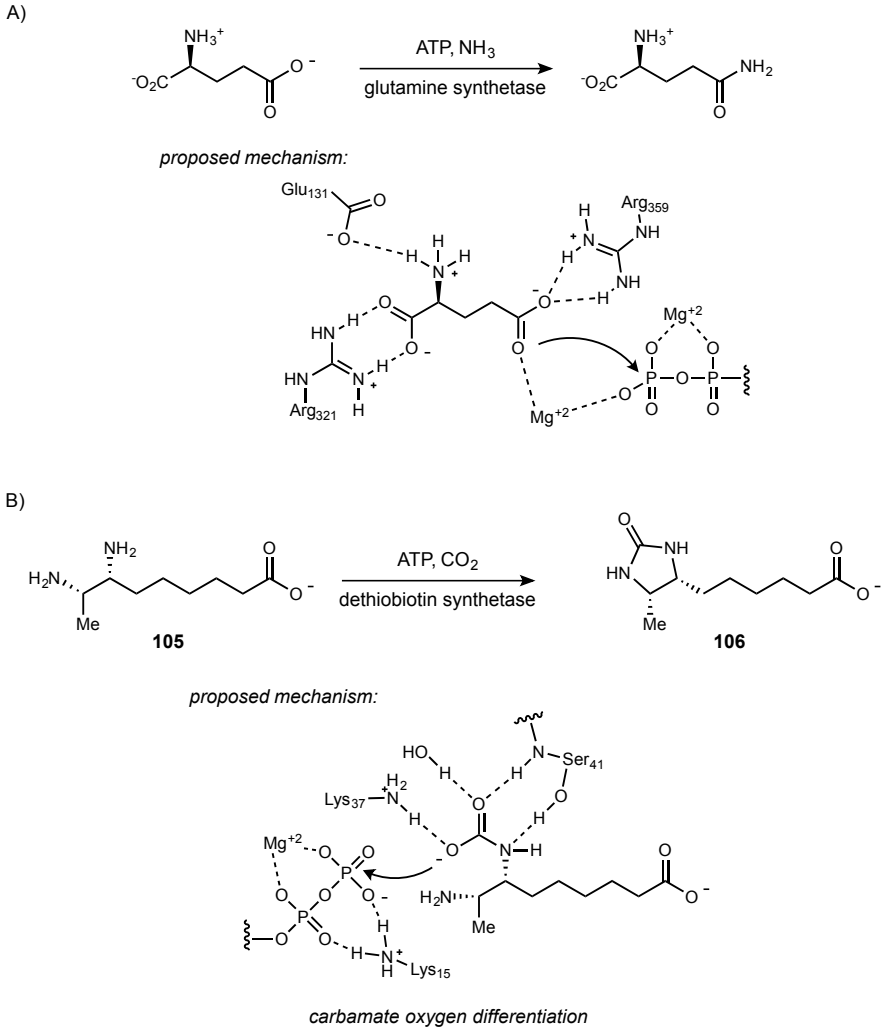

Figure 28: A) Enzymatic control of a carboxylate, and B) dethiobiotin synthetase selectively functionalizes one of the two oxygens in a carbamate.

1.2 Development of an enantioselective lactonization of symmetric carboxylic acids, and mechanistic evidence of Brønsted base catalysis

1.2.1 Mechanistic proposal for enantioselection in cyclopentene carboxylic acids

With the desymmetrization of prochiral phosphoric acid derivatives accomplished, the desymmetrization of prochiral carboxylic acids **107** by bisamidine methodology was investigated (Figure 29A).[99] Cyclopentene carboxylic acids would offer a unique challenge to an organocatalyst for a stereoselective halocyclization. Since the molecule is symmetric through the carboxylic acid, a very subtle desymmetrization would be required for enantioselectivity. As shown in Figure 29B, upon deprotonation by a chiral Brønsted base (**B:**), *chiral* carboxylate (**108**) is generated. The enantiomer of product (**109**) produced is determined by which oxygen of the carboxylate adds to the alkene. Essentially, a catalyst must *differentiate* the carboxylate oxygens for enantioselectivity to be achieved. During the course of optimization, a secondary parameter for which a chiral catalyst must account was

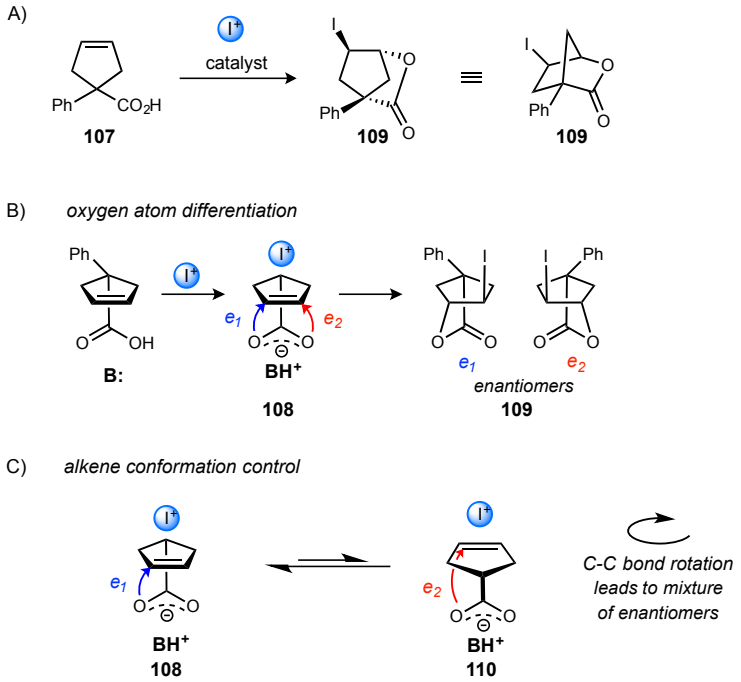

Figure 29: A) Iodocyclization of cyclopentene carboxylic acids, B) depiction of required oxygen atom selectivity for enantioselectivity, and C) added necessity of conformational restraint for success.

[99] Knowe, M. T.; Danneman, M. W.; Sun, S.; Pink, M.; Johnston, J. N. *J. Am. Chem. Soc.* **2018**, *140*, 1998.

discovered (Figure 29C). Two major orientations of the alkene relative to the carboxylate can be envisioned (**108** and**110**). In **108**, cyclization of the "left-hand" oxygen would lead to e_1-**109**. Alternatively, if that same oxygen reacts with the alkene in the reversed conformation, then e_2-**109** would be the major enantiomer produced. In summary, *oxygen differentiation* and *alkene conformation* must be accounted for simultaneously.

1.2.2 Initial investigation into reaction optimization

The background reaction of **107** with NIS was determined to be minimal, delivering less than 5% yield due to poor conversion (Table 1, entry 1). Using 10 mol % of previously developed **14** • $HNTf_2$,[37] iodolactone **109** was not able to be isolated (Table 1, entry 2). Increasing the reaction temperature from -20 ºC to 25 ºC allowed the production of an isolable amount of product, albeit in 16% ee (Table 1, entry 3). Changing to the free base form (**14**) produced **109** in 25% yield and 48% ee (Table 1, entry 4). The free base of the cyclohexane diamine-derived **13** performed much worse, producing racemic product in low yield (Table 1, entry 5). Returning to catalyst **14** at colder temperature increased to 62% ee (Table 1, entry 6).[100] These results contradicted the electrophilic control hypothesis at the time (Figure 21A), but was a promising beginning nonetheless.

Table 1: Exploratory experiments in the iodocyclization of **107.**

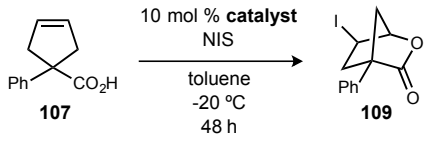

entry	catalyst	temp. (ºC)	yield (%)[a]	ee (%)
1	none	-20	<5	–
2	**14** • $HNTf_2$	-20	<5	–
3	**14** • $HNTf_2$	25	trace	16
4	**14**	25	25	48
5	**13** (PBAM)	25	9	<5
6	**14**	-20	50	62

[a] Yield determined by ^{1}HNMR analysis relative to an internal standard (CH_2Br_2).

The impact of other solvents was then examined. Aprotic solvents typically have the most success in BAM catalysis, as they are unable to disrupt hydrogen bonding between catalyst and substrate. Toluene has traditionally been the optimal solvent for BAM catalysis, as it has a low freezing point, solubilizes BAM catalysts well, and is aprotic. It

[100] Absolute configuration determined by X-ray crystallography.

provided the product in promising yield and selectivity (Table 2, entry 1). Structurally similar xylenes showed diminished selectivity and yield (Table 2, entry 2). Dichloromethane has previously been found to increase reactivity in other lactonization systems,[101] although this was not the case here (Table 2, entry 3). Polar variations of toluene, trifluoro-toluene (Table 2, entry 4) and anisole (Table 2, entry 5) were drastically inferior. Increasing the reaction concentration from 0.05 M to 0.2 M did increase conversion and yield, however the enantioselectivity suffered (Table 2, entry 6). Thus, toluene was the solvent of choice moving forward.

Table 2: Screening of solvent conditions

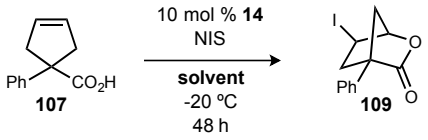

entry	solvent	conc. (M)	conv. (%)[a]	yield (%)	ee (%)
1	toluene	0.05	79	50	62
2	xylenes	0.05	82	27	47
3	CH_2Cl_2	0.05	70	15	11
4	CF_3Ph	0.05	69	13	7
5	anisole	0.05	52	3	<5
6	toluene	0.2	91	58	46

[a] Conversion and yield determined by ^{1}HNMR analysis relative to an internal standard (CH_2Br_2).

Next, an examination of halogenating agents was undertaken. *N*-Iodosuccinimide had already been determined to provide decent yield and selectivity (50% and 62%, respectively; Table 3, entry 1). Bromonium sources were also screened, with neither *N*-bromosuccinimide nor dibromodimethylhydantoin producing product **111** with enantioselection (Table 3, entries 2 and 3). *N*-Chlorosuccinimide was even less reactive and did not yield enough product (**112**) to measure enantioselectivity (Table 3, entry 4). As a result, other iodionium sources had to be evaluated. Diiododimethylhydantoin gave slightly worse results relative to NIS (Table 3, entries 5 and 1). Unlike Jacobsen's methodology, the addition of a catalytic amount of elemental iodine to NIS did not enhance the selectivity either (34% yield, 38% ee; Table 3, entry 6).[61] An iodine source that showed promising results in an enantioselective 7-exo iodolactonization, (diacetoxyiodo)benzene and potassium iodide, was not electrophilic enough to convert the starting material at room temperature (Table 3, entry 8). Finally, the slightly larger and more electrophilic iodonium source, *N*-iodophthalimide, was tested and found to have an increased reaction rate and enantioselectivity after just 24 hours (36%

[101] Johnston *et al.*, unpublished work.

yield, 69% ee; Table 3, entry 9). This easily prepared and handled iodonium source was found to be ideal for this lactonization.[102]

Table 3: Enantioselective halolactonizations: Evaluation of halogen sources.

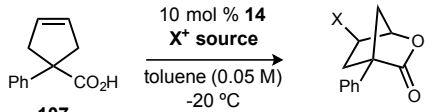

109; X = I
111; X = Br
112; X = Cl

Entry	X^+ source	Conv. (%)[a]	Yield (%)	ee (%)
1	NIS	79	50	62
2	NBS	34	7	<5
3	DBDMH	56	<5	–
4	NCS	14	<5	–
5	DIDMH	49	41	52
6	NIS/10 % I_2	85	34	38
7	I_2/KI	13	8%	–
8[b]	PIDA/KI	0	–	–
9[c]	*N*-iodophthalimide	42	36	69

[a] Conversion and yield determined by ^{1}H NMR analysis relative to an internal standard (CH_2Br_2). [b] Reaction temperature = 25 °C. [c] Reaction time = 24 h.

Since it appeared that none of the other reaction conditions tested had a significant impact on enantioselectivity, catalyst structure was examined next. Since the change from cyclohexane diamine backbone to stilbene diamine was so drastic (Table 1, entries 4 and 5), other chiral diamine backbones were tested (Table 4). When *ortho*-methyl substituents were installed on the phenyl rings of stilbene diamine, the reaction was not drastically impacted, resulting in a slightly increased rate and decreased enantiomeric excess (33% and 57%, respectively; Table 4, entry 2, **113**). Changing from phenyl rings to 1-naphthyl rings proved to be too sterically encumbered, with **114** leading to much lower yield (9%) and further diminished selectivity (43%, Table 4, entry 3). The less conformationally flexible anthracenyl diamine catalyst, **115**, showed poor reactivity and selectivity (Table 4, entry 4). The binaphthyl diamine catalyst **116** had moderate reactivity but produced essentially racemic product (Table 4, entry 5).

[102] Artaryan, A.; Mardyukov, A.; Kulbitski, K.; Avigdori, I.; Nisnevich, G. A.; Schreiner, P. R.; Gandelman, M. *J. Org. Chem.* **2017**, *82*, 7093.

Table 4: Effect of catalyst diamine backbone structure on yield and selectivity.

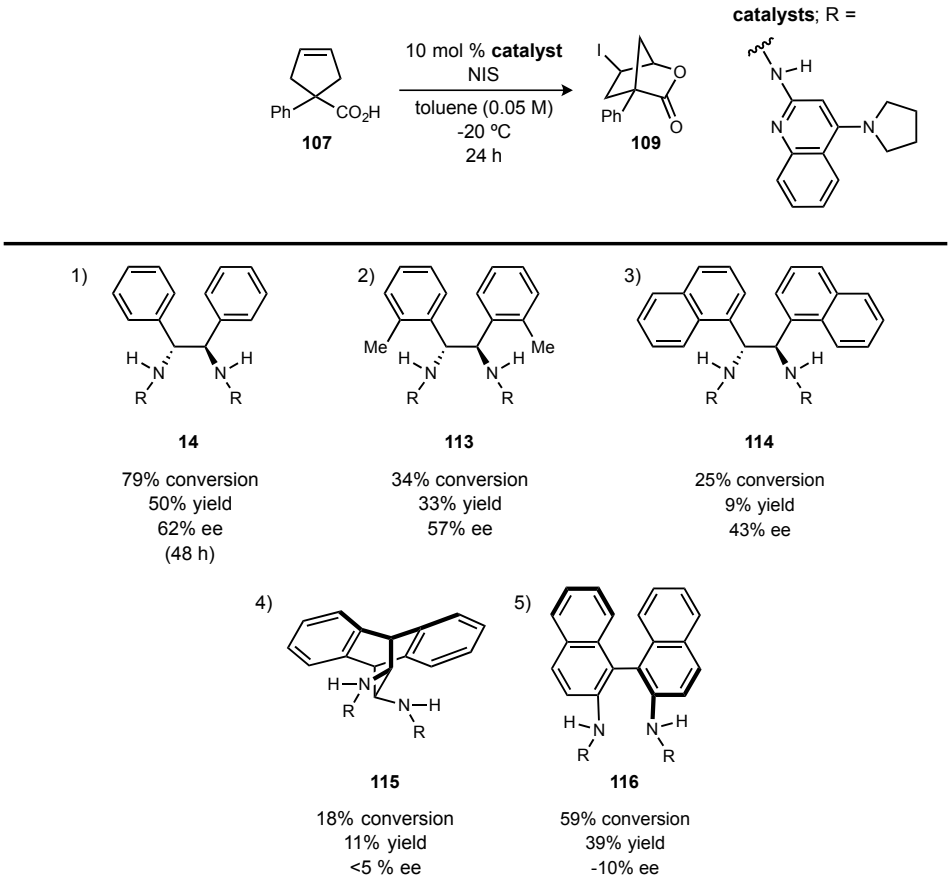

[a] Conversion and yield determined by ^{1}H NMR analysis relative to an internal standard (CH_2Br_2).

Continuing forward with stilbene diamine as the chiral backbone, the electronics of the appended quinoline rings were examined next. Catalysts **14b-14e** were prepared and tested in the iodolactonization reaction (Table 5). The least electron-rich **14b** performed better than 4-MeO bearing **14c** (17% ee vs. no product, Table 5, entries 1 and 2). More electron-rich catalysts, **14d** and **14e**, did not outperform **14a** either (Table 5, entries 4 and 5). Adding a 7-MeO substituent decreased the enantioselectivity to 21%, whereas adding methoxy substituents at the catalyst 6- and 7-positions rescued some of the selectivity (45% ee). No clear significance can be drawn from these results, except that pyrrolidine appears necessary, and a substituent at the catalyst 6-position may be able to increase selectivity slightly. The catalyst activity may be more controlled by quinoline steric changes.

Table 5: Impact of catalyst's quinoline electronic character on enantioselectivity.

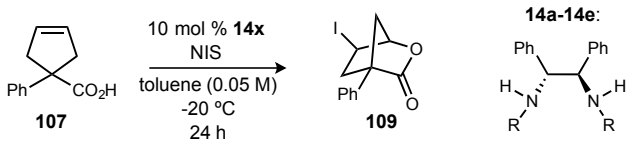

1) **14b**; R =	2) **14c**; R =	3) **14a**; R =	4) **14d**; R =	5) **14e**; R =
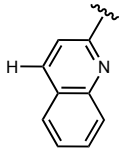	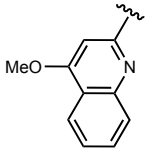	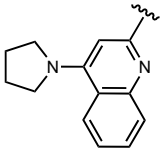	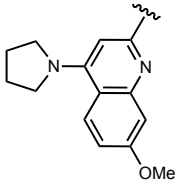	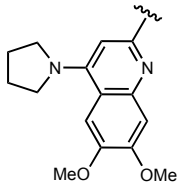
30% conversion 13% yield 17% ee	24% conversion <5% yield	79% conversion 50% yield 62% ee	44% conversion 18% yield 21% ee	35% conversion 24% yield 45% ee

[a] Conversion and yield determined by ^{1}H NMR analysis relative to an internal standard (CH_2Br_2).

A series of catalysts substituted around the quinoline rings were then synthesized and used in the reaction (Table 6). A 3-methyl substituent on the catalyst hampered reactivity and selectivity (**14f**, Table 6, entry 1). Methyl substitutions at the 5- and 7-position entirely inhibited reactivity, possibly due to the $A^{1,3}$ strain of the 5-methyl substituent forcing the pyrrolidine nitrogen out of conjugation with the quinoline ring, effectively decreasing basicity of the catalyst (**14g**, Table 6, entry 2,). Additionally, substituents at the 7-position did not perform well previously (see Table 5, entry 4).

Table 6: Steric effects of quinoline substituents on the reaction outcome.

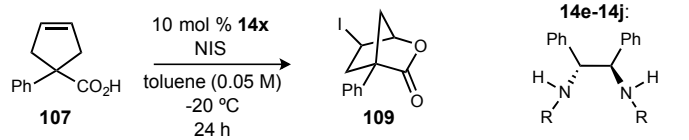

1) **14f**; R =	2) **14g**; R =	3) **14h**; R =	4) **14i**; R =	5) **14j**; R =
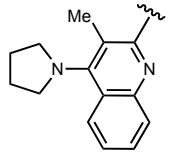	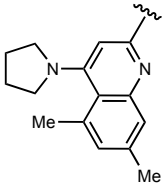	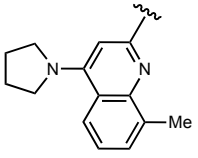	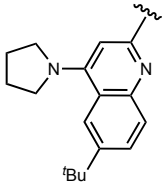	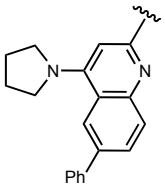
10% yield 33% ee	<5% yield	8% yield 20% ee	34% yield 68% ee (75% ee with NIP)	28% yield 74% ee (with NIP)

[a] Conversion and yield determined by ^{1}H NMR analysis relative to an internal standard (CH_2Br_2).

Installation of an 8-methyl substituent (**14h**) allowed for some product formation, though it was nearly racemic (Table 6, entry 3,). Surprisingly, a *tert*-butyl group at the quinoline

6-position (**14i**) showed improved performance over StilbPBAM (**14a**), increasing enantiomeric excess from 62% to 68% (Table 6, entry 4,). This 6-position appeared to be very far from the reactive site, and its role was unclear until a later time. When combined with the optimized iodine source, *N*-iodophthalimide, catalyst **14i** further increased selectivity to 75% ee. The similar 6-phenyl catalyst, **14j**, performed equally well (74% ee, Table 6, entry 5).

Table 7: Commercially available organocatalysts in the desymmetrization of **107**.

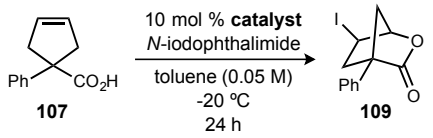

catalysts:

1)

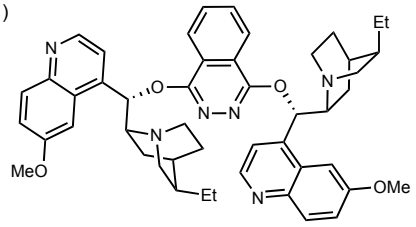

$(DHQD)_2PHAL$
no reaction

2)

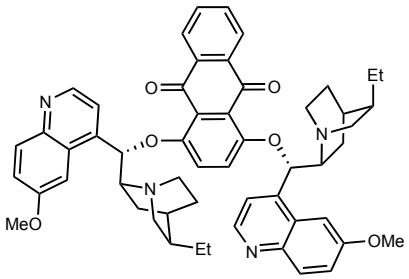

$(DHQD)_2AQN$
no reaction

3)

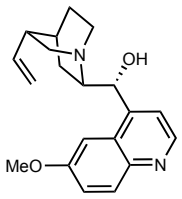

cinchonidine
no reaction

4)

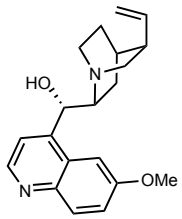

quinidine
8% yield
<5% ee
(25 ºC)

5)

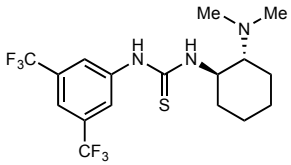

Takemoto Thiourea
no reaction

[a] Conversion and yield determined by ^1H NMR analysis relative to an internal standard (CH_2Br_2).

Other organocatalysts that have previously had success in halocyclizations were screened for comparative analysis. Commercially available $(DHQD)_2PHAL$ and $(DHQD)_2AQN$ were both tested, but neither one was able to convert the starting material (Table 7, entries 1 and 2). Cinchonidine was also unable to catalyze the reaction (Table 7, entry 3). Quinidine was only able to catalyze the reaction when run at room temperature, yielding a small amount of racemic product (Table 7, entry 4). Finally, Takemoto's bifunctional thiourea catalyst also failed to promote the reaction.

A range of 2,2'-substituted chiral phosphoric acid catalysts were examined, due to their previous success in activation of carboxylic acids (Table 8).[91] Unfortunately, the bulky

tri-*iso*-propyl phenyl catalyst (**45**, TRIP) was unable to catalyze the reaction at -50 ºC or even at 25 ºC (Table 8, entries 1 and 2). The 9-anthracenyl and 9-phenanthrene catalysts, **117** and **118**, also did not catalyze the reaction (Table 8, entries 3 and 4). Interestingly, the 4-MeO-2,6-dimethyl-phenyl substituted catalyst **119** was capable of producing enough iodolactone product for HPLC analysis (Table 8, entry 5), but the product was racemic. VAPOL hydrogen phosphate (**120**) was also unable to catalyze the reaction (Table 8, entry 6).

Table 8: Attempts to employ commercially available phosphoric acid catalysts.

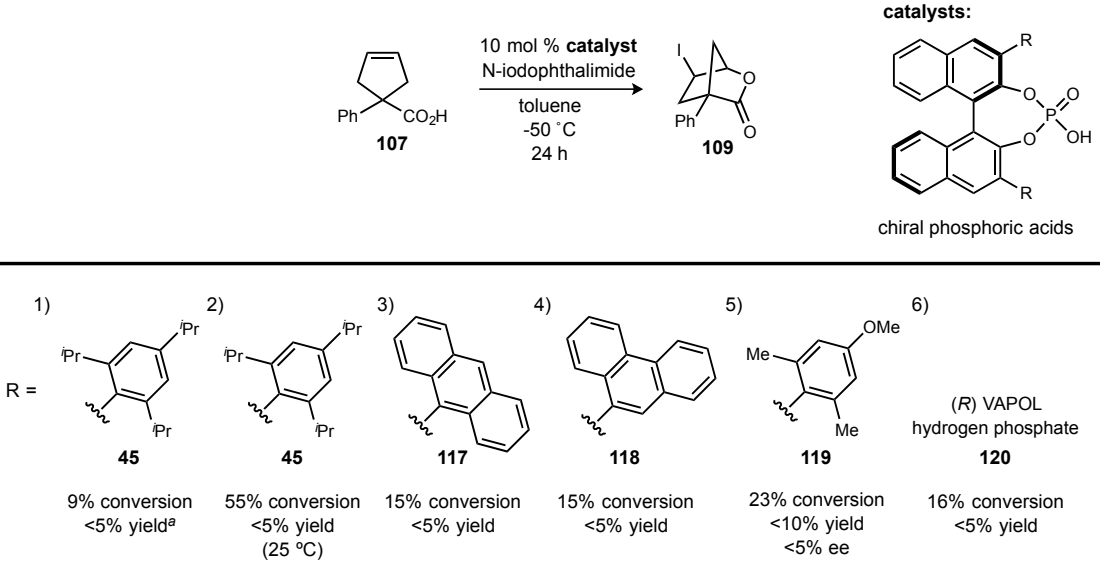

[a] Conversion and yield determined by ^{1}H NMR analysis relative to an internal standard (CH_2Br_2).

With only minor improvements made through steric modification of the catalyst, alterations to the *N*-iodophthalimide iodine source were again examined (Table 9). Electron-poor variations, such as a 5-fluoro and 5-nitro derivatives performed worse (58% and 35% ee, respectively; Table 9, entries 2 and 3) compared to *N*-iodophthalimide. 5-Methyl-*N*-iodophthalimide actually showed an increase in rate but with diminished enantiomeric excess (69%, Table 9, entry 4). More significant changes were explored, but *N*-iodoisatin and *N*-iodosaccharin were unable to afford the product (Table 9, entries 5 and 6). *N*-Iodopyrrolidinone was also unable to improve upon the already optimized results (Table 9, entry 7). Additional options to examine seemed to be exhausted, so insight into the catalyst and substrate interactions was sought in order to inspire new hypotheses.

Table 9: Screening iodine sources based on *N*-iodophthalimide

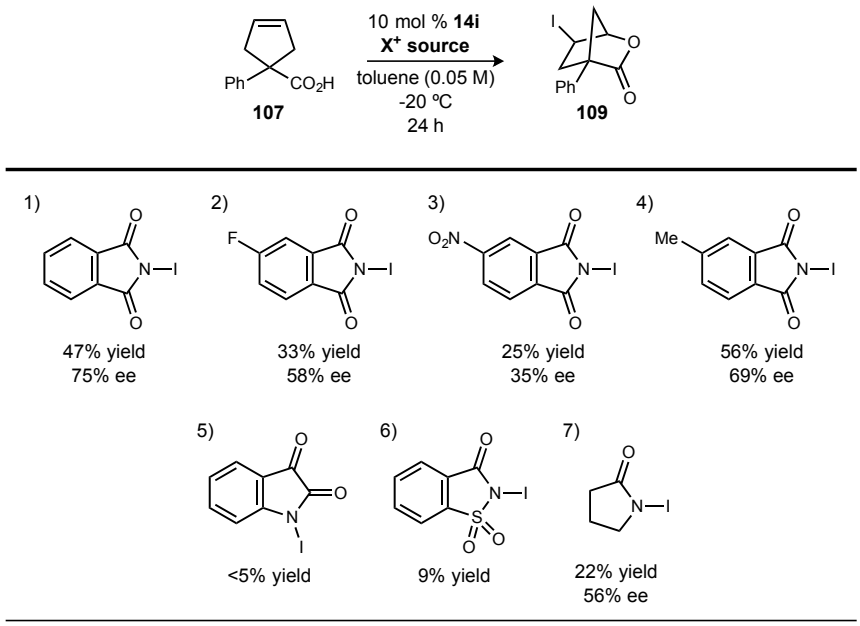

[a] Conversion and yield determined by ^{1}H NMR analysis relative to an internal standard (CH_2Br_2).

*1.2.3 X-Ray crystallographic analysis of a catalyst • substrate (**14 • 107**) complex*

After exhausting these variables to optimize enantioselection without compromising the yield, attempts were made to cocrystallize the substrate and catalyst in order to obtain an X-ray structure. A 1:1 ratio of substrate **107** and catalyst **14** were dissolved in dichloromethane, a layer of hexanes was gently added on top, and the two were allowed to slowly diffuse in a sealed vial. A single crystal was formed and the structure was solved by Maren Pink (Indiana University Molecular Structure Center) (Figure 30). The structure obtained revealed a new mode of binding that had not been hypothesized previously. Immediately obvious is the presence of three hydrogen bonds between the carboxylate and the catalyst. The two hydrogen bonds from one amidine is consistent with previous hypotheses, however the extra hydrogen bond donor is unexpectedly positioned by the twist of the second amidine. The catalyst must be realizing a moderate level of enantioselectivity by donating two hydrogen bonds to one oxygen (N_1-H_1—O_1 and N_2-H_2—O_1, Table 10, entries 1 and 2) and only one hydrogen bond to the other one oxygen (N_3-H_3—O_2, Table 10, entry 3). The singly bound oxygen may be more nucleophilic than the doubly bound oxygen, leading to its enhanced reactivity, however this is a difficult hypothesis to test. In this crystallized conformation, cyclization of the singly bound oxygen would lead to the major enantiomer of the product. It must be stated that a solid-state conformation does not necessarily depict the conformation in solution, and all conclusions derived from a crystal structure need additional evidence for substantiation. Nevertheless, this unexpected binding

pattern gave physical evidence as to *how* BAM catalysis could achieve oxygen differentiation of the carboxylic acid (see Figure 29B). This crystal structure also provided a basis to further improve the enantioselectivity.

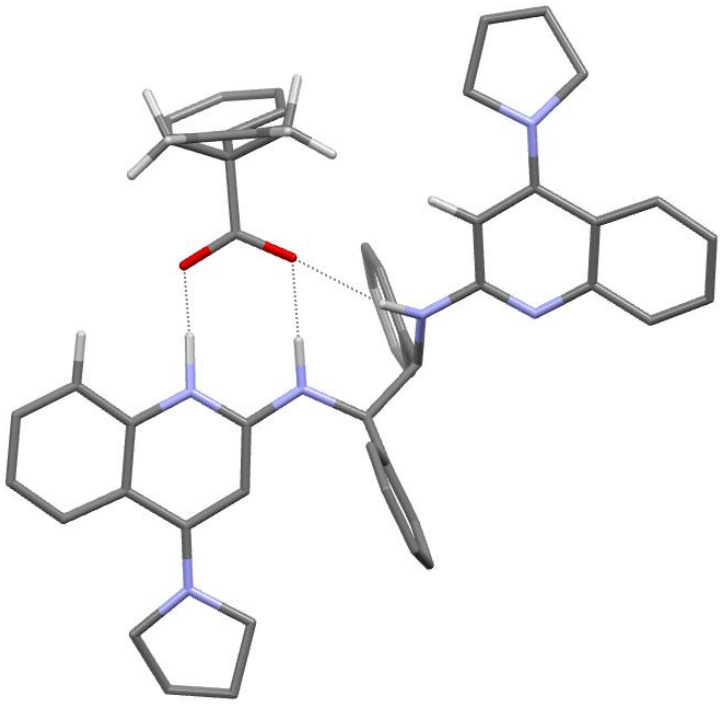

Figure 30: X-Ray co-crystal structure of substrate **107** bound to catalyst **14** (some hydrogens omitted for clarity).

Table 10: Hydrogen bond distances and angles.

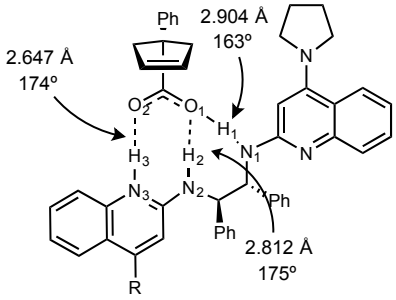

entry	bond	N-H (Å)	O-H (Å)	N-O (Å)	N-H-O (°)
1	N_1-H_1—O_1	0.89	2.04	2.904	163
2	N_2-H_2—O_1	0.85	1.96	2.812	175
3	N_3-H_3—O_2	0.94	1.71	2.647	174

Based on the absolute configuration of the product, the mechanism of product formation could be proposed (Figure 31A). In order to form the major enantiomer, the singly bound oxygen will cyclize onto the alkene which is oxidized by iodonium. The cause of the poor enantioselectivity remained hidden, though. Assuming good selectivity for differentiation of oxygen atoms, a possible explanation for moderate enantioselection was that the alkene conformation was not as restricted as it appeared in the crystal structure. As was alluded to before, the substrate could bind to the catalyst with the alkene forward (as shown in Figure 31A) or with the phenyl forward and the alkene behind (illustrated in Figure 29C). To address this, the catalyst structure was examined for areas that may

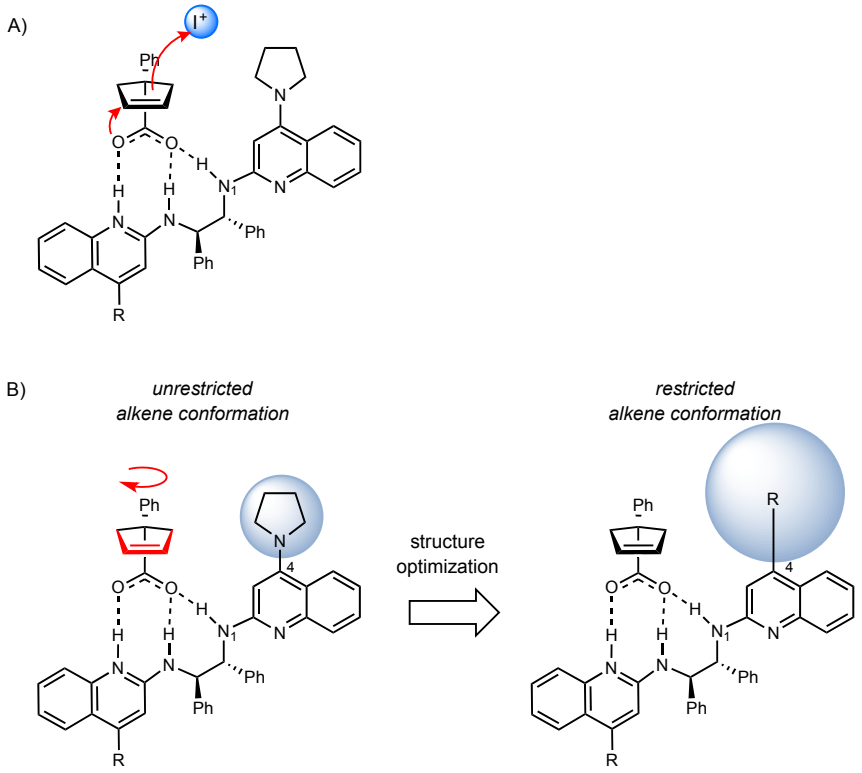

Figure 31: A) Proposed mechanism for formation of the major enantiomer, and B) possible cause of poor enantioselectivity by catalyst **14**, and potential catalyst modifications to improve selectivity.

influence the conformation of the substrate. Fortunately, due to the third hydrogen bonding N-H, one quinoline is twisted with the 4-pyrrolidyl substituent pointing near the substrate (Figure 31B). This substituent may exert a small influence but may not be large enough to effectively discriminate between the two possible alkene conformations, leading to only moderate enantioselectivity. From this observation, larger pyrrolidine surrogates were then installed and tested.

1.2.4 Hypothesis driven catalyst structure optimization

The catalyst-substrate cocyrstal was used as a rational guide to test catalyst derivatives for improved selectivity in this iodolactonization reaction (Table 11). These investigations were initially undertaken on the more readily accessible 4-Cl precursor to catalyst **14a**, as opposed to the more precious 4-Cl, 6-^{t}Bu precursor to the optimal **14i**. Larger heterocyclic rings were surveyed, with piperidine and azepine being installed at the 4-position. Piperidine-containing catalyst **121** demonstrated poorer reactivity and selectivity than its pyrrolidine counterpart, **14a** (Table 11, entries 1 and 2). **122**, with a 4-azepine group, had similar reactivity issues but higher enantioselectivity than expected (51% ee, Table 11, entry 3). Larger rings did not appear beneficial to the reaction, so groups with more flexibility were examined next. Acyclic, dialkyl amines (diethyl amine, dibenzyl amine) were attempted to be installed at the catalyst 4-position. These amines were not nucleophilic enough, however, to accomplish the desired S_NAr reaction and yield the desired catalysts. By chance, *p*-anisidine was installed in the 4-position. Catalyst **123** was anticipated to have lower reactivity than **14a**, because of the weaker electron donating ability of an aniline nitrogen compared to a pyrrolidine nitrogen. Surprisingly, this catalyst performed much better than ever expected (Table 11, entry 4). The enantiomeric excess was 49%, slightly lower than the pyrrolidine based catalyst. However, the yield of product over the course of

Table 11: Catalysts with larger substituents at the quinoline 4-position.

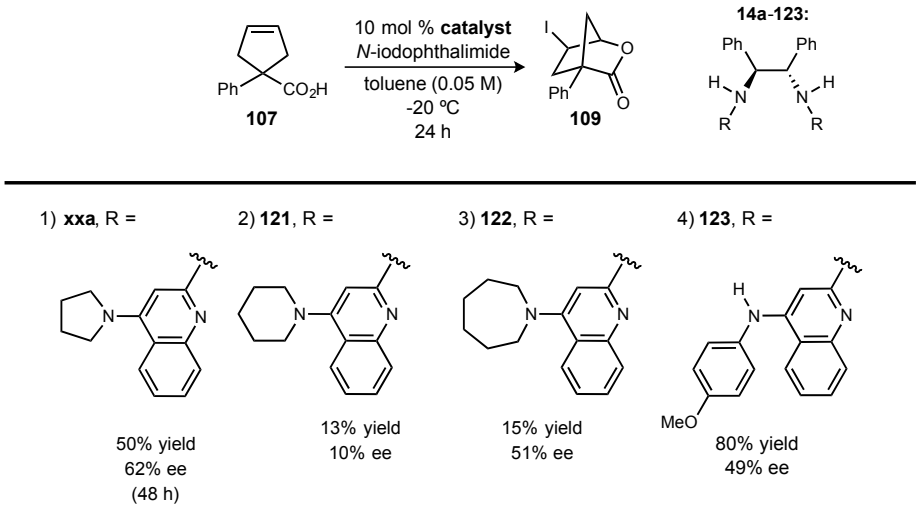

[a] Conversion and yield determined by ^{1}H NMR analysis relative to an internal standard (CH_2Br_2).

one day was almost double that produced by **14a** over two days. The cause of this drastic increase in reaction rate still remains unclear. One would expect a less basic catalyst to be a worse activator of a carboxylic acid, yet this is not the case. This increased rate also opened the possibility for future tests at lower temperatures. Additionally, a wide range of

anilines were commercially available for further examination, in hopes of finding an aniline substituent to deliver high selectivity with increased rate.

Using the readily accessible 4-Cl StilbBAM precursor, **124**,[37] a small library of aniline-substituted catalysts could be quickly produced (Figure 32). Trifluoroacetic acid was required to enhance the electrophilicity of the 4-Cl quinoline, and upon heating in a sealed vessel the products were generated. After base washing, the catalysts were tested without further purification. Changing from *p*-anisidine to *o*-anisidine maintained selectivity and lowered the reactivity (**123a** to **123b**; Table 12, entries 1 and 2). Decreasing in electron richness, aniline catalyst **123c** did not react quite as well, but the selectivity increased to 61% ee (Table 12, entry 3). This added selectivity was comparable to the pyrrolidine substituted catalyst (61% versus 62% ee, see Table 11, entry 1), and the yield was still significantly higher (64%). Less electron rich *p*-CF_3- and 3,5$(CF_3)_2$-aniline derivatives were also tested (**123d** and **123e**, respectively). The yields continued to drop as the electron density of the aniline was lowered (62% and 41% yield, Table 12, entries 4 and 5). Selectivity for **123d** remained high (59% ee, Table 12, entry 4), but for the most electron poor **123e**, enantiomeric excess dropped to 20% (Table 12, entry 5). A trend from this data is not obvious, however it appears that extremely electron rich or deficient substituents are not helpful, and that *p*-substituted anilines may be sterically beneficial. The sterically demanding 9-anthracenyl amine substituent was also tested (Table 12, entry 6), providing comparable results to the undecorated aniline **123c** in entry 3 (Table 12). This catalyst was problematic to synthesize and prone to decomposition, so it was not pursued further. The triflimidic acid salt, **123 • HNTf₂**, was found to have similar reactivity and lower enantioselectivity (56% and 43%, respectively, Table 12, entry 7). The enhanced rate of

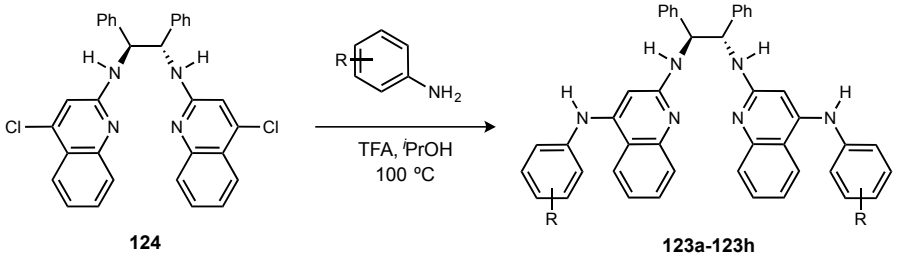

Figure 32: Synthesis of aniline-based catalysts.

these aniline catalysts provoked the synthesis of methylated catalyst, **123h**. The extra N-H donor from the aniline may play a role in substrate binding that allows for higher yield and selectivity. The yield and enantiomeric excess were significantly lowered with this catalyst (Table 12, entry 8). Removal of the N-H donor or the added steric element was detrimental to the reaction.

With the *p*-anisidine substituents (**123a**) and aniline (**123c**) providing the best results, these were combined with previously impactful catalyst changes, namely

substitution at the quinoline 6-position (Table 6). Adding a phenyl substituent at the 6-position (catalyst **125a**, Table 13, entry 1) increased the enantiomeric excess from 49% to 62% (compare Table 12, entry 1). This effect was even greater when combined with the aniline (**125**b), seeing the selectivity rise to 78% from 61% and the yield rise from 64% to 87% (Table 13, entry 2). With such high reactivity being achieved, catalyst **125b** was next tested at -40 ºC for 48 h, and the selectivity increased to 83% ee (Table 13, entry 3). At these same conditions, a 6-*tert*-butyl substituted catalyst, **126a**, provided a slight boost in enantiomeric excess (Table 13, entry 4). This catalyst was combined with the optimal iodine source, *N*-iodophthalimide, to further increase selectivity to 87% ee (Table 13, entry 5). For comparison, 6-*tert*-butyl StilbPBAM (**14i**) could only yield 34% of the product in 68% ee (Table 13, entry 6). Overall, a substitution at the 6-position of the quinoline had a cooperative effect with the 4-aniline substituent, increasing the selectivity. The increased

Table 12: Results from screening aniline derivatives at the catalyst 4-position.

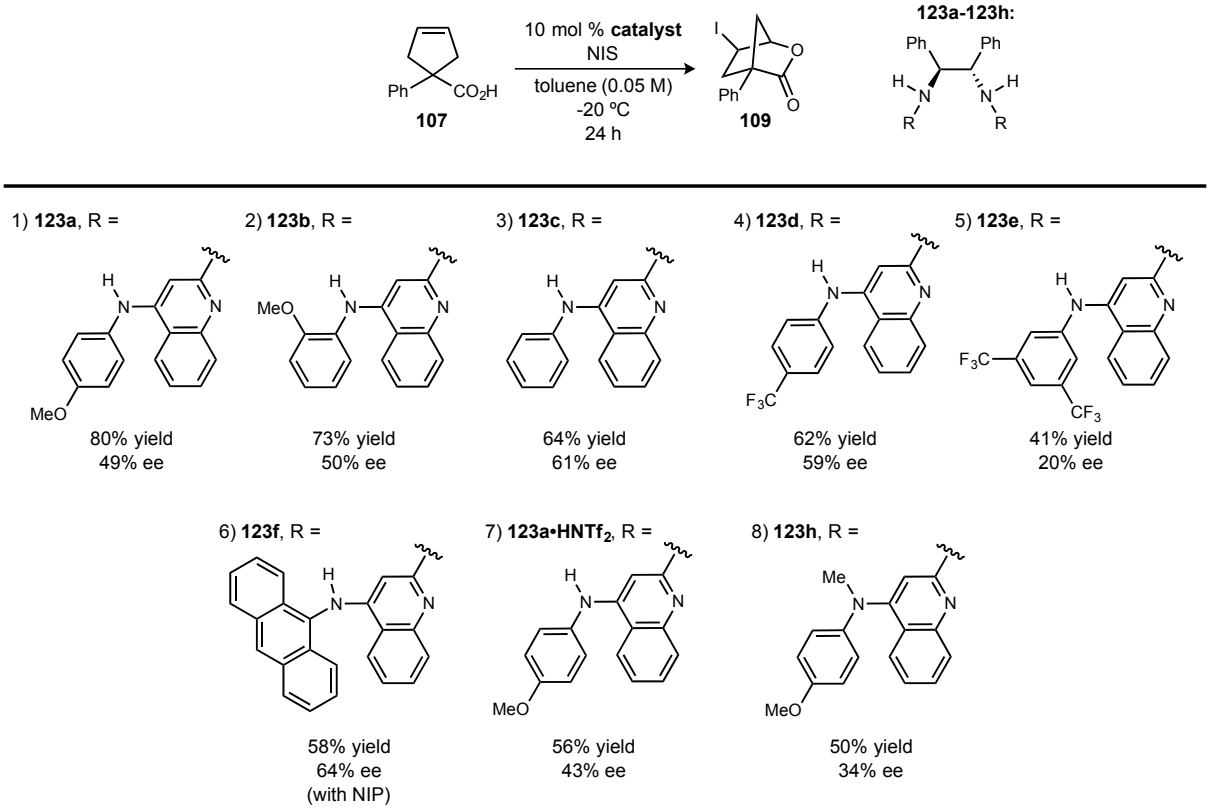

[a] Conversion and yield determined by ^{1}H NMR analysis relative to an internal standard (CH_2Br_2).

reaction rate from the aniline group allowed the reaction to be run for reasonable lengths at colder temperatures to further increase selectivity without sacrifice to conversion.

Table 13: Combination of 4-aniline and quinoline 6-substitutions.

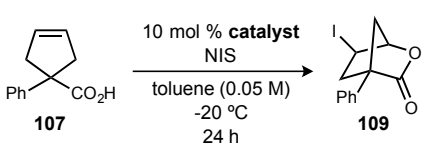

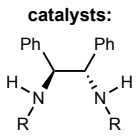

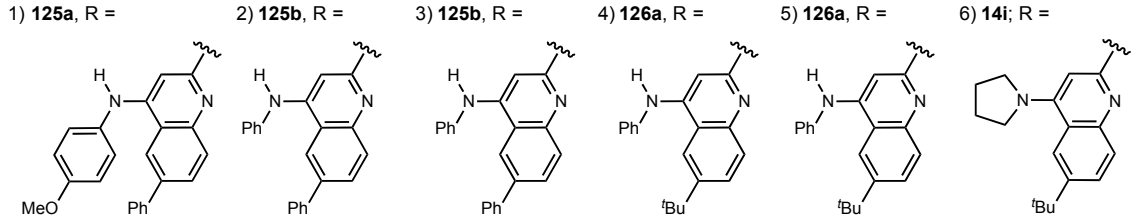

[a] Conversion and yield determined by ^{1}H NMR analysis relative to an internal standard (CH_2Br_2).

These catalysts performed well even at -50 ºC, breaking the 90% enantiomeric excess threshold (Table 14, entry 1). Since substituents at the *para* position of the aniline appeared to impact the reaction, a small study of *p*-anilines was performed to find the right balance of electronics and sterics. A large, *tert*-butyl substituted aniline was installed in catalyst **126b**, however the selectivity dropped to 85% ee (Table 14, entry 2). *p*-Fluoro aniline was then examined, since it is more electron rich than aniline and has no added steric influence,

Table 14: Impact of *para* aniline substituents on reaction outcome.

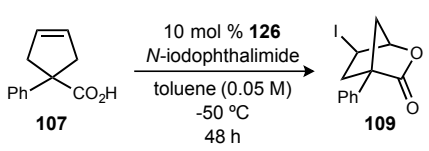

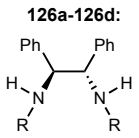

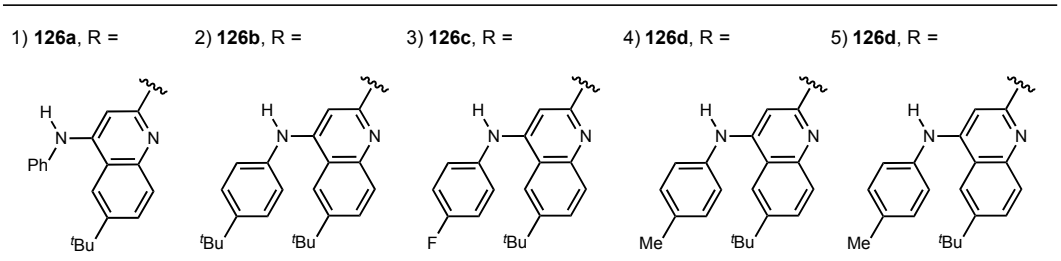

[a] Conversion and yield determined by ^{1}H NMR analysis relative to an internal standard (CH_2Br_2). [b] Reaction stirred in a 2-5 mL round bottomed vial for 24 h.

and the yield and selectivity rose (**126c**, 72% yield, 92% ee, Table 14, entry 3). Then *p*-toluidine was appended in catalyst **126d**, as it would be as electron rich as *p*-fluoro and

have more steric bulk. We were excited to see that it showed an increase in yield (79%) and enantiomeric excess (93%, Table 14, entry 4). After a screen of reaction vessels, a round-bottomed microwave vial provided faster conversion compared to the previously used, flat-bottomed storage vials. The more efficient stirring in a microwave vial yielded the product in 83% after 24 hours, and the enantiomeric excess increased to 94% as well (Table 14, entry 5).

*1.2.5 X-Ray crystallographic analysis of a catalyst • substrate (**126d • 14a**) complex*

The X-ray co-crystal structure of the cyclopentene carboxylic acid substrate bound to StilbPBAM (**14a**) provided a rationale for how moderate enantioselectivity was being achieved by oxygen atom differentiation of the carboxylate (Figure 30). It also provided a foundation on which to build hypotheses for the improvement of enantioselectivity. Most clear of these was that the alkene conformation of the substrate appeared to be too flexible (Figure 29C and Figure 31B). The 4-position of the catalyst seemed conveniently oriented near the substrate, and it could be easily modified to build a library of catalysts for screening. Led by this hypothesis, aniline substituents were found to provide the highest reactivity. Combined with a 6-substituent on the quinoline and fine-tuning of the aniline structure, optimized catalyst **126d** was developed. It is able to desymmetrize carboxylic acid **107** in 83% yield and 94% ee (Table 14, entry 5).

These optimized results were consistent with the hypothesis that led to catalyst **126d**. A second co-crystal structure of substrate **107** and catalyst **126d** would further test this hypothesis. This catalyst and substrate were combined in a 1:1 ratio, and recrystallization conditions were tested. A single co-crystal of sufficient quality was obtained when the complex was dissolved in dichloromethane and heptanes was gently layered on top to allow slow diffusion (Figure 33). A surprisingly similar structure of this complex to that of the suboptimal catalyst and substrate was revealed (compare Figure 30). The substrate orientation relative to the catalyst is the same between the two co-crystal structures. The dihedral angles of the catalyst backbones in both structures were nearly identical (166° and 167°). An analogous hydrogen bonding network (two hydrogen bonds to one oxygen and one hydrogen bond to the other oxygen) is present, indicating a similar mechanism of carboxylate desymmetrization is still operative. In fact, all of the hydrogen bond distances and angles are remarkably similar (Table 15, compare to Table 10). The major differences arise from the added 4-aniline and 6-*tert*-butyl functionalities. The *tert*-butyl may serve to limit the rotational freedom of the 4-subtituent, forcing it closer to the substrate pocket. The aniline is clearly much closer to the substrate than the pyrrolidine was in Figure 30. The substrate alkene also appears to be rotated away from the steric influence of the aniline. The role of the aniline N-H is not clear in this crystal structure, if

it is somehow serving to accelerate the reaction. It should be noted that this N-H does participate in hydrogen bonding with another catalyst-substrate structure, binding to the free quinoline nitrogen of another unit. This additional hydrogen bonding between unit cells is not possible, and is therefore not observed, in the cocrystal structure of **14a • 107**.

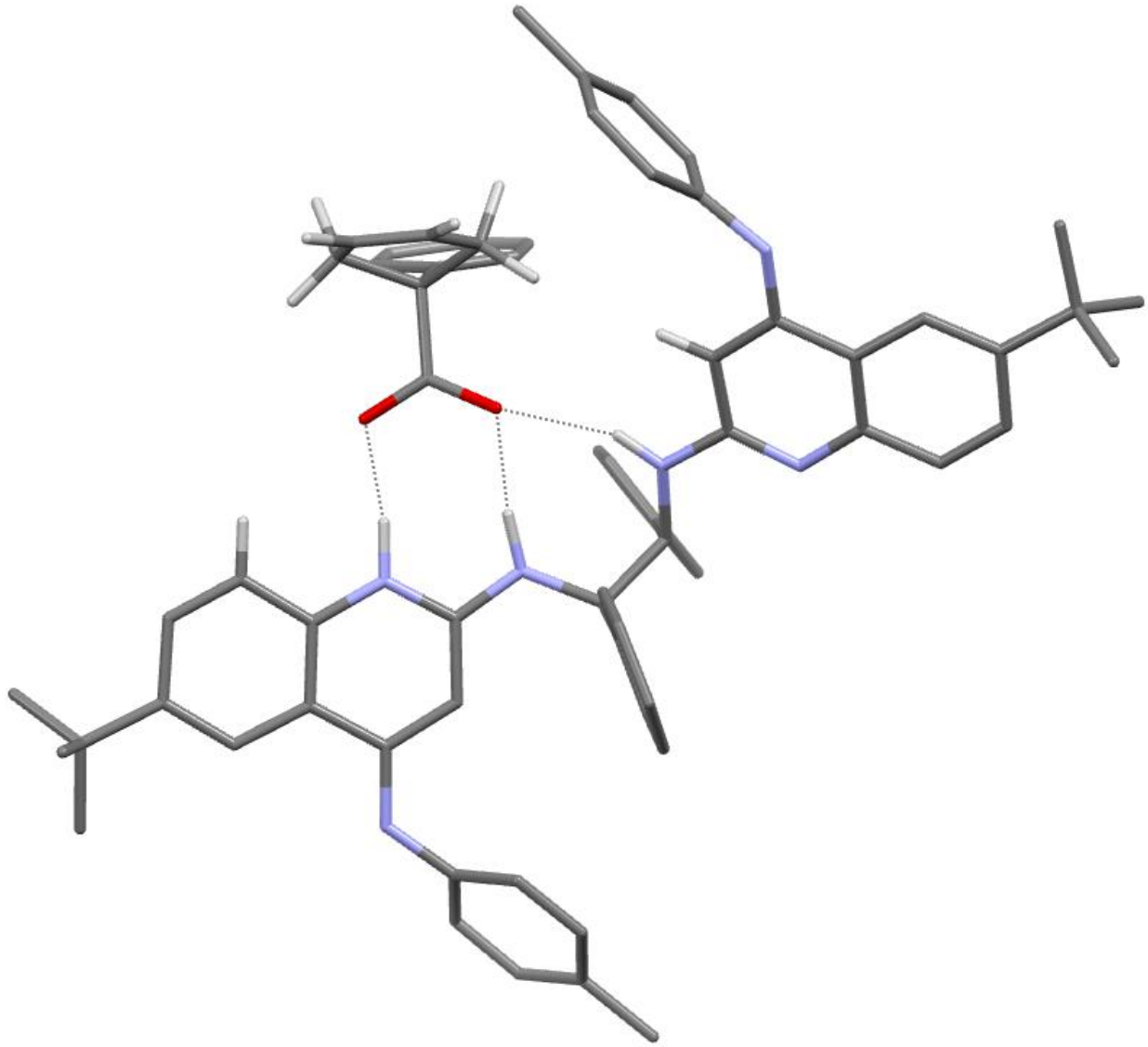

Figure 33: X-Ray co-crystal structure of **107** bound to catalyst **126d** (some hydrogen atoms omitted for clarity).

Table 15: Hydrogen bond distances and angles.

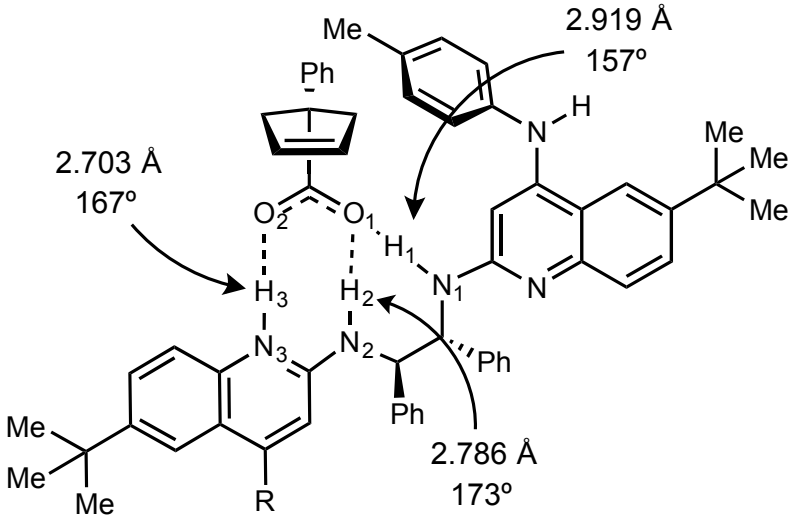

entry	bond	N-H (Å)	O-H (Å)	N-O (Å)	N-H-O (°)
1	N_1-H_1—O_1	0.90	2.07	2.919	157
2	N_2-H_2—O_1	0.97	1.82	2.786	173
3	N_3-H_3—O_2	0.96	1.76	2.703	167

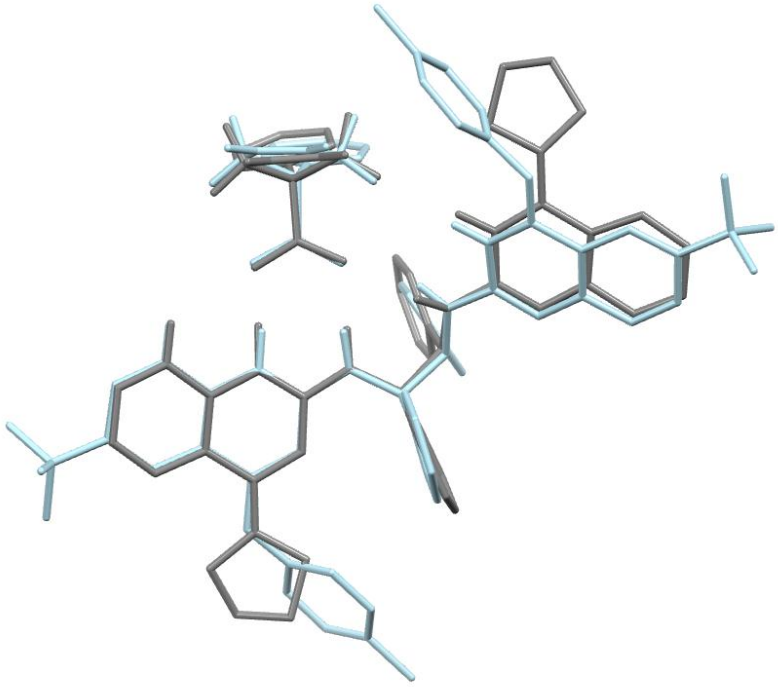

Figure 34: Front view of co-crystals of **126d•107** (cyan) and **14a •107** (grey) overlayed.

To more effectively compare and contrast the two catalyst-substrate co-crystal structures, they were overlayed and aligned along the three nitrogen atoms of the hydrogen bond network (front view, Figure 34; top view, Figure 35; side view, Figure 36). The front and side views show the remarkable similarity between these two separate co-crystal structures (Figure 34 and Figure 36). The top view makes the relative positional differences of the substrates bound to their respective hydrogen bond networks especially evident, with the aniline catalyst appearing to "push" the substrate away. It is hypothesized that this added influence, which twists the substrate just a few extra degrees, was essentially responsible for increasing enantiomeric excess from the 60's to the 90's. The energy difference between substrate binding with alkene forward and binding with the alkene behind was likely increased by the aniline substituent of **126d**. Density functional theory calculations have been undertaken to investigate this hypothesis.

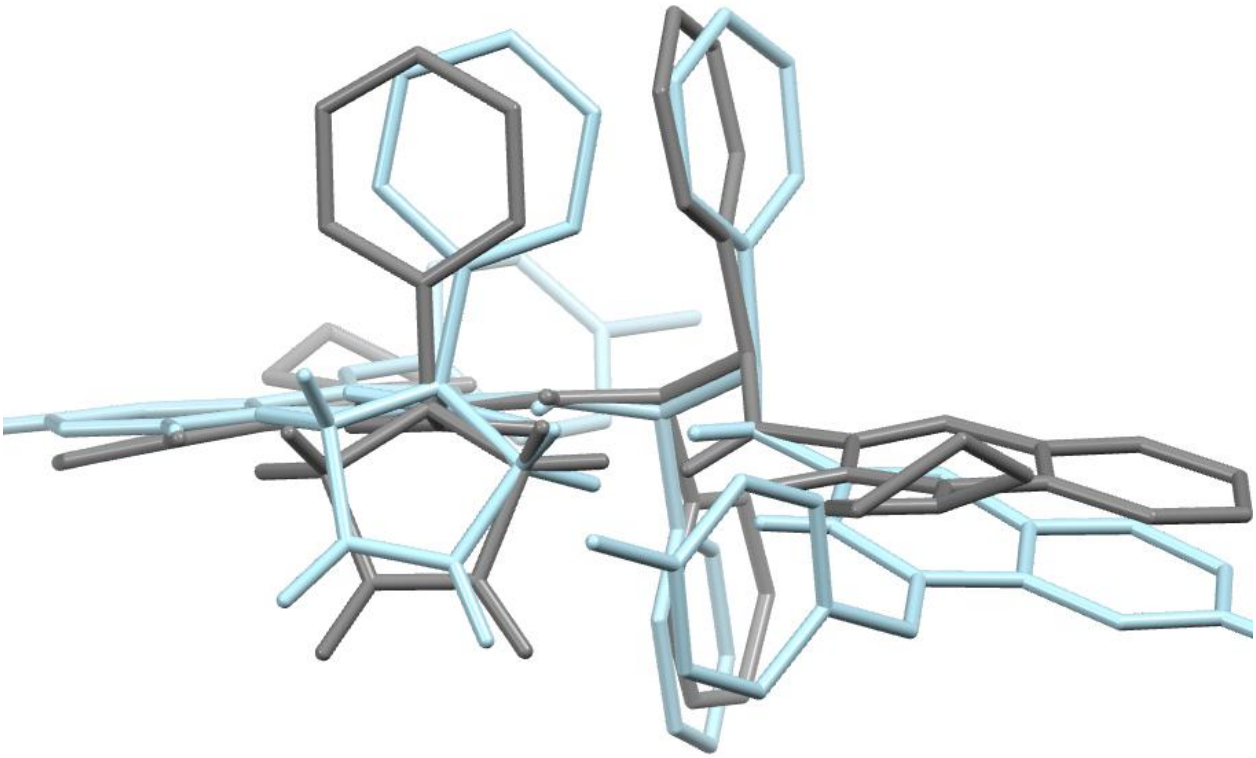

Figure 35: Top view of co-crystals of **126d•107** (cyan) and **14a •107** (grey) overlayed.

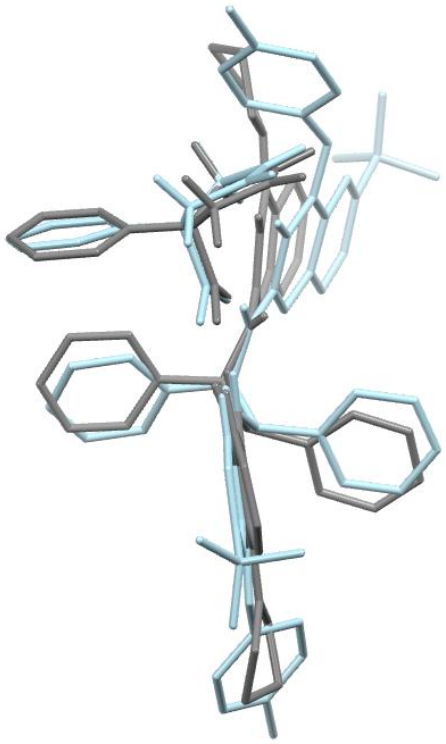

Figure 36: Side view of co-crystals of **126d•107** (cyan) and **14a •107** (grey) overlayed.

In summary, the hypothesis derived from the initial co-crystal structure enabled the development of optimized catalyst, **(*R*,*R*) 126d**, from catalyst **14a** (Figure 37). Including additional optimization of iodine sources, temperature, and reaction container, the reaction was optimized to 86% yield and 94% ee. The optimized catalyst was also co-crystallized, and its structure supports the original hypothesis of the origins of enantioselectivity in this application of BAM catalysis. The broader implications of this work toward other BAM catalyzed reactions is still being realized.

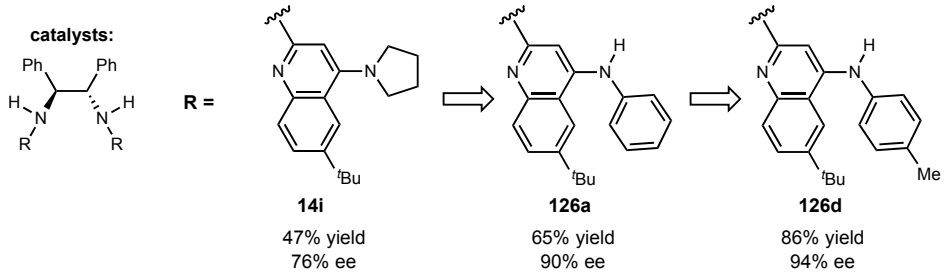

Figure 37: Summary of reaction optimization by catalyst developement.

1.2.6 Analysis of the scope and limitations of the desymmetrization of a carboxylic acid

With an optimized reaction system in hand, exploration of its substrate scope was carried out. A summary of the synthesis of most substrates is in Figure 38. For the synthesis of aryl-cyclopentenecarboxylic acids, a range of commercially available aryl-acetate esters were treated with sodium hydride before bis-alkylation by *cis*-1,4-dichloro-2-butene (Figure 38A). The second, intermolecular alkylation step can either occur by an S_Ni mechanism to create the desired 5-membered ring, or it can cyclize via an S_Ni' mechanism to generate a cyclopropane byproduct. This undesired cyclopropane is generally formed in about 10%, and recrystallization of the final carboxylic acid was typically able to remove it. Synthesis of alkyl substrates were straightforward (Figure 38B). Commercially available 3-cyclopentenecarboxylic acid could be doubly deprotonated by LDA, addition of an alkyl halide electrophile and acidic workup furnished the desired alkyl-cyclopentenecarboxylic acids. Ester substrates were synthesized from LDA deprotonation of 3-cyclopentenecarboxylic esters before quenching by carbon dioxide (Figure 38C).

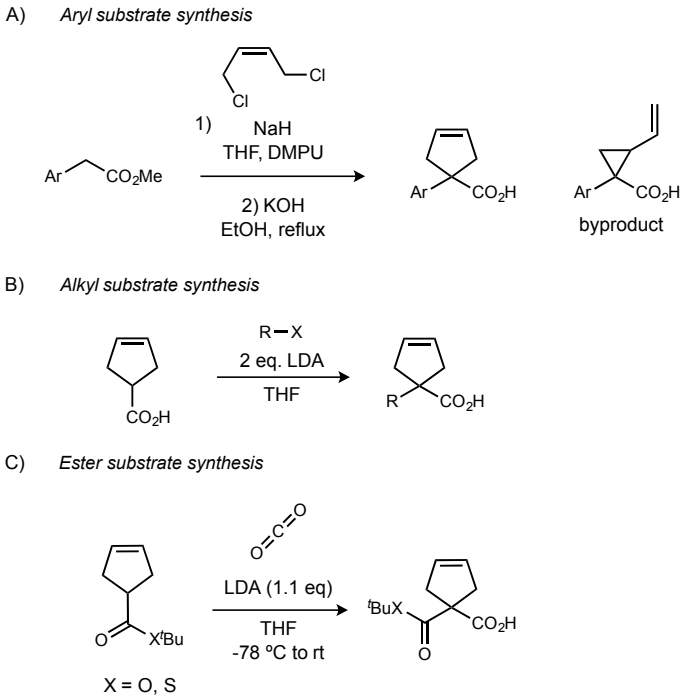

Figure 38: Synthesis of A) aryl-, B) alkyl-, and C) ester-cyclopentene carboxylic acid substrates.

Synthesis of more exotic symmetric carboxylic acid substrates is reported in Figure 39. In an effort to test the viability of this methodology on other ring sizes, phenylacetic acid was doubly alkylated by 4-bromo-1-butene in 14% yield over two steps (Figure 39A).

Diene **127** was then subjected to ring closing metathesis, producing cycloheptene **128** in nearly quantitative yield. A substrate with two symmetric alkenes was also desired. Benzoic acid was subjected to Birch reduction followed by addition of benzyl bromide to generate cyclohexadienecarboxylic acid **129** in good yield (Figure 39B). An attempt was made to explore alkene substitution with tetrasubstituted alkene substrate **130** (Figure 39C), however neither the Grubbs II nor the Stewart-Grubbs[103] catalysts could not promote the ring closing methathesis of these hindered alkenes.

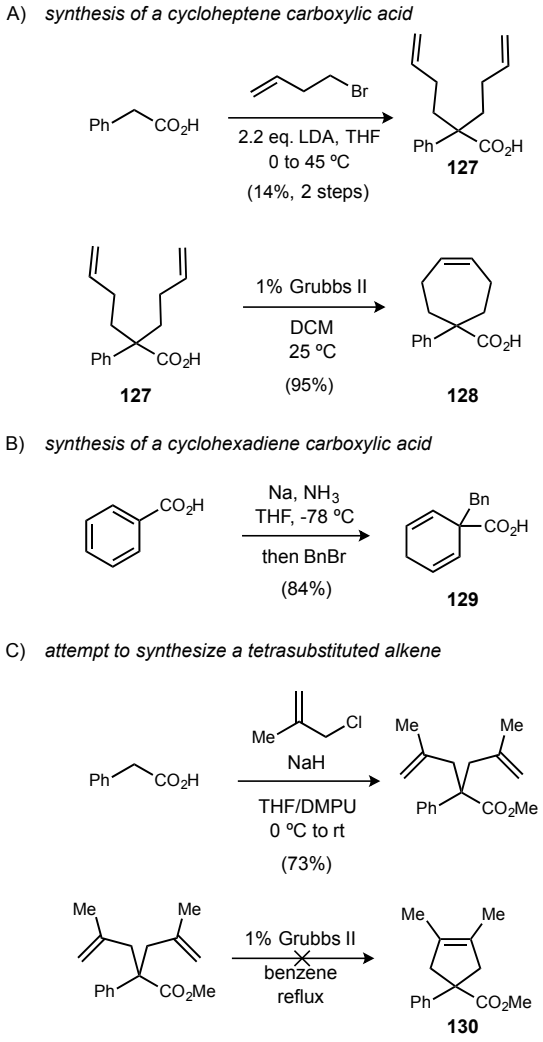

Figure 39: A) synthesis of a phenyl-cycloheptene carboxylic acid substrate; B) synthesis of a symmetric, cyclohexadiene carboxylic acid substrate; C) attempt to synthesize a tetrasubstituted cyclopentene carboxylic acid.

[103] Stewart, I. C.; Douglas, C. J.; Grubbs, R. H. *Org. Lett.* **2008**, *10*, 441.

Overall, the substrate scope revealed a wide tolerance of substituents. Aryl substituents generally performed the best, perhaps due to the reaction optimization on phenyl-cyclopentenecarboxylic acid **107a**. This phenyl substrate could be used on a 1.00 mmol scale, delivering the product **109a** with a longer reaction time and no loss of enantiomeric excess (Table 16, entry 2). A larger, 2-naphthyl substrate was amenable to the reaction conditions, delivering **109b** in 78% yield and 90% ee (Table 16, entry 3). The extremely hindered 1-naphthyl substrate revealed a limitation of this methodology, forming

Table 16: Performance of aryl substrates in the iodolactonization of symmetric carboxylic acids.

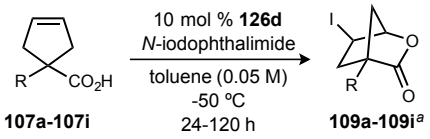

1) 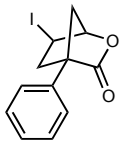 **109a** 87% yield 93% ee 24 h	2) 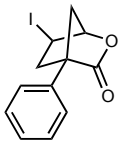 **109a** 66% yield[b] 94% ee 48 h	3) 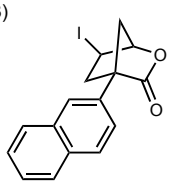 **109b** 78% yield 90% ee 72 h	4) 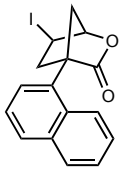 **109c** 72% yield 67% ee 72 h	5) 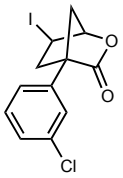 **109d** 69% yield 89% ee 24 h	6) 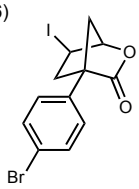 **1091e** 74% yield 89% ee 24 h
7) 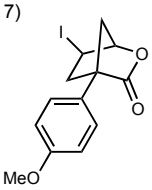 **109f** 65% yield 91% ee 48 h	8) 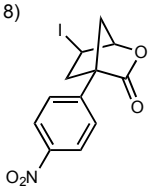 **109g** 78% yield 86% ee 120 h	9) 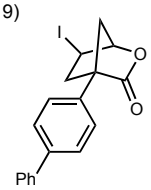 **109h** 55% yield 94% ee 72 h	10) 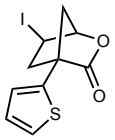 **109i** 69% yield 92% ee 24 h		

[a] Isolated yields reported on 0.10 mmol reaction scale. [b] 1.00 mmol reaction scale.

iodolactone **109c** in much poorer enantiomeric excess (67%, Table 16, entry 4). *Meta*-chloro and *para*-bromo phenyl substitutents performed well under the reaction conditions (89% ee and 89% ee, Table 16, entries 5 and 6). The electron rich *p*-methoxyphenyl iodolactone, **107f**, was also produced in decent yield and 91% ee (Table 16, entry 7). The electron poor **107g**, bearing a *p*-nitrophenyl group, required a five-day reaction time to furnish 78% of product in good enantioselectivity (86%, Table 16, entry 8). Biphenyl substrate **107h** reacted slower, but yielded **109h** in 94% ee (Table 16, entry 9). Finally, the heterocyclic

substrate **107i** reacted well despite the oxidative reaction conditions (69% yield, 92% ee; Table 16, entry 10).

Alkyl substrates also performed well in the reaction, albeit in slightly lower enantioselectivities. Isopropyl-cyclopentenecarboxylic acid was efficiently converted to iodolactone **109j** in 74% yield and 87% ee (Table 17, entry 1). The benzyl and methyl substrates both yielded 66% of product in good enantiomeric excesses (87% and 86% respectivel, Table 17, entries 2 and 3). *tert*-Butyl ester lactone, **109m**, was formed with poor selectivity (64% ee, Table 17, entry 4). Interestingly, the slightly larger *tert*-butyl thioester lactone **109n** was delivered in 10% higher enantioselectivity (74% ee, Table 17, entry 5). The cyclizations of 3-cyclopentenecarboxylic acid (where R = H) and cyano-cyclopentenecarboxylic acid (where R = CN) could not be accomplished (Table 17, entries 6 and 7). It appears that successful substrates require some degree of ground state destabilization. The substituent of the substrate forces the carboxylic acid closer to the alkene, predisposing it to cyclization. If the substituent, R, is too small, then poor reactivity and possibly poor selectivity can be expected.

Table 17: Performance of alkyl and ester substrates in the iodolactonization of symmetric carboxylic acids.

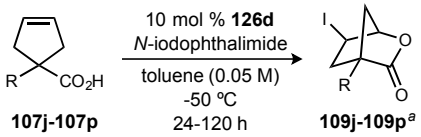

107j-107p **109j-109p**[a]

1)	2)	3)	4)	5)	6)	7)
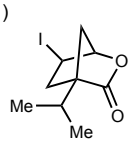	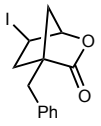	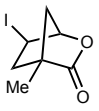	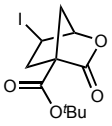	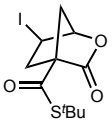	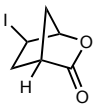	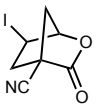
109j	**109k**	**109l**	**109m**	**109n**	**109o**	**109p**
74% yield	66% yield	66% yield	64% yield	66% yield	<5% yield	<5% yield
87% ee	87% ee	86% ee	64% ee	74% ee		
24 h	48 h	72 h	24 h	24 h	72 h	48 h

[a] Isolated yields reported on 0.10 mmol reaction scale.

Several other interesting substrates were screened. Alkenyl substrate **131** was synthesized to test the relative reactivity of the *cis*-alkene and the monosubstituted alkene (Figure 40A). Needless to say, all conversion of starting material was 5-*exo* cyclization upon the monosubstituted alkene. This byproduct, **132**, was produced in relatively high enantioselectivity (79% ee) compared to typical yields on monosubstituted alkenes by BAM catalysis. The reason for this selectivity is unclear, as both alkenes are 5 atoms away from the nucleophile, and the *cis*-alkene ought to be more electron rich. Cyclohexadiene

carboxylic acid **133** could undergo exclusively 4-*exo* cyclization to deliver **134** in 57% yield and 72% ee (Figure 40B). If the reaction was run using a different catalyst or at higher temperatures, an inseparable mixture of 4-*exo* and 5-*endo* products is formed. This product was assigned as the 4-*exo* product by HMBC analysis. Additionally, **134** is slightly unstable at room temperature and isomerizes to the 5-*endo* product, losing enantiomeric excess in the process. The ability of the catalyst to discriminate between two alkenes was gratifying to discover, and opens future avenues in which this catalysis can be further investigated. The cycloheptene carboxylic acid **135** was submitted, and it yielded the [3.2.2] bicyclic lactone **136** in 79% yield but only 39% ee (Figure 40C). The high reactivity was surprising, and the greater alkene flexibility in this ring size likely lead to less conformational control than in the cyclopentene case. Additionally, the previously used 1,1-disubstituted alkene

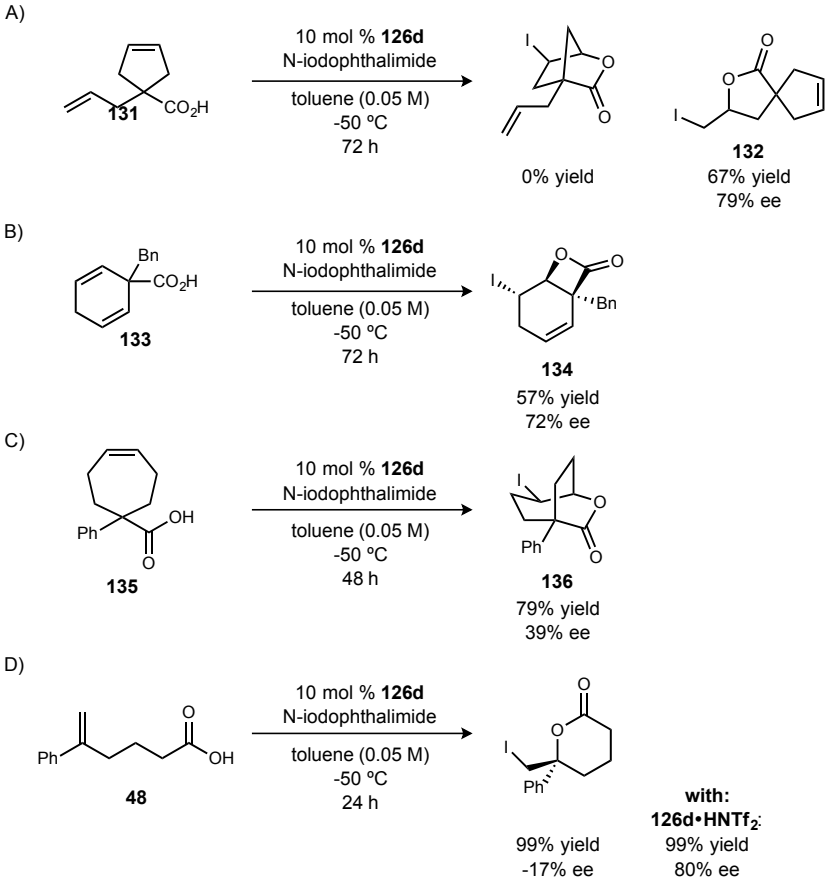

Figure 40: Compatibility of methodology with A) alkene, B) diene, C) heptene, and D) 1,1-disubstituted alkene substrates.

substrate (**48**) was found to react completely in 24 hours, with a slight preference for the minor enantiomer (99% yield. -14% ee, Figure 40D).[37] Since the free base BAM catalyst did not perform well in this system before, the triflimidic acid salt of **126d** was used, and it also provided nearly quantitative yield but with high enantioselectivity for the other

enantiomer (80% ee, Figure 40D). This is an interesting result, and it appears to support the hypothesis that the protonated catalysts are beneficial for 1,1-disubstituted alkenes. The *Z*-alkene substrates are not aided by the acid addition, however.

1.2.7 Mechanistic investigations of the enantioselective desymmetrization of carboxylic acids

The effect of weak acid additives and strong acid additives was examined. This was conducted to determine if the free base of catalyst **126d** was really the most efficient catalyst (Table 18). A range of equivalents from one half to eight of the weakly acidic benzoic acid was added relative to the catalyst. Increasing benzoic acid amounts steadily decreases the selectivity of the catalyst (Table 18, entries 2-5). At eight equivalents of benzoic acid, the reactivity if finally impacted, dropping to 52% yield and 75% ee (Table 18, entry 6). These results contrast with the impact of a strong acid additive. One equivalent of triflimidic acid relative to the catalyst does not impact the reactivity of the catalyst and only diminishes the selectivity by 6% (Table 18, entry 7). The doubly protonated catalyst **126d** • $(HNTf_2)_2$ was unable to promote the reaction (Table 18, entry 8). This appears to indicate that protonation of the free quinoline does not significantly alter the catalyst mode of action. A weakly acidic additive, like benzoic acid, may be exchanged for the weakly acidic substrate carboxylic acid, whereas the strongly acidic additive cannot exchange with the substrate. These findings are consistent with the hypothesis that the free base of the catalyst is operative.

Table 18: Effect of acidic additives on the reaction outcome.

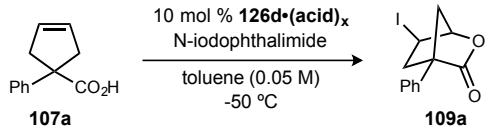

107a **109a**

entry	$(acid)_x$	yield (%)[a]	ee (%)
1	None	83	94
2	$(PhCO_2H)_{1/2}$	85	88
3	$(PhCO_2H)_1$	89	88
4	$(PhCO_2H)_2$	85	81
5	$(PhCO_2H)_4$	87	80
6	$(PhCO_2H)_8$	52	75
7	$(HNTf_2)_1$	85	88
8	$(HNTf_2)_2$	<5	–

[a] Yield determined by ^{1}HNMR analysis relative to an internal standard (CH_2Br_2).

The catalyst could also hypothetically play two distinct roles in catalysis by involving two catalyst molecules in the enantiodetermining step. To investigate this, a non-linear effect study was conducted (Figure 41).[104] Batches of varying enantiopurities of catalyst **126d** were prepared by combination of (*R*,*R*)- and (*S*,*S*)- **126d**. Since a linear correlation of catalyst % ee and product % ee was observed, there is no evidence of two catalyst molecules participating in the enantioselective step. If two catalyst molecules are involved in the enantioselective step, a positive enhancement (an upward curve the line) or negative impedance (a downward curve of the line) of the product ee can be observed relative to the ee of the catalyst batch (i.e. 50% ee catalyst delivering 90% ee product). This arises from a difference in rates between a "homodimeric" catalyst species (i.e. two (*R*,*R*) catalysts) and to a "heterodimeric" catalyst species (i.e. an (*R*,*R*) catalyst and a (*S*,*S*) catalyst), indicating the presence of two catalysts in the selective step. However, no evidence for multiple catalyst molecules was found in this case.

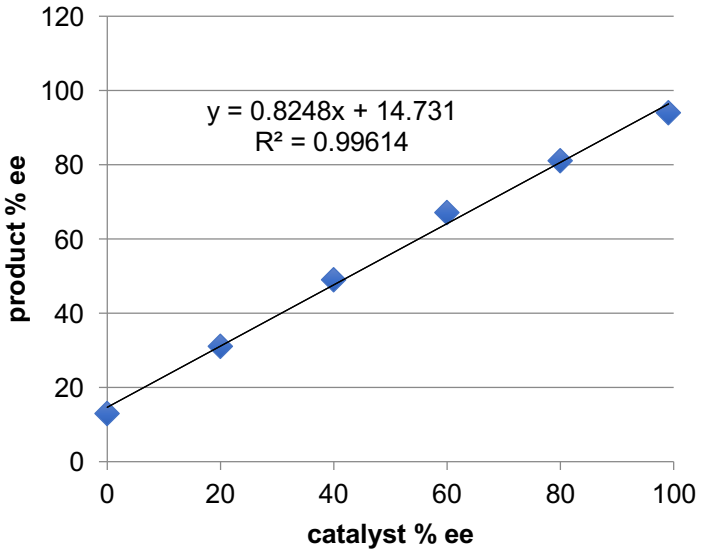

Figure 41: Non-linear effect study of the iodolactonization reaction with catalysts of varying enantiopurities.

Caution is required when information about reactive conformations is derived from crystal structures. Due to crystal packing in the solid state, positions and orientations can deviate from the actual, reactive conformations in solution. A useful technique to compliment the visual information from an X-ray structure is isothermal titration

[104] Guillaneux, D.; Zhao, S.-H.; Samuel, O.; Rainford, D.; Kagan, H. B. *J. Am. Chem. Soc.* **1994**, *116*, 9430.

calorimetry (ITC).[105] ITC is most commonly used to measure protein-ligand interactions, however it is also occasionally applied to investigate small molecule catalyst-substrate binding.[106] In ITC, a known amount of a compound is loaded into a calorimetry cell, and a known amount of another compound is sequentially titrated into the calorimeter. After each injection, the amount of heat generated or absorbed from the interactions of the two compounds is measured, and that change of heat is plotted to generate a titration curve. From this physical measurement, the Gibbs free energy (ΔG), enthalpy of binding (ΔH), and entropy (ΔS) can all be determined. This information gives insight into the interactions of compounds in solution, i.e. the binding constant (K_D), binding stoichiometry, whether a binding event is exothermic or endothermic, and whether complexes of higher order are being formed (which is entropically unfavorable).

Three thermodynamic profiles that are commonly observed in ITC experiments are shown in Figure 42.[107] All three are favorable processes due to their negative overall Gibbs free energy, however, three different combinations of enthalpic and entropic values can lead to a favorable binding process. Each of these scenarios provides information about the nature of binding occurring in solution. For scenario A, a highly exothermic binding event

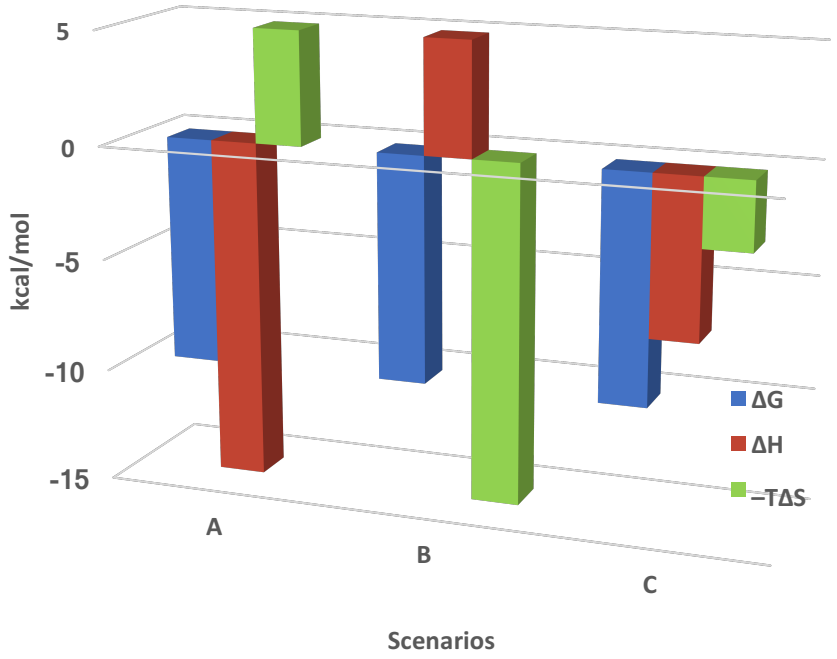

Figure 42: Three thermodynamic scenarios resulting in spontaneous binding events.

[105] Velázquez-Campoy, A.; Ohtaka, H.; Nezami, A.; Muzammil, S.; Freire, E. In *Current Protocols in Cell Biology*; John Wiley & Sons, Inc.: 2001.

[106] Lah, J.; Maier, N. M.; Lindner, W.; Vesnaver, G. *J. Phys. Chem. B* **2001**, *105*, 1670.

[107] Figure adapted from "Introduction to Microcalorimetry" by Malvern.

(-ΔH) is able to overcome an unfavorable entropic change (+TΔS), which is characteristic of strong hydrogen bonding accompanied by an increase in conformational order. The next scenario shows an endothermic binding with a favorable entropic change (-TΔS), which indicates strong hydrophobic interactions (scenario B). Finally, strong hydrogen bonding and hydrophobic interactions can both be operative, leading to an enthalpically and entropically favorable binding (scenario C). Thus, ITC was applied to the titration of substrates **107** into BAM catalysts to compare binding constants and the nature of binding.

Titration of the substrate and the two catalysts for which co-crystal structures could be obtained was performed (Table 19). Titration of substrate **107a** into catalyst **14a**, resulted in a favorable and strong binding constant of 2.52e5 M^{-1} was observed. This is consistent with previously observed carboxylic acids binding to cinchonidine catalysts,[106] and stronger than the binding constant observed between phosphoric acids and carboxylic acids.[91] The binding between **14a** and **107a** is driven by deprotonation and hydrogen bonding (ΔH = -13.0 kcal/mol), which overcomes an entropically unfavorable increase in order (-TΔS = +5.6 kcal/mol, Table 19, entry 1). This strong hydrogen bonding observed by ITC supports a structure in solution similar to the solid-state structure (Figure 30). It should also be noted that only one substrate binding event could be detected. An interesting comparison arises when the same titration is carried out between substrate **107a** and optimized catalyst **126d** (Table 19, entry 2). A weaker binding constant is observed (K_A = 8.40e4 M^{-1}), which correlates with the decreased basicity of the aniline based catalyst relative to pyrrolidyl-catalyst **14a**. Strong hydrogen bonding drives the formation of the substrate-catalyst complex to a similar degree (ΔH = -12.9 kcal/mol, Table 19, entry 2 versus entry 1). Interestingly, a greater increase in order leads to a 0.6 kcal/mol increase in entropy (-TΔS = +6.2 kcal/mol, Table 19, entry 2). This greater entropy value represents formation of a more highly ordered substrate-catalyst complex than in entry 1. This tracks well with the much higher enantioselectivity delivered by catalyst **126d** over **14a**, as well as the greater steric influence of catalyst **126d** on the substrate. Vesnaver and coworkers describe ITC measurements for a similar system of DNB-Leucine binding by cinchona alkaloids as: "the observed highly exothermic values result most likely from the attractive noncovalent intermolecular interactions, such as van der Waals interactions, hydrogen bonding and π-π interaction, whereas the negative entropy contributions apparently reflect the generation of highly ordered bimolecular ionic associates."[106] Therefore, physical measurements of binding in solution support the hypothesized mode of activation provided by X-ray crystal structures.

Table 19: Thermodynamic comparison of the substrate binding between catalyst **14a** and **126d**

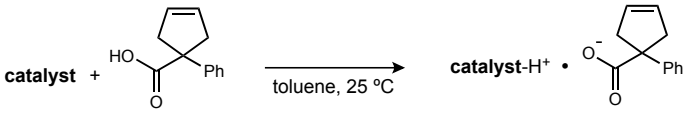

entry	catalyst	ΔH (kcal/mol)	-TΔS (kcal/mol)	ΔG (kcal/mol)	K_A (M^{-1})
1	**14a**	-13.0	+5.6	-7.4	2.52e5
2	**126d**	-12.9	+6.2	-6.7	8.40e4

Binding of several substrates to catalyst **126d** was examined to see if the subtle differences in enantioselectivities could also be represented by differences in entropies of binding. The iodolactonization reaction results are also listed with each titration entry for correlation with the entropies of binding (Table 20). For the phenyl substrate under optimized conditions, 93% ee was achieved and this correlated to a highly unfavorable entropy change (+6.2 kcal/mol, Table 20, entry 1). Another substrate that reacted with high enantiomeric excess (90% ee), 2-naphthyl, had a similar exothermic binding but was less unfavorable (+5.6 kcal/mol, Table 20, entry 2). The results of an alkyl substrate were desired for comparison, and the benzyl substrate was found to be less exothermic than the aryl substrates. It was also less entropically unfavorable (+4.0 kcal/mol, Table 20, entry 3). All three of these substrates reacted well in the lactonization, so poorer substrates were tested next. The *tert*-butyl ester substrate was significantly less exothermic (-7.7 kcal/mol) and also generated a less ordered bimolecular complex (+1.1 kcal/mol, Table 20, entry 4). Thus far, these substrates had appeared to demonstrate a positive correlation between entropy and enantiomeric excess in the lactonization reaction. However, the 1-naphthyl substrate did not fit into this pattern. Although it had similar reactivity (72% yield versus 64% yield) and enantioselectivity (67% versus 64%) to the *tert*-butyl ester substrate (Table 20, entry 5 versus entry 4), the entropy measured was higher than that of the benzyl substrate (4.7 versus 4.0 kcal/mol, Table 20, entry 5 versus entry 3). Perhaps the dramatic steric hindrance of the 1-naphthyl substrate still generates an entropically unfavorable complex, but this obviously does not necessitate high enantioselectivity. Overall, these substrates all display favorable enthalpy and unfavorable entropy values in binding to catalyst **126d**. The magnitude of these values ranges throughout the substrates in a manner that at times correlates with the reaction outcome. Interestingly, despite a range of -12.9 to -7.7 kcal/mol for the measured enthalpies, the Gibb's free energy remains relatively stable, ranging only from -6.7 to -6.5 kcal/mol.

Table 20: Thermodynamics of substrates binding to catalyst **126d**

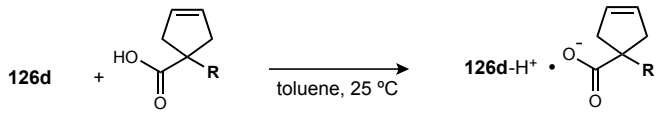

entry	R =	ΔH (kcal/mol)	-TΔS (kcal/mol)	ΔG (kcal/mol)	K_A (M^{-1})	reaction yield (%)	ee (%)
1	-Ph	-12.9	+6.2	-6.7	8.40e4	87	93
2	-2-naphthyl	-13.0	+5.6	-6.5	5.41e4	78	90
3	-Bn	-10.6	+4.0	-6.5	6.13e4	66	87
4	$-CO_2{}^tBu$	-7.7	+1.1	-6.6	6.49e4	64	64
5	-1-naphthyl	-11.3	+4.7	-6.6	4.46e4	72	67

In addition to physical measurements, theoretical calculations have been initiated. The calculations were conducted at the B3LYP level of theory with the 6-311g basis set (adding parameters to account for the large iodine atom). Since no experimental method to determine which oxygen atom was attacking the alkene, DFT calculations were considered to be an insightful alternative. Additionally, the *N*-iodophthalimide could be included in these calculations, which was a limitation of the X-ray crystal structures. Energy and frequency calculations were converged for several conformations of the substrates and products bound to the catalyst. Attempts are ongoing to find transition state structures of the pathways leading to each product enantiomer.

The nature of the substrate binding to catalyst **126d** was investigated first, primarily to understand the difference in energy between binding with the alkene forward (as is shown in the crystal structures) and the alkene reversed (Figure 43A and B, respectively). In these minimized structures, the *N*-iodopthalimide takes up a position above the alkene opposite the nucleophile, and the same hydrogen bonding network from the catalyst to the substrate is observed. As anticipated, an almost indistinguishable energy difference was calculated between the two considered conformations, with the "alkene reversed" conformation being only 0.34 kcal/mol lower in energy.

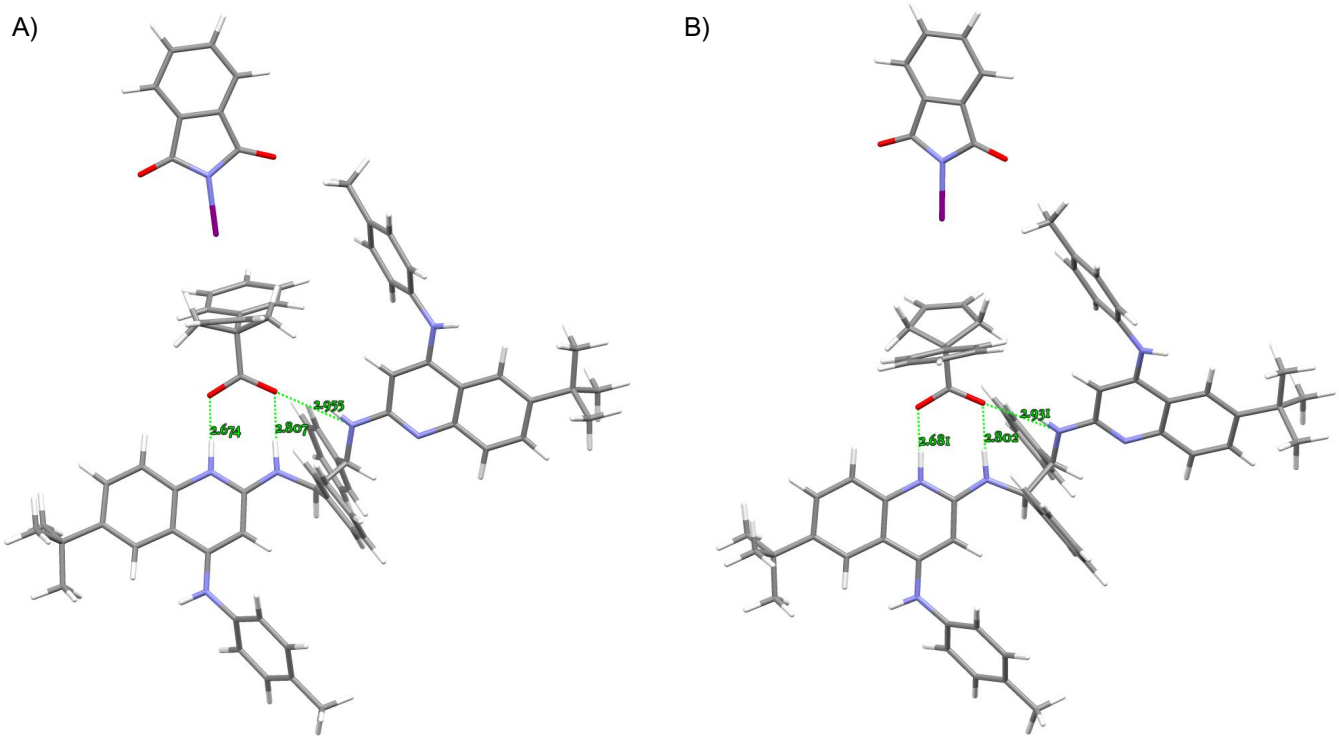

"alkene forward": 0 kcal/mol

"alkene reversed": -0.34 kcal/mol

Figure 43: Calculated structures and relative energies for two plausible alkene conformations of the starting material: A) alkene forward and B) alkene behind.

The products of the reaction were also submitted to structure optimization. The two substrate conformations calculated above were extended to the catalyst bound to the iodolactone major enantiomer and a phthalimide anion (Figure 44). The "product forward" conformation was calculated to be 9.5 kcal/mol *less* stable than the "product reversed" conformation. Three hydrogen bonds exist in each complex, however, the major difference appears to be the ability of succinimide to hydrogen bond to the positively charged N-H in the "product reversed" structure. The product minor enantiomer was examined in an analogous "product behind" type of structure, and it was found to be 1.4 kcal/more less stable than for the major enantiomer (Figure 45). Altogether, the structures of the substrates and products bound to the catalyst appear to indicate that the "reversed" structures may actually be operative in solution, due to their greater stability. This is mere speculation, however, without the calculations converging to transition state structures, yet.

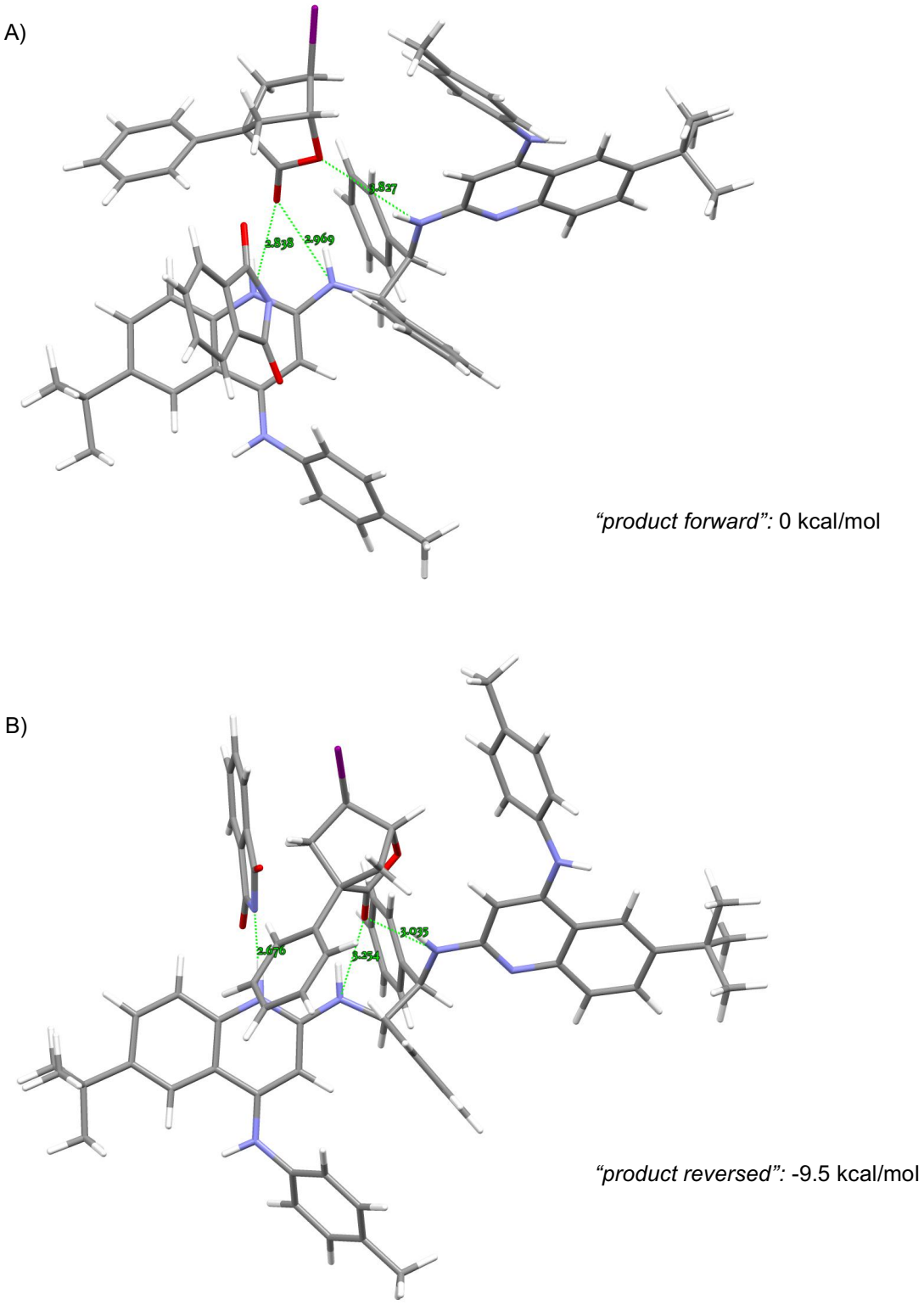

Figure 44: Two optimized structures of iodolactone product and phthalimide bound to catalyst **126d**.

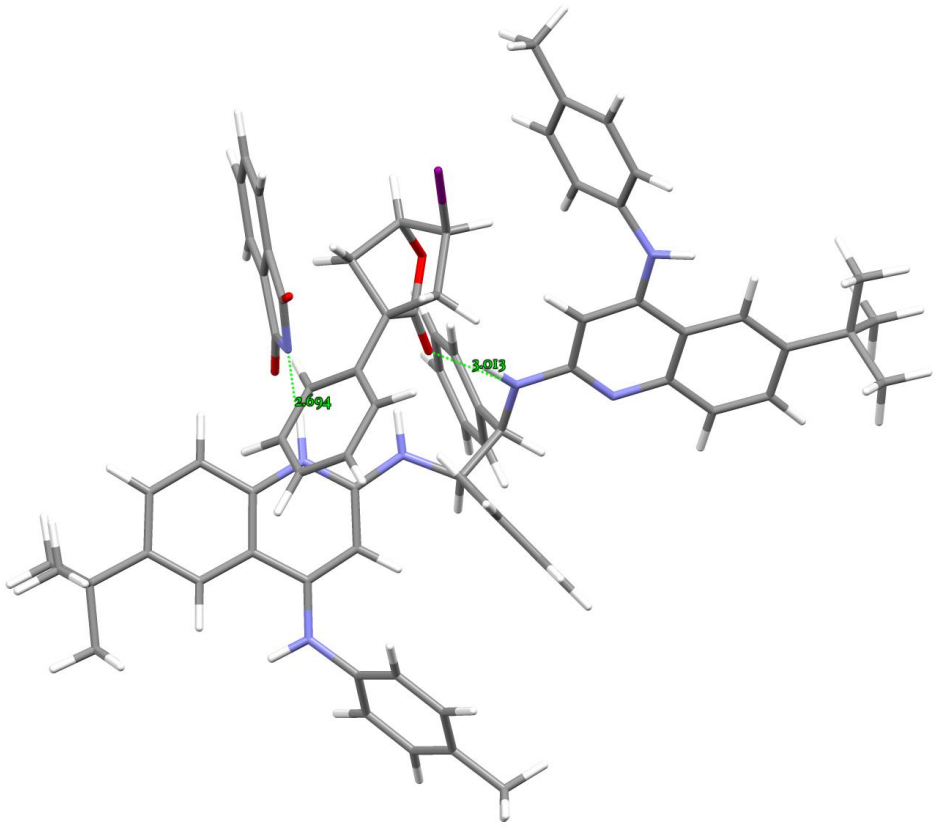

Figure 45: Minor enantiomer of the product bound in a "reversed" fashion.

1.2.8 Derivatization of bicyclic lactones

The bicyclic lactone products generated from this methodology can be derivatized toward a range of functionalized bicycles and cyclopentanes. Several of these methods are demonstrated on enantioenriched iodolactone **109a** in Figure 46. If the lactone is reduced a -78 ^{o}C, diol product **137** can be produced in 42% isolated yield with complete conservation of enantiopurity (Figure 46A). This was surprising, as the lithium alkoxide generated from the reduction was expected to cyclize on the iodine to form a *meso*-epoxide. The relatively low yield was due to the formation of ether **138**, which results from the intramolecular etherification of the primary alcohol on the iodide. When the reduction was run at higher temperatures, this etherification product could be isolated in 59% yield with conversion of enantiomeric excess (Figure 46B). Radical reductions were also feasible, with deiodination (**139**) and allylation (**140**) both reacting well (81% and 53% yield, respectively, Figure 46C and D). The allyation was achieved with moderate levels of diastereoselectivity. All attempts to substitute the iodine with nucleophiles such as azide, cyanide, or alkoxides were unsuccessful. This was typically due to poor conversion, and any conversion was from

nucleophilic acyl substitution at the ester carbon. Deiodinated lactone, **139**, could undergo aminolysis by monosubstituted amines, with the benzyl amine addition proceeding in 70% yield (Figure 46E). Synthesis of this amide product, **141**, opened this methodology to the possibility of being a viable route to carbocyclic nucleoside analogues.[108]

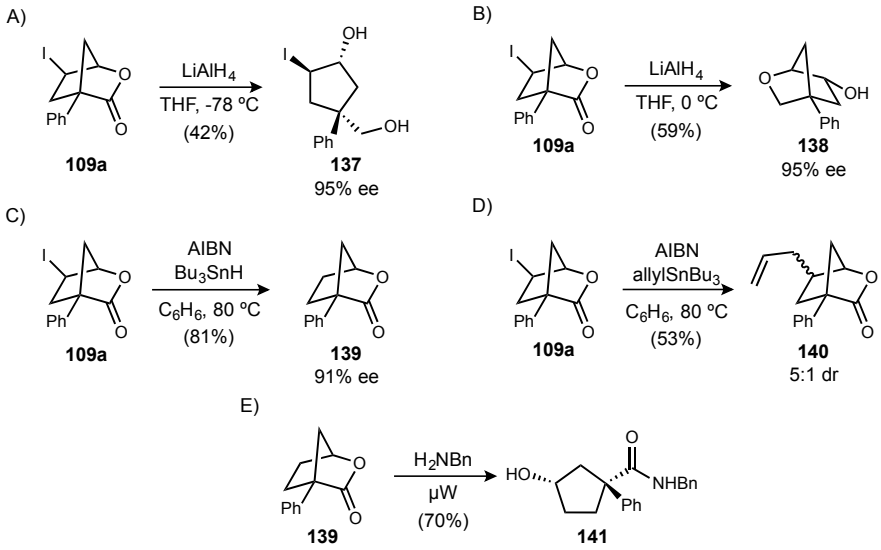

Figure 46: Derivatizations of iodolactone products.

1.2.9 Application towards a biologically active carbocyclic ribonucleoside

Carbocyclic nucleosides are structurally similar to natural nucleosides, with the replacement of the furanose oxygen with a methylene. This alteration gives the molecule greater stability towards enzymatic degradation,[109] while taking advantage of their involvement in numerous biological processes.[110] Nucleoside analogues can target viral telomerases, reverse transcriptases, and DNA polymerases (of HIV, hepatitis B, herpes, etc) by competitive binding to the active site, as well as their termination of DNA chain elongation.

[108] a) Marquez, V. E.; Lim, M.-I. *Med. Res. Rev.* **1986**, *6*, 1. b) Stewart, W. S. *Current Topics in Medicinal Chemistry* **2002**, *2*, 1087.

[109] Stoeckler, J. D.; Cambor, C.; Parks, R. E. *Biochemistry* **1980**, *19*, 102.

[110] Matyugina, E. S.; Khandazhinskaya, A. P.; Sergei, N. K. *Russ. Chem. Rev.* **2012**, *81*, 729.

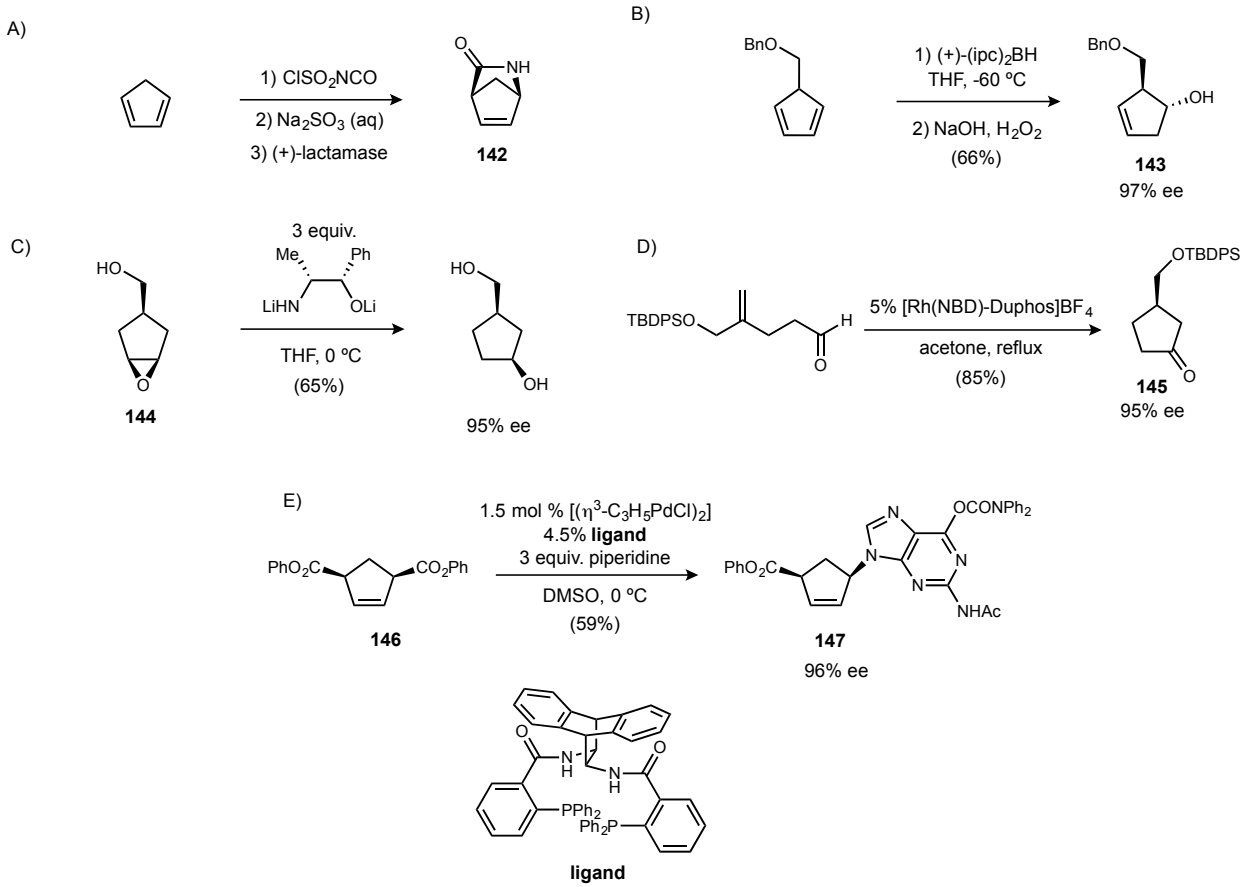

Figure 47: Strategies for the synthesis of enantioenriched carbocyclic nucleoside analogues.

Syntheses of these molecules are typically racemic, however several strategies to access enantioenriched nucleoside analogues exist, such as the elegant enzymatic kinetic resolution to produce Vince lactam (**142**, Figure 47A),[111] kinetic resolution of cyclopentene caroboxylic acids,[112] functionalization of sugars from the chiral pool, or diastereoselective aldol, ring closing metathesis, then palladium coupling with purine bases (as in the syntheses of carbovir and abacavir).[113] Asymmetric hydroboration of cyclopentadiene derivatives has also been employed to generate **143** in good enantioselectivity (Figure 47B).[114] The lithium salt of (1*R*,2*S*)-norephedrine can also be used as a chiral base for the enantioselective opening of *meso*-epoxides **144** (Figure 47C).[115]Asymmetric synthetic methods are generally more limited.[116] The rhodium catalyzed, intramolecular hydroacylation of alkenes provided

[111] Singh, R.; Vince, R. *Chem. Rev.* **2012**, *112*, 4642.

[112] Hildbrand, S.; Troxler, T.; Scheffold, R. *Helv. Chim. Acta* **1994**, *77*, 1236.

[113] Crimmins, M. T.; King, B. W. *J. Org. Chem.* **1996**, *61*, 4192.

[114] Jessel, S.; Meier, C. *Eur. J. Org. Chem.* **2011**, *2011*, 1702.

[115] Hodgson, D. M.; Witherington, J.; Moloney, B. A. *J. Chem. Soc., Perkin Trans. 1* **1994**, 3373.

[116] Boutureira, O.; Matheu, M. I.; Diaz, Y.; Castillon, S. *Chem. Soc. Rev.* **2013**, *42*, 5056.

ketone **145** in 85% yield and 95% ee (Figure 47D).[117] The carbonyl could be converted to the base linkage by reduction and Mitsunobu with adenine. The Trost group reported the enantioselective desymmetrization of diphenylacetate **146** by a palladium catalyzed coupling to provide an advanced intermediate **147** in good yield and excellent enantioselectivity (Figure 47E). Interestingly, authors of a review on enantioselective routes to these analogues assert that "processes based on transition metals are still scarce, and the use of organocatalysts to obtain carbocyclic nucleosides remains unexplored."[116]

(–)-Carbovir, one of the most well-known nucleoside analogue examples, did not succeed in clinical trials, due to poor pharmacokinetic and toxicological properties. However, abacavir (Ziagen) was approved in 1998, and has increased bioavailability and penetration of the central nervous system (Figure 48).[110] Entecavir was approved in 2005 for the treatment of hepatitis B by inhibiting DNA polymerase activity. As of 2012, resistance had still not been developed, and it was effective at treating a lamivudine-resistant strain of HBV. Nucleoside analogues have also been developed as candidates for the treatment of autoimmune diseases by targeting chemokine receptors. For example, MK-0812 was developed as a chemokine receptor antagonist for the treatment of inflammatory diseases, such as rheumatoid arthritis and multiple sclerosis (Figure 48).[118] Chemokines play a major role in inflammation response by recruiting monocytes, T-cells, basophils, and other inflammatory response cells. Chemokine receptor 2 (CCR2) is a G-protein-coupled receptor found on the surface of these cells, and chemokine ligand 2 (CCL2) activates them by binding to CCR2. This ligand and receptor pair are overexpressed in some inflammatory diseases, and knock down experiments indicate that their inhibition may be a useful therapeutic target. MK-0812 failed in clinical trials due to a lack of efficacy, and some believed that it could possibly be due to poor residency time, or the lifetime of the ligand-receptor complex.[119] Vertex optimized a different compound, **148**, for improved residency time while attempting to preserve the potency of MK-0812. These two compounds appeared to be prime targets for desymmetrizing iodolactonization methodology due to the substitution of an isopropyl group at the 4' position, which is required for lactonization to occur (see Table 17, entry 6).

---

[117] Marcé, P.; Díaz, Y.; Matheu, M. I.; Castillón, S. *Org. Lett.* **2008**, *10*, 4735.

[118] Wisniewski, T.; Bayne, E.; Flanagan, J.; Shao, Q.; Wnek, R.; Matheravidathu, S.; Fischer, P.; Forrest, M. J.; Peterson, L.; Song, X.; Yang, L.; DeMartino, J. A.; Struthers, M. *J. Immunol. Methods* **2010**, *352*, 101.

[119] a) Vilums, M.; Zweemer, A. J. M.; Yu, Z.; de Vries, H.; Hillger, J. M.; Wapenaar, H.; Bollen, I. A. E.; Barmare, F.; Gross, R.; Clemens, J.; Krenitsky, P.; Brussee, J.; Stamos, D.; Saunders, J.; Heitman, L. H.; Ijzerman, A. P. *J. Med. Chem.* **2013**, *56*, 7706. b) Vilums, M.; Zweemer, A. J. M.; Barmare, F.; van der Gracht, A. M. F.; Bleeker, D. C. T.; Yu, Z.; de Vries, H.; Gross, R.; Clemens, J.; Krenitsky, P.; Brussee, J.; Stamos, D.; Saunders, J.; Heitman, L. H.; Ijzerman, A. P. *Eur. J. Med. Chem.* **2015**, *93*, 121.

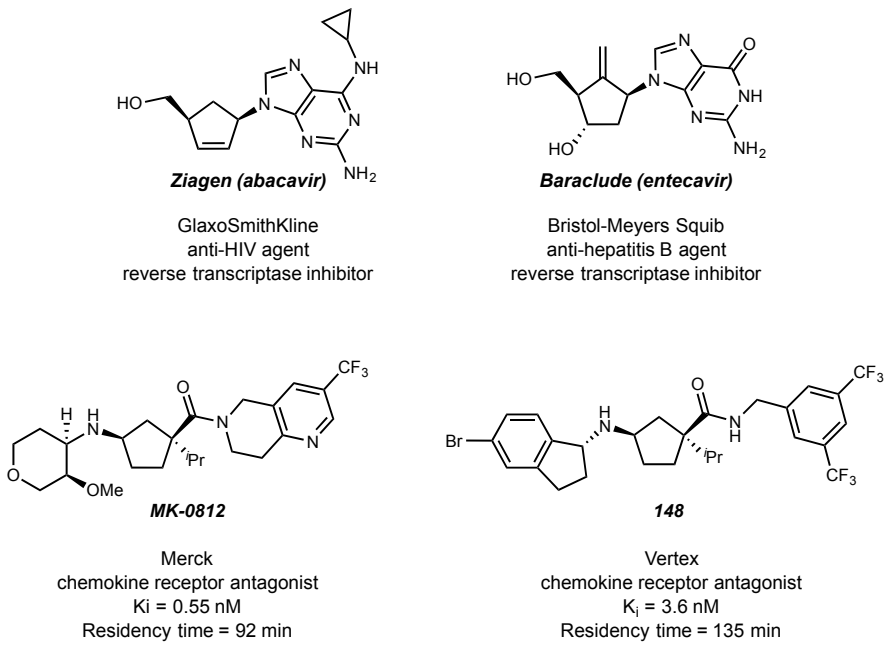

Figure 48: Carbocyclic ribonucleoside based drugs and drug candidates.

Retrosynthetic analysis of MK-0812 provided a highly convergent proposed route to the target molecule (Figure 49A). The amino-pyran could be installed via a substitution of cyclopentane alcohol **149**. This alcohol would be arrived at by a key aminolysis step, wherein lactone **150** is opened by quinuclidine **151**. This lactone results from the deiodination of iodolactone *ent*-**109j**, which was synthesized via iodolactonization of isopropyl cyclopentenecarboxylic acid **107j** by (*S*,*S*)-**126d**. Iodolactonization and deiodination could be readily achieved, as was demonstrated previously (Figure 46C), however aminolysis of this lactone proved quite difficult. Aminolysis had only been previously performed using the monosubstituted benzyl amine, whereas amine **151** was disubstituted. Basic, Brønsted acidic, Lewis acidic, and harsh (microwave in neat **151**) conditions were screened, all to no avail. Quinuclidine **151** would decompose under high enough temperatures, and it was never observed to open the lactone ring. Saponification of the lactone could be performed, however attempts to functionalize the resultant *seco*-acid always resulted in reformation of lactone **150**. These results made the limitation of iodolactone products **109** toward functionalization by nucleophiles, namely disubstituted amines, more evident.

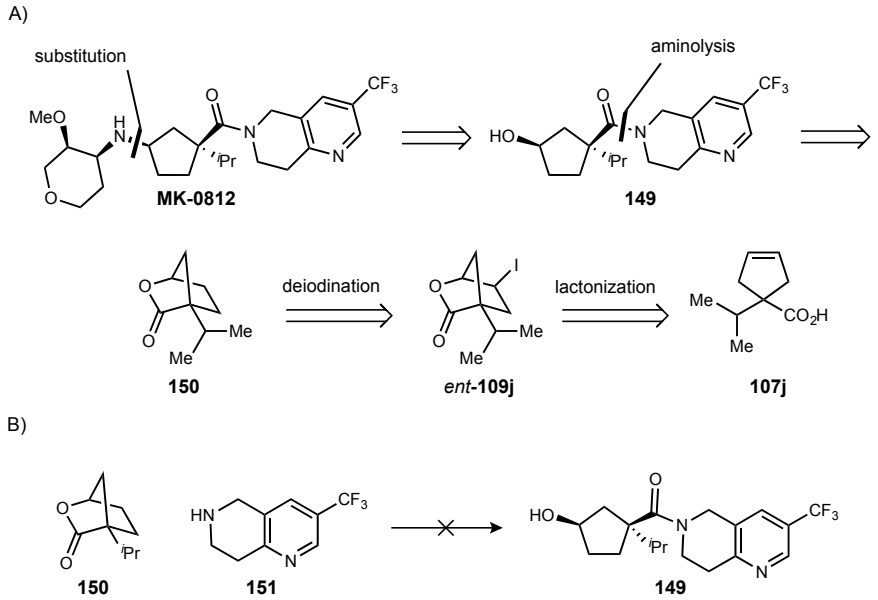

Figure 49: A) Retrosynthetic analysis of MK-0812 incorporating the iodolactonization of cyclopentene carboxylic acids. B) Attempts to open lactone **150** with disubstituted amine **151**.

Efforts were then made toward the synthesis of Vertex compound, **148** (Figure 48). Whereas MK-0812 had been dropped from clinical trials, **148** still had hope of being a more efficacious compound than MK-0812. The same 4' isopropyl substitution was still present, a similar route could be employed, and a monosubstituted benzyl amine could be used for the aminolysis step. Iodolactonization of **107j** proceeded smoothly on gram scale, providing the product in 73% yield and -79% ee, which could be recrystallized to -95%ee with a 56% overall yield (Figure 50). **107j** could be deiodinated with full and clean conversion. This material was carried forward to the aminolysis crude. Aminolysis in neat 3,5-bis(trifluoromethyl)benzyl amine provided the desired *syn*-alcohol **152** in 51% yield over two steps.

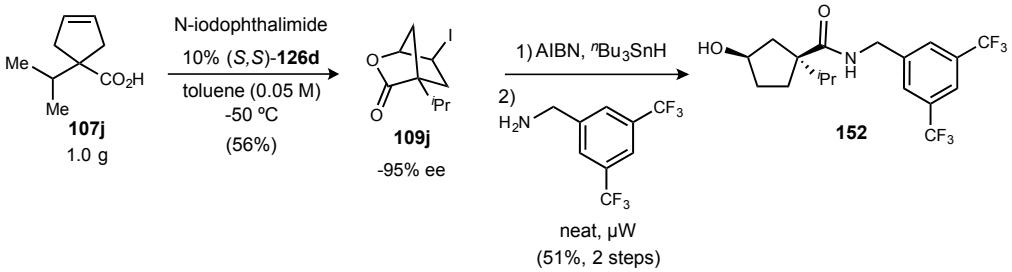

Figure 50: Iodolactonization and aminolysis to alcohol **152**.

The western portion of Vertex compound **148** was synthesized from known compound bromo-indanone **153** (Figure 51).[120] Oxime formation followed by zinc reduction yielded *rac*-**154**. This amine was resolved by salt formation with *N*-acyl-*D*-leucine, and two rounds of recrystallization provided amine **154** in 95% ee.

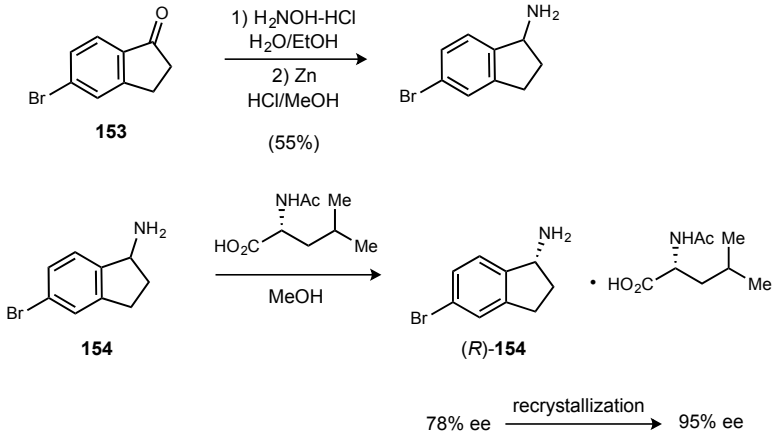

Figure 51: Synthesis and resolution of amine (*R*)-**154**.

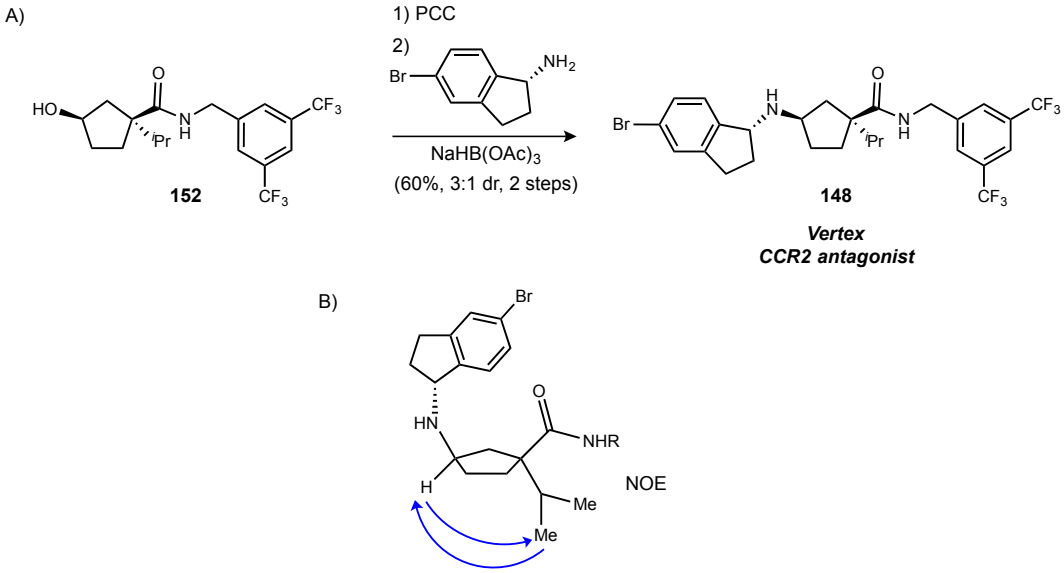

Figure 52: A) Convergence of amine (*R*)-**154** and alcohol **152** to produce CCR2 antagonist, **148**. B) Assignment based on NMR analysis of the major diastereomer.

[120] Taveras, A., *et. al.* Preparation of pyrimidinecarboxamides and analogs thereof as metalloprotease inhibitors. WO 2008002671. 2008.

Alcohol **152** was initially inverted to the corresponding bromide by phosphorous tribromide, however subsequent alkylation attempts by amine (*R*)-**154** yielded only an intramolecular cyclization of the amide functionality onto the bromide. Reductive amination was then employed. Alcohol **152** was oxidized by PCC cleanly, and the ketone was carried into the next step crude. Reduction of the iminium by sodium triacetoxyborohydride yielded the final Vertex compound **148** in 60% and 3:1 diastereomeric ratio (Figure 52A). The identity of the major diastereomer was confirmed as the using COSY and ROESY (Figure 52B). This target molecule could be synthesized in 5 steps (LLS) in 17% overall yield using an organocatalyst as opposed to the previously reported 9 step synthesis from Vince lactam.[119a]

1.3 Conclusions and future directions

Altogether, a methodology for the enantioselective desymmetrization of carboxylic acid substrates by iodolactonization was achieved. Key to the optimization of the reaction rate and selectivity was the acquisition of a catalyst-substrate cocrystal structure. From this structure, a hypothesis for oxygen atom desymmetrization by hydrogen bonding was derived. Additionally, new testable theories for improving the enantioselectivity could also be made. Guided by this crystal structure, a new catalyst **126d** was developed to facilitate the reaction in high enantioselectivity and yield. A second co-crystal structure of the optimized catalyst and substrate corroborated initial hypotheses for the origin of enantioselectivity. Mechanistic investigations using isothermal titration calorimetry allowed for comparisons of the relative binding constants and entropies between different catalysts and substrates. In general, it appeared that the cases with higher enantioselectivity also formed a more ordered complex with the catalyst. The methodology was further applied successfully to a range of aryl and alkyl cyclopentene carboxylic acids. These iodolactones possess three stereocenters, with one being an all carbon quaternary center. Derivatizations provided access to a variety of functionalized cyclopentanes, and a Vertex CCR2 antagonist molecule could be synthesized in 5 steps and 21% overall yield using a novel organocatalytic methodology. Future directions include optimization of an 4-*exo* lactonization on cyclohexadiene carboxylic acid substrates (Figure 40B), as well as continued computational studies to calculate plausible transition state structures of the desymmetrization by catalyst **126d**.

2 Multigram preparation of an arylglycine dipeptide by Umpolung amide synthesis (UmAS)

2.1 Introduction

2.1.1 Arylglycine α-amino amides and their synthesis

Arylglycine α-amino amides are important residues due to their presence in medicinally significant natural products like glycopeptide antibiotics (vancomycin, teicoplanins, and ristomycin) and α-lactam antibiotics (nocardicins A-G, amoxicillin) (Figure 53).[121]

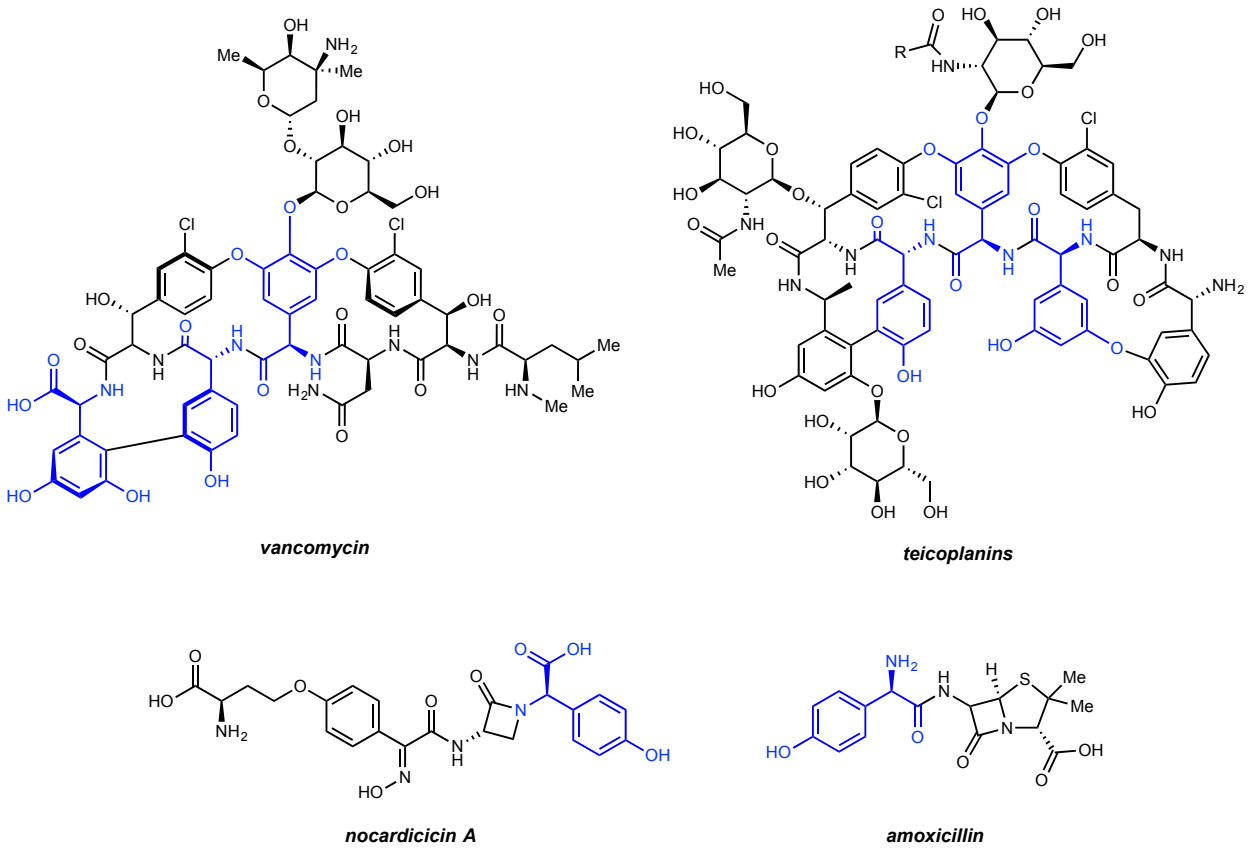

Figure 53: Arylglycine α-amino amides in glycopeptide antibiotics and α-lactam antiobiotics with arylglycine residues highlighted.

[121] a) Williams, R. M.; Hendrix, J. A. *Chem. Rev.* **1992**, *92*, 889. b) Al Toma, R. S.; Brieke, C.; Cryle, M. J.; Sussmuth, R. D. *Nat. Prod. Rep.* **2015**, *32*, 1207. c) Nicolaou, K. C.; Boddy, C. N. C.; Bräse, S.; Winssinger, N. *Angew. Chem. Int. Ed.* **1999**, *38*, 2096. d) Schwieter, K. E.; Johnston, J. N. *J. Am. Chem. Soc.* **2016**, *138*, 14160.

Significant effort has been applied toward the stereoselective synthesis of the corresponding arylglycine amino acids. Evans and coworkers reported one of the earliest routes towards these, using a chiral auxiliary to facilitate a diastereoselective α-azidation of amides (**155**, Figure 54A).[122] An enantioselective route employs the osmium catalyzed aminohydroxylation of styrenes to deliver aminoalcohols **156** in good yield and enantioselectivity (76% and 97%, respectively; Figure 54B).[123] Iminoesters (**157**) have also been used as precursors for the enantioselective, rhodium catalyzed hydrogenation to deliver arylglycine esters **158** in excellent yield (99%) and selectivity (95% ee) (Figure 54C).[124] The Fu group has also reported an N-H insertion for accessing arylglycine amino acids, where copper catalyzes the insertion of boc-carbamate into aryl diazoesters **159** to generate aminoesters **160** in good yield and excellent enantiomeric excess (Figure 54D).[125]

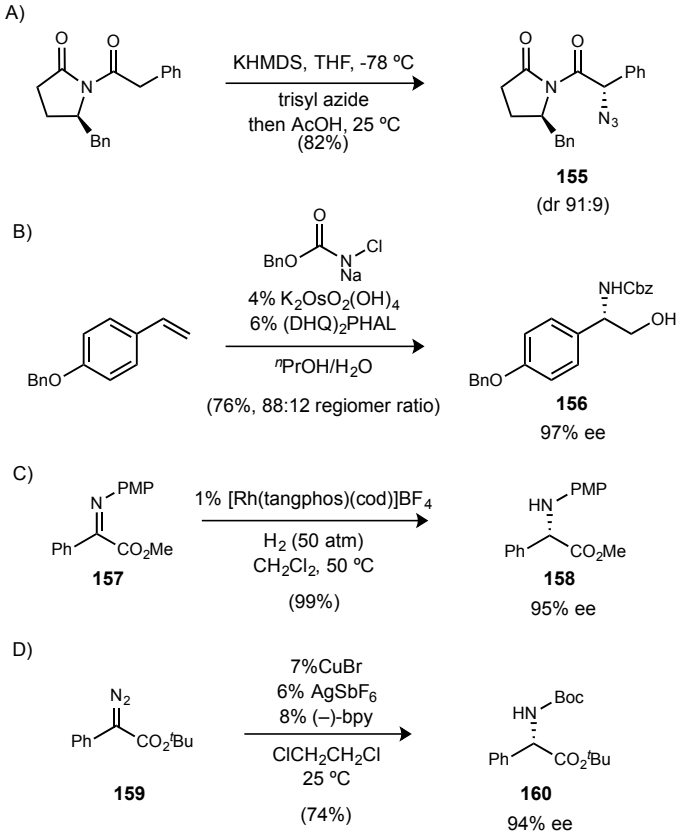

Figure 54: Methods for the synthesis of enantioenriched arylglycine amino acid precursors.

---

[122] Evans, D. A.; Evrad, D. A.; Rychnovsky, S. D.; Früh, T.; Whittingham, W. G.; deVries, K. M. *Tetrahedron Lett.* **1992**, *33*, 1189.

[123] Reddy, K. L.; Sharpless, K. B. *J. Am. Chem. Soc.* **1998**, *120*, 1207.

[124] Shang, G.; Yang, Q.; Zhang, X. *Angew. Chem. Int. Ed.* **2006**, *45*, 6360.

[125] Lee, E. C.; Fu, G. C. *J. Am. Chem. Soc.* **2007**, *129*, 12066.

2.1.2 Incorporation of arylglycine residues by UmAS

Integration of these arylglycine amino acids into peptides has proved challenging due to their increased propensity towards epimerization.[126] The aryl group increases the acidity of the α-proton, and upon activating the carboxylate for coupling, racemization can occur more easily than for canonical amino acids. This issue was circumvented using aza-Henry/UmAS in tandem. α-Bromo nitroalkanes (**161**) are prepared in high enantiopurity by the addition of bromonitromethane into imines by BAM catalysis (Figure 55A).[127] Bromonitroalkanes **161** are then reacted with an amine, base, and oxidant to produce the corresponding amides (**162**, Figure 55B).[128] This unique set of conditions is hypothesized to proceed in an Umpolung fashion relative to standard condensative amide coupling conditions.[129] The bromonitroalkane can be deprotonated and add into the *N*-haloamine generated from amine reaction with NIS. This reversal of nucleophile and electrophile avoids the formation of an acidic, activated ester intermediate, making Umpolung Amide Synthesis (UmAS) a useful tool for incorporating aryglycine amino acids. To improve the utility of this methodology, a highly reproducible procedure for the multigram preparation of an arylglycine peptide was developed.[130]

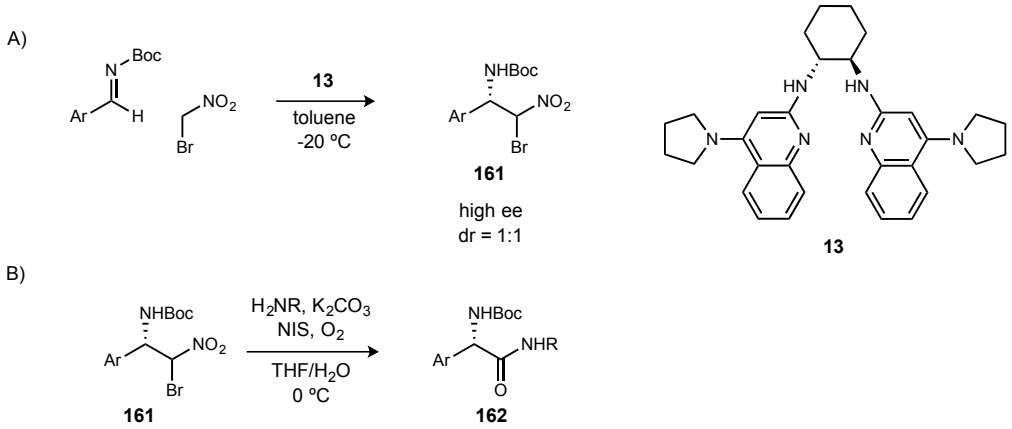

Figure 55: Synthesis of arylglycine containing peptides using BAM catalysis and UmAS.

2.2 Application of UmAS on larger scale preparations

[126] a) Konig, W.; Geiger, R. *Chemische Berichte-Recueil* **1970**, *103*, 2024. b) Han, S.-Y.; Kim, Y.-A. *Tetrahedron* **2004**, *60*, 2447. c) Goodman, M.; McGahren, W. J. *J. Am. Chem. Soc.* **1966**, *88*, 3887. d) Dettner, F.; Hänchen, A.; Schols, D.; Toti, L.; Nußer, A.; Süssmuth, R. D. *Angew. Chem. Int. Ed.* **2009**, *48*, 1856.

[127] Davis, T. A.; Wilt, J. C.; Johnston, J. N. *J. Am. Chem. Soc.* **2010**, *132*, 2880.

[128] Shen, B.; Makley, D. M.; Johnston, J. N. *Nature* **2010**, *465*, 1027.

[129] Shackleford, J. P.; Shen, B.; Johnston, J. N. *Proc. Natl. Acad. Sci. U. S. A.* **2012**, *109*, 44.

[130] Knowe, M.; Tsukanov, S. V.; Johnston, J. N. *Org. Synth.* **2017**, *94*, 388.

The multigram-scale synthesis of α-aryl bromonitroalkane (**163**) was accomplished starting from the *para*-benzyloxy benzaldehyde **164** (Figure 56A).[131] Synthesis of the amido sulfone **165** and subsequent elimination provided grams of the crude Boc-protected imine cleanly (**166**, Figure 56B). This imine could then be used in a large-scale aza-Henry reaction catalyzed by 5 mol % of the PBAM free base (**13**) (Figure 56C). α-Aryl bromonitroalkane (**163**) was produced in good yield and high enantioselectivity. After a silica plug and recrystallization, grams of the product were produced in 36% overall yield and 97%/95% ee of each diastereomer. This procedure describes the chromatography-free production of large amounts of a starting material for further use in the synthesis of α-arylglycine containing peptides.

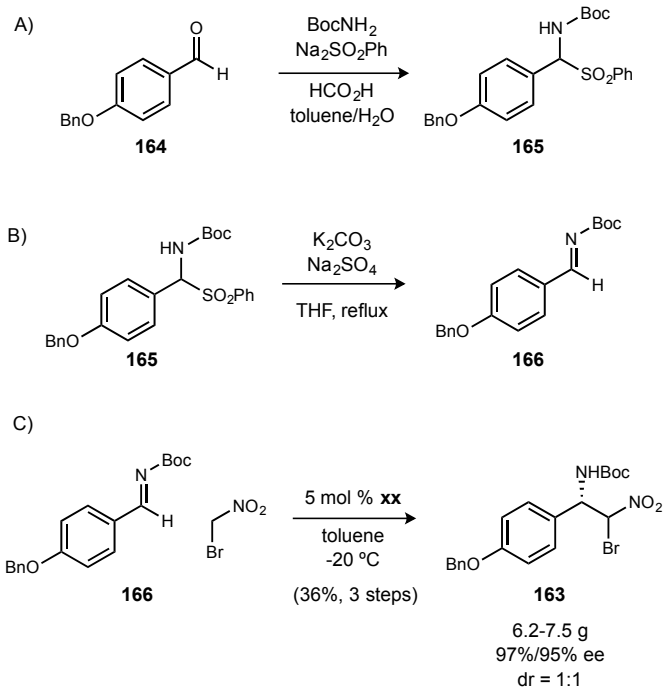

Figure 56: Enantioselective synthesis of an α-aryl bromonitroalkane.

2.2.1 First generation synthesis and purification

Initial investigations for the optimization of the UmAS coupling of aryl bromonitro alkane **163** began on a 1g test scale (Figure 57). The goal was to develop a practical method for the synthesis of useful quantities of arylglycine containing peptides, which was defined as synthesizing and fully purifying 5 g of a peptide in at least 50% yield without any column chromatography.

Phenylalanine methyl ester was chosen as the amine coupling partner for its increased crystallinity within the peptide product (**167**). Cesium carbonate (2 equivalents)

[131] Lim, V.; Tsukanov, S. V.; Doody, A.; Johnston, J. N. *Org. Synth.* **2016**, *93*, 88.

was used as the base, and recrystallized NIS was used as the oxidant. An oxygen balloon was included as well to aid in reaction conversion.[132] A biphasic solvent system of 2-methyl THF and water was used to ensure solubility of all reaction components. Vigorous stirring was required to mix the two phases. UmAS reactions have been typically run at 0 ºC, so a cryocool was used to control the reaction temperature. The reaction was run for two days before reductive quenching with saturated aqueous sodium thiosulfate. An acid wash could also be used to remove any remaining phenylalanine. Concentration of the extracts afforded a viscous red oil from which crystalline product could not be easily obtained. Polar impurities were removed by filtration through a silica plug, and off white, solid material was obtained. At this stage, the crude material was primarily unreacted starting material, product, and succinimide. This material could be recrystallized by dissolving in hot benzene/cyclohexane (3:2) to provide product in 56% isolated yield and 93% purity. It should be noted that conversion on this small scale was essentially complete, simplifying purification of the crude reaction mixture.

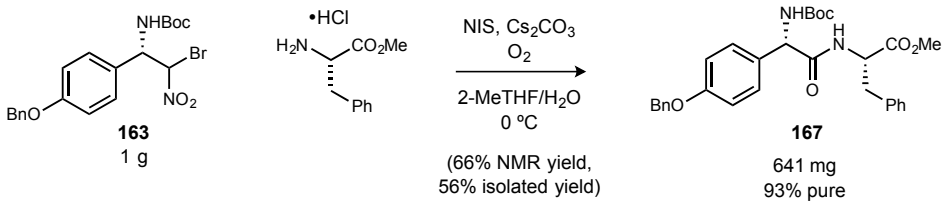

Figure 57: Synthesis of peptide **167** by UmAS on 1g scale.

To achieve the goal of 5 g of peptide **167** with an estimated 50% yield, the reaction was scaled up to 8.9 g of starting material. In a larger reaction flask, conversion was much worse, achieving only 40% yield by NMR after two days. A mechanical stirrer was used with a dimpled flask for maximized phase mixture (Figure 58). A typical case for this large-scale reaction is shown in Figure 59. After two days, conversion was not complete and appeared to stall out. The ratio of starting material to product was monitored by ^{1}H NMR analysis of reaction aliquots over the course of eleven days (Table 21). Additions of extra equivalents of NIS, refilling the oxygen balloon, increasing reaction temperature, or extending reaction times did not improve the conversion. A balance between yield and purity in the isolation procedure was therefore difficult to achieve. The recrystallization could provide over 5 grams of material in lower purity (5.4 g, 83% pure, Figure 59), but to obtain pure material the recrystallization would need to be filtered early, providing less than the 5 g goal. Second rounds of recrystallization were never able to compensate the pure material.

[132] Schwieter, K. E.; Shen, B.; Shackleford, J. P.; Leighty, M. W.; Johnston, J. N. *Org. Lett.* **2014**, *16*, 4714.

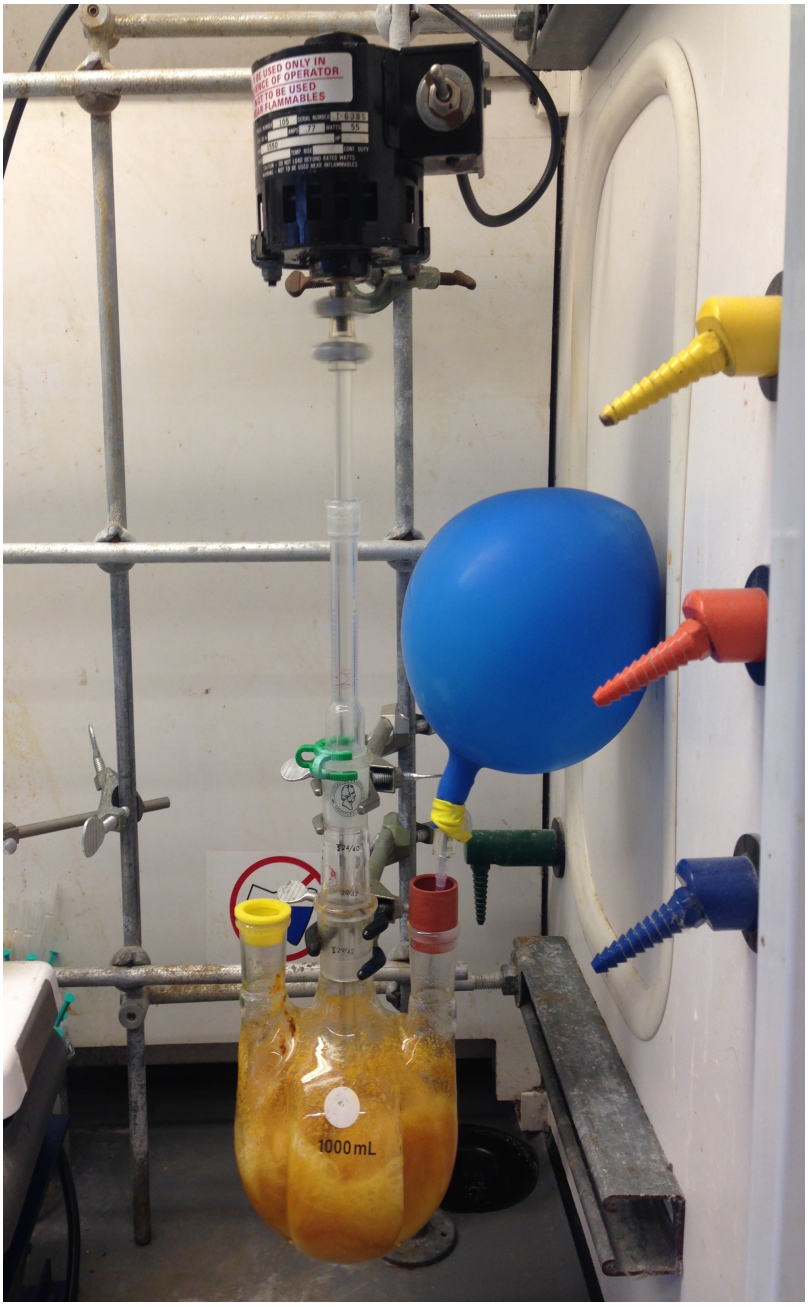

Figure 58: Reaction set up for the large scale UmAS of am arylglycine containing peptide.

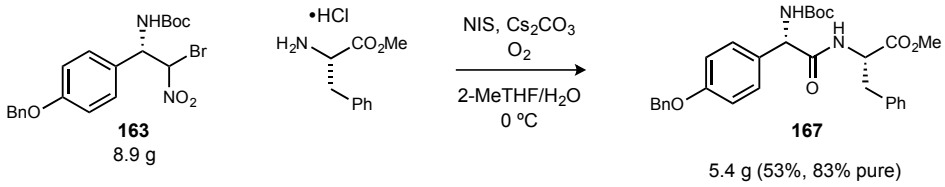

Figure 59: A common result from large scale reaction.

Table 21: Conversion compared to reaction time estimated from ratio of product to starting material.

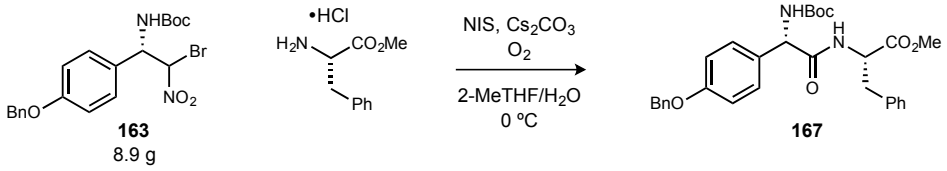

Entry	Reaction time (d)	Starting material : product[a]
1	2	1:2.8
2	3	1:3.6
3	4	1:3.7
4	5	1:4.5
5	6	1:6.5
6	11	1:7.7

[a] Measured by ^{1}H NMR analysis of reaction aliquots.

2.2.2 Second generation synthesis and purification

In a hopeful bid to synthesize the peptide in large quantities with high purity, the benzyl ester of phenylalanine (**168**) was used instead of the methyl ester (Figure 60A). Unlike the methyl ester, this ester provided favorable results at room temperature after only one day, simplifying the procedure drastically. Additionally, commercially available NIS could be used without further purification. It performed well on small scale and was

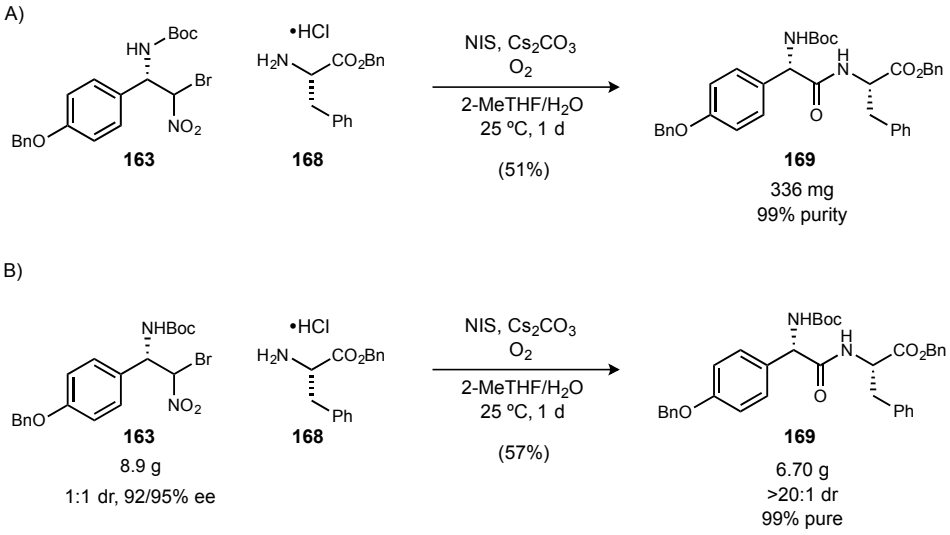

Figure 60: A) Performance of phenylalanine benzyl ester in the UmAS reaction, and B) results of a scaled up reaction.

recrystallized easily to provide pure peptide **169** in 51% yield. Gratifyingly, the large-scale reaction using a mechanical stirrer reached full conversion after one day at room temperature. An aqueous thiosulfate quench followed by silica plug quickly provided the solid crude material. Recrystallization from toluene/cyclohexane (3:2) provided 6.7 g of the product in greater than 20:1 dr and 99% purity (Figure 60B). This procedure was additionally repeated and validated by a third party, completing the first large-scale preparation of a peptide using UmAS methodology.[130]

In summary, a method was developed for the incorporation of aryl glycine residues into dipeptides, enabling the straightforward production of relevant quantities. Alterations to previously developed UmAS conditions to improve the practicality of this methodology include: raising the reaction temperature to 25 °C, using commercially available NIS as-is rather than recrystallized, and shortening reaction times to one day. Unfortunately, the use of the more expensive cesium carbonate could not be avoided. The use of large quantities of distilled 2-methyl THF could not be circumvented either. Due to the heterogeneous conditions of the reaction, vigorous stirring by a mechanical stirrer was required. Ultimately, however, a benzyl ester of phenylalanine (rather than a methyl ester) was required for fastest conversion and ease of purification. The reason for the faster conversion has not been investigated yet, however it is logical that the benzyl ester could make the product more crystalline, allowing for a more reproducible purification. It also remains to be investigated if this robust procedure is amenable to other amino acid benzyl esters.

3 Progress toward the total synthesis of *(+)-zwittermicin A*

3.1 Background

3.1.1 Isolation and biological activity of (+)-zwittermicin A

Scientific and technological advance is intimately connected to the improvement of society, and total synthesis of biologically relevant molecules not only advances understanding in the chemical community but also in global society, providing solutions to practical problems. With the population of the earth increasing, consumption rising, and natural resources diminishing, more efficient global food production needs to be developed, and a part of addressing this complex problem relies on chemical innovation to control diseases and pests that threaten food production.[133a] An estimated 10-16%, or $220 billion, of the global food harvest is lost to plant diseases, and 6-10% is also lost after harvest for various reasons.[133b] Food insecurity, defined as a reduced quality, variety, desirability, or availability of diet, is a problem currently faced by 24% of the world (802 million people in 2012) and 14.5% of Americans, according to the US Department of Agriculture.[134] The identification of antibiotics that can protect food supplies from a variety of threats is instrumental in addressing food insecurity worldwide, and it can combat the development of resistance to current antibiotics.

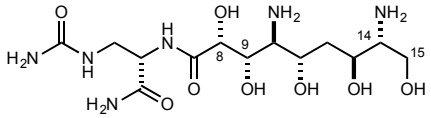

(+)-zwittermicin A

170

Figure 61: Structure of (+)-zwittermicin A, highlighting the pseudo-C_2 symmetric core from carbons 9 to 15.

(+)-Zwittermicin A (**170**, zwA; Figure 61) represents the first of its kind as an aminopolyol antibiotic. It is a synthetically challenging, linear, and highly oxidized natural product with a *pseudo* C_2-symmetric C9-C15 core and seven stereocenters in close proximity. It was first isolated in 1994 from *Bacillus cereus* UW85, a very common and widespread

[133] a) Godfray, H. C. J.; Beddington, J. R.; Crute, I. R.; Haddad, L.; Lawrence, D.; Muir, J. F.; Pretty, J.; Robinson, S.; Thomas, S. M.; Toulmin, C. *Science* **2010**, *327*, 812. b) Chakraborty, S.; Newton, A. C. *Plant Pathology* **2011**, *60*, 2.

[134] http://www.ers.usda.gov/topics/food-nutrition-assistance/food-security-in-the-us/

bacterium.[135] This bacterium was found to suppress a variety of diseases in a range of agricultural crops, and it became an attractive organism for identification of new drugs and antibiotics.[136] From culturing this bacterium, zwittermicin A was able to be isolated in an average yield of 2-4 mg/L culture.[135] It was found to be responsible for growth inhibition of the alfalfa pathogen *Phytophtora medicaginis*, a protist, and inhibits a plethora of fungi responsible for the destruction of beets, corn, grasses, berries, apples, and general stored fruits and vegetables, as well as several gram-negative and gram-positive bacteria, and enhances the insecticidal activity of *Bacillus thuringiensis*.[136] ZwA producing organisms are pervasive in soil, and ZwA is unique in its broad range of biological activity, suggesting that it acts upon a evolutionarily conserved pathway across many organisms.[137,138] It has potential for development of antibiotics that are agriculturally relevant across large geographic regions as well as environmentally friendly. An attempt to investigate the mechanism of action through studying resistant strains of bacteria identified a correlation between resistance and an inability to maintain electrical membrane potential properly. It also identified DNA transcription, replication, and DNA gyrase or topoisomerase as possible targets but the authors were unable to observe any alteration in the amount of DNA or RNA processing, which together could suggest a novel mechanism of action.[138]

3.1.2 Structural elucidation and previous formal total synthesis

The structure of (+)-Zwittermicin A was originally determined by mass spectrometry and NMR studies, and the relative stereochemistry at carbons 8, 9, and 10 was determined by nOe of a cyclized derivative,[133] however the remaining stereochemistry was unknown until 2007 when a series of 8 diastereomeric compounds resembling the C9-C15 core were synthesized by Molinski and coworkers.[139] The ^{13}C NMR shifts were compared pairwise with the natural product, thereby determining the relative stereochemistry of the C8-C15 core of ZwA. The proposed absolute stereochemistry was based on the sequence of the non-ribosomal peptide synthetase—polyketide synthase megasynthese responsible for synthesis of ZwA, which identified the starting unit as serine.[140,141,142] Since L-serine is naturally occurring and epimerase domains were absent from the cluster, the absolute stereochemistry was assigned (**171**, Figure 62) assuming the configuration of C14 was derived from L-serine.

---

[135] He, H.; Silo-Suh, L. A.; Handelsman, J.; Clardy, J. *Tetrahedron Lett.* **1994**, *35*, 2499.
[136] Silo-Suh, L. A.; Stabb, E. V.; Raffel, S. J.; Handelsman, J. *Curr. Microbiol.* **1998**, *37*, 6.
[137] Stabb, E. V.; Jacobson, L. M.; Handelsman, J. *Appl. Environ. Microbiol.* **1994**, *60*, 4404.
[138] Stabb, E. V.; Handelsman, J. *Mol. Microbiol.* **1998**, *27*, 311.
[139] Rogers, E. W.; Molinski, T. F. *Org. Lett.* **2007**, *9*, 437.
[140] Emmert, E. A.; Klimowicz, A. K.; Thomas, M. G.; Handelsman, J. *Appl. Environ. Microbiol.* **2004**, *70*, 104.
[141] Stohl, E. A.; Milner, J. L.; Handelsman, J. *Gene* **1999**, *237*, 403.
[142] Kevany, B. M.; Rasko, D. A.; Thomas, M. G. *Appl. Environ. Microbiol.* **2009**, *75*, 1144.

The C4 stereocenter was determined by hydrolysis of the natural product, derivatizing the liberated amino acid, and comparing to known *S*-albizziin.

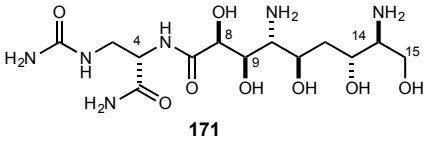

171

Figure 62: Original stereochemical assignment of zwA.

In 2008, Molinski and coworkers published their first attempt at total synthesis of (+)-zwA, based on their proposed absolute stereochemical assignment (**171**, Figure 63).[143] Suprisingly, their assignment based on L-serine proved wrong, and they revised the natural product configuration based on synthesis of the enantiomer, (-)-zwA. Their synthesis begins with azidodiol **172** which they prepared previously (Scheme 1.2).[139] This is selectively protected at the terminal alcohol, before the secondary alcohol is MOM protected and the silyl group removed. Azide **173** is reduced, benzyl protected, and the terminal alcohol oxidized to prepare for the Evans aldol with **174**. The reaction proceeds with good yield and diastereoselection, and the chiral auxiliary is removed in good yield over the two steps.

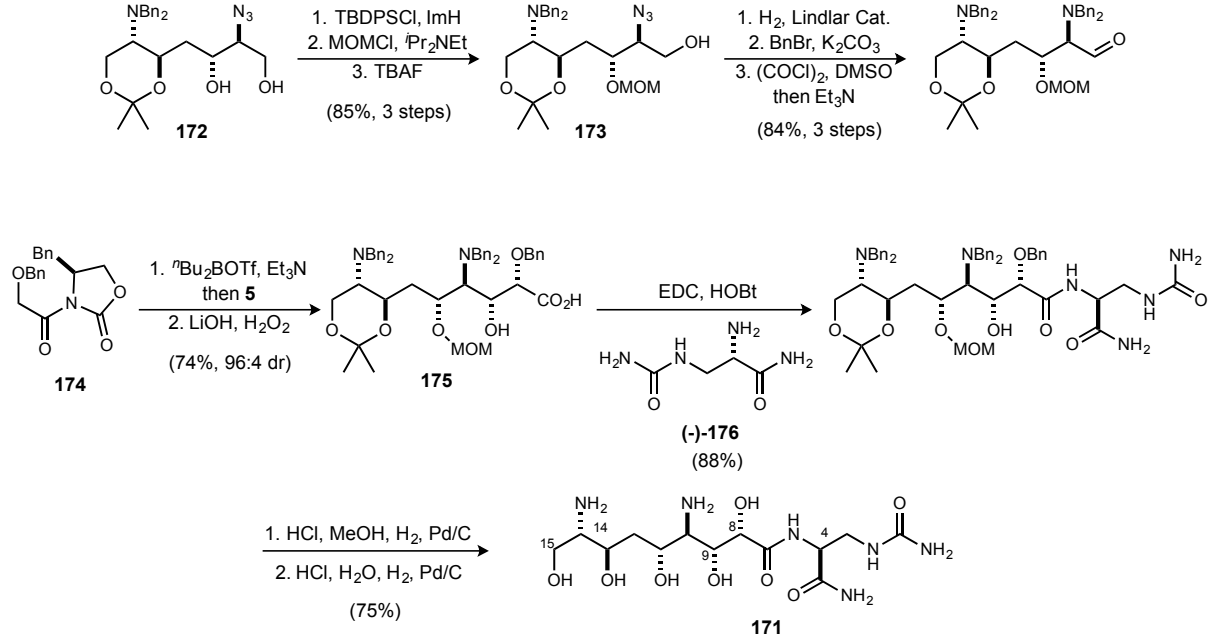

Figure 63: Total synthesis of **171**.

The requisite carboxylic acid **175** is coupled in high yield to amide (-)-**176**, and global deprotection affords **171** in good yield. When compared with the natural product, the NMR

[143] Rogers, E. W.; Dalisay, D. S.; Molinski, T. F. *Angew. Chem. Int. Ed.* **2008**, *47*, 8086.

spectra of **171** were slightly different, and the specific rotation was opposite and greater in magnitude than for (+)-zwittermicin A, suggesting they had synthesized a diastereomer.

They hypothesized that their assumption based on L-serine as the starting material was incorrect, and adjusted their synthesis to make (-)-zwittermicin A.[143] By coupling acid **175** with (+)-**176** then deprotecting, they synthesized (-)-zwittermicin in 24 steps from an L-serine derivative, and it had an identical NMR spectrum with and exactly opposite specific rotation to the natural product. This proved the absolute configuration of (+)-zwittermicin A to be that depicted as (+)-**170**, and indicated the biosynthetic incorporation of D-serine. In 2009, Molinski and Rogers published a shorter route to the opposite enantiomer of **173**, which completed the first formal total synthesis of (+)-zwittermicin A in 19 steps.[144]

(-)-Zwittermicin A was tested for biological activity against several fungal strains in comparison to (+)-zwittermicin A and was found to be inactive.[143] Molinski and coworkers synthesized a series of thirteen analogues and diastereomers of (+)-zwittermicin A to test for biological activity and structure-activity relationships.[145] None of the aminopolyol derivatives and analogues showed any activity, however, indicating (+)-zwittermicin A has a highly stereospecific mechanism of action, with every stereocenter playing a vital role.

3.2 Approach to (+)-zwittermicin A

3.2.1 Retrosynthetic analysis

A bidirectional, convergent, and stereoselective synthetic strategy was planned for the total synthesis of (+)-zwittermicin A **170**, using key Brønsted acid-promoted azide-olefin [3+2] cycloaddition, desymmetrization, and diastereoselective Passerini steps.[146] A key disconnection between C7 and C8 that could be achieved by this diastereoselective Passerini reaction with isonitrile **177** and alcohol **178** (Figure 64). This would form the C7 α-oxy amide and convergently unite the western urea fragment with the eastern aminoalcohol fragment. Primed for all final functional group manipulations, isonitrile **177** could be synthesized from L-Aspartic Acid. Alcohol **178** would be obtained from fragmentation and desymetritization of C_2 symmetric bis(oxazolidine) dione **179**. This protected aminoalcohol intermediate is the goal of the stereoselective, bidirectional approach to the pseudo-symmetric core of (+)-zwittermicin A from C9-C15.

---

[144] Rogers, E. W.; Molinski, T. F. *J. Org. Chem.* **2009**, *74*, 7660.

[145] Rogers, E. W.; Dalisay, D. S.; Molinski, T. F. *Bioorg. Med. Chem. Lett.* **2010**, *20*, 2183.

[146] Muchalski, H. Stereospecific Reactions of α-Amino-β-Diazonium Intermediates; Mechanistic Studies, New Reaction Discovery and their Application to a Two-Directional Total Synthesis of (+)-Zwittermicin A, *PhD Dissertation*, Vanderbilt University, **2012**.

This bidirectional strategy to bis(oxazolidine dione) **179** (Figure 64) would be achieved using methodology for the Brønsted acid-promoted, formal aminohydroxylation of olefins.[147,148,149] **179** could be formed by the acid promoted fragmentation of bis(triazoline) **180**, which would be acquired from the diastereoselective [3+2] addition of benzyl azide to bisimide **181**. This could result from the HWE olefination of diene **182** with phosphonoimide **183**. Diene **182** could be synthesized according to known procedures from readily available acetylacetone.

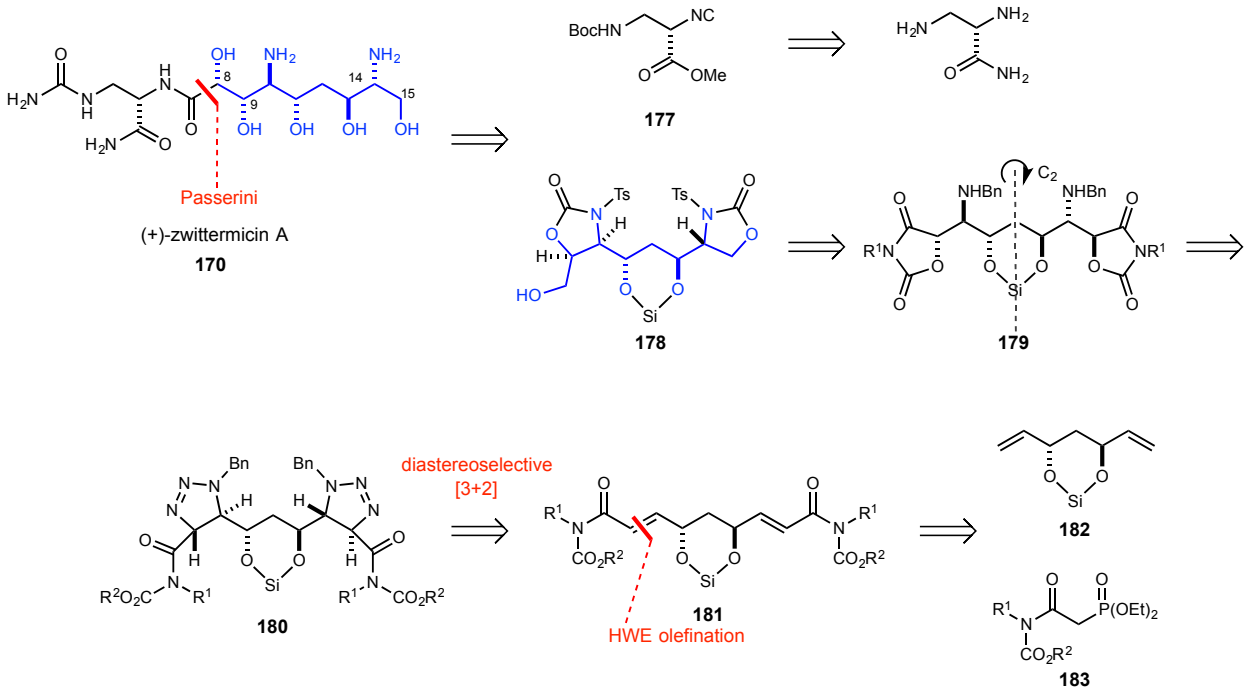

Figure 64: Retrosynthetic analysis.

3.2.2 Acid-promoted formal aminohydroxylation

The methodology that led to the pursuit of a total synthesis of (+)-zwittermicin A was Brønsted acid-promoted olefin aziridination (Figure 65).[147] This was achieved by the addition of nucleophilic alkyl azide to an electron deficient olefin to produce the corresponding triazoline **184** (Figure 65A). Triazolines were known to decompose under various conditions, with the exception of acid promoted decomposition. This work's contribution included the first example of their useful acid promoted decomposition to

[147] Mahoney, J. M.; Smith, C. R.; Johnston, J. N. *J. Am. Chem. Soc.* **2005**, *127*, 1354.
[148] Hong, K. B.; Donahue, M. G.; Johnston, J. N. *J. Am. Chem. Soc.* **2008**, *130*, 2323.
[149] Muchalski, H.; Hong, K. B.; Johnston, J. N. *Beilstein J. Org. Chem.* **2010**, *6*, 1206.

aziridines **185**. When ester **186**, bearing an activating group possessing a Lewis basic oxygen, was submitted to the same reaction conditions, triazoline **187** would decompose to deliver **188** with α,β-substituted *anti*-amino hydroxylation (Figure 65B). This participation in the decomposition by the carbonyl oxygen occurs in a stereospecific fashion capable of producing diastereomeric ratios greater than 20:1. Further investigations into the mechanism were carried out, confirming the presence of a triazoline intermediate and gathering mechanistic evidence by *in situ* IR for its formation and decomposition to oxazolidine dione.[148,150]

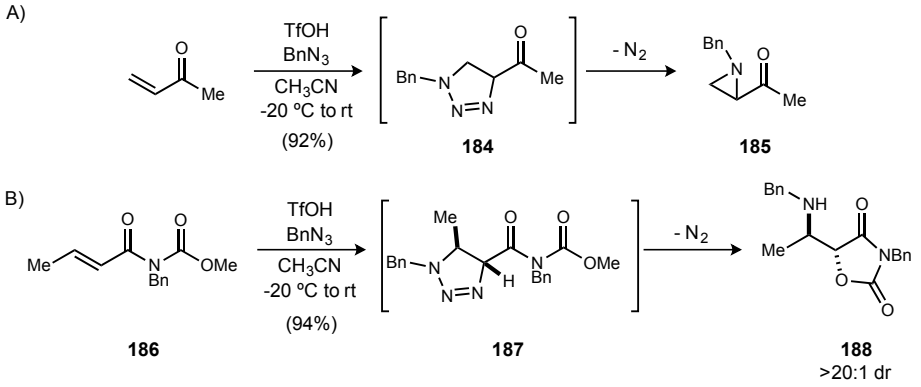

Figure 65: Brønsted acid-promoted reactions of azide with olefins.

2.2.2 Model system for synthesis of (+)-zwittermicin A core

With a robust methodology to provide aminohydroxylated products in high diastereoselection and under relatively mild conditions, a synthesis of a complex natural product was pursued to display its viability and utility. Zwittermicin A became an attractive candidate, as it contains a complex, C_2 symmetric aminopolyol core that could be synthesized in a bidirectional fashion utilizing a novel substrate controlled *anti*-diastereoselective azide olefin reaction.[151] The assembly of this core diastereoselectively was tested on imide **189** bearing a chiral center similar to that in the natural product.[152] The alcohol bore a bulky TBDPS group to aid in selectivity (Figure 66). Under thermal conditions (Figure 66A) the yield of **190** is modest, and the diastereoselectivity is minimal. But under the acid promoted conditions, the yield is slightly higher, and the selectivity is much better, but produces the S_N2' product **191** in almost equal amount (Figure 66B).

[150] Donahue, M. G.; Hong, K. B.; Johnston, J. N. *Bioorg. Med. Chem. Lett.* **2009**, *19*, 4971.

[151] At the time of this study, the absolute stereochemistry of (+)- zwittermicin A had not been confirmed. Therefore, the opposite enantiomer is shown in the schemes of this section.

[152] Hong, K. B. Brønsted Acid Promoted Olefin Functionalization (Anti-Aminohydroxylation) and Progress Toward (+)-Zwittermicin A. *PhD Dissertation*, Vanderbilt University, **2010.**

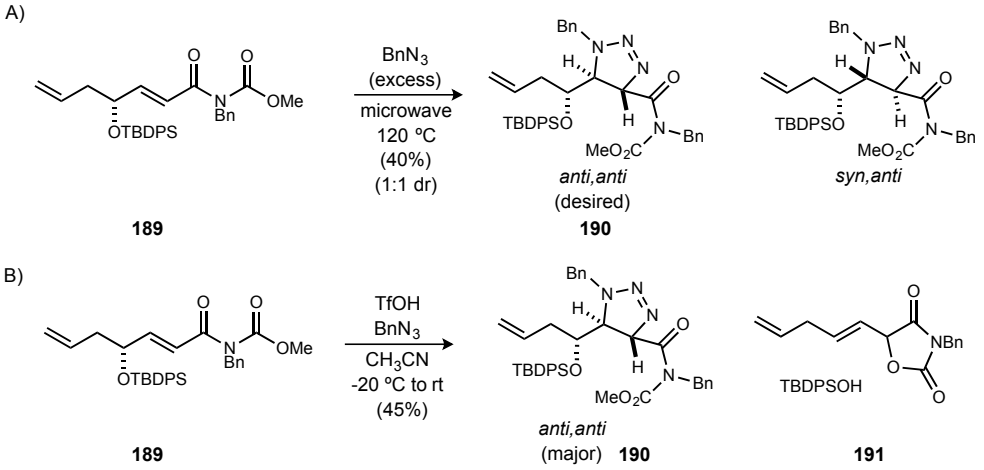

Figure 66: Model system for diastereoselective [3+2] cycloaddition.

Both the *anti,anti*-**190** and *syn,anti*-**190** products were subjected to fragmentation conditions, and provided the corresponding diastereomeric oxazolidine diones **192** and **193** in 68% and 60% yields, respectively (Figure 67). This model study showed promise for the assembly of the core of (+)-zwittermicin A and synthesis was begun.

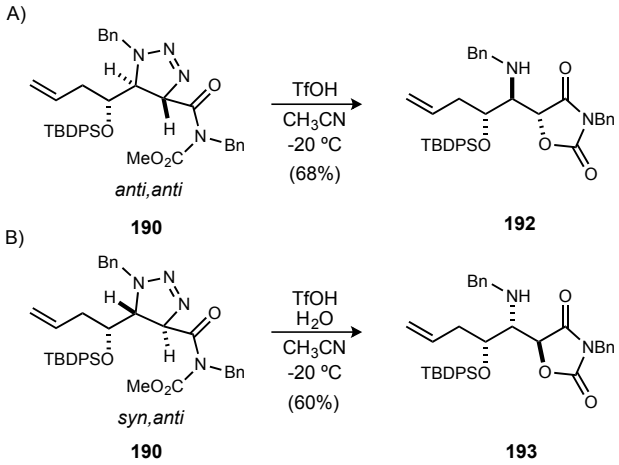

Figure 67: Fragmentation of model system triazoline.

3.2.3 Synthesis of bis(Imide) 181

The bidirectional synthesis of (+)-zwittermicin A begins with the known preparation of the C_2 symmetric diol **194** (Figure 68).[153] Pentanedione is activated by a Lewis acid and undergoes nucleophilic acyl substitution with two equivalents of chloroacetyl chloride. The

[153] Rychnovsky, S.; Griesgraber, G.; Powers, J. *Org. Synth.* **2004**, *Col l. Vol. 10*, 276.

conversion of this intermediate is then driven to completion by removal of acetyl chloride by distillation from the mixture. The resulting dichloropentanedione is unstable, and must be stabilized by coordination with copper(II). This copper complex is formed in 58% yield (88 g) on up to 750 mmol scale.

Complex **195** (Figure 68) can be deprotected under aqueous acid conditions, then immediately subjected to Noyori reduction by ruthenium(II), (*R*) BINAP, and a hydrogen atmosphere to yield chiral diol **194** as a single enantiomer.[153] This reduction originally appeared problematic, with yields of **194** averaging around 18% on 80 mmol scale, while the reported yield is 40%. This difference in yield was originally attributed solely to an increased presence of oxygen and water, as it was not performed in a glove box. Yet, in previous preparations, neither the toluene used for catalyst preparation nor the methanol used during the reduction were dried or degassed. After formation, the Noyori catalyst also must be heated and dissolved in the reaction solvent, or else poor solubility likely leads to poor conversion. In addition, the reaction bomb was previously used without a glass insert and was therefore incapable of holding a stir bar. Without stirring, the surface area between the reaction mixture and hydrogen was limited during the reaction, leading to poor conversion. Making these adaptions increased the yield of **194** to 29% on the same scale. This reduction is the lone enantioselective reaction of the synthesis, and the chirality of this substrate is the basis of all future stereoselection.

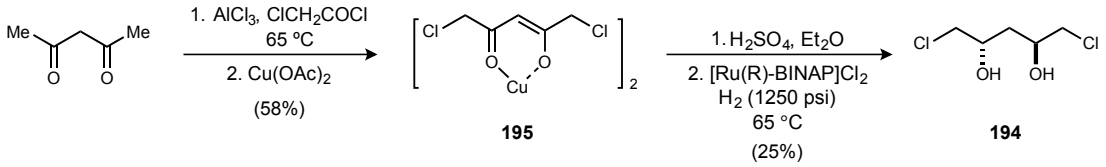

Figure 68: Enantioselective preparation of chiral diol precursor **194**.

To prepare the substrate for the Horner-Wadsworth-Emmons olefination, diol **194** is then treated with trimethyl sulfonium iodide and strong base to effect bis(olefination) yielding compound **196** (Figure 69).[154] Again, this known reaction was originally yielding half of the expected 80%, with poor conversion of starting material and decomposition of product. This was initially addressed by using THF dried over sieves so maximal ylide could be generated. Additionally, this reaction requires 10 equivalents of trimethyl sulfonium iodide, and with that amount of salt in the reaction slurry, magnetic stirring becomes ineffective. To remedy this, a dimpled flask equipped with a mechanical stirrer was used to maximize turbulence and temperature consistency throughout the mixture. Elimination of sulfonium to olefin **196** is hypothesized to be the slow step, and these sulfonium

[154] Whitehead, A.; McReynolds, M. D.; Moore, J. D.; Hanson, P. R. *Org. Lett.* **2005**, *7*, 3375.

intermediates may be sensitive at temperatures above -40 °C, so the reaction was kept at -50 °C to ensure minimal decomposition before slowly warming to room temperature. The concentration was also lowered to discourage any intermolecular decomposition pathways. These changes increased the yield of diene **196** from 45% to 73% on 300 mmol scale, relieving a major bottleneck in the synthesis. The diol moiety of diene **196** was next silyl protected prior to oxidative cleavage of the olefins. Tetraisopropyldisiloxane (-TIPDS-) was employed because of its high diastereoselectivity in the azide-olefin [3+2] cycloaddition.[139] After extraction, crude **182** appeared very clean, however the mass balance was too high, possibly due to excess $TIPDSCl_2$. Column chromatography of **182** revealed a significant amount of a byproduct, possibly from methanol opening of the siloxane ring.

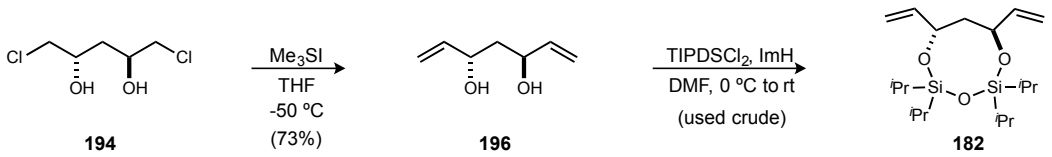

Figure 69: Preparation of TIPDS protected diene **196**.

Diene **182** was converted to bis(aldehyde) **197** by a two-step procedure, as direct ozonolysis led to complex reaction mixtures with little aldehyde observed by ^1H NMR.[146] Muchalski found that a two-step procedure utilizing an Upjohn dihydroxylation[155] followed by Johnson-Lemieux oxidation,[156] was able to provide bis(aldehyde) **197** cleanly. When

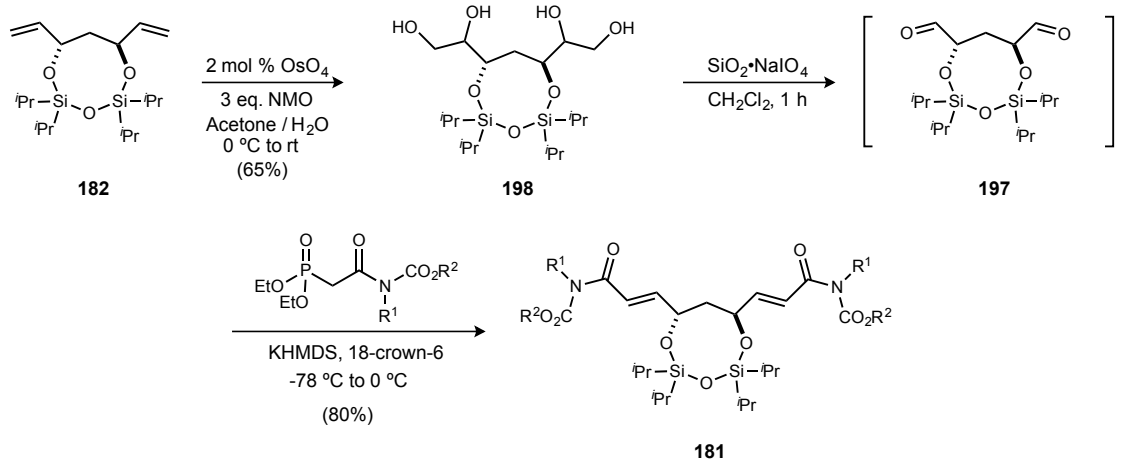

Figure 70: Optimized synthesis of bis(imide) **181**.

crude diene **182** was dihydroxylated with catalytic OsO_4 and NMO, a mixture of diastereomers **198** was isolated in 65% yield (Figure 70). When **196** was purified prior to dihydroxylation, yields were as high as 82%, but the unwanted byproduct generated by its

[155] Zhong, Y.-L.; Shing, T. K. M. *J. Org. Chem.* **1997**, *62*, 2622.

[156] Pappo, R.; Allen, J. D. S.; Lemieux, R. U.; Johnson, W. S. *J. Org. Chem.* **1956**, *21*, 478.

purification led to use of **182** crude. Reacting **199** with silica-gel supported $NaIO_4$ yielded bis(aldehyde) **197**, which was unstable and used immediately in unpurified form. Treatment with the stabilized phosphonate ester anion effected the Horner-Wadsworth-Emmons olefination yielding 80% of the *E,E*–bis(imide) **181** after purification. This approach convergently and bidirectionally provided **181** in 7 steps and 10% overall yield from 2,4 pentanedione.

3.2.4 Synthesis of bis(acid) ***208***

With an efficient route to bis(imide) **181** in hand, Muchalski screened a range of imide substituents, as well as cyclic and acyclic silyl protecting groups for their effect on the diastereoselection and yield of the [3+2] azide-olefin cycloaddition (Table 22).[146,149] Acyclic silyl protecting groups (TIPS, TBS, TBDPS) could not be used in ozonolysis or Johnson-Lemiuex oxidative cleavage due to decomposition. Cyclic silyl groups, TIPDS and DTBS, were then examined because of their increased conformational restraint and steric hindrance, which could improve stability of bis(aldehyde) **197** while also improving diastereoselection in the subsequent cycloaddition. DTPS protected methyl carbamate **199a** was formed in good yield (79%). However, TIPDS protected methyl carbamate **199b** formed in low yield. Byproduct **200** was isolated and hypothesized to form from fast acyl transfer over the slower oxaphosphetane formation. By changing R^2 to *tert*-butyl, **199c** could be synthesized in good yield. However, the *tert*-butyl carbamate was labile in the strongly-acidic conditions of the [3+2], yielding only the bis(amide) byproduct **201**. Therefore, the *iso*-propyl carbamate **199d** was chosen for its steric deterrence of acyl transfer in the HWE and its stability under acidic conditions.

Table 22: Imide substituent and silyl group screen

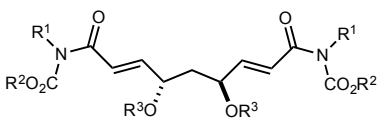

199a-d

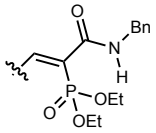

200

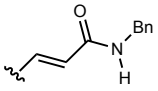

201

Entry	**199**	R^1	R^2	R^3
1	**199a**	Bn	Me	-DTBS-
2	**199b**	Bn	Me	-TIPDS-
3	**199c**	Bn	^{t}Bu	-TIPDS-
4	**199d**	Bn	^{i}Pr	-TIPDS-

Muchalski found when the various (bis)imides were screened under both thermal and acidic conditions for triazoline formation, **199d** was found to be the optimal substrate under acidic conditions (Figure 71).[146,149] It yielded the desired *anti,anti* diastereomer **180a** in an 18:1:1 ratio over the *anti,syn*-**180a** and *syn,syn*-**180a** diastereomers (as determined by NOESY). Use of the DTBS protecting group (**199a**) gave lower yield and a 1:9:9 ratio of diastereomers under the same conditions, suggesting that the flexibility provided by the 8 membered disiloxane ring was important for adopting a conformation conducive to high diastereoselection.

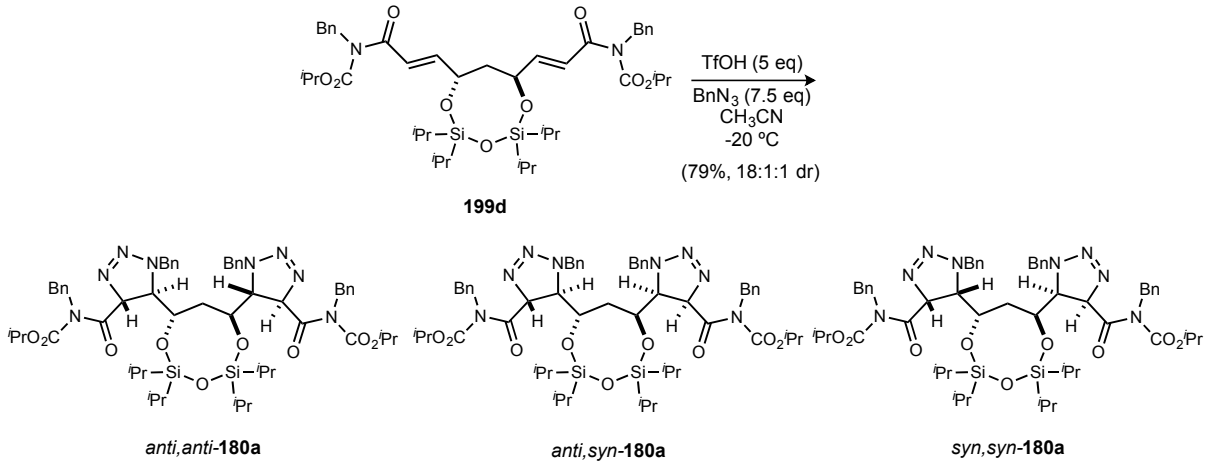

Figure 71: Triflic acid promoted, diastereoselective [3+2] cycloaddition.

Triazoline **180a** was treated with triflic acid at room temperature to induce fragmentation of the triazoline ring, releasing dinitrogen, and forming the bis(oxazolidine dione) **202a** in 71% yield (Figure 72). For the next conversion, a variety of hydroxide sources, Brønsted acid, hydrides, and Lewis acids were tested for opening the bis(oxazolidine dione) rings to yield bis(amide), however, none were successful.[146]

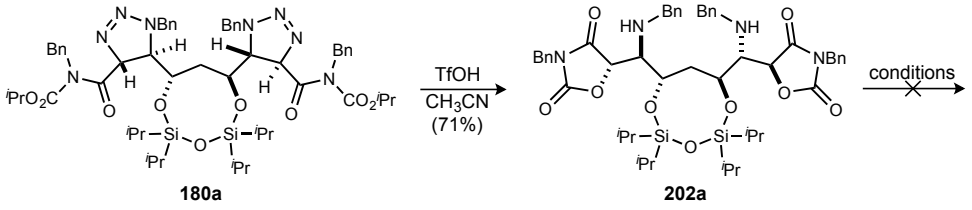

Figure 72: Triazoline fragmentation and functionalization.

Believing this poor reactivity was due to the electron donating effect of the benzyl substituent, the route was adjusted by Muchalski to interchange it with a phenyl substituent (Figure 73). Diethylphosphonoacetic acid **203** was converted to the acid chloride prior to coupling with aniline to form amide **204**. This amide was deprotonated with LHMDS and

then added into isopropyl chloroformate to yield imide **205** in 70% yield over the four steps. This imide is highly susceptible to hydrolytic decomposition at the amide carbon, thus the complete purification must be carried out immediately after quenching the reaction. Muchalski also developed a more cost-effective protocol for the HWE olefination to give bis(imide) **199e** in similar yields. The [3+2] cycloaddition converted faster and in similar yields and diastereoselction. The equivalents of benzyl azide could be reduced without diminishing yield or selectivity. Bis(triazoline) **180b** was problematic in the subsequent fragmentation. Use of triflic acid could no longer accelerate the reaction of **180b** as it did with **180a**, and decomposition was observed at higher temperatures. Weaker acids such as methanesulfonic and *para*-toluene sulfonic acid provided much faster conversion, and using *para*-toluene sulfonic acid allowed for simple chromatographic purification of bis(oxazolidine dione) **202b** in 70-90% yield.

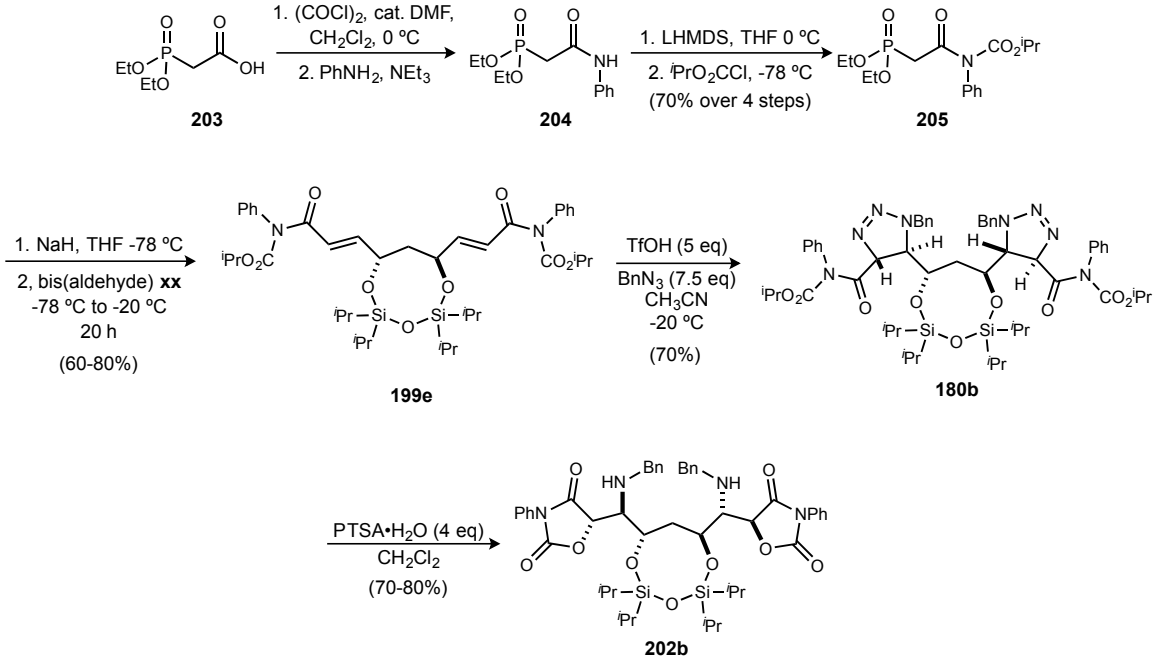

Figure 73: Adjusted route to N-Ph bis(oxazolidine dione) **202b**.

With phenyl substituted bis(oxazolidine dione) **202b** prepared, opening of the oxazolidine dione rings was attempted again.[146] Hydroxides and alkoxides only caused decomposition or epimerization. A Lewis acid, $Ti(O^iPr)_4$, was mildly successful, causing ring opening in 55% yield but with low conversion, irreproducibility, and an inseparable mixture of starting material and product. When treated with methanol and ammonia (Figure 74), both starting material and product were converted to bis(amide) **206**, which not only opens the oxazolidine dione rings with methoxide, but also cyclizes the requisite carbonate with the benzyl amine to form the bis(amide). This mechanism is evidenced by isolation of

partially cyclized intermediate **207**. The ^{1}H NMR of the crude reaction mixture generally indicated that **202b** cleanly converted to **206**. After concentration, however, the ^{1}H NMR showed significant degradation to unknown byproducts, and chromatography was very difficult, never yielding more than 42%. It was hypothesized that this decomposition was due to the remaining ammonia before concentration. The protocol was altered to include an argon purge of the reaction mixture after full conversion was reached, and consequently, yields increased to 66% of **206**. This mechanism in one step effectively reveals the terminal carbons for later functionalization as well as protects the secondary amines as oxazolidinone rings.

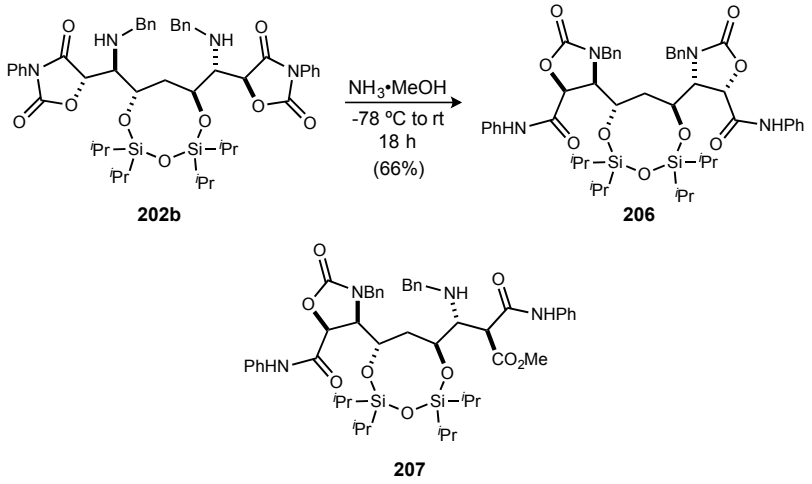

Figure 74: Isomerization to bis(amide) **206**.

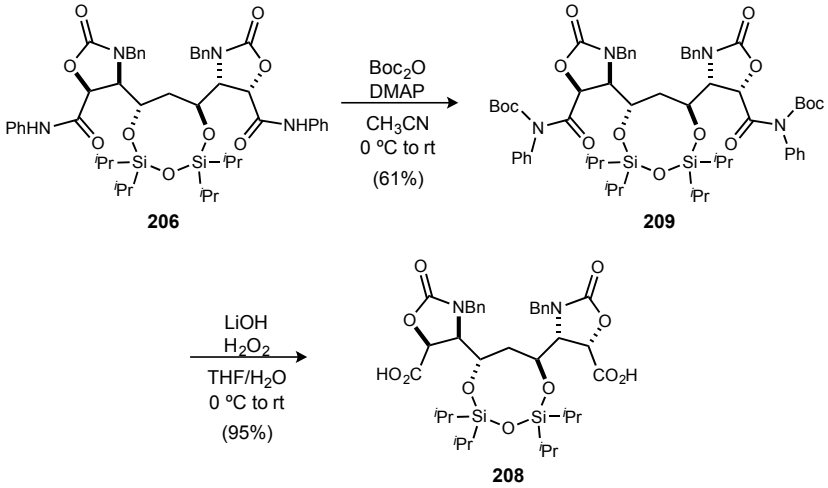

Figure 75: Preparation of bis(acid) **208**.

Bis(amide) **206** could not be directly converted to bis(acid) **208** using ammonium hydroxide, but could by a two-step procedure (Figure 75). Boc protection proceeded well, then **209** is saponified to bis(acid) **208**, which had to be used crude, due to its high polarity.

*3.2.5 Synthesis of isonitrile **177** and initial route to an advanced intermediate*

With a route established to synthesize bis(acid) **208** efficiently, the *pseudo* C_2-symmetric core of (+)-zwittermicin A was complete, and five of seven stereocenters are established. Desymmetrization, removal of one of the terminal carbons, and a diastereoselective Passerini reaction still remained.

First, preparation of isonitrile **210** (Figure 76) was attempted by Muchalski for coupling in the Passerini reaction. This isonitrile would allow for the most convergent route possible, as no further functional group manipulations would be necessary after the Passerini. However, preparation of this proved difficult, due to incompatible preparations for the urea, amide, and isonitrile functional groups. When the urea was formed first, the amide could not subsequently be formed. By protecting the secondary amine, the urea and amide could be constructed, however this amine could not then be formylated in route to the isonitrile. When isonitrile preparation was attempted after installation of the urea, the compound could not be isolated. The urea amine was even brought in as an azide, which was also incompatible with isonitrile formation. At the expense of convergence, the urea would need to be formed after the Passerini from the Boc-protected amine. Thus, synthesis of isonitrile **177** was begun with the conversion of L-aspartic acid to L-DAP **211** by a Schmidt reaction (Figure 76). The acid was then converted to methyl ester **212**, which was selectively Boc-protected in 73% yield. The free amine could then be formylated to yield compound **213**. Triphosgene and NMM effect the dehydration of the formamide, and

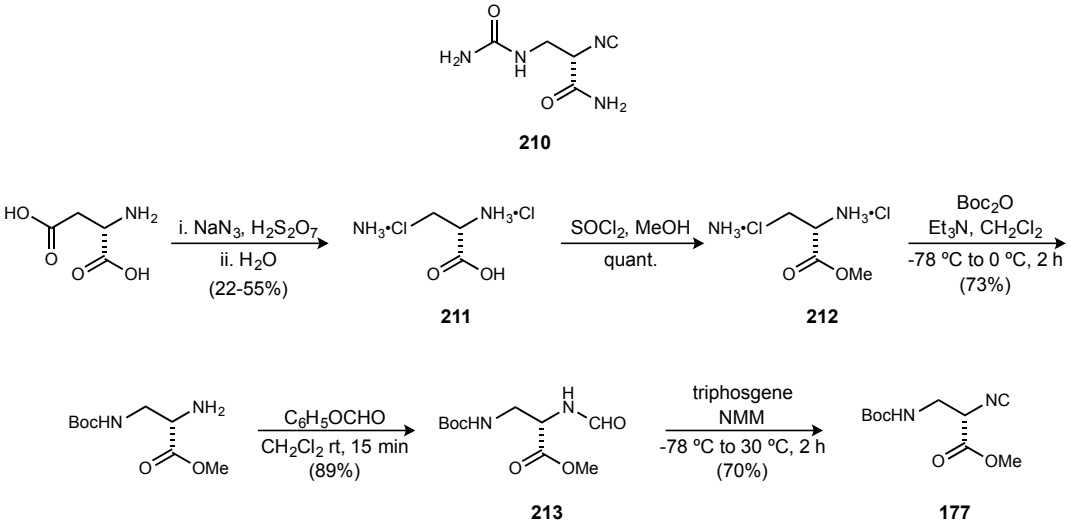

Figure 76: Synthesis of isonitrile **177**.

isonitrile **177** was formed in 70% yield. Attempts to convert the methyl ester to an amide failed, indicating that this would need to take place after the Passerini as well. Methodology

for the main convergent connection could be developed to employ a diastereoselective Henry reaction with nitromethane. Oxidation of the resultant nitroalkane to a carboxylic acid would allow for a simple amide coupling with a more highly functionalized western piece. This could possibly shorten the longest linear sequence dramatically.

At this point, Muchalski explored a route that was not ultimately successful, but was vastly significant in developing the current one. From bis(acid) **208**, reduction to the alcohols, followed by trityl protection, yielded desymmetrized mono alcohol **214** in 30% (86% brsm) (Figure 77). Swern oxidation was found to be the best method for aldehyde formation, which had to be used immediately in the Passerini reaction with isonitrile **177** due to aldehyde instability. The Passerini provided adduct **215** in 65% yield and modest 2:1 dr. The identities of the diasteromers could not be determined, and will need to be assigned by comparison to the natural product.

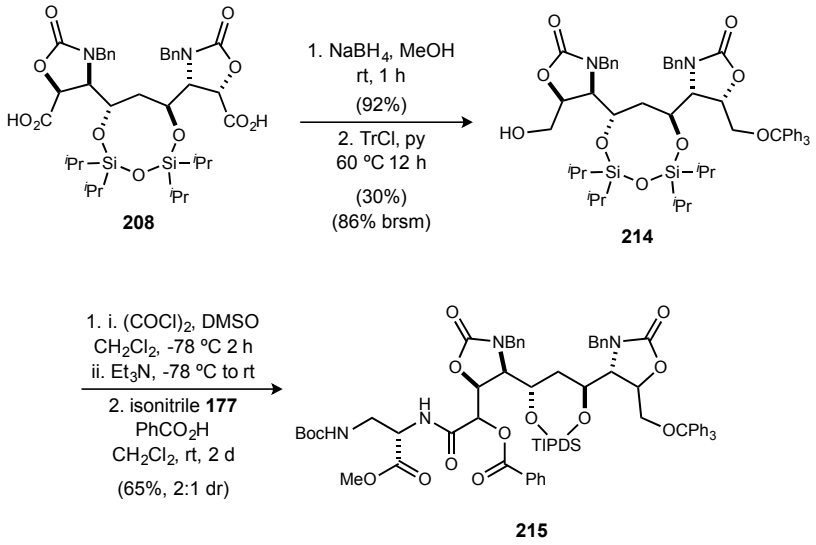

Figure 77: Initial route to Passerini adduct **215**.

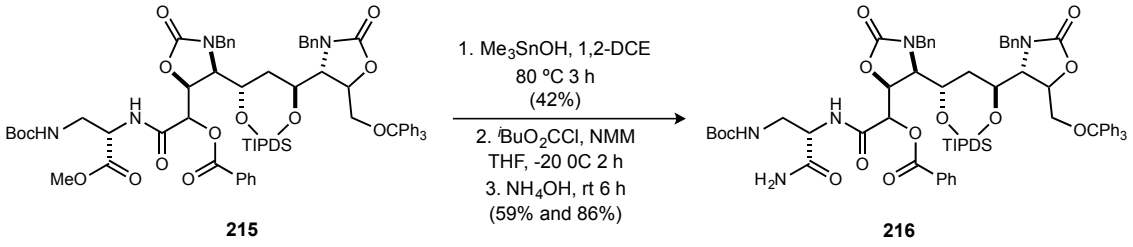

Figure 78: Amide **216** formation.

With all stereocenters now set, decarbonylation, several functional group manipulations, and global deprotection remained. Conversion of methyl ester **215** to the free amide could be achieved by saponification with trimethyltin hydroxide, which was effective at avoiding epimerization (Figure 78). Diastereomers were separated, then

converted to the mixed anhydride before amide formation by ammonium hydroxide to yield **216**.

Boc deprotection of the terminal amine was attempted with TFA but caused epimerization of the product. Thus, Muchalski attempted to globally deprotect the methyl ester, the benzoate ester and the oxazolidinone rings of **216** at once using a variety of strongly basic conditions (Figure 79), however the oxazolidinone rings were never reactive.

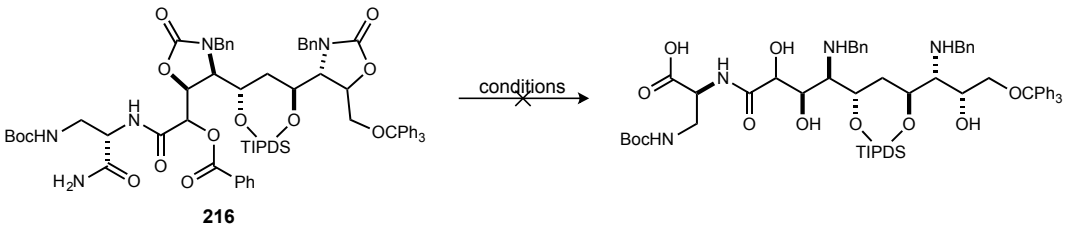

216

Figure 79: Attempted deprotection of **216**.

Again, this poor reactivity was attributed to the *N*-benzyl substituent's electron rich character, decreasing the electrophilicity of the carbamate. Using a model system (Figure 80), Muchalski determined that a protecting group exchange to the more electron withdrawing *N*-tosyl would allow for oxazolidinone deprotection. However, seeing the difficulty of the amide formation and deprotections, it was decided to remove a terminal carbon prior to the Passerini. The conclusions drawn from this initial pass through the final stages of the synthesis were tremendously useful in shaping the current route towards (+)-zwittermicin A.

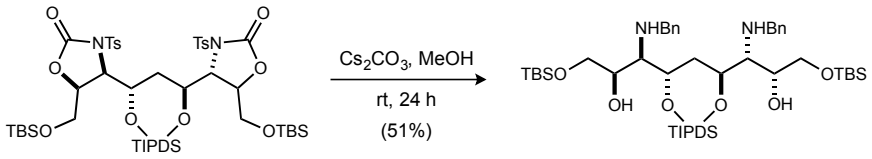

Figure 80: Model system for *N*-tosyl carbamate deprotection.

*3.2.6 Desymmetrization, decarbonylation, and preparation of Passerini substrate **178***

The knowledge gained from the initial route indicated the molecule must not only be desymmetrized before the Passerini, but must lose one carbon as well. Therefore bis(acid) **208** needed to be monoprotected prior to radical decarbonylation at the free carboxylic acid. Muchalski attempted several monoesterification methods, and the most effective one

found was developed by Nishiguchi for dicarboxylic acids of 4-14 carbon units.[157,158] The bis(acid) was subjected to a toluene-$HCO_2{}^n$Bu mixture with DOWEX 50WX8 resin at high temperatures to yield the purified monoprotected ester in up to 57% yield. Since the resin is about 50% water by weight, the bis(acid) is more soluble and reactive at the resin surface. This allows the bis(acid) to react faster than the monoprotected product **217** (Figure 81). An added benefit to this method was that bis(ester) **218** could be easily isolated in 40-60% yield and treated with LiOH to recover additional bis(acid) **208** for recycling.

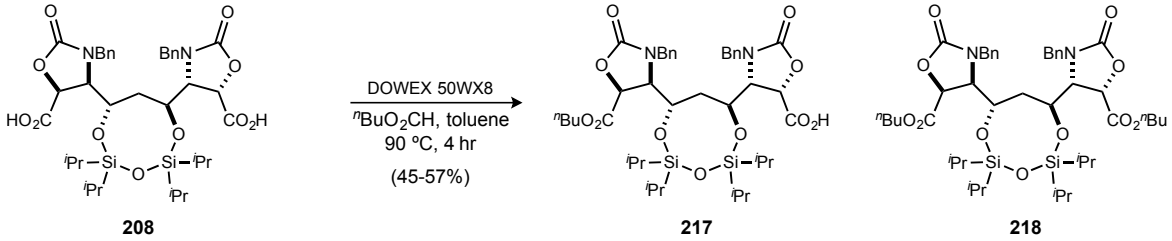

208 **217** **218**

Figure 81: Desymmetrization and monoprotection of bis(acid) **208**.

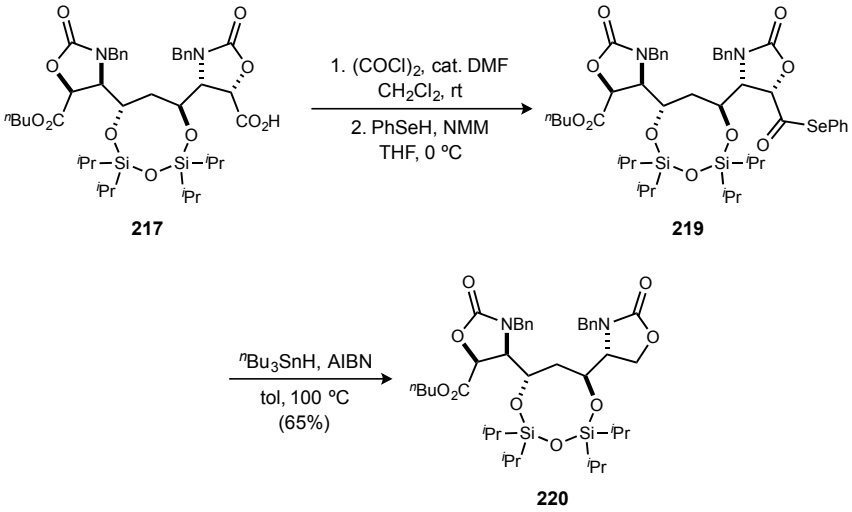

217 **219** **220**

Figure 82: Synthesis of decarbonylated ester **220**.

With desymmetrization accomplished, removal of the terminal carboxylic acid carbon could be undertaken. Several trials were required to determine that activation of the acid before treatment with benzeneselenol gave the best conversion of starting material to selenoester **219** (Figure 82). Without isolation, the selenoester was dried over P_2O_5 then treated with 2 equivalents of ^{n}Bu$_3$SnH and 1 equivalent of AIBN at high temperature to cause decarbonylation in yields averaging 65%. Product **220** cannot be produced if the selenoester is not sufficiently dried and if the AIBN has not been recently recrystallized.

[157] Saitoh, M.; Fujisaki, S.; Ishii, Y.; Nishiguchi, T. *Tetrahedron Lett.* **1996**, *37*, 6733.

[158] Nishiguchi, T.; Ishii, Y.; Fujisaki, S. *J. Chem. Soc., Perkin Trans. 1* **1999**, 3023.

As previously determined by Muchalski's first route, the carbamate benzyl group needed to be converted to tosyl to provide for facile deprotection after the Passerini. Thus, ester **220** had to be reduced and protected (Figure 83). Several stronger reducing agents were examined in the initial route, however only the milder $NaBH_4$ could convert the ester to the alcohol. This was carried out and then protected by MOMCl to yield the MOM ether. Now the benzyl groups could be removed by Birch reduction to yield unprotected carbamate **221** in 78% yield over three steps. This was deprotonated with ^{n}BuLi and quenched with tosyl chloride. The MOM ether could then be removed with TFA to provide the Passerini substrate **178** in 82% yield.

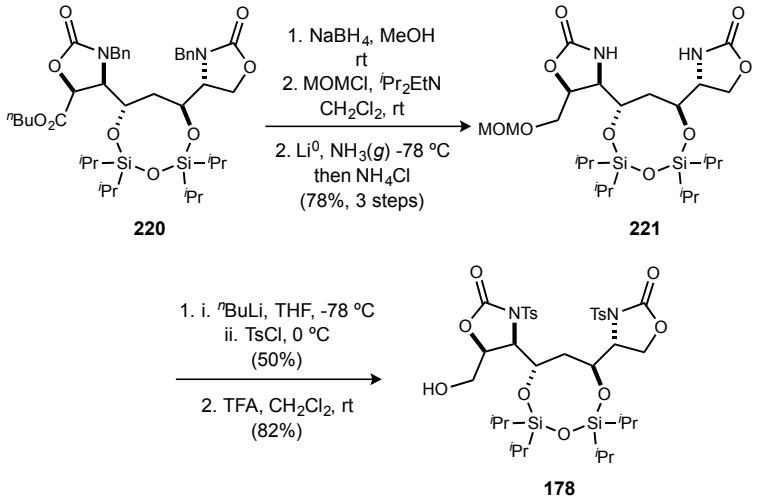

Figure 83: Preparation of Passerini precursor **178**.

3.2.7 Passerini and final steps twowards (+)-zwittermicin A

With the stage set for the Passerini, the oxidation of the primary alcohol again needed optimization. Many conditions using DMP, DMSO, PCC, TPAP, and TEMPO were examined before an NMR study with DMP was conducted. This showed that the alcohol was completely consumed in fifteen minutes to produce the aldehyde product. The reagents for the Passerini could be added directly to the reaction mixture, and complete conversion was achieved quickly. The aldehyde is extremely reactive and therefore very sensitive to water and air. Passerini adduct **222** could be isolated from the reaction in 50% yield in a 4:1 diastereomeric ratio (Figure 84), however the configuration of the major diastereomer will remain unknown until comparison with the natural product.

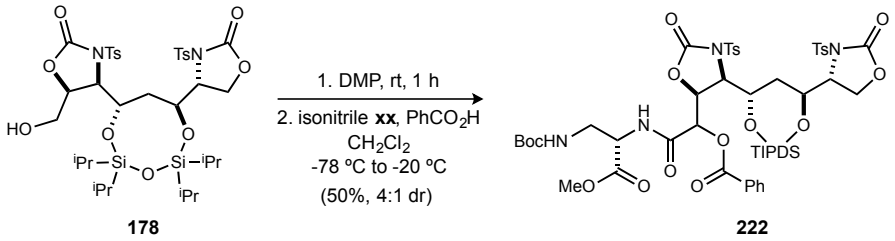

Figure 84: Optimized oxidation and Passerini to yield compound **222**.

The proposed model for the Passerini reaction is shown in Figure 85. This model positions the more electronegative oxygen substituent perpendicular to the carbonyl and opposite the approach of the nucleophile regardless of the steric influences of the largest substituent, as dictated by the Felkin-Anh model.[159] This relieves the dipole-dipole repulsion that would occur in the transition state as the nucleophile-carbon bond is forming, and would provide conformation A (Figure 85). It is hypothesized, however, that the steric interaction of the large, amino methine substituent with the carbonyl will cause conformation B to predominate, with the oxygen substituent still perpendicular, but the largest group furthest from the carbonyl, as dictated by the Cram model.[160] If predicted correctly, conformation B would lead to the correct configuration found in (+)-zwittermicin A. If incorrect, the counterion could be modified, perhaps to a chiral acid, to modulate the diastereoselectivity. If still unsuccessful, either epimerization by Mitsunobu reaction can be employed, or the Passerini can be run at higher temperature to afford a diastereomeric ratio closer to 1:1.

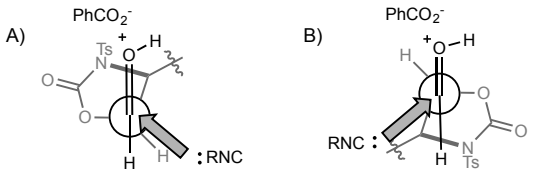

Figure 85: Proposed model for the diastereoselective Passerini.

With the final key reaction accomplished, all that remained were several functional group manipulations and deprotections (Figure 86). First, as found in Muchalski's initial route, methyl ester **222** had to be converted to the amide by a two-step procedure. Saponification with trimethyltin hydroxide successfully avoided epimerization at the position α to the amide, but proceeded only in moderate yield due to poor conversion. Formation of the mixed anhydride allowed for amide **223** formation in 49% yield. Next, the urea was installed, since it could not be formed in the presence of the isonitrile prior to the

[159] Chérest, M.; Felkin, H.; Prudent, N. *Tetrahedron Lett.* **1968**, *9*, 2199.

[160] Cram, D. J.; Wilson, D. R. *J. Am. Chem. Soc.* **1963**, *85*, 1245.

Passerini. This was accomplished by first deprotecting the Boc amine with trifluoroacetic acid, then the crude amine was treated with trimethylsilyl isocyanate to yield urea **224** in 50%. The tosylated oxazolidine rings will be opened with Cs_2CO_3, as was successfully done by Muchalski in 51% yield with a model system. Removal of the cyclic silyl protecting group, TIPDS, from **225** will be effected by HF • pyridine to afford **226**. Finally, the tosyl groups will be removed by Birch reduction to complete the total synthesis of (+)-zwittermicin A.

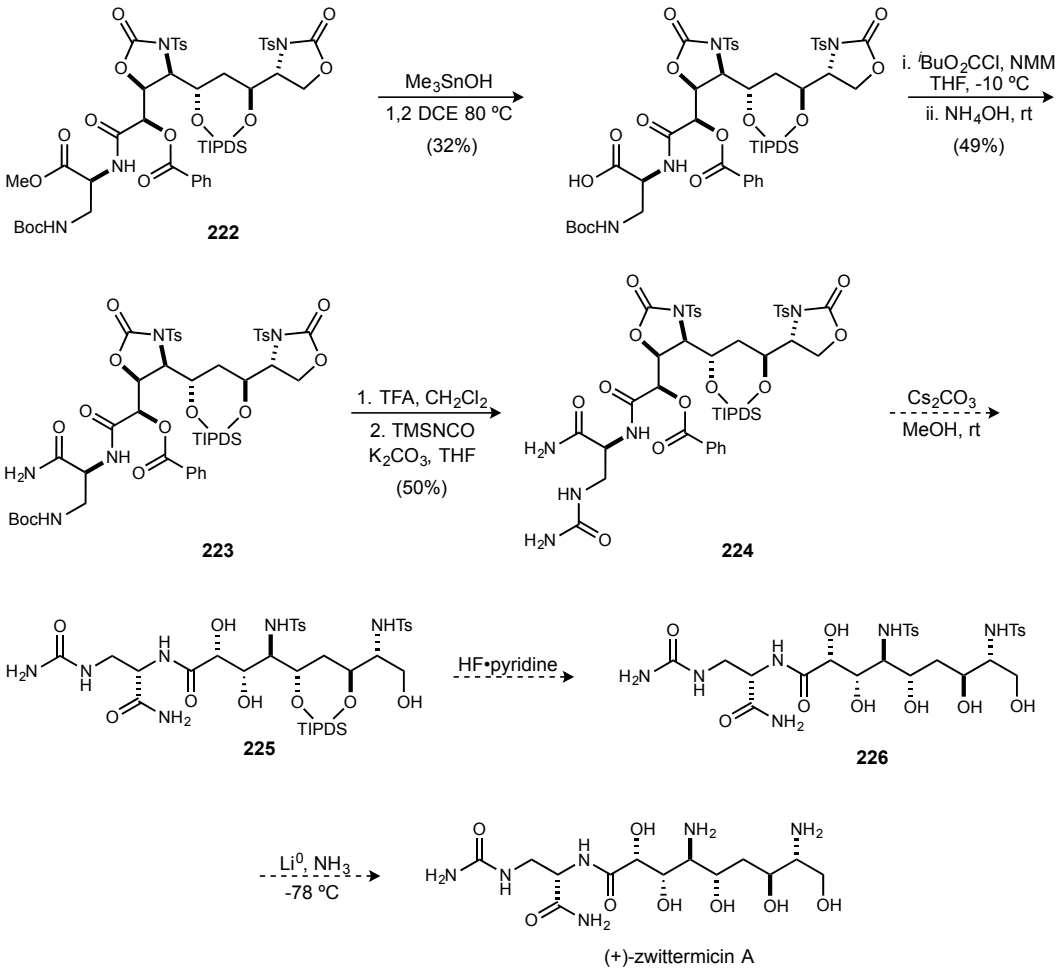

Figure 86: Final manipulations for the synthesis of (+)-zwittermicin A.

In summary of this author's throughput, copper complex **195** was prepared on a half mol scale (Figure 87). This was converted to 150 mmol of chiral diol after the Noyori reduction was optimized up to 25% yield. Careful alteration of the olefination reaction procedure increased the yield to 70% and yielded 22g of the bis(olefin) product, **196**. 74 mmol (58 g) of the HWE product **199e** was produced, as opposed to 22g previously. Increased yield over the next several steps allowed for an increase from the previous 18% yield over those same steps. Conversion of all material to the desymmetrized mono acid

217 provided 10 g of the product, which was passed along to coworkers specializing in the backend of the synthesis. If the final two steps can be optimized, this material could be enough to provide several milligrams of (+)-zwittermicin A.

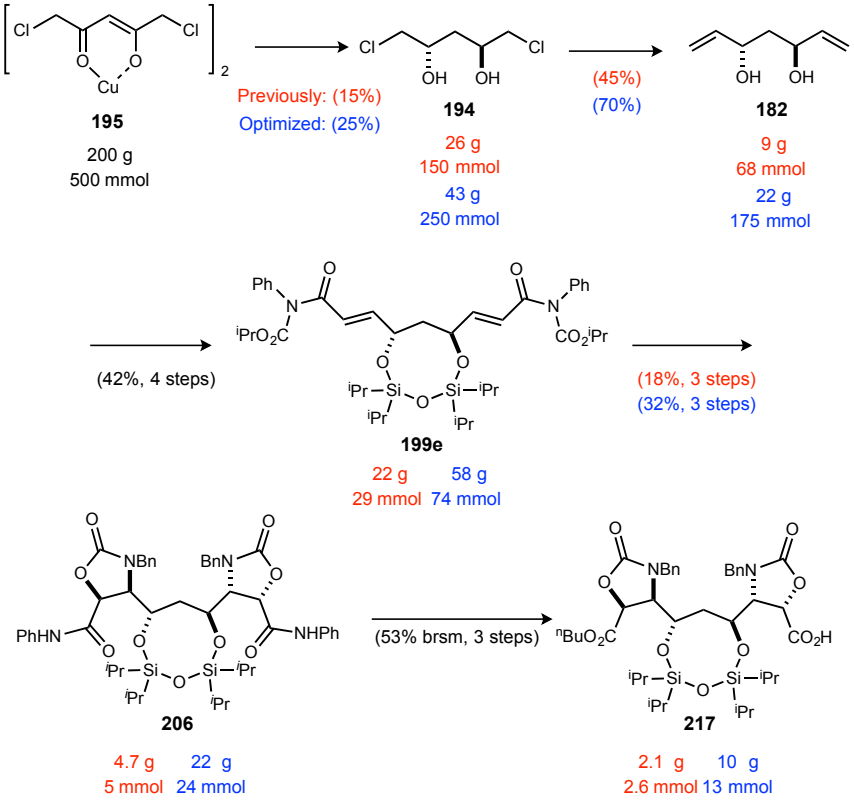

Figure 87: Summary of synthetic sequence with optimized yields and material throughput.

4 Experimental appendix

A Characterization of organic molecules

General Experimental Details

All reagents and solvents were commercial grade and purified prior to use when necessary. Toluene and tetrahydrofuran was dried by passage through a column of activated alumina as described by Grubbs.[i] N-Iodosuccinimide was recrystallized from dioxane and carbon tetrachloride. Thin layer chromatography (TLC) was performed using glass-backed silica gel (250 μm) plates and flash chromatography utilized 230–400 mesh silica gel from Sorbent Technologies.

UV light, and/or the use of iodine/SiO_2 were used to visualize products. Nuclear magnetic resonance spectra (NMR) were acquired on a Bruker DRX-500 (500 MHz), Bruker AV- 400 (400 MHz) or Bruker AV II-600 (600 MHz) instrument. Chemical shifts are measured relative to residual solvent peaks as an internal standard set to δ 7.26 (^{1}H) and δ 77.0 (^{13}C) ($CDCl_3$) and δ 2.50 (^{1}H) and δ 39.52 (^{13}C) (DMSO-d_6). IR spectra were recorded on a Thermo Nicolet IR100 spectrophotometer and are reported in wavenumbers (cm^{-1}). Compounds were analyzed as neat films on a NaCl plate (transmission). Mass spectra were recorded on a Waters LCT spectrometer by use of the ionization method noted.

Catalyst Synthesis

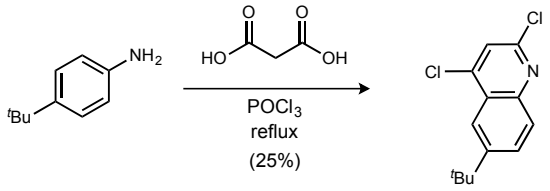

6-(*tert*-Butyl)-2,4-dichloroquinoline (S1).

To a 50 mL round-bottom flask in an ice bath was added malonic acid (3.85 g, 37.0 mmol) and $POCl_3$ (15.0 mL, 160 mmol). After stirring for five minutes, 4-*tert*-butyl aniline (5.90 mL, 37.0 mmol) was added slowly. The flask was then moved to an oil bath, equipped with a condenser and argon balloon, and stirred for 6 hours at reflux. The reaction was then removed from the oil bath and poured into a 500 mL beaker containing 250 mL of ice-water. Water was used to rinse the reaction flask into the beaker. The mixture was stirred vigorously and solid NaOH was added slowly until the pH was neutral. The mixture was filtered, and the collected solid was transferred to a 500 mL round-bottom flask. Hexanes was added to the flask, and the mixture was triturated by stirring in a warm water bath

for 15 minutes. The mixture was filtered, and the filtrate was concentrated to a yellow oil. The oil was purified by flash column chromatography (SiO_2, 0-10% ethyl acetate in hexanes) to yield 2.38 g (25%) as a yellow solid. Mp 45-47 °C; R_f = 0.58 (10% EtOAc/hexanes); IR (film) 2960, 2870, 1563, 1494, 1390, 1263, 1195 cm^{-1}; ^1H NMR (400 MHz, $CDCl_3$) δ8.09 (d, J = 2.1 Hz, 1H), 7.96 (d, J = 8.9 Hz, 1H), 7.87 (dd, J = 8.9, 2.1 Hz, 1H), 7.46 (s, 1H), 1.43 (s, 9H); ^{13}C NMR (100 MHz, $CDCl_3$) ppm 151.3, 149.2, 146.8, 144.3, 130.6, 128.7, 124.8, 121.8, 119.3, 35.4, 31.2; HRMS (EI): Exact mass calcd for $C_{13}H_{14}Cl_2N$ $[M+H]^+$ 254.0503, found 254.0498. MTK-4-176.

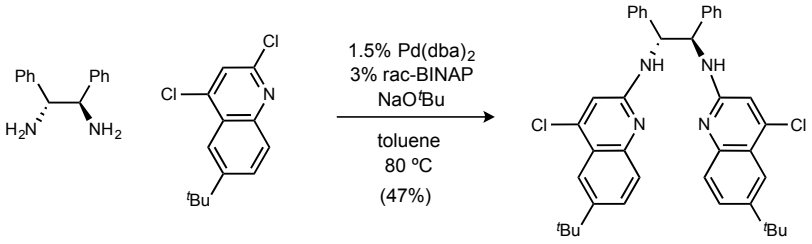

(1*R*,2*R*)-*N*1,*N*2-bis(6-(*tert*-Butyl)-4-chloroquinolin-2-yl)-1,2-diphenylethane-1,2-diamine (S2).

To a 100 mL, flame-dried round-bottom flask was added $Pd(dba)_2$ (34 mg, 59 µmol), *rac*-BINAP (73 mg, 120 µmol) and NaO^{t}Bu (944 mg, 9.83 mmol) in a glovebox. The flask was removed from the glovebox and charged with diamine (835 mg, 3.93 mmol), quinoline (2.00 g, 7.87 mmol) and toluene (40 mL). The flask was heated at 80 ºC under argon atmosphere for 22 hours, and then removed from heat and quenched with 10 mL of satd aq NH_4Cl. The mixture was transferred to a separatory funnel and the layers were separated. The aqueous layer was extracted with ethyl acetate, and the organic layers were combined, dried with Mg_2SO_4, filtered, and concentrated to an orange oil. The oil was purified by flash column chromatography (SiO_2, 5-10% ethyl acetate in hexanes) to yield 1.20 g (47%) as a yellow solid. Mp 135-138 °C; $[\alpha]_D^{20}$ +7.60 (c 1.12, $CHCl_3$); R_f = 0.35 (10% EtOAc/hexanes); IR (film) 3236, 3063, 2961, 1599, 1479, 1396, 1252 cm^{-1}; ^1H NMR (400 MHz, DMSO-d_6/$CDCl_3$, 10:1) δ7.88 (br d, J = 6.8 Hz, 2H), 7.75 (d, J = 2.0 Hz, 2H), 7.62 (dd, J = 8.8, 2.0 Hz, 2H), 7.47 (d, J = 8.8 Hz, 2H), 7.33 (d, J = 7.6 Hz, 4H), 7.14 (t, J = 7.6 Hz, 4H), 7.05 (t, J = 7.6 Hz, 2H), 7.02 (s, 2H), 5.63 (br d, J = 5.2 Hz, 2H), 1.32 (s, 18H); ^{13}C NMR (100 MHz, DMSO-d_6/$CDCl_3$, 10:1) ppm 155.8, 146.5, 144.5, 141.5, 140.5, 128.6, 127.7, 127.5, 126.5, 126.0, 119.8, 118.1, 112.1, 59.2, 34.2, 31.0; HRMS (EI): Exact mass calcd for $C_{40}H_{41}Cl_2N_4$ $[M+H]^+$ 647.2708, found 647.2728. MTK-4-181.

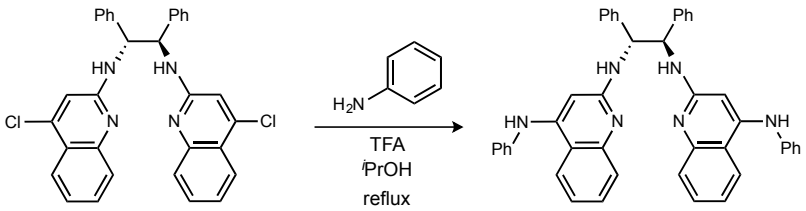

_N_2,_N_2'-((1_R_,2_R_)-1,2-Diphenylethane-1,2-diyl)bis(_N_4-phenylquinoline-2,4-diamine) (123c).

To a 2-5 mL microwave vial with a stir bar was added 4-Cl quinoline (95 mg, 180 µmol), isopropanol (1.8 mL), trifluoroacetic acid (35 µL, 440 µmol) and aniline (65 µL, 710 µmol). The vial was sealed (which was less than half-filled), placed behind a blast shield and heated in an oil bath at 110 °C for 18 hours, and then removed from heat. The mixture was concentrated under reduced pressure, and then dissolved in dichloromethane (20 mL) and transferred to a separatory funnel. The organic layer was washed with 2 M HCl (20 mL), and the aqueous layer was extracted with dichloromethane. The combined organic layers were washed with 6 M NaOH (20 mL), and the aqueous layer was extracted with dichloromethane. The organic layers were combined, dried (Mg_2SO_4), filtered, and concentrated to an off-white solid (20 mg, 17%). Mp 109-111 °C; $[\alpha]_D^{20}$ +5.36 (*c* 1.00, $CHCl_3$); R_f = 0.37 (20% MeOH/CH_2Cl_2); IR (film) 3235, 3056, 2923, 2856, 1589, 1526, 1500, 1437, 1254, 1083, 1033 cm^{-1}; ^1H NMR (400 MHz, DMSO-d_6/$CDCl_3$, 10:1) δ 8.38 (br s, 2H), 7.99 (br d, *J* = 8.3 Hz, 2H), 7.40-7.29 (m, 14H), 7.17-7.13 (m, 8H), 7.09-7.02 (m, 6H), 6.30 (br s, 2H), 5.52 (br s, 2H); ^{13}C NMR (125 MHz, DMSO-d_6/$CDCl_3$, 10:1) ppm 157.6, 148.7, 147.3, 142.4, 141.2, 129.1 (2C), 128.9, 127.6, 127.5, 126.3, 126.0, 122.6, 121.7, 121.6, 119.9, 116.6, 90.7; HRMS (EI): Exact mass calcd for $C_{44}H_{37}N_6$ $[M+H]^+$ 649.3074, found 649.3076. MTK-6-128.

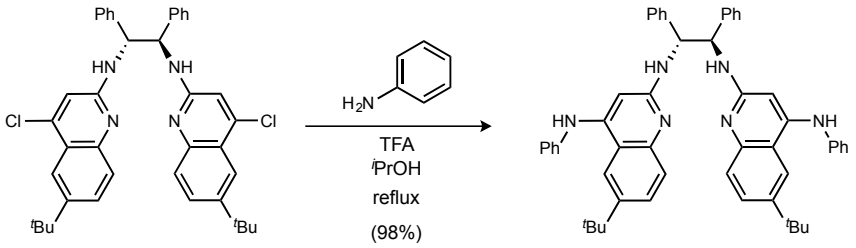

_N_2,_N_2'-((1_R_,2_R_)-1,2-Diphenylethane-1,2-diyl)bis(6-(*tert*-butyl)-_N_4-phenylquinoline-2,4-diamine) (126a).

To a 10-20 mL microwave vial with a stir bar was added 4-Cl quinoline (500 mg, 770 µmol), isopropanol (7 mL), trifluoroacetic acid (150 µL, 1.93 mmol) and aniline (280

µL, 3.09 mmol). The vial was sealed (which was less than half filled), placed behind a blast shield and heated in an oil bath at 110 °C for 18 hours, and then removed from heat. The mixture was concentrated under reduced pressure, and then dissolved in dichloromethane (20 mL) and transferred to a separatory funnel. The organic layer was washed with 2 M HCl (20 mL), and the aqueous layer was extracted with dichloromethane. The combined organic layers were washed with 6 M NaOH (20 mL), and the aqueous layer was extracted with dichloromethane. The organic layers were combined, dried with Mg_2SO_4, filtered, and concentrated to an off white solid (573 mg, 98%). Mp 165-168 °C; $[\alpha]_D^{20}$ +4.80 (*c* 1.58, $CHCl_3$); R_f = 0.63 (20% MeOH/CH_2Cl_2); IR (film) 3249, 3055, 2958, 1589, 1498, 1260 cm^{-1}; ^1H NMR (400 MHz, DMSO-d_6/$CDCl_3$, 10:1) δ8.42 (br s, 2H), 7.92 (br s, 2H), 7.48 (d, J = 8.8 Hz, 2H), 7.36-7.31 (m, 12H), 7.17 (m, 8H), 7.06 (m, 4H), 6.26 (br s, 2H), 5.51 (br s, 2H), 1.34 (s, 18H); ^{13}C NMR (100 MHz, DMSO-d_6/$CDCl_3$, 10:1) ppm 157.3, 147.5, 146.9, 142.4, 141.3, 129.2 (2C), 127.6, 127.5, 127.1, 126.3, 125.6, 122.7, 122.0, 117.1, 115.9, 90.8, 59.7, 34.5, 31.4; HRMS (EI): Exact mass calcd for $C_{52}H_{53}N_6$ $[M+H]^+$ 761.4332, found 761.4331. MTK-4-186.

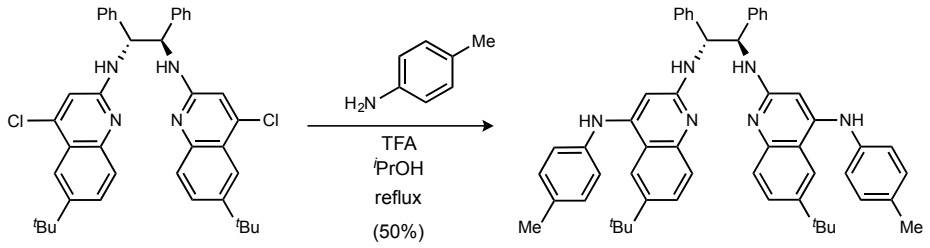

N2,N2'-((1R,2R)-1,2-Diphenylethane-1,2-diyl)bis(6-(*tert*-butyl)-N4-(p-tolyl)quinoline-2,4-diamine) (126d).

To a 10 mL microwave vial with a stir bar was added 4-Cl quinoline (1.00 g, 1.54 mmol), isopropanol (6 mL), trifluoroacetic acid (295 µL, 3.85 mmol) and *p*-toluidine (662 mg, 6.18 mmol). The vial was sealed and heated at 110 °C for 18 hours, and then removed from the oil bath. The mixture was concentrated by rotary evaporator, and then dissolved in dichloromethane (20 mL) and transferred to a separatory funnel. The organic layer was washed with 2 M HCl (20 mL), and the aqueous layer was extracted with dichloromethane. The combined organic layers were washed with 6 M NaOH (20 mL) by vigorous stirring for 2 h, and the aqueous layer was extracted with dichloromethane. The organic layers were combined, dried with Mg_2SO_4, filtered, and concentrated to an off-white solid. The solid was recrystallized from CH_2Cl_2/heptanes to yield colorless crystals (610 mg, 50%). Note that prior to use of this highly crystalline material, it must be dissolved in hot toluene or ethyl acetate and then be reconcentrated to enhance solubility. Mp 175-178 °C; $[\alpha]_D^{20}$ +58.7 (*c* 1.02, $CHCl_3$); R_f = 0.39 (20% MeOH/CH_2Cl_2); IR (film) 3249, 3055, 2958, 1589, 1498,

1260 cm^{-1}; ^{1}H NMR (400 MHz, DMSO-d_6/$CDCl_3$, 10:1) δ 8.31 (br s, 2H), 7.92 (br s, 2H), 7.46 (d, J = 8.8 Hz, 2H), 7.32-7.27 (m, 6H), 7.18-7.05 (m, 16H), 6.12 (br s, 2H), 5.52 (br s, 2H), 2.32 (s, 6H), 1.34 (s, 18H); ^{13}C NMR (100 MHz, DMSO-d_6/$CDCl_3$, 10:1) ppm 157.3, 147.5, 146.9, 142.4, 141.3, 129.2, 127.6, 127.5, 127.1, 126.3, 125.6, 122.7, 122.0, 117.1, 115.9, 90.8, 59.7, 34.5, 31.4; HRMS (EI): Exact mass calcd for $C_{54}H_{57}N_6$ $[M+H]^+$ 789.4645, found 789.4684. MTK-4-232.

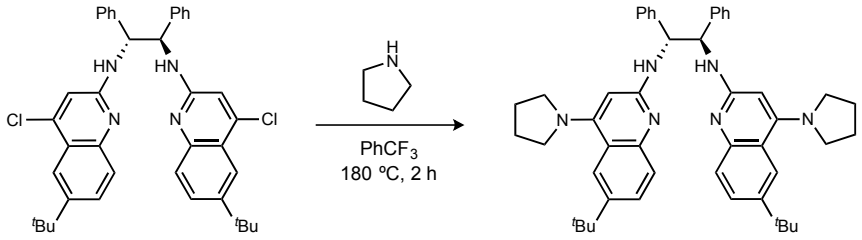

(1*R*,2*R*)-*N*1,*N*2-bis(6-(*tert*-Butyl)-4-(pyrrolidin-1-yl)quinolin-2-yl)-1,2-diphenylethane-1,2-diamine (14i).

A 2-5 mL microwave vial equipped with a stir bar was charged with 4-Cl, 6-^{t}BuStilb-BAM (100 mg, 150 µmol), pyrrolidine (60 µL, 770 µmol), and trifluoromethylbenzene (1.5 mL). The vial was sealed, and this solution was heated with stirring at 180 °C in the microwave for 2 h. The reaction mixture was diluted with dichloromethane and transferred to a separatory funnel, and washed with 4 M NaOH (50 mL). The resulting organic layer was dispensed into a 125 mL Erlenmeyer flask and dried (Mg_2SO_4). The solution was removed in vacuo to provide a light brown powder (101 mg, 92%). Mp 261-263 °C; $[\alpha]_D^{20}$ +26.8 (*c* 1.00, $CHCl_3$); R_f = 0.34 (10% MeOH/CH_2Cl_2); IR (film) 3239, 2959, 2866, 1582, 1438, 1361, 1277 cm^{-1}; ^{1}H NMR (400 MHz, DMSO-d_6) δ 7.82 (br d, J = 1.3 Hz, 2H), 7.46-7.35 (m, 10H), 7.18 (d, J = 7.4 Hz, 2H), 7.16 (d, J = 7.4 Hz, 2H), 7.07 (dd, J = 7.2, 7.2 Hz, 2H), 5.84 (br s, 2H), 5.59 (br s, 2H), 3.46-3.41 (br m, 4H), 3.36-3.31 (br m, 4H), 1.88 (br s, 8H), 1.30 (s, 18H); ^{13}C NMR (100 MHz, DMSO-d_6) ppm 157.1, 153.0, 142.4, 141.2, 127.7 (3C), 126.5, 126.4, 125.6, 120.0, 117.3, 92.3, 60.1, 51.5, 34.1, 31.3, 25.3; HRMS (EI): Exact mass calcd for $C_{48}H_{57}N_6$ $[M+H]^+$ 717.4639, found 717.4638. MTK-6-130.

Preparation of Cyclopentene Carboxylic Acids

Known compounds were synthesized according to published procedures.

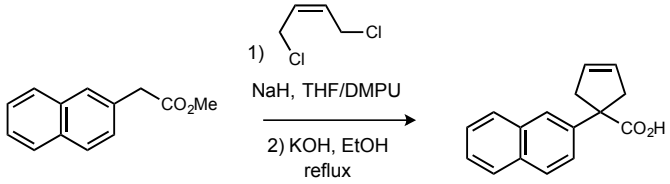

1-(Naphthalen-2-yl)cyclopent-3-ene-1-carboxylic acid (107b).

To a flame-dried round-bottom flask under nitrogen atmosphere was added NaH (60 mg, 2.5 mmol, 2.0 eq), THF (2.5 mL) and DMPU (600 µL). The mixture was cooled to 0 ºC while stirring, upon which the methyl ester (250 mg, 1.25 mmol, 1 eq) was added. The mixture was warmed to room temperature for 10 minutes before recooling to 0 ºC. Dichlorobutene (160 µL, 1.50 mmol, 1.2 eq) was then added dropwise, and the reaction was stirred at room temperature overnight. The reaction was quenched by careful addition of of water (5 mL). The layers were separated, and the aqueous layer was extracted with ethyl acetate. The organic layers were combined, dried, filtered and concentrated to an oil. The oil was purified by flash column chromatography (SiO_2, 10% ethyl acetate in hexanes) to yield an inseparable mixture of the methyl ester cyclopentene and cyclopropane (~10:1 ratio) as a colorless oil (270mg, 85%). This mixture was then dissolved in EtOH (11 mL), combined with KOH (300 mg, 5.29 mmol, 5 eq) and stirred under reflux overnight. The reaction was cooled to room temperature and acidified to pH 2 with 2 M H_2SO_4. The aqueous layer was extracted with ethyl acetate, and the combined organic layers were dried, filtered, and concentrated to a colorless solid. The solid was recrystallized from CH_2Cl_2/hexanes to yield the pure cyclopentene carboxylic acid as colorless crystals (180 mg, 60%, two steps). Mp 162-164 °C; R_f = 0.31 (25% EtOAc/hexanes); IR (film) 3500-2500, 3418, 3061, 2902, 1690, 1272 cm^{-1}; ^1H NMR (400 MHz, $CDCl_3$) δ7.81-7.28 (m, 4H), 7.50-7.43 (m, 3H), 5.80 (s, 2H), 3.52 (d, J = 15.2 Hz, 2H), 2.88 (d, J = 14.6 Hz, 2H), no CO_2H observed; ^{13}C NMR (100 MHz, $CDCl_3$) ppm 181.9, 140.2, 133.3, 132.5, 129.3, 128.3, 128.2, 127.6, 126.3, 126.1, 125.51, 125.47, 58.5, 42.6; HRMS (CI): Exact mass calcd for $C_{16}H_{14}O_2$ $[M]^+$ 238.0988, found 238.0977. MTK-4-018.

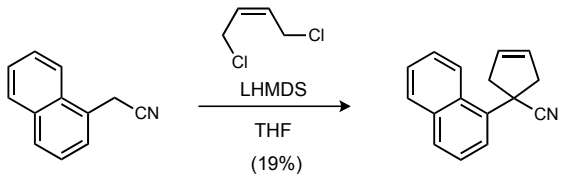

1-(Naphthalen-1-yl)cyclopent-3-ene-1-carbonitrile (S3).

To a flame-dried round-bottom flask under nitrogen atmosphere was added LHMDS (4.51 g, 27.0 mmol, 3.5 eq) and THF (40 mL). The mixture was cooled to 0 ºC while stirring, at which time the nitrile (1.29 g, 7.70 mmol, 1 eq) was added. The mixture was warmed to room temperature for 10 minutes before recooling to 0 ºC. Dichlorobutene (810 µL, 7.70 mmol, 1 eq) was then added dropwise, and the reaction was stirred at room temperature overnight. The reaction was quenched by addition of water (5 mL) and ethyl acetate (5 mL). The layers were separated, and the aqueous layers were extracted with ethyl acetate.

The organic layers were combined, dried, filtered and concentrated to an oil. The oil was purified by flash column chromatography (SiO_2, 5% ethyl acetate in hexanes) to yield the pure cyclopentene nitrile as a yellow oil (325 mg, 19%). R_f = 0.58 (25% EtOAc/hexanes); IR (film) 3059, 2934, 2868, 2234, 1601, 1512, 1448, 1252 cm^{-1}; ^1H NMR (400 MHz, $CDCl_3$) δ7.96-7.91 (m, 2H), 7.84 (d, J = 7.7 Hz, 2H), 7.55-7.51 (m, 2H), 7.45 (dd, J = 7.8, 7.8 Hz, 1H), 5.96 (s, 2H), 3.40 (m, 4H), no CO_2H observed; ^{13}C NMR (100 MHz, $CDCl_3$) ppm 134.9, 134.3, 129.9, 129.5, 128.8 (2C), 126.4, 125.9, 125.6, 125.2, 125.0, 123.8, 47.4, 45.9; HRMS (CI): Exact mass calcd for $C_{16}H_{13}N$ $[M]^+$ 219.1043, found 219.1042. MTK-4-084.

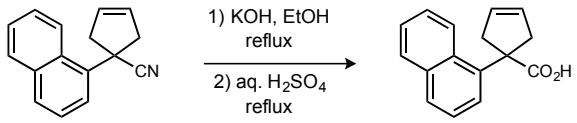

1-(Naphthalen-1-yl)cyclopent-3-ene-1-carboxylic acid (107c).

To a round-bottom flask was added cyclopentene nitrile (325 mg, 1.50 mmol, 1 eq), EtOH (15 mL) and KOH (270 mg, 4.70 mmol, 3.2 eq). The reaction was stirred at reflux for three days, and then cooled to room temperature. Water (5 mL) and ethyl acetate (5 mL) were added. The layers were separated, and the aqueous layer was extracted with ethyl acetate. The organic layers were combined, dried, filtered and concentrated to provide the cyclopentene amide (204 mg, 58%). The amide material was refluxed with EtOH (1 mL) and 6 M HCl (1 mL) overnight, after which the reaction was cooled to room temperature, basified with aq. KOH, and diluted with dichloromethane (10 mL). The layers were separated, and the aqueous layer was acidified with 2 M H_2SO_4 and extracted with DCM. The combined organic layers were dried, filtered and concentrated to yield the carboxylic acid product as a colorless solid (57 mg, 16%). Mp 141-143°C; R_f = 0.32 (25% EtOAc/hexanes); IR (film) 3426, 3040, 2926, 2859, 1699, 1262 cm^{-1}; ^1H NMR (400 MHz, $CDCl_3$) δ7.96-7.91 (m, 2H), 7.84 (d, J = 7.7 Hz, 2H), 7.55-7.51 (m, 2H), 7.45 (t, J = 7.8 Hz, 2H), 5.96 (s, 2H), 3.40 (m, 4H); ^{13}C NMR (100 MHz, $CDCl_3$) ppm 182.0, 138.5, 134.7, 131.5, 129.5, 128.51, 128.47, 126.3, 125.5, 125.2, 124.5, 124.1, 57.2, 44.1; HRMS (CI): Exact mass calcd for $C_{16}H_{14}O_2$ $[M]^+$ 238.0988, found 238.0983. MTK-4-183.

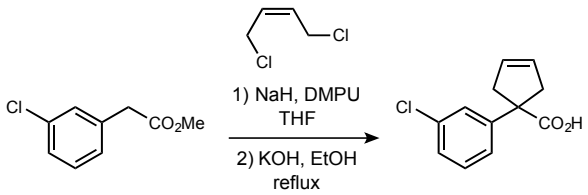

1-(3-Chlorophenyl)cyclopent-3-ene-1-carboxylic acid (107d).

To a flame-dried round-bottom flask under nitrogen atmosphere was added NaH (485 mg, 20.2 mmol, 2.1 eq), THF (20 mL) and DMPU (5 mL). The mixture was cooled to 0 ºC while stirring, upon which the methyl ester (1.50 mL, 10.0 mmol, 1 eq) was added. The mixture was warmed to room temperature for 10 minutes then cooled to 0 ºC again. Dichlorobutene (1.26 mL, 12.0 mmol, 1.2 eq) was then added dropwise, and the reaction was stirred at room temperature for three days. The reaction was quenched by addition of water (5 mL). The layers were separated, and the aqueous layer was extracted with ethyl acetate. The organic layers were combined, dried, filtered and concentrated to an oil. The oil was purified by flash column chromatography (SiO_2, 10% ethyl acetate in hexanes) to yield an inseparable mixture of the methyl ester cyclopentene and cyclopropane (~10:1 ratio) as a colorless oil (1.54 g). This mixture was then dissolved in EtOH (15 mL), combined with KOH (1.70 g, 29.6 mmol, 5 eq) and stirred under reflux overnight. The reaction was cooled to room temperature and acidified to pH 2 with 2 M HCl. The aqueous layer was extracted with ethyl acetate, and the combined organic layers were dried, filtered, and concentrated to a colorless solid. The solid was recrystallized from DCM/hexanes to yield the pure cyclopentene carboxylic acid as pale yellow crystals (565 mg, 13% two steps). Mp 124-128 °C; R_f = 0.41 (20% EtOAc/hexanes); IR (film) 3300-2500, 3066, 2975, 2891, 2651, 1691, 1586, 1473, 1407, 1288, 1199 cm^{-1}; ^1H NMR (400 MHz, $CDCl_3$) δ7.34 (s, 1H), 7.24 (br s, 3H), 5.76 (s, 2H), 3.40 (d, 15.2 Hz, 2H), 2.73 (d, 15.2 Hz, 2H), no CO_2H observed; ^{13}C NMR (100 MHz, $CDCl_3$) ppm 181.7, 144.8, 134.5, 129.8 (2C), 129.2, 127.4, 125.4, 58.3, 42.5; HRMS (CI): Exact mass calcd for $C_{12}H_{11}ClO_2$ $[M]^+$ 222.0442, found 222.0447. SS224.

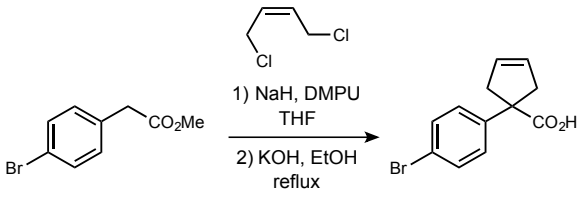

1-(4-Bromophenyl)cyclopent-3-ene-1-carboxylic acid (107e).

To a flame-dried round-bottom flask under nitrogen atmosphere was added NaH (330 mg, 13.8 mmol, 2.1 eq), THF (13 mL) and DMPU (3 mL). The mixture was cooled to 0 ºC while stirring, upon which the methyl ester (1.50 g, 6.55 mmol, 1 eq) was added. The mixture was warmed to room temperature for 10 minutes then cooled to 0 ºC again. Dichlorobutene (830 µL, 7.86 mmol, 1.2 eq) was then added dropwise, and the reaction was stirred at room temperature overnight. The reaction was quenched by addition of water (5 mL). The layers were separated, and the aqueous layer was extracted with ethyl acetate. The organic layers were combined, dried, filtered and concentrated to an oil. The oil was purified by flash column chromatography (SiO_2, 10% ethyl acetate in hexanes) to yield an

inseparable mixture of the methyl ester cyclopentene and cyclopropane (~10:1 ratio) as a colorless oil (1.0 g). This mixture was then dissolved in EtOH (15 mL), combined with KOH (1.00 g, 17.8 mmol, 5 eq) and stirred at reflux temperature (18 hours). The reaction was cooled to room temperature and acidified to pH 2 with 2 M H_2SO_4. The aqueous layer was extracted with ethyl acetate, and the combined organic layers were dried, filtered, and concentrated to a colorless solid. The solid was recrystallized from DCM/hexanes to yield the pure cyclopentene carboxylic acid as colorless crystals (475 mg, 28%, two steps). Mp 169-172 °C; R_f = 0.41 (25% EtOAc/hexanes); IR (film) 3068, 2973, 2884, 1681, 1485, 1399, 1284 cm^{-1}; ^1H NMR (400 MHz, $CDCl_3$) δ7.44 (d, J = 8.6 Hz, 2H), 7.23 (d, J = 8.6 Hz, 2H), 5.76 (s, 2H), 3.40 (d, J = 15.0 Hz, 2H), 2.71 (d, J = 14.7 Hz, 2H), no CO_2H observed; ^{13}C NMR (100 MHz, $CDCl_3$) ppm 181.8, 141.9, 131.7, 129.3, 128.9, 121.3, 58.1, 42.5; HRMS (EI): Exact mass calcd for $C_{12}H_{11}BrO_2$ $[M]^+$ 391.8909, found 391.8906. MTK-5-072.

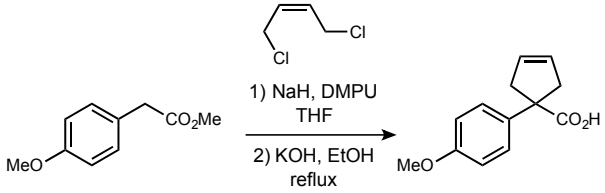

1-(4-Methoxyphenyl)cyclopent-3-ene-1-carboxylic acid (107f).

A 100 mL round-bottom flask with stir bar was flame-dried and backfilled with argon. To the flask was added NaH (484 mg, 20.2 mmol). The flask was equipped with an argon balloon, then DMPU (5.0 mL) and THF (20 mL) were added. The flask was cooled to 0 °C in an ice bath and the ester (1.27 mL, 8.00 mmol) was added dropwise. The flask was warmed to room temperature for 10 minutes, then cooled again to 0 °C. Dichlorobutene (850 µL, 8.00 mmol) was added dropwise, and the flask was removed from the ice bath and stirred for one day. The mixture was quenched with water, the layers were separated, and the aqueous layer was extracted with ethyl acetate. The organic layers were combined, dried, filtered and concentrated to an oil. The oil was purified by flash column chromatography (SiO_2, 10% ethyl acetate in hexanes) to yield an inseparable mixture of the methyl ester cyclopentene and cyclopropane (SiO_2, 5-10% ethyl acetate in hexanes) as a yellow oil (1.26 g). In a 50 mL round-bottomed flask, the ester (630 mg, 2.70 mmol) was dissolved in EtOH (20 mL) before KOH (760 mg, 13.6 mmol) was added. The mixture was stirred for 24 hours at reflux temperature, cooled to room temperature, and acidified to pH 2 with 2 M HCl. The aqueous layer was extracted with CH_2Cl_2, and the combined organic layers were dried, filtered, and concentrated to a colorless solid. The solid was recrystallized in hexanes and DCM to yield a white solid (638 mg, 22%). Mp 117-118 °C, R_f = 0.17 (20% EtOAc/hexanes); IR (film) 3500-2800, 3060, 2951, 1699, 1512, 1250, 1181 cm^{-1}; ^1H NMR

(400 MHz, $CDCl_3$) δ7.28 (d, J = 8.8 Hz, 2H), 6.85 (d, J = 8.8 Hz, 2H), 5.77 (s, 2H), 3.79 (s, 3H), 3.40 (d, J = 14.8 Hz, 2H), 2.74 (d, J = 14.8 Hz, 2H), CO_2H not observed; ^{13}C NMR (100 MHz, $CDCl_3$) ppm 180.7, 158.6, 134.8, 129.4, 128.2, 114.0, 57.7, 55.4, 42.6; HRMS (CI): Exact mass calcd for $C_{13}H_{14}O_3$ $[M]^+$ 218.0943, found 218.0941. SS238.

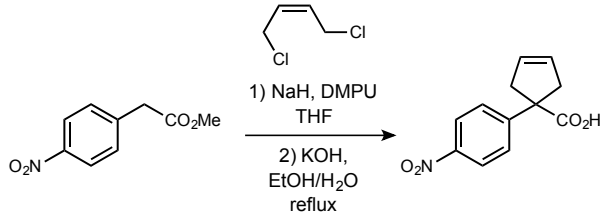

1-(4-Nitrophenyl)cyclopent-3-ene-1-carboxylic acid (107g).

A 100 mL round-bottom flask with stir bar was flame-dried and backfilled with argon. To the flask was added NaH (484 mg, 20.2 mmol, 2.1 eq). The flask was equipped with an argon balloon, then DMPU (5.0 mL) and THF (20 mL) were added. The flask was cooled to 0°C in an ice bath and the ester (1.95 g, 10.0 mmol) was added dropwise. The flask was warmed to room temperature for 10 minutes, then cooled again to 0 °C. Dichlorobutene (1.26 mL, 12.0 mmol, 1.2 eq) was next added dropwise, then the flask was removed from the ice bath and stirred for one day. The mixture was quenched with water, the layers were separated, and the aqueous layer was extracted with ethyl acetate. The organic layers were combined, dried, filtered and concentrated to an oil. The oil was purified by flash column chromatography (SiO_2, 10% ethyl acetate in hexanes) to yield an inseparable mixture of the methyl ester cyclopentene and cyclopropane (SiO_2, 5-10% ethyl acetate in hexanes) to yield a yellow oil (2.09 g. In a 50 mL round-bottomed flask, the ester (1.00 g, 4.10 mmol) was dissolved in EtOH (10 mL) and H_2O (10 mL) before KOH (1.16 g, 20.6 mmol) was added and stirred for 30 minutes at reflux. The reaction was cooled to room temperature and acidified to pH 2 with 2 M HCl. The aqueous layer was extracted with CH_2Cl_2, and the combined organic layers were dried, filtered, and concentrated to a colorless solid. The solid was recrystallized in hexanes and DCM to yield a yellow solid (216 mg, 23%). Mp 145-150 ºC, R_f = 0.03 (20% EtOAc/hexanes); IR (film) 3600-2600, 3412, 3071, 2960, 1693, 1596, 1515, 1443, 1405, 1351, 1289, 1231, 1110 cm^{-1}; ^1H NMR (400 MHz, $CDCl_3$) δ8.18 (d, J = 9.2 Hz, 2H), 7.52 (d, J = 8.8 Hz, 2H), 5.79 (s, 2H), 3.46 (d, J = 14.8 Hz, 2H), 2.78 (d, J = 14.8 Hz, 2H), no CO_2H observed; ^{13}C NMR (100 MHz, $CDCl_3$) ppm 179.6, 150.2, 147.1, 129.1, 128.0, 123.8, 58.4, 42.8; HRMS (CI): Exact mass calcd for $C_{12}H_{12}O_4N$ $[M+H]^+$ 234.0766, found 234.0758. SS255.

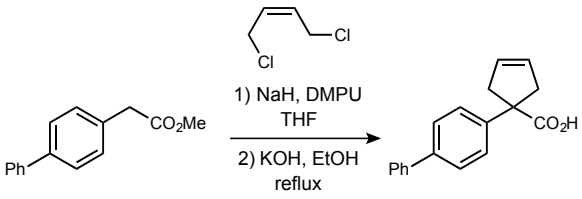

1-([1,1'-Biphenyl]-4-yl)cyclopent-3-ene-1-carboxylic acid (107h).

To a flame-dried round-bottom flask under nitrogen atmosphere was added NaH (170 mg, 7.05 mmol), THF (7 mL) and DMPU (1.5 mL). The mixture was cooled to 0 ºC while stirring, to which the methyl ester (760 mg, 3.36 mmol) was added. The mixture was warmed to room temperature for 10 minutes then cooled to 0 ºC again. Dichlorobutene (430 µL, 4.0 mmol) was then added dropwise, and the reaction was stirred at room temperature overnight. The reaction was quenched by the addition of water (5 mL). The layers were separated, and the aqueous layer was extracted with EtOAc. The organic layers were combined, dried, filtered and concentrated to an oil. The oil was purified by flash column chromatography (SiO_2, 10% ethyl acetate in hexanes) to yield an inseparable mixture of the methyl ester cyclopentene and cyclopropane (~10:1 ratio) as a colorless oil (590 mg). This mixture was then dissolved in EtOH (15 mL), combined with KOH (595 mg, 10.6 mmol, 5 eq) and stirred at reflux temperature overnight. The reaction was cooled to room temperature and acidified to pH 2 with 2 M aq H_2SO_4. The aqueous layer was extracted with ethyl acetate, and the combined organic layers were dried, filtered, and concentrated to a colorless solid. The solid was recrystallized from DCM/hexanes to yield the pure cyclopentene carboxylic acid as gray crystals (242 mg, 43% two steps). Mp 188-190 °C; R_f = 0.37 (25% EtOAc/hexanes); IR (film) 3400-2800, 3271, 3068, 2924, 2858, 1690, 1277 cm^{-1}; ^1H NMR (400 MHz, DMSO-d_6) δ7.66-7.61 (m, 4H), 7.48-7.34 (m, 5H), 5.79 (s, 2H), 3.33 (d, J = 14.8 Hz, 2H), 2.67 (d, J = 14.8 Hz, 2H), no CO_2H observed; ^{13}C NMR (100 MHz, DMSO-d_6) ppm 176.7, 143.0, 139.8, 138.4, 129.2, 128.9, 127.4, 127.1, 126.60, 126.58, 57.6, 42.3; HRMS (CI): Exact mass calcd for $C_{18}H_{17}O_2$ $[M+H]^+$ 265.1229, found 265.1229. MTK-5-097.

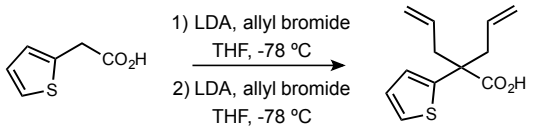

2-Allyl-2-(thiophen-2-yl)pent-4-enoic acid (S5).

To a flame-dried round-bottom flask under nitrogen atmosphere was added distilled diisopropyl amine (2.20 mL, 15.5 mmol) and THF (30 mL). The solution was cooled to -78 ºC and treated with ^{n}BuLi (7.4 mL, 15.0 mmol) added dropwise, before stirring for 15

minutes. The carboxylic acid (1.00 g, 7.03 mmol) was added, and the reaction was removed from the ice bath and stirred at room temperature for 10 minutes. The reaction was placed in an ice bath and allyl bromide (670 µL, 7.70 mmol) was added. The reaction was removed from the ice bath and stirred at room temperature for 4 hours. To the reaction was added water (5 mL) and Et_2O (20 mL). The organic and aqueous layers were separated, and the aqueous layer was acidified to pH 1 by 2 M H_2SO_4. This aqueous solution was extracted by Et_2O. The combined organic layers were dried, filtered and concentrated to an oil. This oil was then alkylated a second time using the same procedure as above, and was purified by flash column chromatography (SiO_2, 50% ethyl acetate in hexanes) to yield the product as a white solid (380 mg, 24%). Mp 89-91 ºC; R_f = 0.47 (50% EtOAc/hexanes); IR 3300-2500, 3077, 2971, 2914, 2668, 1701, 1283, 1235 (film) cm^{-1}; ^1H NMR (400 MHz, $CDCl_3$) δ7.25 (dd, J = 5.0, 1.3 Hz, 1H), 7.01-6.97 (m, 2H), 5.64 (dddd, J = 17.2, 10.2, 7.1, 7.1 Hz, 2H), 5.16-5.09 (m, 4H), 2.88 (dd, J = 14.0, 7.4 Hz, 2H), 2.80 (dd, J = 14.0, 7.4 Hz, 2H), no CO_2H observed; ^{13}C NMR (100 MHz, $CDCl_3$) ppm 178.6, 145.2, 132.8, 126.8, 125.2, 124.8, 119.4, 51.7, 40.4; HRMS (EI): Exact mass calcd for $C_{12}H_{14}O_2S$ $[M]^+$ 222.0715, found 222.0705. MTK-5-021.

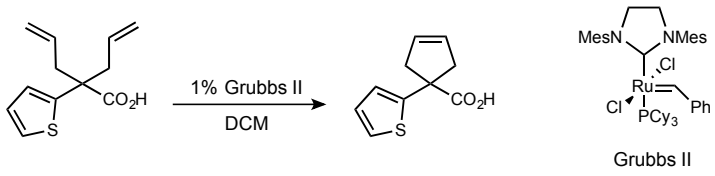

1-(Thiophen-2-yl)cyclopent-3-ene-1-carboxylic acid (107i).

To a flame-dried round-bottom flask under nitrogen atmosphere was added diene (200 mg, 900 µmol), CH_2Cl_2 (9 mL) and Grubbs II[ii] (8 mg, 10 µmol), and the solution was stirred for 24 h at room temperature. The solution was loaded onto a silica plug, flushed with ethyl acetate, and concentrated to a solid. This solid was purified by flash column chromatography (SiO_2, 15% ethyl acetate in hexanes) to yield the product as a white solid (150 mg, 87%). Mp 118-121 ºC; R_f = 0.19 (25% EtOAc/hexanes); IR 3200-2500, 3068, 2962, 2861, 1649, 1545, 1693, 1281, 1214 (film) cm^{-1}; ^1H NMR (400 MHz, $CDCl_3$) δ7.18 (dd, J = 5.1, 1.2 Hz, 1H), 7.01 (dd, J = 3.6, 1.2 Hz, 1H), 6.94 (dd, J = 5.1, 3.6 Hz, 1H), 5.74 (s, 2H), 3.40 (d, J = 14.7 Hz, 2H), 2.88 (d, J = 14.6 Hz, 2H), no CO_2H observed; ^{13}C NMR (100 MHz, $CDCl_3$) ppm 180.5, 147.0, 129.0, 126.9, 125.0, 124.3, 55.3, 44.7; HRMS (EI): Exact mass calcd for $C_{10}H_{10}O_2S$ $[M]^+$ 194.0402, found 194.0393. MTK-5-022.

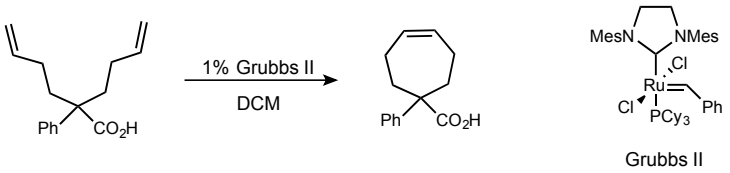

1-Phenylcyclohept-4-ene-1-carboxylic acid (128).

To a flame-dried round-bottom flask under nitrogen atmosphere was added diene (100 mg, 410 µmol), CH_2Cl_2 (5 mL) and Grubbs II[ii] (3 mg, 4 µmol), and the solution was stirred for 24 h at room temperature. The solution was loaded onto a silica plug, flushed with ethyl acetate, and concentrated to a solid. This solid was purified by flash column chromatography (SiO_2, 25% ethyl acetate in hexanes) to yield the product as an off-white solid (89 mg, 99%). Mp 109-111 ºC; R_f = 0.52 (75% EtOAc/hexanes); IR (film) 3200-2500, 3017, 2920, 2848, 1689, 1444, 1299, 1267 cm^{-1}; ^1H NMR (400 MHz, $CDCl_3$) δ 7.18 (dd, J = 5.1, 1.2 Hz, 1H), 7.01 (dd, J = 3.6, 1.2 Hz, 1H), 6.94 (dd, J = 5.1, 3.6 Hz, 1H), 5.74 (s, 2H), 3.40 (d, J = 14.7 Hz, 2H), 2.88 (d, J = 14.6 Hz, 2H), no CO_2H observed; ^{13}C NMR (100 MHz, $CDCl_3$) ppm 180.5, 147.0, 129.0, 126.9, 125.0, 124.3, 55.3, 44.7; HRMS (EI): Exact mass calcd for $C_{10}H_{10}O_2S$ $[M]^+$ 217.1223, found 217.1233. MTK-4-284.

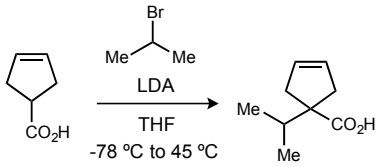

1-Isopropylcyclopent-3-ene-1-carboxylic acid (107j).

To a flame-dried round-bottom flask under nitrogen atmosphere was added diisopropyl amine (1.60 mL, 11.5 mmol) and THF (8 mL), and then cooled to -78 ºC. ^{n}BuLi (5.30 mL, 11.0 mmol, 2.07 M in hexanes) was added dropwise. The solution was warmed to 0 ºC for 10 min and then recooled to -78 ºC. The cyclopentene carboxylic acid (560 mg, 5.00 mmol) was then added dropwise and allowed to stir for 10 minutes. 2-Bromopropane (700 µL, 7.50 mmol) was added dropwise and the reaction was allowed to warm to room temperature and then stirred at 45 ºC for 12 hours. The reaction was quenched by addition of 5 mL of water and 5 mL Et_2O. The layers were separated and the aqueous layer was acidified by addition of 2M H_2SO_4, and then extracted with Et_2O. The organic extracts were combined, dried, filtered and concentrated to an oil. The oil was purified by flash column chromatography (SiO_2, 10% ethyl acetate in hexanes) to yield a colorless oil (235 mg, 30%). R_f = 0.52 (25% EtOAc/hexanes); IR (film) 3400-2600, 2968, 2924, 1690 cm^{-1}; ^1H NMR (400 MHz, $CDCl_3$) δ 5.59 (s, 2H), 2.88 (d, J = 14.8 Hz, 2H), 2.36 (d, J = 14.7 Hz, 2H), 2.12 (sept, J = 6.8 Hz, 1H), 0.88 (d, J = 6.8 Hz, 6H), no CO_2H observed; ^{13}C NMR (100 MHz,

$CDCl_3$) ppm 184.7, 128.9, 56.7, 39.4, 35.0, 18.0; HRMS (CI): Exact mass calcd for $C_9H_{14}O_2$ $[M]^+$ 154.0988, found 154.0987. MTK-5-042.

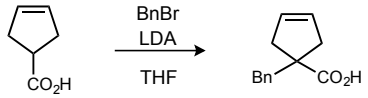

1-Benzylcyclopent-3-ene-1-carboxylic acid (107k).

To a flame-dried round-bottom flask under nitrogen atmosphere was added diisopropyl amine (1.40 mL, 6.96 mmol) and THF (23 mL), and then cooled to -78 ºC. ^{n}BuLi (2.80 mL, 6.15 mmol, 2.20 M in hexanes) was added dropwise. The solution was warmed to 0 ºC for 10 minutes and then recooled to -78 ºC. The cyclopentene carboxylic acid (300 mg, 2.68 mmol, 1 eq) was then added dropwise as a solution in THF (2 mL) and allowed to stir for 10 minutes. Benzyl bromide (480 µL, 4.01 mmol, 1.5 eq) was added dropwise and the reaction was allowed to stir at room temperature overnight. The reaction was quenched by addition of water (5 mL) and Et_2O (5 mL). The layers were separated and the aqueous layer was acidified by the addition of 2 M H_2SO_4, and then extracted with Et_2O. The organic extracts were combined, dried, filtered and concentrated to an oil. The oil was purified by flash column chromatography (SiO_2, 10% ethyl acetate in hexanes) to yield a yellow oil (50 mg, 17%). R_f= 0.35 (25% EtOAc/hexanes); IR (film) 3600-2400, 3032, 2925, 2608, 1699, 1444, 1412, 1282, 1224 cm^{-1}; ^{1}H NMR (400 MHz, $CDCl_3$) δ 7.33-7.23 (m, 5H), 5.69 (s, 2H), 3.10 (s, 2H), 2.91 (d, J = 15.2 Hz, 2H), 2.52 (d, J = 15.0 Hz, 2H), no CO_2H observed; ^{13}C NMR (100 MHz, $CDCl_3$) ppm 183.8, 138.0, 129.9, 128.6, 128.3, 126.8, 54.0, 44.0, 41.8; HRMS (CI): Exact mass calcd for $C_{13}H_{14}O_2$ $[M]^+$ 202.0988, found 202.0992. MTK-3-245.

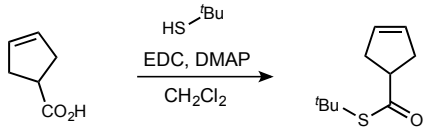

***S*-(*tert*-Butyl) cyclopent-3-ene-1-carbothioate (S6).**

To a round-bottom flask under nitrogen atmosphere was added carboxylic acid (500 µL, 4.8 mmol), DCM (20 mL), EDC (1.11 g, 5.81 mmol), DMAP (710 mg, 5.81 mmol) and stirred at room temperature for 5 minutes. Then *tert*-butyl thiol (650 µL, 5.8 mmol) was added, and the reaction was stirred for 18 hours. The reaction was quenched by the addition of 1 M aq HCl (10 mL). The organic and aqueous layers were separated, and the aqueous layer was further extracted by DCM. The combined organic layers were dried, filtered, and concentrated to an oil. The oil was purified by flash column chromatography (SiO_2, 100%

hexanes) to yield the product as an oil (670 mg, 75%). R_f = 0.56 (100% hexanes); IR (film) 3061, 2955, 2862, 1681, 1453, 1168, 1017 cm^{-1}; ^1H NMR (400 MHz, $CDCl_3$) δ5.64 (s, 2H), 3.26 (tt, J = 6.8, 6.7 Hz, 1H), 2.69-2.55 (m, 4H), 1.47 (s, 9H); ^{13}C NMR (100 MHz, $CDCl_3$) 203.3, 128.9, 51.1, 47.9, 36.9, 30.0 ppm; HRMS (TIC): Exact mass calcd for $C_{10}H_{17}OS$ $[M+H]^+$ 185.0995, found 185.0995. MTK-5-075

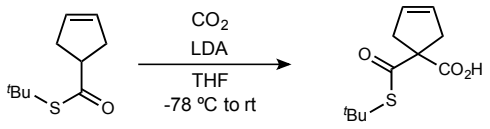

1-((*tert*-Butylthio)carbonyl)cyclopent-3-ene-1-carboxylic acid (107n).

To a flame-dried round-bottom flask under nitrogen atmosphere was added distilled diisopropyl amine (310 µL, 2.2 mmol) and THF (10 mL) and stirred in a dry ice bath for 15 minutes. Then ^{n}BuLi (1.0 mL, 2.1 mmol) was added dropwise and the solution was stirred for 15 minutes. The thioester (370 mg, 2.00 mmol) was added dropwise, and the nitrogen line was exchanged for a balloon of CO_2. The reaction was allowed to warm to room temperature and stirred for 18 hours. To the reaction was added water (5 mL) and Et_2O (10 mL). The organic and aqueous layers were separated, and the aqueous layer was acidified to pH 1 by 2 M H_2SO_4. This aqueous solution was extracted with Et_2O. The combined organic layers were dried, filtered, and concentrated to an oil. The oil was purified by flash column chromatography (SiO_2, 50% ethyl acetate in hexanes) to g the product as a white solid (70 mg, 16%). Mp 126-128 ºC; R_f = 0.26 (75% EtOAc/hexanes); IR (film) 3200-2800, 3071, 2963, 2919, 1675, 1404, 1281, 1090 cm^{-1}; ^1H NMR (400 MHz, $CDCl_3$) δ5.61 (s, 2H), 3.07 (s, 4H), 1.47 (s, 9H), no CO_2H observed; ^{13}C NMR (100 MHz, $CDCl_3$) ppm 198.8, 78.1, 128.0, 67.5, 49.0, 41.0, 29.9; HRMS (CI): Exact mass calcd for $C_{11}H_{17}O_2S$ $[M+H]^+$ 229.0898, found 229.0898. MTK-5-077

Enantioselective Iodobicyclization

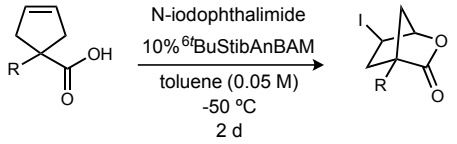

General Procedure for Enantioselective Iodobicyclization

To a 0.5-2 mL microwave vial with stir bar is added carboxylic acid (100 µmol), ^{6t}BuStilb(^{p}MeAn)BAM **3a** (7.9 mg, 10 µmol) and toluene (2 mL, 0.05 M). The solution was stirred at -50 ºC for 30 minutes before *N*-iodophthalimide (28.4 mg, 104 µmol) was added and the mixture was stirred for 1 day. The reaction mixture was then quenched by adding

50 mg of 15% $Na_2S_2O_3/SiO_2$, and allowing the slurry to stir for 15 minutes as it warmed to room temperature. The slurry was loaded onto a 15% $Na_2S_2O_3/SiO_2$ plug and flushed with 5 mL of 50% ethyl acetate in hexanes. The eluent was concentrated, and the residue was purified by flash column chromatography (SiO_2, ethyl acetate in hexanes) to yield the product.

General Procedure for Iodobicyclization to Racemic Product

Racemic products were produced using the general procedure with racemic ^{6t}BuStilb(^{p}MeAn)BAM **3a**, which was produced by mixing equal amounts of (*R,R*)-**3a** and (*S,S*)-**3a**.

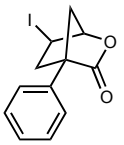

(1*R*,4*R*,6*R*)-6-Iodo-4-phenyl-2-oxabicyclo[2.2.1]heptan-3-one (109a).

This substrate was treated at 1.0 mmol scale. The carboxylic acid (188 mg, 1.0 mmol) was treated according to the general procedure to give the lactone as a yellow solid (207 mg, 66%). The product was determined to be 94% ee by chiral HPLC analysis (Chiralpak IA, 10% ^{i}PrOH/hexanes, 1 mL/min, t_r(e_1 minor) = 7.9 min, t_r(e_2 major) = 11.3 min. Mp 54-56 ^{o}C. $[\alpha]_D^{20}$ 83.6 (*c* 1.37, $CHCl_3$); R_f= 0.36 (10% EtOAc/hexanes); IR (film) 3030, 2927, 2860, 1786 cm^{-1}; ^{1}H NMR (600 MHz, $CDCl_3$) δ7.43-7.34 (m, 5H), 5.05 (d, *J* = 1.2 Hz, 1H), 4.28 (dddd, *J* = 6.6, 4.2, 2.4, 0.6 Hz, 1H), 2.97 (ddd, *J* = 13.8, 7.8, 1.8 Hz, 1H), 2.90 (d, *J* = 10.8, 1H), 2.72 (br dddd, *J* = 10.8, 2.4, 2.4, 2.4 Hz, 1H), 2.62 (dd, *J* = 13.8, 4.2 Hz, 1H); ^{13}C NMR (150.9 MHz, $CDCl_3$) ppm 176.0, 134.0, 128.7, 128.2, 127.2, 83.3, 56.2, 42.9, 41.1, 16.8; Exact mass calcd for $C_{12}H_{12}IO_2$ $[M+H]^+$ 314.9876, found 314.9872. MTK-5-010.

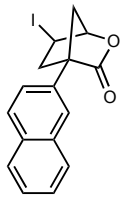

(1*R*,4*R*,6*R*)-6-Iodo-4-(naphthalen-2-yl)-2-oxabicyclo[2.2.1]heptan-3-one (109b).

The carboxylic acid (24 mg, 100 µmol) was treated according to the general procedure to give the lactone as a white solid (28.3 mg, 73%) which was determined to be 90% ee by chiral HPLC analysis (Chiralpak IA, 10% ^{i}PrOH/hexanes, 1 mL/min, t_r(e_1 minor) = 11.2 min, t_r(e_2 major) = 12.4 min). Mp 107-110 ^{o}C. $[\alpha]_D^{20}$ -82.0 (*c* 1.42, $CHCl_3$); R_f=

0.55 (25% EtOAc/hexanes); IR (film) 3053, 2926, 1784, 1098 cm^{-1}; ^1H NMR (400 MHz, $CDCl_3$) δ7.89-7.83 (m, 4H), 7.52-7.47 (m, 3H), 5.09 (d, J = 0.9 Hz, 1H), 4.32 (dddd, J = 7.5, 4.2, 2.0, 0.8 Hz, 1H), 3.07 (ddd, J = 14.2, 7.9, 2.1 Hz, 1H), 2.99 (d, J = 10.9 Hz, 1H), 2.83 (br dddd, J = 10.9, 2.1, 2.1, 2.1 Hz, 1H), 2.71 (dd, J = 14.2, 4.2 Hz, 1H); ^{13}C NMR (100 MHz, $CDCl_3$) ppm 176.16, 133.2, 133.1, 131.6, 128.6, 128.1, 127.8, 126.6, 126.6, 126.3, 125.1, 83.6, 56.5, 43.0, 41.5, 17.0; HRMS (CI): Exact mass calcd for $C_{16}H_{14}IO_2$ $[M+H]^+$ 365.0033, found 365.0032. MTK-5-120.

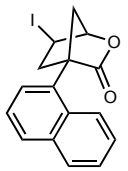

(1*R*,4*R*,6*R*)-6-Iodo-4-(naphthalen-1-yl)-2-oxabicyclo[2.2.1]heptan-3-one (109c).

The carboxylic acid (24 mg, 100 µmol) was treated according to the general procedure to give the lactone as a foam (26.1 mg, 72%) which was determined to be 67% ee by chiral HPLC analysis (Chiralpak IA, 20% EtOH/hexanes, 1 mL/min, t_r(e_1 minor) = 9.1 min, t_r(e_2 major) = 10.7 min). $[\alpha]_D^{20}$ -76.1 (c 1.31, $CHCl_3$); R_f = 0.38 (25% EtOAc/hexanes); IR (film) 2924, 1784, 1082, 779 cm^{-1}; ^1H NMR (400 MHz, $CDCl_3$) δ7.92-7.86 (m, 3H), 7.54-7.49 (m, 2H), 7.47-7.38 (m, 2H), 5.15 (d, J = 1.7 Hz, 1H), 4.38 (dddd, J = 7.6, 4.4, 2.0, 0.7 Hz, 1H), 3.38 (ddd, J = 14.1, 7.8, 2.4 Hz, 1H), 3.19 (br dddd, J = 11.1, 2.2, 2.2, 2.2 Hz, 1H), 2.89 (d, J = 11.1 Hz, 1H), 2.85 (dd, J = 14.2, 4.4 Hz, 1H); ^{13}C NMR (100 MHz, $CDCl_3$) ppm 175.7, 134.6, 131.5, 130.5, 129.9, 129.4, 126.1, 125.9, 125.7, 125.6, 125.1, 83.8, 57.3, 42.7, 42.3, 16.7; HRMS (CI): Exact mass calcd for $C_{16}H_{13}IO_2$ $[M]^+$ 363.9955, found 363.9942. MTK-5-111.

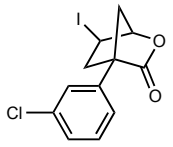

(1*R*,4*R*,6*R*)-4-(3-Chlorophenyl)-6-iodo-2-oxabicyclo[2.2.1]heptan-3-one (109d).

The carboxylic acid (22 mg, 100 µmol) was treated according to the general procedure to give the lactone as a white foam (24.1 mg, 69%) which was determined to be 89% ee by chiral HPLC analysis (Chiralpak IA, 10% ^{i}PrOH/hexanes, 1 mL/min, t_r(e_1 minor) = 8.1 min, t_r(e_2 major) = 11.3 min). $[\alpha]_D^{20}$ -81.9 (c 1.21, $CHCl_3$); R_f = 0.58 (20% EtOAc/hexanes); IR (film) 2923, 1785, 1597, 1477, 1102 cm^{-1}; ^1H NMR (400 MHz, $CDCl_3$) δ7.31 (m, 4H), 5.05 (dd, J = 1.6, 0.8 Hz, 1H), 4.27 (dddd, J = 7.6, 4.3, 2.2, 0.9 Hz, 1H), 2.94 (ddd, J = 14.2, 7.9, 2.2 Hz, 1H), 2.90 (d, J = 10.9 Hz, 1H), 2.70 (br dddd, J = 10.8,

2.1, 2.1, 2.1 Hz, 1H), 2.58 (dd, J = 14.2, 4.3 Hz, 1H); ^{13}C NMR (100 MHz, $CDCl_3$) ppm 175.5, 136.2, 134.8, 130.1, 128.6, 127.6, 125.6, 83.5, 56.0, 43.1, 41.2, 16.5; HRMS (CI): Exact mass calcd for $C_{12}H_{10}ClIO_2$ $[M]^+$ 347.9409, found 347.9394. MTK-5-107, SS225.

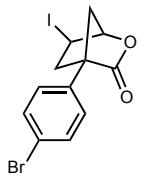

(1*R*,4*R*,6*R*)-1-(4-Bromophenyl)cyclopent-3-ene-1-carboxylic acid (109e).

The carboxylic acid (27 mg, 100 µmol) was treated according to the general procedure to give the lactone as a white solid (29.1 mg, 74%) which was determined to be 89% ee by chiral HPLC analysis (Chiralpak IA, 10% ^{i}PrOH/hexanes, 1 mL/min, t_r(e_1 minor) = 9.6 min, t_r(e_2 major) = 13.0 min). Mp 169-172 ^{o}C; $[\alpha]_D^{20}$ -67.3 (c 1.46, $CHCl_3$); R_f = 0.53 (25% EtOAc/hexanes); IR (film) 3010, 2928, 1772, 1489, 1103 cm^{-1}; ^{1}H NMR (400 MHz, $CDCl_3$) δ7.53 (d, J = 8.5 Hz, 2H), 7.25 (d, J = 8.5 Hz, 2H), 5.04 (d, J = 1.3 Hz, 1H), 4.27 (dddd, J = 7.5, 4.1, 2.1, 0.9 Hz, 1H), 2.94 (ddd, J = 14.2, 7.9, 2.2 Hz, 1H), 2.89 (d, J = 10.9 Hz, 1H), 2.68 (br dddd, J = 10.9, 2.2, 2.2, 2.2 Hz, 1H), 2.57 (dd, J = 14.2, 4.3 Hz, 1H); ^{13}C NMR (100 MHz, $CDCl_3$) ppm 175.6, 133.2, 132.0, 129.0, 122.5, 83.5, 55.9, 43.0, 41.1, 16.6; HRMS (EI): Exact mass calcd for $C_{12}H_{10}BrIO_2$ $[M]^+$ 391.8909, found 391.8906. MTK-5-100.

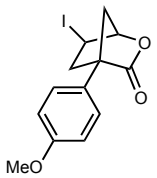

(1*R*,4*R*,6*R*)-6-Iodo-4-(4-methoxyphenyl)-2-oxabicyclo[2.2.1]heptan-3-one (109f).

The carboxylic acid (22 mg, 100 µmol) was treated according to the general procedure to give the lactone as a white solid (22.3 mg, 65%) which was determined to be 91% ee by chiral HPLC analysis (Chiralpak IA, 10% ^{i}PrOH/hexanes, 1 mL/min, t_r(e_1 minor) = 11.8 min, t_r(e_2 major) = 13.4 min). Mp 166-168 ^{o}C; $[\alpha]_D^{20}$ -80.9 (c 1.12, $CHCl_3$); R_f = 0.32 (20% EtOAc/hexanes); IR (film) 2930, 2845, 1785, 113, 1518, 1251, 1100 cm^{-1}; ^{1}H NMR (400 MHz, $CDCl_3$) δ 7.29 (d, J = 8.8 Hz, 2H), 6.92 (d, J = 8.8 Hz, 2H), 5.02 (d, J = 1.2 Hz, 1H), 4.26 (dddd, J = 7.4, 4.2, 2.1, 0.8 Hz, 1H), 3.81 (s, 3H), 2.93 (ddd, J = 15.2, 7.9, 2.2 Hz, 1H), 2.86 (d, J = 10.9 Hz, 1H), 2.68 (br dddd, J = 10.8, 2.2, 2.2, 2.2 Hz, 1H), 2.59 (dd, J = 14.2, 4.2 Hz, 1H); ^{13}C NMR (100 MHz, $CDCl_3$) ppm 176.5, 159.6, 128.4, 126.2,

114.3, 83.5, 55.8, 55.5, 43.1, 41.4, 17.1; HRMS (EI): Exact mass calcd for $C_{12}H_{10}BrIO_2$ $[M]^+$ 391.8909, found 391.8906. MTK-5-099.

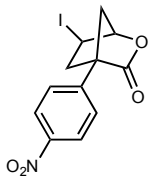

(1*R*,4*R*,6*R*)-6-Iodo-4-(4-nitrophenyl)-2-oxabicyclo[2.2.1]heptan-3-one (109g).

The carboxylic acid (23 mg, 100 µmol) was treated according to the general procedure to give the lactone as a white solid (27.9 mg, 78%) which was determined to be 86% ee by chiral HPLC analysis (Chiralpak IA, 30% ^{i}PrOH/hexanes, 1 mL/min, t_r(e_1 minor) = 12.3 min, t_r(e_2 major) = 18.5 min). Mp 109-111 ^{o}C; $[\alpha]_D^{20}$ -58.4 (*c* 1.40, $CHCl_3$); R_f= 0.27 (20% EtOAc/hexanes); IR (film) 3118, 2923, 2855, 1779, 1512, 1350 cm^{-1}; ^{1}H NMR (400 MHz, $CDCl_3$) δ 8.26 (d, *J* = 8.7 Hz, 2H), 7.58 (d, *J* = 8.7 Hz, 2H), 5.10 (s, 1H), 4.27 (br ddd, *J* = 5.9, 3.6, 1.6 Hz, 1H), 3.04-2.97 (m, 2H), 2.75 (br dddd, *J* = 10.8, 2.2, 2.2, 2.2 Hz, 1H), 2.60 (dd, *J* = 14.1, 4.1 Hz, 1H); ^{13}C NMR (100 MHz, $CDCl_3$) ppm 174.8, 147.9, 141.3, 128.5, 124.0, 83.6, 56.2, 43.3, 41.1, 29.8; HRMS (EI): Exact mass calcd for $C_{12}H_{10}INO_4$ $[M]^+$ 359.9733, found 359.9724. MTK-5-101.

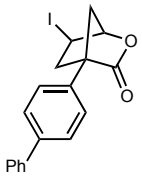

(1*R*,4*R*,6*R*)-4-([1,1'-Biphenyl]-4-yl)-6-iodo-2-oxabicyclo[2.2.1]heptan-3-one (109h).

The carboxylic acid (26 mg, 100 µmol) was treated according to the general procedure to give the lactone as a white solid (21.4 mg, 55%) which was determined to be 94% ee by chiral HPLC analysis (Chiralpak IA, 10% ^{i}PrOH/hexanes, 1 mL/min, t_r(e_1 minor) = 12.5 min, t_r(e_2 major) = 14.9 min). Mp 158-160 ^{o}C; $[\alpha]_D^{20}$ -58.3 (*c* 1.07, $CHCl_3$); R_f= 0.44 (25% EtOAc/hexanes); IR (film) 3030, 2931, 1779, 1318, 1186, 1099, 907 cm^{-1}; ^{1}H NMR (400 MHz, $CDCl_3$) δ7.65-7.58 (m, 4H), 7.47-7.44 (m, 4H), 7.37 (dddd, *J* = 7.4, 7.4, 1.2, 1.2 Hz, 1H), 5.07 (d, *J* = 1.6 Hz, 1H), 4.30 (dddd, *J* = 7.4, 4.1, 2.0, 0.7 Hz, 1H), 3.01 (ddd, *J* = 14.2, 7.9, 2.2 Hz, 1H), 2.93 (d, *J* = 10.8 Hz, 1H), 2.76 (br dddd, *J* = 10.9, 2.1, 2.1, 2.1 Hz, 1H), 2.66 (dd, *J* = 14.2, 4.3 Hz, 1H); ^{13}C NMR (100 MHz, $CDCl_3$) ppm 176.2, 141.3, 140.6, 133.1, 129.0, 127.74, 127.67, 127.6, 127.3, 83.5, 56.2, 43.0, 41.3, 16.9; HRMS (CI): Exact mass calcd for $C_{18}H_{15}IO_2$ $[M]^+$ 390.0117, found 390.0109. MTK-5-103.

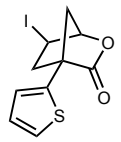

(1*R*,4*S*,6*R*)-6-Iodo-4-(Thiophen-2-yl)-2-oxabicyclo[2.2.1]heptan-3-one (109i).

The carboxylic acid (19 mg, 100 µmol) was treated according to the general procedure to give the lactone as a colorless oil (22.0 mg, 69%). The product was determined to be 92% ee by chiral HPLC analysis (Chiralpak IA, 10% ^{i}PrOH/hexanes, 1 mL/min, t_r(e_1 minor) = 7.2 min, t_r(e_2 major) = 12.4 min). $[\alpha]_D^{20}$ -63.7 (*c* 1.10, $CHCl_3$); R_f = 0.39 (25% EtOAc/hexanes); IR (film) 3103, 2924, 2857, 1758, 1446, 1313, 1187, 1096 cm^{-1}; ^{1}H NMR (400 MHz, $CDCl_3$) δ7.32 (dd, *J* = 5.1, 1.1 Hz, 1H), 7.11 (dd, *J* = 3.6, 1.1 Hz, 1H), 7.04 (dd, *J* = 5.1, 3.6 Hz, 1H), 5.03 (d, *J* = 1.5 Hz, 1H), 4.25 (dddd, *J* = 7.6, 5.4, 2.2, 0.8 Hz, 1H), 2.99-2.93 (m, 2H), 2.70-2.66 (m, 2H); ^{13}C NMR (100 MHz, $CDCl_3$) ppm 175.1, 136.4, 127.2, 126.1, 125.7, 83.9, 54.5, 44.3, 43.5, 16.4; HRMS (EI): Exact mass calcd for $C_{10}H_9IO_2S$ $[M]^+$ 319.9368, found 319.9363. MTK-5-096.

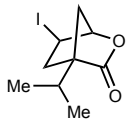

(1R,4R,6R)-6-Iodo-4-isopropyl-2-oxabicyclo[2.2.1]heptan-3-one (109j).

The carboxylic acid (15 mg, 100 µmol) was treated according to the general procedure to give the lactone as a white solid (20.7 mg, 74%) which was determined to be 87% ee by chiral HPLC analysis (Chiralpak IA, 10% ^{i}PrOH/hexanes, 1 mL/min, t_r(e_1 minor) = 4.8 min, t_r(e_2 major) = 6.5 min). Mp 51-53 ^{o}C; $[\alpha]_D^{20}$ -75.1 (*c* 1.04, $CHCl_3$); R_f = 0.65 (25% EtOAc/hexanes); IR (film) 2956, 2925, 2865, 1787 cm^{-1}; ^{1}H NMR (400 MHz, $CDCl_3$) δ4.87 (d, *J* = 1.4 Hz, 1H), 4.13 (dddd, *J* = 7.2, 4.0, 2.1, 0.9 Hz, 1H), 2.43 (ddd, *J* = 14.3, 7.9, 2.0 Hz, 1H), 2.49 (d, *J* = 10.9 Hz, 1H), 2.31 (dd, *J* = 14.3, 4.2 Hz, 1H), 2.18 (br dddd, *J* = 10.8, 2.1, 2.1, 2.1 Hz, 1H), 2.12 (sept, *J* = 6.8 Hz, 1H), 1.04 (d, *J* = 6.9 Hz, 6H); ^{13}C NMR (100 MHz, $CDCl_3$) ppm 177.3, 83.2, 57.2, 38.8, 38.1, 26.5, 18.9, 18.3, 17.7; HRMS (EI): Exact mass calcd for $C_9H_{13}IO_2$ $[M]^+$ 279.9960, found 279.9966. MTK-5-116.

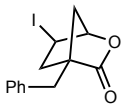

(1*R*,4*R*,6*R*)-4-Benzyl-6-iodo-2-oxabicyclo[2.2.1]heptan-3-one (109k).

The carboxylic acid (20 mg, 100 µmol) was treated according to the general procedure to give the lactone as an oil (21.8 mg, 66%) which was determined to be 87% ee by chiral HPLC analysis (Chiralpak IA, 5% EtOH/hexanes, 1 mL/min, t_r(e_1 minor) = 9.4 min, t_r(e_2 major) = 14.0 min). $[\alpha]_D^{20}$ -93.0 (c 1.09, $CHCl_3$); R_f = 0.47 (25% EtOAc/hexanes); IR (film) 2925, 1785, 1089, 913 cm^{-1}; ^1H NMR (400 MHz, $CDCl_3$) δ 7.33-7.20 (m, 5H), 4.85 (d, J = 1.4 Hz, 1H), 4.10 (dddd, J = 7.2, 5.2, 3.1, 0.9 Hz, 1H), 3.16 (d, J = 14.2 Hz, 1H), 2.92 (d, J = 14.1 Hz, 1H), 2.47 (ddd, J = 14.2, 7.9, 2.2 Hz, 1H), 2.32 (d, J = 11.0 Hz, 1H), 2.19 (dd, J = 14.2, 4.2 Hz, 1H), 2.07 (br dddd, J = 11.0, 2.1, 2.1, 2.1 Hz, 1H); ^{13}C NMR (100 MHz, $CDCl_3$) ppm 177.5, 136.8, 129.9, 128.7, 127.1, 83.6, 54.1, 41.0, 40.1, 34.5, 17.1; HRMS (CI): Exact mass calcd for $C_{13}H_{15}IO_2$ $[M+H]^+$ 329.0033, found 329.0042. MTK-5-105.

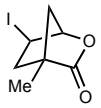

(1*R*,4*R*,6*R*)-6-Iodo-4-methyl-2-oxabicyclo[2.2.1]heptan-3-one (109l).

The carboxylic acid (13 mg, 100 µmol) was treated according to the general procedure to give the lactone as a white solid (16.6 mg, 66%) which was determined to be 86% ee by chiral HPLC analysis (Chiralpak IA, 10% ^{i}PrOH/hexanes, 1 mL/min, t_r(e_1 minor) = 5.6 min, t_r(e_2 major) = 8.5 min). Mp 56-58 °C; $[\alpha]_D^{20}$ -71.6 (c 0.83, $CHCl_3$); R_f = 0.28 (25% EtOAc/hexanes); IR (film) 2927, 2862, 1787 cm^{-1}; ^1H NMR (400 MHz, $CDCl_3$) δ 4.89 (d, J = 1.2 Hz, 1H), 4.12 (dddd, J = 7.5, 4.2, 2.2, 0.8 Hz, 1H), 2.50 (ddd, J = 14.3, 7.9, 2.2 Hz, 1H), 2.49 (d, J = 10.7 Hz, 1H), 2.23 (dd, J = 14.2, 4.2 Hz, 1H), 2.18 (br dddd, J = 10.9, 2.1, 2.1, 2.1 Hz, 1H), 1.37 (s, 3H); ^{13}C NMR (100 MHz, $CDCl_3$) ppm 178.4, 83.9, 49.0, 43.0, 42.6, 17.4, 13.8; HRMS (EI): Exact mass calcd for $C_7H_9IO_2$ $[M]^+$ 251.9647, found 251.9652. MTK-5-108.

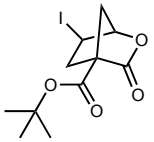

***tert*-Butyl (1*R*,4*S*,6*R*)-6-iodo-3-oxo-2-oxabicyclo[2.2.1]heptane-4-carboxylate (109m).**

The carboxylic acid (21 mg, 100 µmol) was treated according to the general procedure to give the lactone as a white solid (21.7 mg, 64%). The product was determined to be 64% ee by chiral HPLC analysis (Chiralpak IA, 3% ^{i}PrOH/hexanes, 1 mL/min, t_r(e_1 minor) = 7.8 min, t_r(e_2 major) = 8.1 min. Mp 124-127 °C. $[\alpha]_D^{20}$ -35.3 (c 1.09, $CHCl_3$); R_f = 0.31 (25% EtOAc/hexanes); IR (film) 2975, 2923, 1783, 1725, 1337, 1166, 1058, 910 cm^{-1};

^{1}H NMR (400 MHz, $CDCl_3$) δ 4.94 (d, J = 1.3 Hz, 1H), 4.13 (dddd, J = 7.6, 4.3, 2.1, 0.9 Hz, 1H), 2.78 (ddd, J = 14.7, 7.9, 2.0 Hz, 1H), 2.74 (d, J = 10.8 Hz, 1H), 2.66-2.59 (m, 2H), 1.50 (s, 9H); ^{13}C NMR (100 MHz, $CDCl_3$) ppm 172.5, 165.8, 84.1, 83.3, 58.4, 40.2, 38.4, 28.1, 15.8; HRMS (EI): Exact mass calcd for $C_{11}H_{15}IO_4Na$ $[M+Na]^+$ 360.9913, found 360.9925. MTK-5-112.

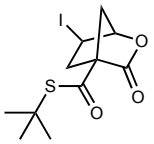

_S_-(_tert_-Butyl)-(1_R_,4_S_,6_R_)-6-iodo-3-oxo-2-oxabicyclo[2.2.1]heptane-4-carbothioate (109n).

The carboxylic acid (23 mg, 100 µmol) was treated according to the general procedure to give the lactone as a white solid (23.4 mg, 66%) which was determined to be 74% ee by chiral HPLC analysis (Chiralpak IA, 5% ^{i}PrOH/hexanes, 1 mL/min, t_r(e_1 minor) = 7.2 min, t_r(e_2 major) = 8.3 min). Mp 127-132 ^{o}C (decomp); $[\alpha]_D^{20}$ -37.3 (c 1.17, $CHCl_3$); R_f= 0.31 (25% EtOAc/hexanes); IR (film) 2956, 2918, 2863, 1779, 1661, 1447, 1163, 1081, 846 cm^{-1}; ^{1}H NMR (400 MHz, $CDCl_3$) δ 4.94 (d, J = 1.3 Hz, 1H), 4.14 (dddd, J = 7.5, 4.1, 2.1, 0.8 Hz, 1H), 2.84 (ddd, J = 14.4, 7.9, 2.0 Hz, 1H), 2.77 (d, J = 11.0 Hz, 1H), 2.69 (br dddd, J = 11.1, 2.0, 2.0, 2.0 Hz, 1H), 2.64 (dd, J = 14.4, 4.2 Hz, 1H), 1.52 (s, 9H); ^{13}C NMR (100 MHz, $CDCl_3$) ppm 193.0, 171.8, 83.6, 64.3, 49.8, 40.4, 39.1, 29.8, 15.4; HRMS (EI): Exact mass calcd for $C_{11}H_{15}IO_4SNa$ $[M+Na]^+$ 376.9684, found 376.9701. MTK-5-113.

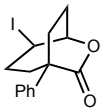

(1_S_,4_R_,5_R_)-4-Iodo-1-phenyl-6-oxabicyclo[3.2.2]nonan-7-one (136).

The carboxylic acid (22 mg, 100 µmol) was treated according to the general procedure to give the lactone as an oil (25.0 mg, 73%) which was determined to be 41% ee by chiral HPLC analysis (Chiralpak IA, 10% ^{i}PrOH/hexanes, 1 mL/min, t_r(e_1 minor) = 11.7 min, t_r(e_2 major) = 13.8 min. $[\alpha]_D^{20}$ -18.2 (c 1.25, $CHCl_3$); R_f= 0.52 (25% EtOAc/hexanes); IR (film) 3060, 2944, 1742, 1594, 1447, 1377, 1139 cm^{-1}; ^{1}H NMR (400 MHz, $CDCl_3$) δ 7.38-7.33 (m, 4H), 7.30-7.25 (m, 1H), 5.04 (d, J = 5.8 Hz, 1H), 4.53 (dddd, J = 9.0, 8.4, 1.3, 1.2 Hz, 1H), 2.65-2.53 (m, 4H), 2.42-2.27 (m, 3H), 2.31 (ddd, J = 14.5, 4.4, 4.0 Hz, 1H); ^{13}C NMR (100 MHz, $CDCl_3$) 174.9, 142.9, 128.2, 127.2, 126.8, 81.9, 47.0, 37.9, 35.0, 27.9, 27.2, 19.1 ppm; HRMS (EI): Exact mass calcd for $C_{14}H_{15}IO_2$ $[M]^+$ 342.0117, found 342.0118. MTK-5-128.

Derivatization of Bicyclic Iodolactones

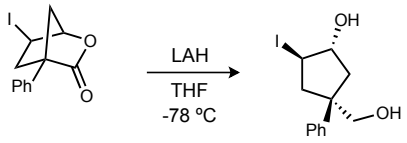

(1*R*,2*R*,4*S*)-4-(Hydroxymethyl)-2-iodo-4-phenylcyclopentan-1-ol (137).

To a flame died vial with stir bar was added $LiAlH_4$ (6 mg, 150 µmol) and THF (1 mL). The mixture was cooled to -78 ºC, the iodolactone (31 mg, 100 µmol, 95% ee) was added slowly, and the mixture was stirred at -78 ºC for 30 minutes. The reaction was quenched by addition of satd aq $NaHCO_3$ (1 mL) and Et_2O (1 mL). The layers were separated and the aqueous layer was extracted with Et_2O. The combined organic layers were dried, filtered, and concentrated. The product was purified by flash column chromatography (SiO_2, 20% ethyl acetate in hexanes) to yield a colorless oil (13.1 mg, 42 %). The product was determined to be 95% ee by chiral HPLC analysis (Chiralpak IA, 10% ^{i}PrOH/hexanes, 1 mL/min, $t_r(e_1$ minor) = 9.21 min, $t_r(e_2$ major) = 12.0 min). $[\alpha]_D^{20}$ -24.9 (*c* 0.63, $CHCl_3$); R_f = 0.37 (50% EtOAc/hexanes); IR (film) 3332, 3062, 2927, 2870, 1493, 1445, 1042 cm^{-1}; ^{1}H NMR (400 MHz, $CDCl_3$) δ 7.31-7.27 (m, 2H), 7.21-7.17 (m, 3H), 4.41 (ddd, J = 7.2, 5.0, 5.0 Hz, 1H), 4.19 (br ddd, J = 7.2, 7.2, 5.5 Hz, 1H), 3.51 (d, J = 10.4 Hz, 1H), 3.45 (d, J = 10.4 Hz, 1H), 2.91 (dd, J = 14.3, 6.8 Hz, 1H), 2.67 (dd, J = 14.1, 7.2 Hz, 1H), 2.53 (dd, J = 14.3, 8.0 Hz, 1H), 2.01 (dd, J = 14.1, 4.5 Hz, 1H); ^{13}C NMR (100 MHz, $CDCl_3$) ppm 145.9, 128.7, 126.9, 126.7, 71.8, 72.1, 51.8, 44.4, 41.5, 31.5; HRMS (CI): Exact mass calcd for $C_{12}H_{15}O_2$ $[M\text{-}I]^+$ 191.1072, found 191.1070. MTK-5-297.

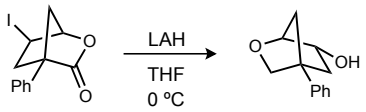

(1*S*,4*R*,6*R*)-4-Phenyl-2-oxabicyclo[2.2.1]heptan-6-ol (138).

To a flame-dried vial with stir bar was added $LiAlH_4$ (6 mg, 150 µmol) and THF (1 mL). The mixture was cooled to 0 ºC, iodolactone (31 mg, 100 µmol, 95% ee) was added slowly, and the mixture was stirred at 0 ºC for 30 minutes. The reaction was quenched by addition of satd aq $NaHCO_3$ (1 mL) and Et_2O (1 mL). The layers were separated and the aqueous layer was extracted with Et_2O. The combined organic layers were dried, filtered, and concentrated. The product was purified by flash column chromatography (SiO_2, 10% ethyl acetate in hexanes) to yield a colorless solid (11.2 mg, 59%). The product was determined to be 95% ee by chiral HPLC analysis (Chiralpak IA, 15% ^{i}PrOH/hexanes, 1 mL/min, $t_r(e_1$ major) = 7.4 min, $t_r(e_2$ minor) = 8.1 min). Mp 129-131 ºC. $[\alpha]_D^{20}$ +21.9 (*c*

1.12, $CHCl_3$); R_f = 0.38 (75% EtOAc/hexanes); IR (film) 3425, 2926, 2871, 1446, 1406, 1114 cm^{-1}; ^1H NMR (400 MHz, $CDCl_3$) δ7.35-7.32 (m, 2H), 7.27-7.21 (m, 3H), 4.32 (dd, J = 2.5, 2.5 Hz, 1H), 4.23 (br d, J = 9.5 Hz, 1H), 3.91 (d, J = 6.9 Hz, 1H), 3.83 (dd, J = 6.8, 3.5 Hz, 1H), 2.81 (br s, 1H), 2.26-2.20 (m, 2H), 1.89 (d, J = 10.5 Hz, 1H), 1.65 (ddd, J = 13.3, 3.6, 2.9 Hz, 1H); ^{13}C NMR (100 MHz, $CDCl_3$) ppm 140.2, 128.7, 127.2, 126.4, 80.2, 78.3, 72.9, 52.9, 44.9, 40.7; HRMS (EI): Exact mass calcd for $C_{14}H_{15}IO_2$ $[M]^+$ 190.0994, found 190.1037. MTK-5-132.

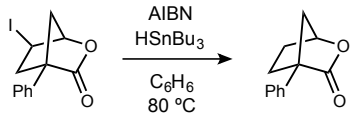

(1*S*,4*S*)-4-Phenyl-2-oxabicyclo[2.2.1]heptan-3-one (139).

To a flame-dried microwave vial with stir bar was added iodolactone (60 mg, 0.20 mmol, 93% ee), Bu_3SnH (110 µL, 0.40 mmol), and benzene (2.0 mL). The mixture was degassed (freeze-pump-thaw, 3 cycles) and then heated to 80 °C. One portion of AIBN (2 mg, 0.05 eq) was added, and the mixture was stirred for 30 minutes. A second portion of AIBN (2 mg, 0.05 eq) was added, and the mixture was stirred for another 30 minutes until full conversion was achieved. The reaction was cooled to room temperature, and the mixture was loaded onto a 15% K_2CO_3/SiO_2 pipette column and flushed with Et_2O. The eluent was concentrated to an oil that was purified by column chromatography (SiO_2, 20% ethyl acetate in hexanes) to yield a colorless solid (30.3 mg, 81%). The product was determined to be 91% ee by chiral HPLC analysis (Chiralpak IA, 3% ^{i}PrOH/hexanes, 1 mL/min, t_r(e_1 minor) = 14.1 min, t_r(e_2 major) = 14.8 min). Mp 67-70 °C; $[\alpha]_D^{20}$ -103 (c 1.52, $CHCl_3$); R_f = 0.24 (25% EtOAc/hexanes); IR (film) 3027, 2952, 2873, 1772, 1501, 1449, 1324, 1102 cm^{-1}; ^1H NMR (400 MHz, $CDCl_3$) 7.44-7.31 (m, 5H), 4.98 (d, J = 1.3 Hz, 1H), 2.56 (dd, J = 10.2, 1.5 Hz, 1H), 2.16-2.09 (m, 4H), 2.03 (d, J = 10.3 Hz, 1H); ^{13}C NMR (100 MHz, $CDCl_3$) ppm 177.8, 135.9, 128.6, 127.8, 127.4, 79.1, 55.3, 44.3, 30.2, 30.0; HRMS (EI): Exact mass calcd for $C_{12}H_{12}O_2Na$ $[M+Na]^+$ 211.0735, found 211.0745. MTK-5-153.

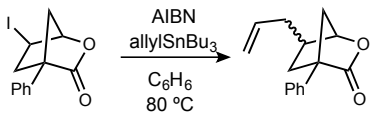

(1*R*,4*S*)-6-Allyl-4-phenyl-2-oxabicyclo[2.2.1]heptan-3-one (140).

To a flame-dried microwave vial with stir bar was added iodolactone (16 mg, 0.05 mmol, 93% ee), allyl$SnBu_3$ (60 µL, 0.20 mmol), and benzene (1.0 mL). The mixture was degassed (freeze-pump-thaw, 3 cycles) and then heated to 80 °C. One portion of AIBN (1

mg, 0.05 eq) was added, and the mixture was stirred for 30 minutes. A second portion of AIBN (1 mg, 0.05 eq) was added, and the mixture was stirred for 4 hours until full conversion was achieved. The reaction was cooled to room temperature, and the mixture was loaded onto a 15% K_2CO_3/SiO_2 pipette column and flushed with Et_2O. The eluent was concentrated to an oil that was purified by column chromatography (SiO_2, 20% ethyl acetate in hexanes) to yield a colorless oil (5.3 mg, 46%, 5:1 dr). $[\alpha]_D^{20}$ -55.9 (*c* 0.58, $CHCl_3$); R_f = 0.47 (25% EtOAc/hexanes); IR (film) 3066, 2925, 2857, 1777, 1451, 1317, 1232, 1103 cm^{-1}; ^1H NMR (400 MHz, $CDCl_3$) 7.39-7.31 (m, 5H), 5.85-5.75 (m, 1H), 5.09 (dd, *J* = 13.8, 1.9 Hz, 2H), 4.73 (d, *J* = 1.6 Hz, 1H), 2.54 (br dddd, *J* = 10.5, 2.2, 2.2, 2.2 Hz, 1H), 2.48-2.41 (m, 1H), 2.37 (dd, *J* = 12.4, 2.1 Hz, 1H), 2.28-2.21 (m, 1H), 2.17 (d, *J* = 10.4 Hz, 1H), 2.16-2.11 (m, 1H), 1.69 (dd, *J* = 12.5, 4.9 Hz, 1H); ^{13}C NMR (100 MHz, $CDCl_3$) ppm 177.7, 135.8, 135.1, 128.6, 127.9, 127.4, 117.1, 81.6, 55.1, 42.1, 41.5, 38.0, 37.1; HRMS (EI): Exact mass calcd for $C_{15}H_{16}O_2$ $[M]^+$ 228.1155, found 228.1150. MTK-5-063.

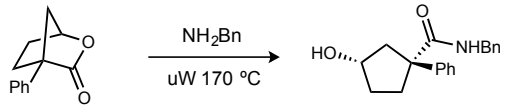

(1*R*,3*S*)-*N*-Benzyl-3-hydroxy-1-phenylcyclopentane-1-carboxamide (141).

To a flame-dried 100-500 µL microwave vial with stir bar was added lactone (19 mg, 0.10 mmol) and benzyl amine (100 µL). The mixture microwaved at 170 ºC for 20 minutes. The reaction mixture was purified directly by column chromatography (SiO_2, 40% ethyl acetate in hexanes) to yield a colorless solid (20.5 mg, 70%). Mp 77-79ºC; $[\alpha]_D^{20}$ -191 (*c* 1.03, $CHCl_3$); R_f = 0.38 (100% EtOAc); IR (film) 3340, 3059, 3033, 2928, 1644, 1526, 1448, 1276 cm^{-1}; ^1H NMR (400 MHz, $CDCl_3$) 7.57-7.51 (m, 4H), 7.48-7.40 (m, 4H), 7.24 (d, *J* = 6.6 Hz, 2H), 5.77 (br s, 1H), 4.85 (br s, 1H), 4.60-4.54 (m, 2H), 4.52 (dd, *J* = 15.2, 5.8 Hz, 1H), 2.90 (dd, *J* = 14.1, 0.9 Hz, 1H), 2.79-2.72 (m, 1H), 2.48-2.29 (m, 3H), 2.13-2.05 (m, 1H); ^{13}C NMR (100 MHz, $CDCl_3$) ppm 179.0, 144.1, 138.1, 129.2, 128.8, 127.6, 127.5, 127.3, 127.1, 73.1, 58.6, 47.2, 43.9, 36.4, 36.2; HRMS (EI): Exact mass calcd for $C_{19}H_{21}NO_2$ $[M+H]^+$ 296.1651, found 296.1161. MTK-5-279.

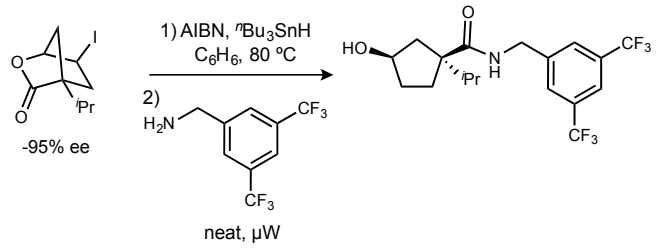

(1*S*,3*R*)-*N*-(3,5-bis(trifluoromethyl)benzyl)-3-hydroxy-1-isopropylcyclopentane-1-carboxamide (152).

To a flame-dried microwave vial with stir bar was added iodolactone (150 mg, 540 µmol, 95% ee), Bu_3SnH (290 µL, 1.08 mmol), and benzene (3.0 mL). The mixture was degassed (freeze-pump-thaw, 3 cycles) and then heated to 80 °C. One portion of AIBN (2 mg, 0.05 eq) was added, and the mixture was stirred for 30 minutes. A second portion of AIBN (5 mg, 0.05 eq) was added, and the mixture was stirred for another 30 minutes until full conversion was achieved. The reaction was cooled to room temperature, and the mixture was loaded onto a 15% K_2CO_3/SiO_2 pipette column and flushed with Et_2O. The eluent was concentrated to an oil. This oil was transferred to a 2-5 mL microwave vial and 3,5-bis(trifluoromethyl)benzylamine (1.3 g, 5.4 mmol) was added. The reaction was microwaved neat at 220 °C for 2 h. After completion, the contents were washed into a separatory funnel with dichloromethane (5 mL) and 3M HCl (5 mL). The layers were separated and the aqueous layer was extracted with dichloromethane. The combined organic layers were dried, filtered, and concentrated. The product was purified by flash column chromatography (SiO_2, 10% ethyl acetate in hexanes) to yield a colorless solid (109 mg, 56%). Mp 99-102 °C; $[\alpha]_D^{20}$ + 1.75 (*c* 0.93, $CHCl_3$); R_f = 0.30 (50% EtOAc/hexanes); IR (film) 3328, 2931, 1637, 1533 cm^{-1}; ^1H NMR (400 MHz, $CDCl_3$) 7.75-7.73 (m, 3H), 7.14 (br dd, J = 5.6, 5.0 Hz, 1H), 4.58 (dd, J = 15.6, 6.2 Hz, 1H), 4.51 (dd, J = 15.7, 5.7 Hz, 1H), 4.43 (br m, 1H), 2.69 (br s, 1H), 2.18 (sept, J = 6.8 Hz, 1H), 2.22-2.02 (m, 2H), 1.82-1.68 (m, 4H), 0.87 (d, J = 6.9 Hz, 3H), 0.85 (d, J = 6.8 Hz, 3H); ^{13}C NMR (100 MHz, $CDCl_3$) ppm 179.5, 141.9, 131.9 (q, $^2J_{CF}$ = 33.1 Hz), 127.6 (br q, $^3J_{CF}$ = 3.0 Hz), 123.3 (q, $^1J_{CF}$ = 271 Hz), 121.3 (dq, $^3J_{CF}$ = 3.6, 3.6 Hz), 74.1, 57.1, 43.0, 38.5, 36.3, 34.5, 34.2, 19.2, 17.2; HRMS (EI): Exact mass calcd for $C_{18}H_{22}F_6NO_2$ $[M+H]^+$ 398.1549, found 398.1555. MTK-6-192 and 193.

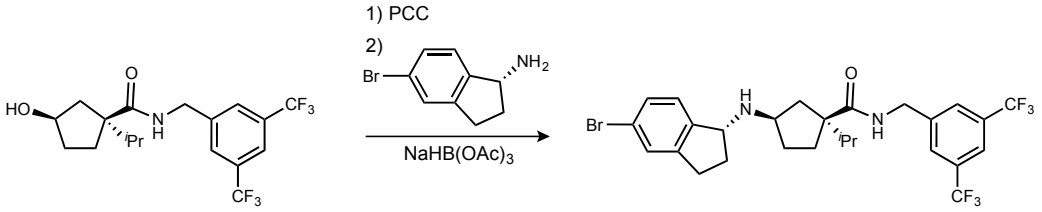

(1*S*,3*R*)-*N*-(3,5-Bis(trifluoromethyl)benzyl)-3-(((*R*)-5-bromo-2,3-dihydro-1*H*-inden-1-yl)amino)-1-isopropylcyclopentane-1-carboxamide (148)

To a 10 mL round bottomed flask with stir bar was added alcohol (73 mg, 180 µmol), PCC (79 mg, 370 µmol), and dichloromethane (2.0 mL). The mixture was stirred for 18 hours until full conversion was achieved. The reaction was transferred onto a silica pad and flushed with diethyl ether (20 mL). The eluent was concentrated to a colorless oil (52.4 mg), of which 28.9 mg of the crude material was transferred to a 2-5 mL microwave vial. (*R*)-5-bromo-2,3-dihydro-1H-inden-1-amine (15.5 mg, 73 µmol), methanol (1 mL), acetic acid (5 µL, 73 µL), and molecular sieves were added. The reaction was allowed to stir for 30 minutes, then $NaBH_3CN$ (14 mg, 220 µmol) was added and stirred at room temperature

for 18 hours. After completion, the reaction was quenched by the addition of water (2 mL) and diethyl ether (2 mL). The layers were separated and the aqueous layer was extracted with diethyl ether. The combined organic layers were dried, filtered, and concentrated. The product was purified by flash column chromatography (SiO_2, 30% ethyl acetate, 1% Et_3N in hexanes) to yield an oil (25.9 mg, 60%, 2 steps, 3:1 dr). $[\alpha]_D^{20}$ +10.7 (*c* 0.65, $CHCl_3$, 2.30 equiv TFA added); R_f = 0.39 (1% Et_3N/EtOAc); IR (film) 3340, 2960, 2876, 1643, 1525, 1465, 1378, 1281, 1174, 1137 cm^{-1}; ^1H NMR (600 MHz, DMSO-*d*6) 8.54 (t, *J* = 5.7 Hz, 1H), 7.96 (br s, 1H), 7.94 (br s, 2H), 7.39 (br s, 1H), 7.27 (br d, *J* = 7.7 Hz, 1H), 7.12 (br d, *J* = 7.6 Hz, 1H), 4.49 (dd, *J* = 10.4, 5.8 Hz, 1H), 4.41 (dd, *J* = 10.4, 5.6 Hz, 1H), 4.04 (br s, 1H), 3.18 (br dddd, *J* = 6.8, 6.8, 6.1, 6.1 Hz, 1H), 2.90-2.86 (m, 1H), 2.70 (ddd, *J* = 16.0, 7.7, 7.7 Hz, 1H), 2.32-2.27 (m, 1H), 2.11 (br ddd, *J* = 11.9, 7.1, 4.0 Hz, 1H), 2.01 (sept, *J* = 6.7 Hz, 1H), 1.86 (d, *J* = 6.3 Hz, 2H), 1.83-1.78 (m, 1H), 1.68-1.63 (m, 1H), 1.51-1.46 (m, 1H), 1.34-1.28 (m, 1H), 0.79 (d, *J* = 6.7 Hz, 3H), 0.76 (d, *J* = 6.7 Hz, 3H); ^{13}C NMR (125 MHz, DMSO-*d*6) ppm 177.4, 146.0, 144.1 (2C), 130.0 (q, $^2J_{CF}$ = 27.2 Hz), 128.6, 127.9, 127.3, 125.9, 123.4 (q, $^1J_{CF}$ = 272 Hz), 120.3 (dq, $^3J_{CF}$ = 3.4, 3.4 Hz), 60.4, 56.8, 56.4, 41.8, 34.2, 32.7, 30.2, 29.7, 29.0, 18.4, 17.9; HRMS (EI): Exact mass calcd for $C_{27}H_{30}N_2O_1BrF_6$ $[M+H]^+$ 591.1440, found 591.1440. MTK-6-195, 200, and 201.

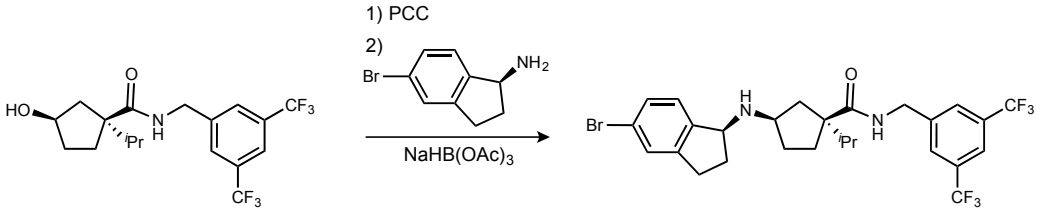

(1*S*,3*R*)-*N*-(3,5-Bis(trifluoromethyl)benzyl)-3-(((*S*)-5-bromo-2,3-dihydro-1*H*-inden-1-yl)amino)-1-isopropylcyclopentane-1-carboxamide (*epi*-148)

To a 10 mL round bottomed flask with stir bar was added alcohol (35 mg, 90 µmol), PCC (38 mg, 180 µmol), and dichloromethane (2.0 mL). The mixture was stirred for 18 hours until full conversion was achieved. The reaction was transferred onto a silica pad and flushed with diethyl ether (10 mL). The eluent was concentrated to a colorless oil (33 mg), which was transferred to a 2-5 mL microwave vial. (*S*)-5-bromo-2,3-dihydro-1H-inden-1-amine (18 mg, 80 µmol), methanol (1 mL), acetic acid (5 µL, 80 µL), and molecular sieves were added. The reaction was allowed to stir for 30 minutes, then $NaBH_3CN$ (16 mg, 250 µmol) was added and stirred at room temperature for 18 hours. After completion, the reaction was quenched by the addition of water (2 mL) and diethyl ether (2 mL). The layers were separated and the aqueous layer was extracted with diethyl ether. The combined organic layers were dried, filtered, and concentrated. The product was purified by flash column chromatography (SiO_2, 30% ethyl acetate, 1% Et_3N in hexanes) to yield an oil (45.0 mg, 92%, 2 steps, 2:1 dr). $[\alpha]_D^{20}$ -19.2 (*c* 0.76, $CHCl_3$, 2.75 equiv TFA added); R_f = 0.39 (1%

Et_3N/EtOAc); IR (film) 3341, 2925, 2858, 1643, 1525, 1462, 1377, 1280 cm^{-1}; ^1H NMR (600 MHz, DMSO-*d*6) 8.54 (t, J = 5.9 Hz, 1H), 7.94 (s, 2H), 7.92 (d, J = 7.4 Hz, 1H), 7.39 (br s, 1H), 7.24 (br d, J = 7.8 Hz, 1H), 7.10 (br d, J = 7.9 Hz, 1H), 4.51 (dd, J = 15.8, 5.9 Hz, 1H), 4.42 (dd, J = 15.8, 5.9 Hz, 1H), 4.05 (br s, 1H), 3.19 (br dddd, J = 6.8, 6.8, 5.9, 5.9 Hz, 1H), 2.88 (dddd, J = 15.4, 12.1, 8.1, 3.7 Hz, 1H), 2.70 (ddd, J = 16.1, 7.9, 7.9 Hz, 1H), 2.32-2.27 (m, 1H), 2.15-2.11 (m, 1H), 2.00 (sept, J = 6.7 Hz, 1H), 1.97-1.92 (m, 1H), 1.83-1.76 (m, 2H), 1.68-1.62 (m, 1H), 1.49 (dt, J = 13.2, 8.5 Hz), 1.31-1.27 (m, 1H), 0.79 (d, J = 6.9 Hz, 3H), 0.76 (d, J = 6.8 Hz, 3H); ^{13}C NMR (125 MHz, DMSO-*d*6) ppm 177.4, 145.9, 144.1 (2C), 130.0 (q, $^2J_{CF}$ = 27.2 Hz), 128.7, 127.9, 127.3, 126.0, 123.4 (q, $^1J_{CF}$ = 226 Hz), 120.3 (dq, $^3J_{CF}$ = 3.4, 3.4 Hz), 60.5, 56.7, 56.4, 41.8, 34.4, 33.6, 30.5, 29.7, 29.0, 18.4, 17.9; HRMS (EI): Exact mass calcd for $C_{27}H_{30}N_2O_1BrF_6$ $[M+H]^+$ 591.1440, found 591.1443. MTK-6-184.

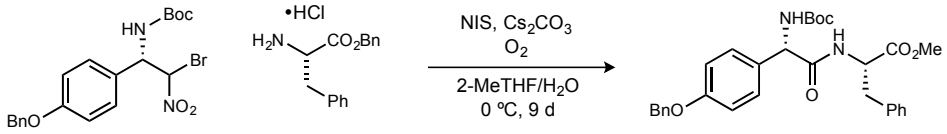

Methyl((*S*)-2-(4-(benzyloxy)phenyl)-2-((*tert*-butoxycarbonyl)amino)acetyl)-L-phenylalaninate (167).

A three-necked (24/40, 29/42, and 24/40 joints), dimpled 1-L round bottom flasked was equipped with an overhead mechanical stirrer in the central neck and placed into a temperature controlled isopropanol bath. A thermometer adapter and thermometer were placed in a 24/40 neck. Bromonitroalkane (8.90 g, 19.7 mmol, 1.0 equiv, 92/95% ee), *L*-phenylalanine methyl ester (4.24 g, 23.7 mmol, 1.2 equiv), and cesium carbonate (14.14 g, 43.4 mmol, 2.2 equiv) were loaded into the flask. Deionized water (35 mL) and 2-Me-THF (200 mL) were poured into the vessel. A septum and oxygen balloon were then placed in the open neck, and the mixture was stirred in the 0 °C isopropanol bath until the internal reaction temperature reached 0 °C. *N*-iodosuccinimide (4.44 g, 19.7 mmol, 1.0 equiv) was then added in one portion through the neck bearing a septum. The reaction mixture was stirred for 9 d refilling the oxygen balloon as needed, until full consumption of starting material was observed by ^1H NMR. To quench the reaction, satd aq $Na_2S_2O_3$ (50 mL) was poured into the stirring reaction, and the mixture was then gradually warmed to room temperature by turning off the cold finger and continuing stirring. The mixture was then poured into a 1-L separatory funnel, using ethyl acetate (50 mL) to rinse the remaining mixture into the funnel. The organic and aqueous layers were separated, and the latter was extracted with ethyl acetate (2 x 50 mL). The combined organic layers were dried over $MgSO_4$ (25 g), filtered, and concentrated to a red oil in a 1-L round-bottomed flask by rotary evaporation (25 °C, 23 mm Hg). The oil was transferred onto a pad of silica (8 cm

tall by 7 cm wide), using 10 mL of dichloromethane to retrieve the residual oil. The silica was then flushed with 50% ethyl acetate and hexanes (600 mL) into a 1-L round bottom flask and was concentrated to a red solid by rotary evaporation (25 °C, 23 mm Hg). The material was subjected to high vacuum (0.01 mm Hg) for 1 h. To the crude solid was added 50 mL of 60% toluene/cyclohexane and stirred in a warm water bath (70 °C) until all solids dissolved. The flask was then removed from the water bath, capped with a plastic stopper, and allowed to cool to room temperature (25 °C) for 6 h. The suspension was vacuum filtered through a Büchner funnel (7 cm diameter), fitted with filter paper. Cyclohexane (2 x 25 mL) was used to rinse the remaining powder from the round-bottomed flask onto the filter cake. The solid was transferred into a tared 100 mL round bottom flask and dried by high vacuum (0.1 mm Hg) for 10 h to give an off white solid (5.25 g, 51% yield). $R_f = 0.46$ (30% EtOAc/hexanes); mp = 125-127 °C; $R_f = 0.47$ (50% EtOAc/hexanes); IR (film) 3322, 3033, 2976, 1669, 1507, 1237, 1170 cm^{-1}; ^1H NMR (400 MHz, $CDCl_3$) δ 7.42-7.31 (m, 5H), 7.28-7.18 (m, 5H), 7.05 (d, $J = 7.6$ Hz, 2H), 6.90 (d, $J = 8.8$ Hz, 2H), 6.29 (br d, $J = 6.8$ Hz, 1H), 5.60 (br s, 1H), 5.05 (br s, 1H), 5.03 (s, 2H), 4.80 (dd, $J = 13.2$, 7.2 Hz, 1H), 3.64 (s, 3H), 3.14 (dd, $J = 14.0$, 6.0 Hz, 1H), 3.04 (dd, $J = 14.0$, 6.0 Hz, 1H), 1.41 (s, 9H); ^{13}C NMR (125 MHz, $CDCl_3$) ppm 171.5, 170.2, 158.9, 155.2, 136.9, 135.7, 130.1, 129.4, 128.7 (2C), 128.6, 128.1, 127.6, 127.3 (2C), 115.4, 80.2, 70.1, 53.6, 52.4, 37.8, 28.4; HRMS (EI): Exact mass calcd for $C_{30}H_{34}N_2O_6Na$ $[M+Na]^+$ 541.2315, found 541.2295.

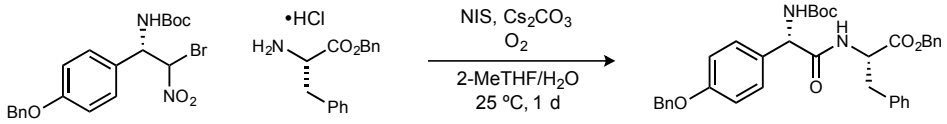

Benzyl((*S*)-2-(4-(benzyloxy)phenyl)-2-((*tert*-butoxycarbonyl)amino)acetyl)-L-phenylalaninate (169).

A three-necked (24/40, 29/42, and 24/40 joints), dimpled 1-L round bottom flasked was equipped with an overhead mechanical stirrer in the central neck. A septum and plastic stopper were placed in the other two necks. Bromonitroalkane (8.90 g, 19.7 mmol, 1.0 equiv, 92/95% ee), *L*-phenylalanine benzyl ester hydrochloride (6.90 g, 23.7 mmol, 1.2 equiv), and cesium carbonate (20.6 g, 63.1 mmol, 3.2 equiv) were loaded into the flask. Deionized water (35 mL) and 2-Me-THF (200 mL) were poured into the vessel. An oxygen balloon was then placed in the septum, and the mixture was stirred at room temperature for 5 minutes. *N*-Iodosuccinimide (4.44 g, 19.7 mmol, 1.0 equiv) was then added in one portion through the neck bearing the plastic stopper. The reaction mixture was stirred for 24 hours. To quench the reaction, satd aq $Na_2S_2O_3$ (50 mL) was poured into the stirring reaction and allowed to stir for 1 hour. The mixture was then poured into a 1-L separatory funnel, using ethyl acetate (50 mL) to rinse the remaining mixture into the funnel. The organic and aqueous

layers were separated, and the latter was extracted with ethyl acetate (2 x 50 mL). The combined organic layers were dried over $MgSO_4$ (25 g), filtered, and concentrated to a red oil in a 1-L round-bottomed flask by rotary evaporation (25 °C, 23 mm Hg). The oil was transferred onto a pad of silica (8 cm tall by 7 cm wide), using 10 mL of dichloromethane to retrieve the residual oil. The silica was then flushed with 50% ethyl acetate and hexanes (600 mL) into a 1-L round bottom flask and was concentrated to a red solid by rotary evaporation (25 °C, 23 mm Hg). The material was subjected to high vacuum (0.01 mm Hg) for 1 h. To the crude solid was added 50 mL of 60% toluene/cyclohexane and heated in a warm water bath (70 °C) until all solids dissolved. The flask was then removed from the water bath, capped with a plastic stopper, and allowed to cool to room temperature (25 °C) for 2 h. The flask was cooled to 0 ºC in a freezer for 18 h. The suspension was vacuum filtered through a Büchner funnel (7 cm diameter), fitted with filter paper. Cold cyclohexane (2 x 25 mL) was used to rinse the remaining powder from the round-bottomed flask onto the filter cake. The solid was transferred into a tared 100 mL round bottom flask and dried by high vacuum (0.1 mm Hg) for 10 h to give an off-white solid (6.70 g, 57% yield). R_f = 0.44 (25% EtOAc/hexanes); 99% purity (Q NMR, DMF internal standard); mp = 126-128 °C; IR (film) 3321, 3034, 2974, 2929, 1668, 1507, 1240, 1172 cm^{-1}; ^1H NMR (400 MHz, $CDCl_3$) δ 7.43-7.33 (m, 8H), 7.24-7.16 (m, 7H), 6.97-6.95 (m, 2H), 6.88 (d, J = 8.7 Hz, 2H), 6.14 (br d, J = 6.9 Hz, 1H), 5.57 (br s, 1H), 5.11-5.03 (br m, 5H), 4.84 (dd, J = 7.6, 5.8 Hz, 1H), 3.14 (dd, J = 14.0, 5.8 Hz, 1H), 3.06 (dd, J = 14.0, 5.7 Hz, 1H), 1.41 (s, 9H); ^{13}C NMR (125 MHz, DMSO-d_6) 170.9, 170.2, 157.6, 154.7, 137.1, 136.9, 135.6, 130.8, 129.1, 128.4 (2C), 128.3, 128.2, 127.9, 127.7 (2C), 127.5, 126.4, 114.3, 78.3, 69.1, 65.9, 56.7, 53.7, 36.5, 28.1 ppm; HRMS (EI): Exact mass calcd for $C_{36}H_{39}N_2O_6$ $[M+H]^+$ 595.2808, found 595.2816.

---

[i] Pangborn, A. B.; Giardello, M. A.; Grubbs, R. H.; Rosen, R. K.; Timmers, F. J. *Organometallics* **1996**, *15*, 1518-1520.

[ii] Scholl, M.; Ding, S.; Lee, C. W.; Grubbs, R. H. *Org. Lett.* **1999**, *1*, 953.

B Spectral data

Figure B 1: ^{1}H NMR (400 MHz, CDCl3) of **S1**

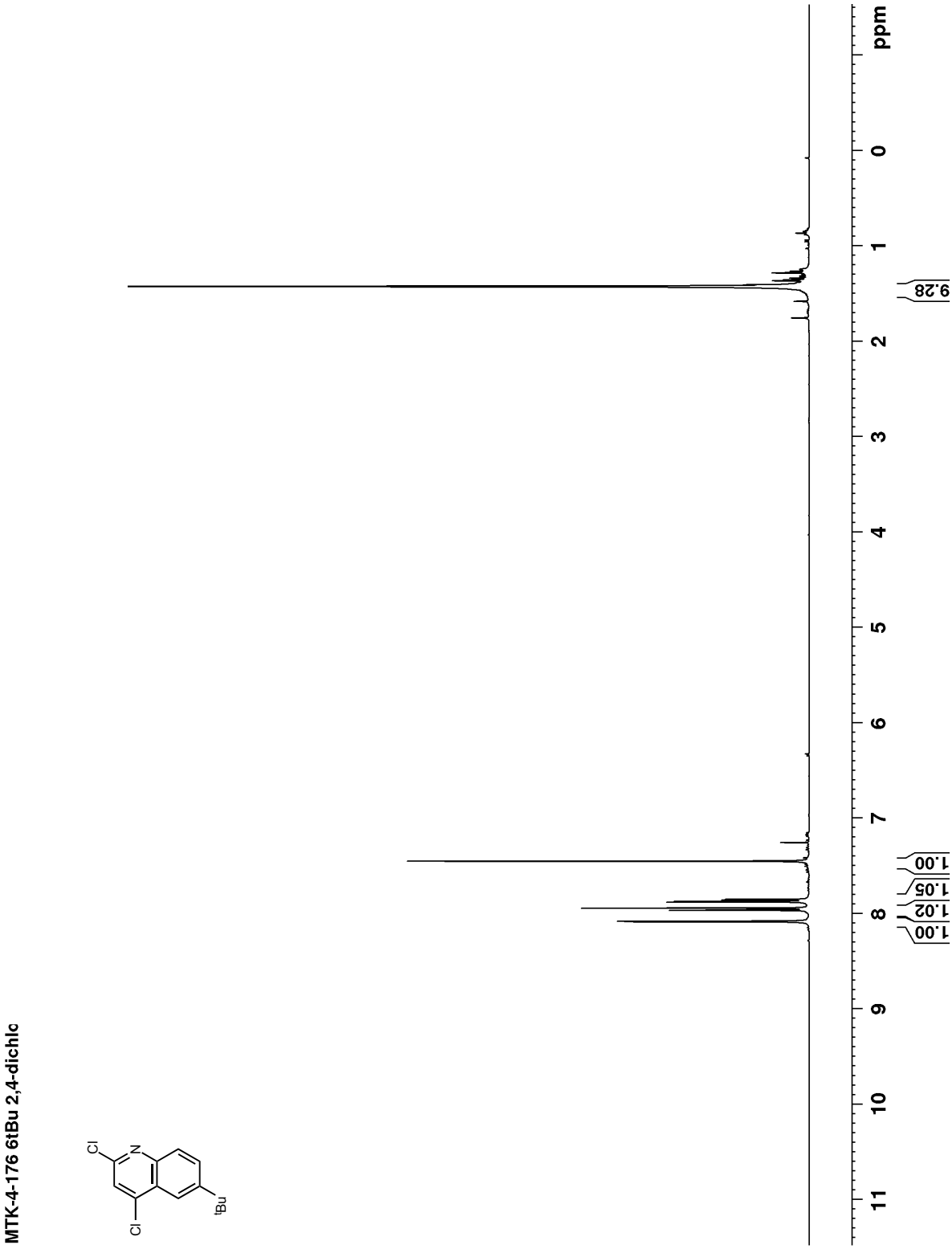

Figure B 2: ^{13}C NMR (100 MHz, $CDCl_3$) of **S1**

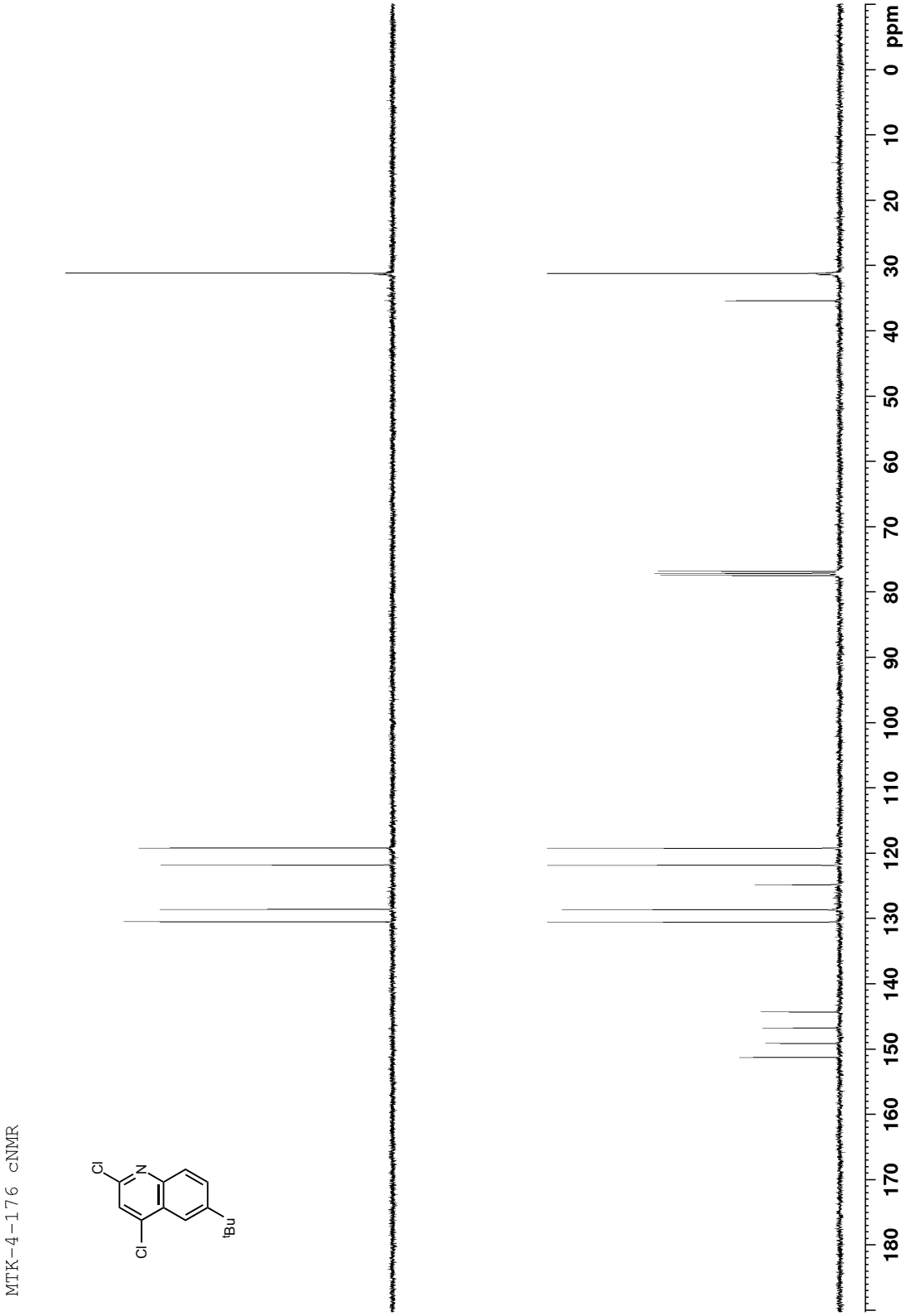

Figure B 3: ^{1}H NMR (400 MHz, $CDCl_3$) of **S2**

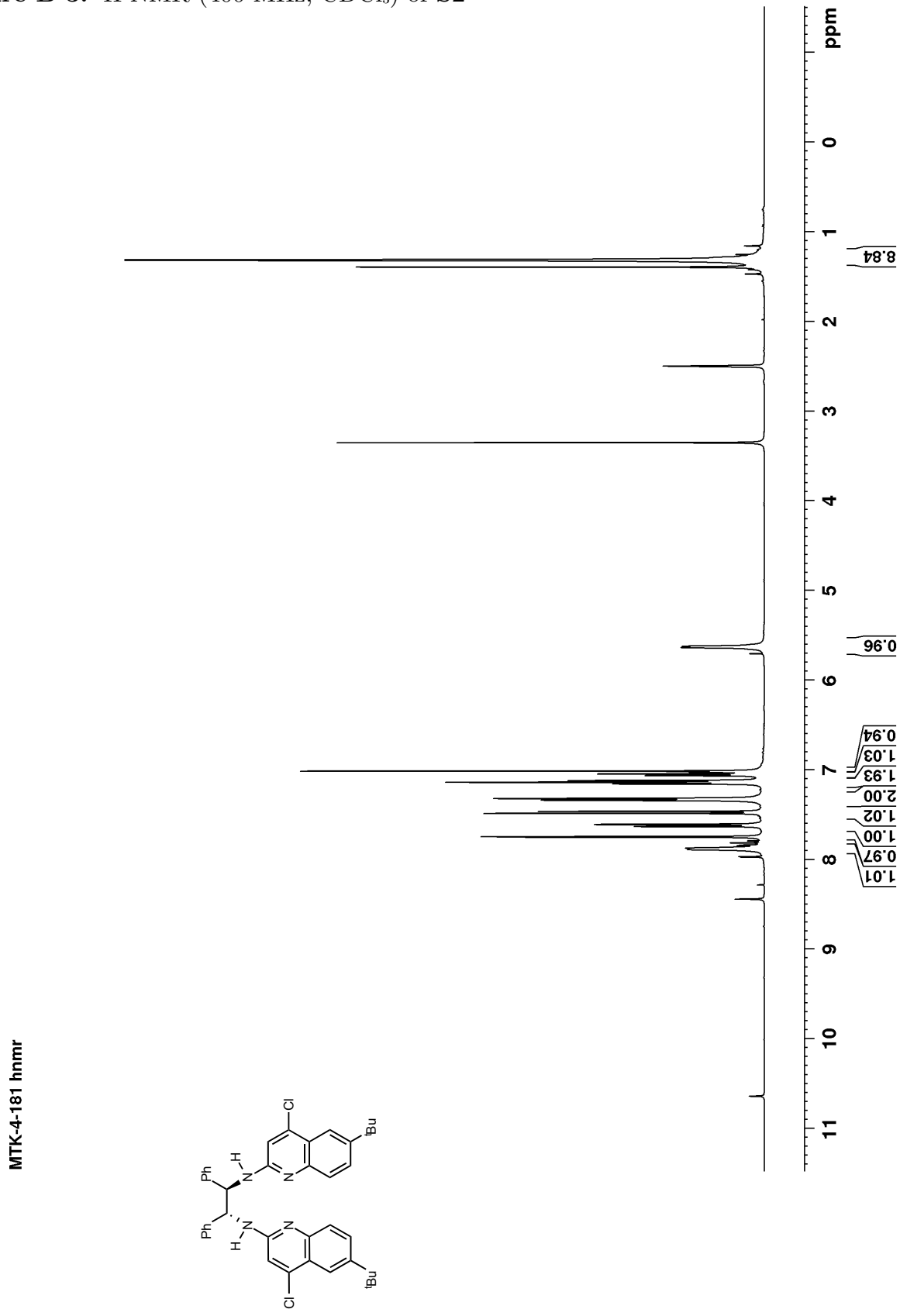

Figure B 4: ^{13}C NMR (100 MHz, $CDCl_3$) of S2

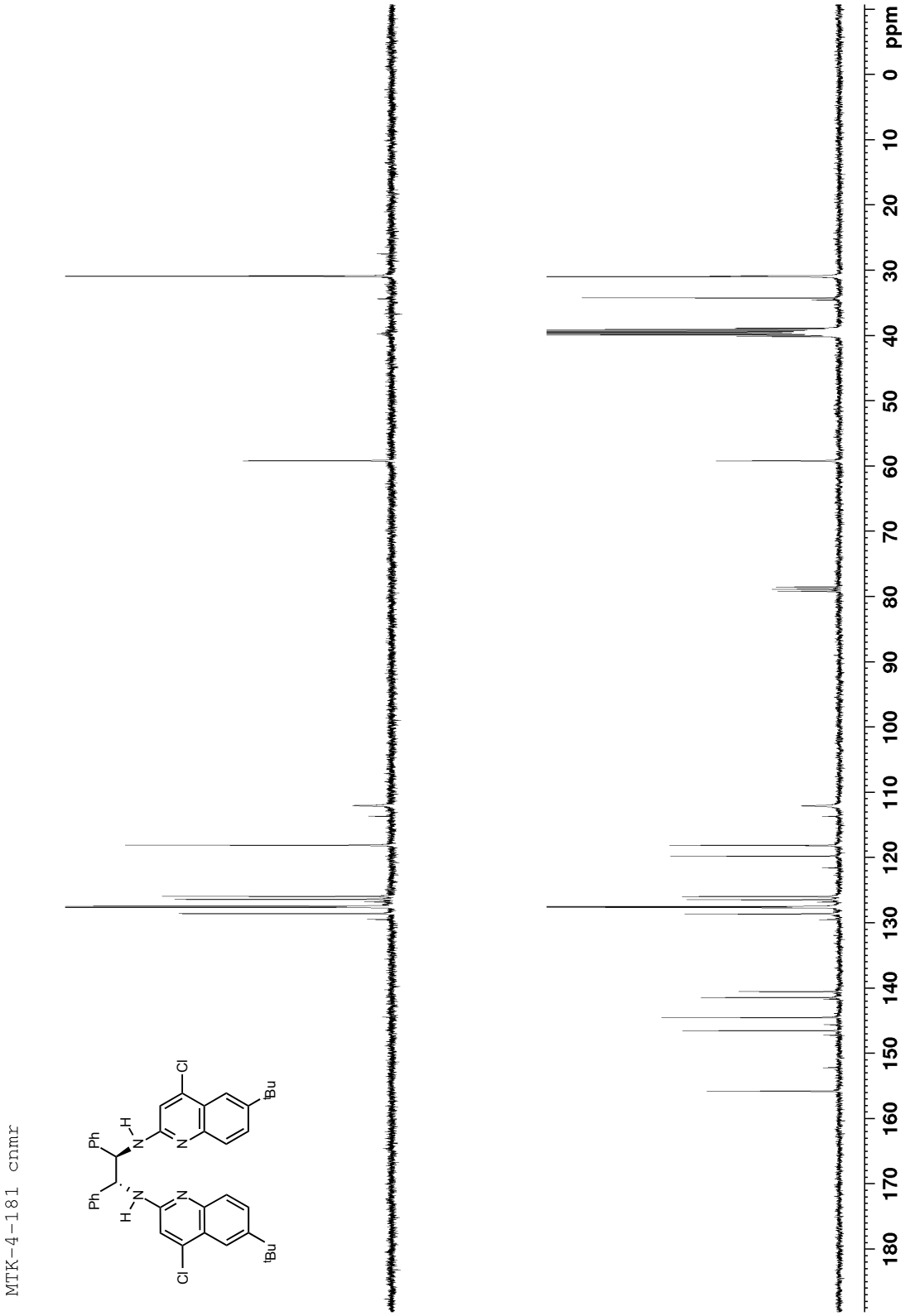

Figure B 5: ^{1}H NMR (400 MHz, d_6-DMSO/$CDCl_3$ 10:1) of **123c**

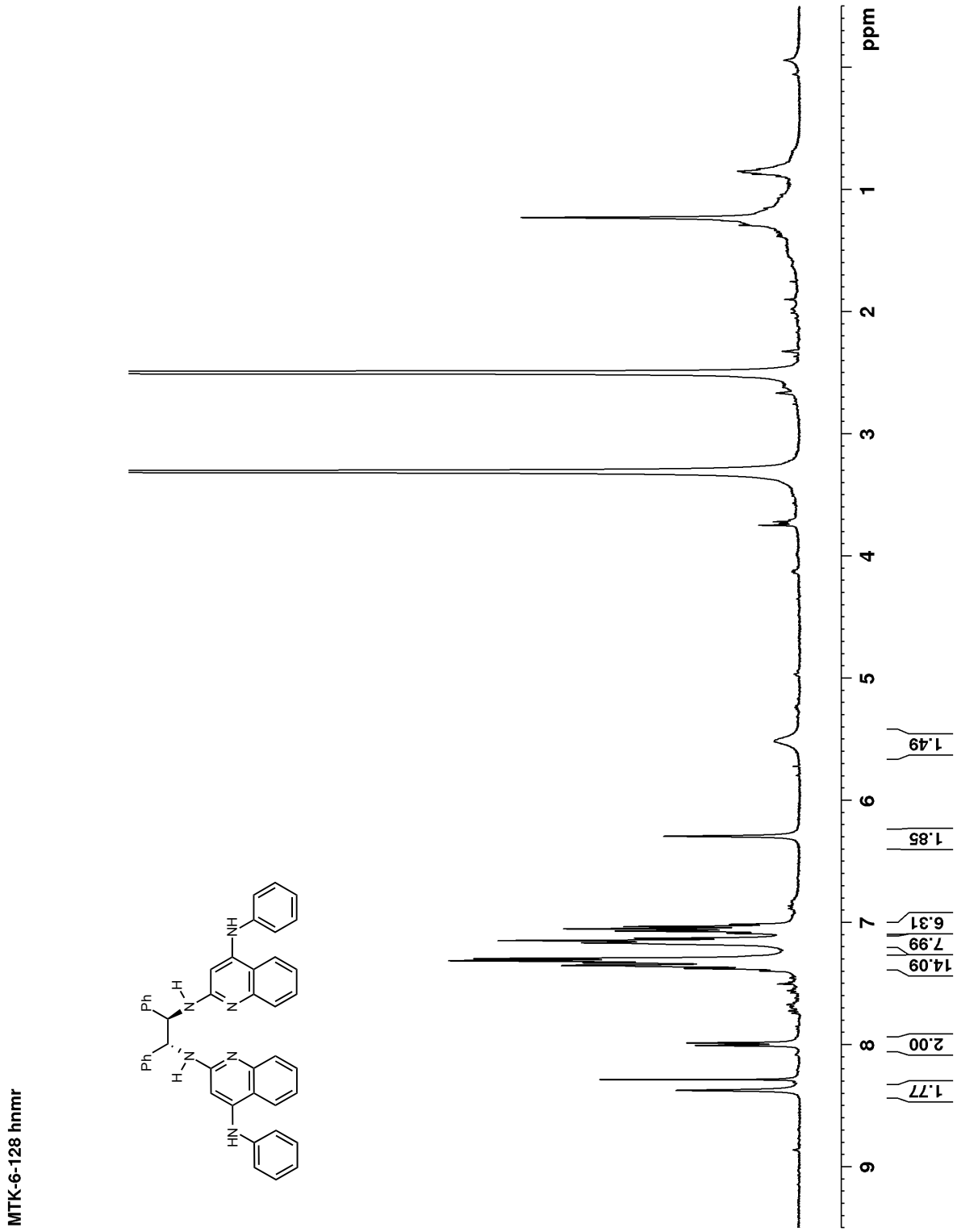

Figure B 6: ^{13}C NMR (125 MHz, d_6-DMSO/$CDCl_3$ 10:1) of **123c**

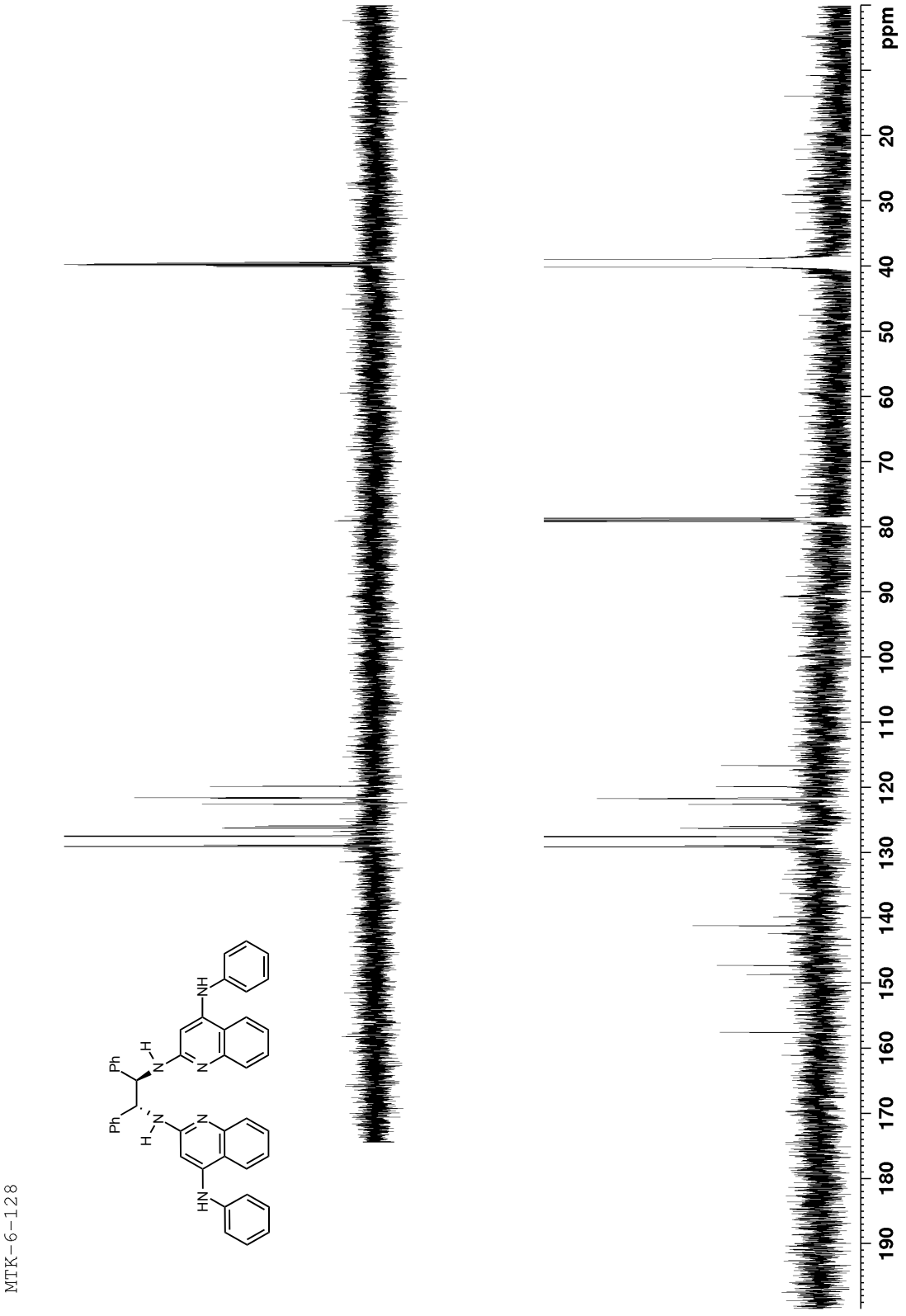

Figure B 7: ^{1}H NMR (400 MHz, d_6-DMSO) of **126a**

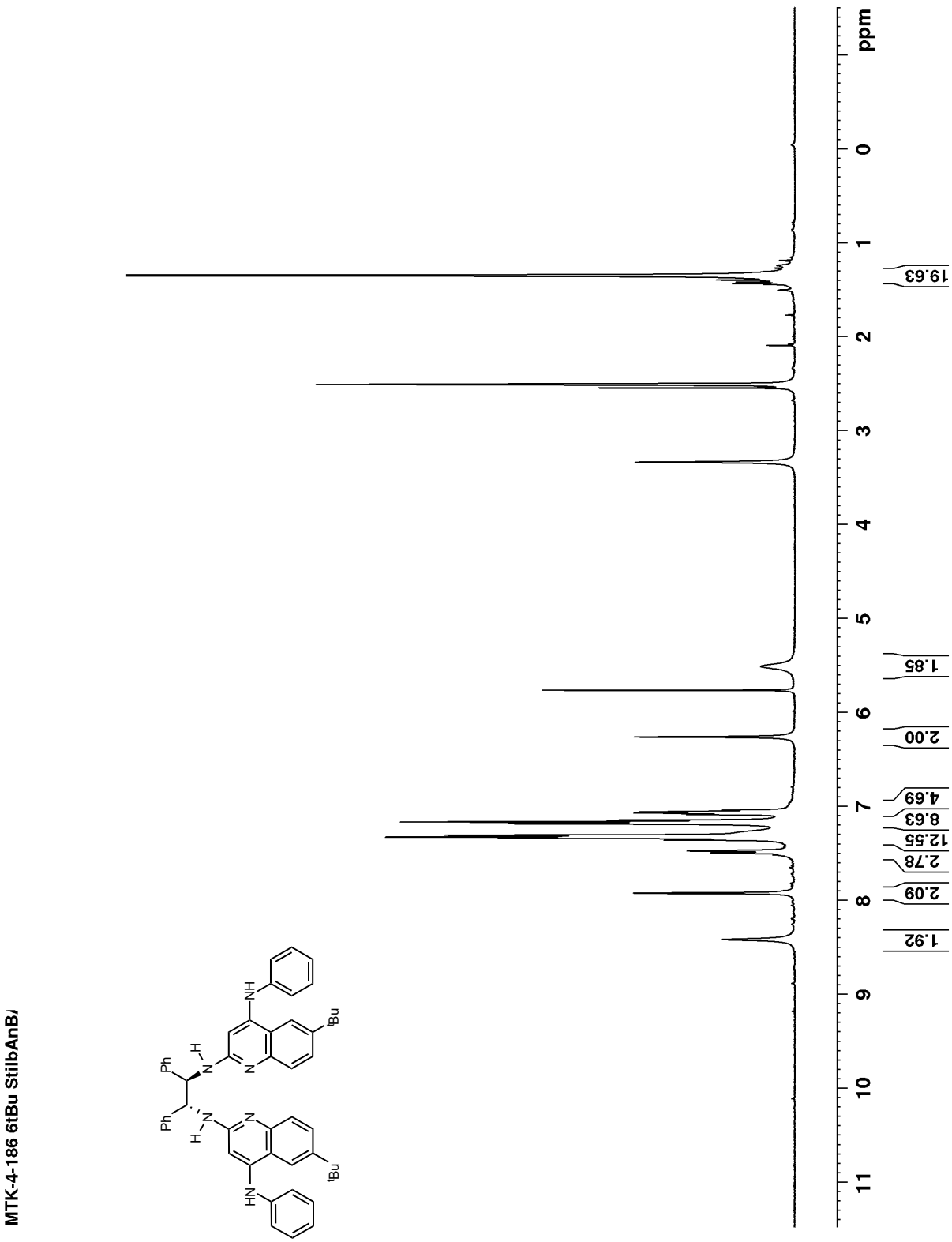

Figure B 8: ^{13}C NMR (100 MHz, d_6-DMSO) of **126a**

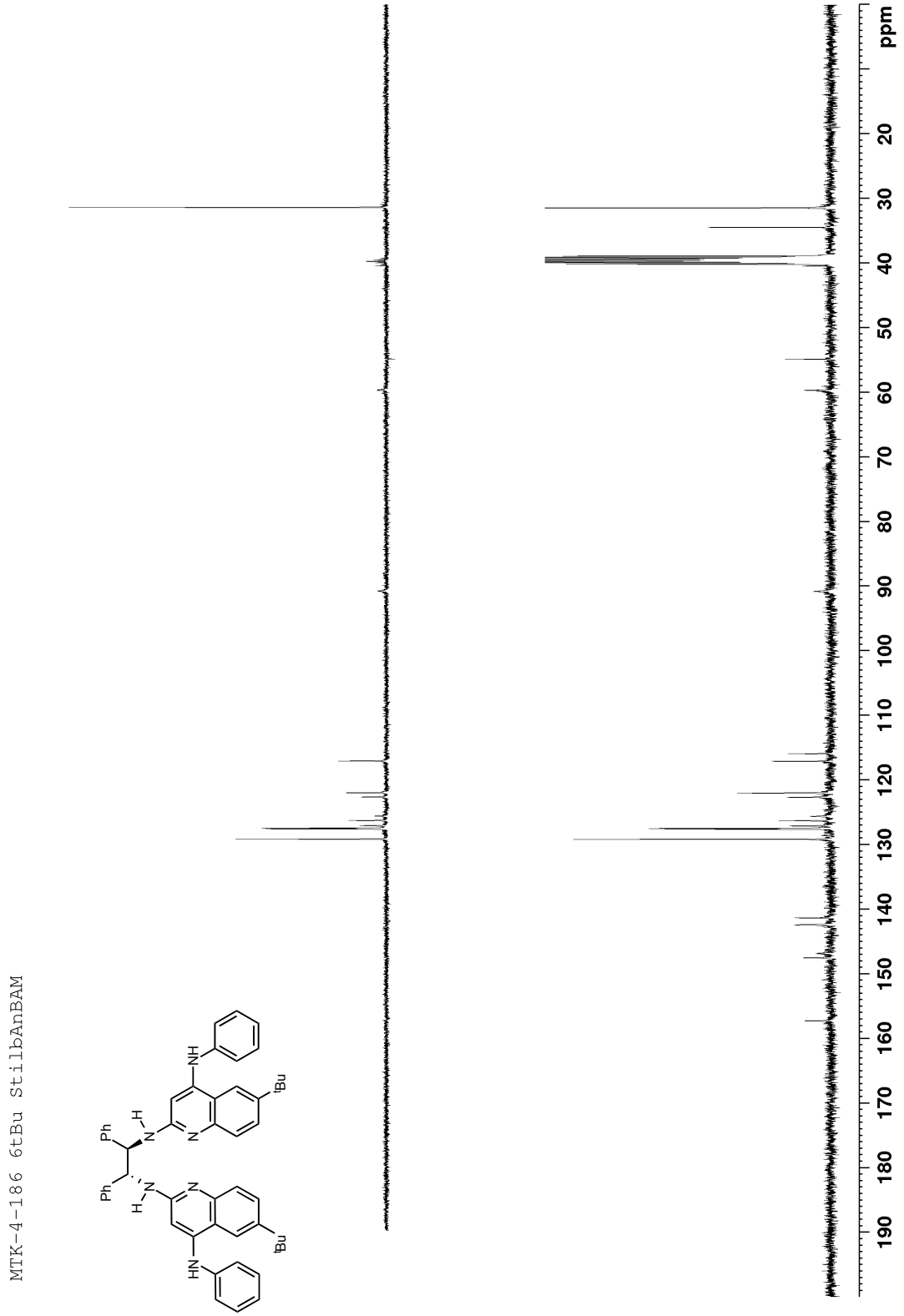

Figure B 9: ^{1}H NMR (400 MHz, d_6-DMSO) of **126d**

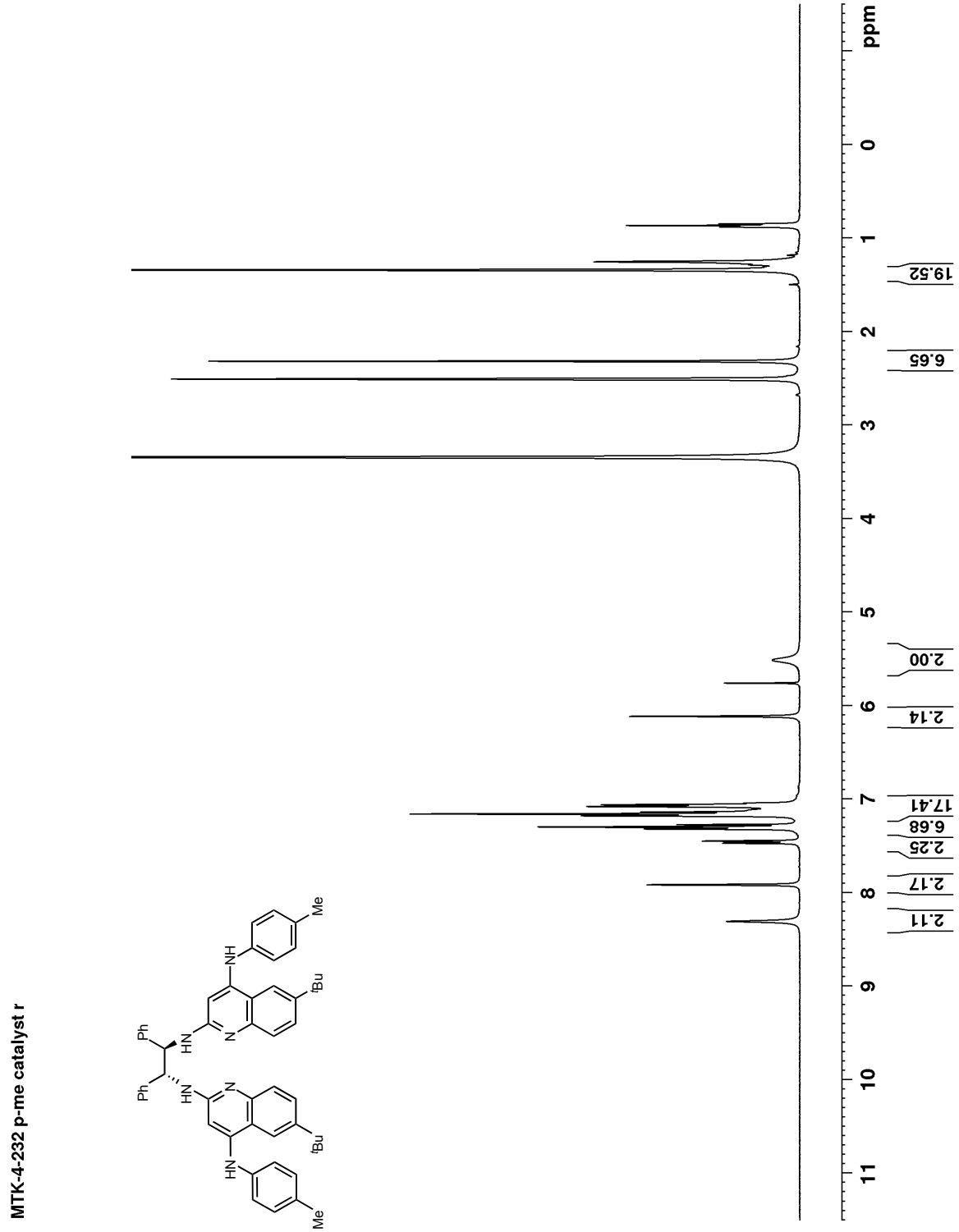

Figure B 10: ^{13}C NMR (100 MHz, d6-DMSO) of **126d**

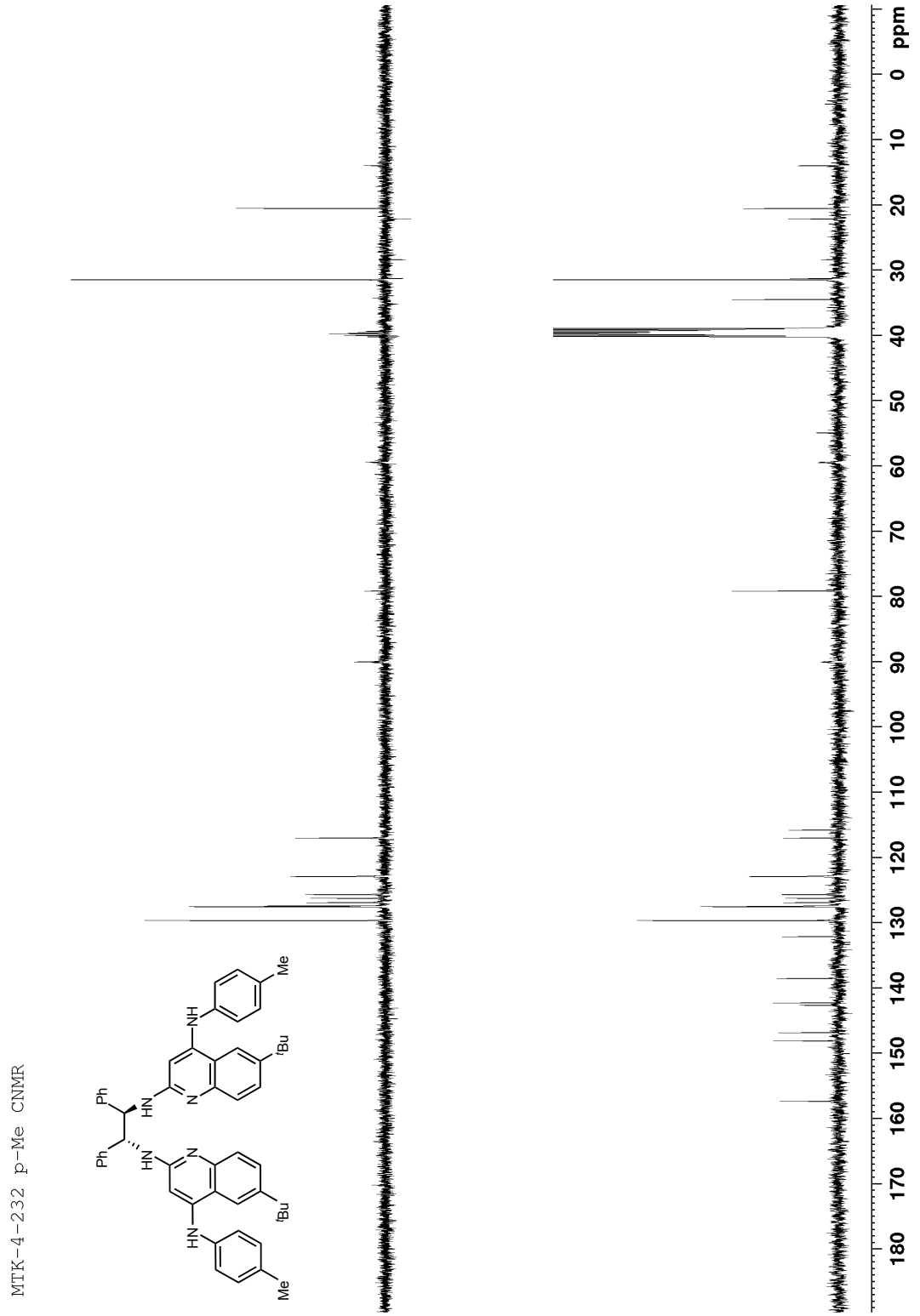

Figure B 11: ^{1}H NMR (400 MHz, d_6-DMSO) of **14i**

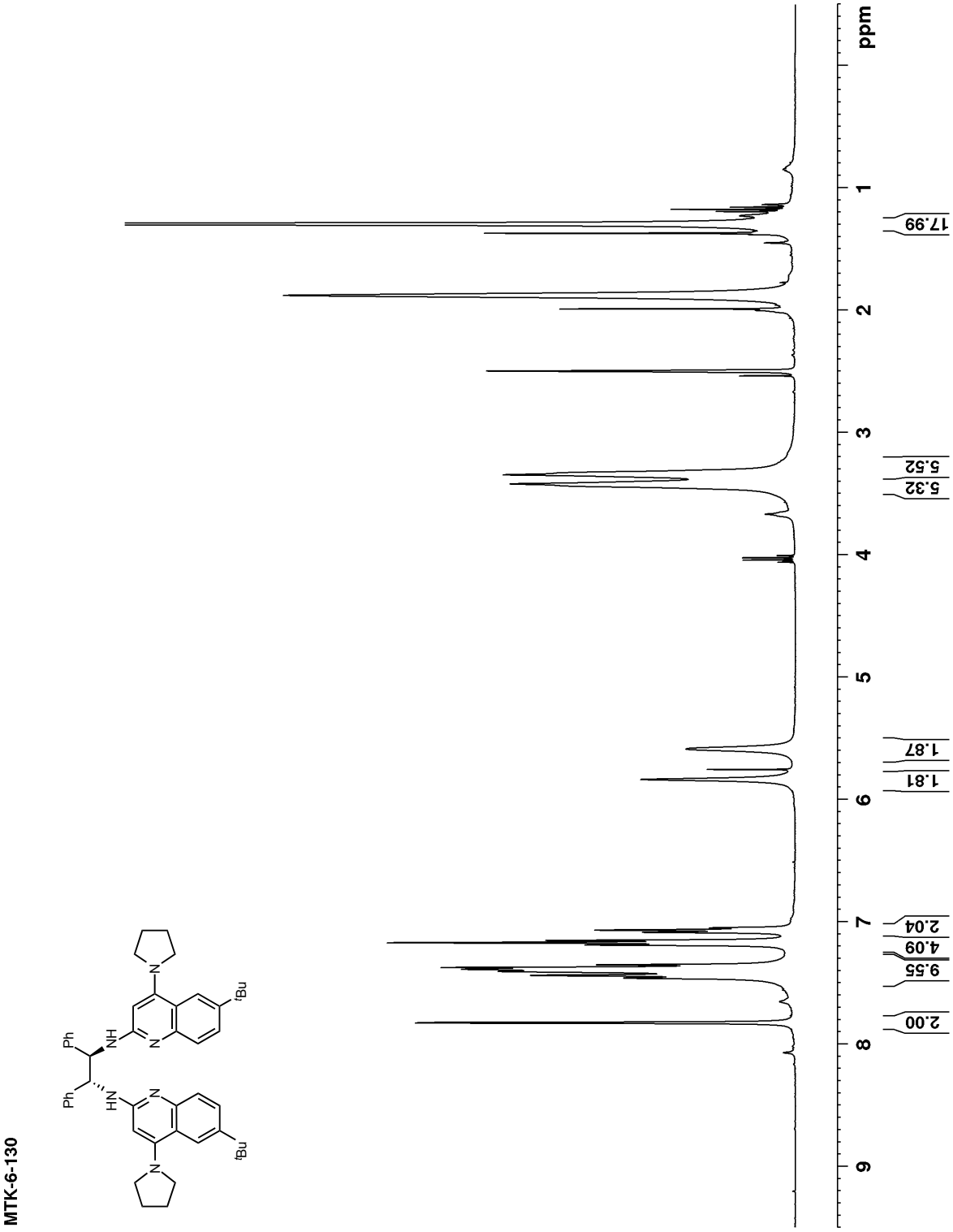

Figure B 12: ^{13}C NMR (100 MHz, d_6-DMSO) of **14i**

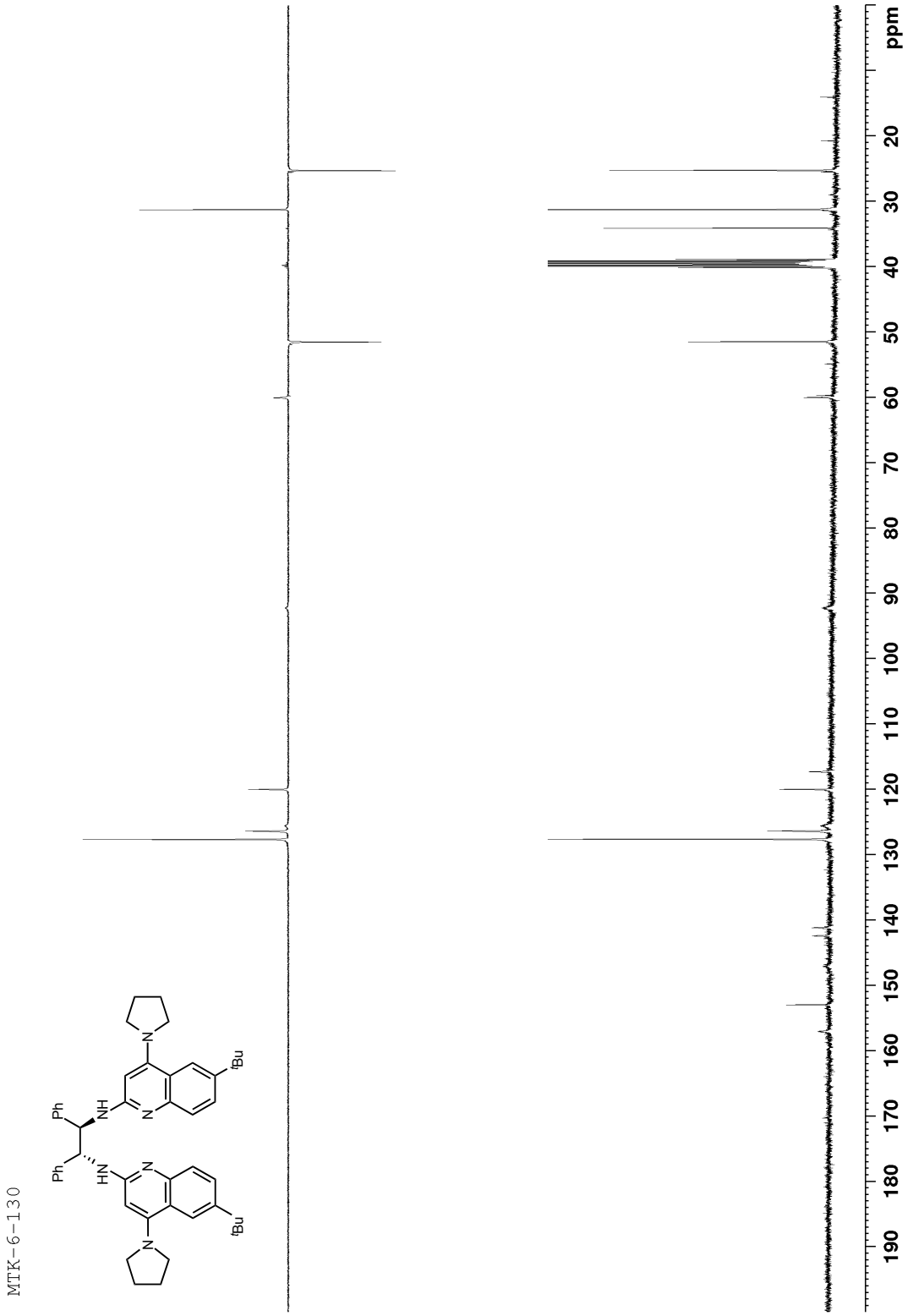

Figure B 13: ^{1}H NMR (400 MHz, $CDCl_3$) of **107b**

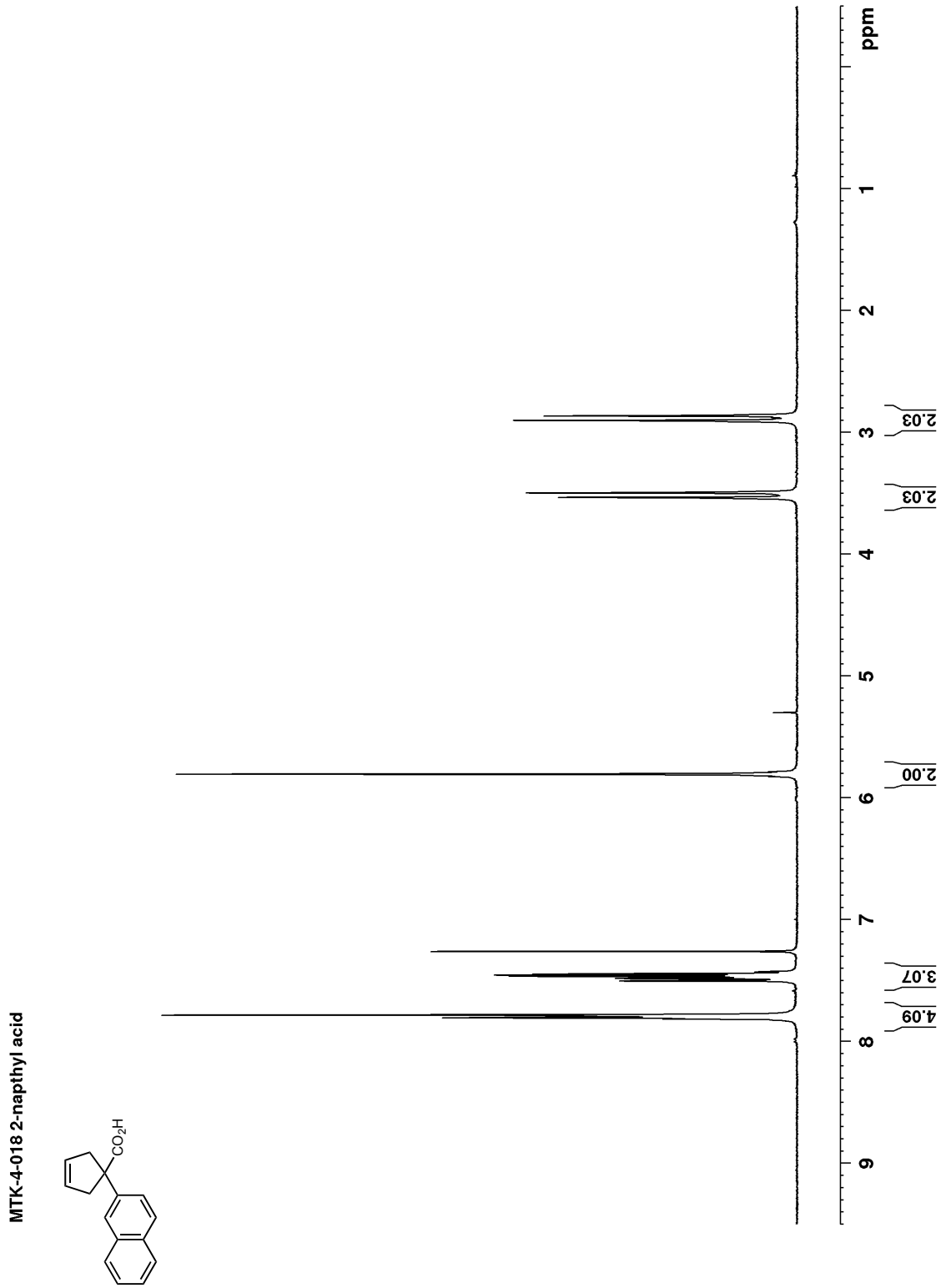

Figure B 14: ^{13}C NMR (100 MHz, $CDCl_3$) of **107b**

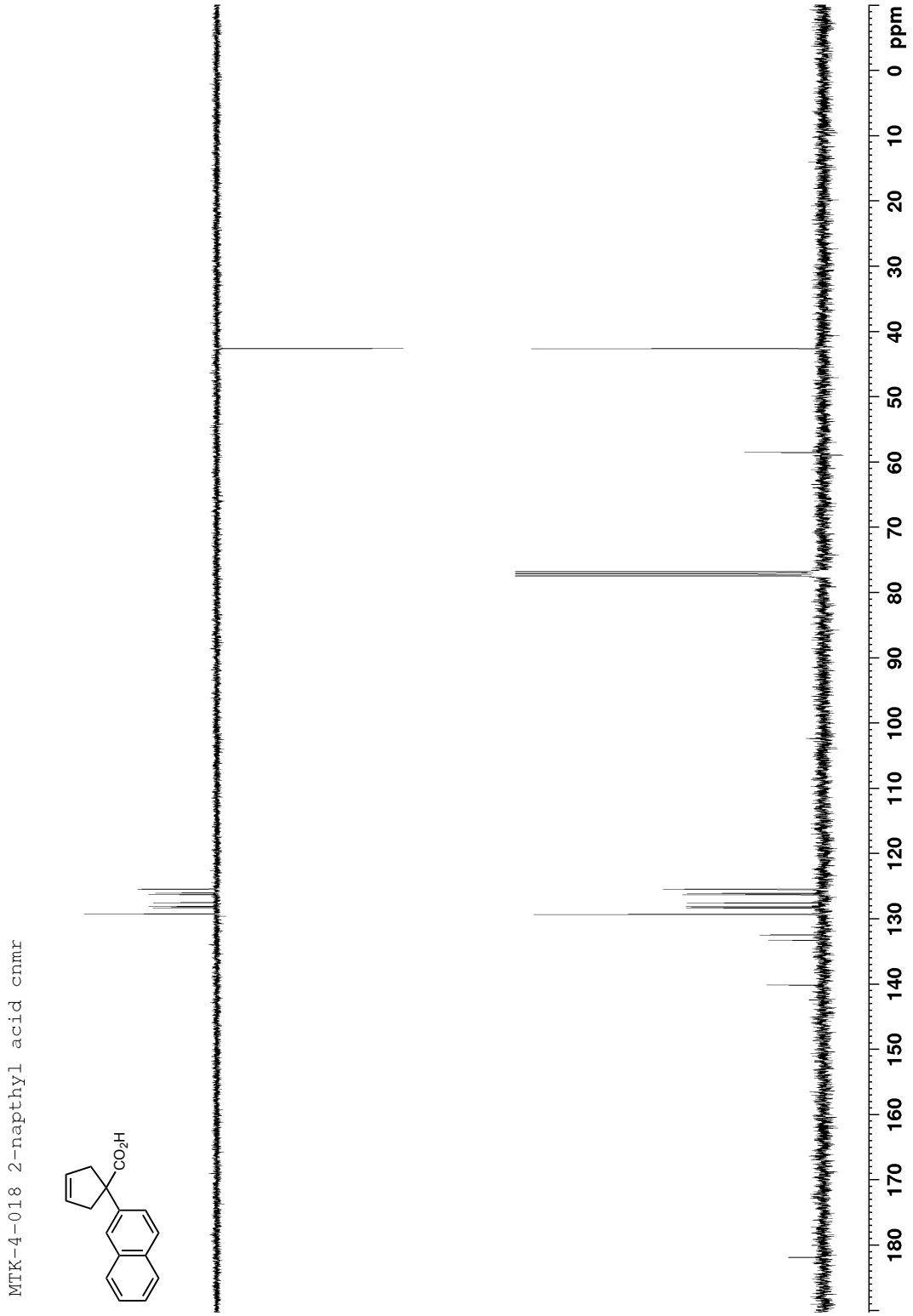

Figure B 15: ^{1}H NMR (400 MHz, $CDCl_3$) of **S3**

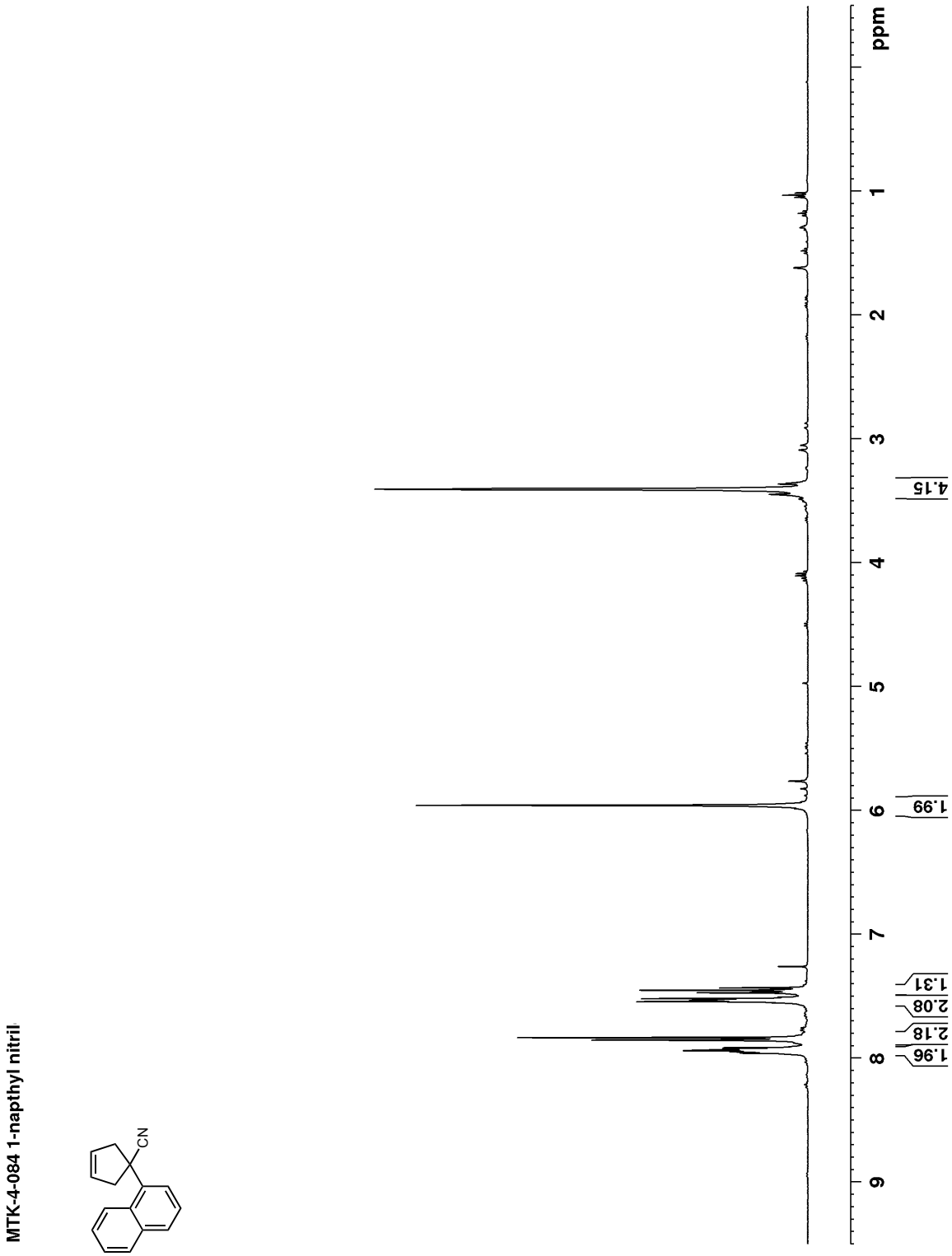

Figure B 16: ^{13}C NMR (100 MHz, $CDCl_3$) of **S3**

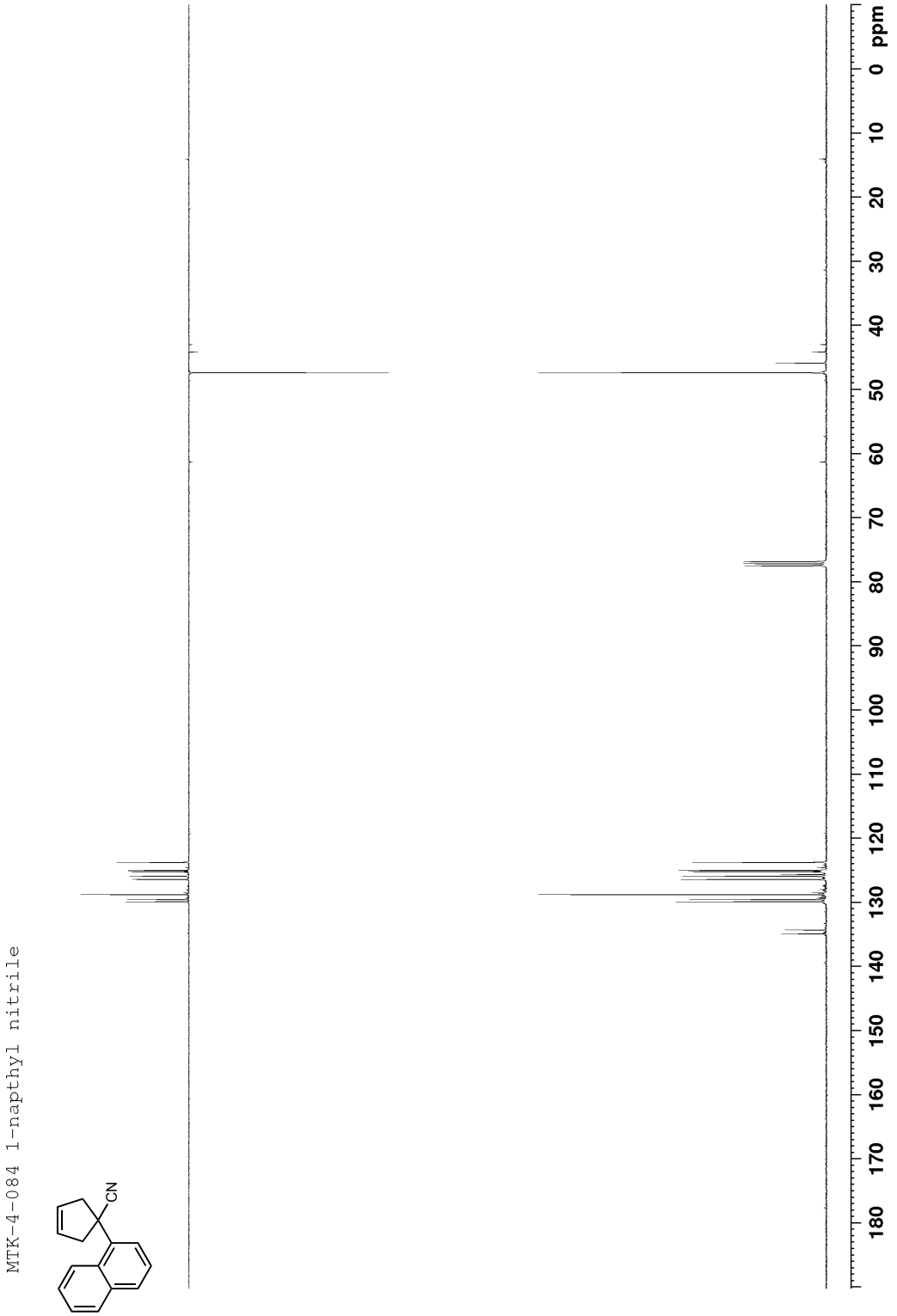

Figure B 17: ^{1}H NMR (400 MHz, $CDCl_3$) of **107c**

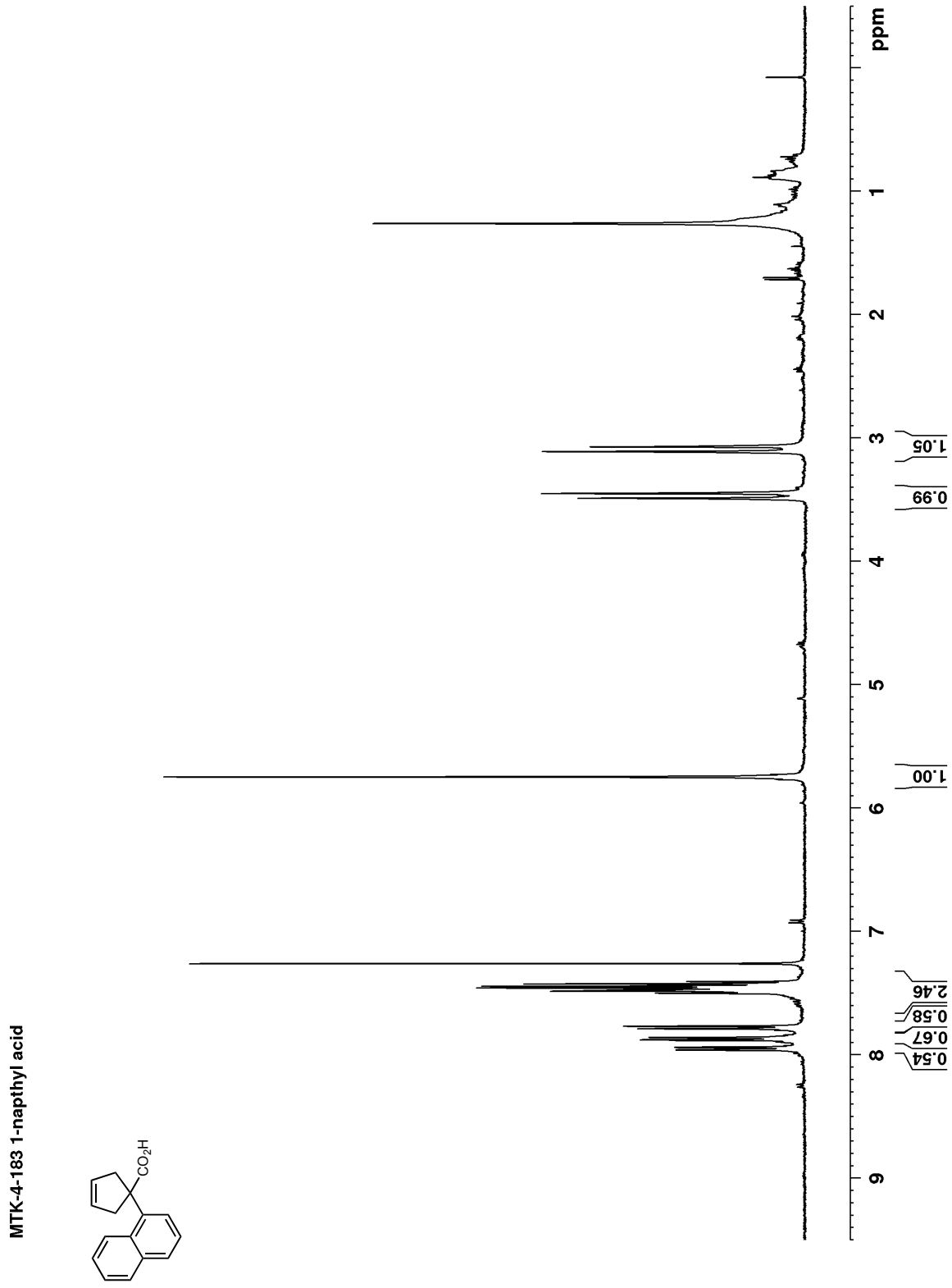

Figure B 18: ^{13}C NMR (100 MHz, CDCl3) of **107c**

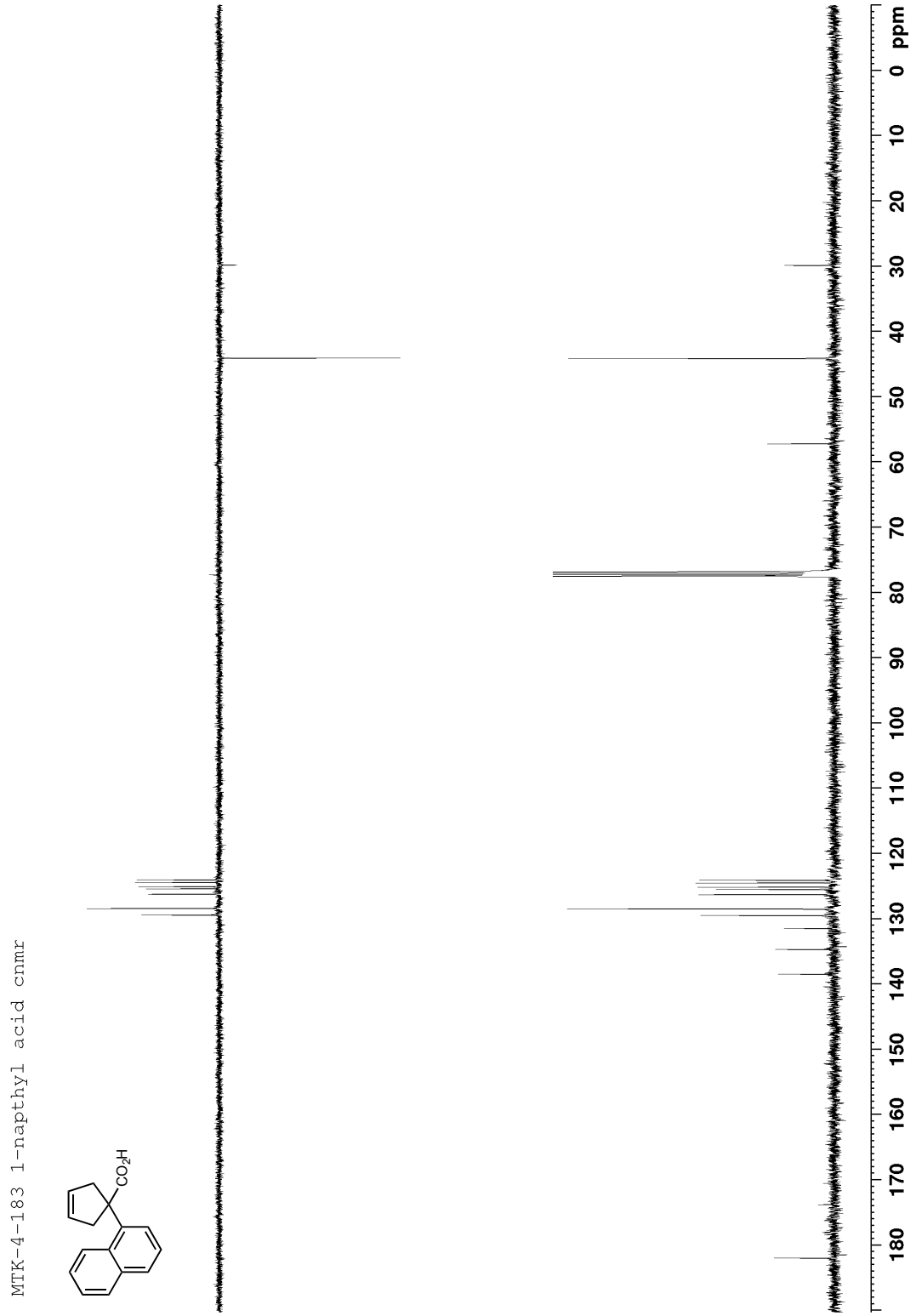

Figure B 19: [1]H NMR (400 MHz, CDCl3) of **107d**

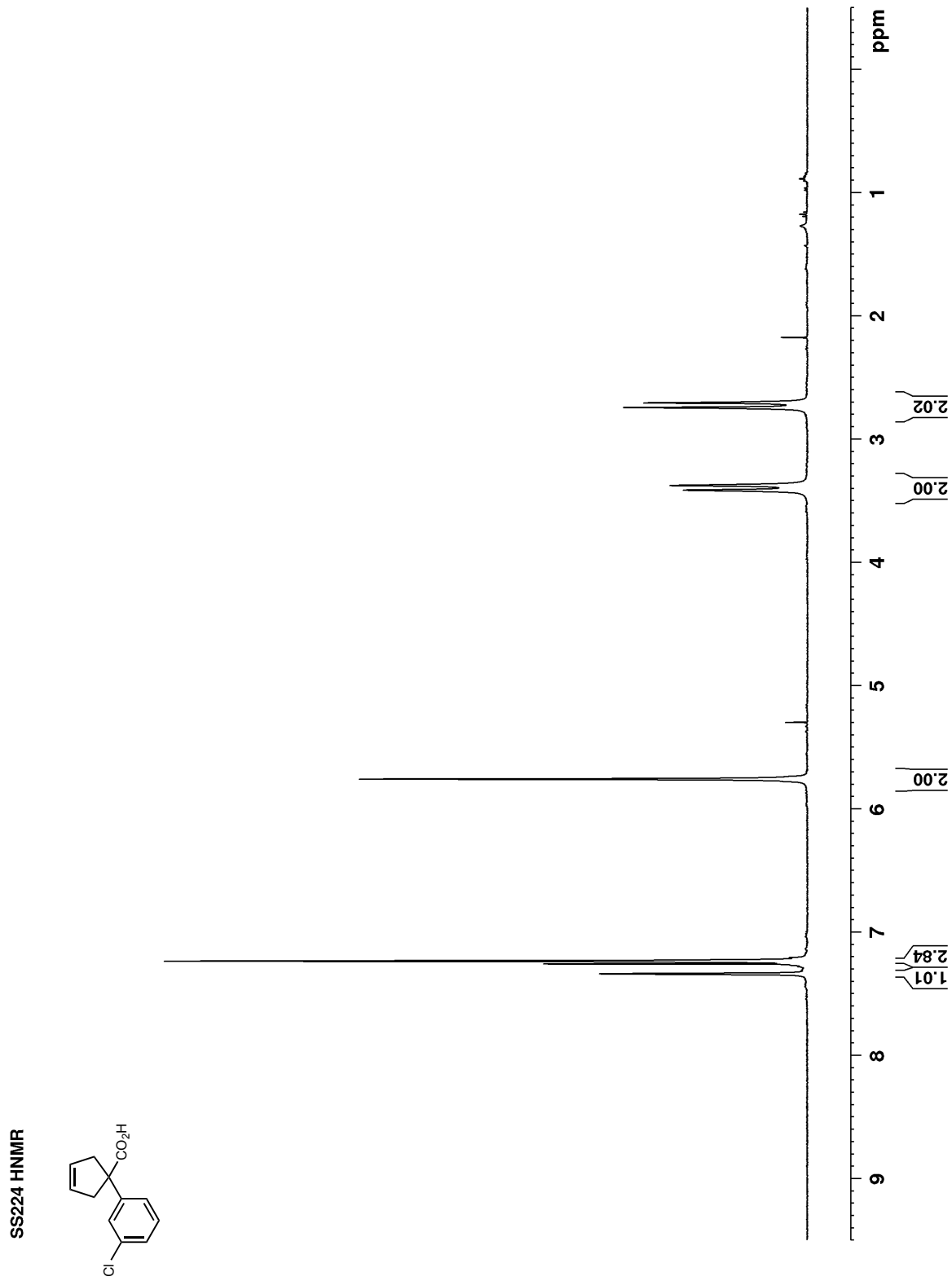

Figure B 20: ^{13}C NMR (100 MHz, CDCl3) of **107d**

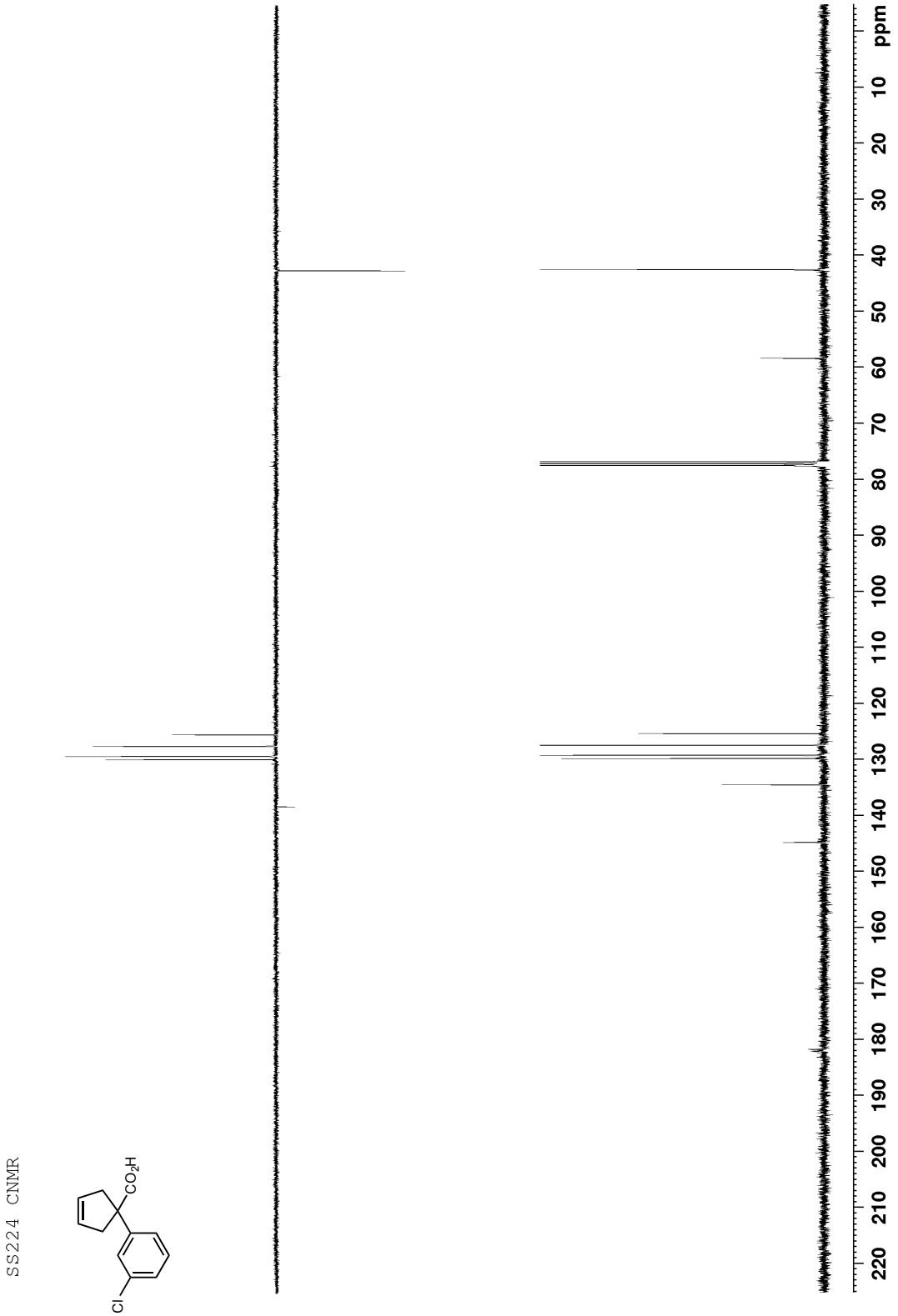

Figure B 21: ^{1}H NMR (400 MHz, CDCl3) of **107e**

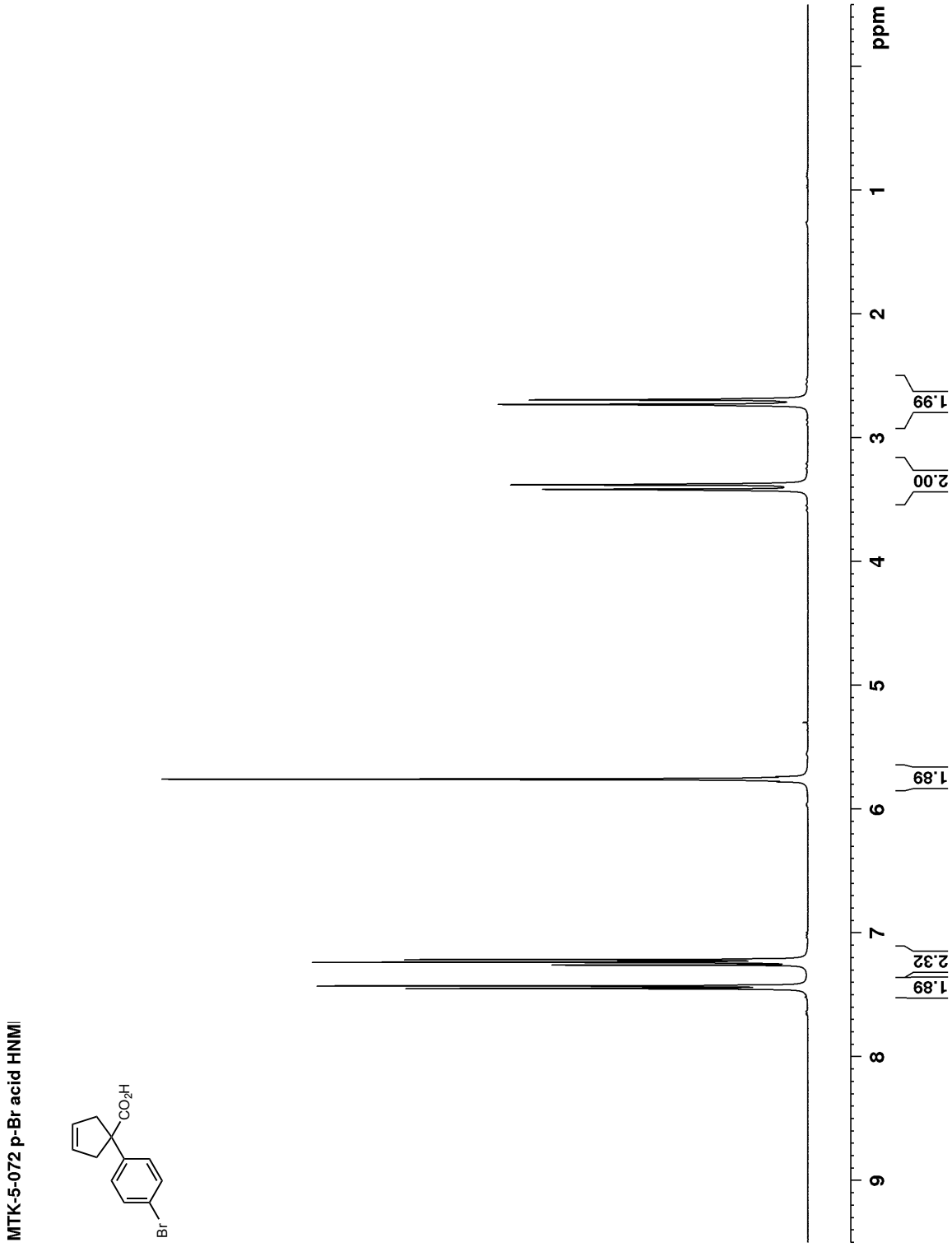

Figure B 22: ^{13}C NMR (100 MHz, CDCl3) of **107e**

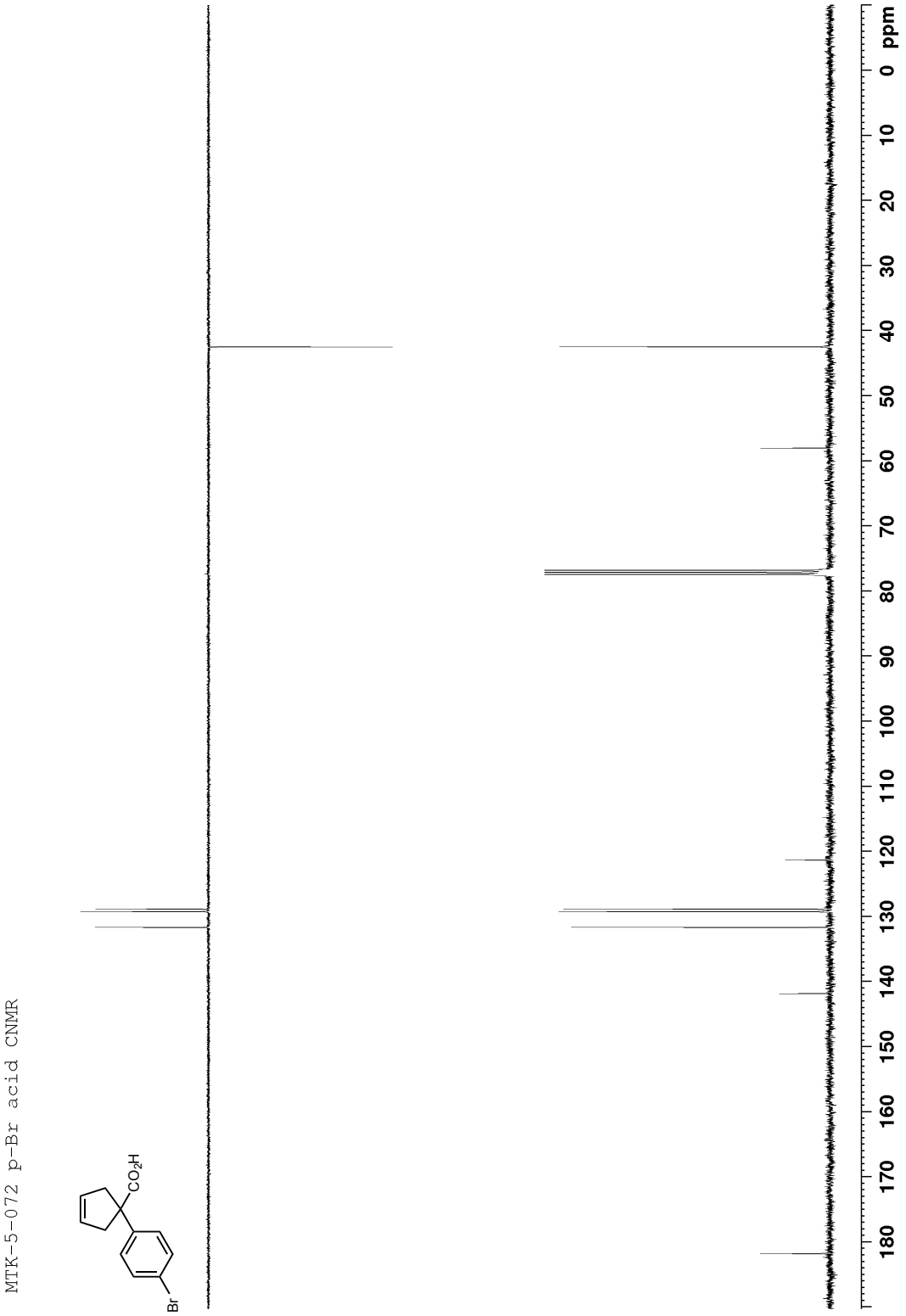

Figure B 23: ^{1}H NMR (400 MHz, CDCl3) of **107f**

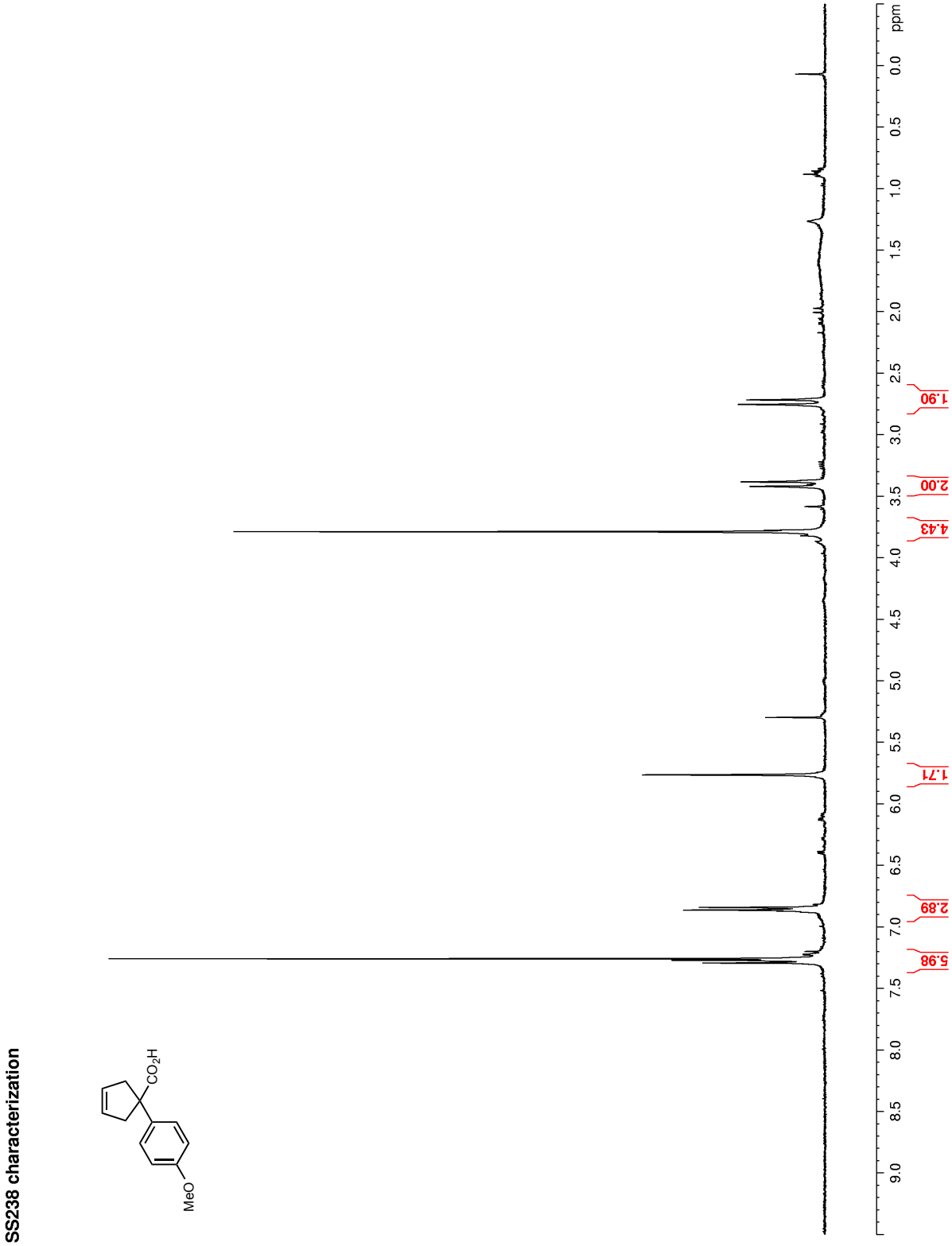

Figure B 24: ^{13}C NMR (100 MHz, $CDCl_3$) of **107f**

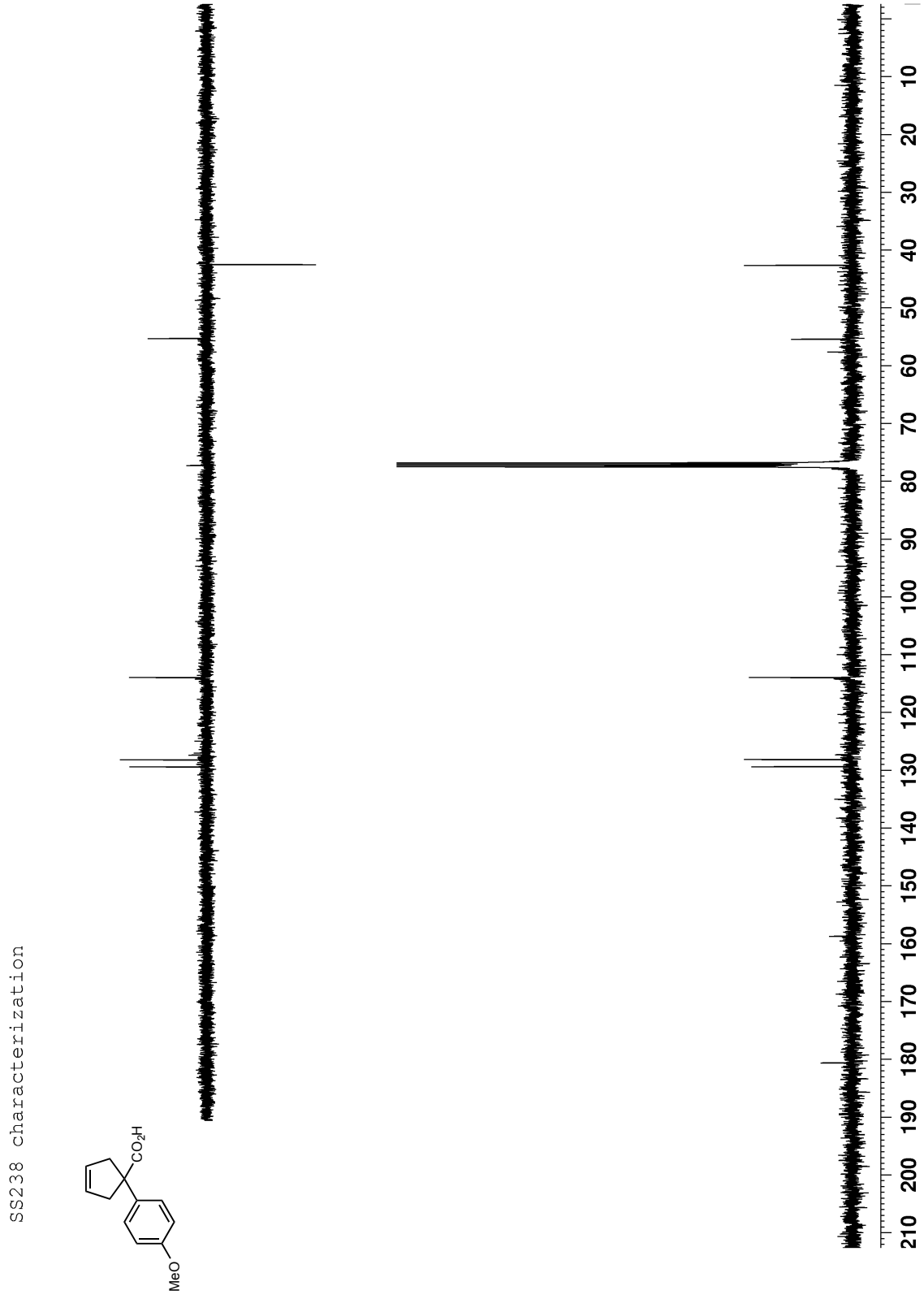

Figure B 25 ^{1}H NMR (400 MHz, $CDCl_3$) of **107g**

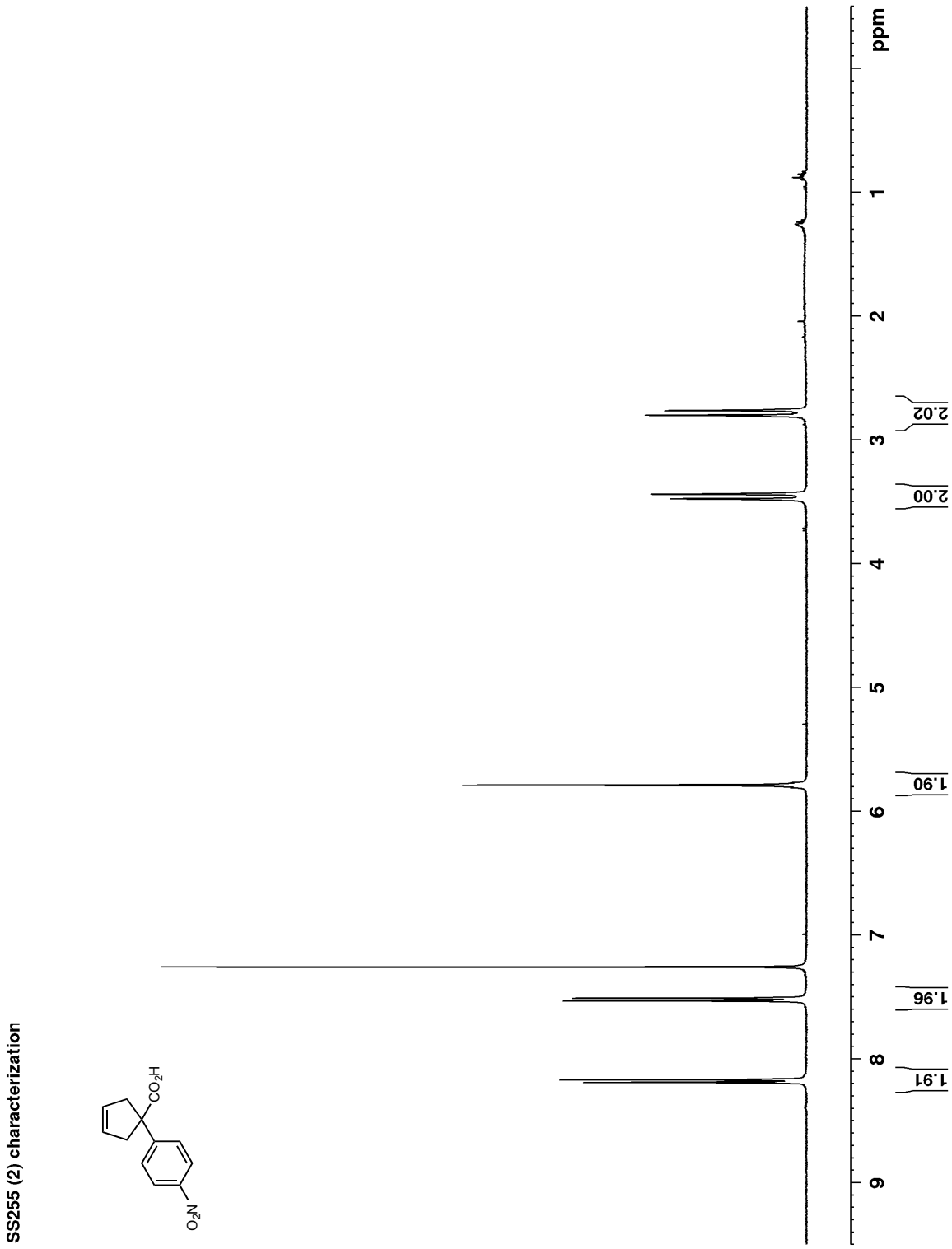

Figure B 26: ^{13}C NMR (100 MHz, $CDCl_3$) of **107g**

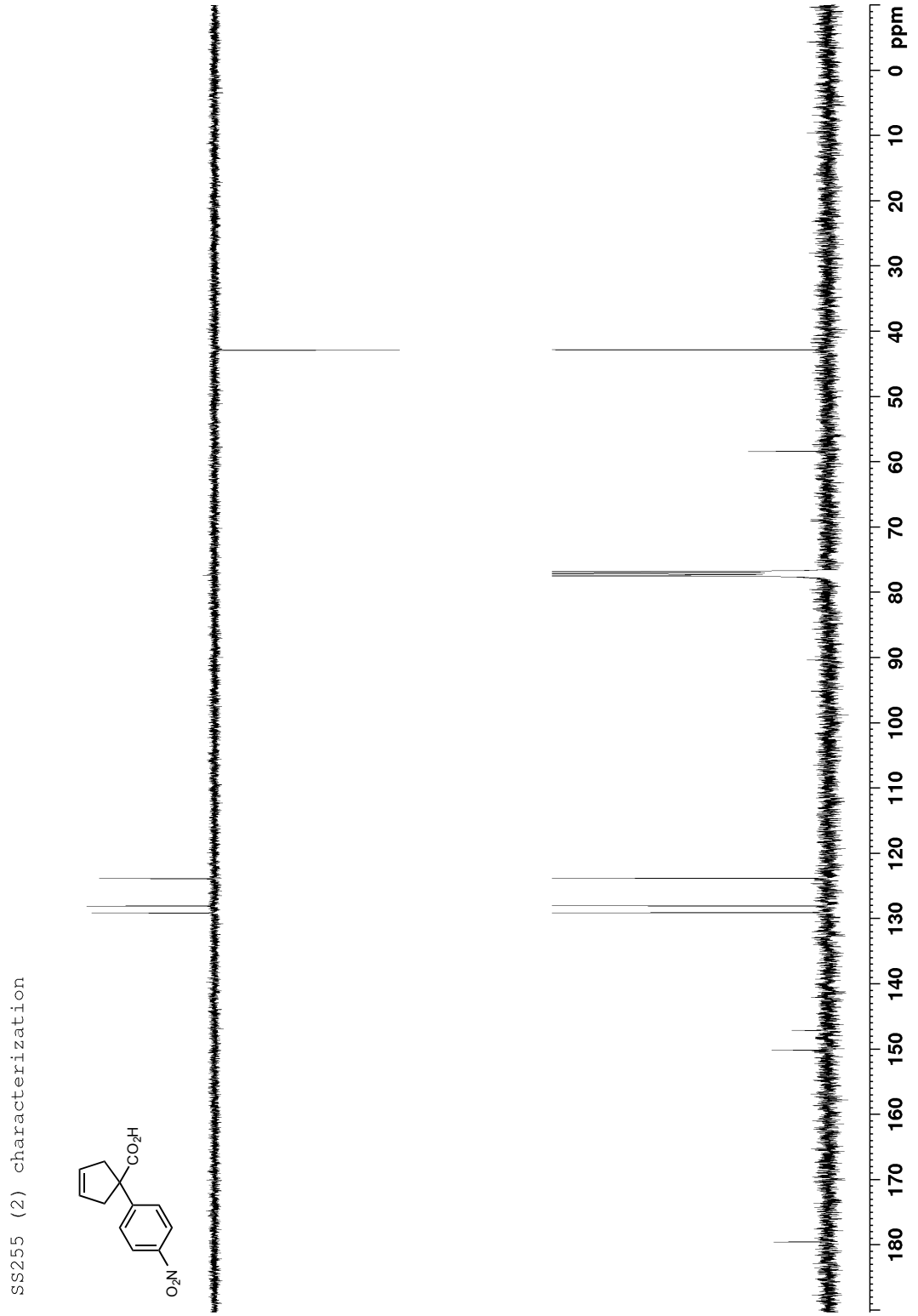

Figure B 27: ^{1}H NMR (400 MHz, $CDCl_3$) of **107h**

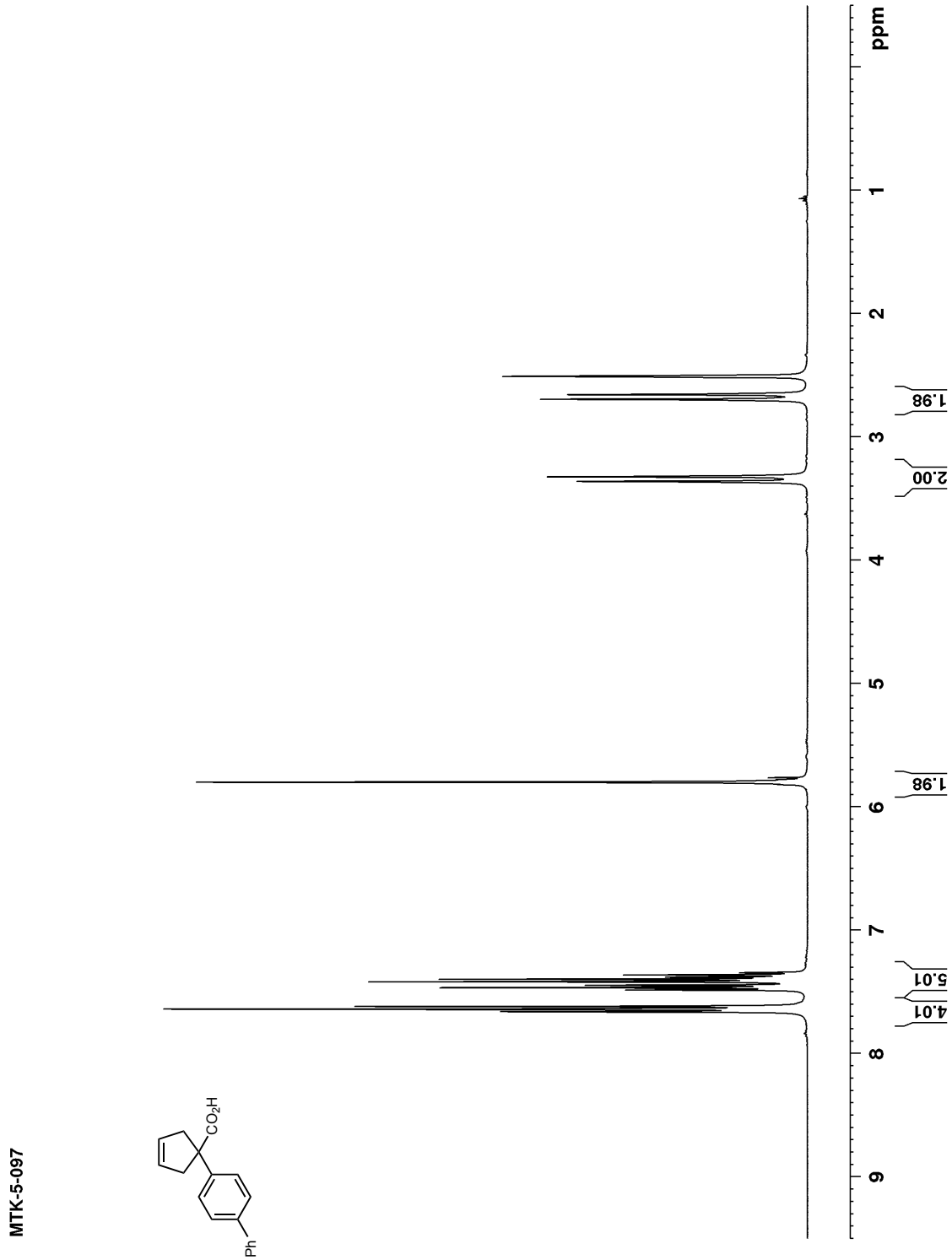

Figure B 28: ^{13}C NMR (100 MHz, $CDCl_3$) of **107h**

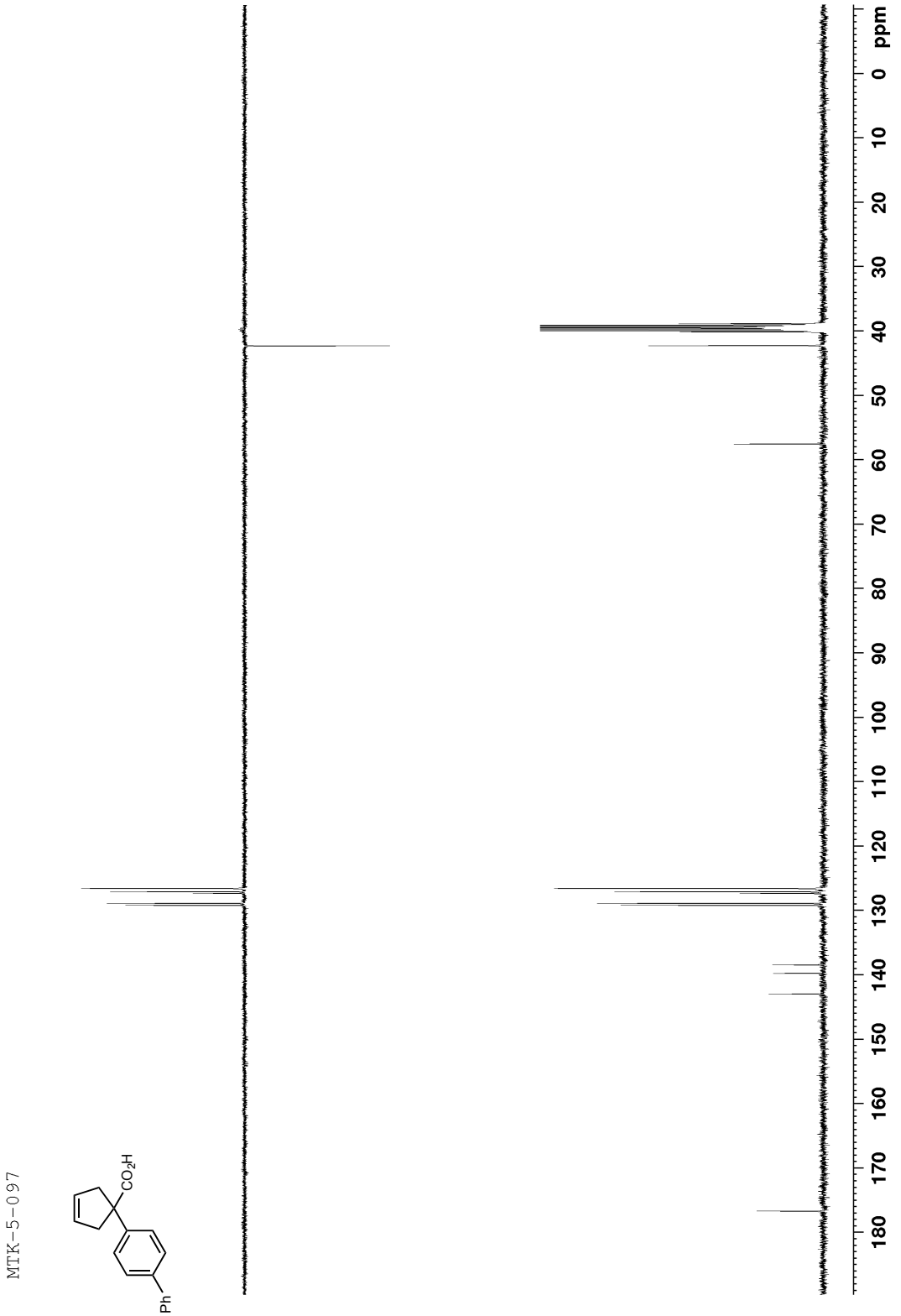

Figure B 29: ^{1}H NMR (400 MHz, $CDCl_3$) of **S5**

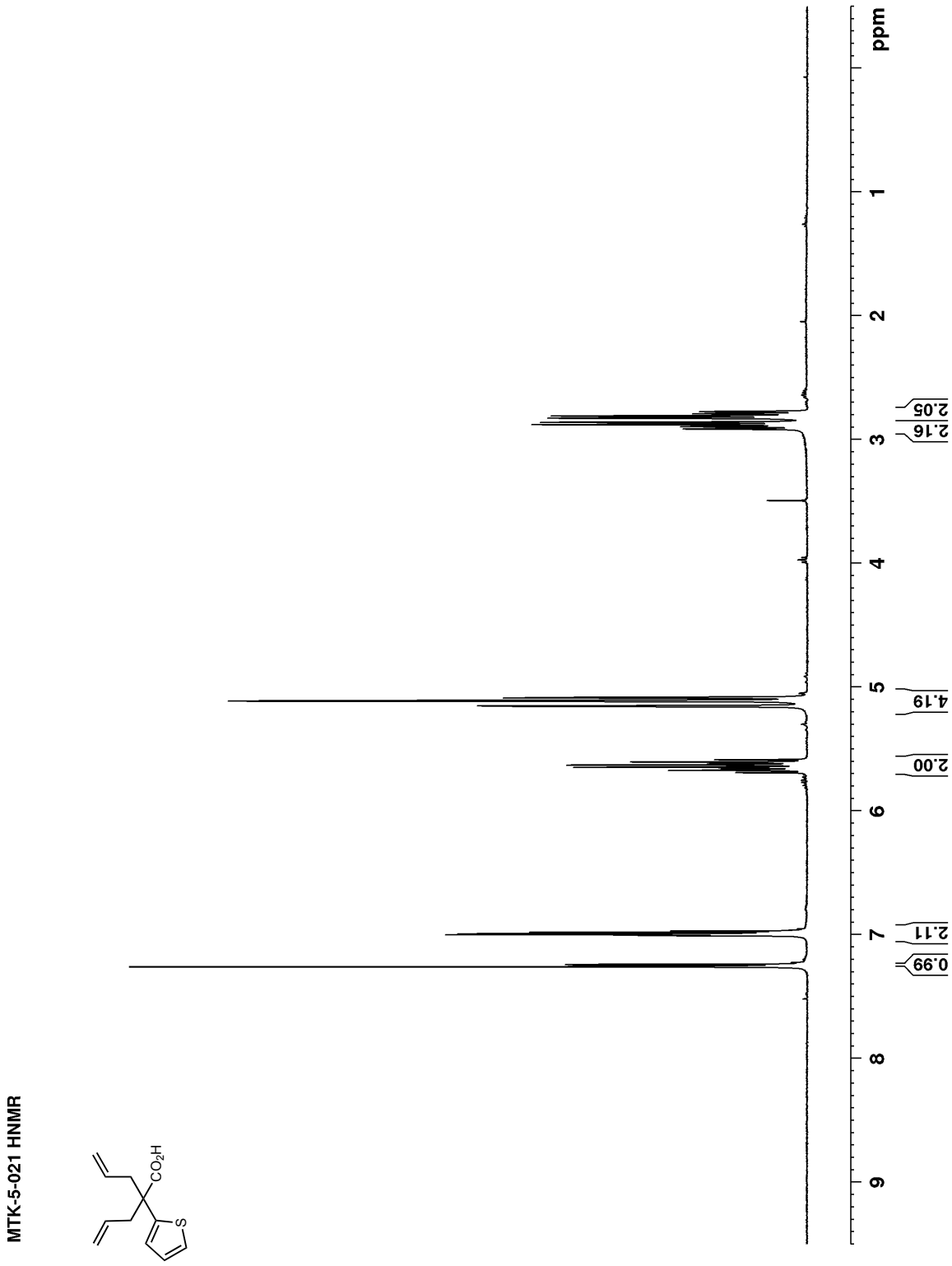

Figure B 30: ^{13}C NMR (100 MHz, $CDCl_3$) of **S5**

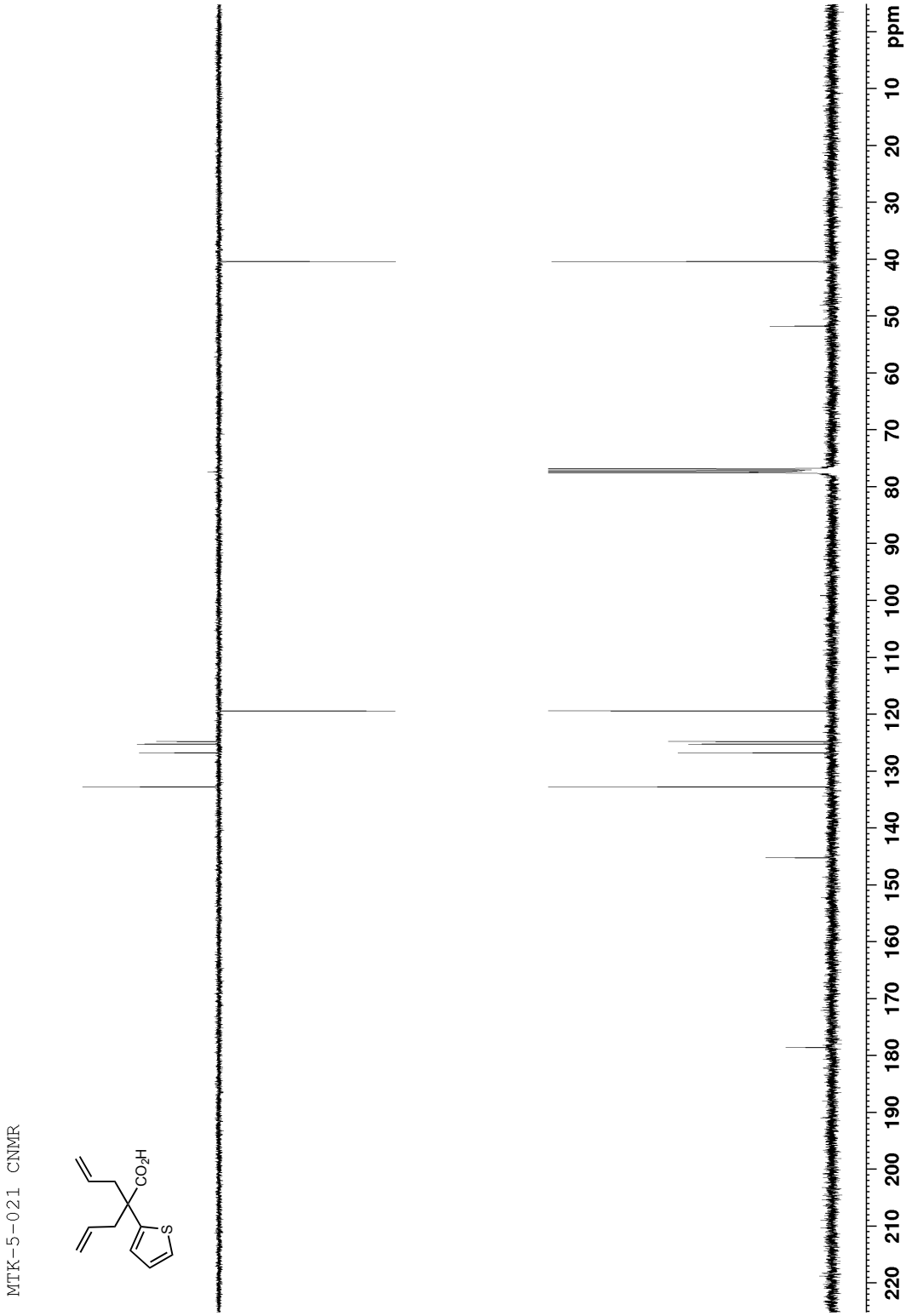

Figure B 31: ^{1}H NMR (400 MHz, $CDCl_3$) of **107i**

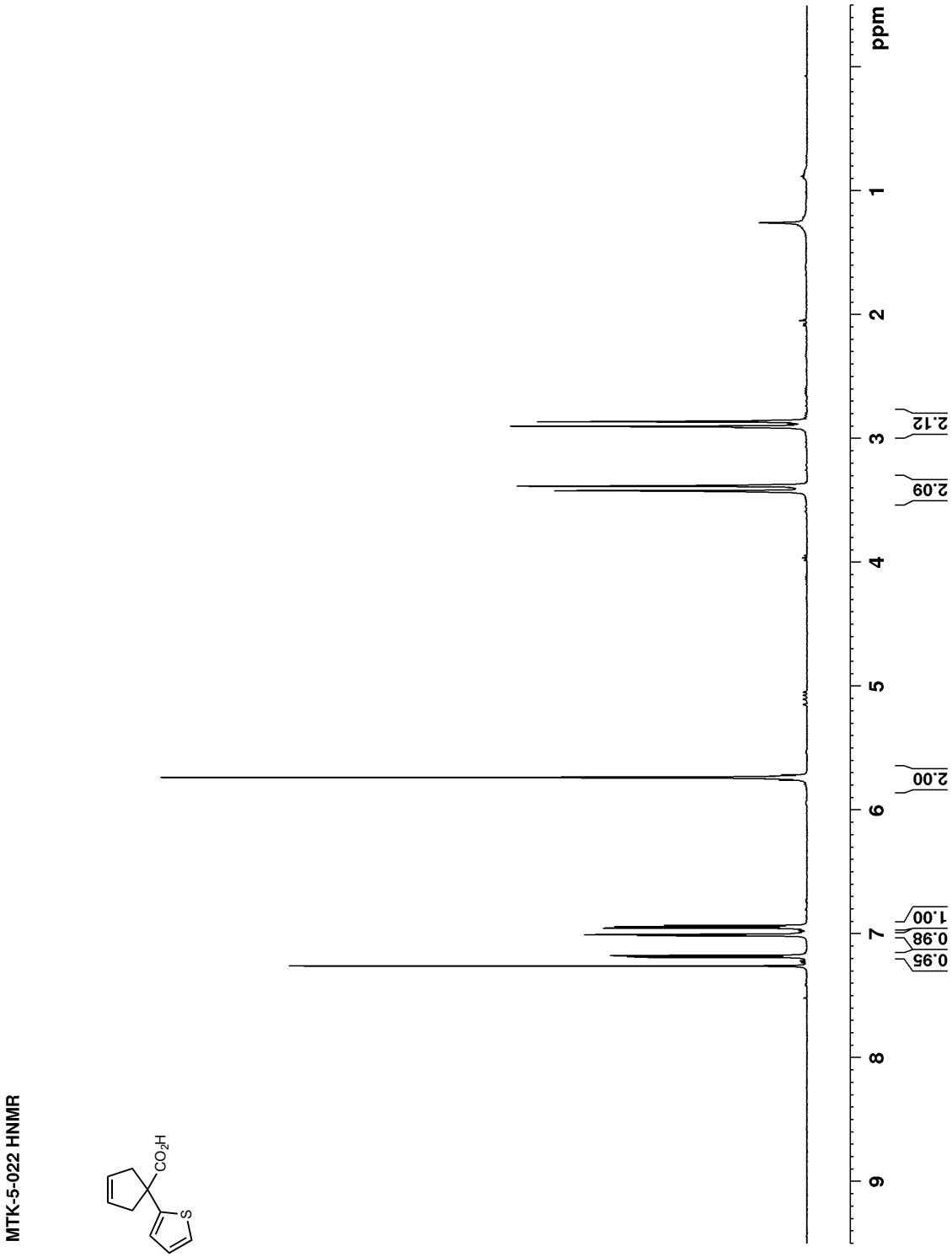

Figure B 32: ^{13}C NMR (100 MHz, $CDCl_3$) of **107i**

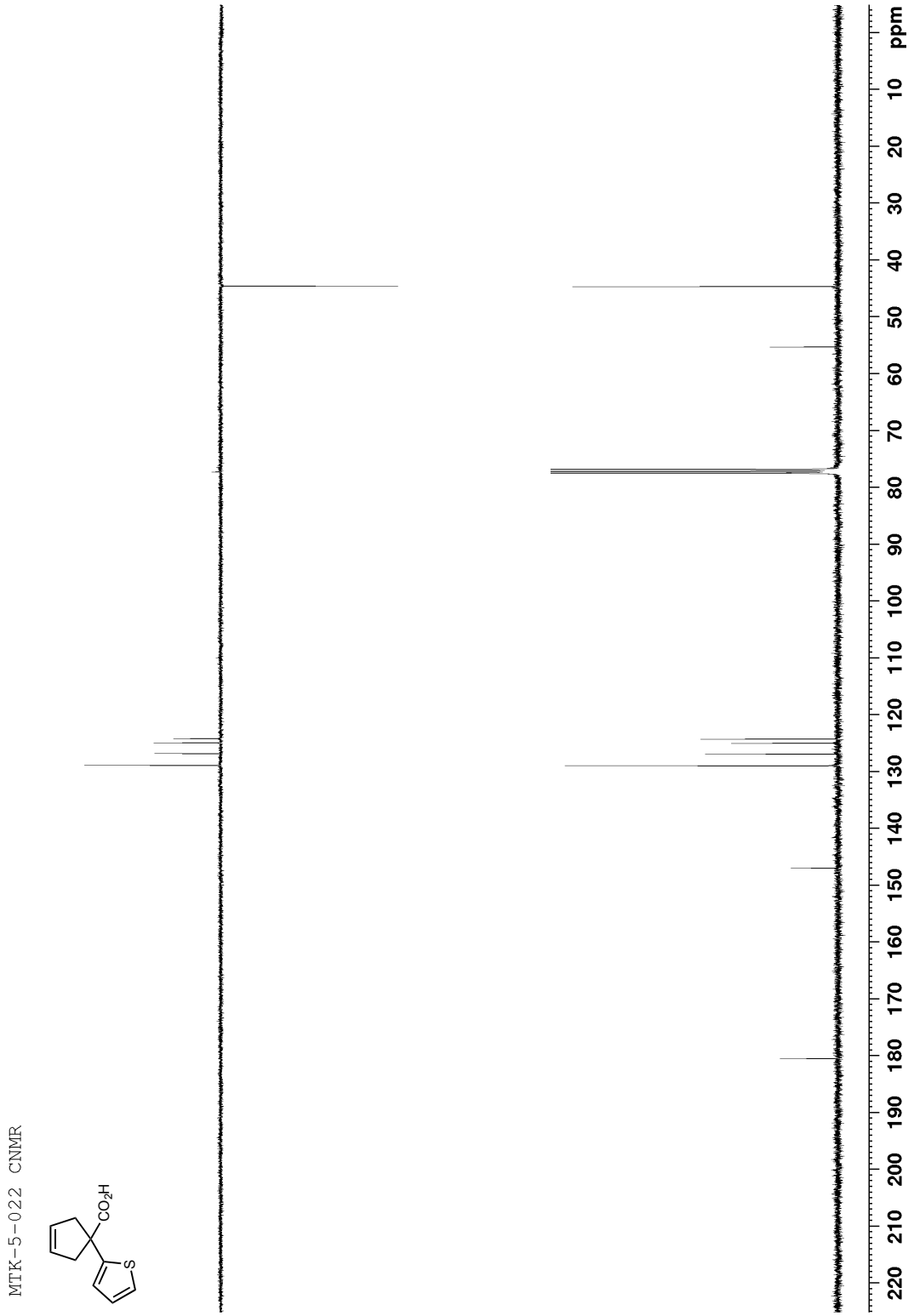

Figure B 33: ^{1}H NMR (400 MHz, $CDCl_3$) of **128**

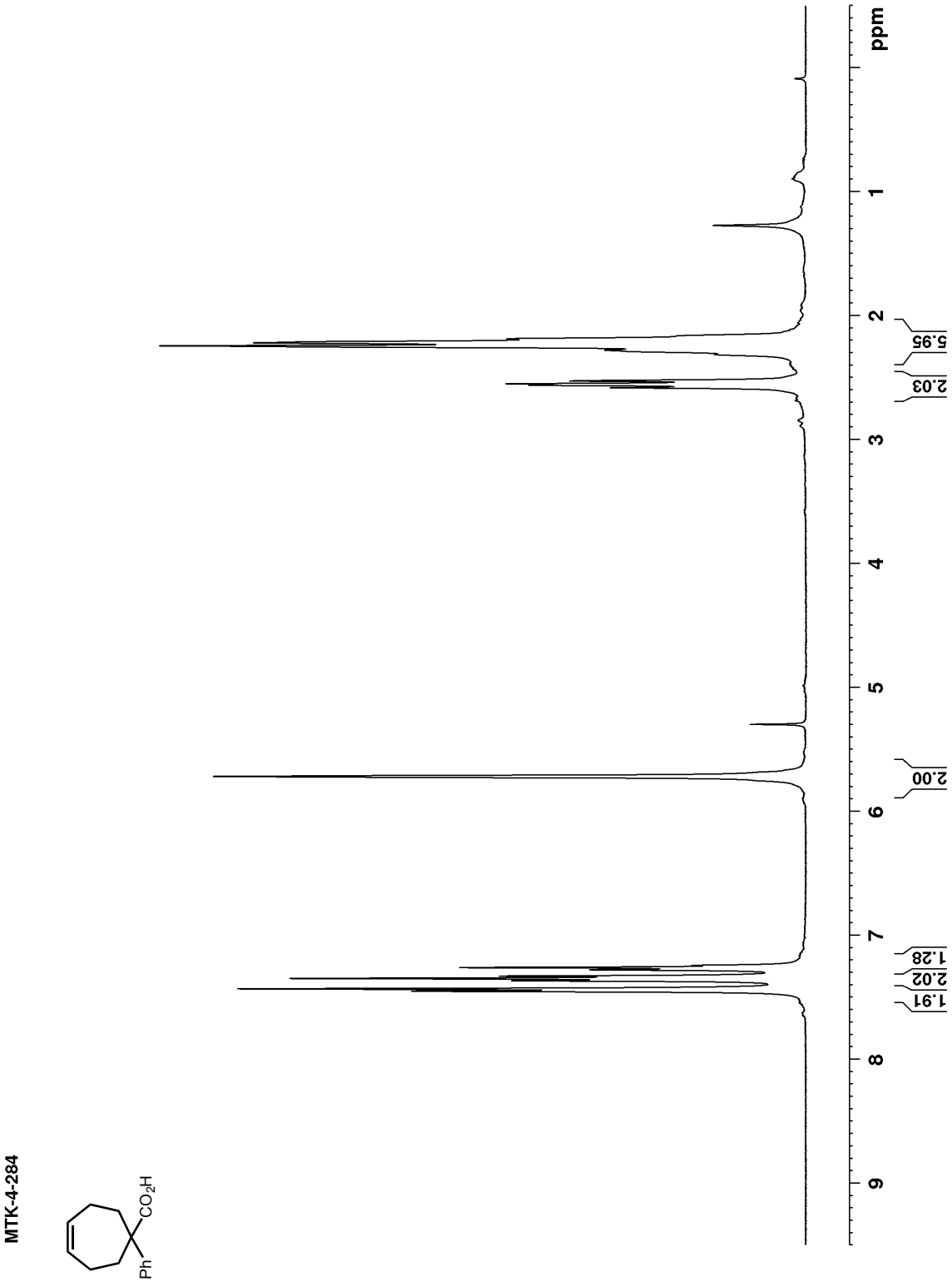

Figure B 34: ^{13}C NMR (100 MHz, $CDCl_3$) of **128**

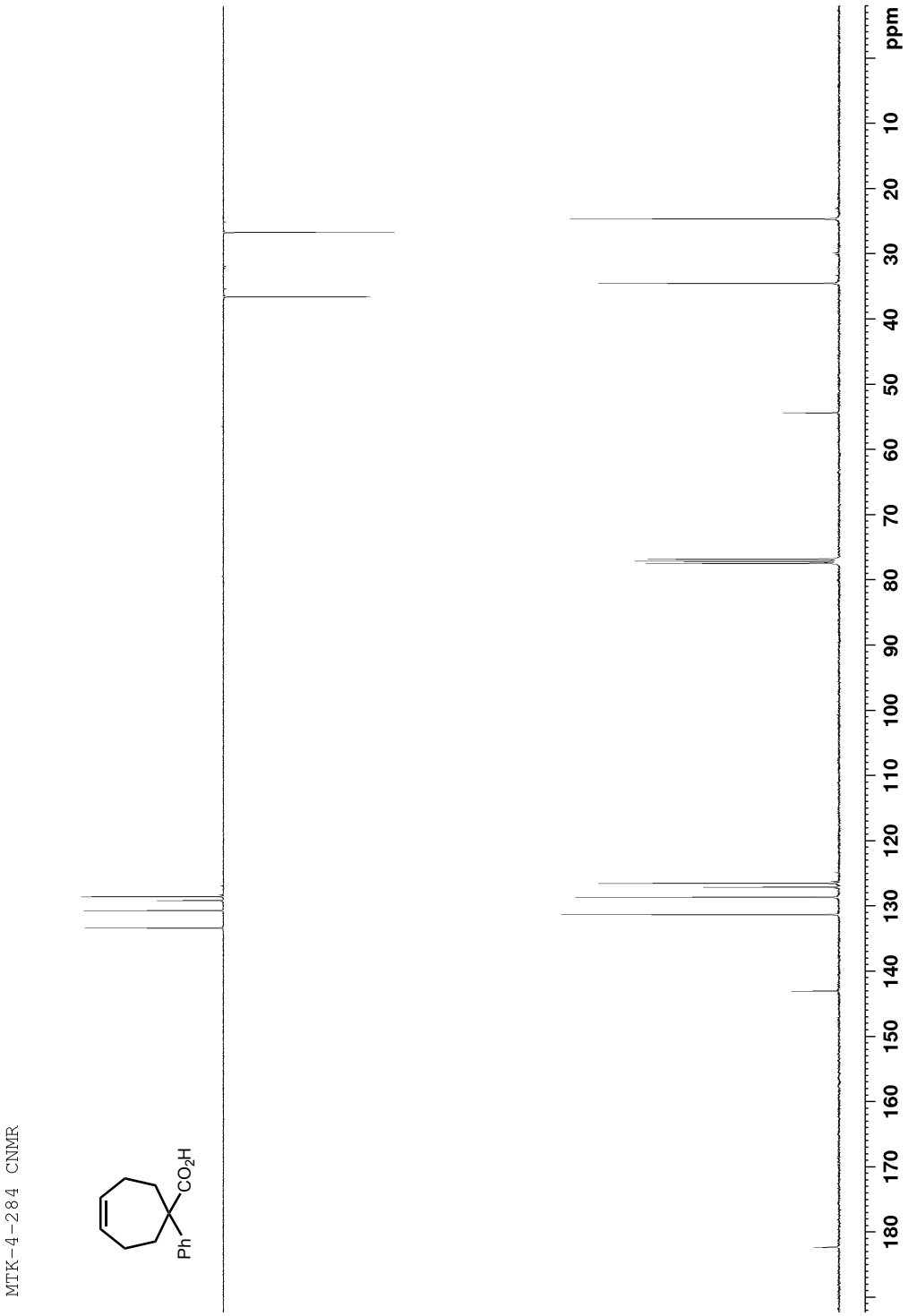

Figure B 35: ^{1}H NMR (400 MHz, $CDCl_3$) of **107j**

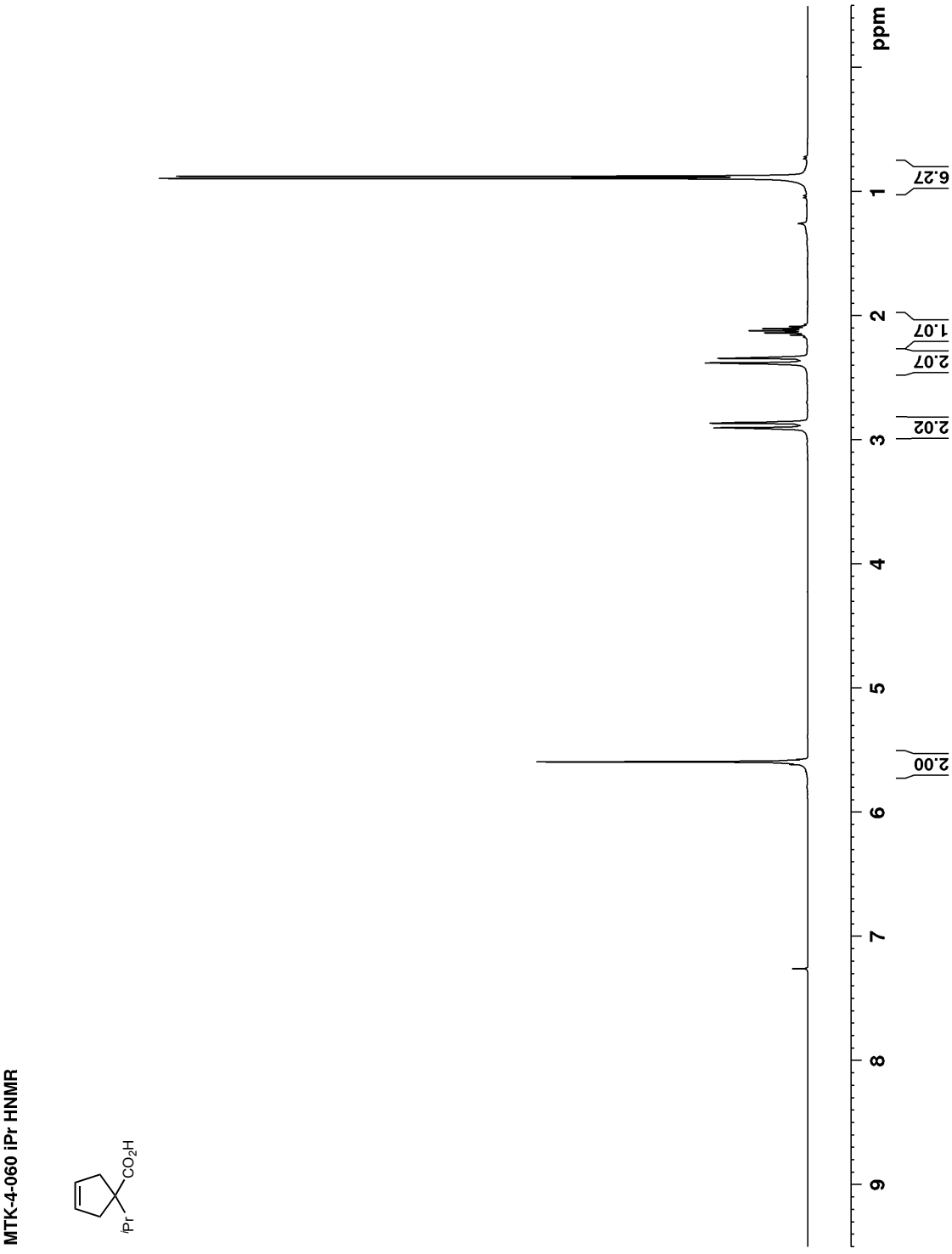

Figure B 36: ^{13}C NMR (100 MHz, $CDCl_3$) of **107j**

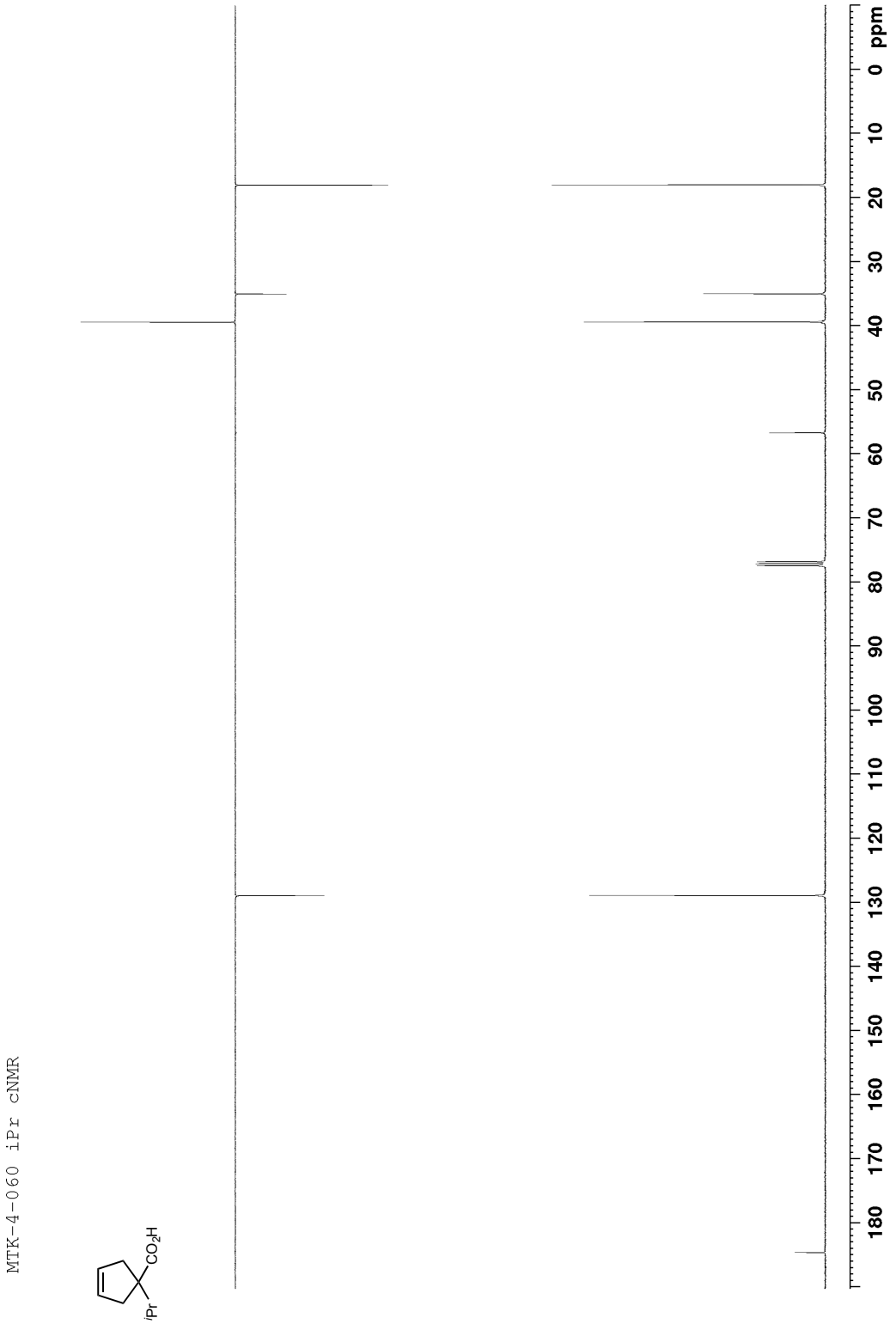

Figure B 37: ^{1}H NMR (400 MHz, $CDCl_3$) of **107k**

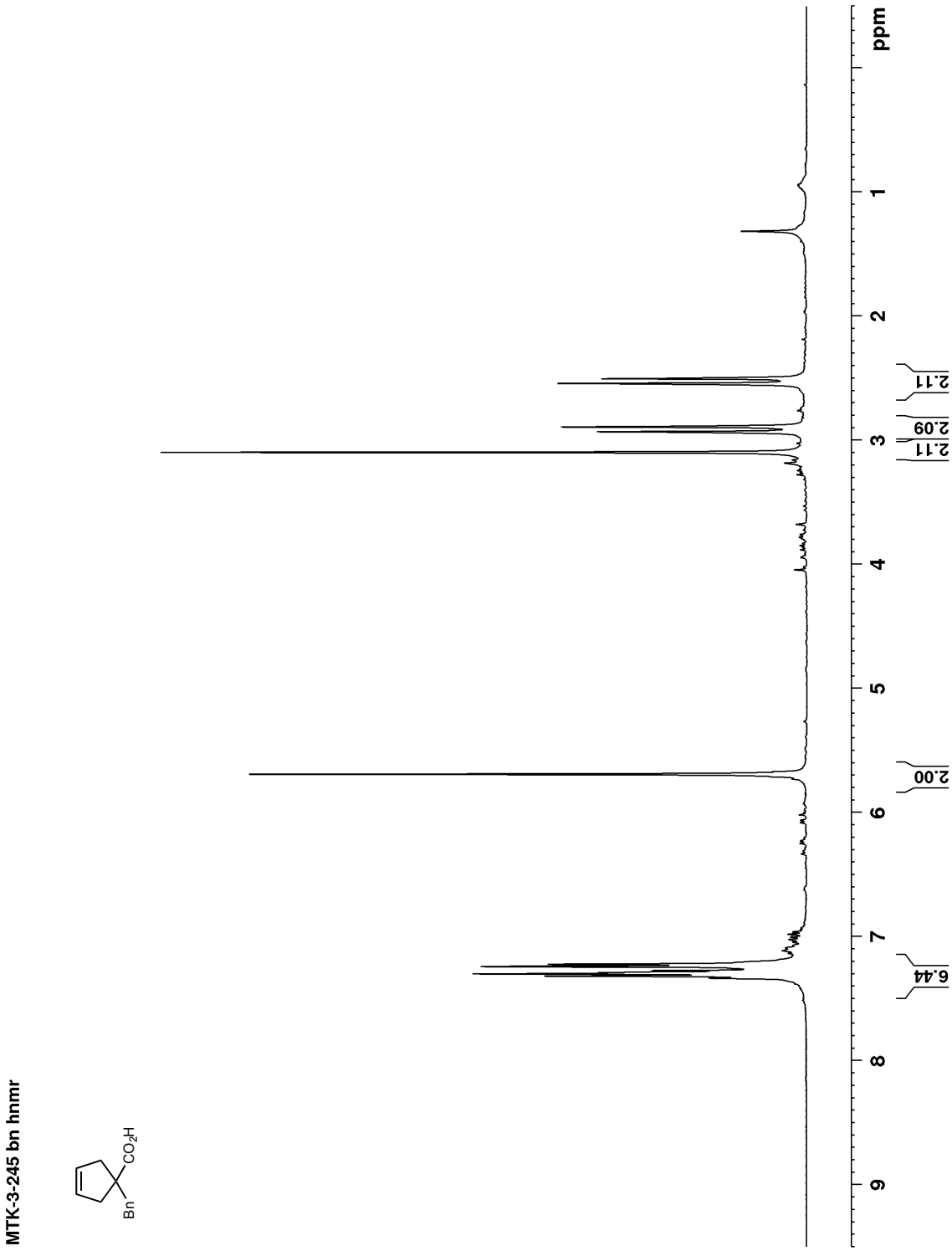

Figure B 38: ^{13}C NMR (100 MHz, $CDCl_3$) of **107k**

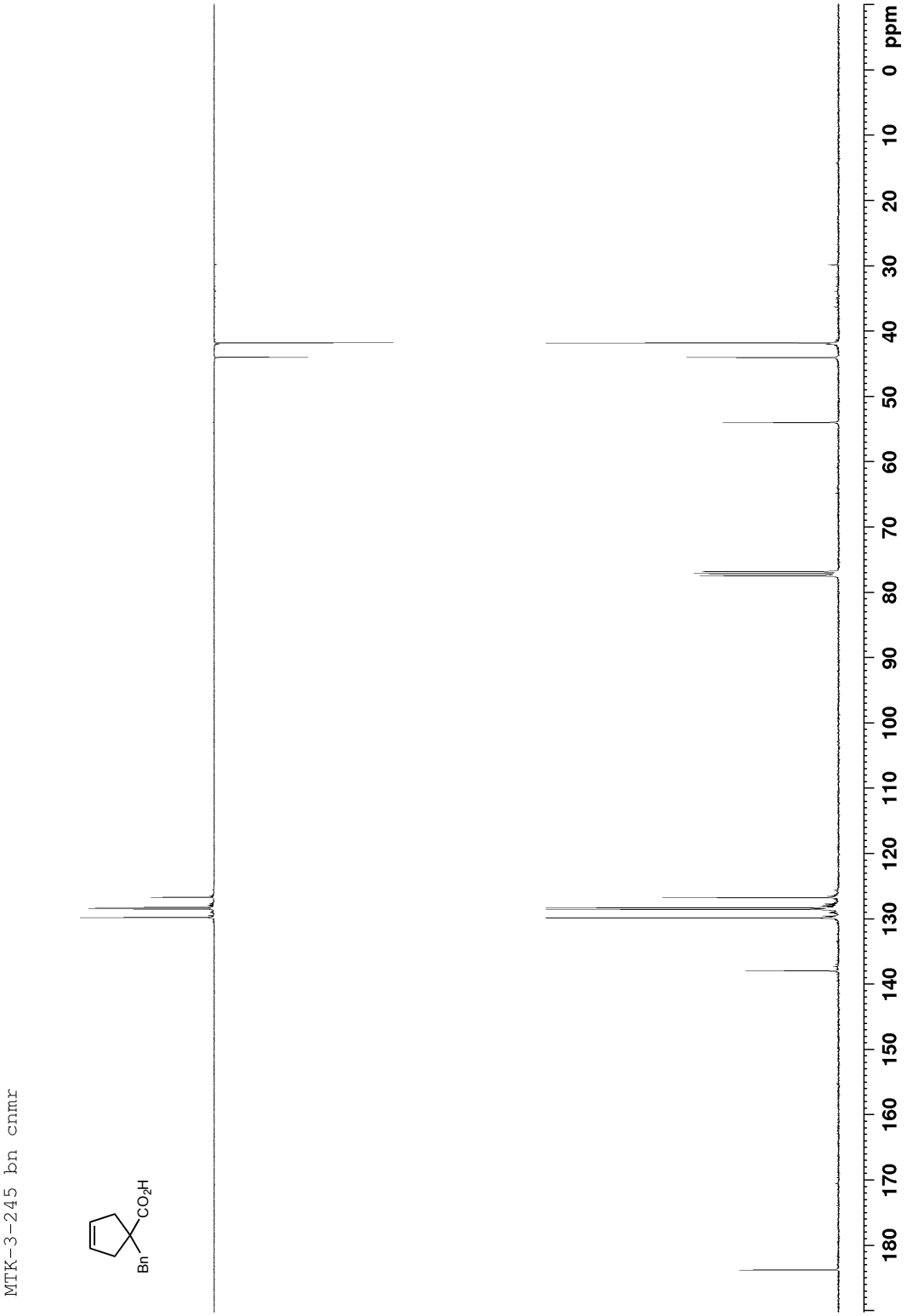

Figure B 39: ^{1}H NMR (400 MHz, $CDCl_3$) of **S6**

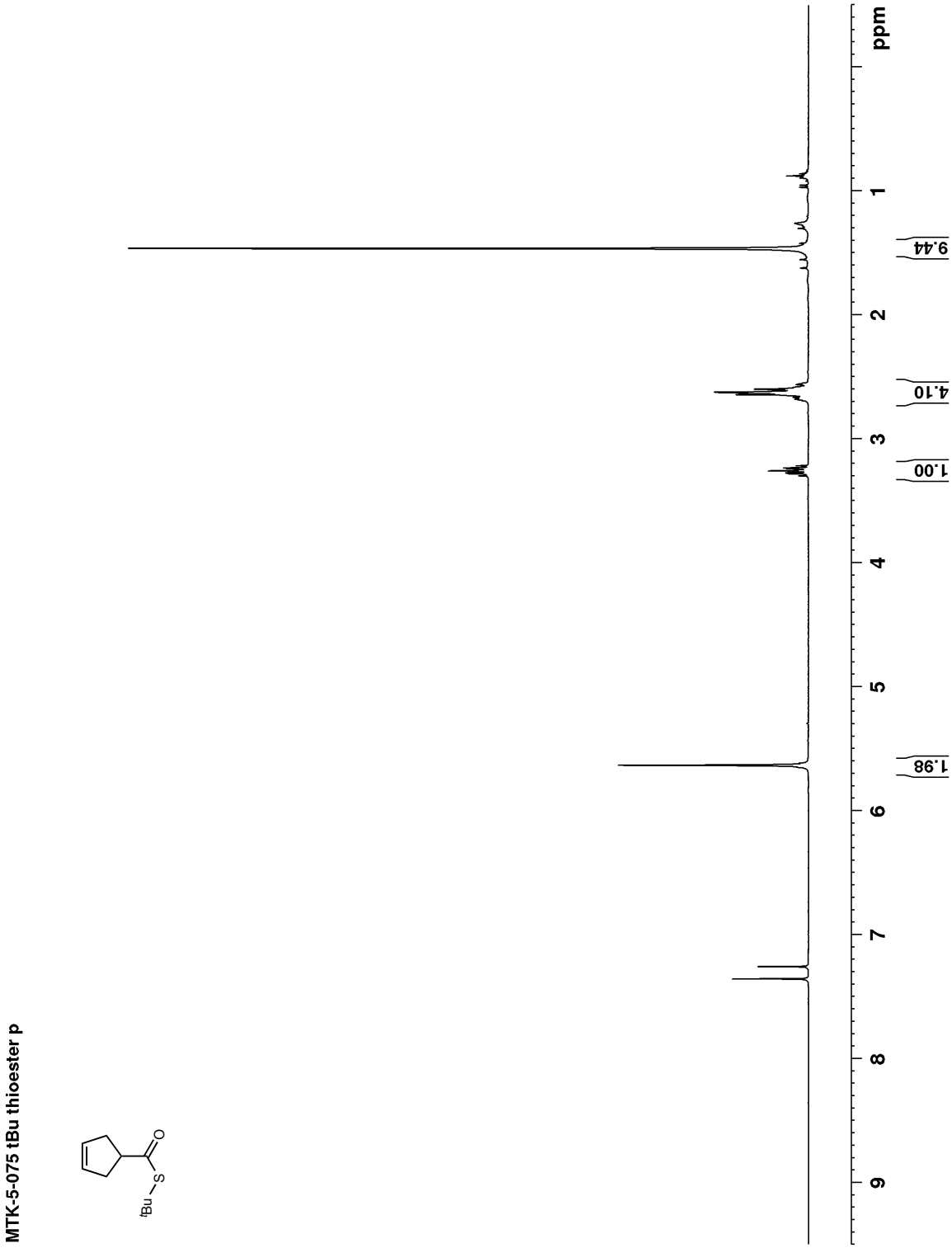

Figure B 40: ^{13}C NMR (100 MHz, $CDCl_3$) of **S6**

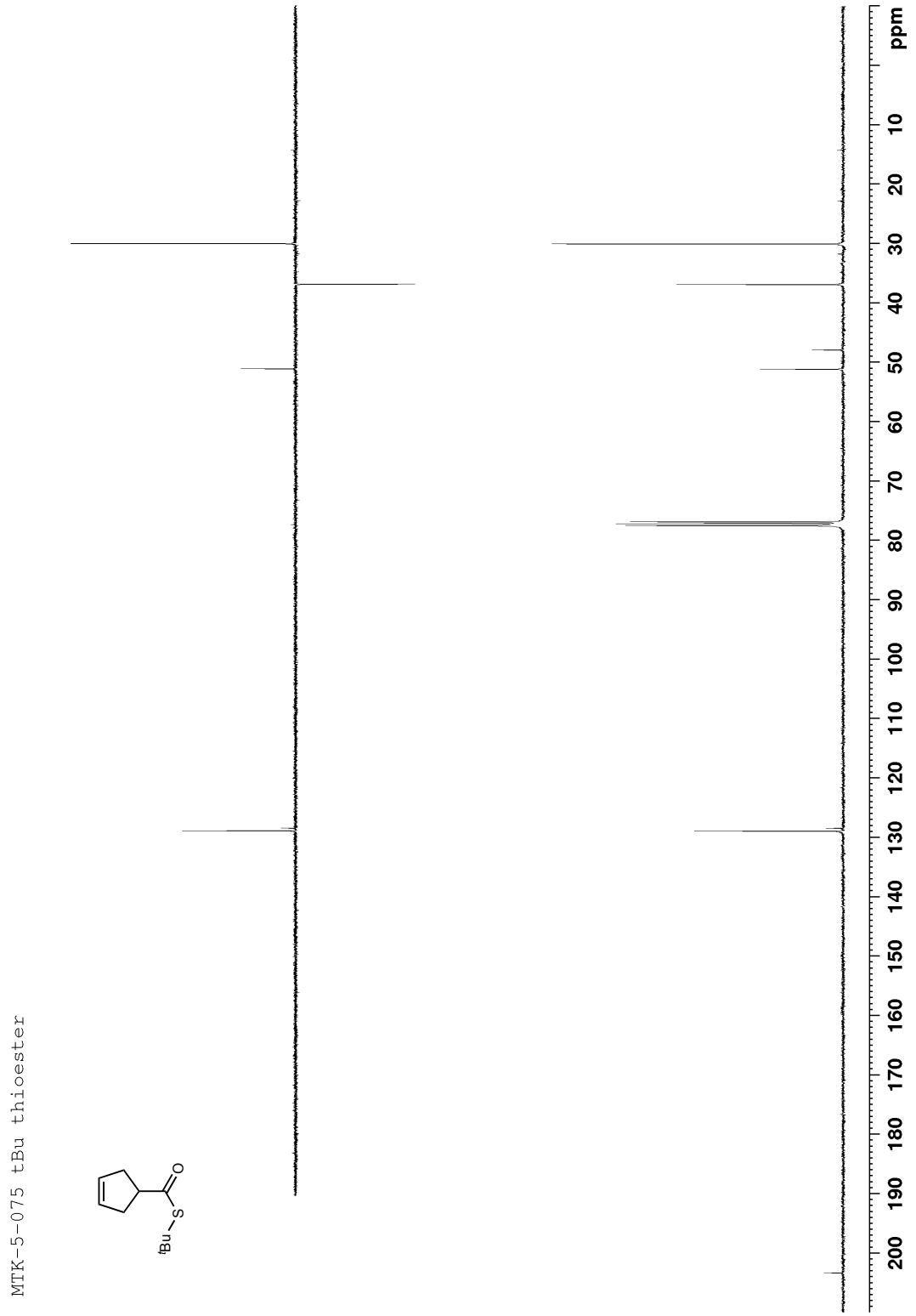

Figure B 41: ^{1}H NMR (400 MHz, $CDCl_3$) of **107n**

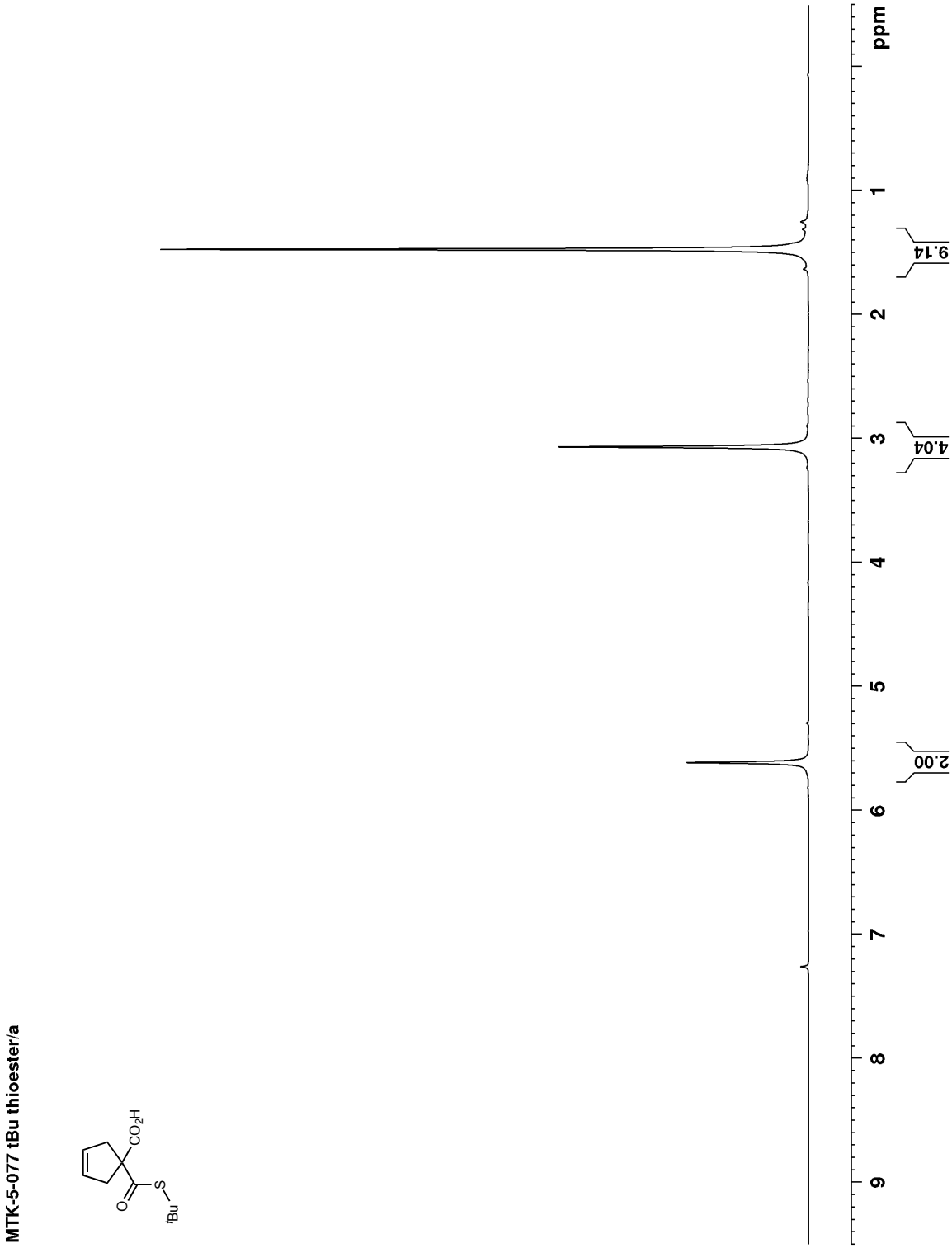

Figure B 42: ^{13}C NMR (100 MHz, $CDCl_3$) of **107n**

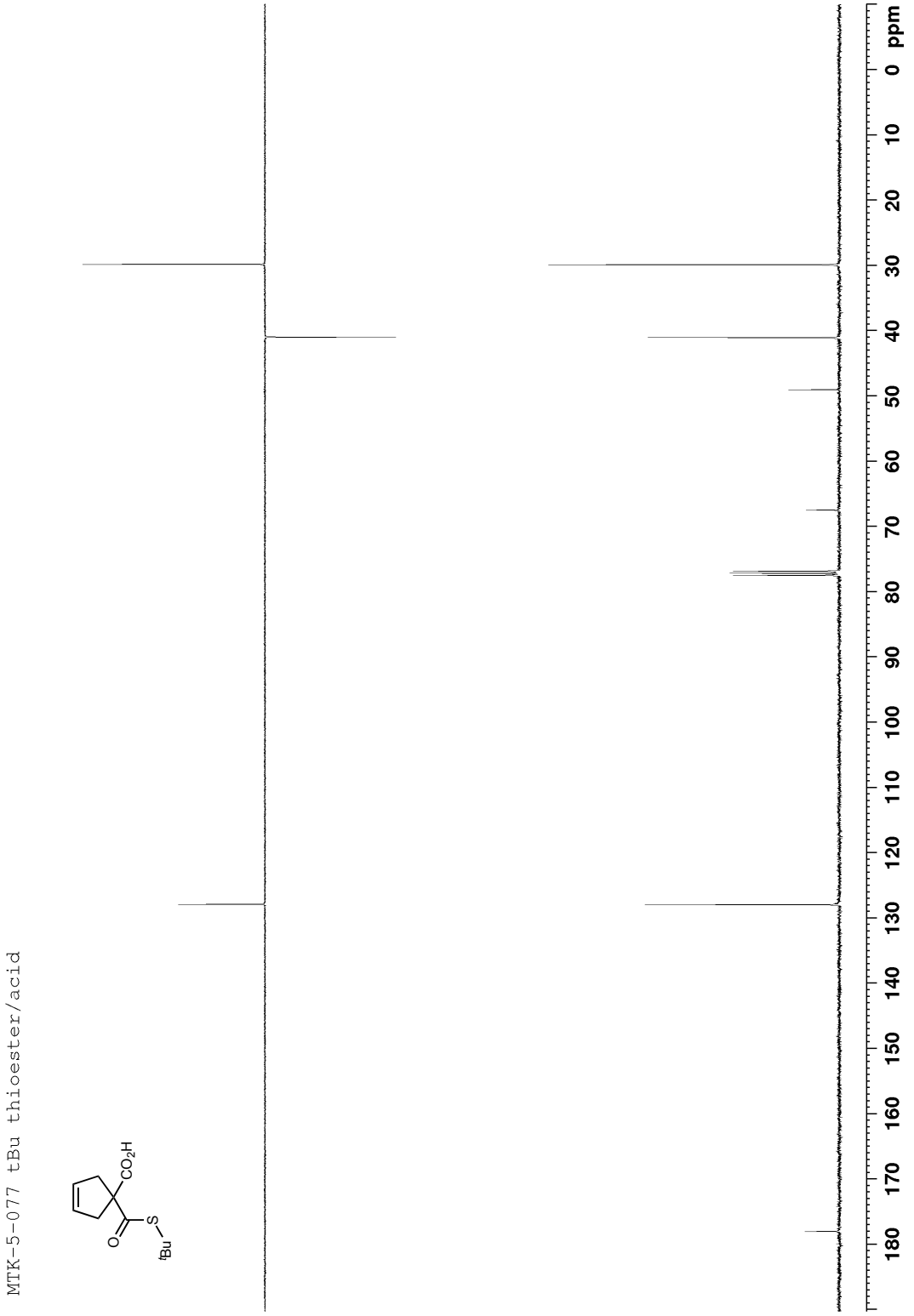

Figure B 43: ^{1}H NMR (500 MHz, $CDCl_3$) of **109a**

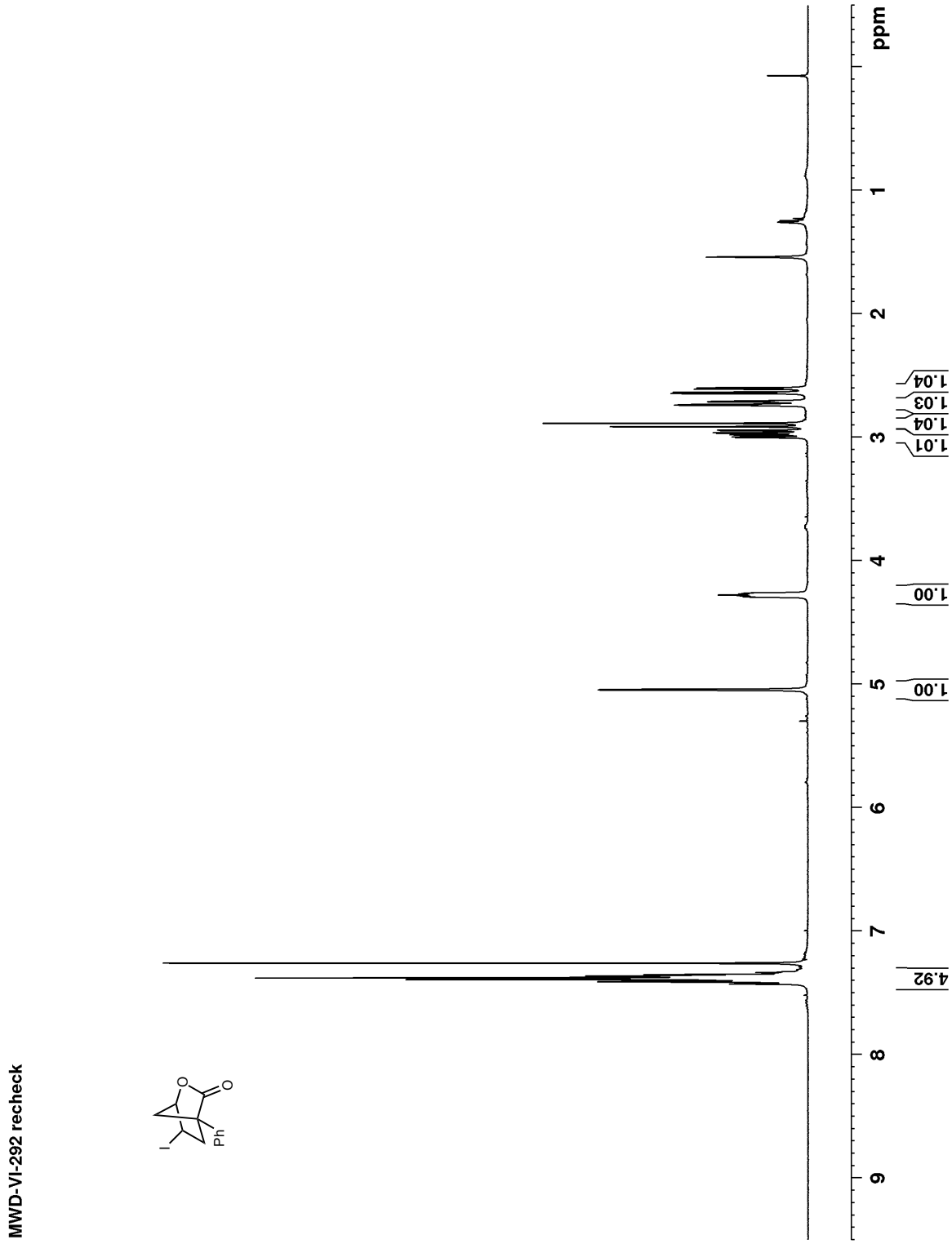

Figure B 44: ^{13}C NMR (125 MHz, $CDCl_3$) of **109a**

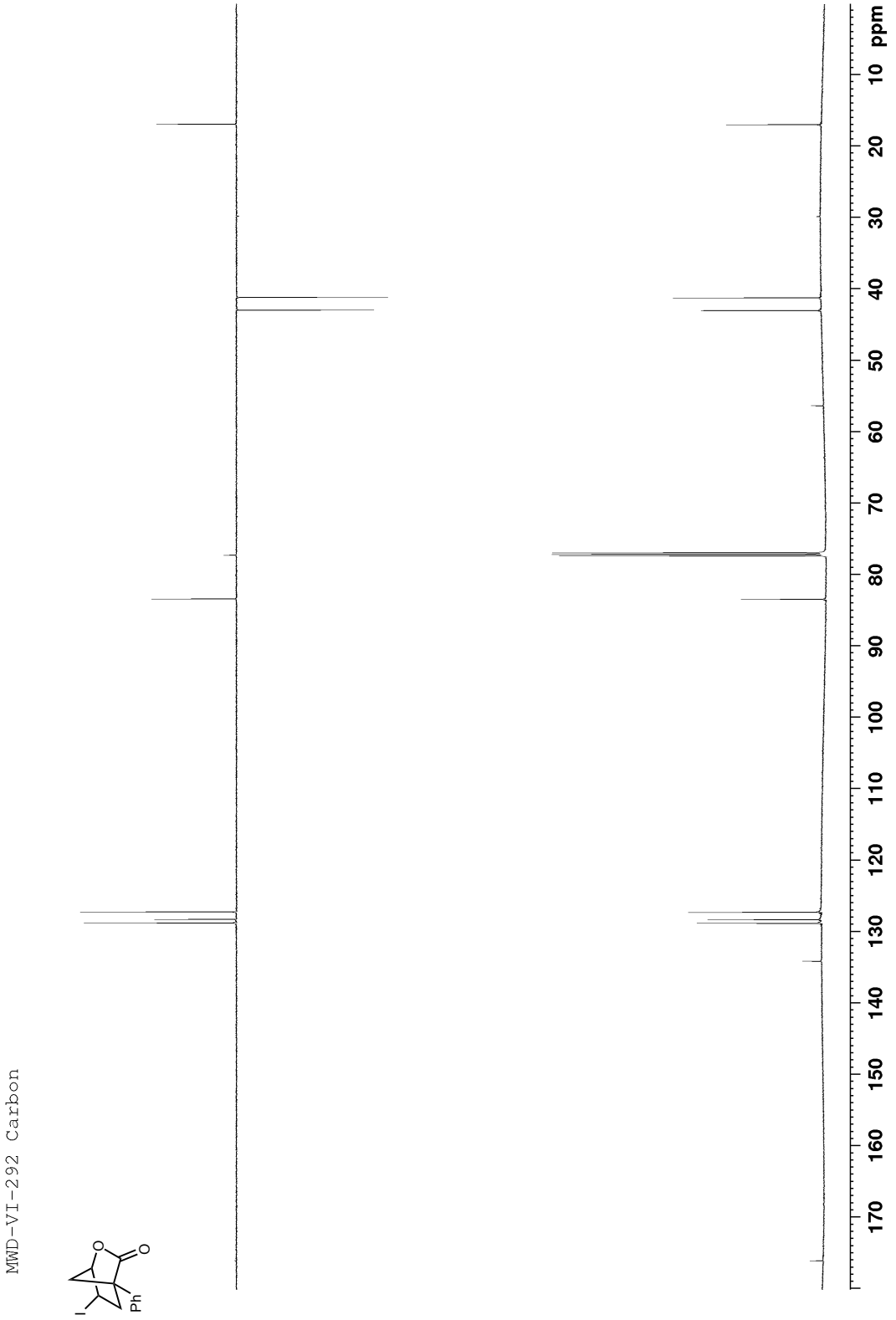

Figure B 45: COSY (600 MHz, $CDCl_3$) of **109a**

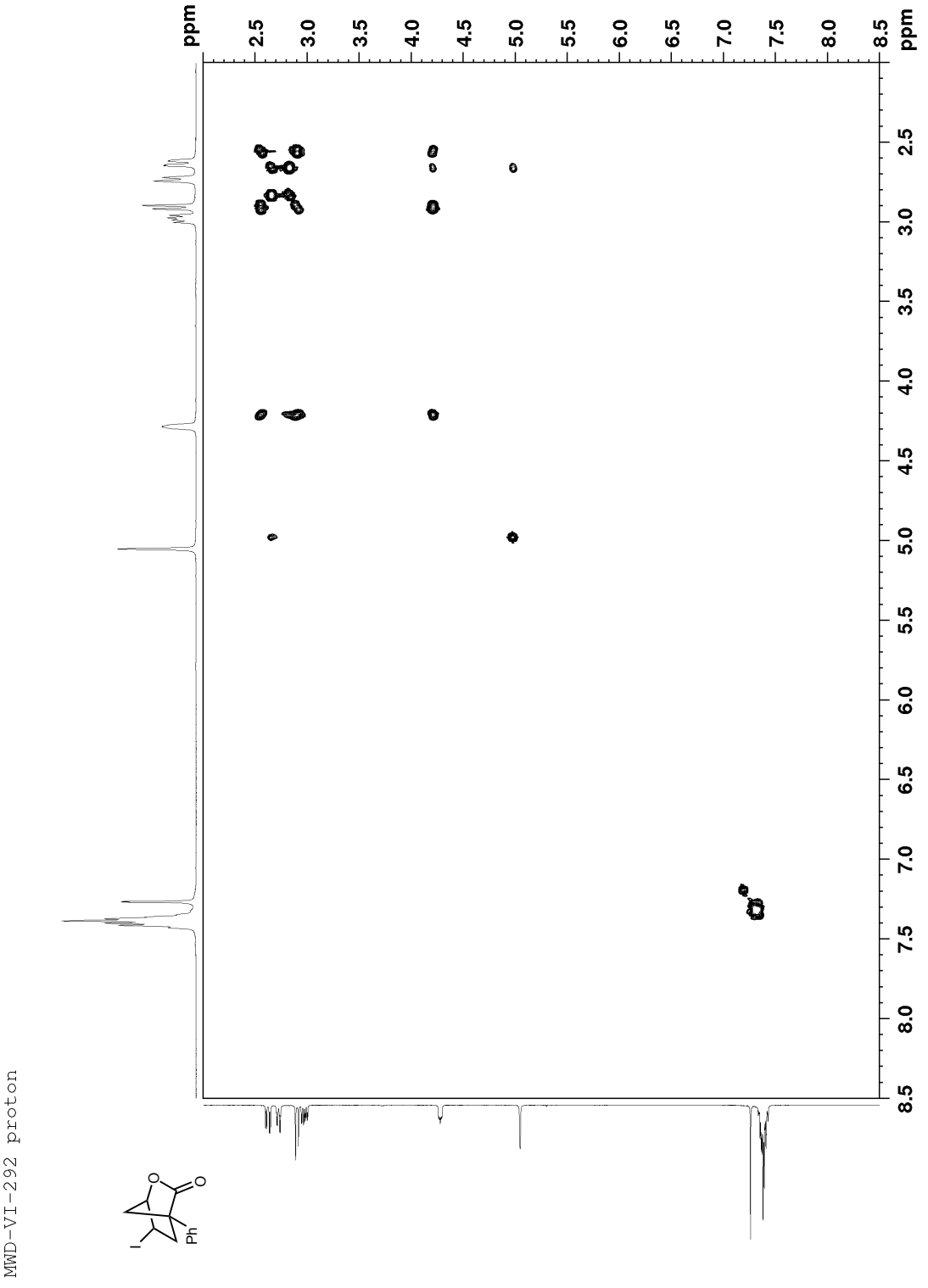

Figure B 46: HMBC (600 MHz, $CDCl_3$) of **109a**

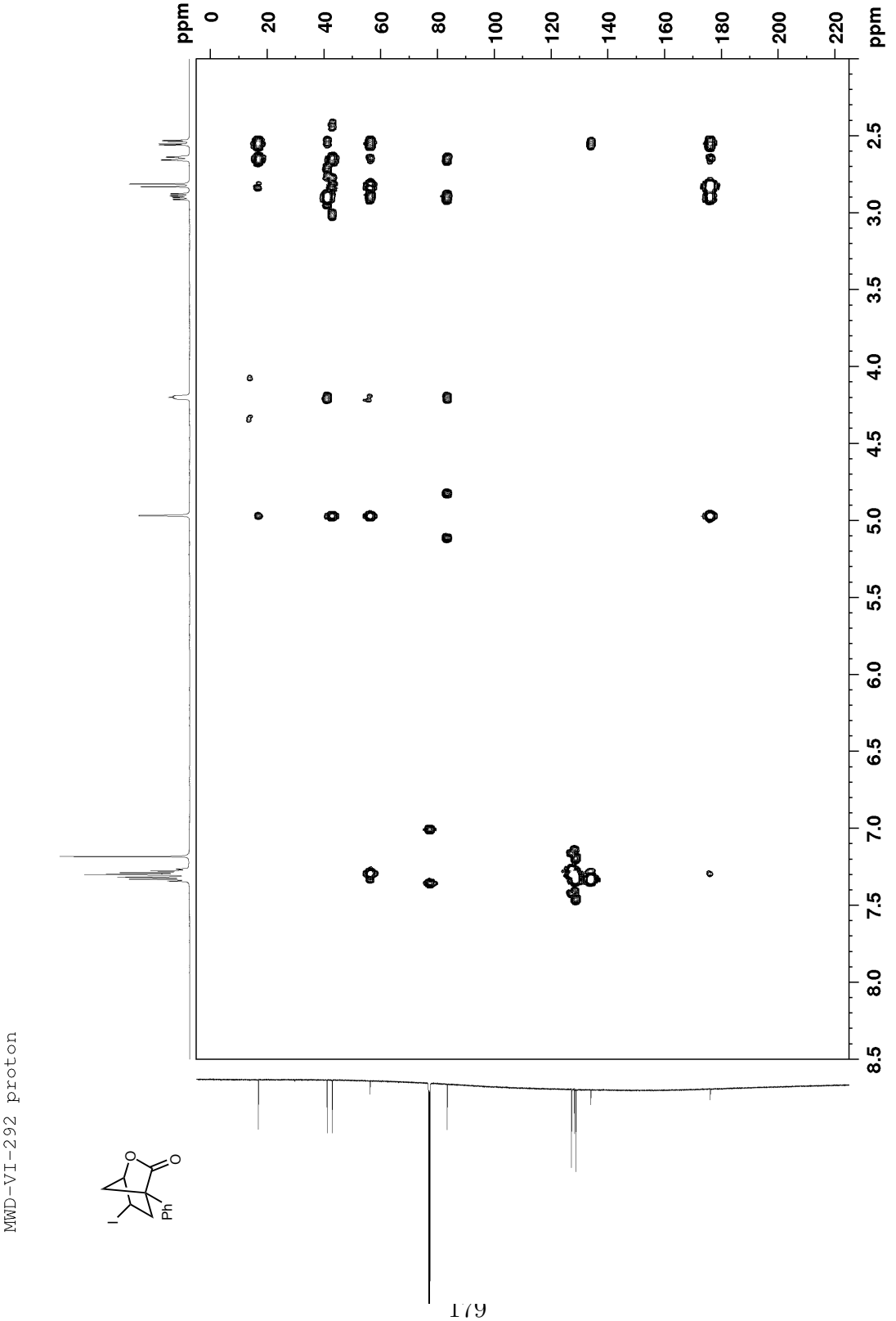

Figure B 47: Proton-proton couplings of **109a**

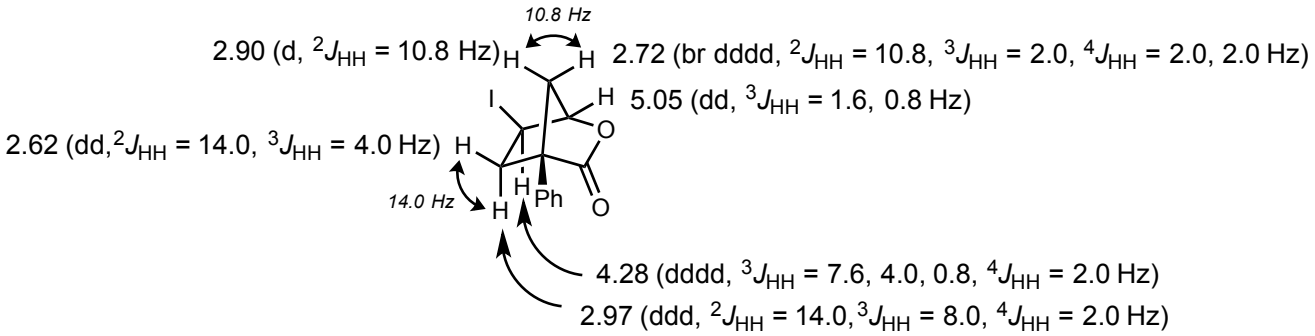

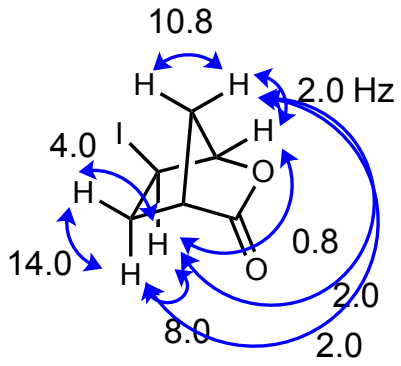

Figure B 48: ^{1}H NMR (400 MHz, $CDCl_3$) of **109b**

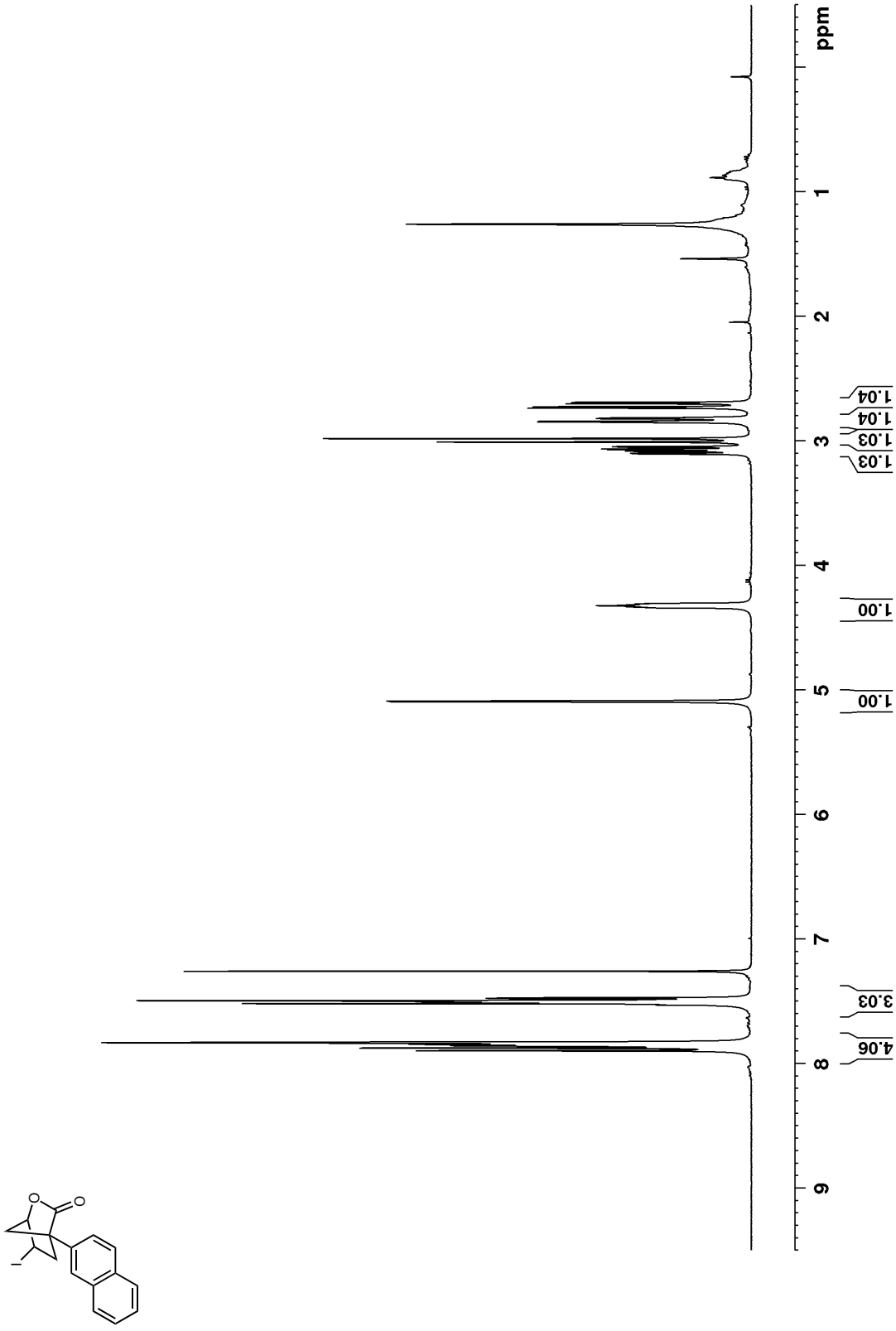

Figure B 49: ^{13}C NMR (100 MHz, $CDCl_3$) of **109b**

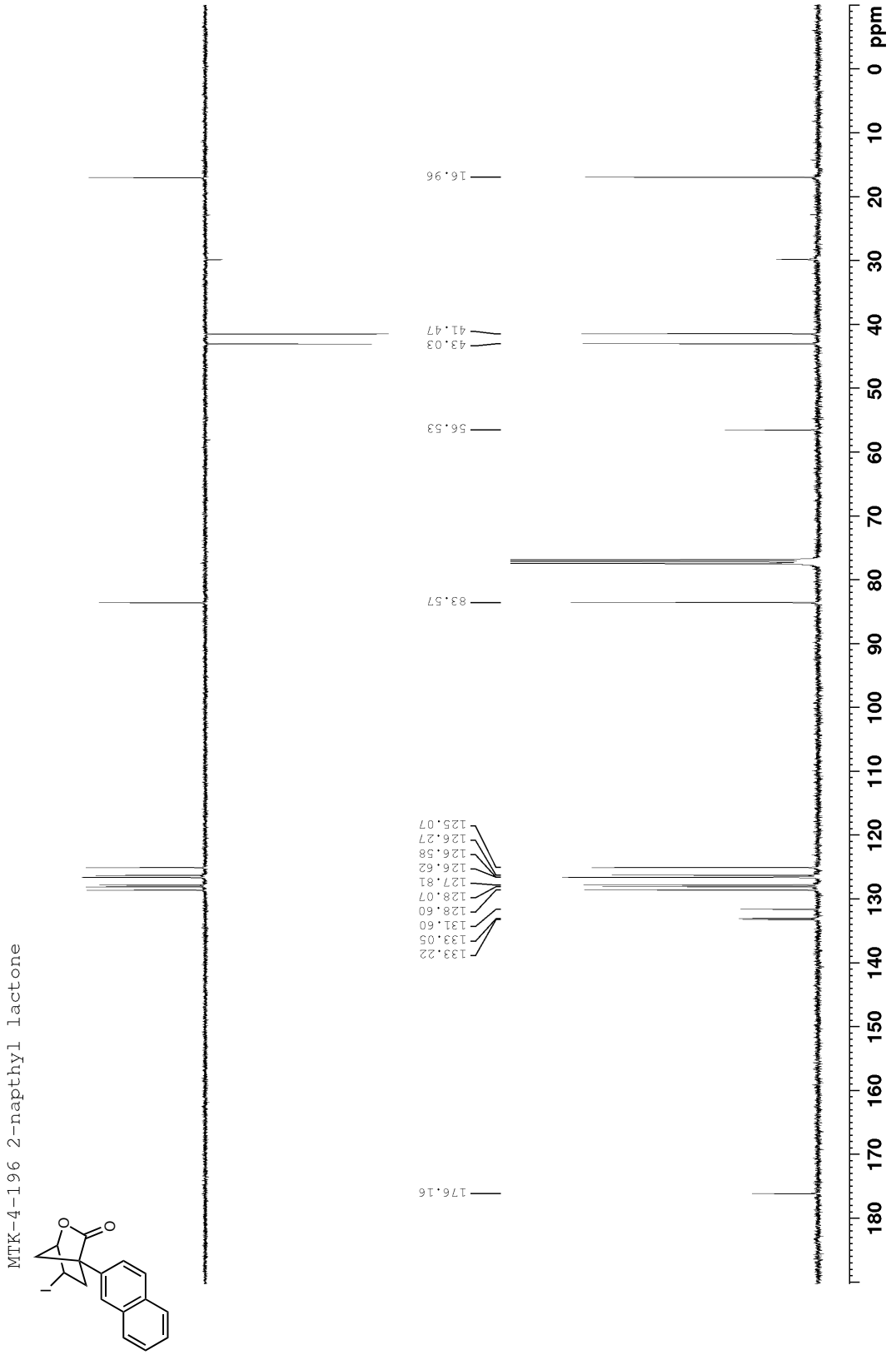

Figure B 50: ^{1}H NMR (400 MHz, $CDCl_3$) of **109c**

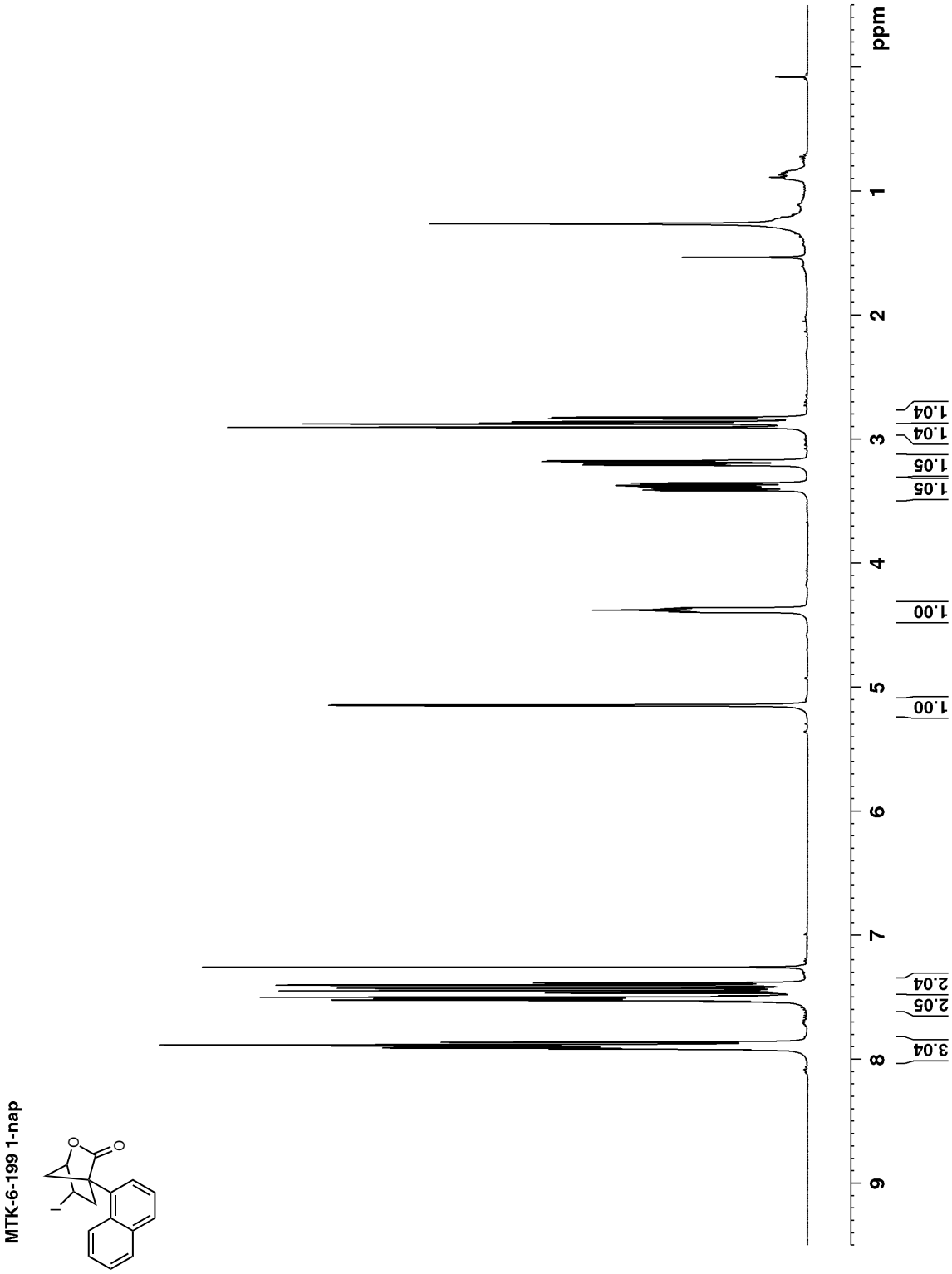

Figure B 51: ^{13}C NMR (100 MHz, $CDCl_3$) of **109c**

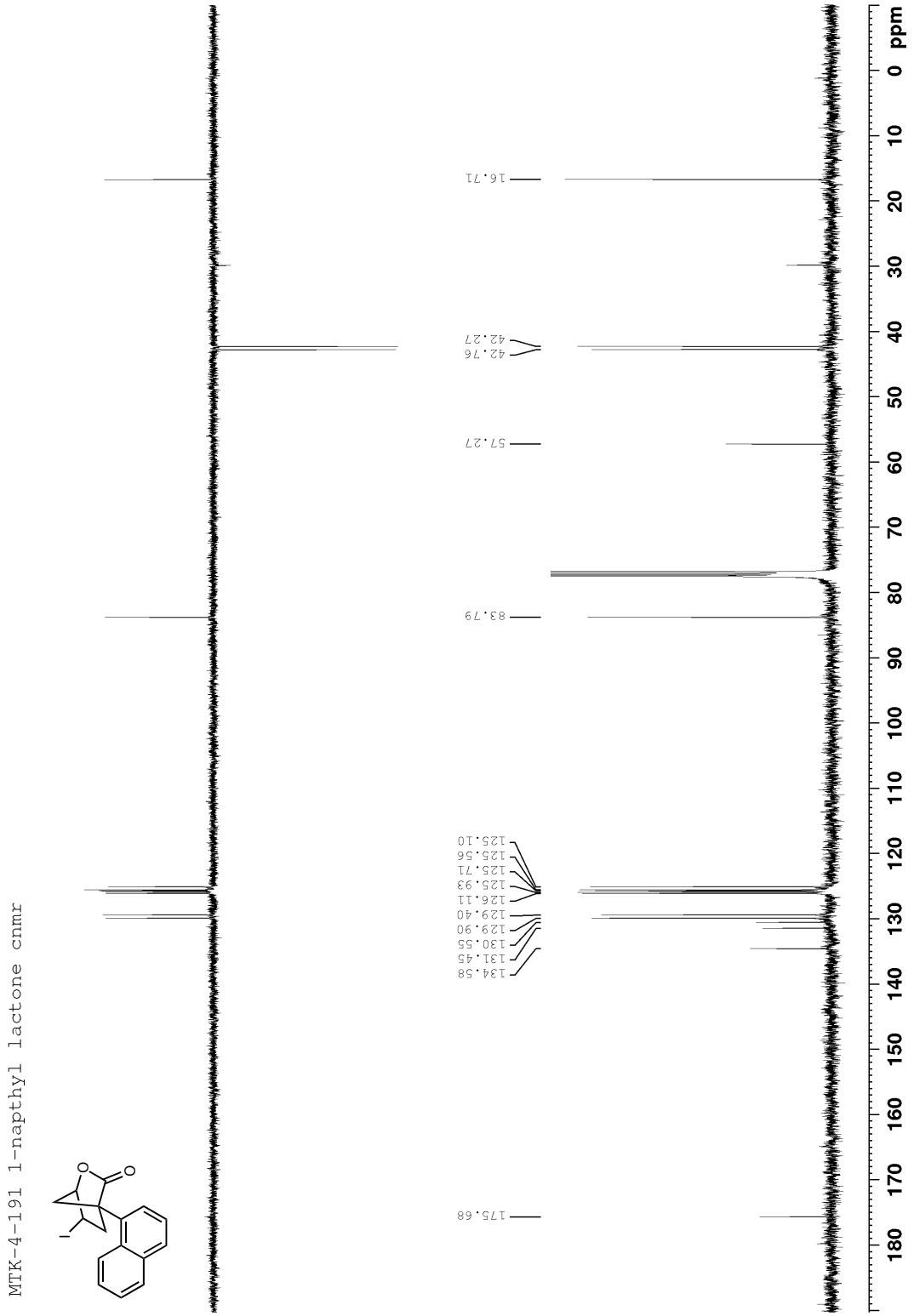

Figure B 52: ^{1}H NMR (400 MHz, $CDCl_3$) of **109d**

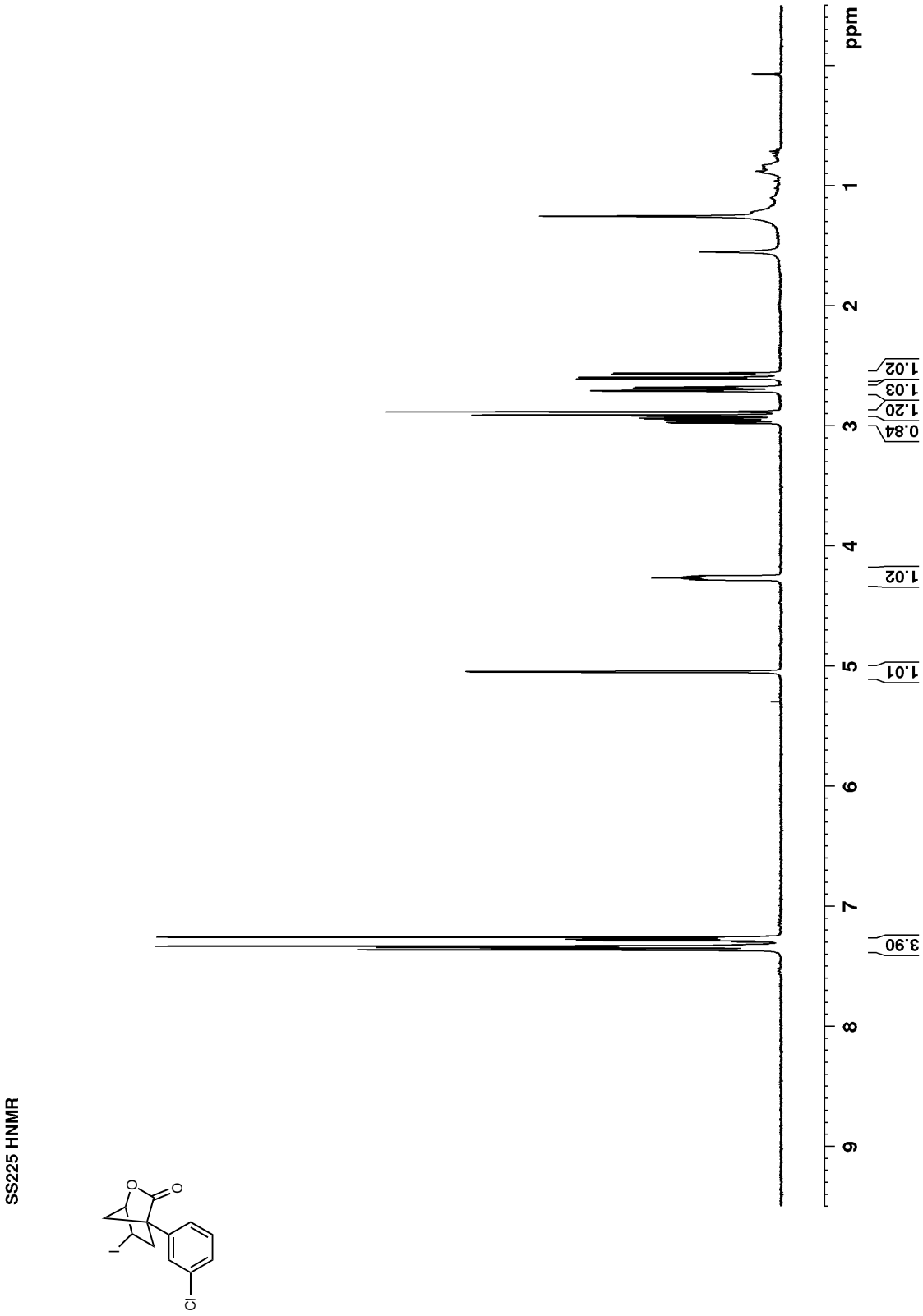

Figure B 53: ^{13}C NMR (100 MHz, $CDCl_3$) of **109d**

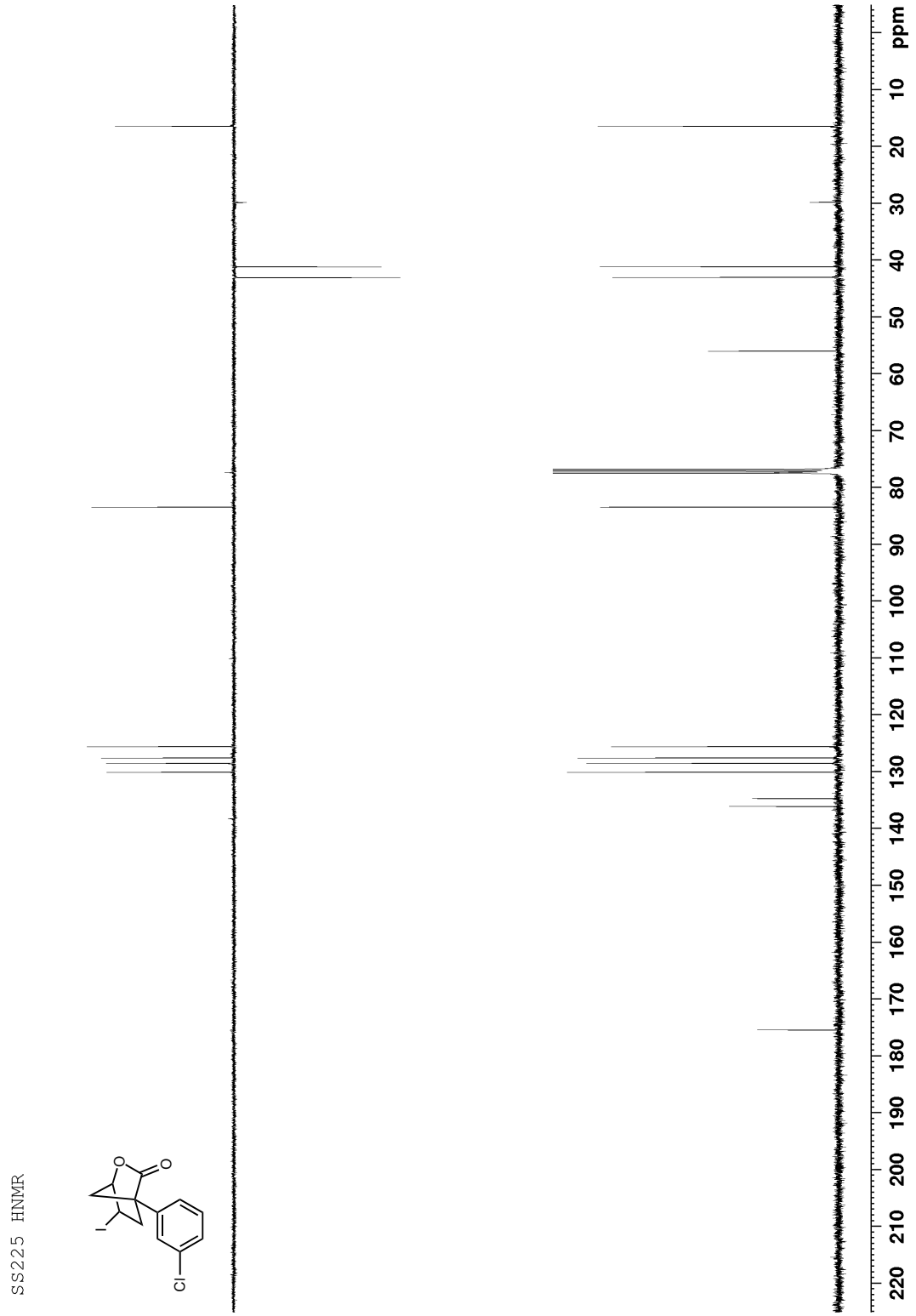

Figure B 54: ^{1}H NMR (400 MHz, $CDCl_3$) of **109e**

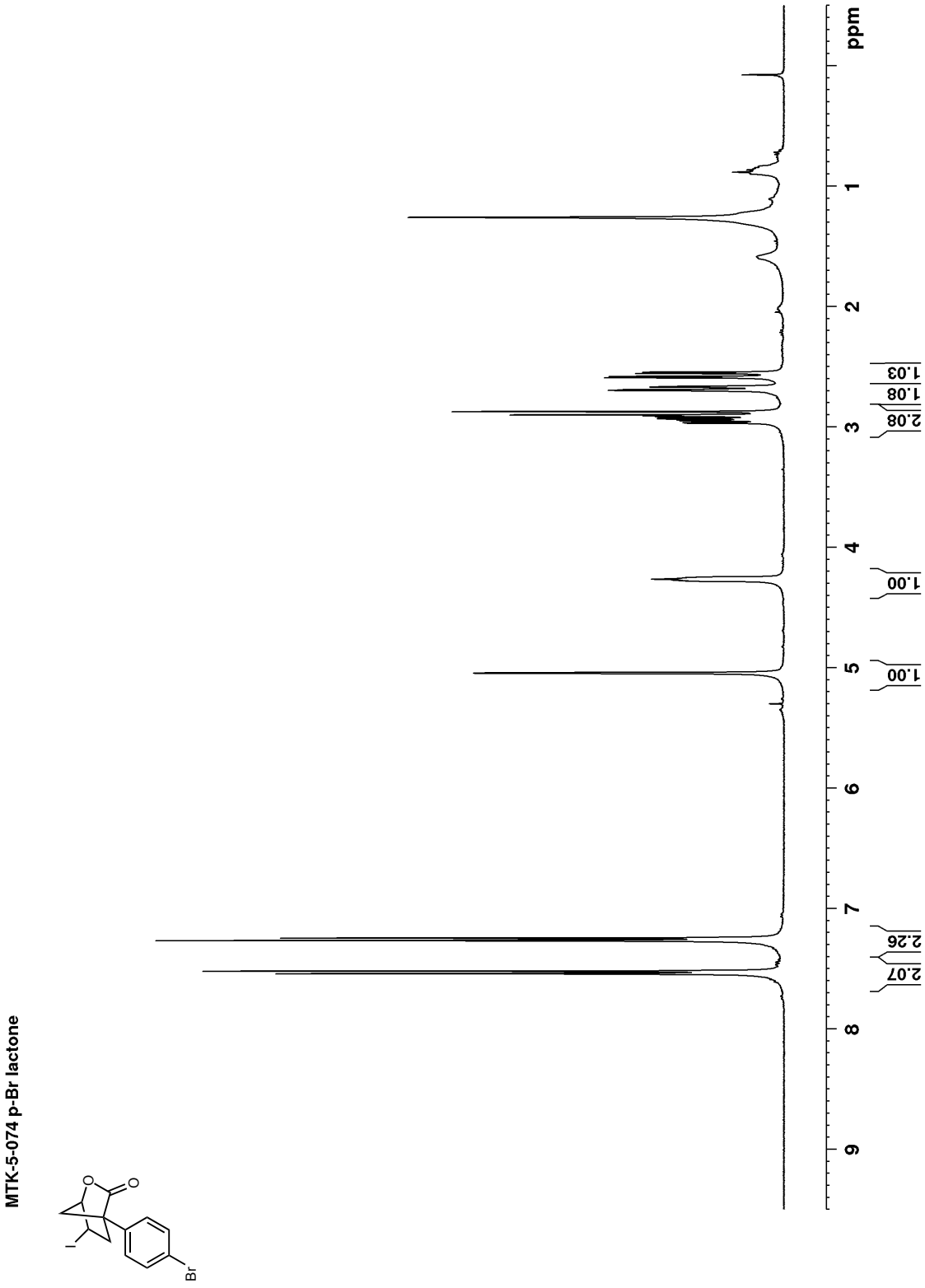

Figure B 55: ^{13}C NMR (100 MHz, $CDCl_3$) of **109e**

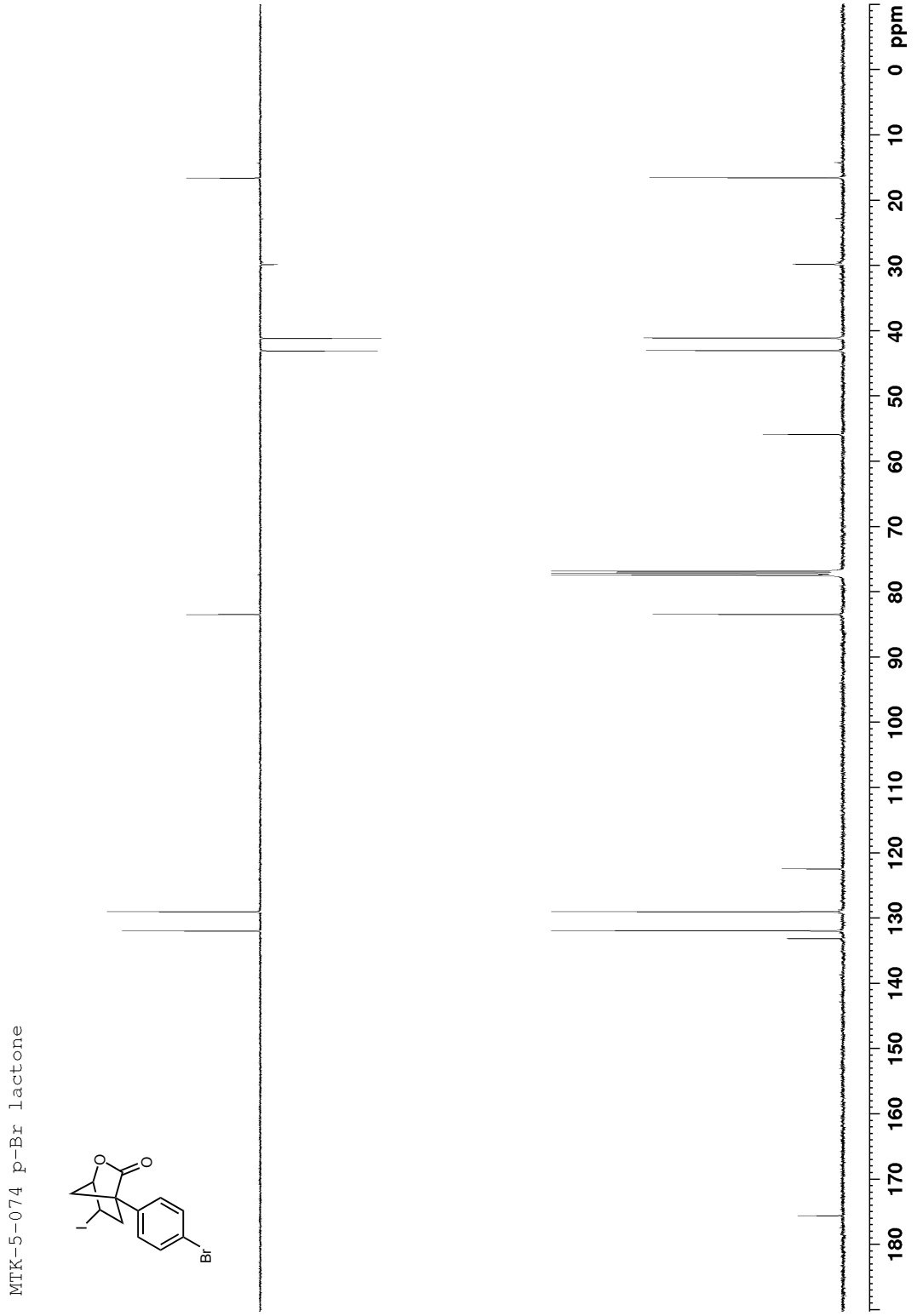

Figure B 56: ^{1}H NMR (400 MHz, $CDCl_3$) of **109f**

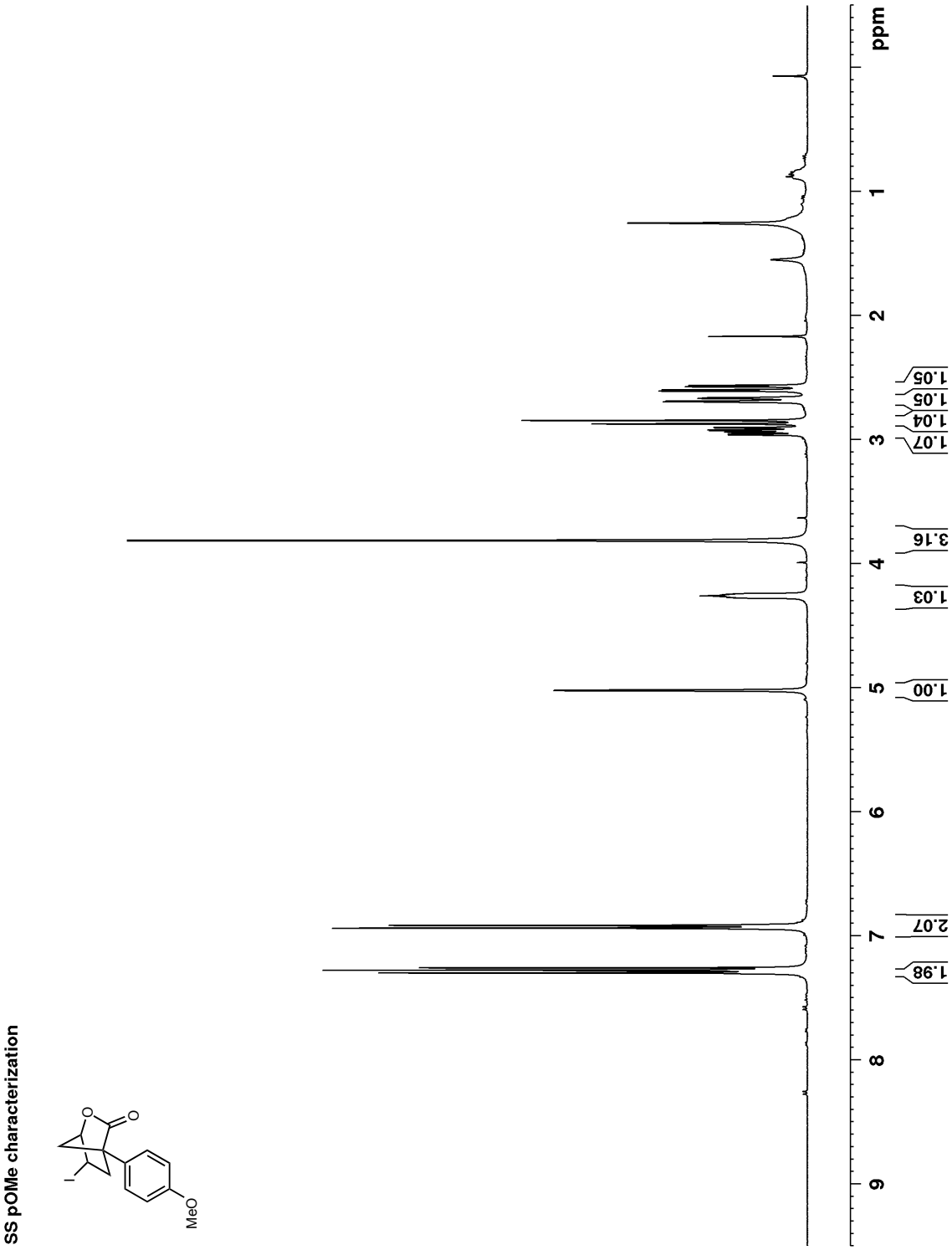

Figure B 57: ^{13}C NMR (100 MHz, $CDCl_3$) of **109f**

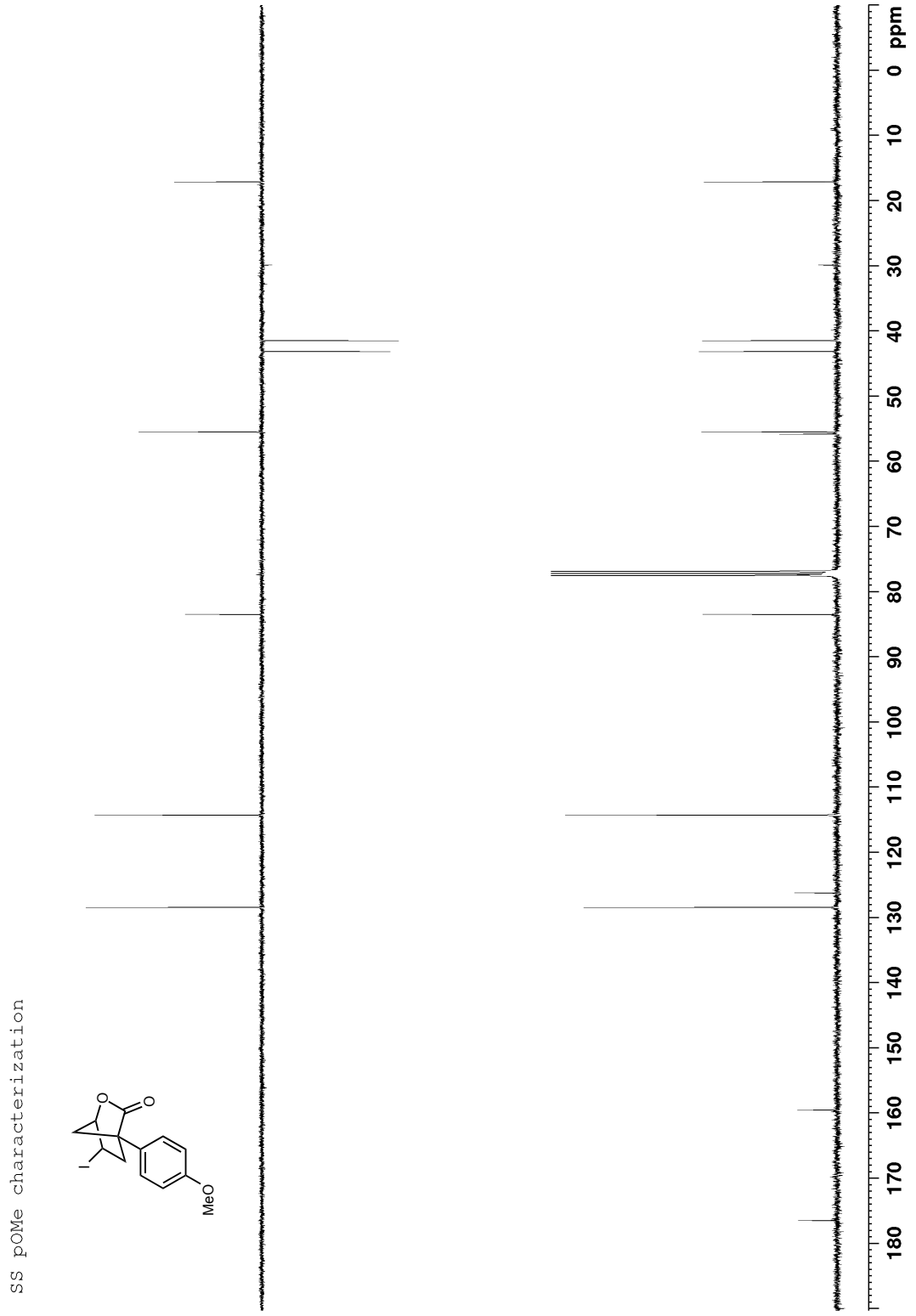

Figure B 58: ^{1}H NMR (400 MHz, $CDCl_3$) of **109g**

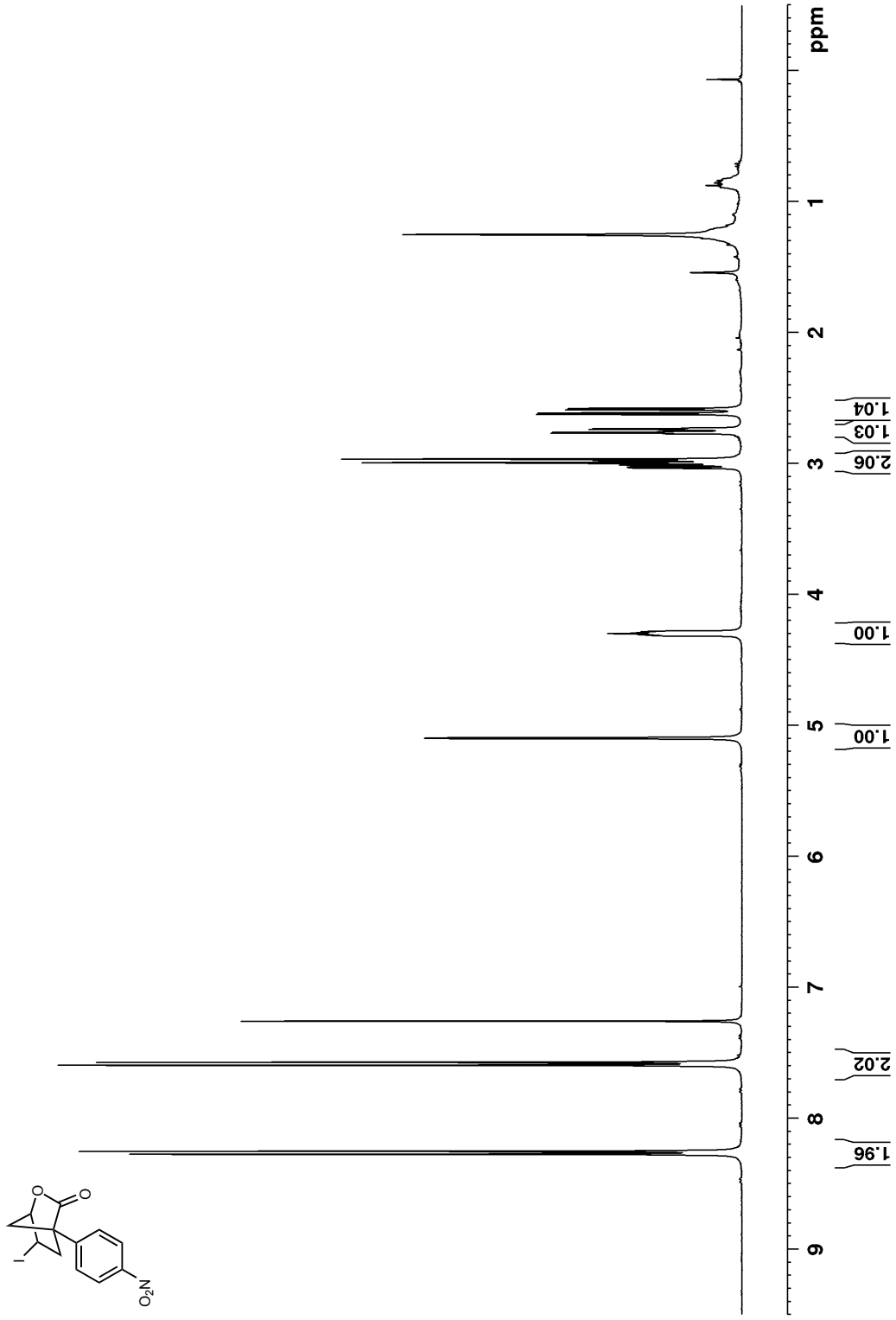

Figure B 59: ^{13}C NMR (100 MHz, $CDCl_3$) of **109g**

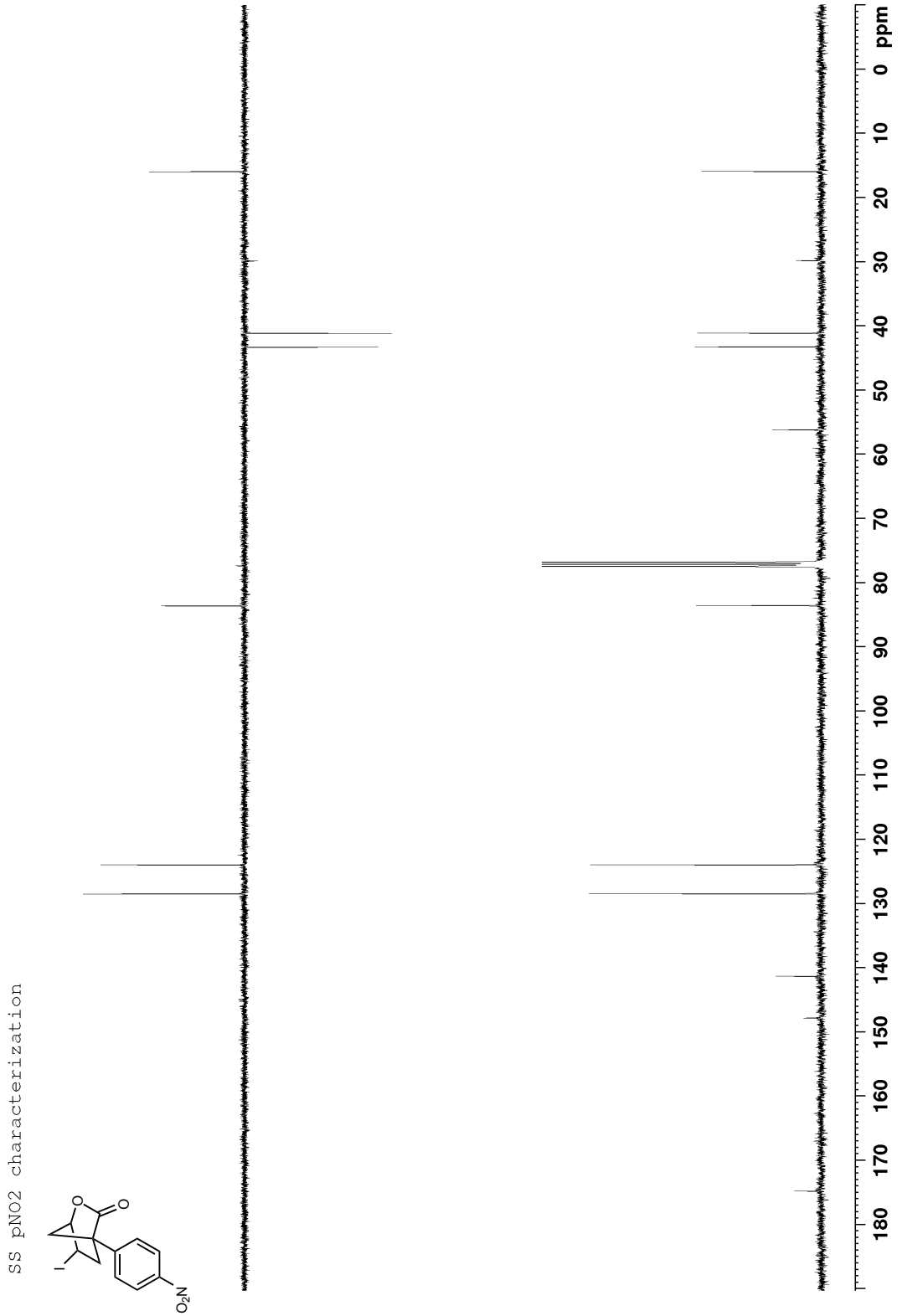

Figure B 60: ^{1}H NMR (400 MHz, $CDCl_3$) of **109h**

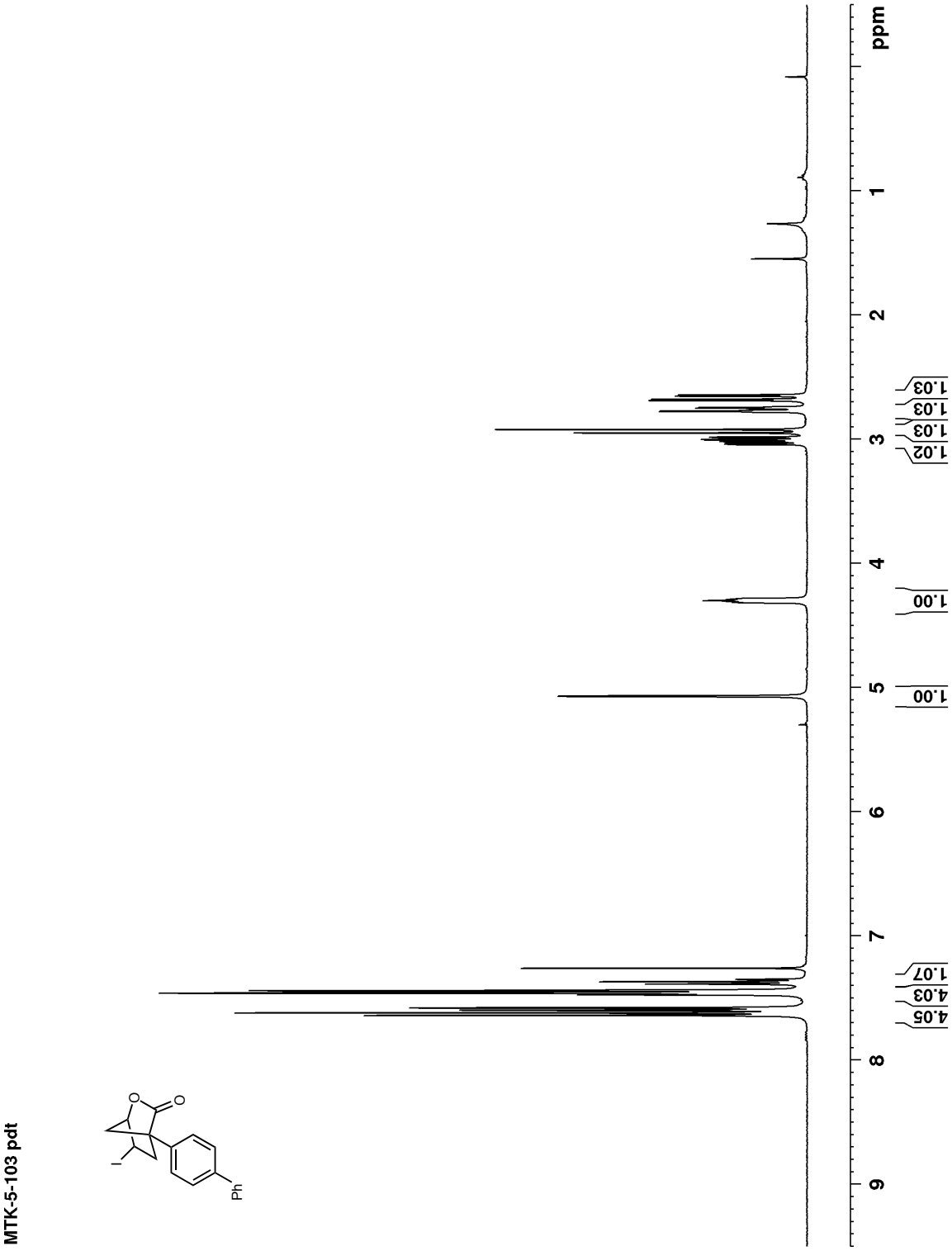

Figure B 61: ^{13}C NMR (100 MHz, $CDCl_3$) of **109h**

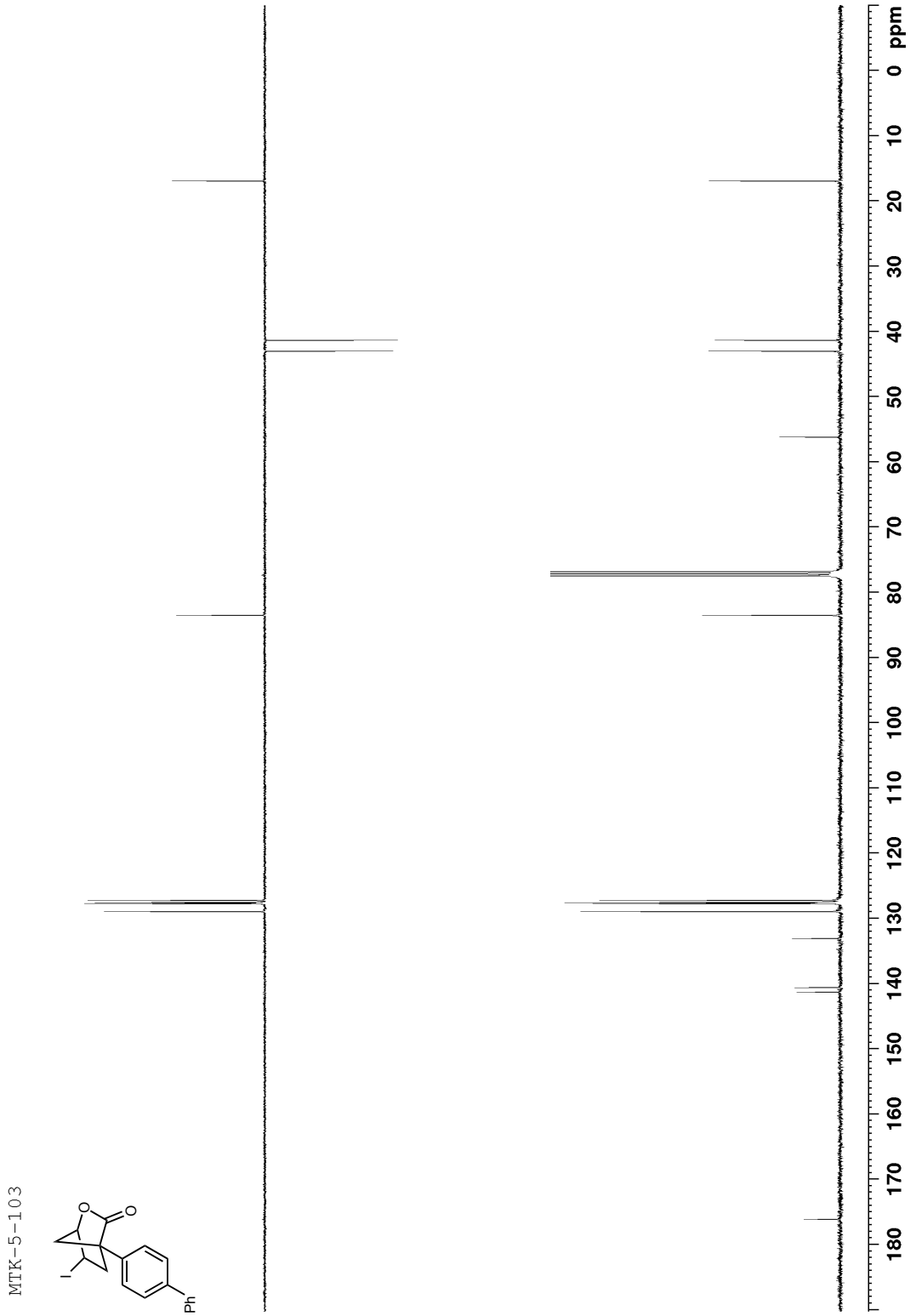

Figure B 62: ^{1}H NMR (400 MHz, $CDCl_3$) of **109i**

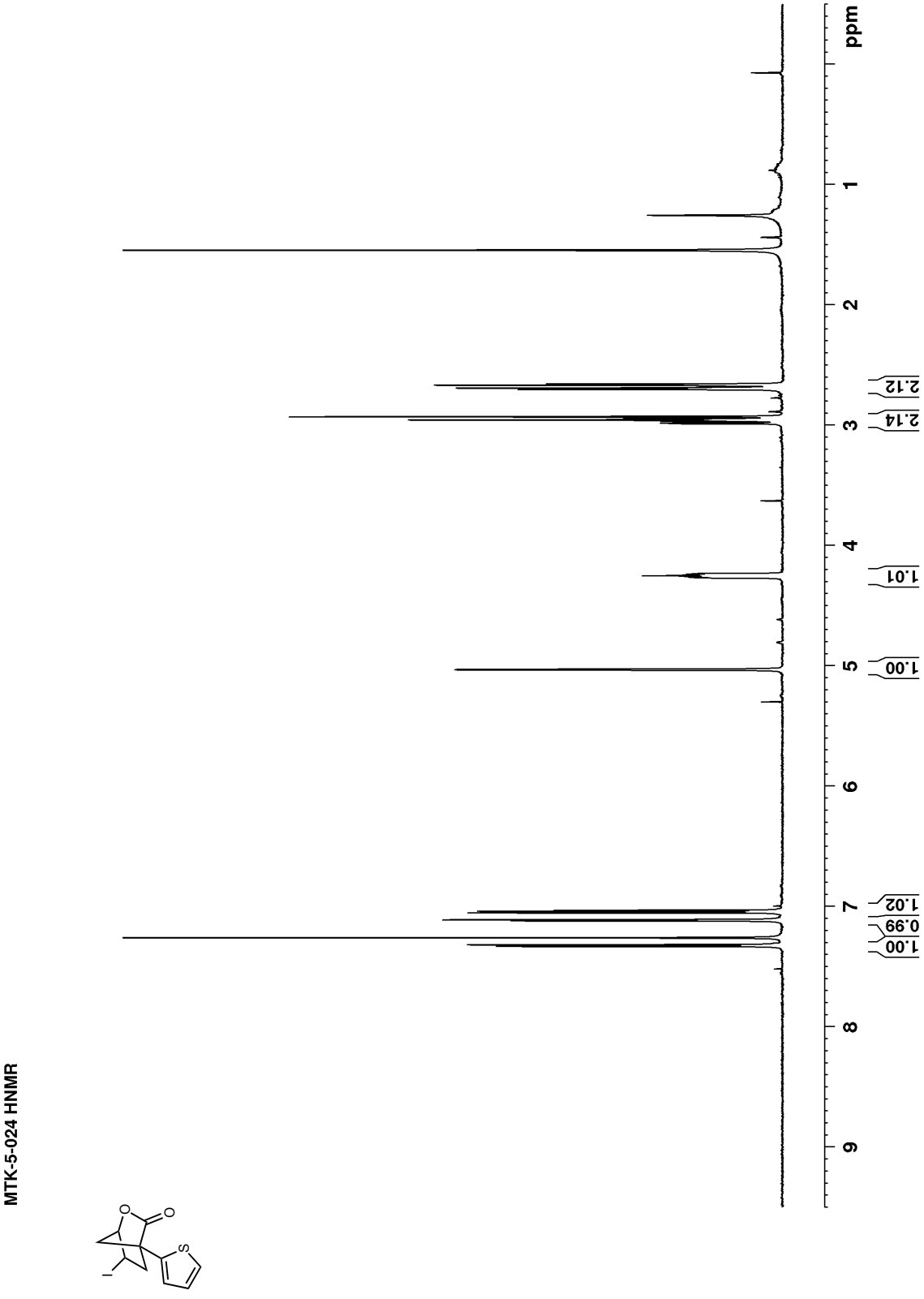

Figure B 63: ^{13}C NMR (100 MHz, $CDCl_3$) of **109i**

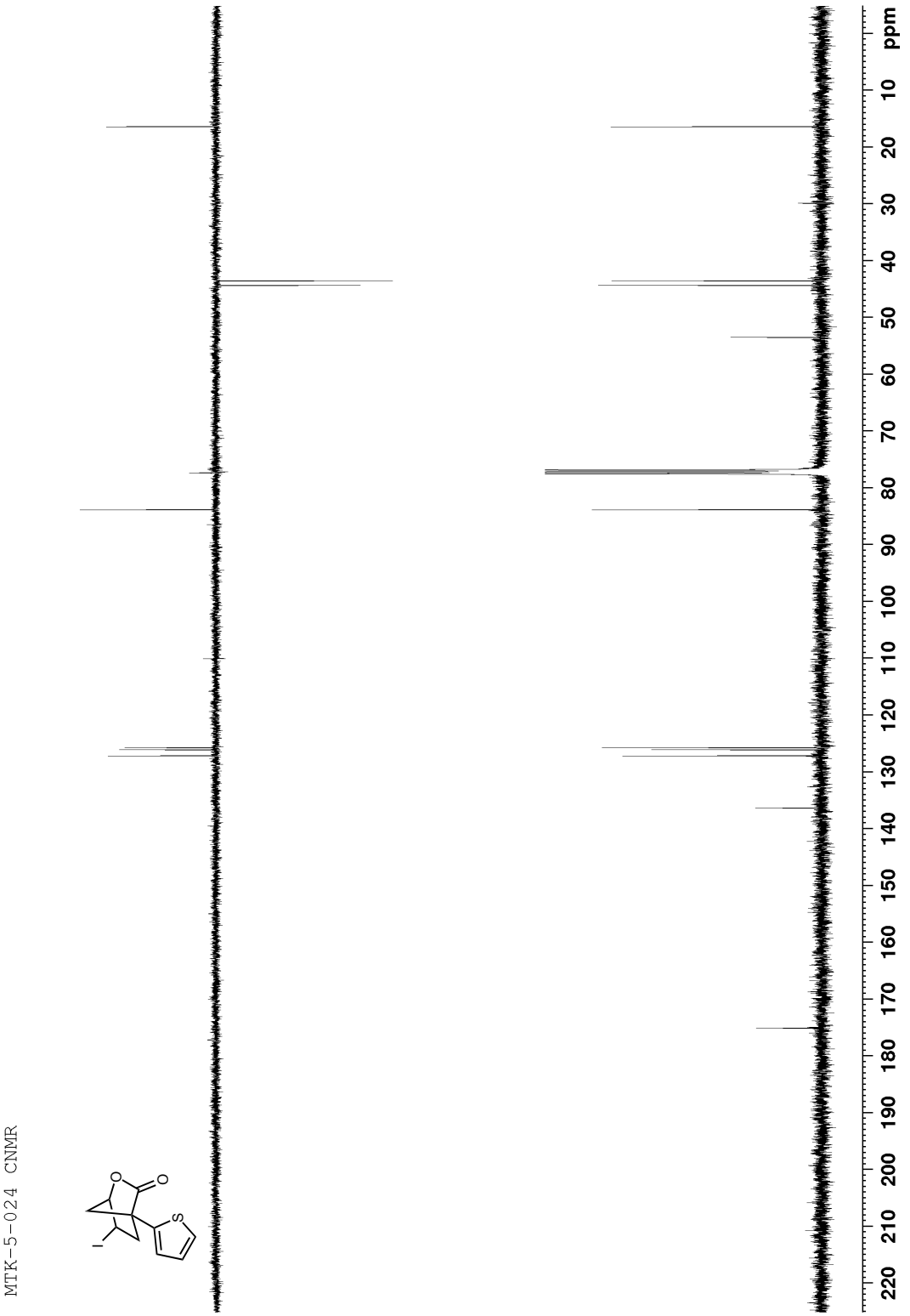

Figure B 64: ^{1}H NMR (400 MHz, $CDCl_3$) of **109j**

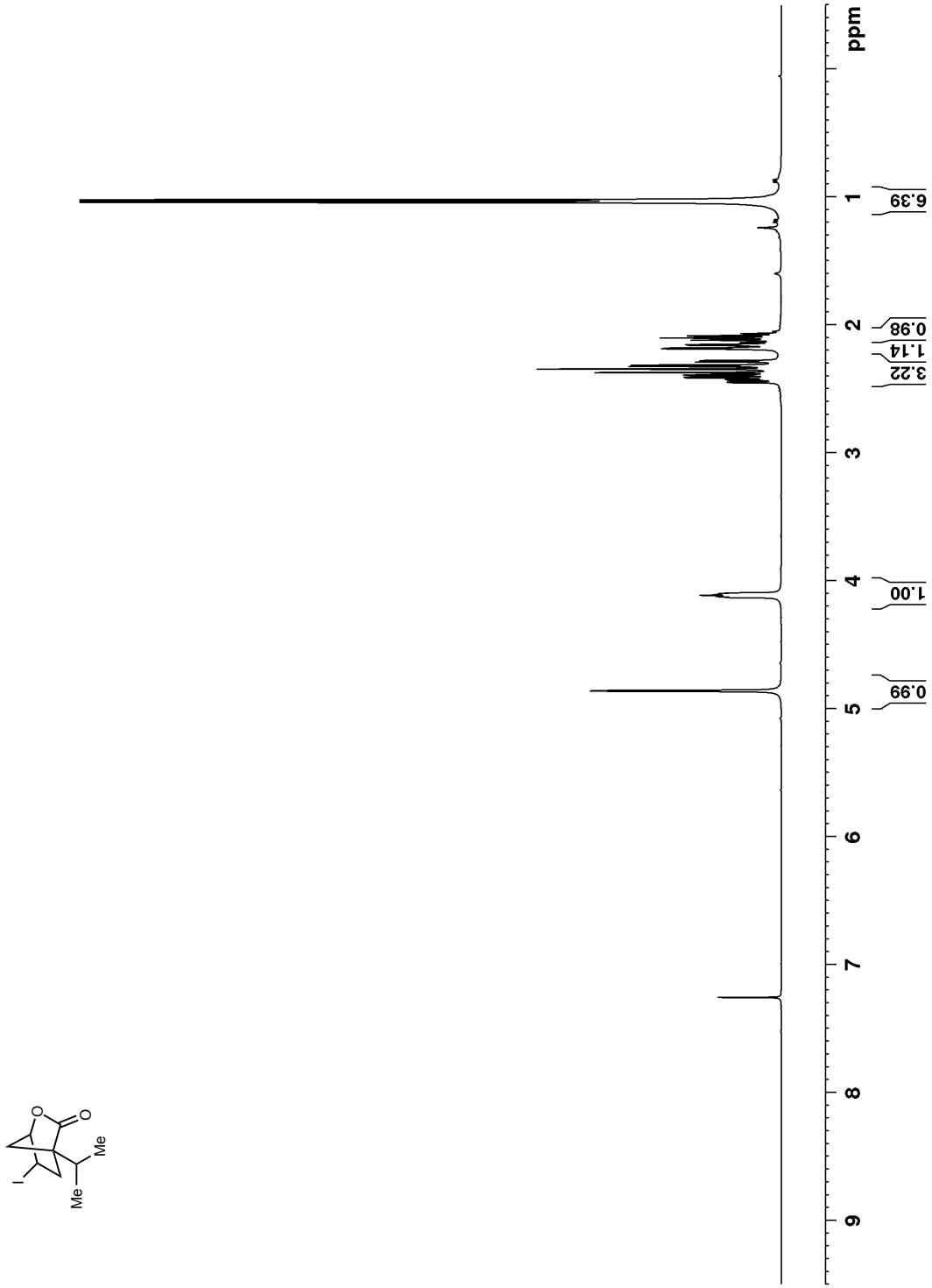

Figure B 65: ^{13}C NMR (100 MHz, $CDCl_3$) of **109j**

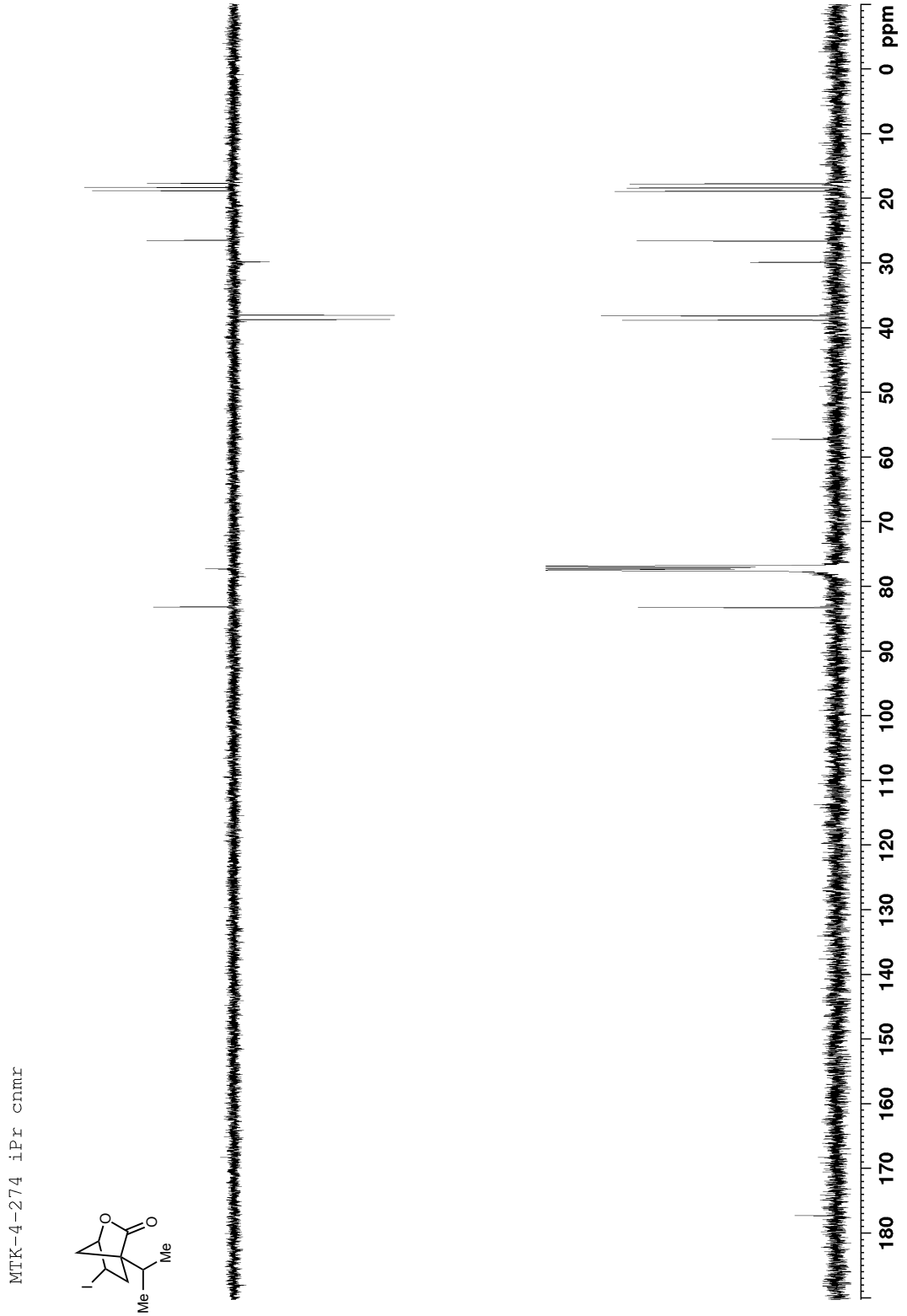

Figure B 66: ^{1}H NMR (400 MHz, $CDCl_3$) of **109k**

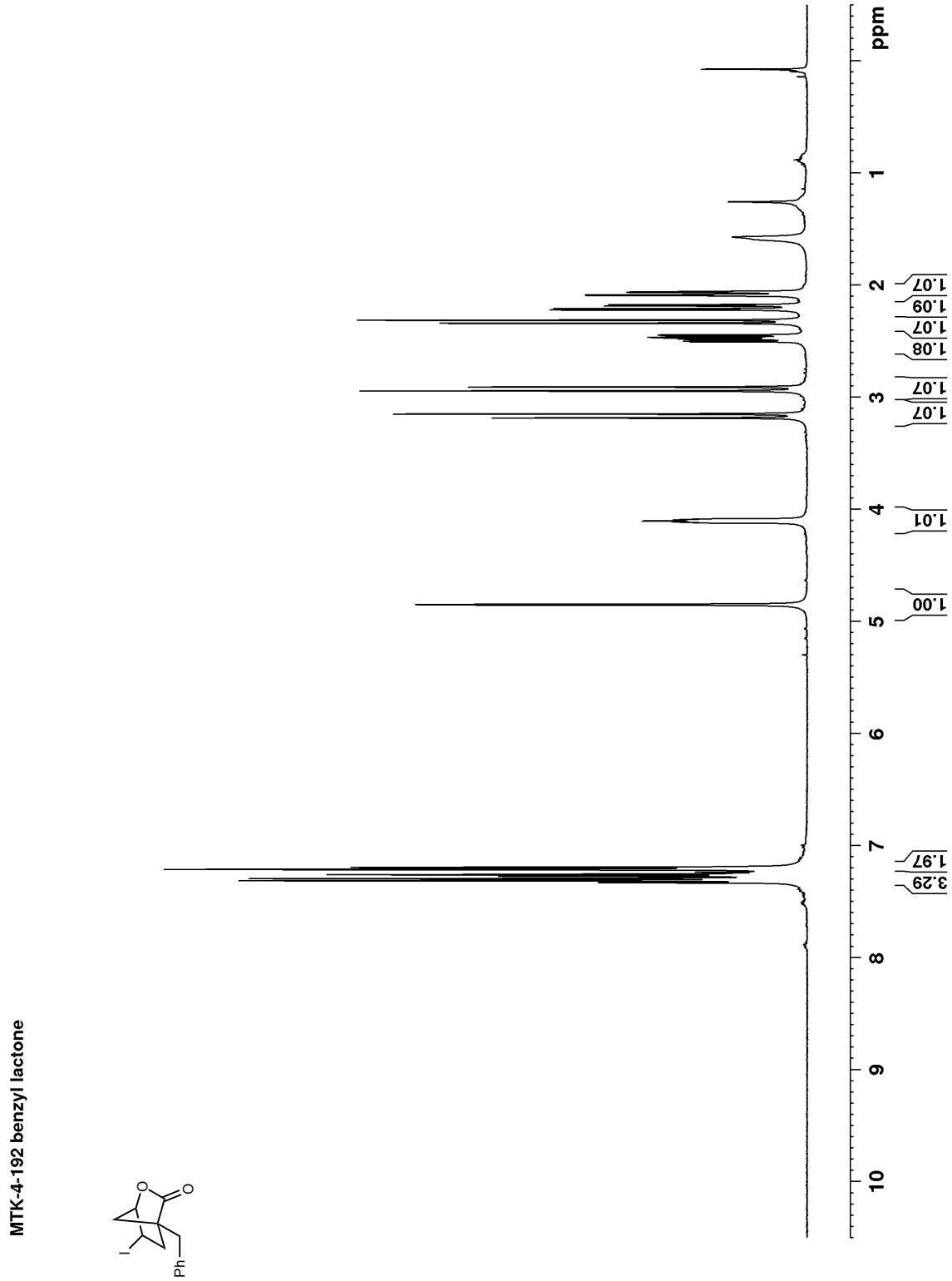

Figure B 67: ^{13}C NMR (100 MHz, $CDCl_3$) of **109k**

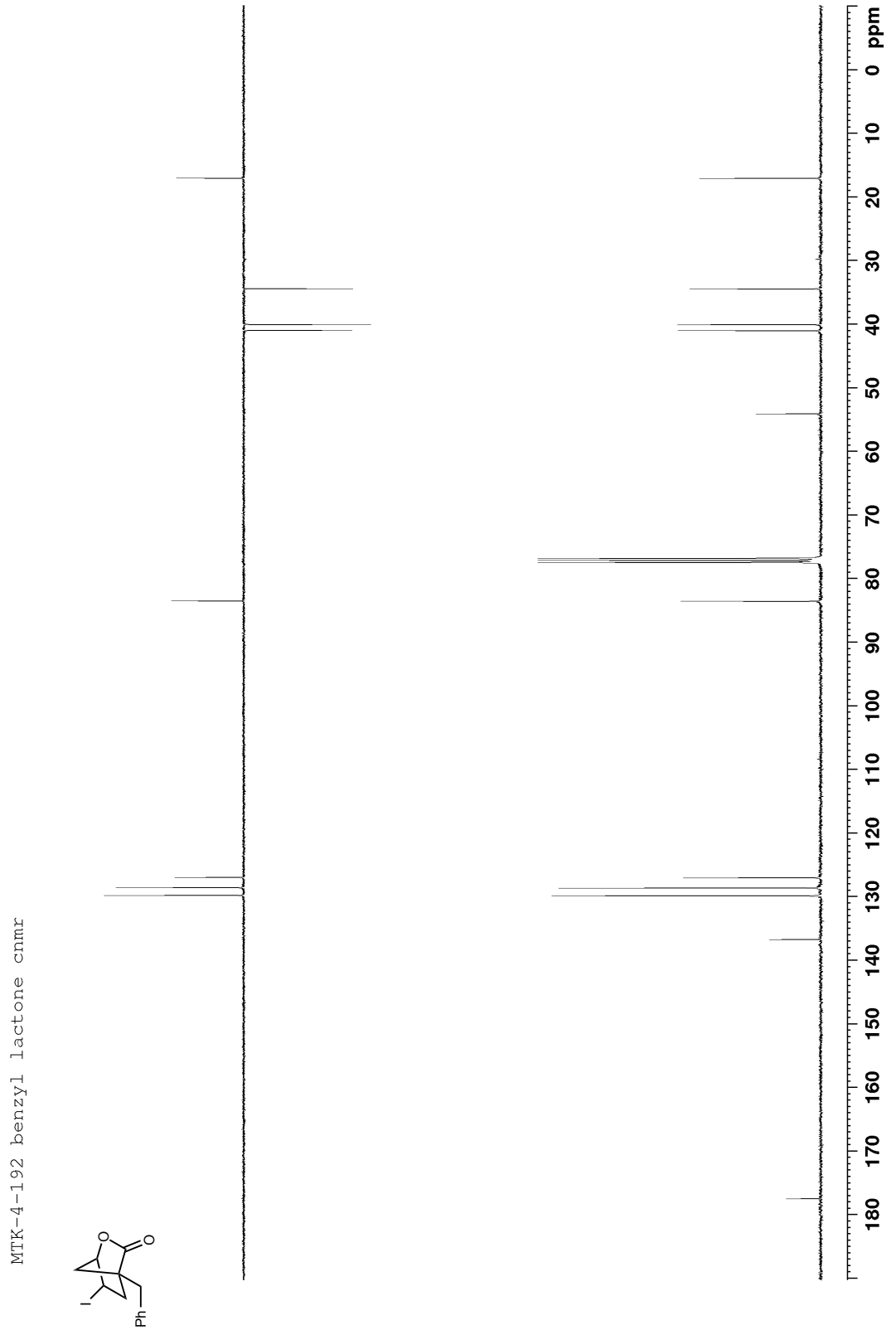

Figure B 68: ^{1}H NMR (400 MHz, $CDCl_3$) of **109l**

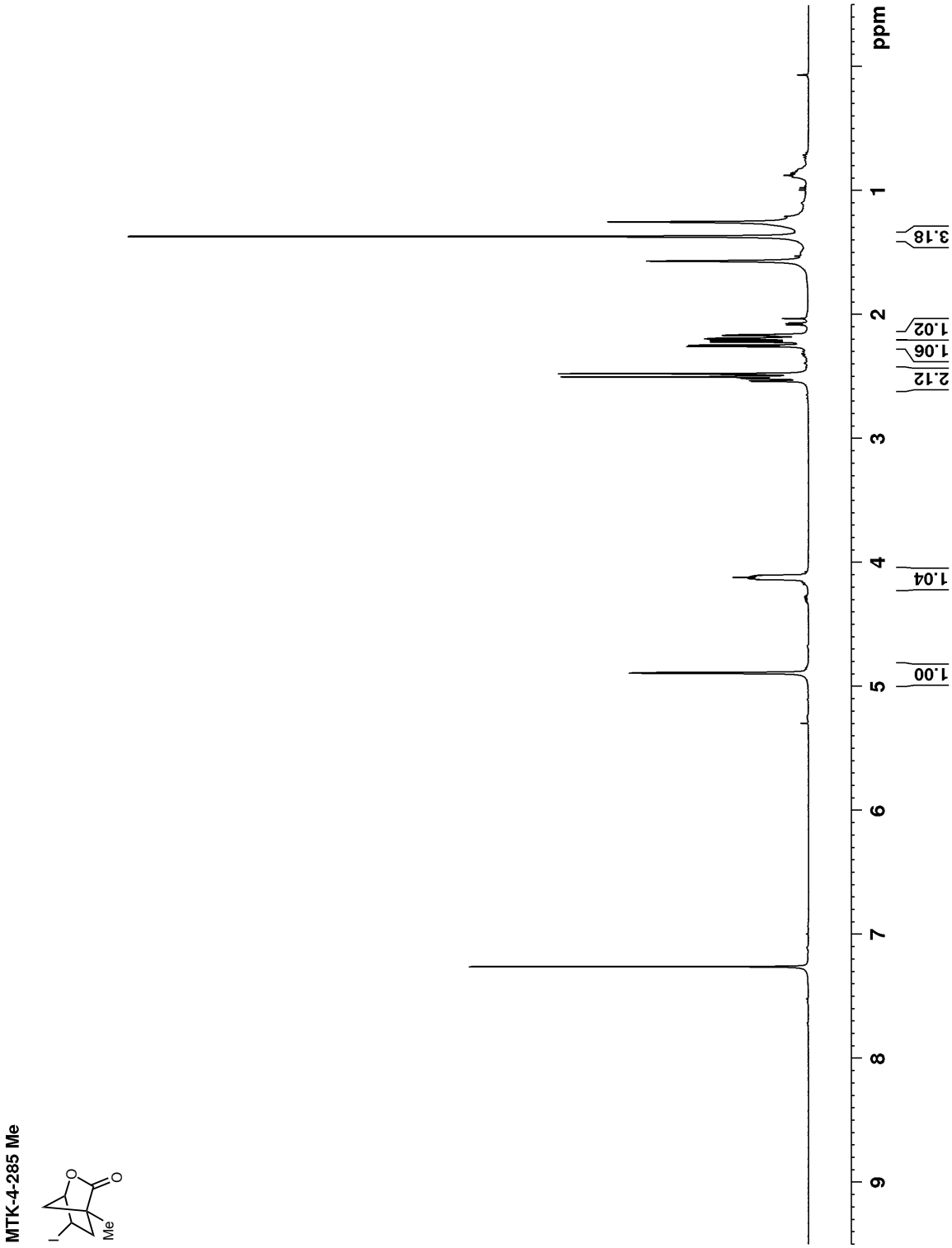

Figure B 69: ^{13}C NMR (100 MHz, $CDCl_3$) of **109l**

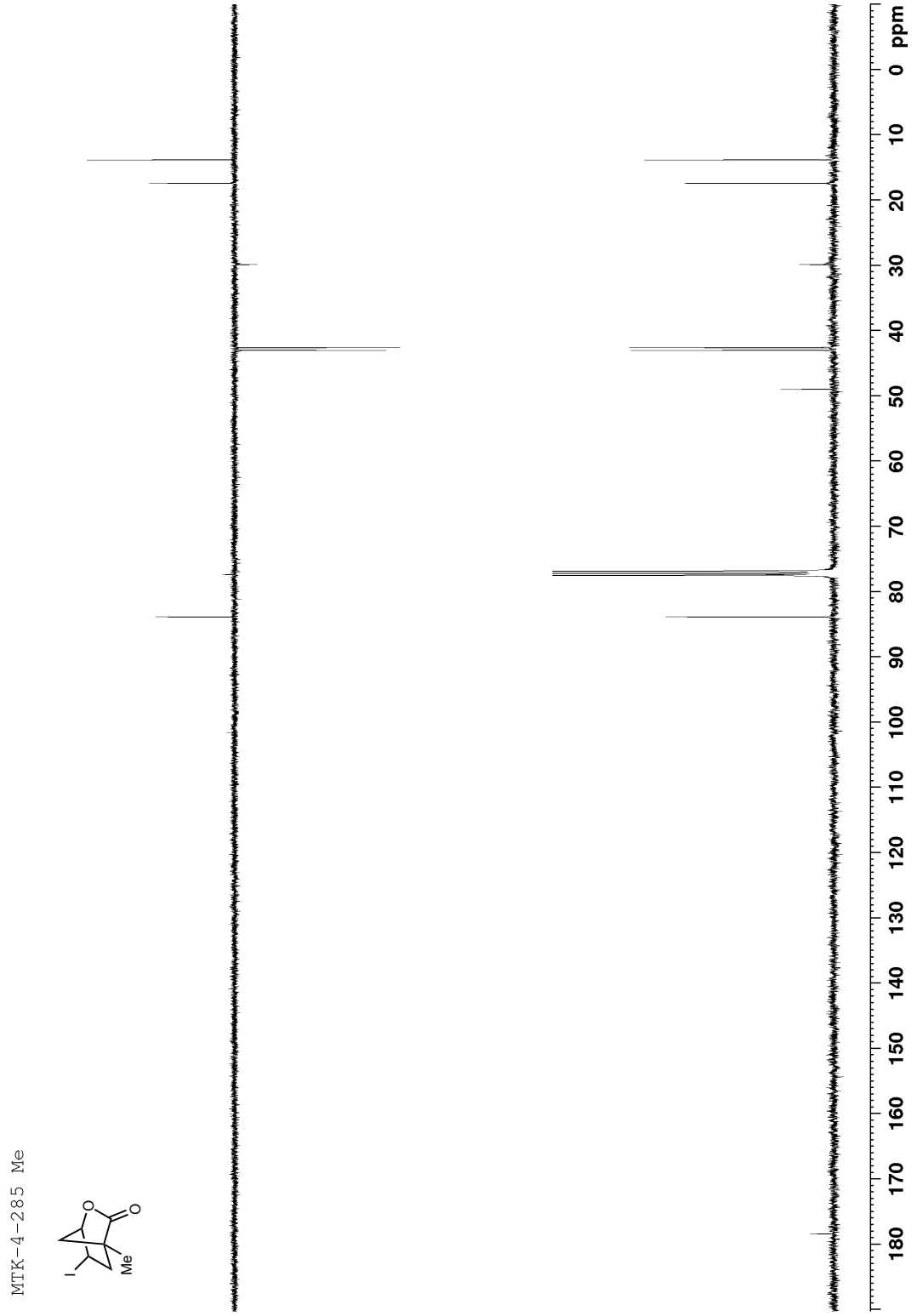

Figure B 70: ^{1}H NMR (400 MHz, $CDCl_3$) of **109m**

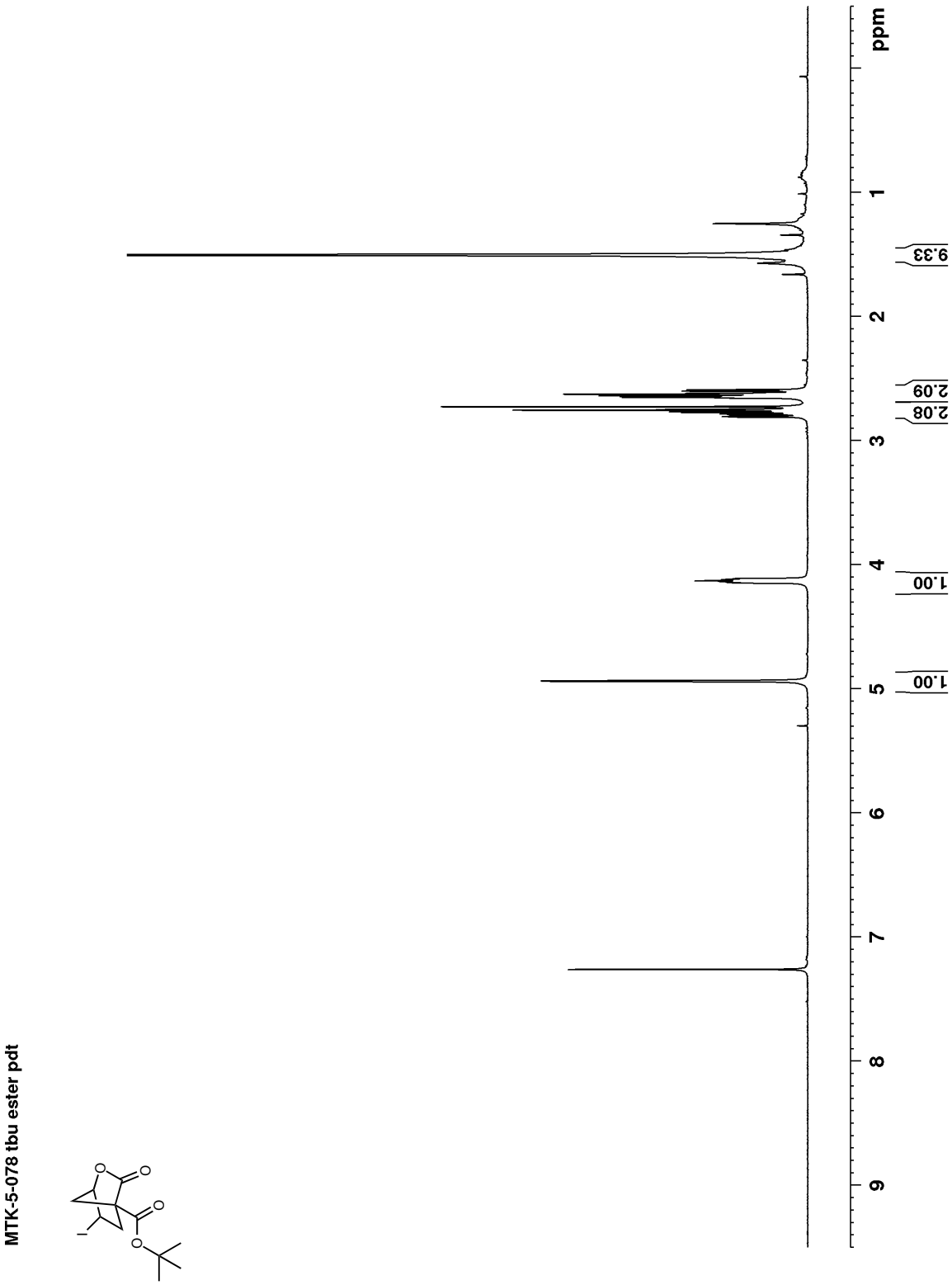

Figure B 71: ^{13}C NMR (100 MHz, $CDCl_3$) of **109m**

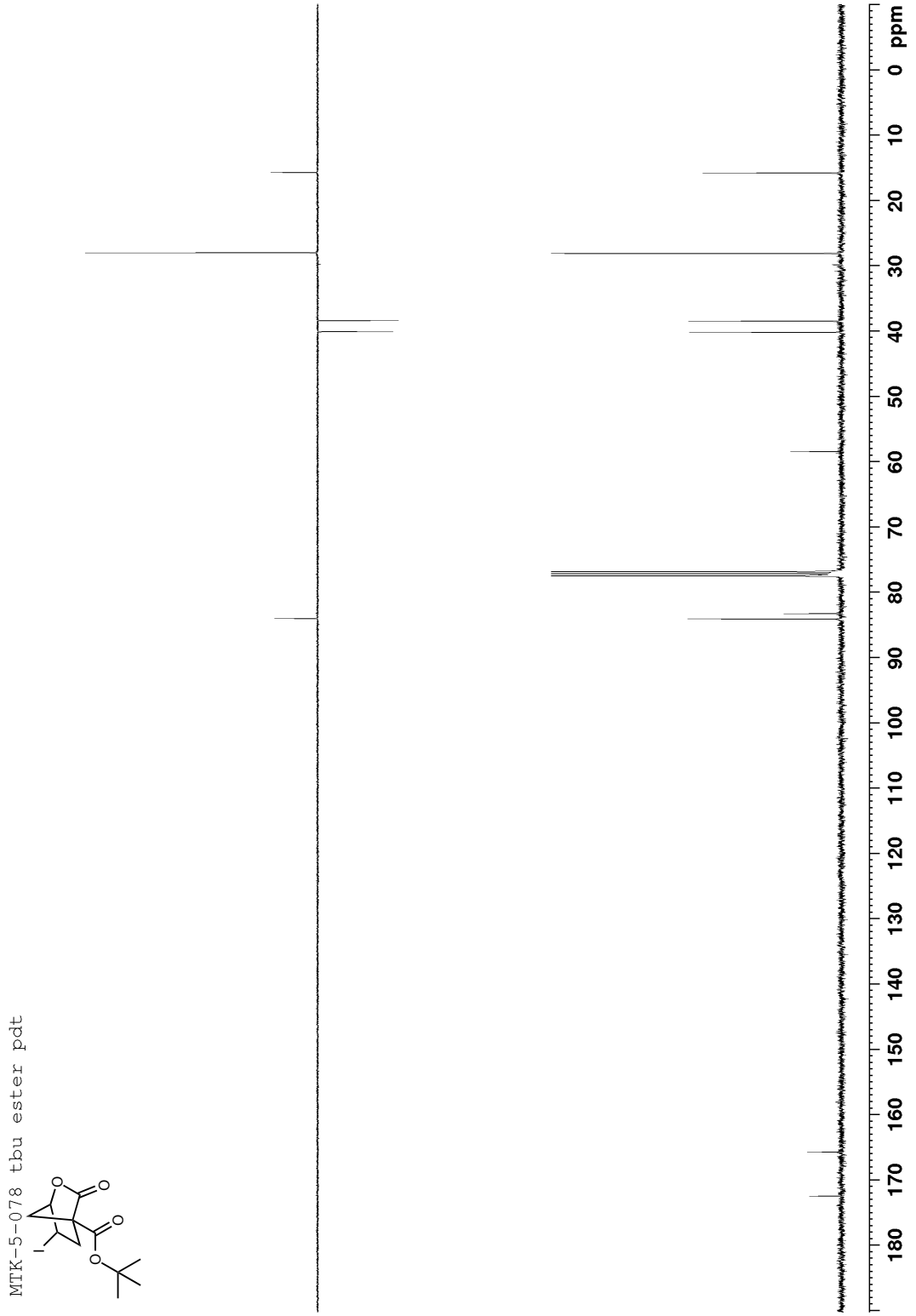

Figure B 72: ^{1}H NMR (400 MHz, $CDCl_3$) of **109n**

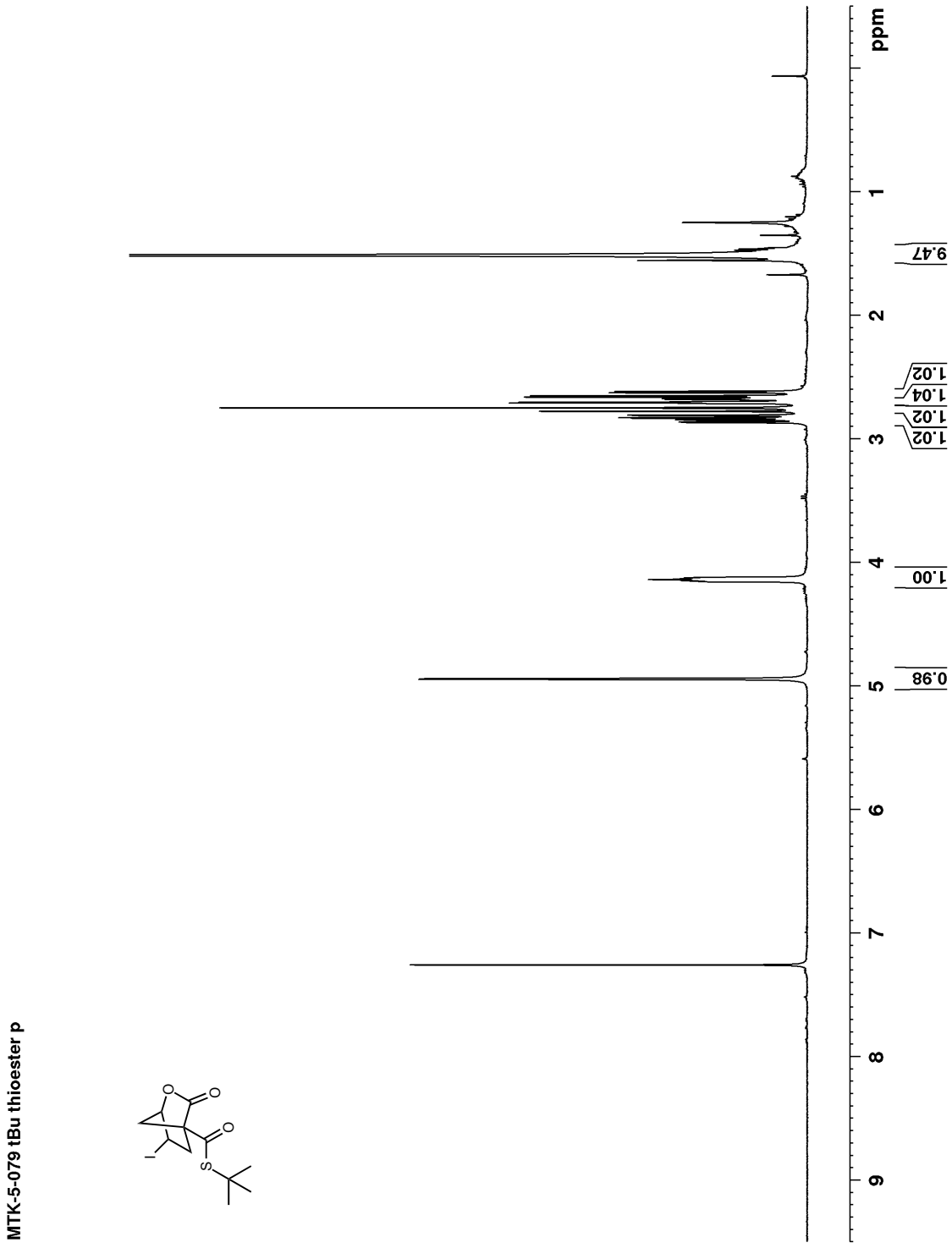

Figure B 73: ^{13}C NMR (100 MHz, $CDCl_3$) of **109n**

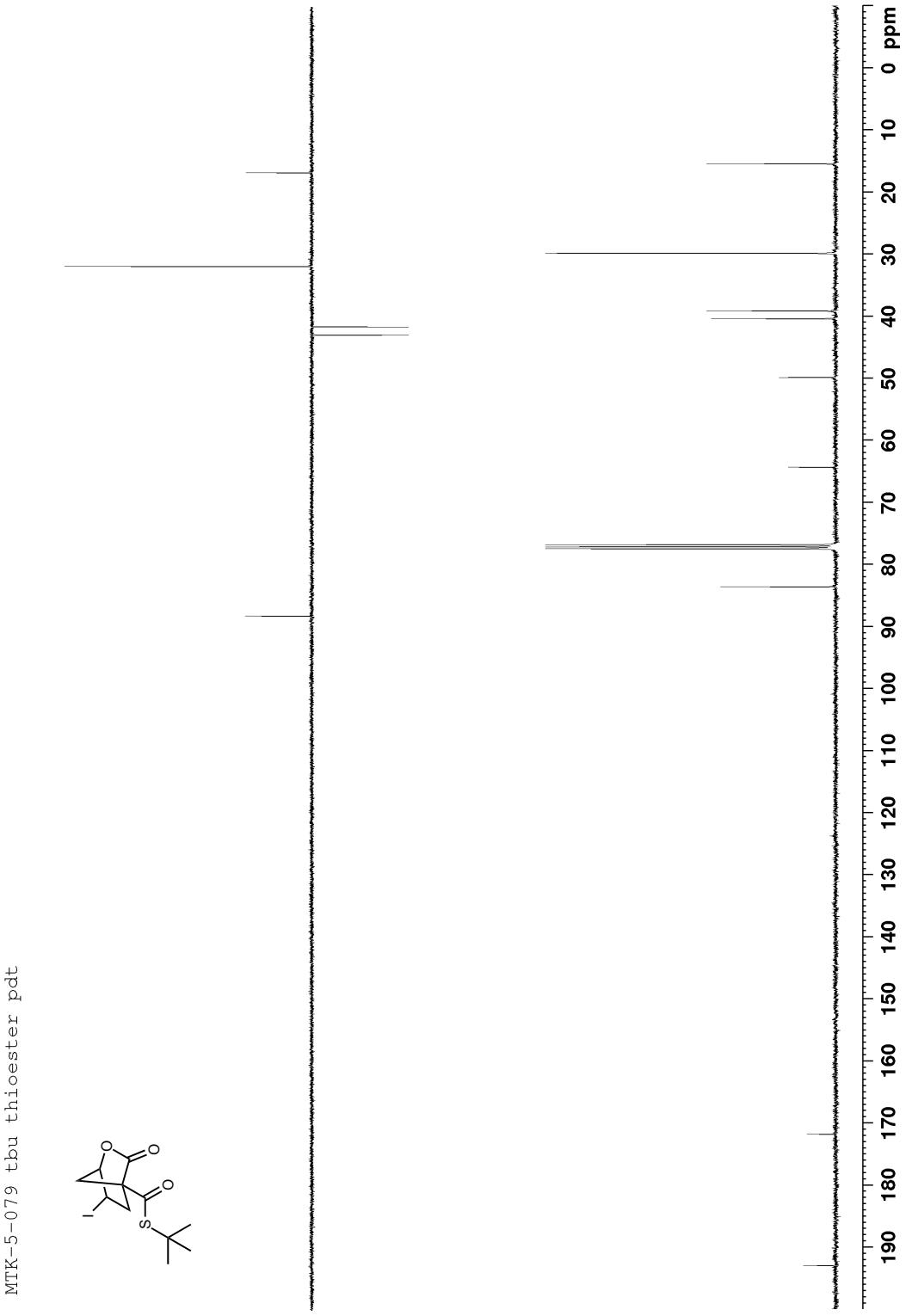

Figure B 74: ^{1}H NMR (400 MHz, $CDCl_3$) of **134**

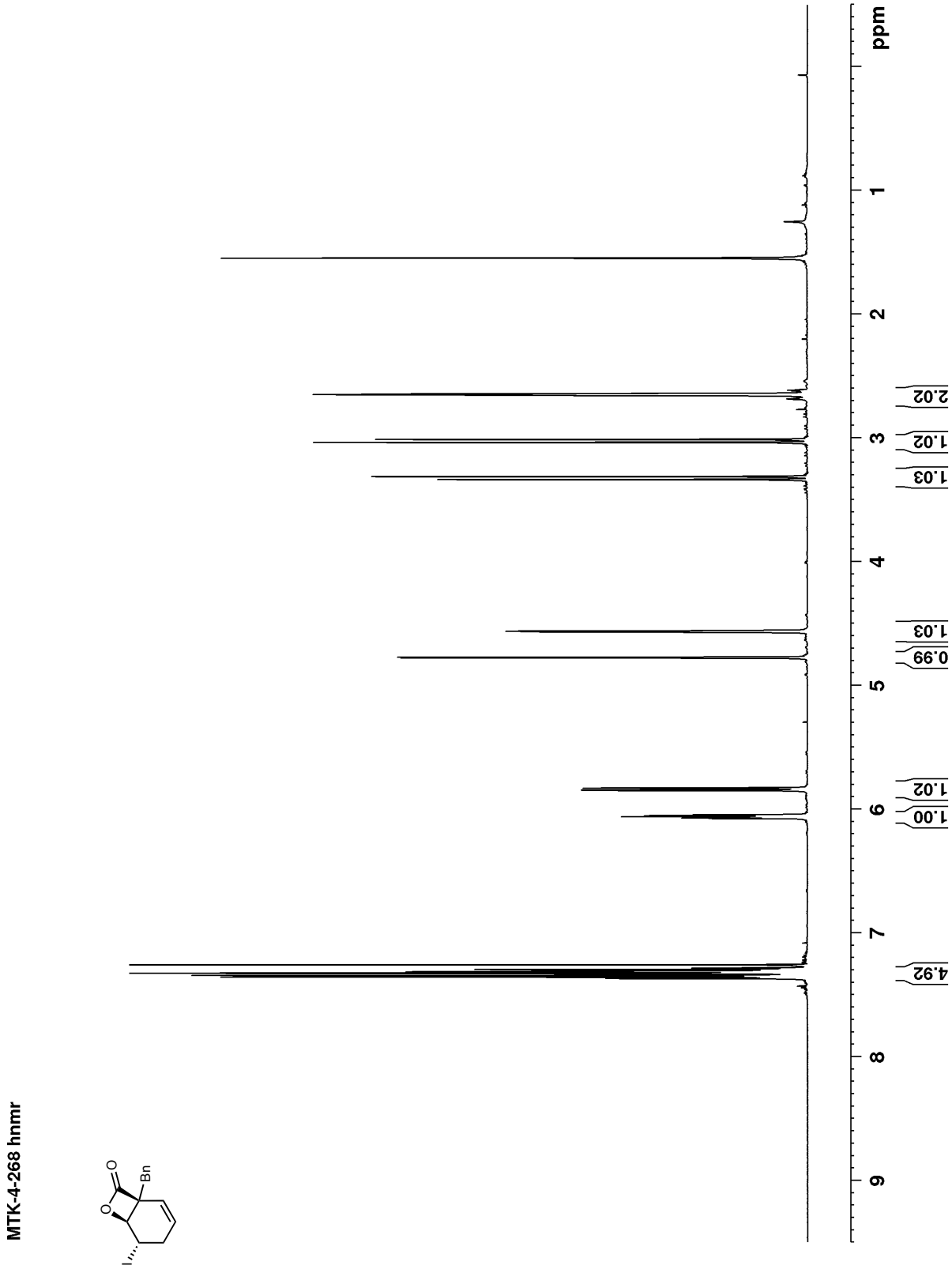

Figure B 75: ^{13}C NMR (100 MHz, $CDCl_3$) of **134**

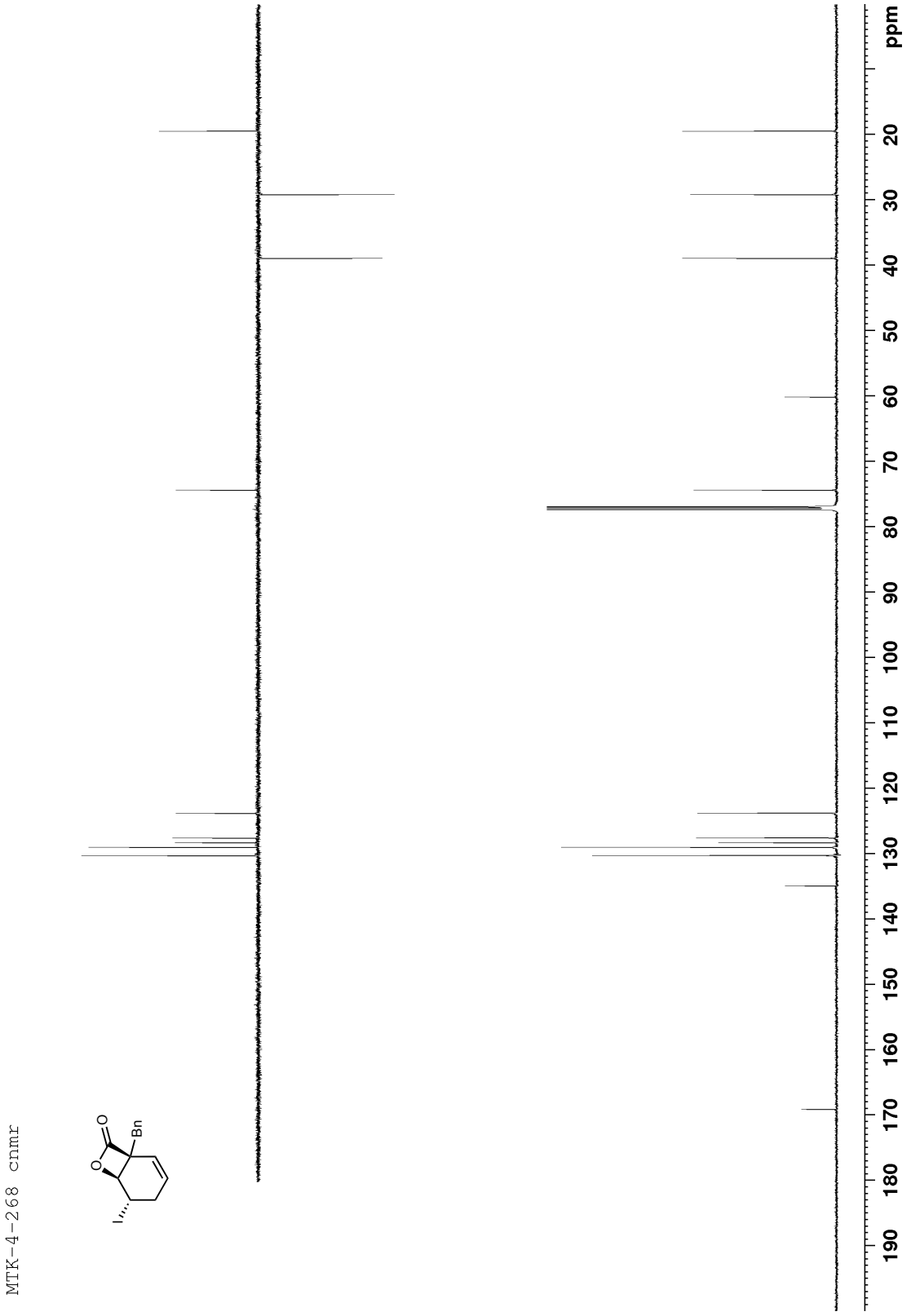

Figure B 76: HMBC (100 MHz, $CDCl_3$) of **134**

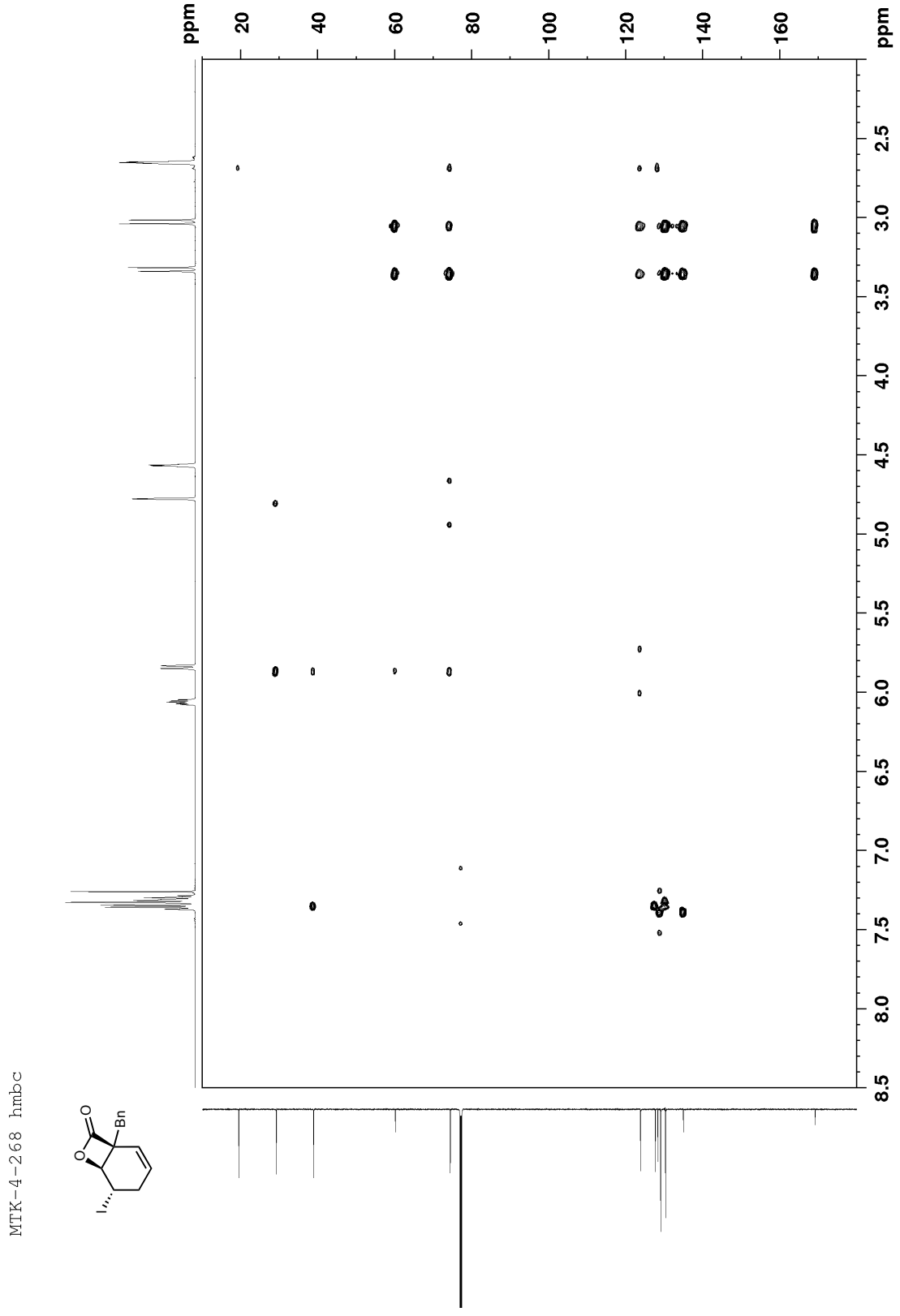

Figure B 77: ^{1}H NMR (400 MHz, $CDCl_3$) of **136**

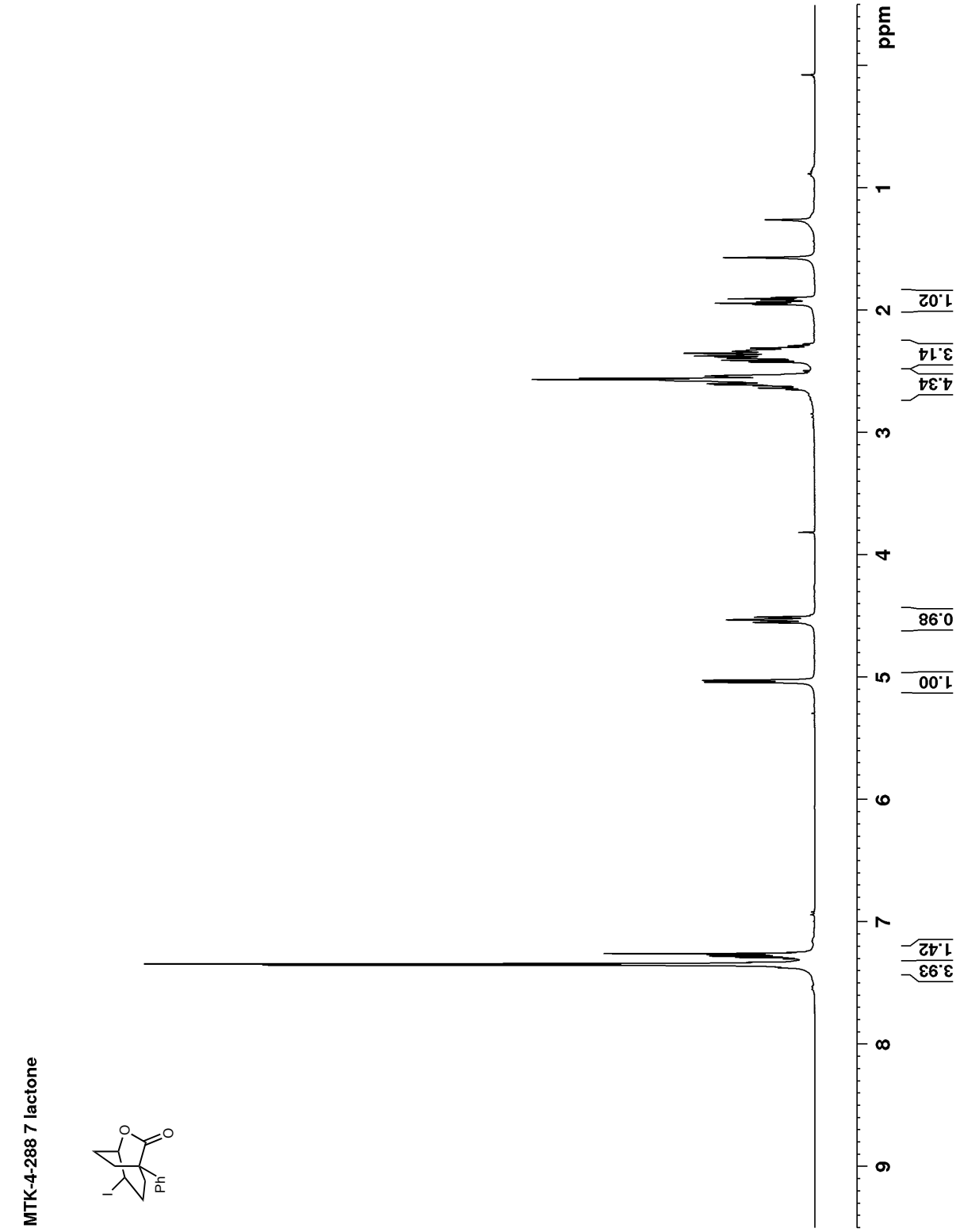

Figure B 78: ^{13}C NMR (100 MHz, $CDCl_3$) of **136**

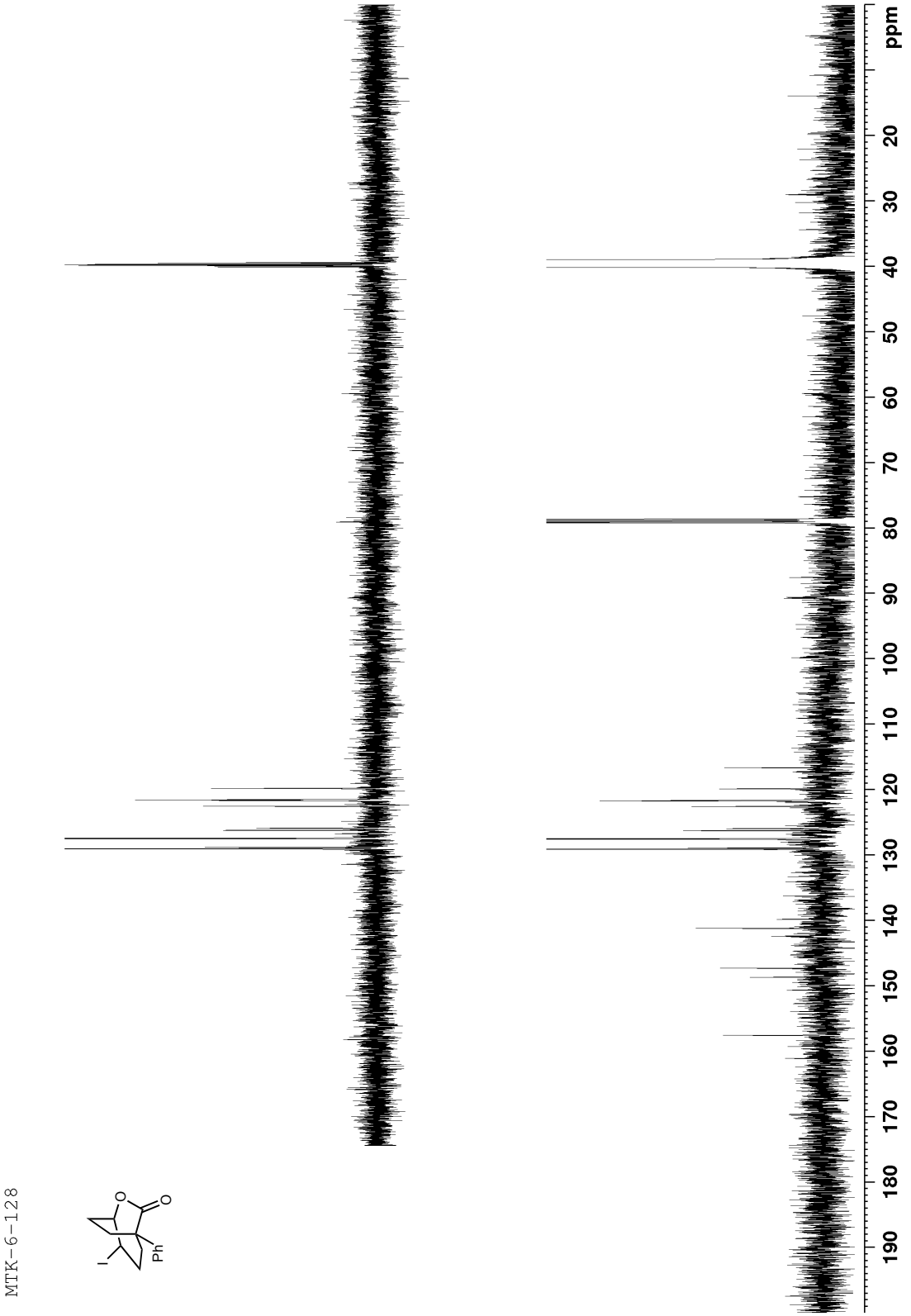

Figure B 79: ^{1}H NMR (400 MHz, $CDCl_3$) of **137**

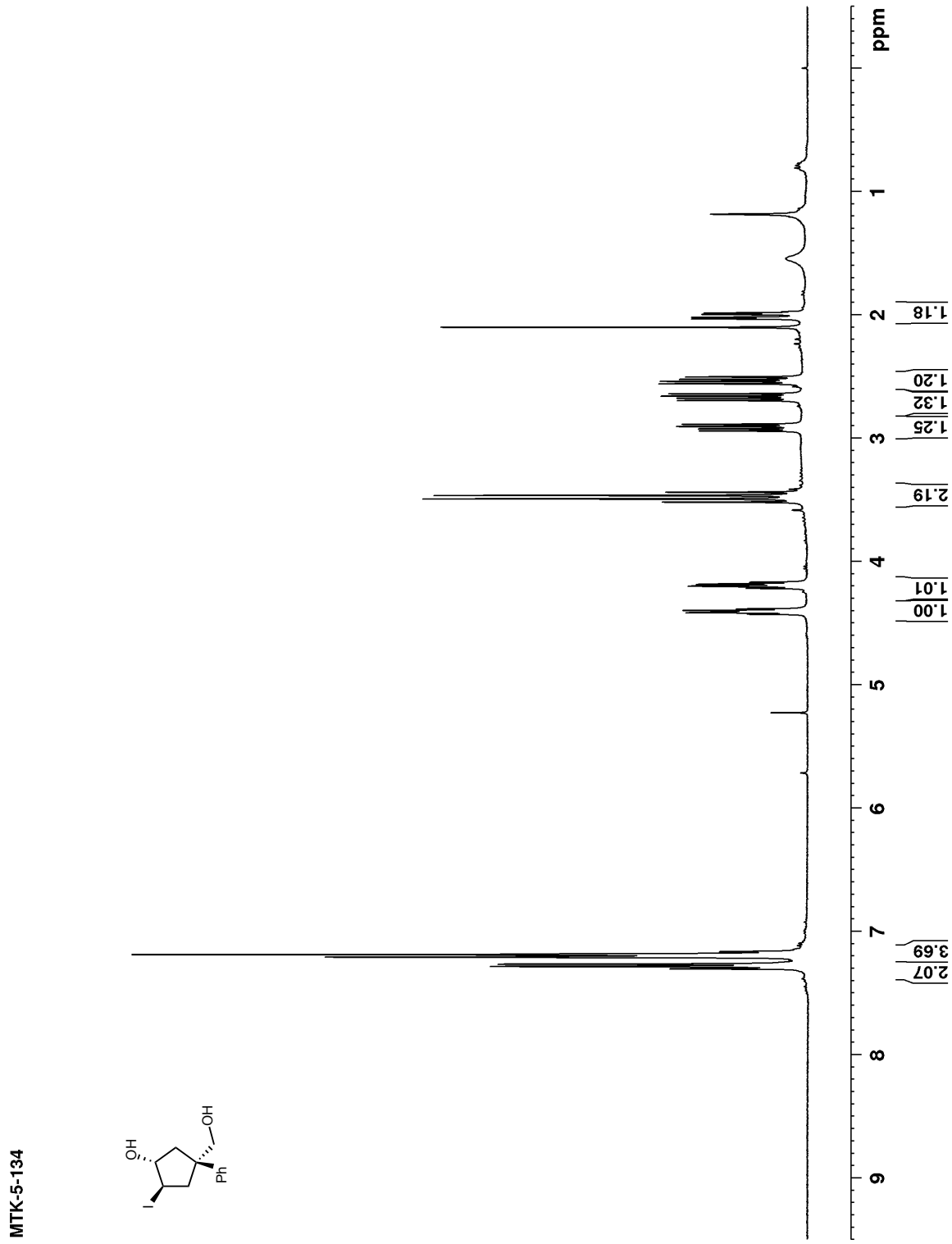

Figure B 80: ^{13}C NMR (100 MHz, $CDCl_3$) of **137**

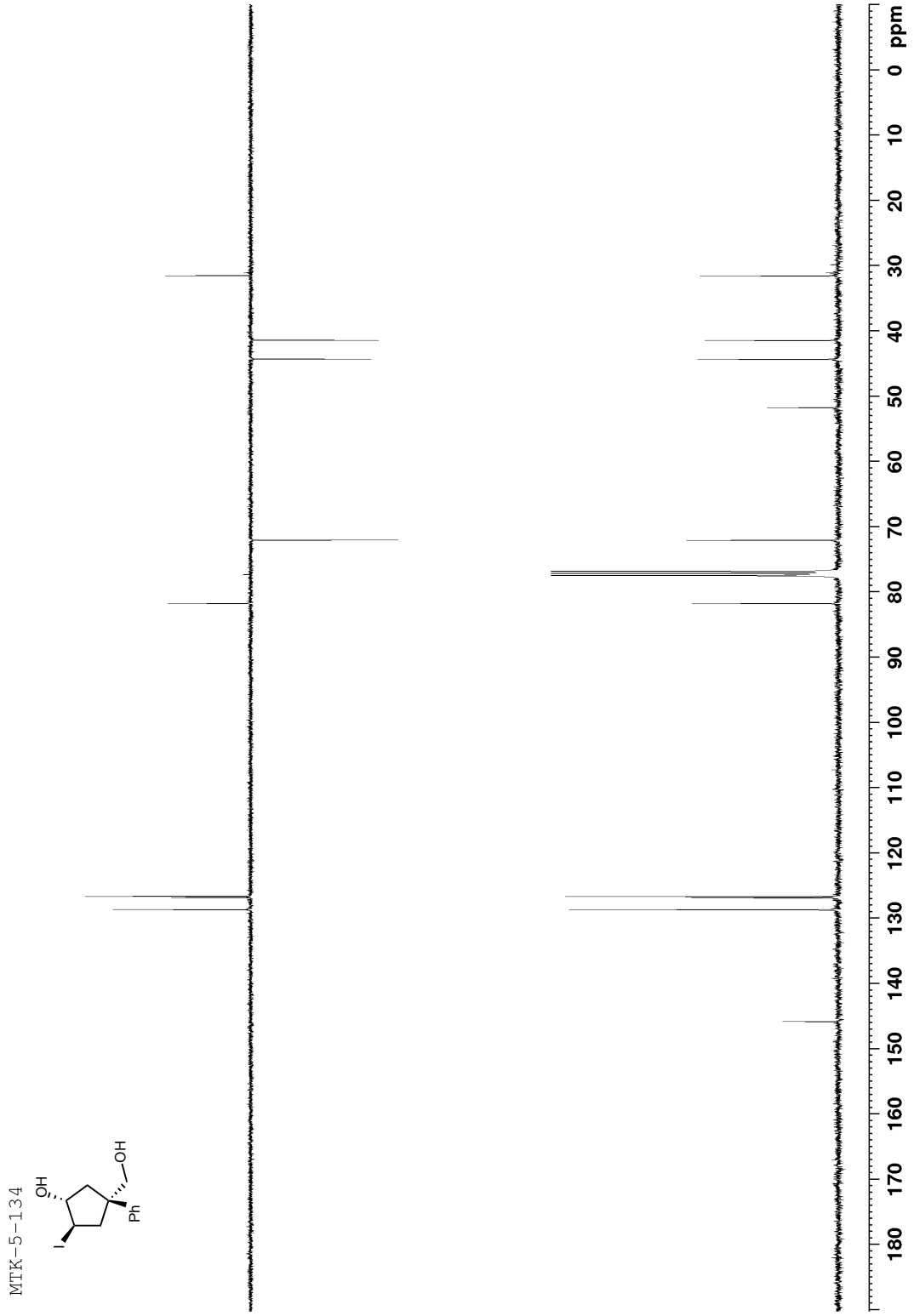

Figure B 81: ^{1}H NMR (600 MHz, $CDCl_3$) of **138**

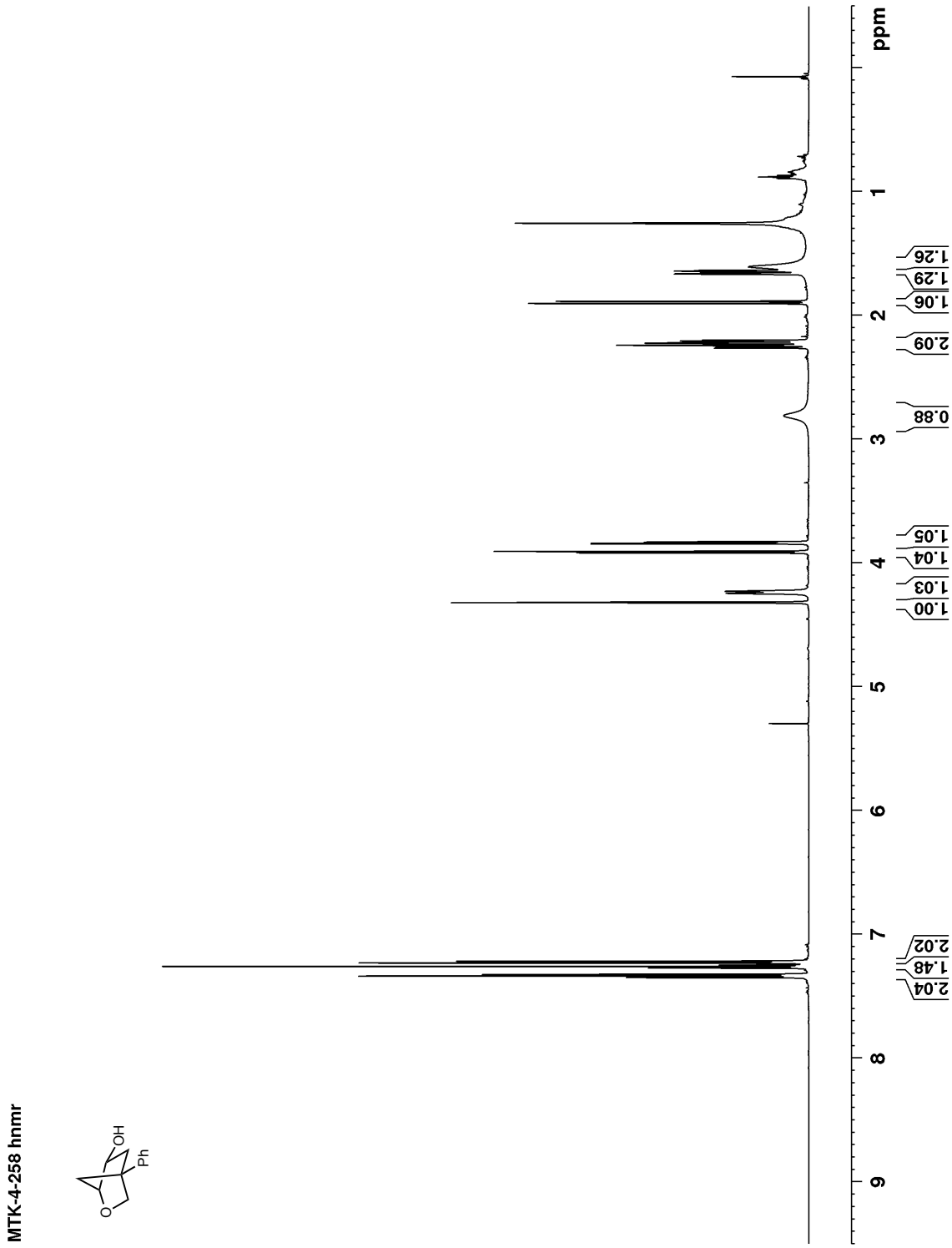

Figure B 82: ^{13}C NMR (125 MHz, $CDCl_3$) of **138**

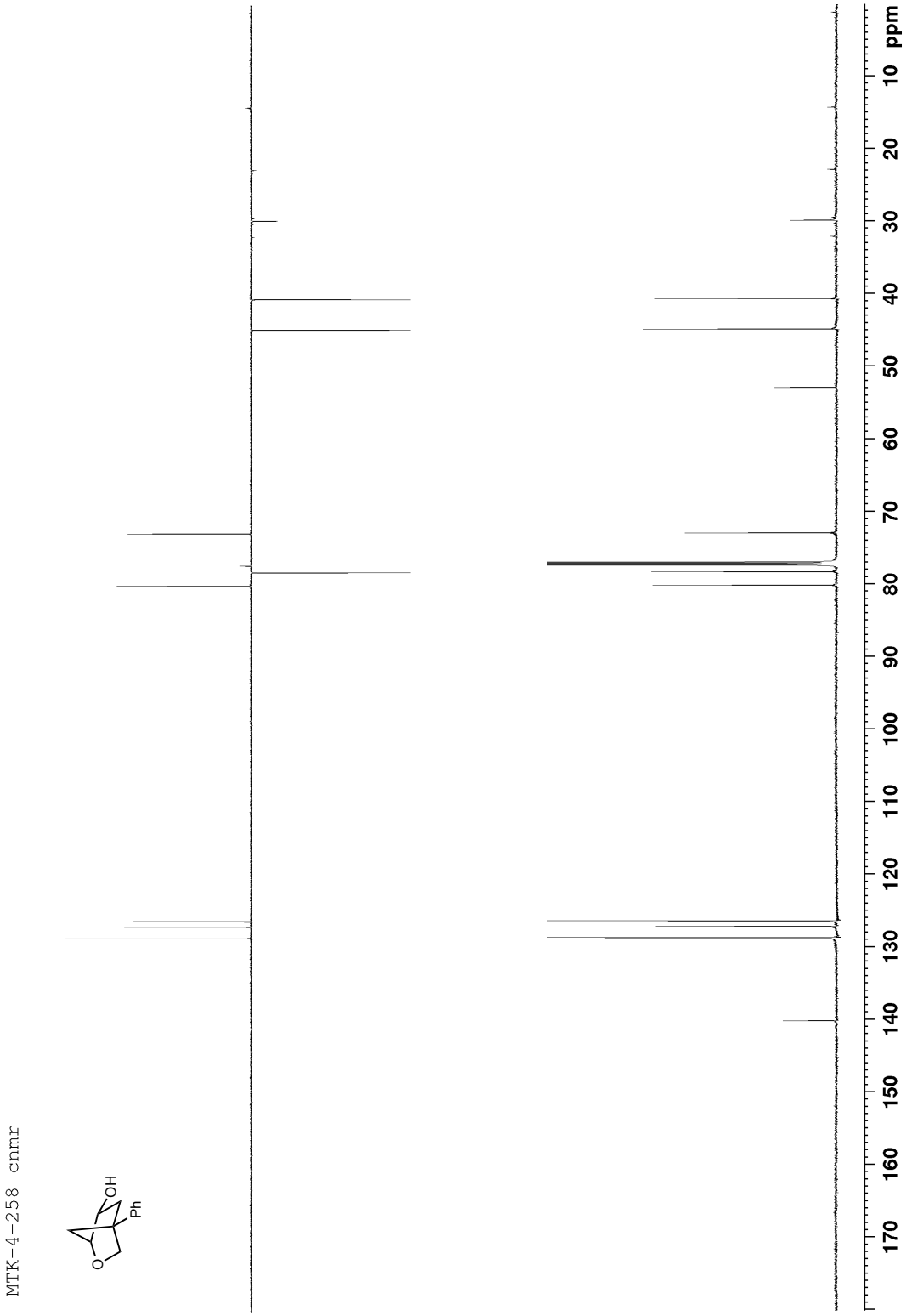

Figure B 83: HMBC (125 MHz, $CDCl_3$) of **139**

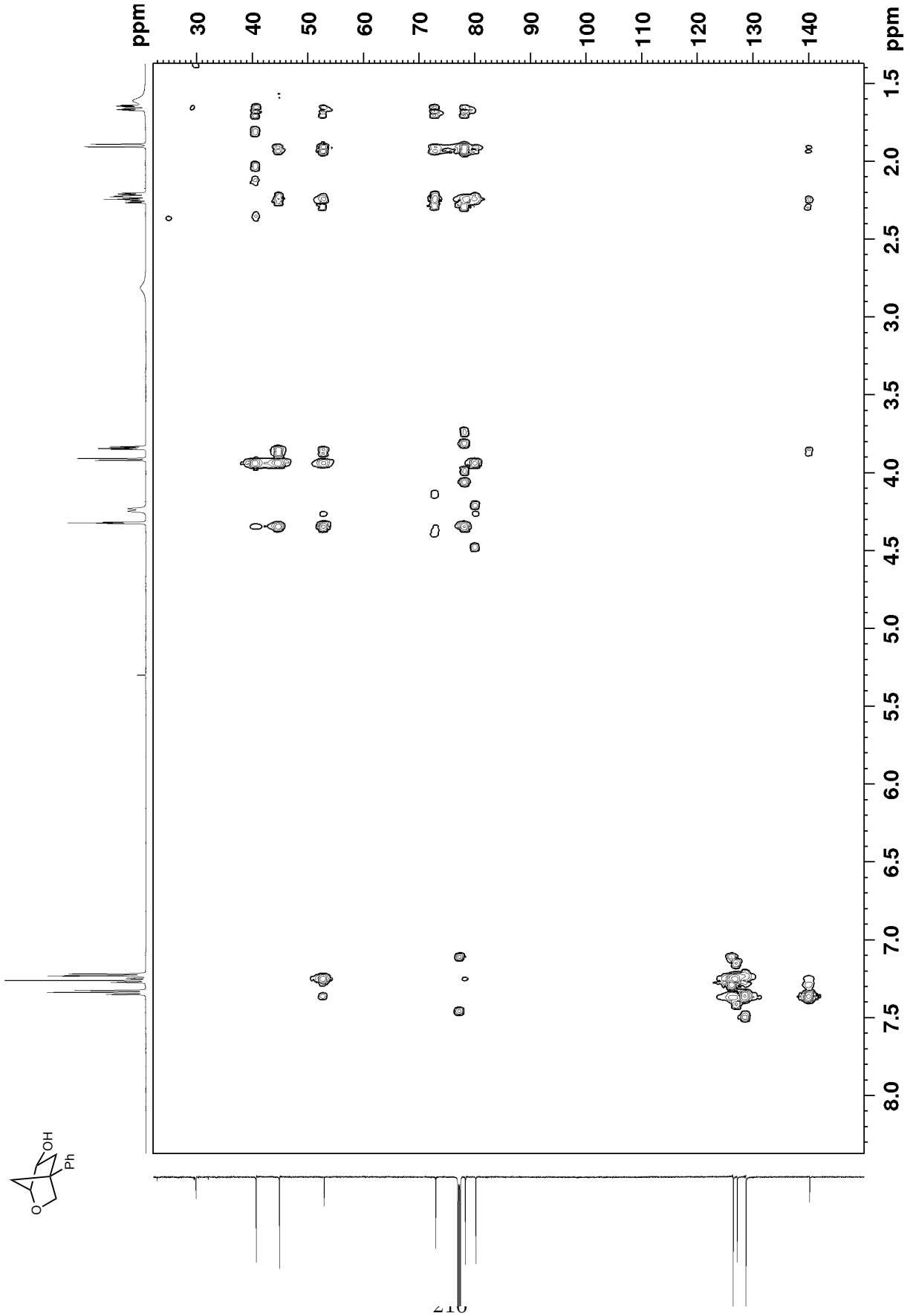

Figure B 84: ^{1}H NMR (400 MHz, $CDCl_3$) of **139**

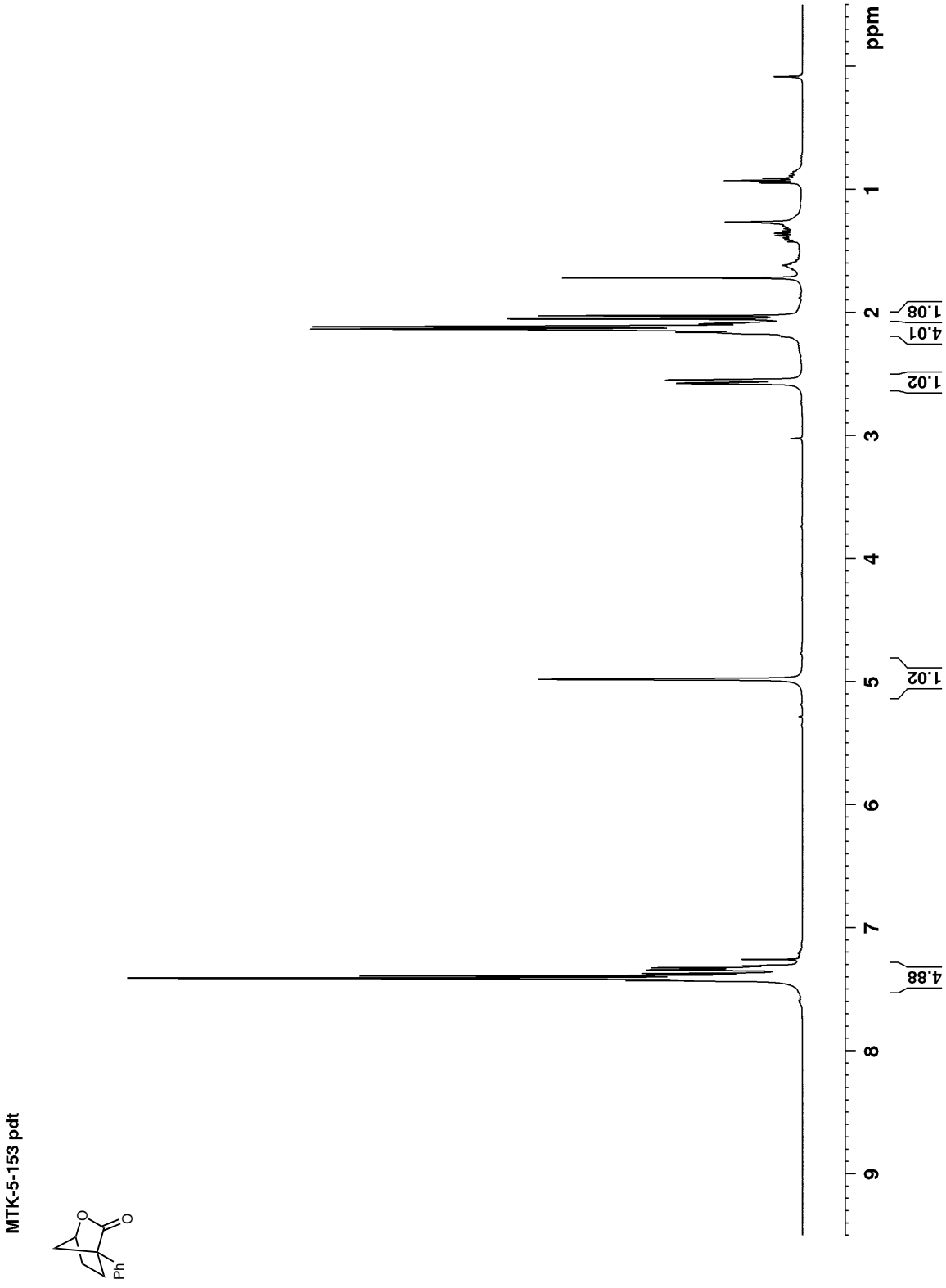

Figure B 85: ^{13}C NMR (100 MHz, $CDCl_3$) of **139**

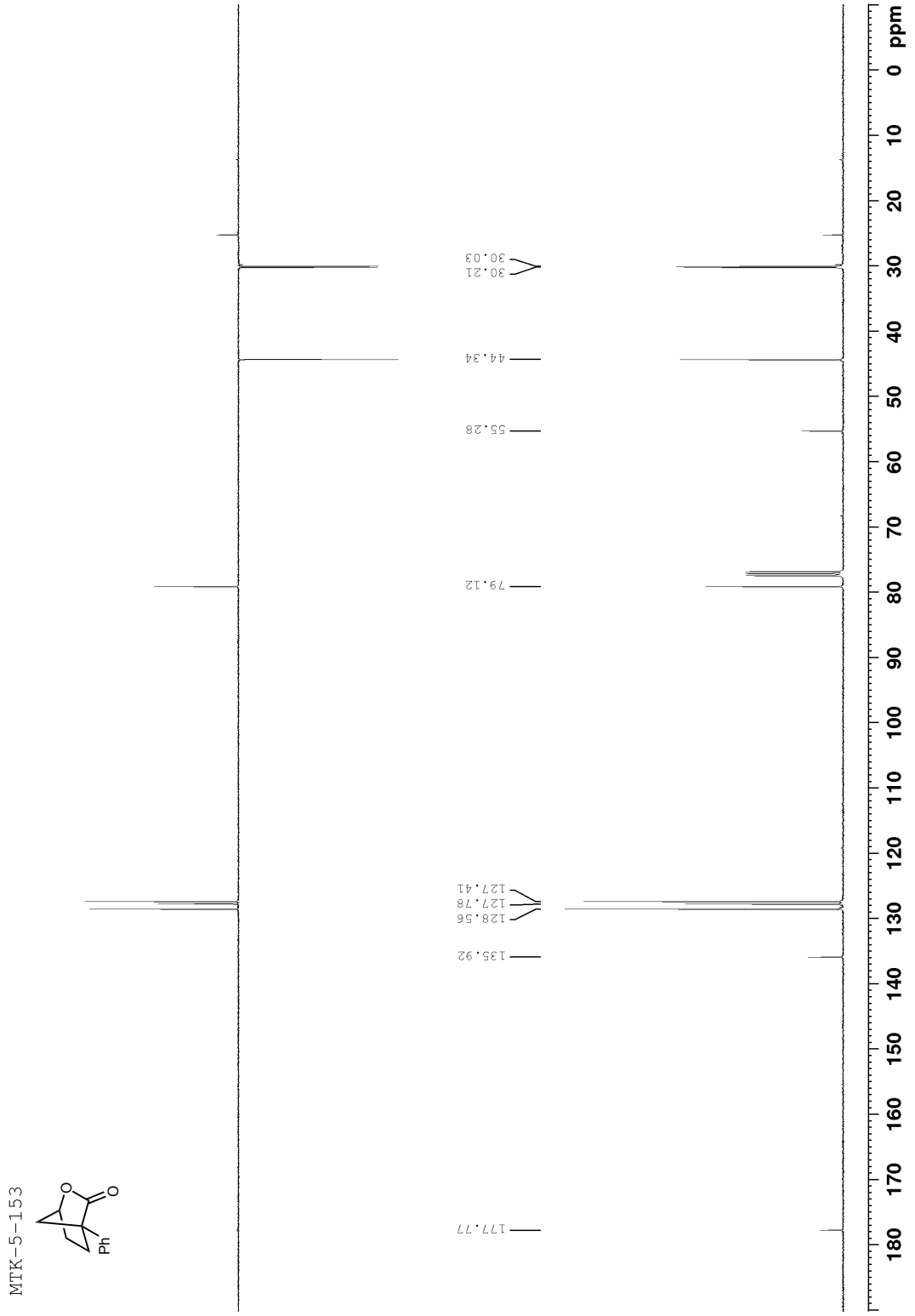

Figure B 86: ^{1}H NMR (400 MHz, $CDCl_3$) of **140**

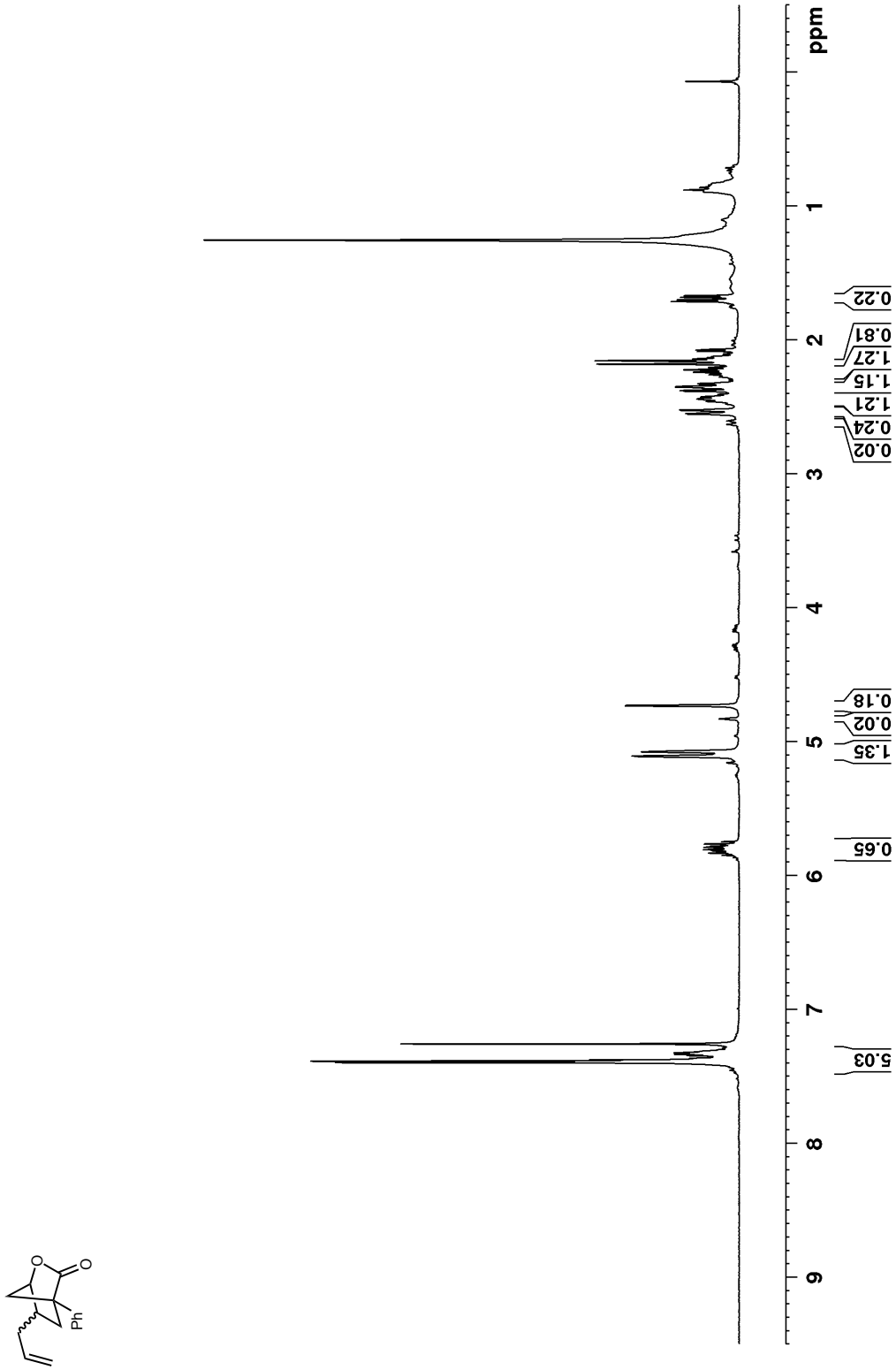

Figure B 87: ^{13}C NMR (100 MHz, $CDCl_3$) of **140**

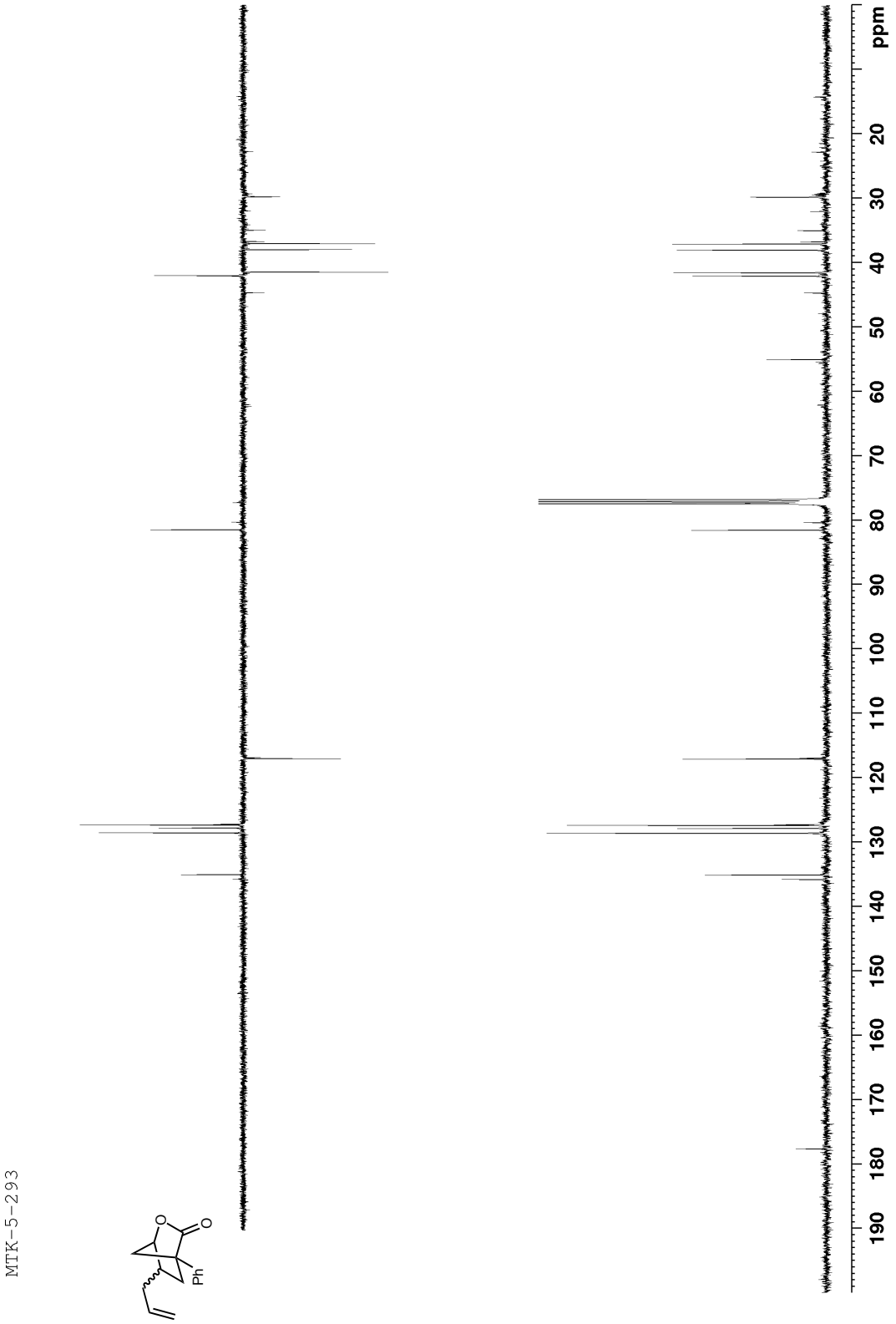

Figure B 88: ^{1}H NMR (400 MHz, $CDCl_3$) of **141**

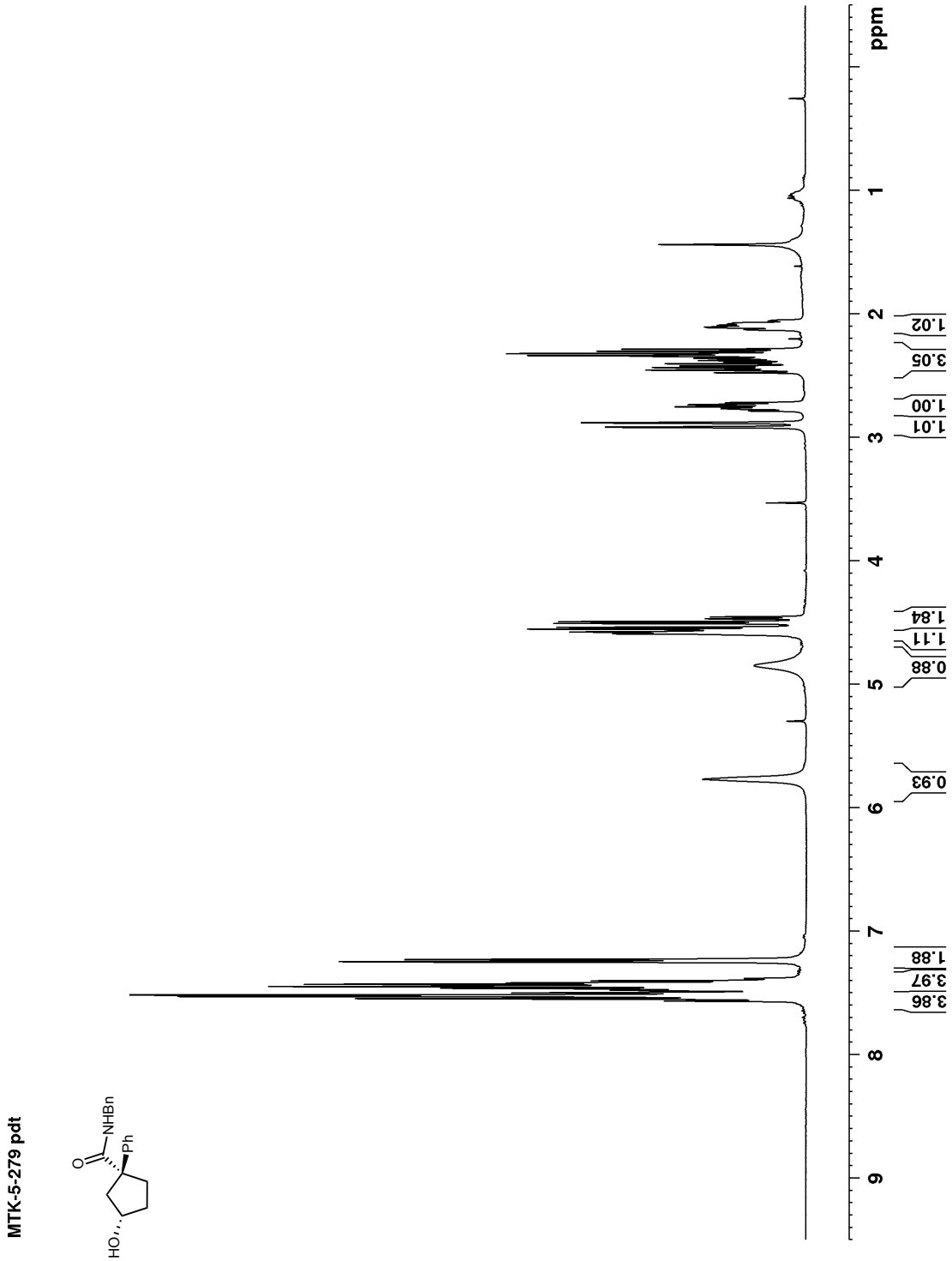

Figure B 89: ^{13}C NMR (100 MHz, $CDCl_3$) of **141**

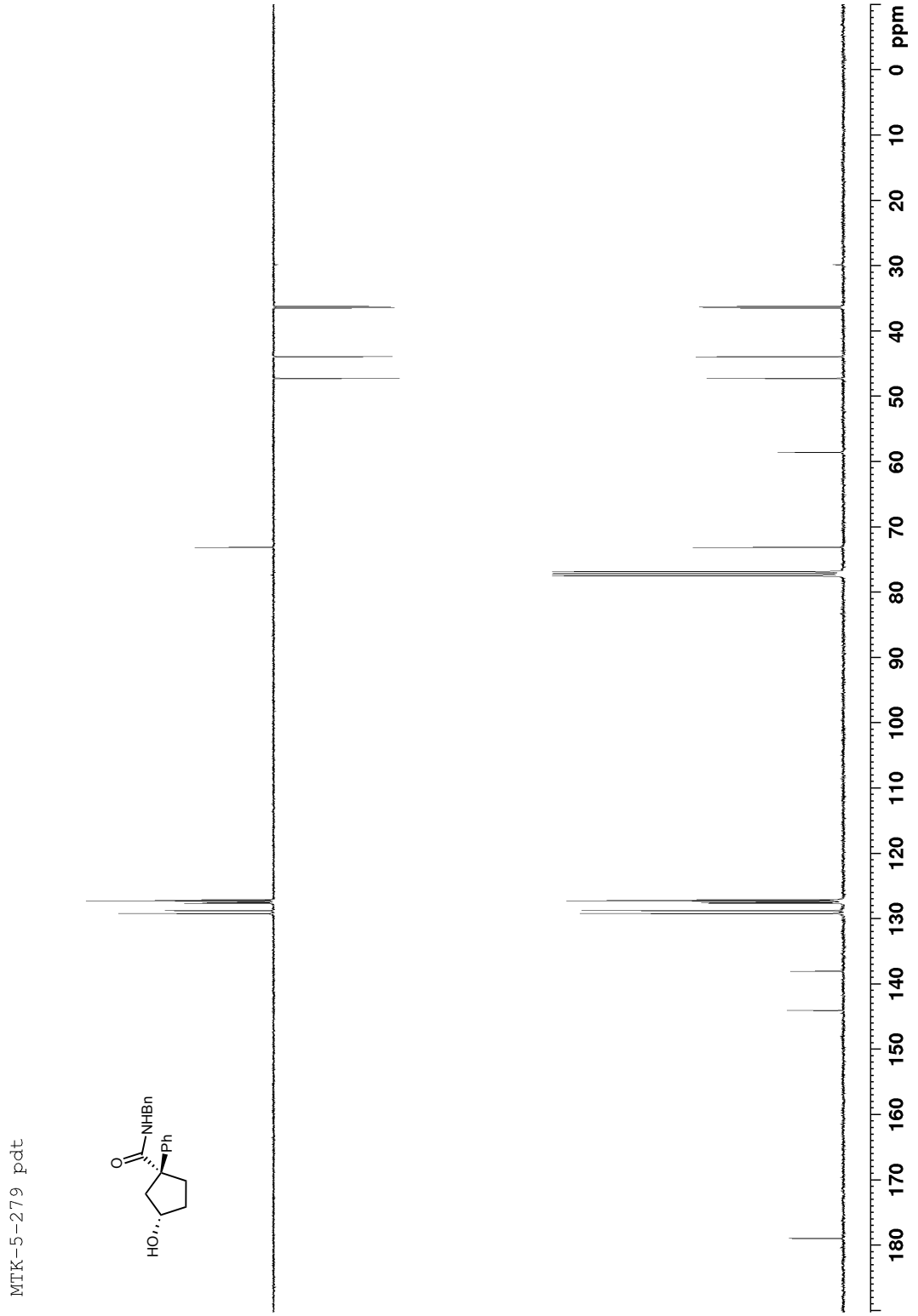

Figure B 90: ^{1}H NMR (400 MHz, $CDCl_3$) of **152**

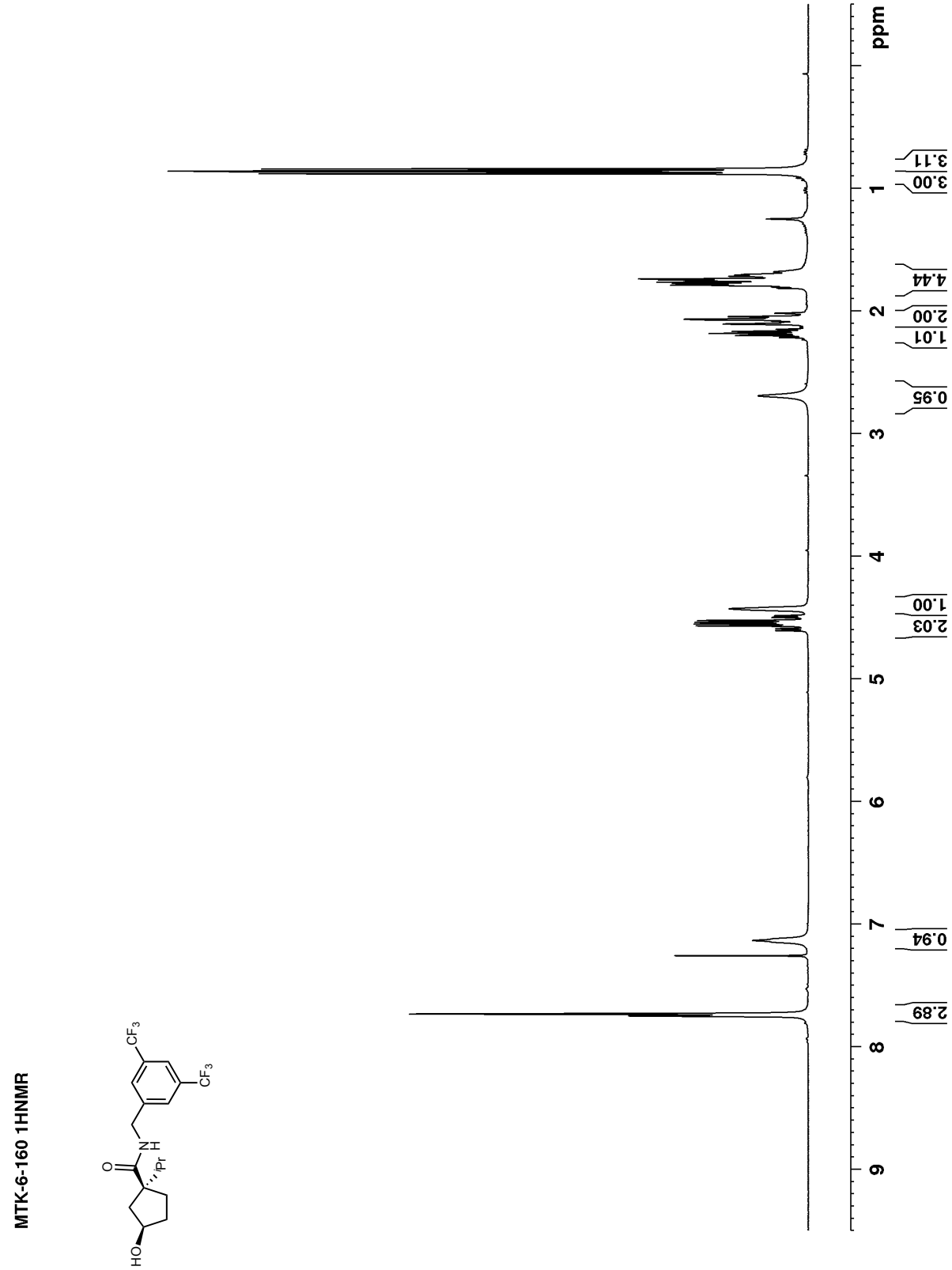

Figure B 91: ^{13}C NMR (100 MHz, $CDCl_3$) of **152**

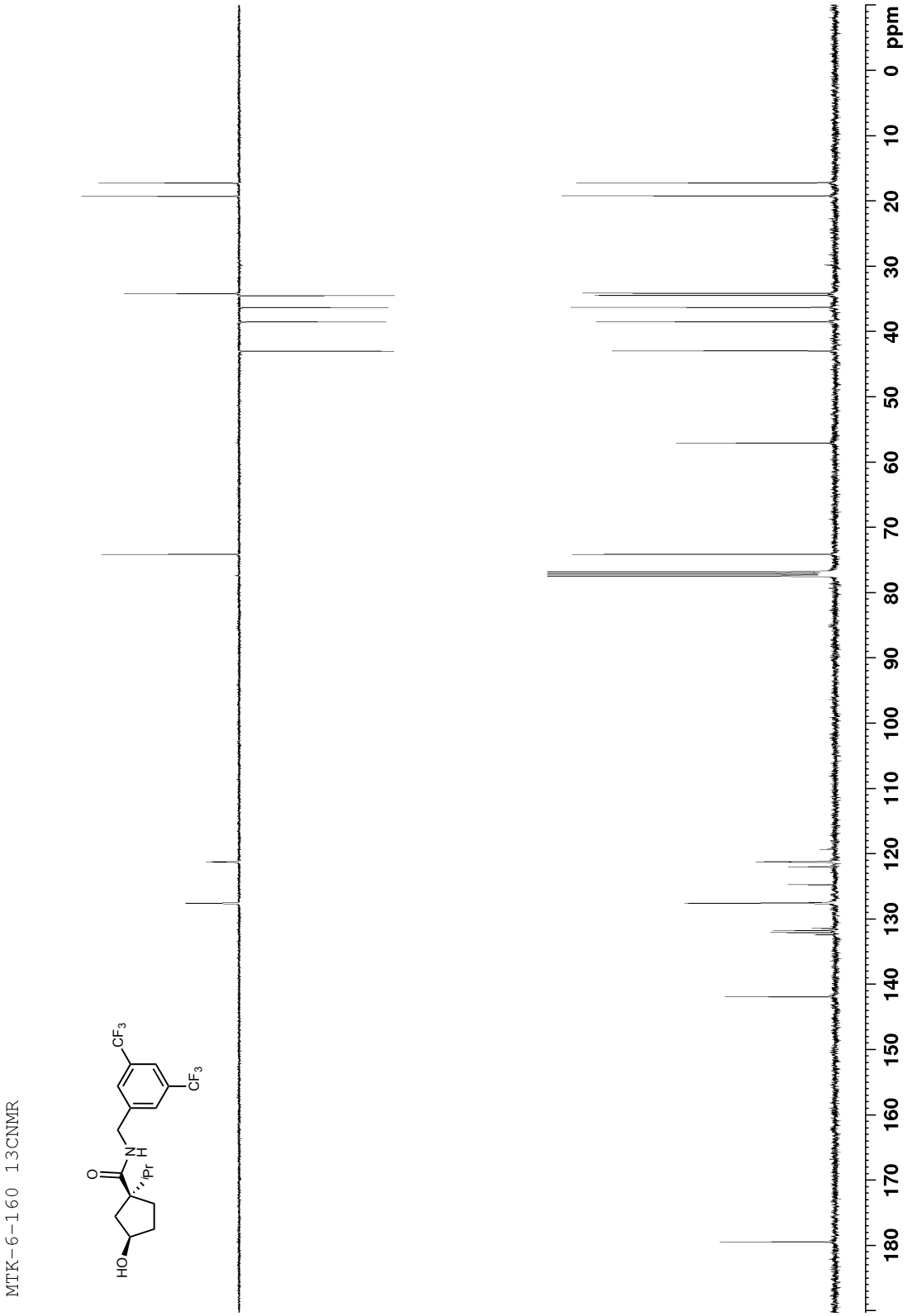

Figure B 92: ^{1}H NMR (600 MHz, DMSO-*d*6) of **148**

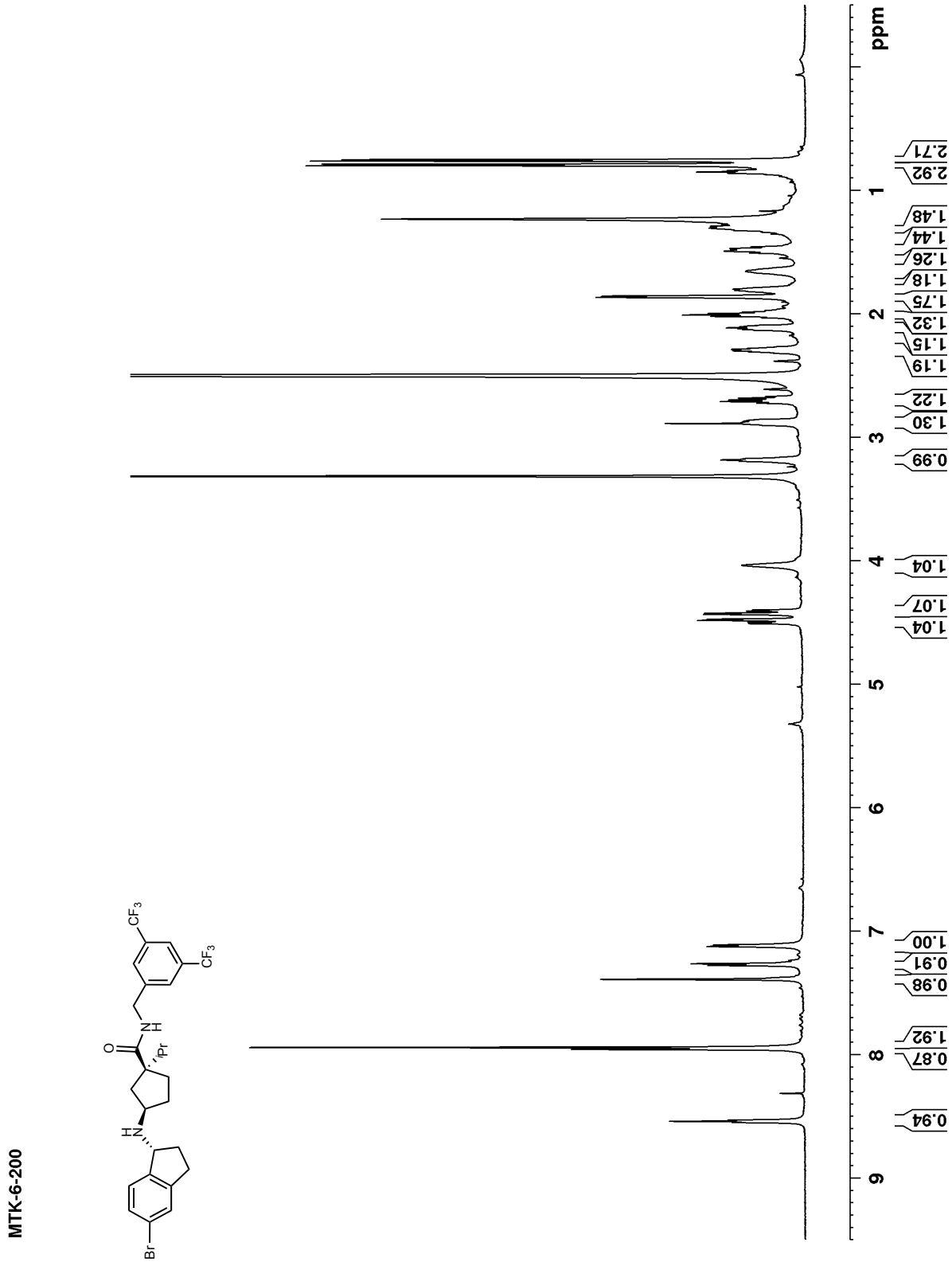

Figure B 93: ^{13}C NMR (125 MHz, DMSO-*d*6) of **148**

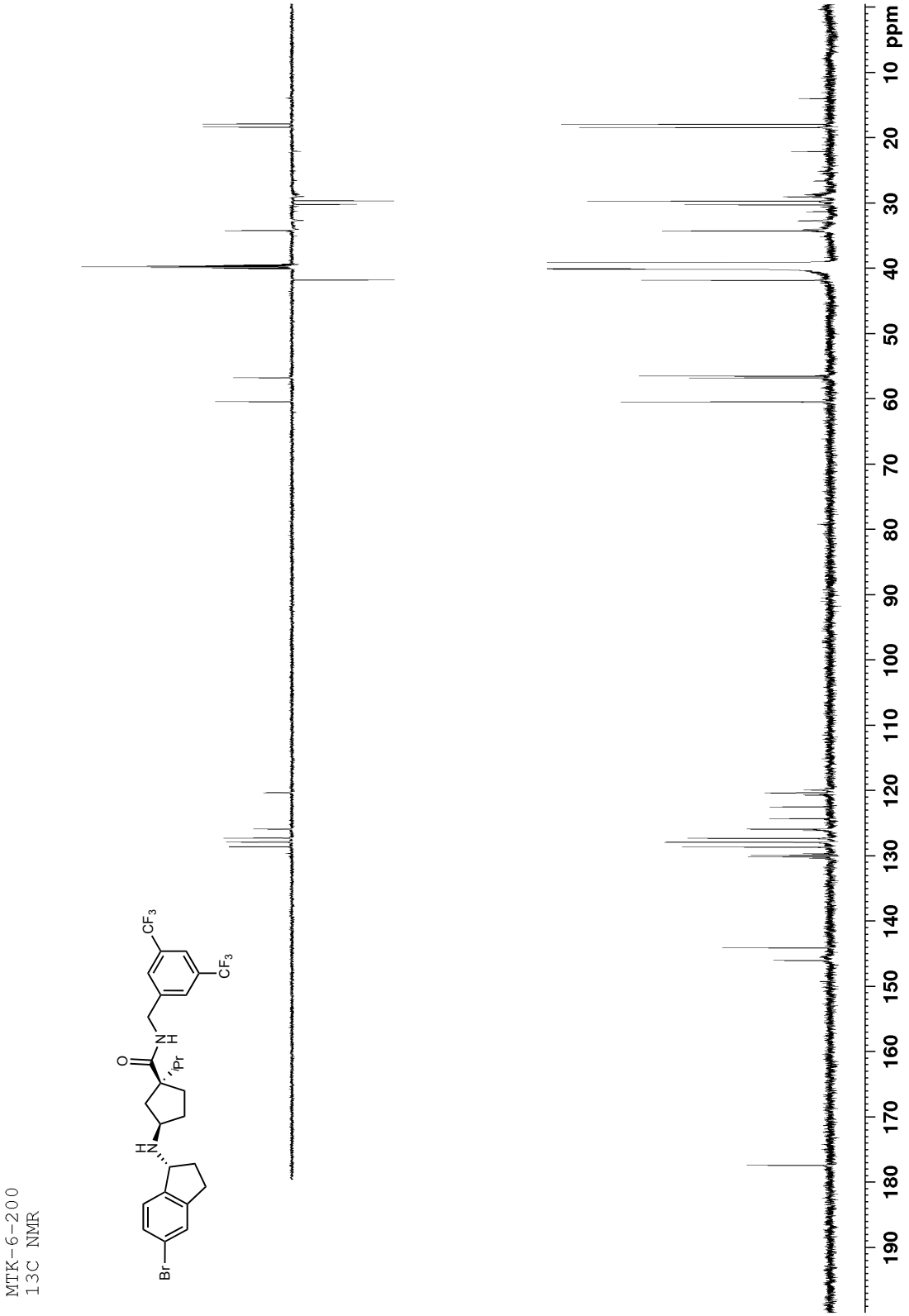

Figure B 94: 1D selective ROESY (600 MHz, DMSO-*d*6) of **148**

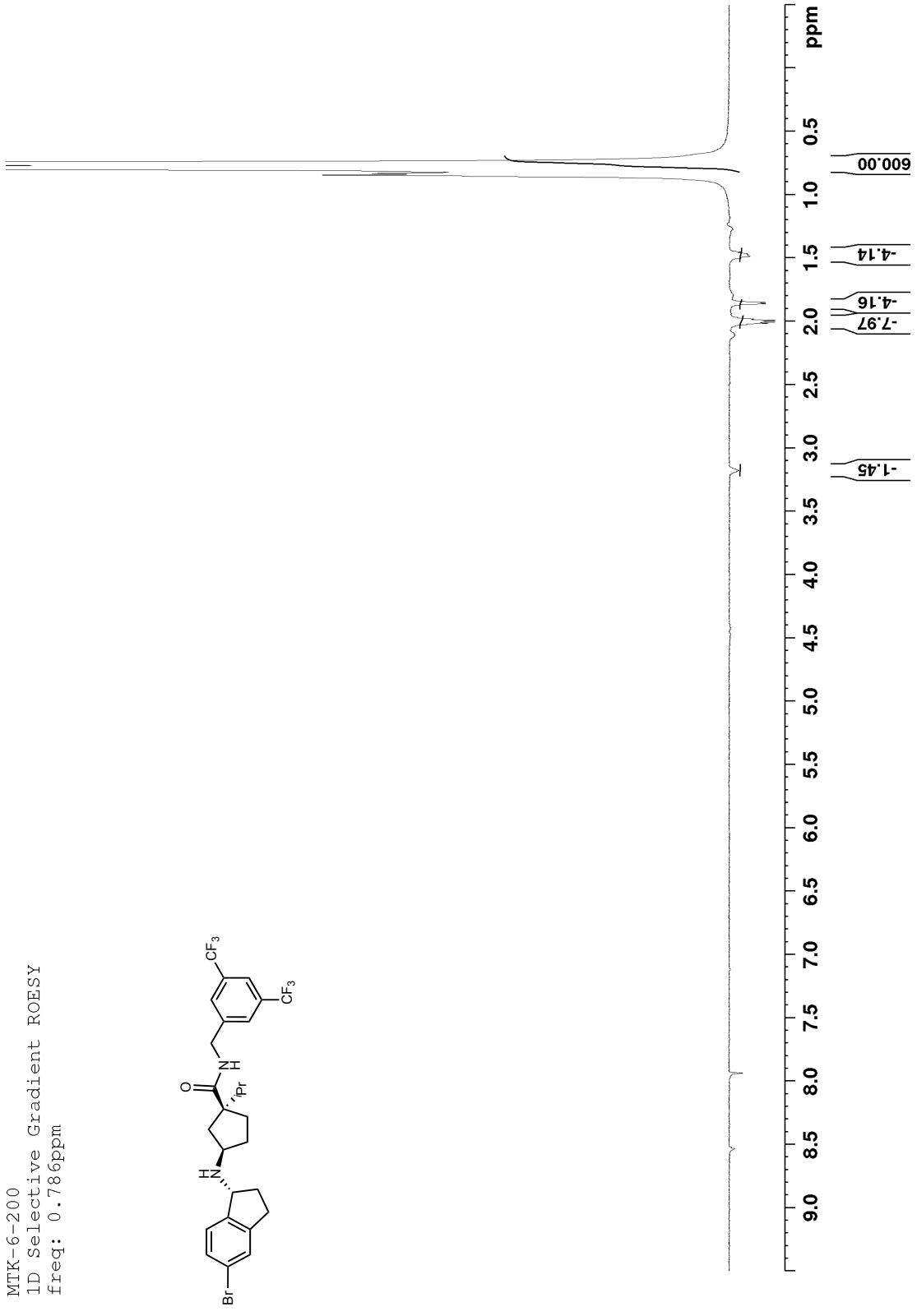

Figure B 95: 1D selective ROESY (600 MHz, DMSO-*d*6) of **148**

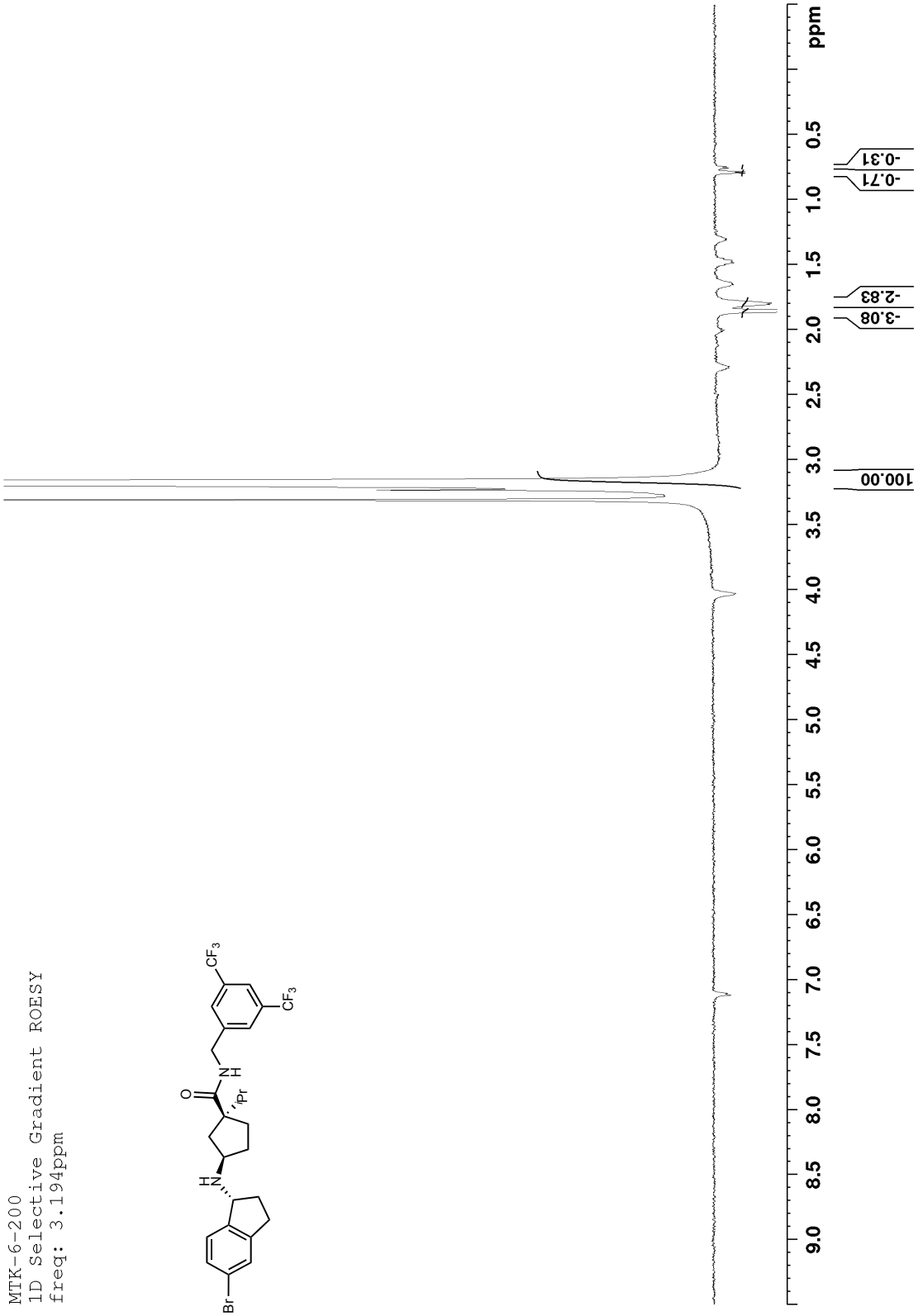

Figure B 96: ^{1}H NMR (600 MHz, DMSO-*d*6) of *epi*-**148**

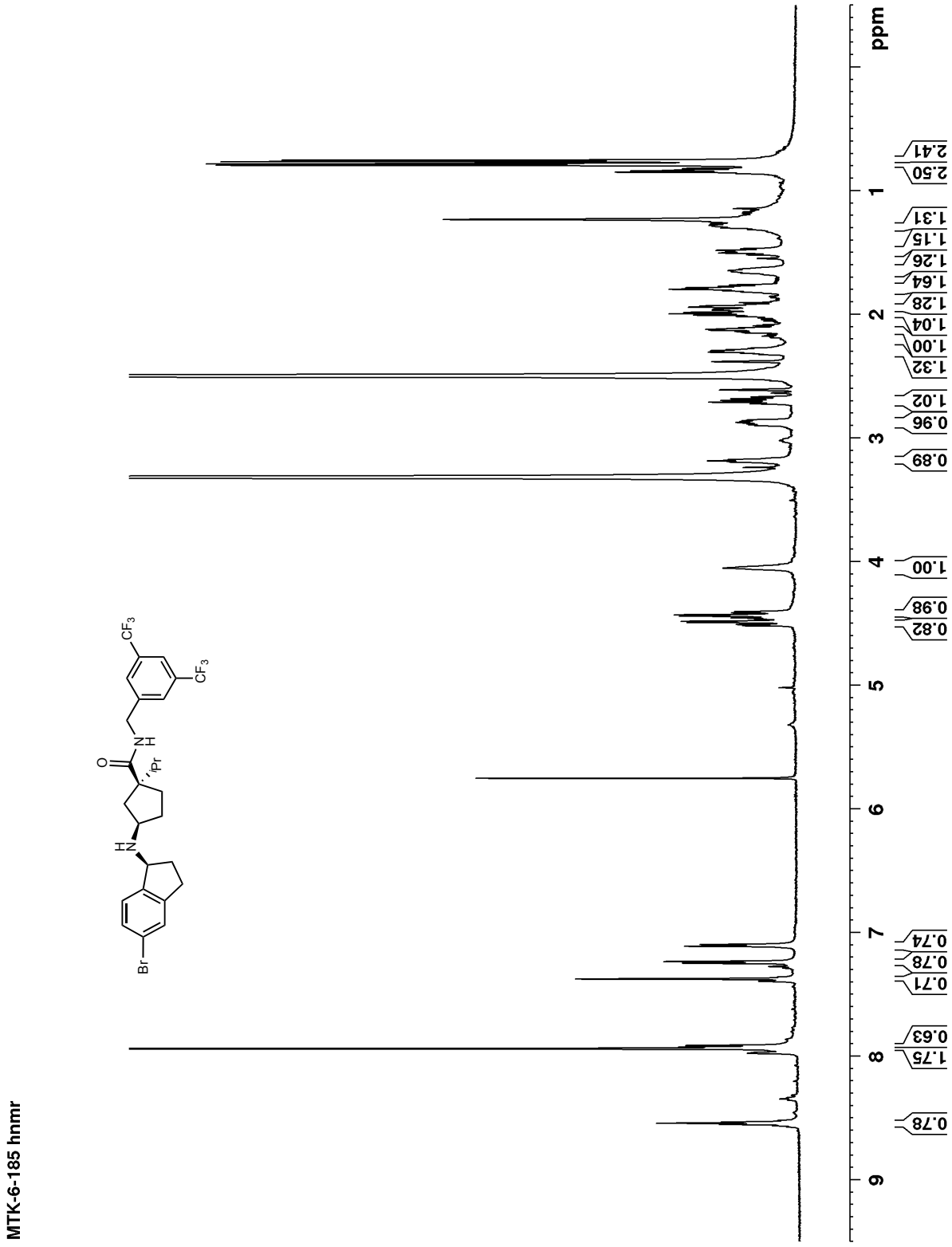

Figure B 97: ^{13}C NMR (125 MHz, DMSO-*d*6) of *epi*-**148**

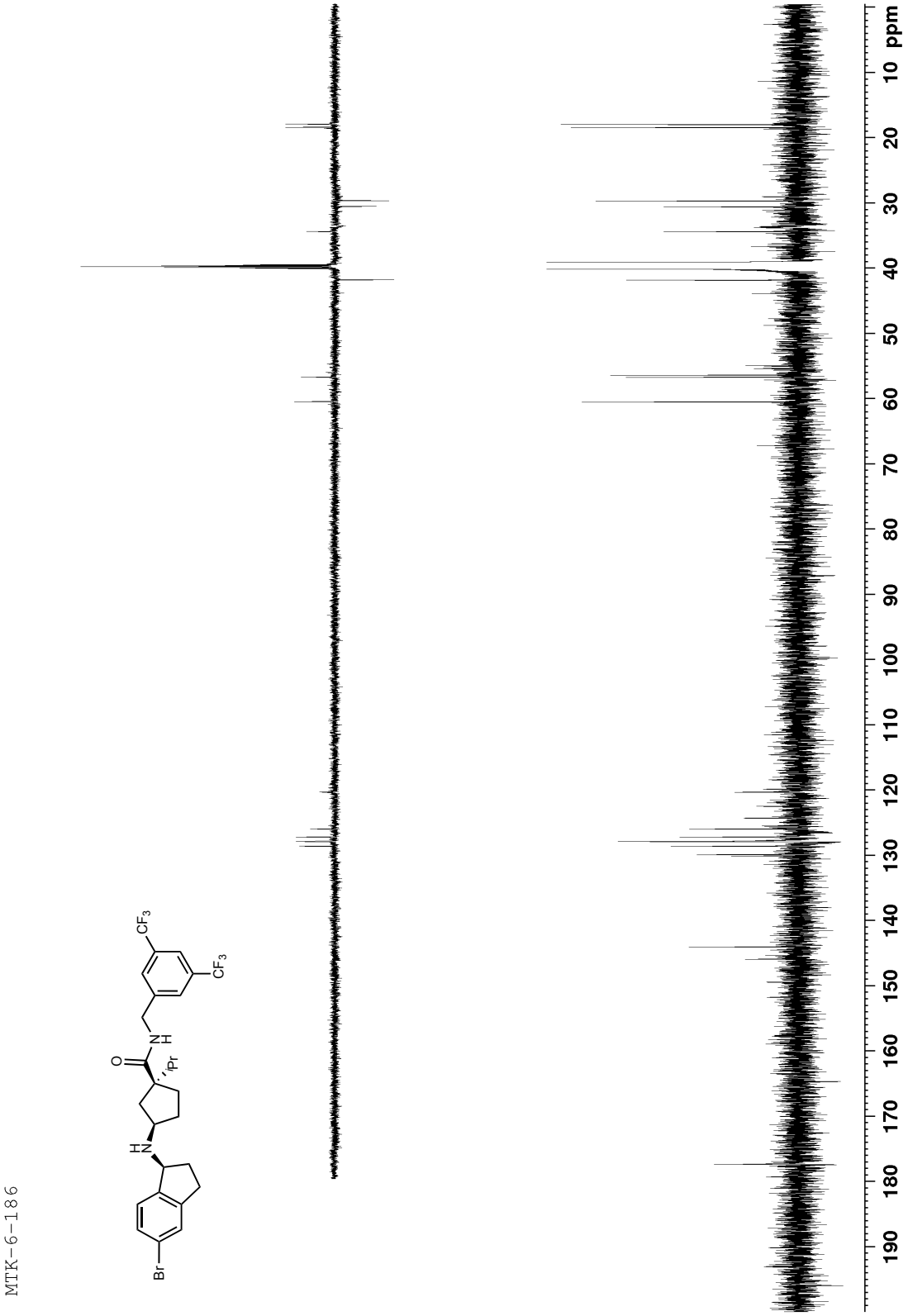

Figure B 98: 1D selective ROESY (600 MHz, DMSO-*d*6) of *epi*-**148**

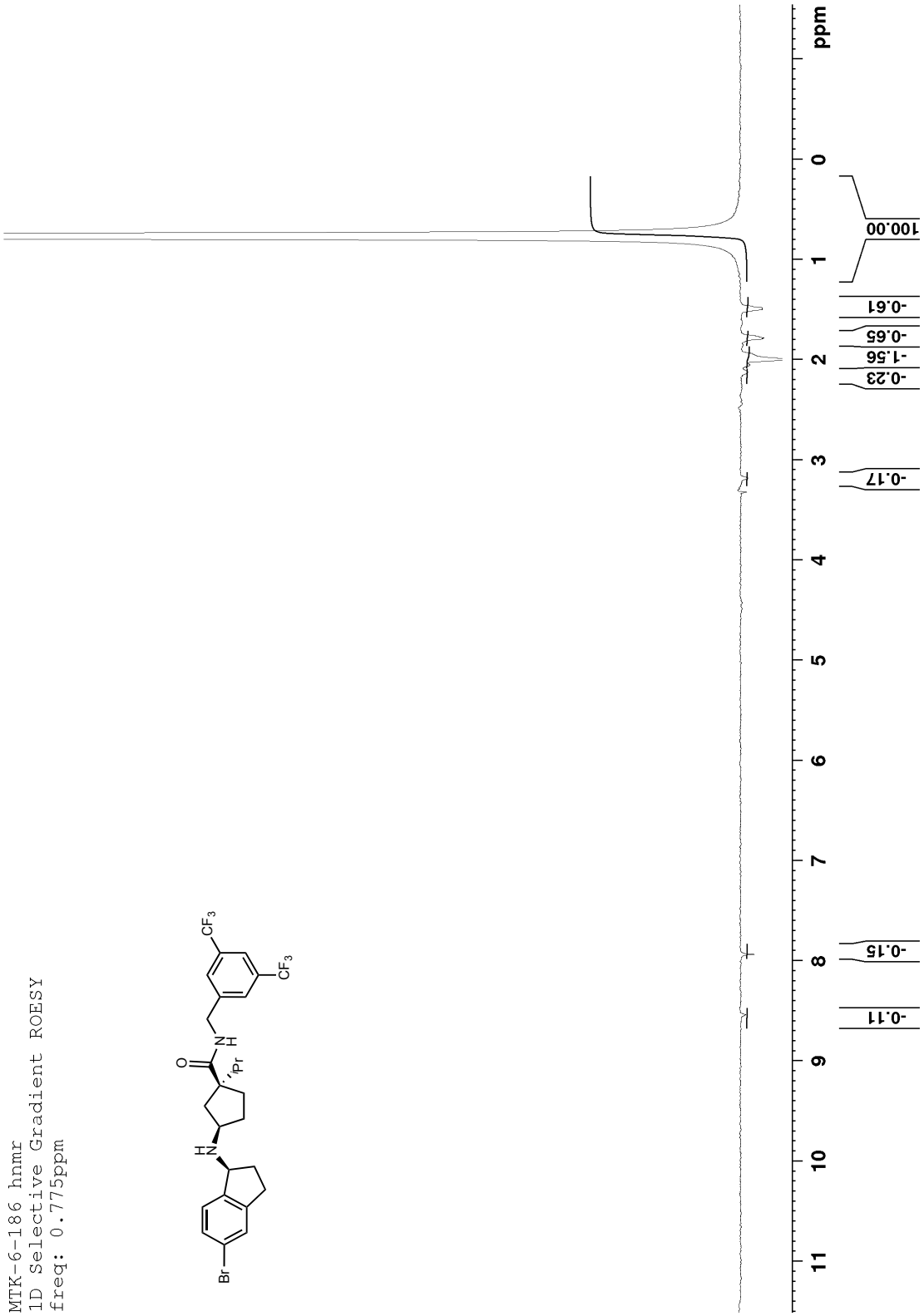

Figure B 99: 1D selective ROESY (600 MHz, DMSO-*d*6) of *epi*-**148**

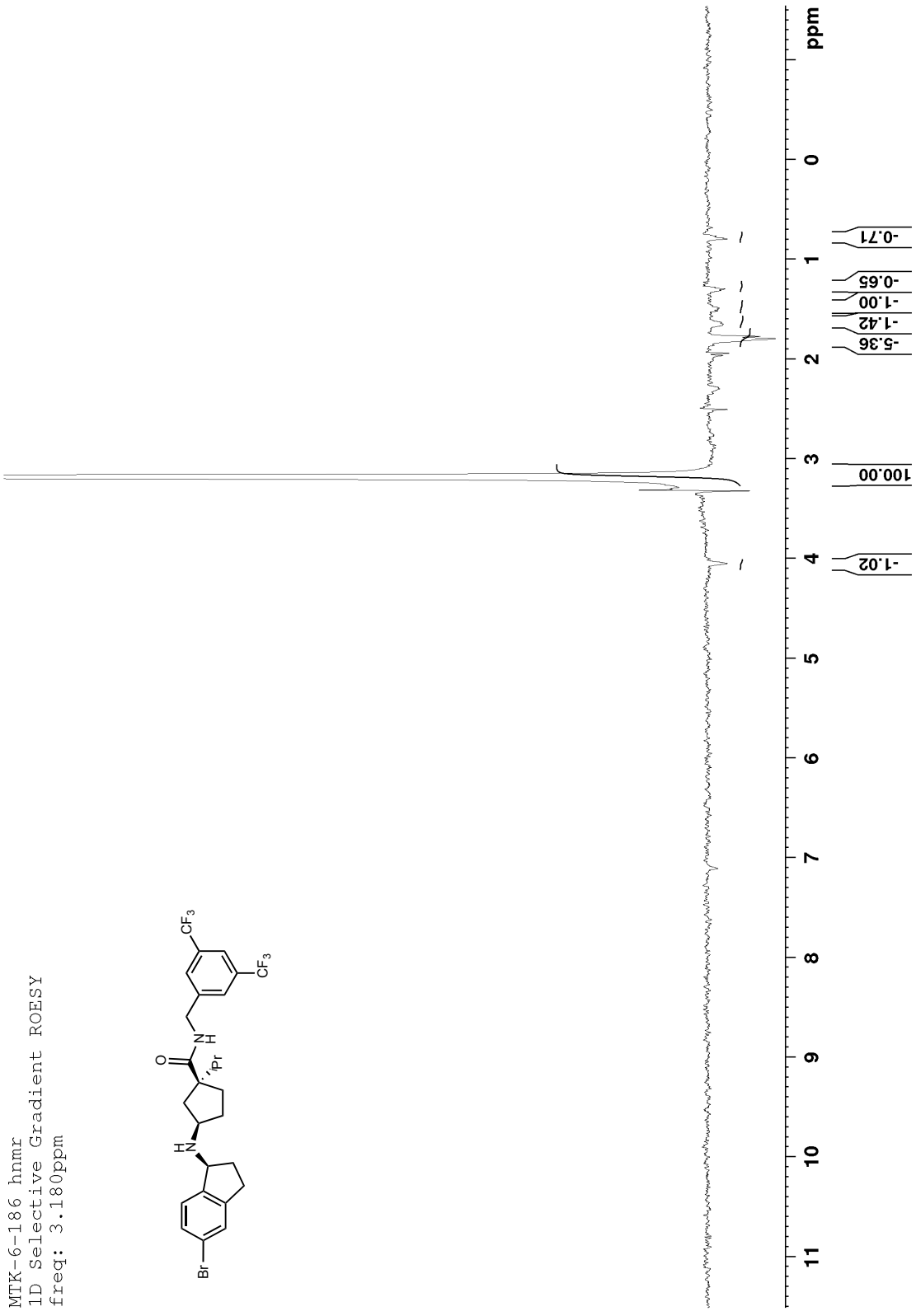

Figure B 100: ^{1}H NMR (400 MHz, $CDCl_3$) of **167**

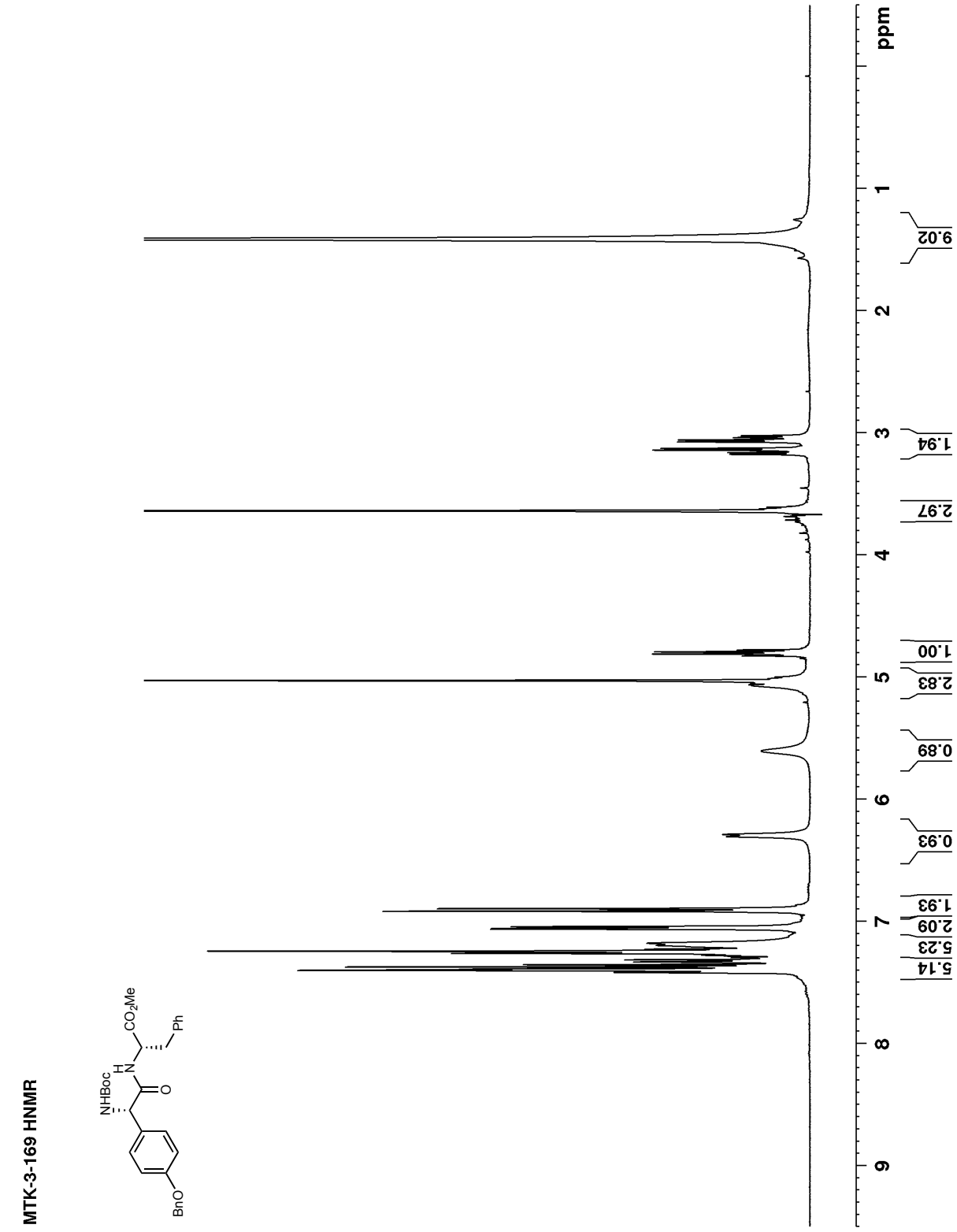

Figure B 101: ^{13}C NMR (100 MHz, $CDCl_3$) of **167**

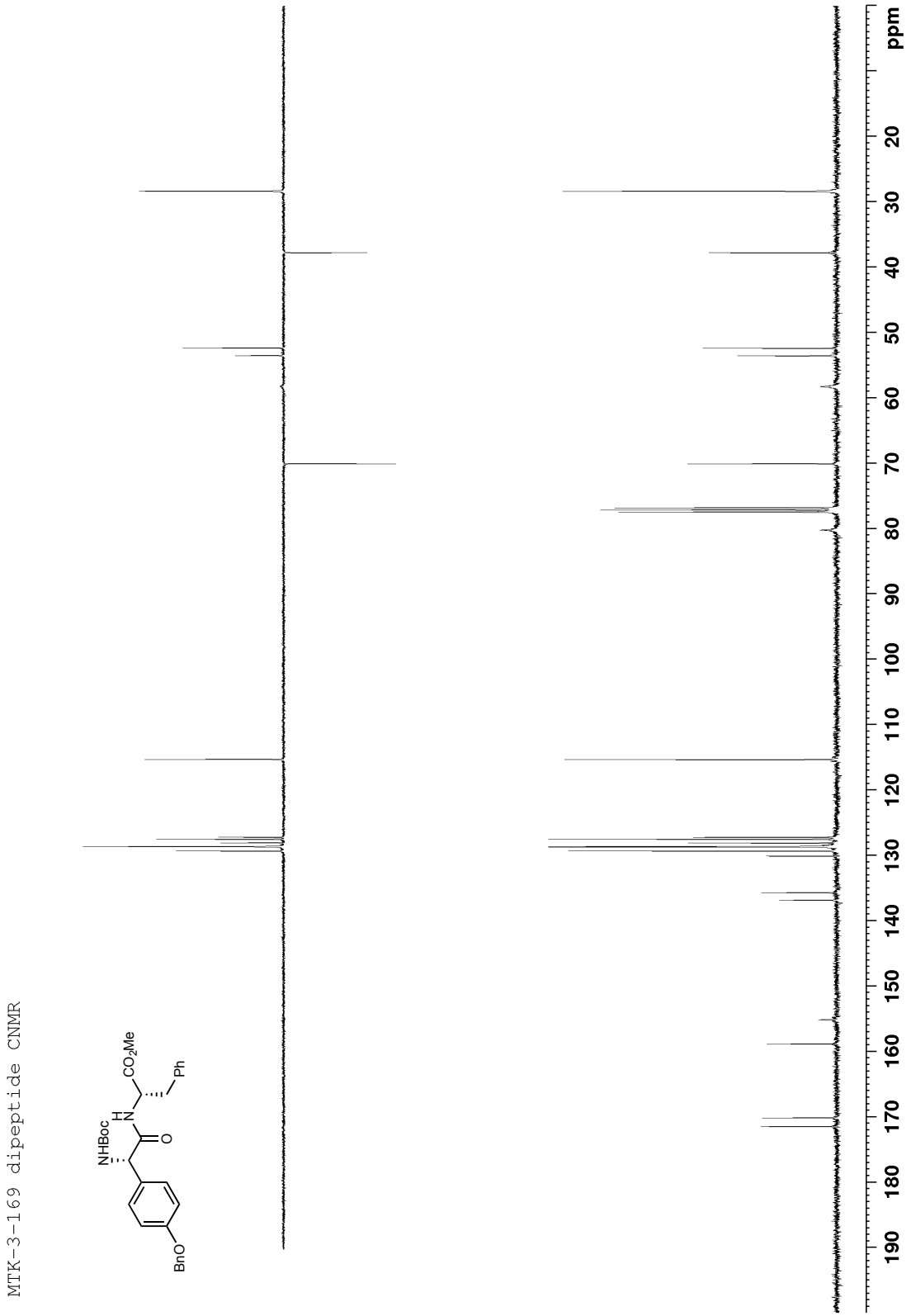

Figure B 102: ^{1}H NMR (400 MHz, $CDCl_3$) of **169**

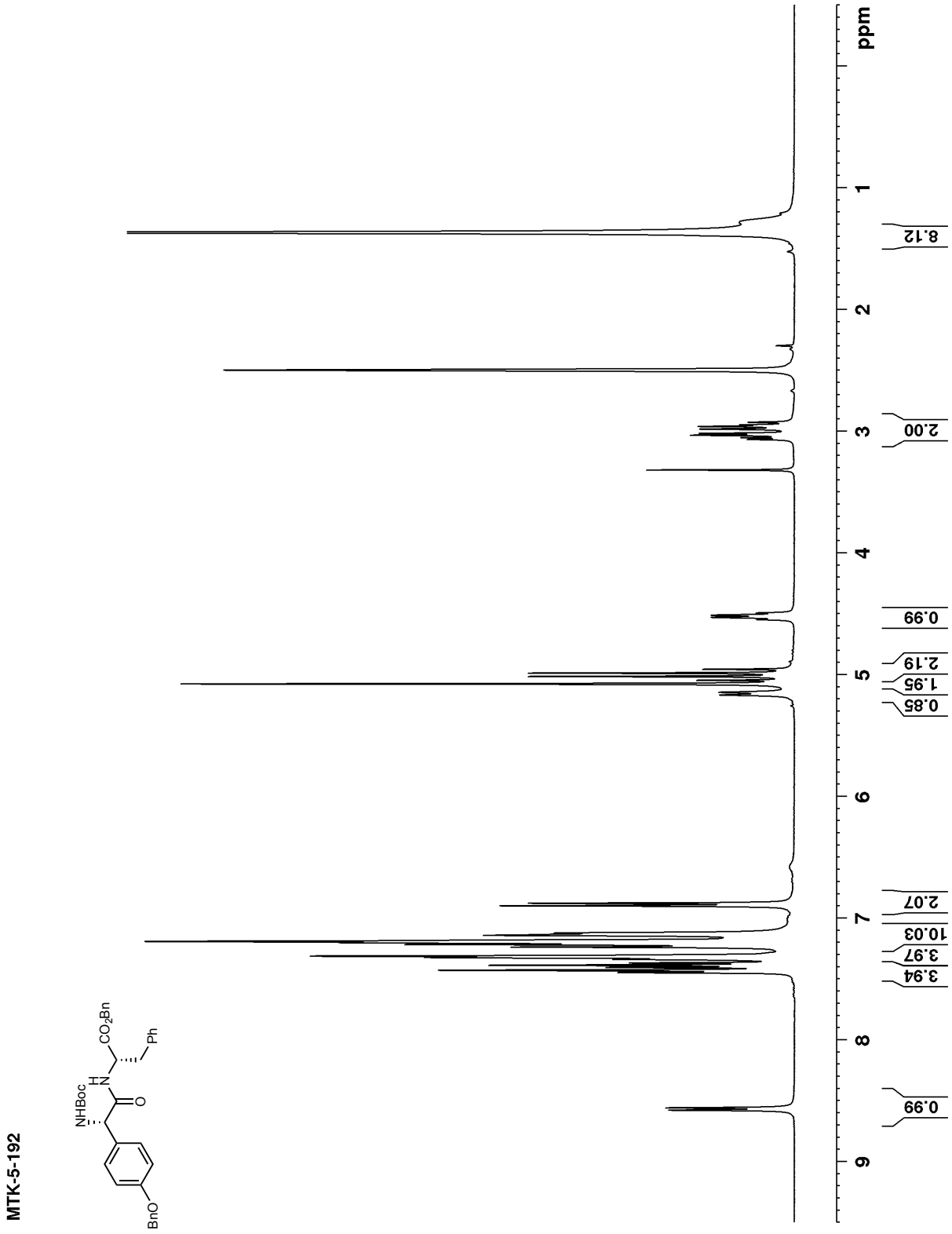

Figure B 103: ^{13}C NMR (125 MHz, $CDCl_3$) of **169**

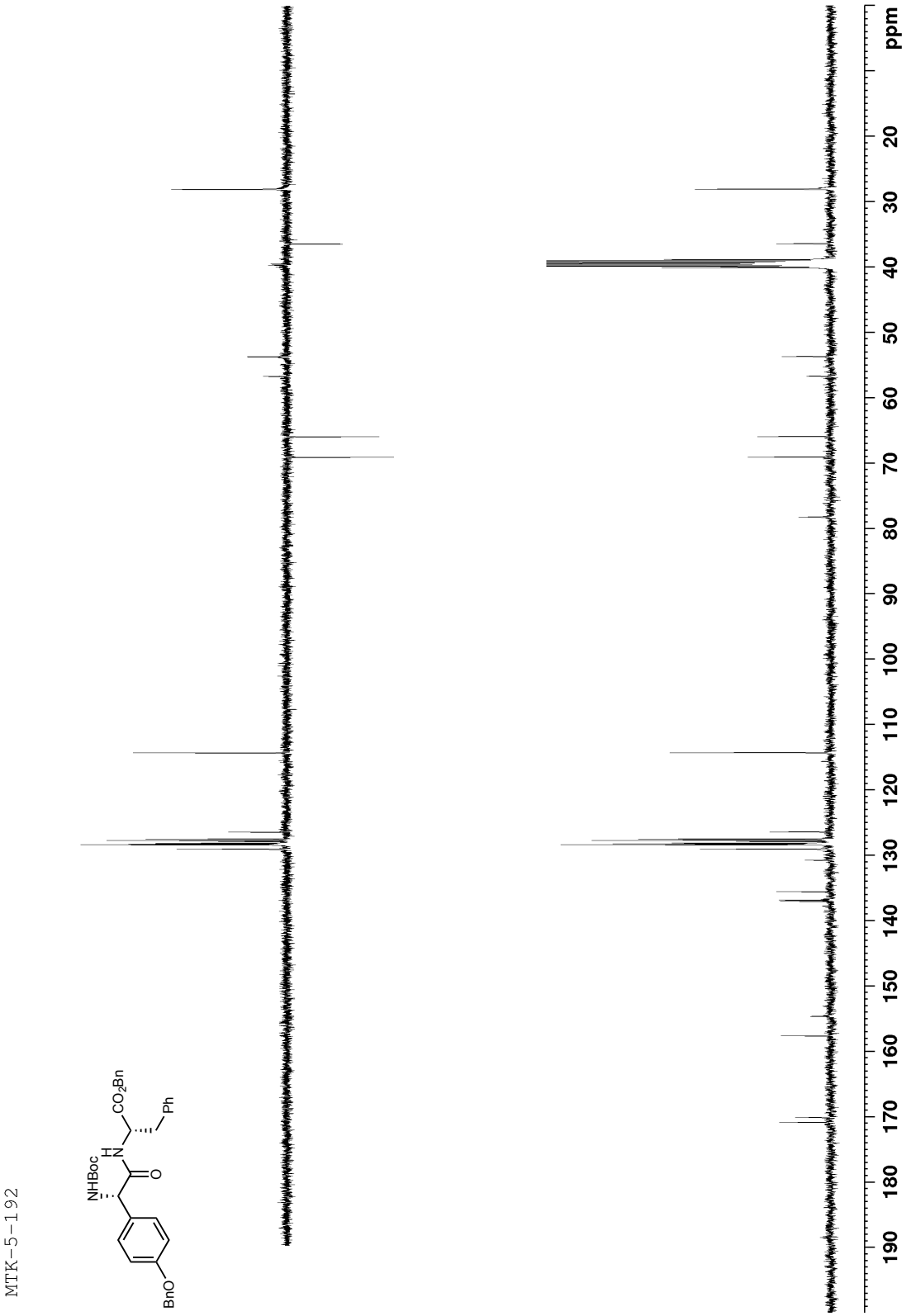

C HPLC traces

Figure C 1: HPLC trace of **109a**

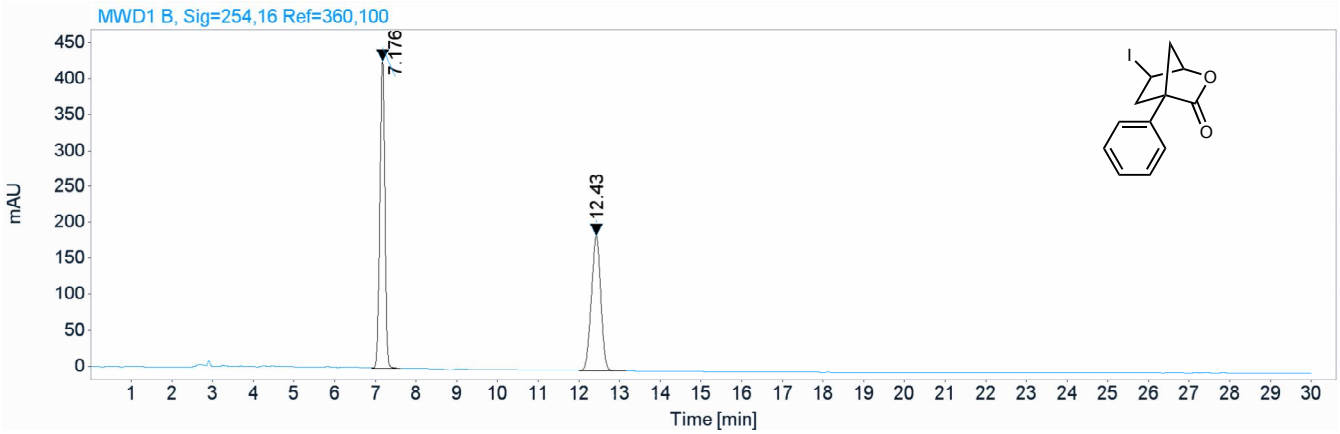

Signal: MWD1 B, Sig=254,16 Ref=360,100

RT [min]	Type	Width [min]	Area	Height	Area%	Name
7.176	VV	0.1327	3625.7966	428.5378	54.5180	
12.430	VB	0.2453	3024.8416	188.3916	45.4820	
		Sum	6650.6382			

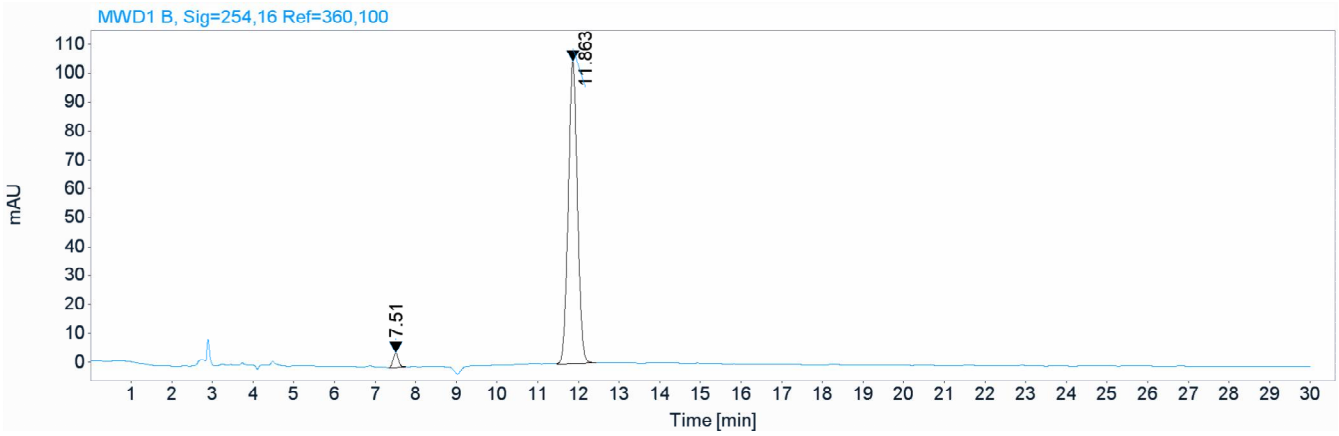

Signal: MWD1 B, Sig=254,16 Ref=360,100

RT [min]	Type	Width [min]	Area	Height	Area%	Name
7.510	BB	0.1384	43.8737	4.9008	2.6122	
11.863	BB	0.2361	1635.6903	104.7975	97.3878	
		Sum	1679.5640			

Figure C 2: HPLC trace of **109b**

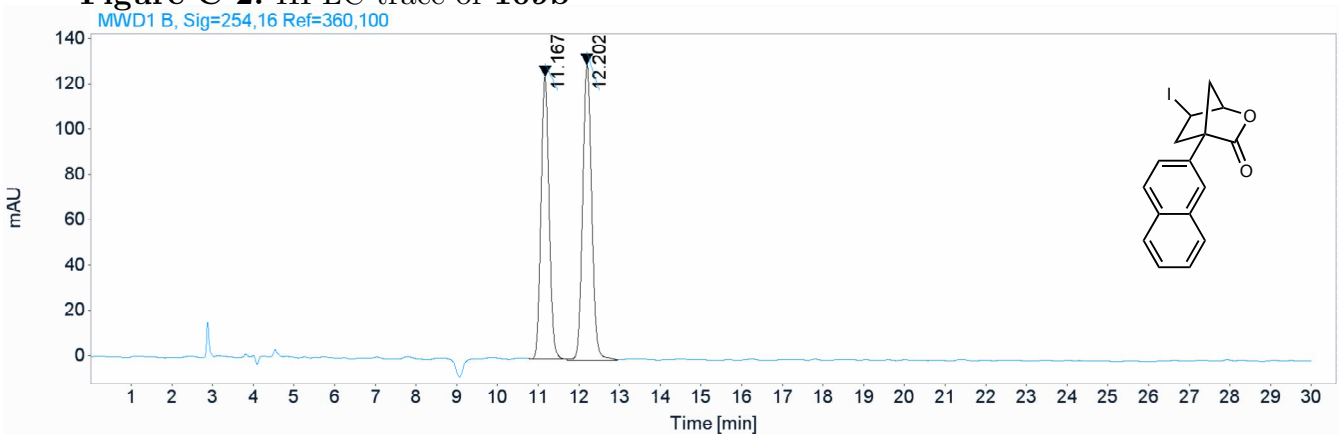

Signal: MWD1 B, Sig=254,16 Ref=360,100

RT [min]	Type	Width [min]	Area	Height	Area%	Name
11.167	MM	0.2303	1724.1740	124.7827	45.8646	
12.202	MM	0.2593	2035.0994	130.7970	54.1354	
		Sum	3759.2733			

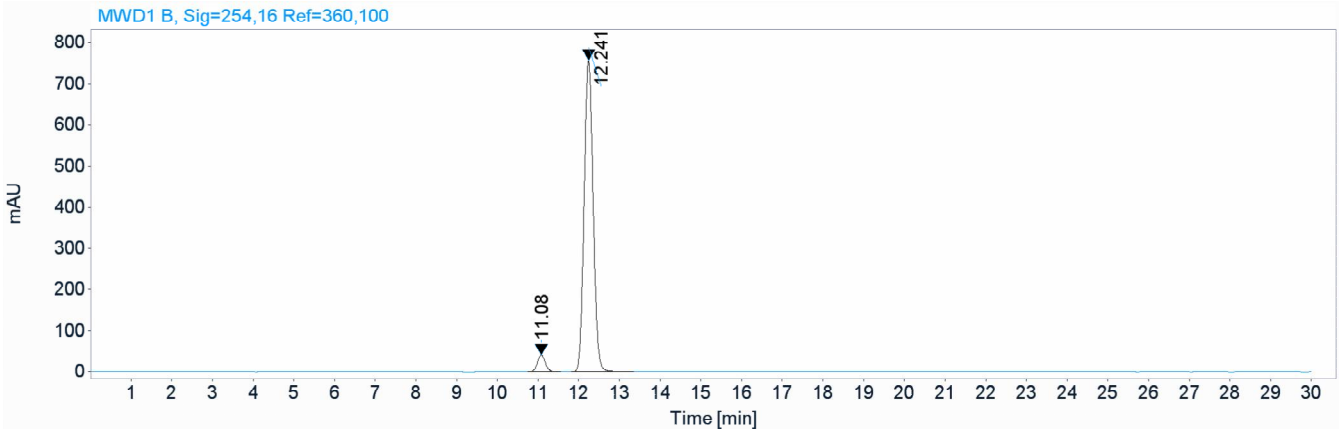

Signal: MWD1 B, Sig=254,16 Ref=360,100

RT [min]	Type	Width [min]	Area	Height	Area%	Name
11.080	BB	0.2134	573.3398	41.9578	4.6814	
12.241	BB	0.2418	11673.7402	757.5051	95.3186	
		Sum	12247.0801			

Figure C 3: HPLC trace of **109c**

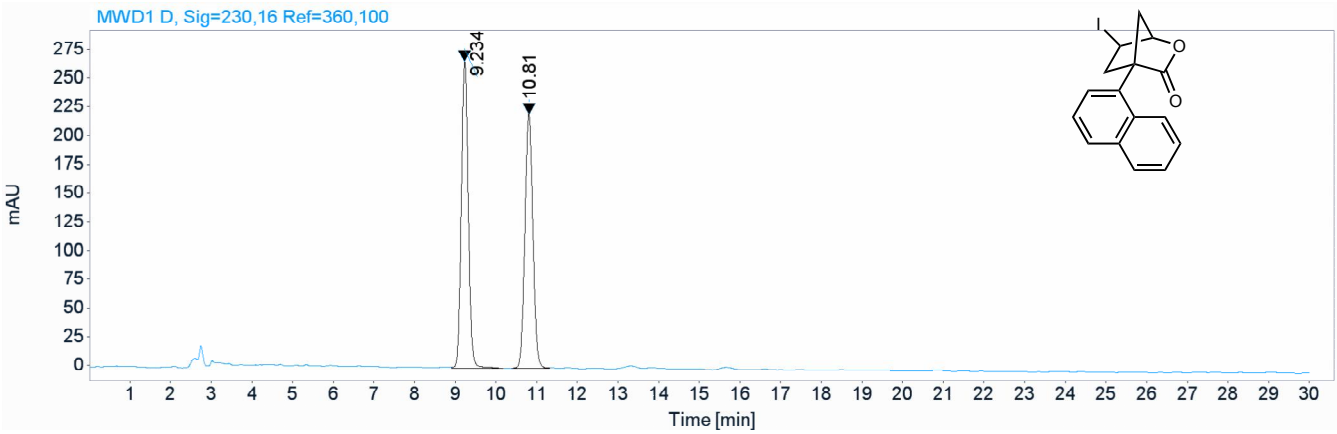

Signal: MWD1 D, Sig=230,16 Ref=360,100

RT [min]	Type	Width [min]	Area	Height	Area%	Name
9.234	BB	0.1850	3182.3850	267.1710	51.3730	
10.810	BB	0.2130	3012.2837	220.9678	48.6270	
		Sum	6194.6687			

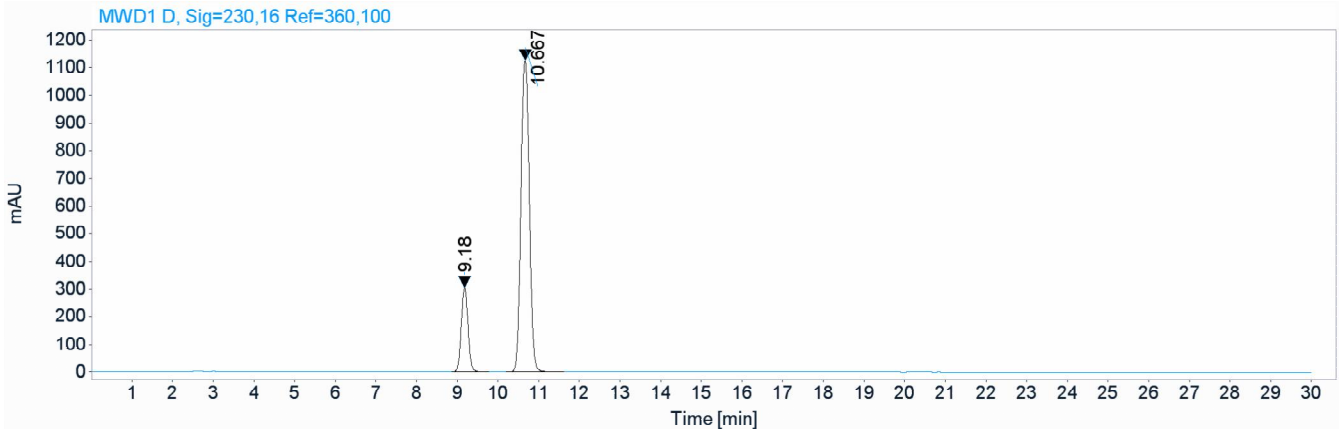

Signal: MWD1 D, Sig=230,16 Ref=360,100

RT [min]	Type	Width [min]	Area	Height	Area%	Name
9.180	MM	0.1920	3534.2861	306.7835	17.9740	
10.667	MM	0.2383	16128.9902	1127.9482	82.0260	
		Sum	19663.2764			

Figure C 4: HPLC trace of **109d**

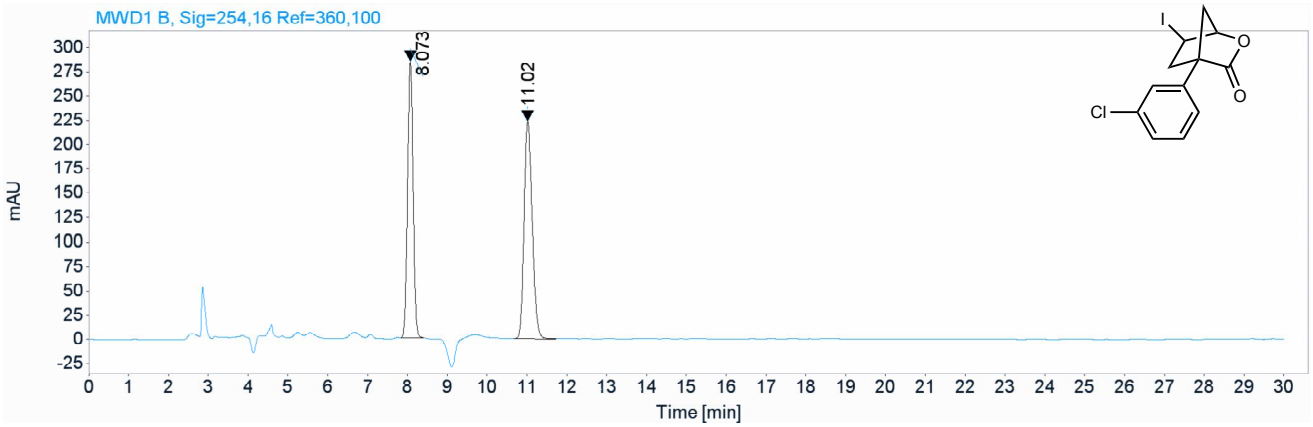

Signal: MWD1 B, Sig=254,16 Ref=360,100

RT [min]	Type	Width [min]	Area	Height	Area%	Name
8.073	MM	0.1613	2758.0833	285.0321	46.5111	
11.020	MM	0.2361	3171.8628	223.9151	53.4889	
		Sum	5929.9460			

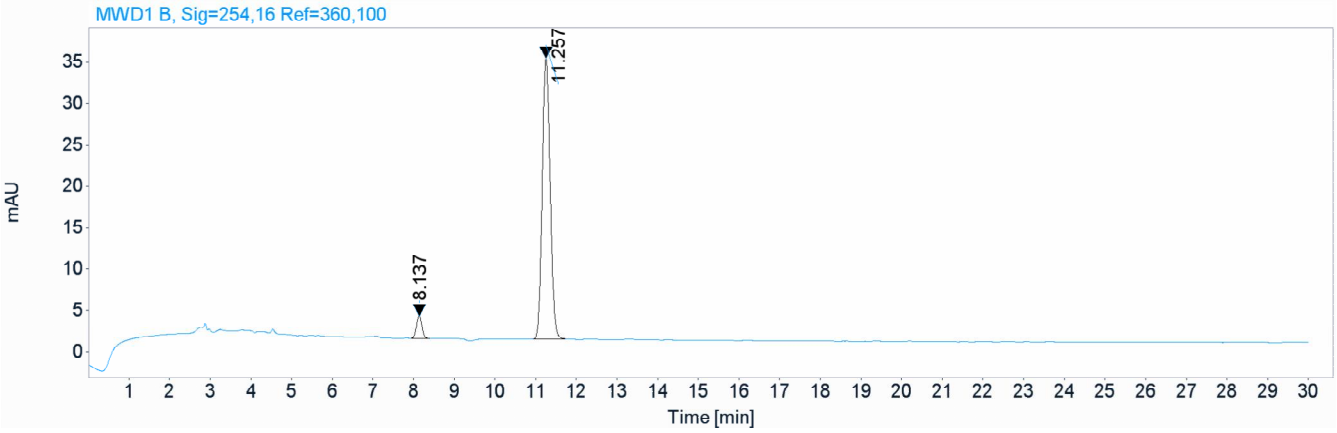

Signal: MWD1 B, Sig=254,16 Ref=360,100

RT [min]	Type	Width [min]	Area	Height	Area%	Name
8.137	BB	0.1464	26.0882	2.7575	5.3571	
11.257	BB	0.2105	460.8923	33.9166	94.6429	
		Sum	486.9806			

Figure C 5: HPLC trace of **109e**

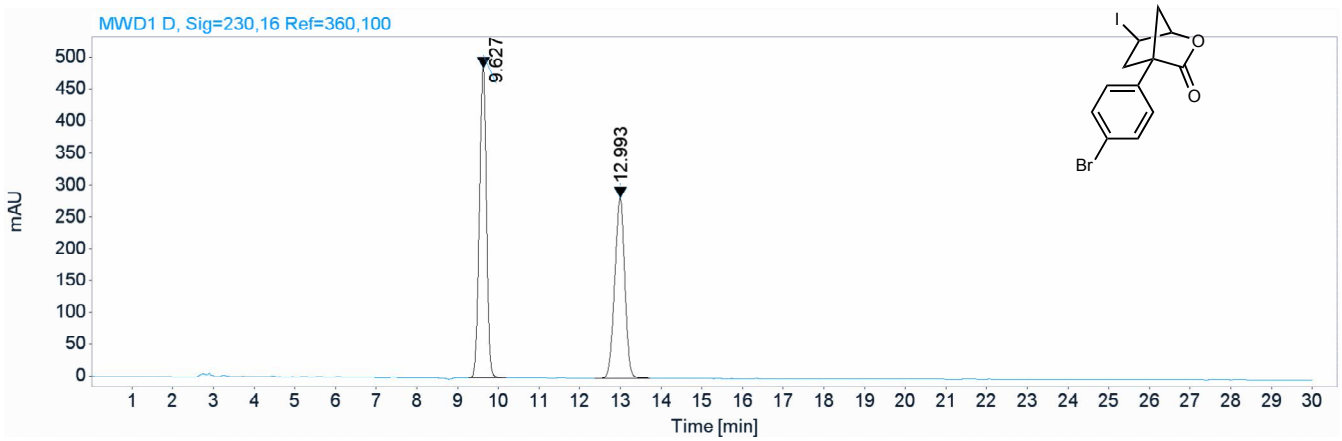

Signal: MWD1 D, Sig=230,16 Ref=360,100

RT [min]	Type	Width [min]	Area	Height	Area%	Name
9.627	MM	0.2011	5883.9355	487.6227	54.6965	
12.993	VB	0.2666	4873.4849	283.3961	45.3035	

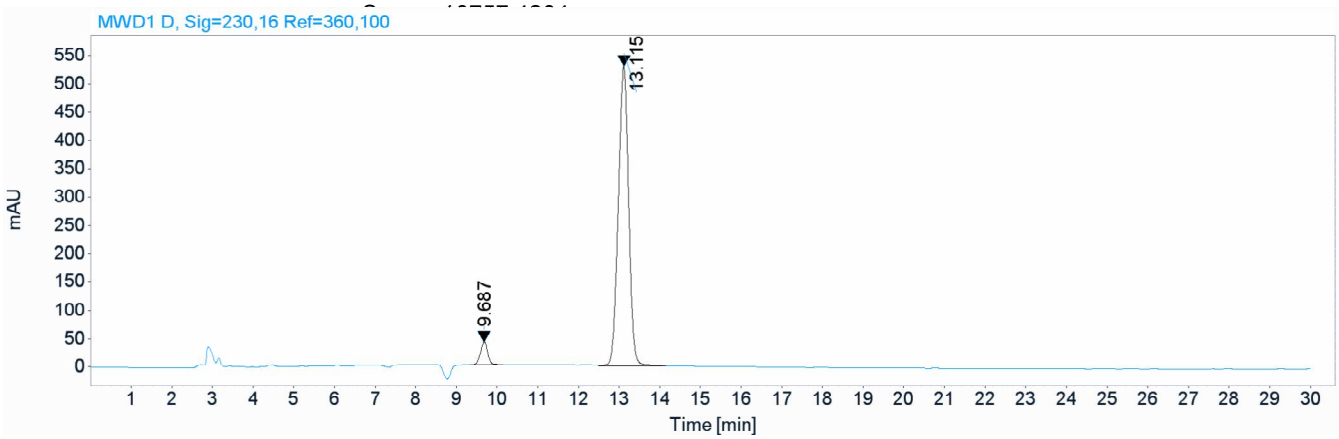

Signal: MWD1 D, Sig=230,16 Ref=360,100

RT [min]	Type	Width [min]	Area	Height	Area%	Name
9.687	MM	0.2061	508.6172	41.1241	5.1444	
13.115	MM	0.2952	9378.2842	529.5397	94.8556	
		Sum	9886.9014			

Figure C 6: HPLC trace of **109f**

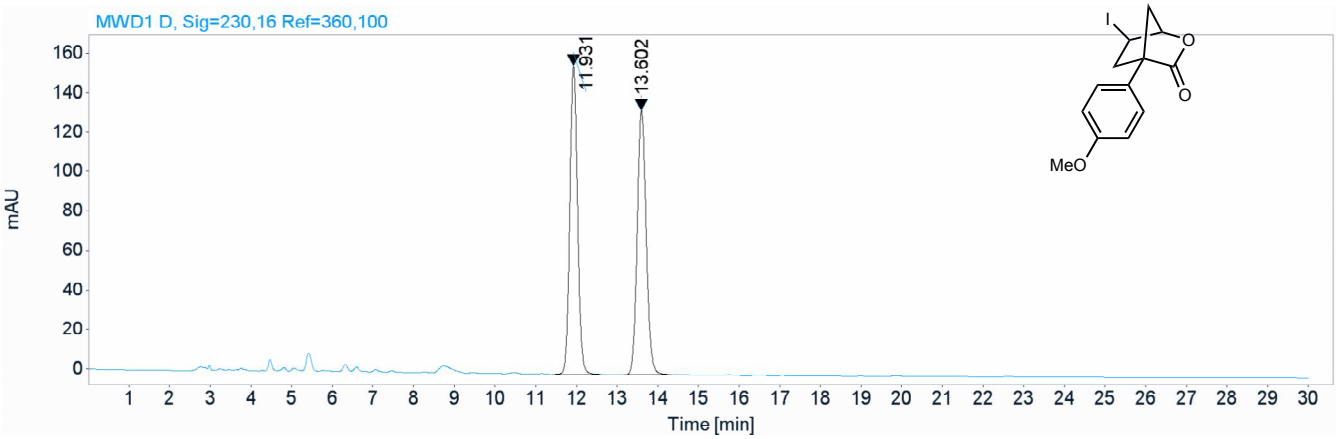

Signal: MWD1 D, Sig=230,16 Ref=360,100

RT [min]	Type	Width [min]	Area	Height	Area%	Name
11.931	VB	0.2038	2063.2578	156.5276	50.0449	
13.602	BB	0.2371	2059.5540	134.1978	49.9551	

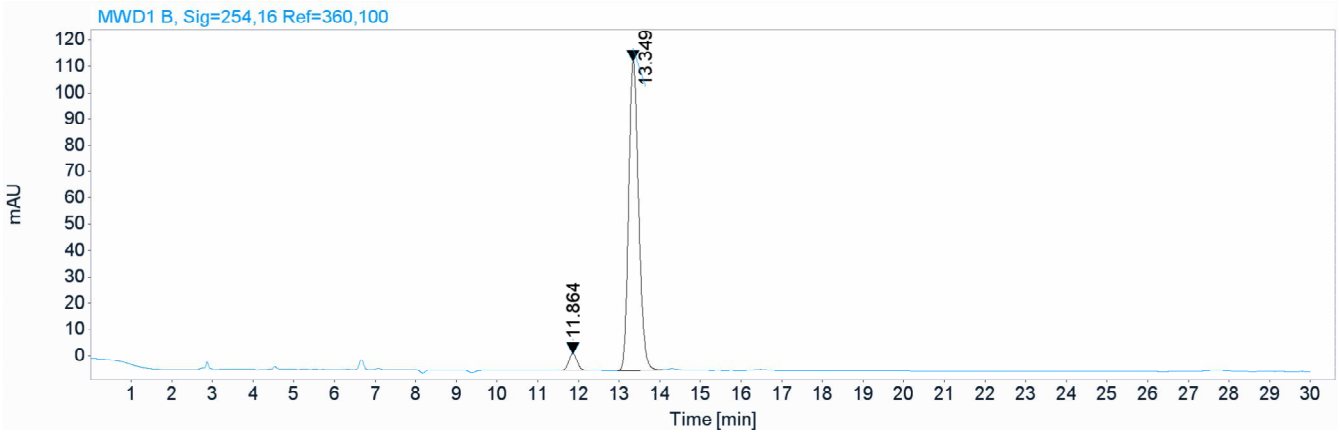

Signal: MWD1 B, Sig=254,16 Ref=360,100

RT [min]	Type	Width [min]	Area	Height	Area%	Name
11.864	BB	0.2232	93.3749	6.5168	4.4524	
13.349	BB	0.2643	2003.8063	117.8705	95.5476	
		Sum	2097.1812			

Figure C 7: HPLC trace of **109g**

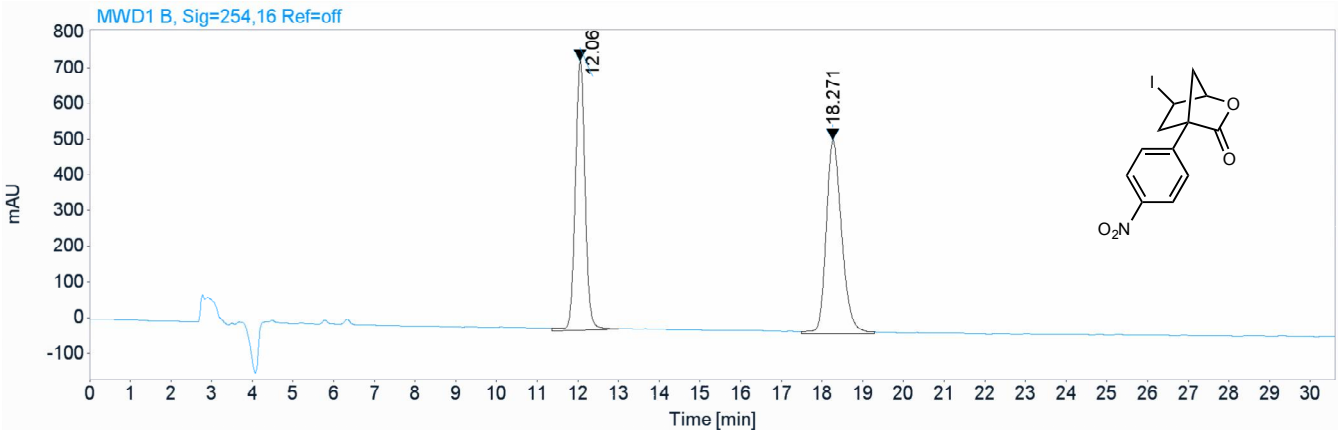

Signal: MWD1 B, Sig=254,16 Ref=off

RT [min]	Type	Width [min]	Area	Height	Area%	Name
12.060	MM	0.2810	12769.3418	757.4849	46.9234	
18.271	MM	0.4442	14443.8447	541.9376	53.0766	
		Sum	27213.1865			

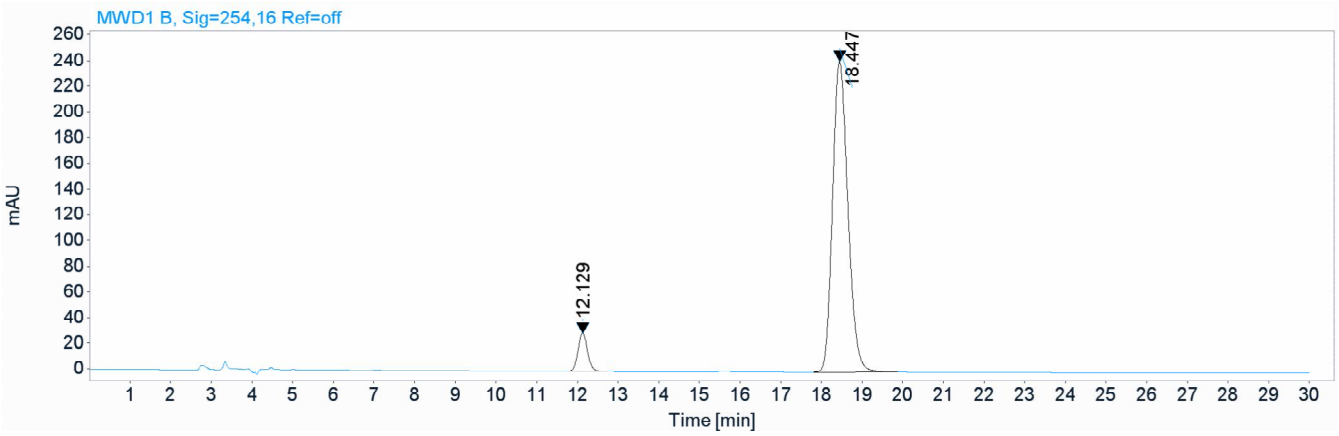

Signal: MWD1 B, Sig=254,16 Ref=off

RT [min]	Type	Width [min]	Area	Height	Area%	Name
12.129	BB	0.2553	487.4927	29.7299	7.1260	
18.447	BB	0.4067	6353.5059	241.7000	92.8740	
		Sum	6840.9986			

Figure C 8: HPLC trace of **109h**

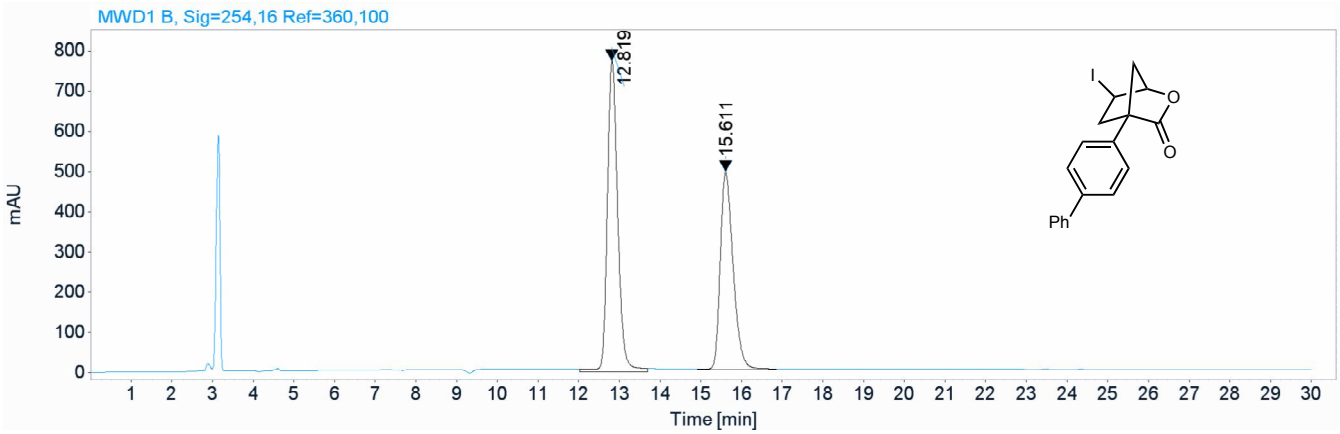

Signal: MWD1 B, Sig=254,16 Ref=360,100

RT [min]	Type	Width [min]	Area	Height	Area%	Name
12.819	MM	0.2986	13858.5752	773.4414	55.9036	
15.611	MM	0.3701	10931.5391	492.2958	44.0964	
		Sum	24790.1143			

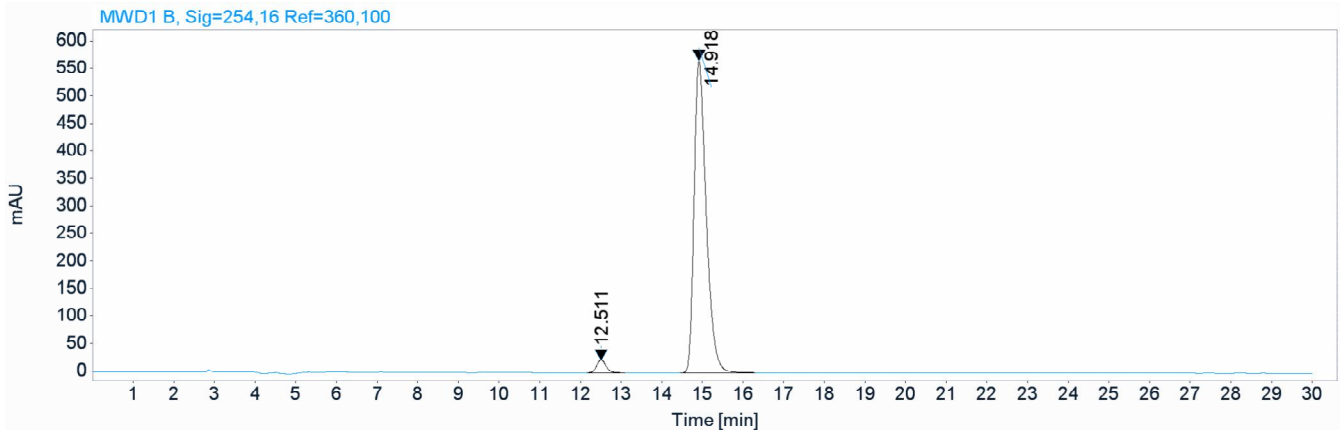

Signal: MWD1 B, Sig=254,16 Ref=360,100

RT [min]	Type	Width [min]	Area	Height	Area%	Name
12.511	BB	0.2526	361.7747	22.1391	2.9929	
14.918	BB	0.3133	11726.1328	566.9210	97.0071	
		Sum	12087.9075			

Figure C 9: HPLC trace of **109i**

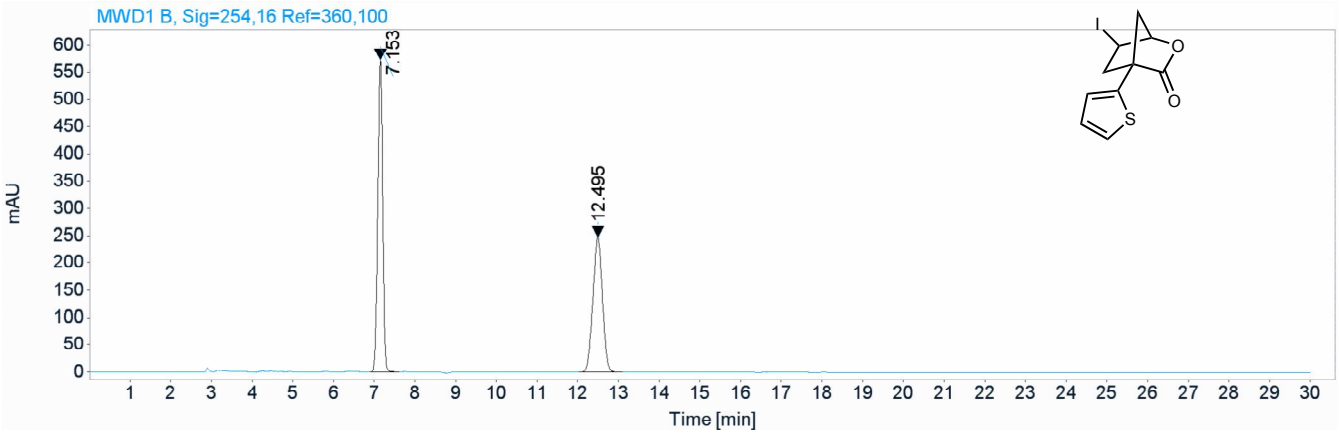

Signal: MWD1 B, Sig=254,16 Ref=360,100

RT [min]	Type	Width [min]	Area	Height	Area%	Name
7.153	VB	0.1325	4835.1460	572.4946	54.4409	
12.495	VB	0.2479	4046.3152	248.5837	45.5591	
		Sum	8881.4612			

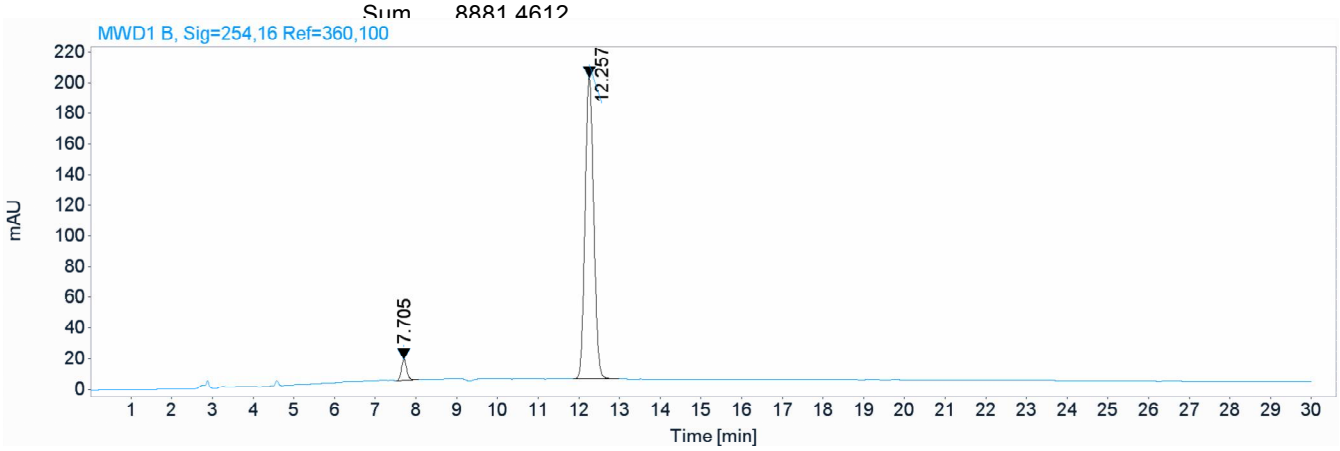

Signal: MWD1 B, Sig=254,16 Ref=360,100

RT [min]	Type	Width [min]	Area	Height	Area%	Name
7.705	VB	0.1394	126.4164	13.9976	4.1650	
12.257	BB	0.2324	2908.7844	196.8011	95.8350	
		Sum	3035.2008			

Figure C 10: HPLC trace of **109j**

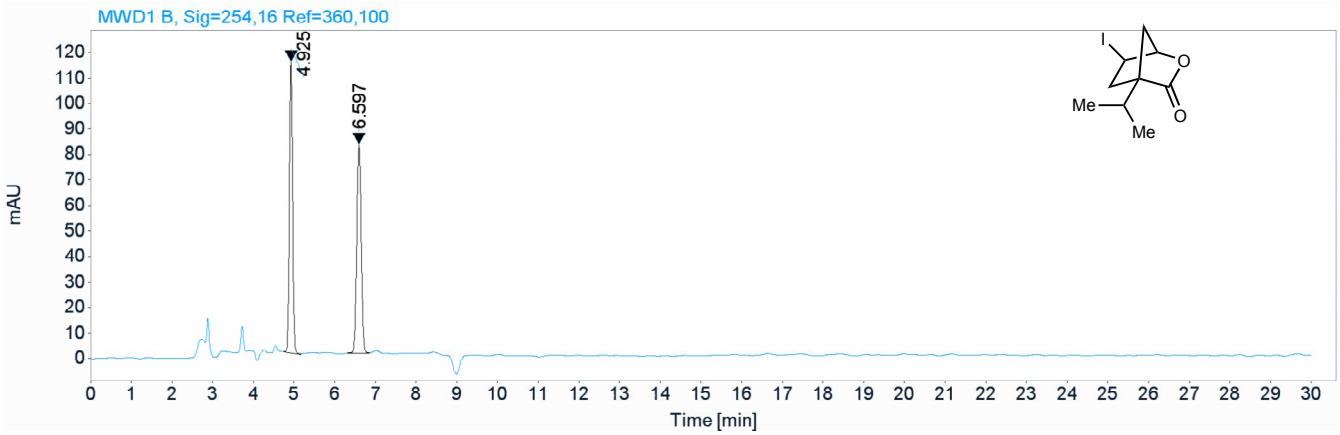

Signal: MWD1 B, Sig=254,16 Ref=360,100

RT [min]	Type	Width [min]	Area	Height	Area%	Name
4.925	MM	0.0899	619.3856	114.8271	49.8345	
6.597	MM	0.1262	623.5004	82.3372	50.1655	
		Sum	1242.8859			

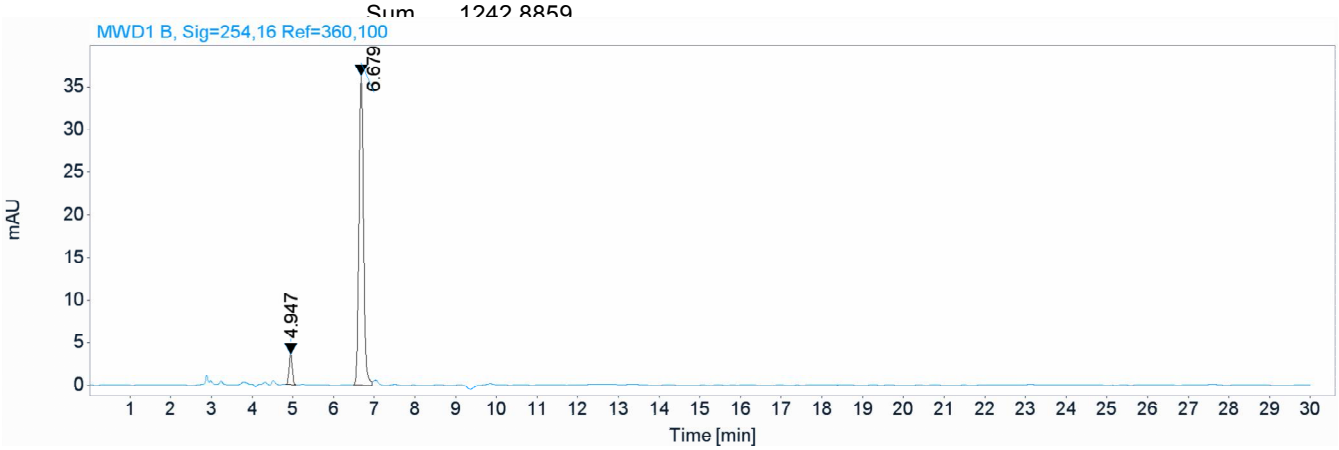

Signal: MWD1 B, Sig=254,16 Ref=360,100

RT [min]	Type	Width [min]	Area	Height	Area%	Name
4.947	MM	0.0885	19.0293	3.5837	6.3418	
6.679	BV	0.1206	281.0329	36.1773	93.6582	
		Sum	300.0623			

Figure C 11: HPLC trace of **109k**

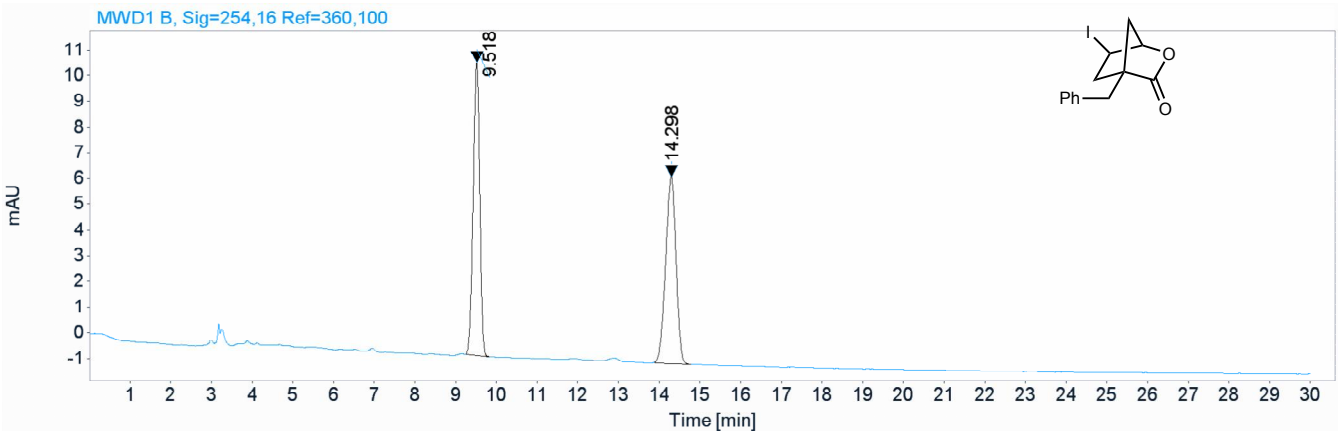

Signal: MWD1 B, Sig=254,16 Ref=360,100

RT [min]	Type	Width [min]	Area	Height	Area%	Name
9.518	BB	0.1751	128.1288	11.4057	49.7644	
14.298	BB	0.2755	129.3422	7.2710	50.2356	

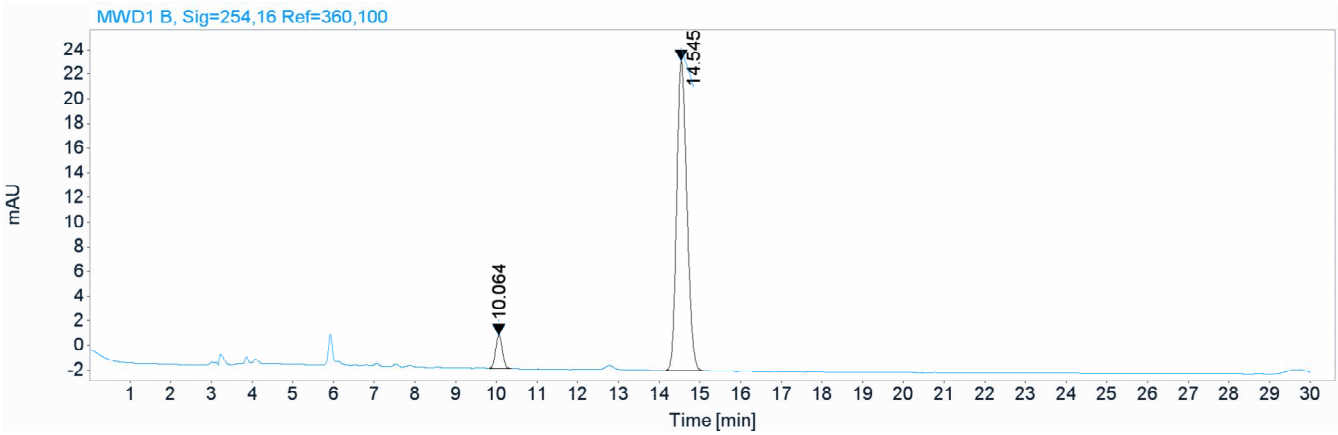

Signal: MWD1 B, Sig=254,16 Ref=360,100

RT [min]	Type	Width [min]	Area	Height	Area%	Name
10.064	BB	0.1747	30.2189	2.6970	6.4921	
14.545	BB	0.2704	435.2518	25.0936	93.5079	
		Sum	465.4707			

Figure C 12: HPLC trace of **109l**

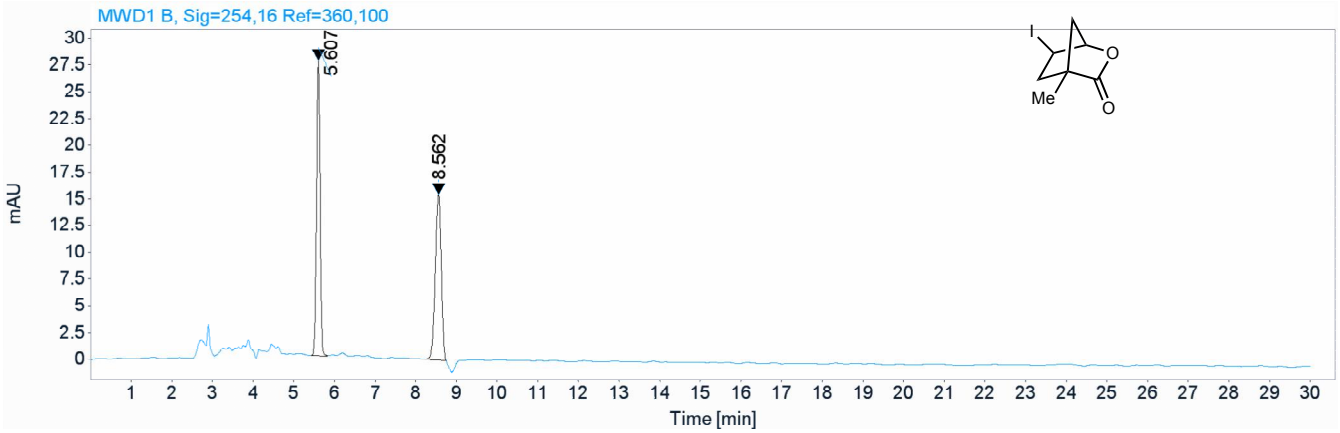

Signal: MWD1 B, Sig=254,16 Ref=360,100

RT [min]	Type	Width [min]	Area	Height	Area%	Name
5.607	BB	0.0952	168.9962	27.6781	51.5838	
8.562	MM	0.1706	158.6190	15.5002	48.4162	
		Sum	327.6152			

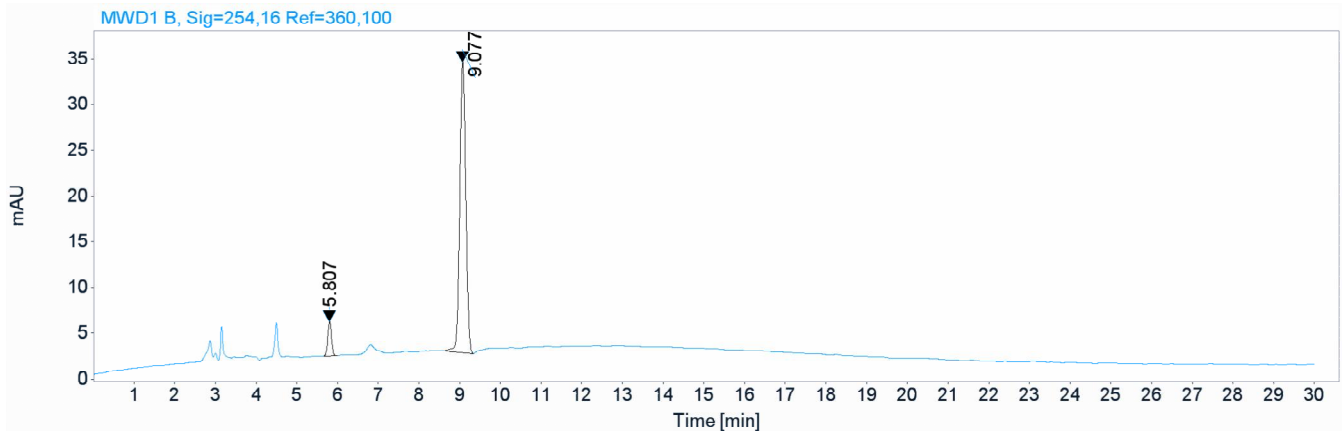

Signal: MWD1 B, Sig=254,16 Ref=360,100

RT [min]	Type	Width [min]	Area	Height	Area%	Name
5.807	BB	0.1000	23.7754	3.7470	6.7797	
9.077	BV	0.1600	326.9082	31.7891	93.2203	
		Sum	350.6836			

Figure C 13: HPLC trace of **109m**

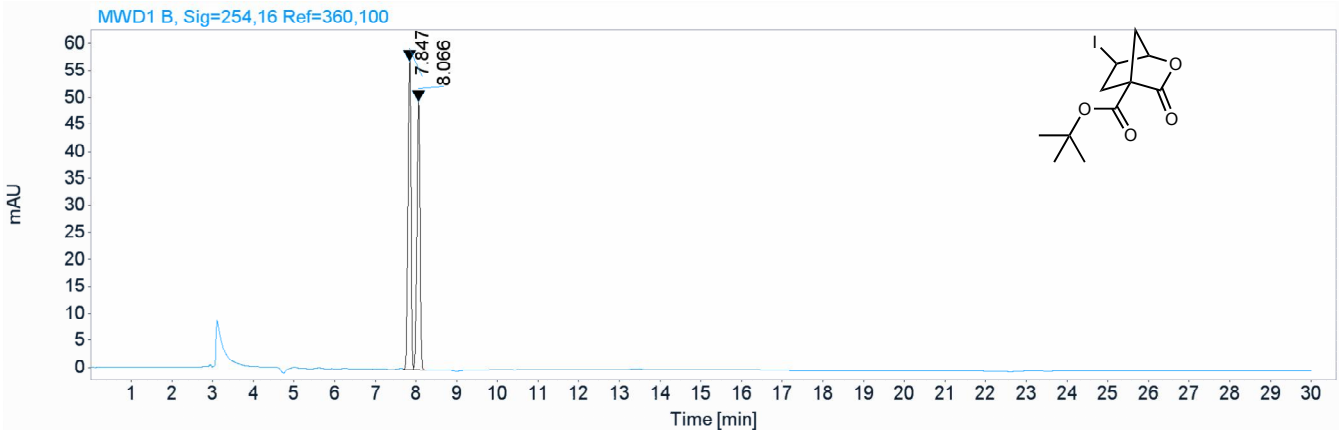

Signal: MWD1 B, Sig=254,16 Ref=360,100

RT [min]	Type	Width [min]	Area	Height	Area%	Name
7.847	VV	0.0855	302.3685	57.3134	53.0315	
8.066	VB	0.0844	267.7996	50.0367	46.9685	
		Sum	570.1681			

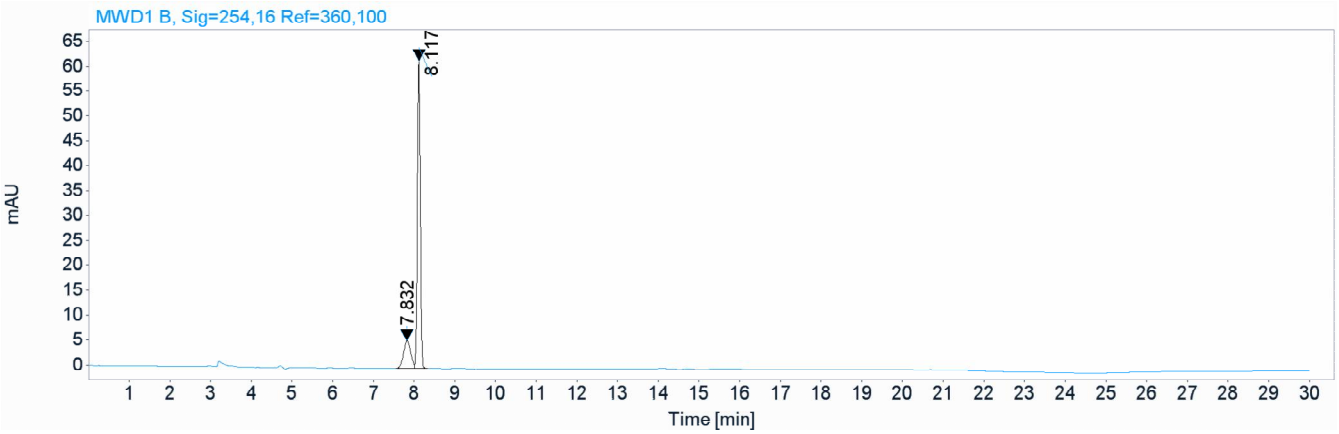

Signal: MWD1 B, Sig=254,16 Ref=360,100

RT [min]	Type	Width [min]	Area	Height	Area%	Name
7.832	BV	0.1876	67.5972	5.4923	17.9892	
8.117	VB	0.0781	308.1693	61.8659	82.0108	
		Sum	375.7665			

Figure C 14: HPLC trace of **109n**

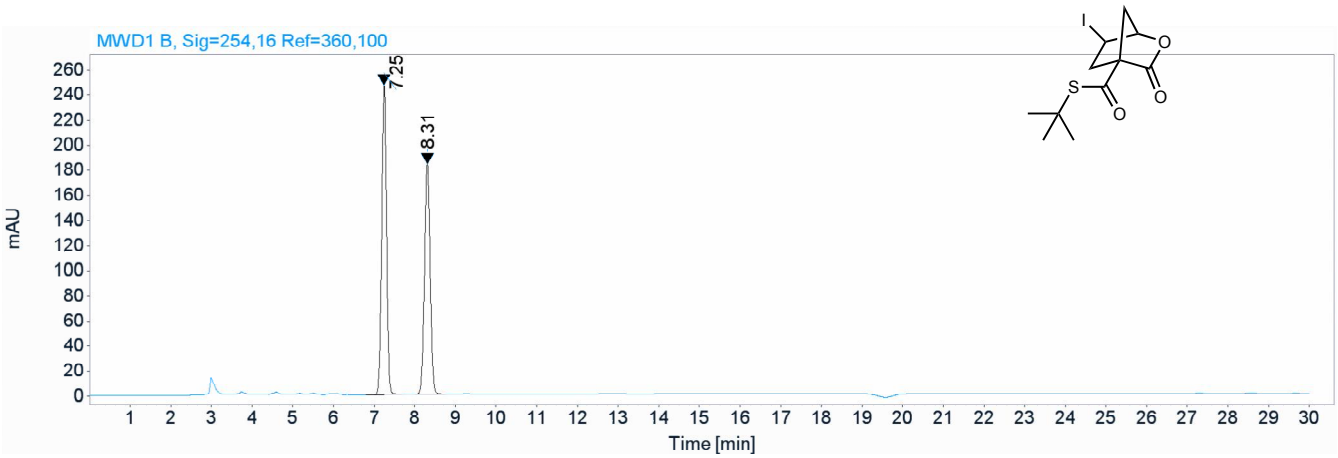

Signal: MWD1 B, Sig=254,16 Ref=360,100

RT [min]	Type	Width [min]	Area	Height	Area%	Name
7.250	BB	0.1287	2048.6560	247.1414	53.4241	
8.310	BB	0.1492	1786.0481	184.1522	46.5759	
		Sum	3834.7041			

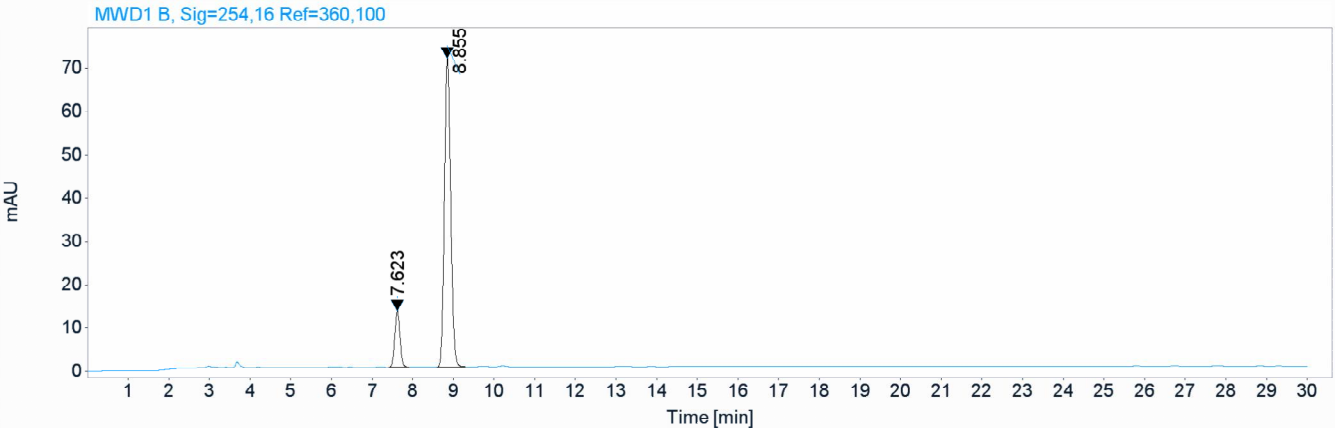

Signal: MWD1 B, Sig=254,16 Ref=360,100

RT [min]	Type	Width [min]	Area	Height	Area%	Name
7.623	BB	0.1383	115.4892	12.9238	13.1013	
8.855	BB	0.1673	766.0233	71.3417	86.8987	
		Sum	881.5125			

Figure C 15: HPLC trace of **137**

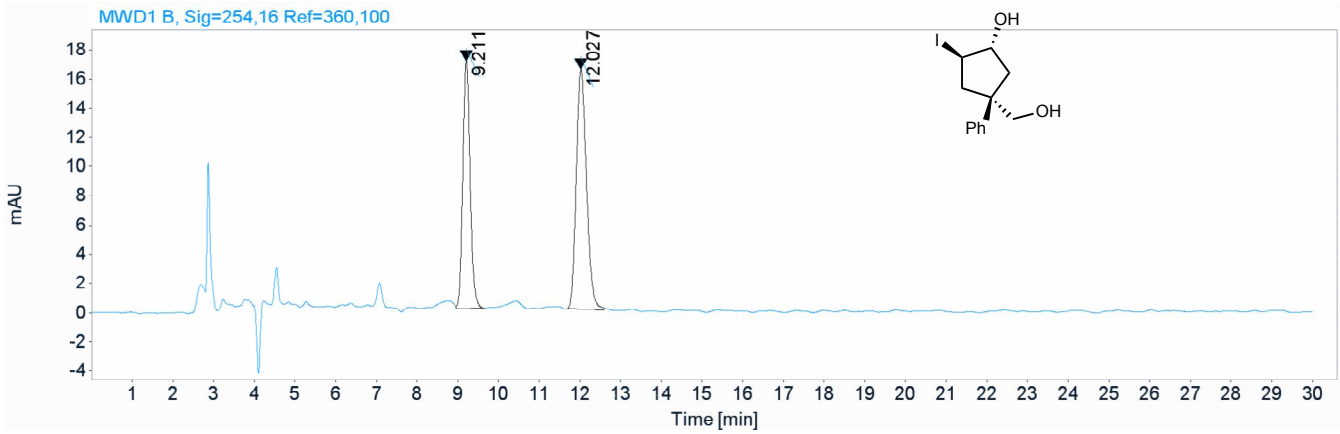

Signal: MWD1 B, Sig=254,16 Ref=360,100

RT [min]	Type	Width [min]	Area	Height	Area%	Name
9.211	VB	0.1953	210.6861	16.9173	42.4698	
12.027	BB	0.2714	285.3990	16.3683	57.5302	
		Sum	496.0850			

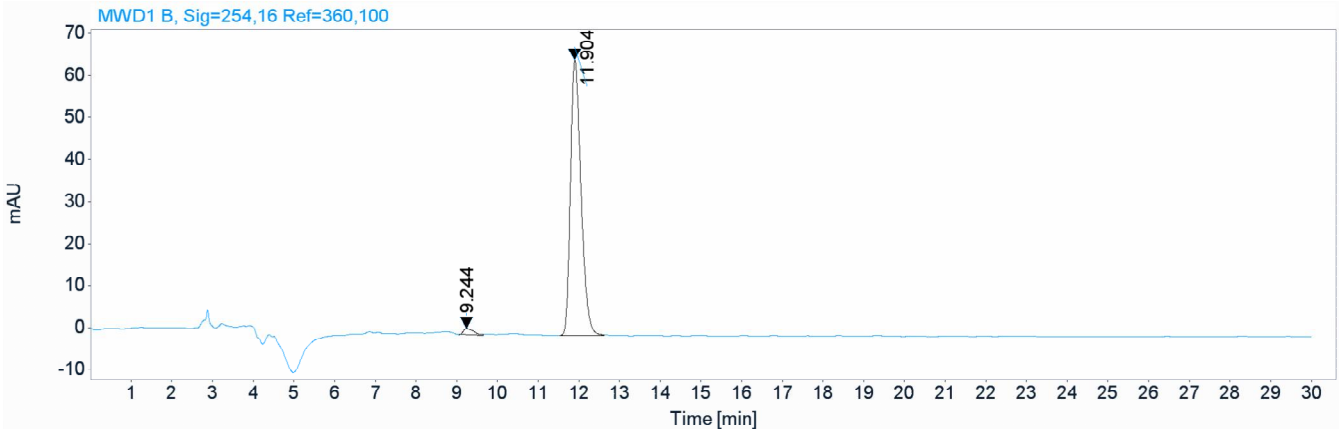

Signal: MWD1 B, Sig=254,16 Ref=360,100

RT [min]	Type	Width [min]	Area	Height	Area%	Name
9.244	MM	0.3058	27.2807	1.4869	2.2719	
11.904	BB	0.2756	1173.5099	65.3102	97.7281	
		Sum	1200.7906			

Figure C 16: HPLC trace of **138**

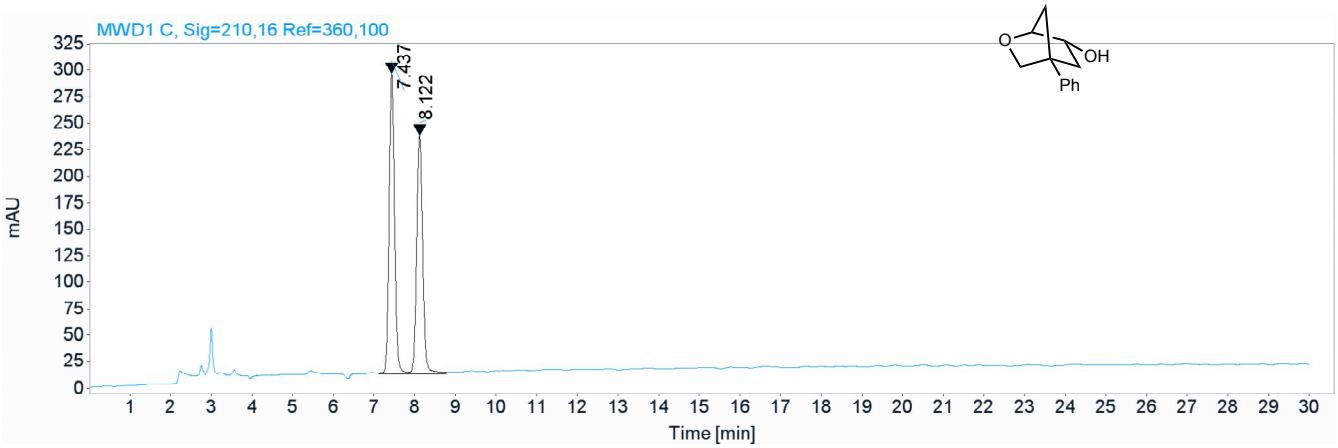

Signal: MWD1 C, Sig=210,16 Ref=360,100

RT [min]	Type	Width [min]	Area	Height	Area%	Name
7.437	MF	0.1558	2646.9331	283.1826	53.0807	
8.122	FM	0.1729	2339.6848	225.4895	46.9193	
		Sum	4986.6179			

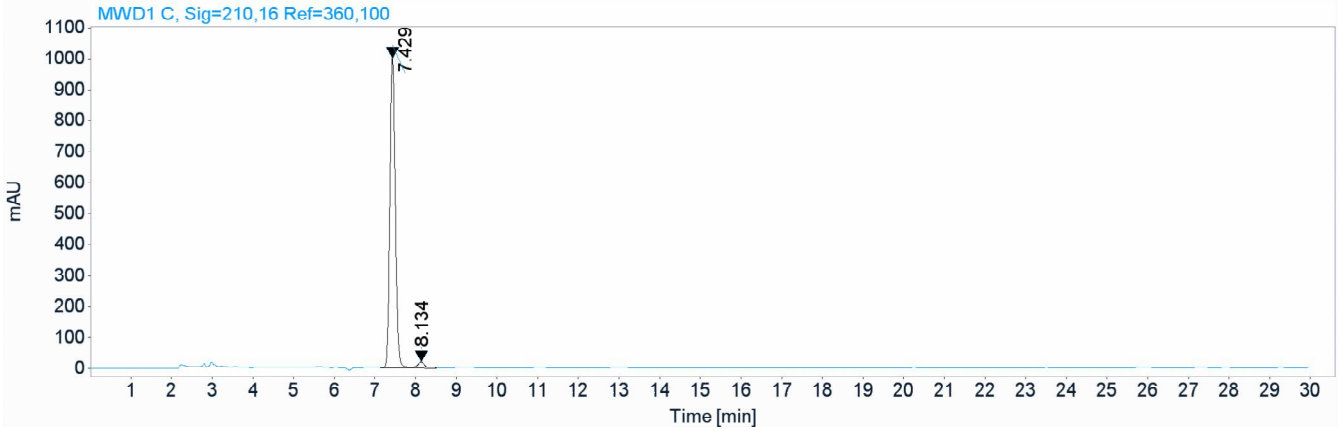

Signal: MWD1 C, Sig=210,16 Ref=360,100

RT [min]	Type	Width [min]	Area	Height	Area%	Name
7.429	MF	0.1552	9334.4229	1002.3060	97.2534	
8.134	FM	0.2139	263.6217	20.5368	2.7466	
		Sum	9598.0446			

Figure C 17: HPLC trace of **139**

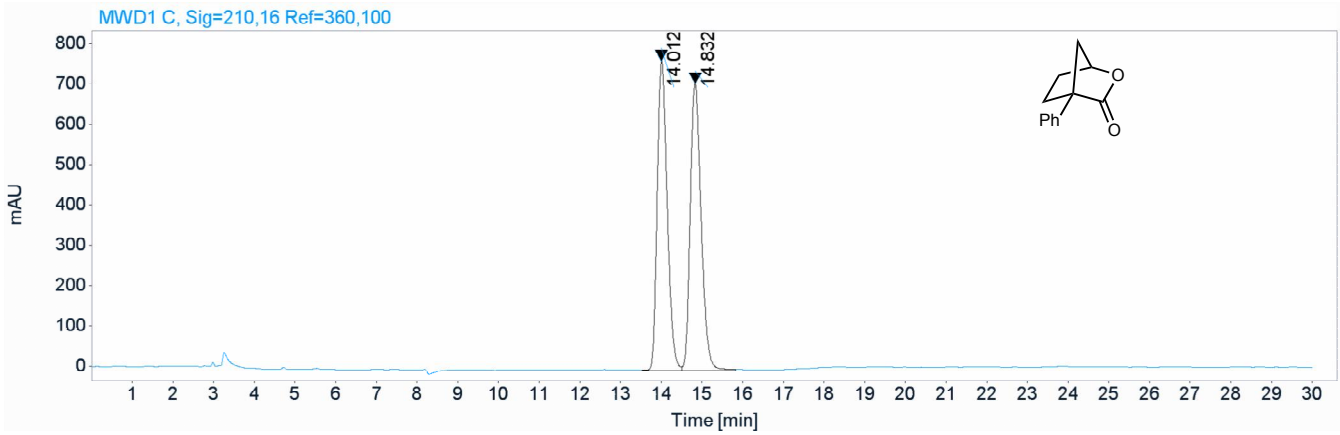

Signal: MWD1 C, Sig=210,16 Ref=360,100

RT [min]	Type	Width [min]	Area	Height	Area%	Name
14.012	MF	0.2851	13137.0547	768.0323	49.6503	
14.832	FM	0.3115	13322.1143	712.7924	50.3497	
		Sum	26459.1689			

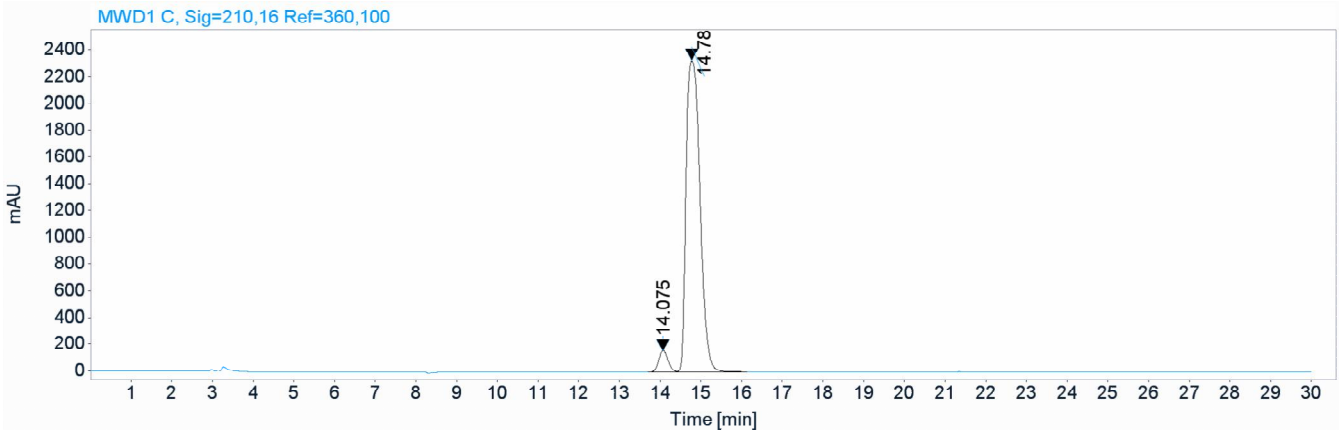

Signal: MWD1 C, Sig=210,16 Ref=360,100

RT [min]	Type	Width [min]	Area	Height	Area%	Name
14.075	VV	0.2574	2604.9226	158.7713	4.5134	
14.780	VB	0.3780	55111.0156	2329.8367	95.4866	
		Sum	57715.9382			

D Isothermal titration calorimetry

Figure D 1: Ph substrate titrated into StilbPBAM (**14**)

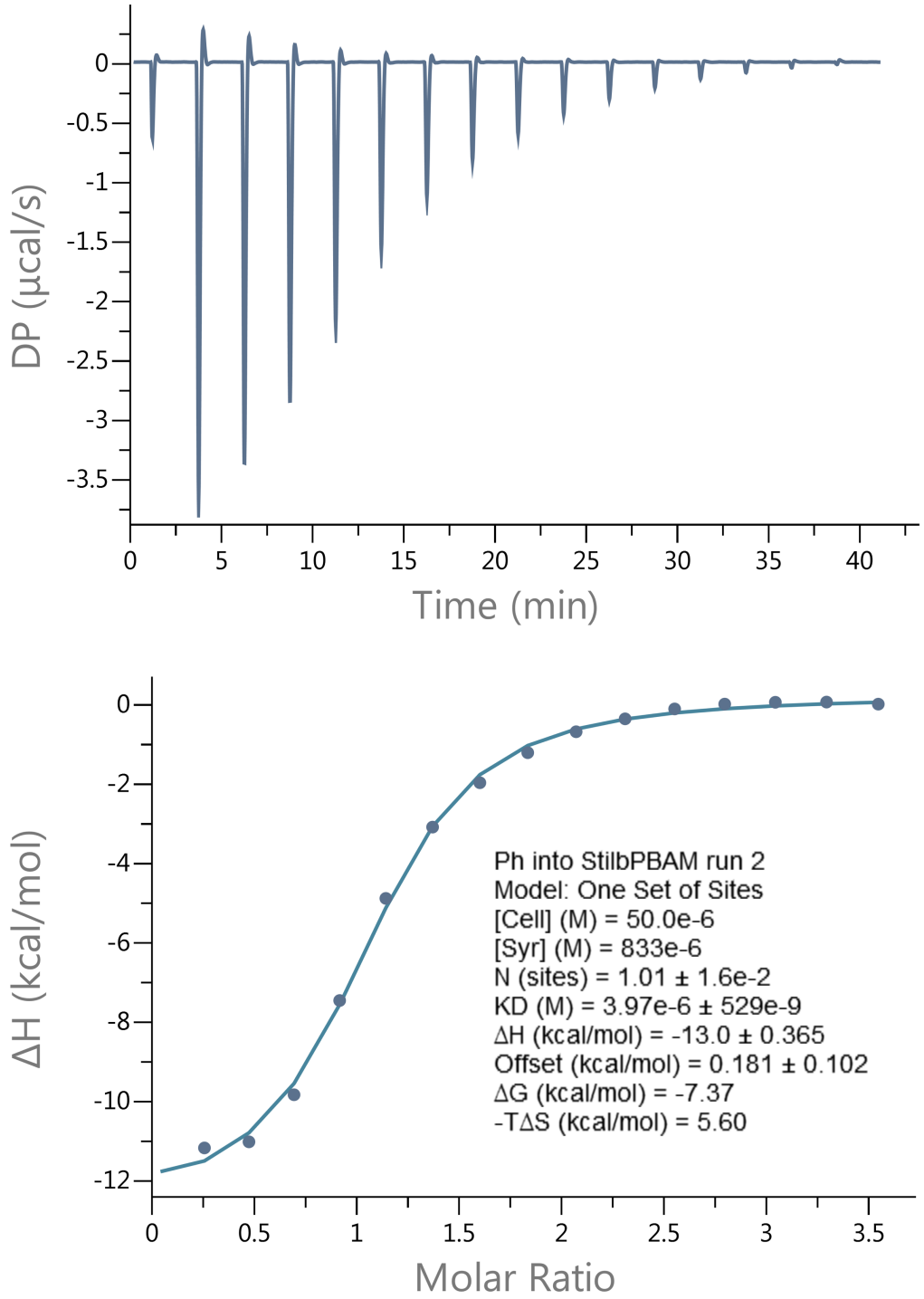

Figure D 2: Ph substrate titrated into StilbAnBAM (**126d**)

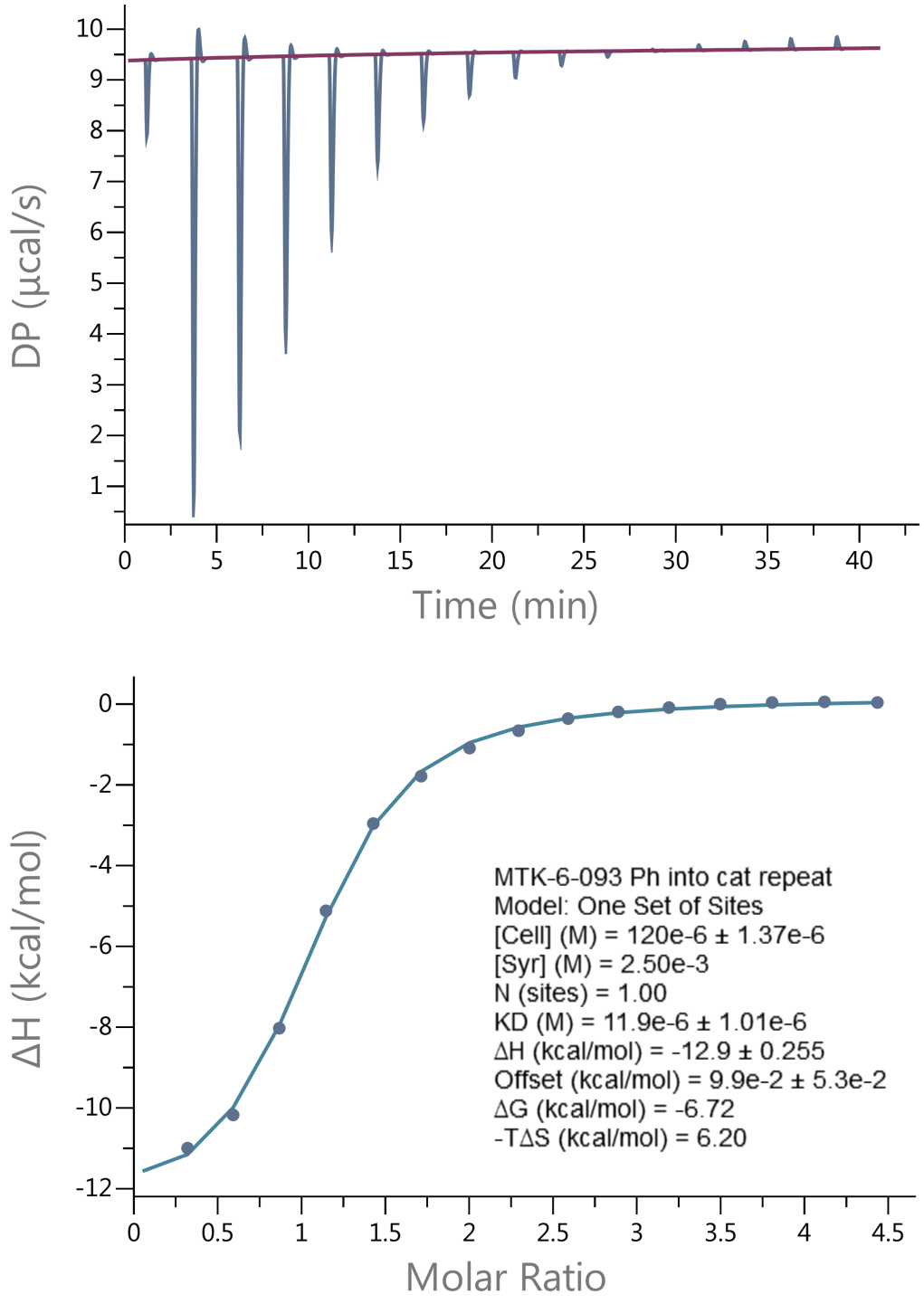

Figure D 3: 2-Naphthyl substrate titrated into StilbAnBAM (**126d**)

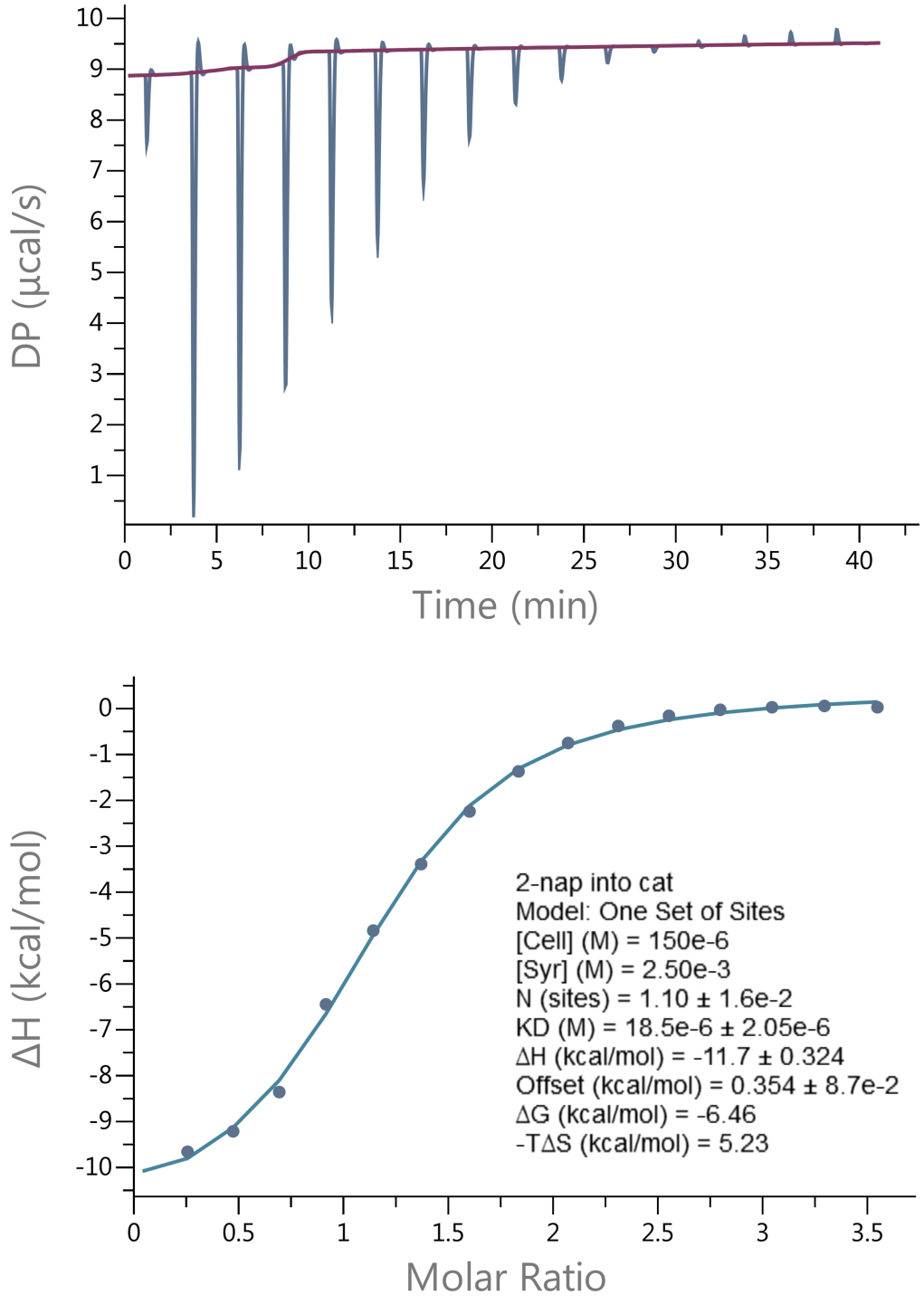

Figure D 4: Bn substrate titrated into StilbAnBAM (**126d**).

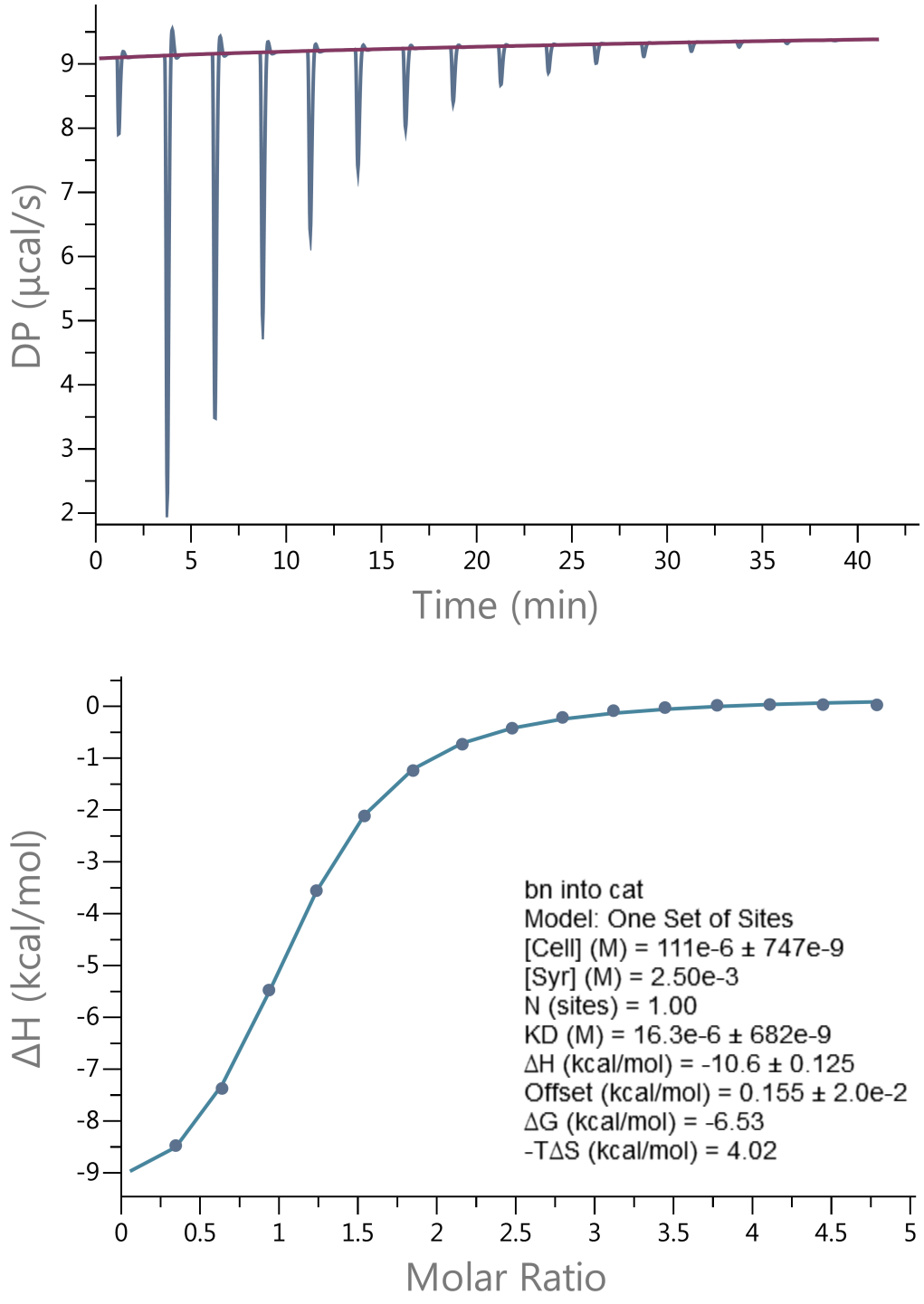

Figure D 5: $CO_2{}^t$Bu substrate titrated into StilbAnBAM (**126d**).

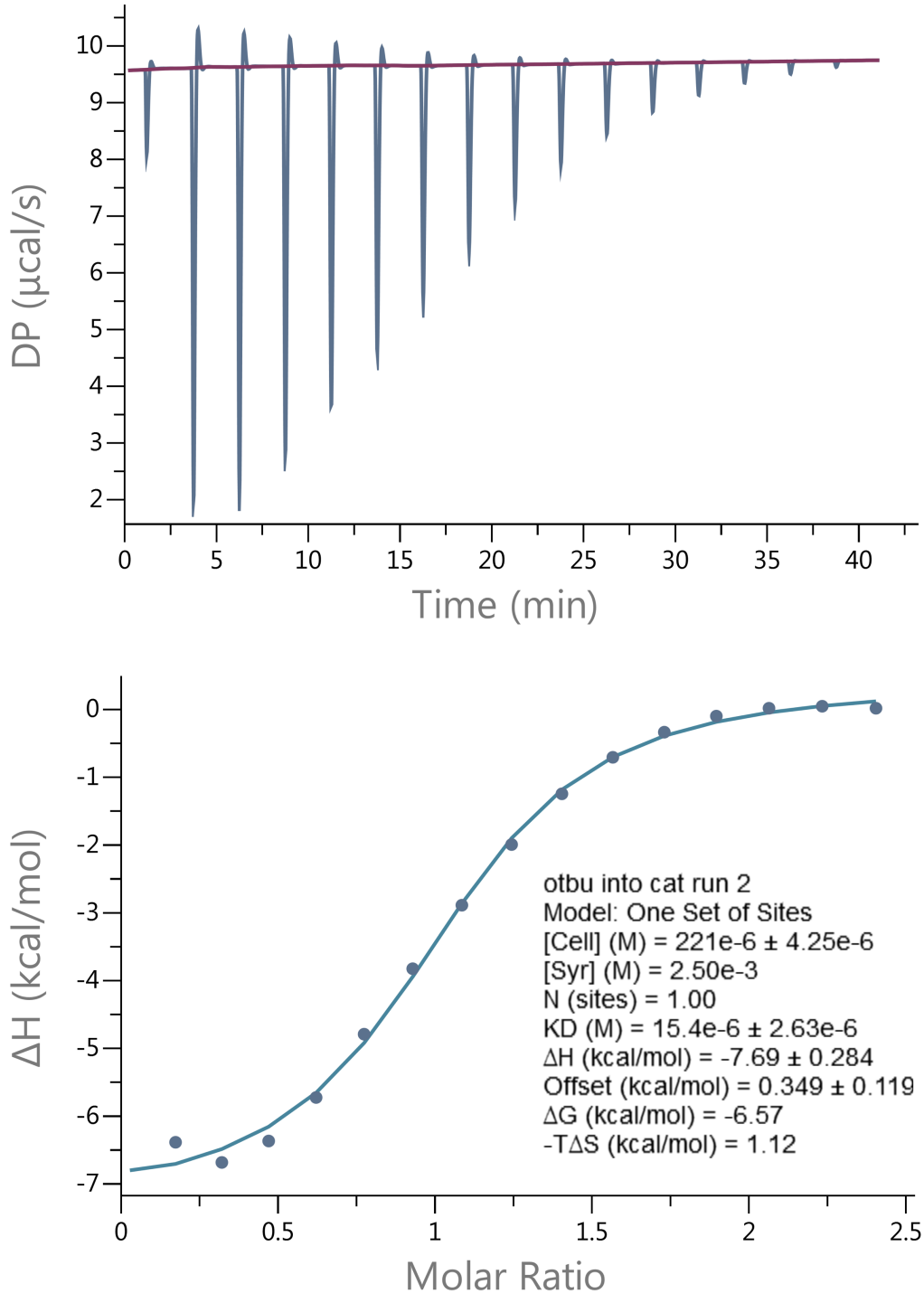

Figure D 6: 1-Naphthyl substrate titrated into StilbAnBAM (**126d**).

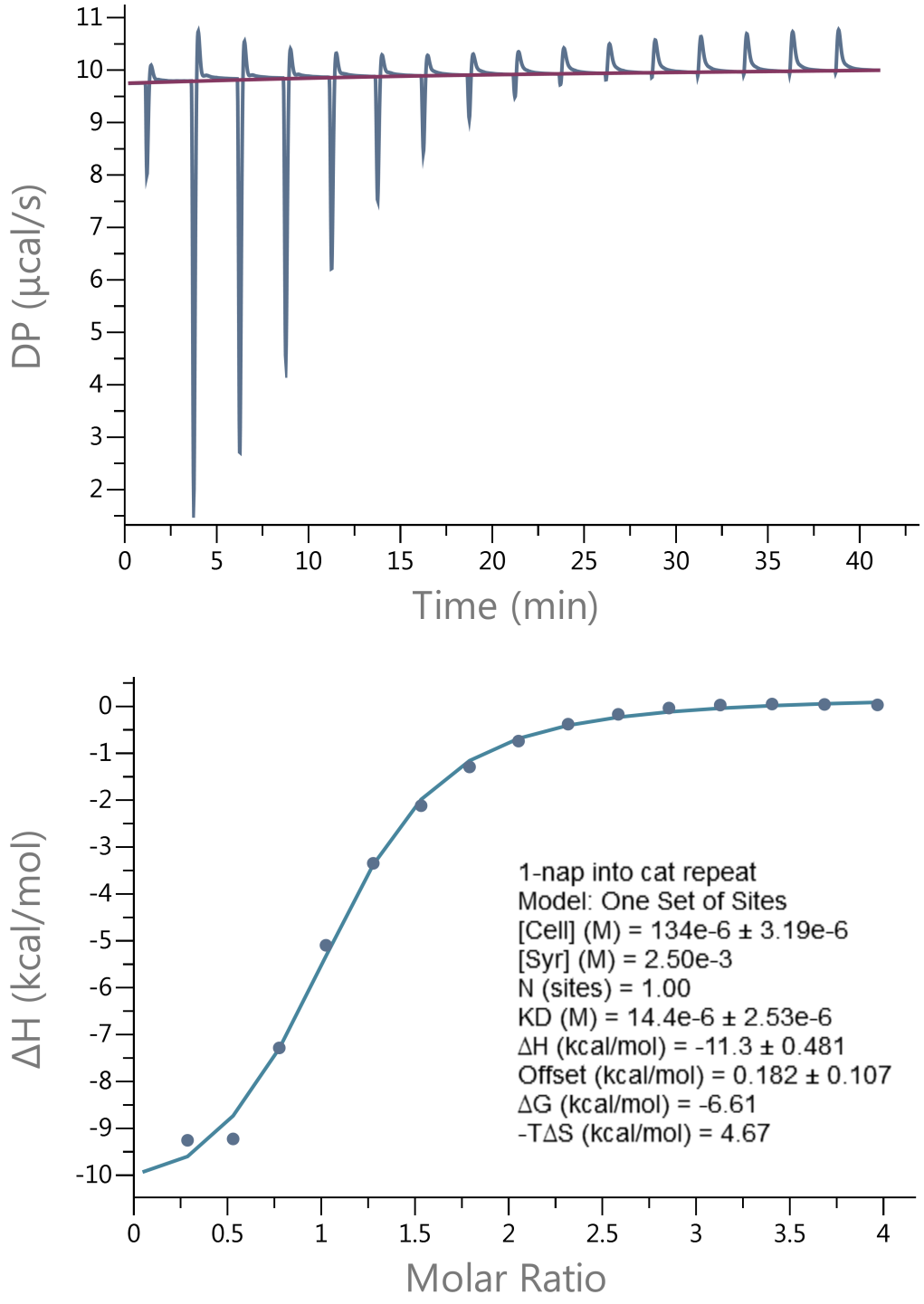

E X-Ray Crystallography of cocrystal structures

INDIANA UNIVERSITY DEPARTMENT OF CHEMISTRY

Molecular Structure Center

Report No. 16042

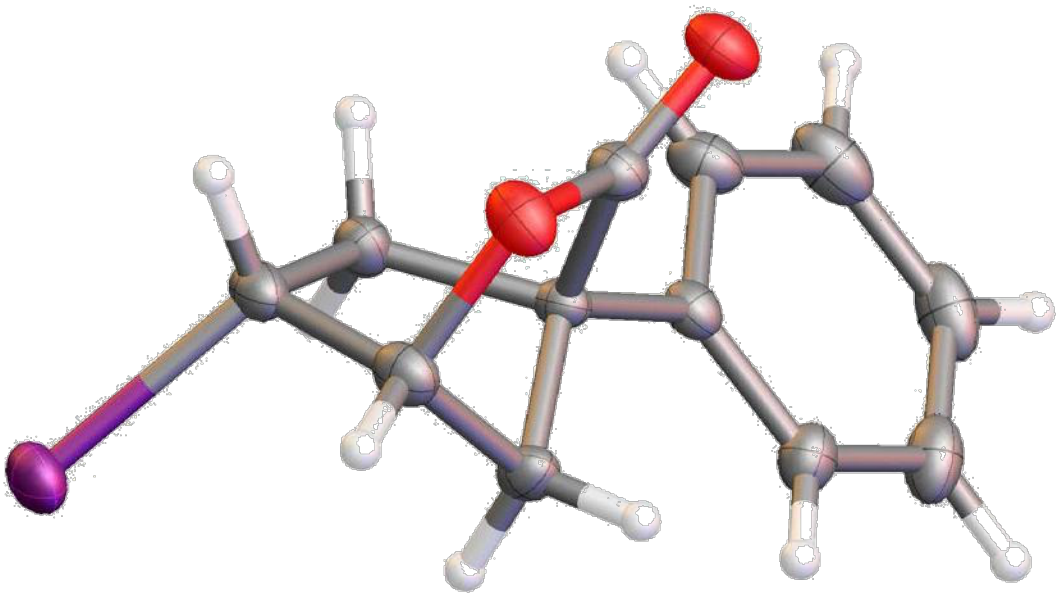

$C_{12}H_{11}I_1O_2$

Prepared for
Matthew Knowe and Professor J. Johnston

by M. Pink

May 9, 2016

IUMSC
Molecular Structure Center

E 1: *X-ray structure of 109a.*

The sample was submitted by Matthew Knowe (research group of Jeff Johnston, Department of Chemistry, Vanderbilt University). A colorless crystal (approximate dimensions 0.31 × 0.14 × 0.05 mm^3) was placed onto the tip of a 0.05 mm diameter glass capillary and mounted on a Bruker APEX II Kappa Duo diffractometer equipped with an APEX II detector at 150(2) K.

Data collection

The data collection was carried out using Mo Kα radiation (graphite monochromator) with a frame time of 20 seconds and a detector distance of 40 mm. A collection strategy was calculated and complete data to a resolution of 0.50 Å with a redundancy of 4 were collected. Eight major sections of frames were collected with 0.50º ω and φ scans. The total exposure time was 17.59 hours. The frames were integrated with the Bruker SAINT software package[1] using a narrow-frame algorithm. The integration of the data using a monoclinic unit cell yielded a total of 26319 reflections to a maximum θ angle of 30.13° (0.71 Å resolution), of which 6227 were independent (average redundancy 4.227, completeness = 99.6%, Rint = 2.56%, Rsig = 2.45%) and 5978 (96.00%) were greater than 2σ(F2). The final cell constants of a = 12.2856(8) Å, b = 6.1896(4) Å, c = 15.4428(11) Å, β = 103.702(4)°, volume = 1140.90(13) $Å^3$, are based upon the refinement of the XYZ-centroids of 9859 reflections above 20 σ(I) with 4.838° < 2θ < 60.02°. Data were corrected for absorption effects using the multi-scan method (SADABS).[2] The ratio of minimum to maximum apparent transmission was 0.765. The calculated minimum and maximum transmission coefficients (based on crystal size) are 0.4790 and 0.8730. Please refer to Table 1 for additional crystal and refinement information.

Structure solution and refinement

The space group $P2_1$ was determined based on intensity statistics and systematic absences. The structure was solved and refined using the SHELX suite of programs.[3] An intrinsic-methods solution was calculated, which provided most non-hydrogen atoms from the E-map. Full-matrix least squares / difference Fourier cycles were performed, which located the remaining non-hydrogen atoms. All non-hydrogen atoms were refined with anisotropic displacement parameters. The hydrogen atoms were placed in ideal positions and refined as riding atoms with relative isotropic displacement parameters. The final anisotropic full-matrix least-squares refinement on F2 with 271 variables converged at R1 = 1.86%, for the observed data and wR2 = 4.34% for all data. The goodness-of-fit was 1.056. The largest peak in the final difference electron density synthesis was 0.638 $e^-/Å^3$ and the largest hole was -0.833 $e^-/Å^3$ with an RMS deviation of 0.067 $e^-/Å^3$. On the basis of the final model, the calculated density was 1.829 g/cm^3 and F(000), 608 e^-. The absolute configuration was determined for anomalous dispersion effects.

1 SAINT, Bruker Analytical X-Ray Systems, Madison, WI, current version.
2 SADABS, Bruker Analytical X-Ray Systems, Madison, WI, current version.
3 A short history of *SHELX*, G. M. Sheldrick, *Acta Cryst*. A64, 112 - 122 (2008).

Bulk material.

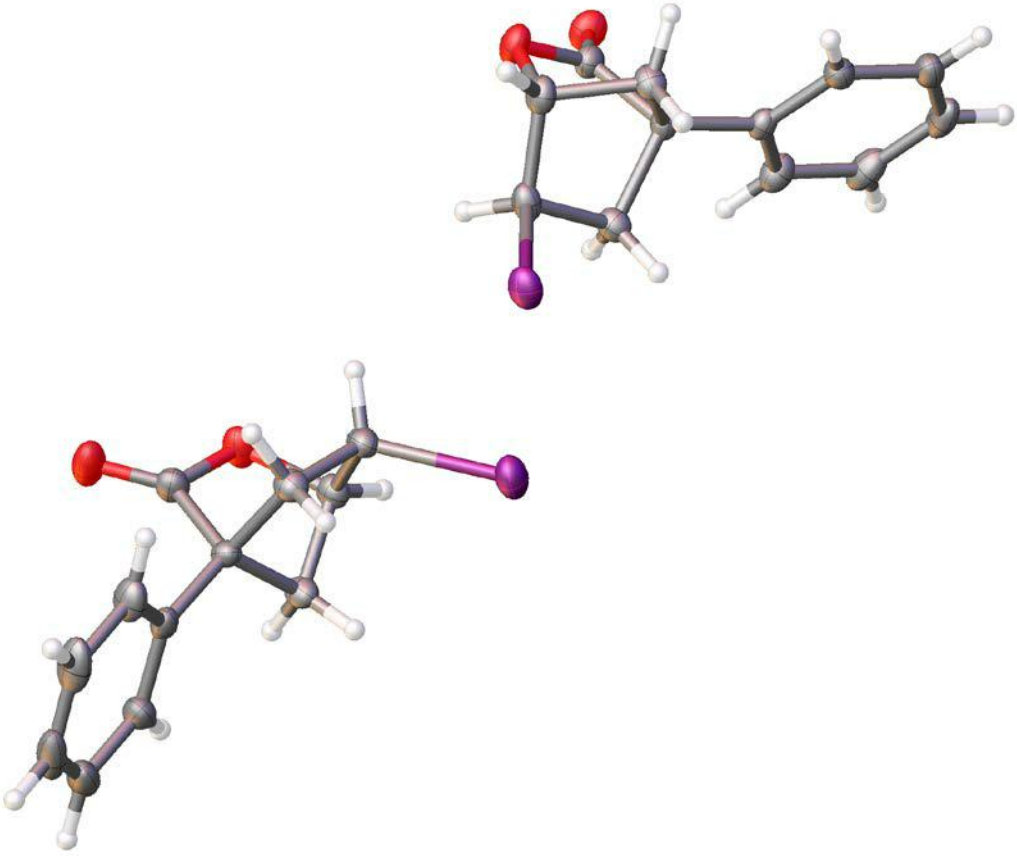

Asymmetric unit (two independent molecules).

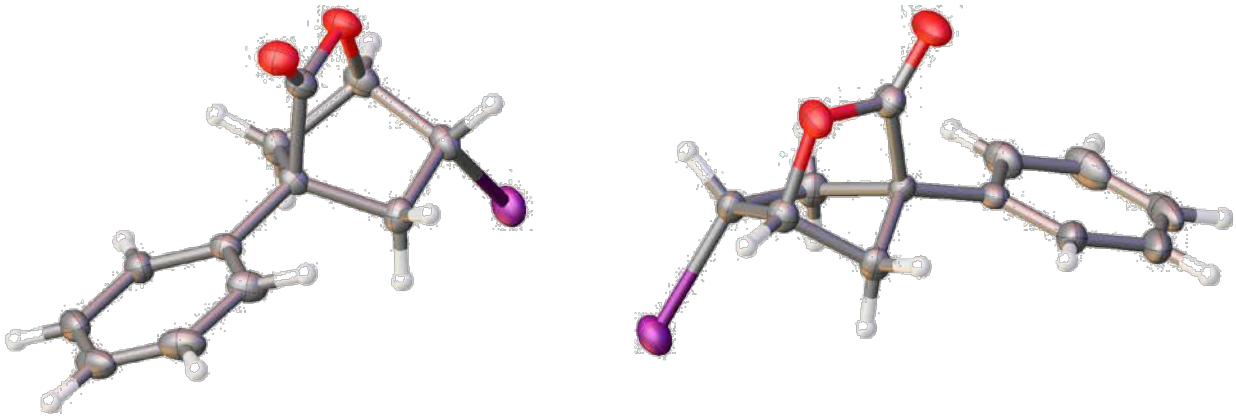

Asymmetric unit (two independent molecules).

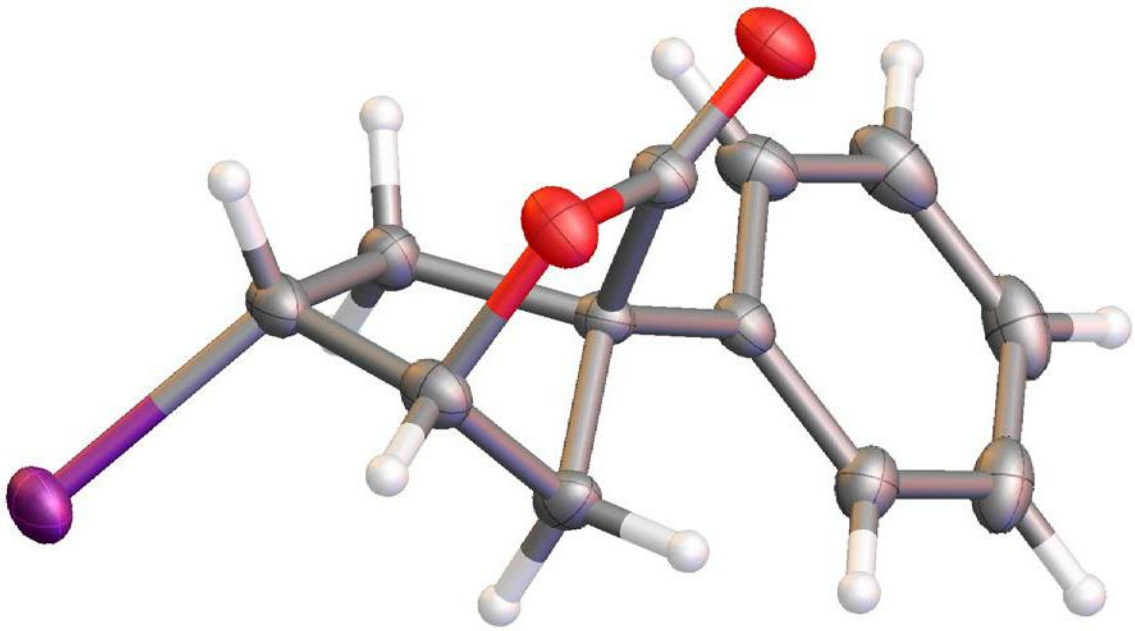

Formula unit.

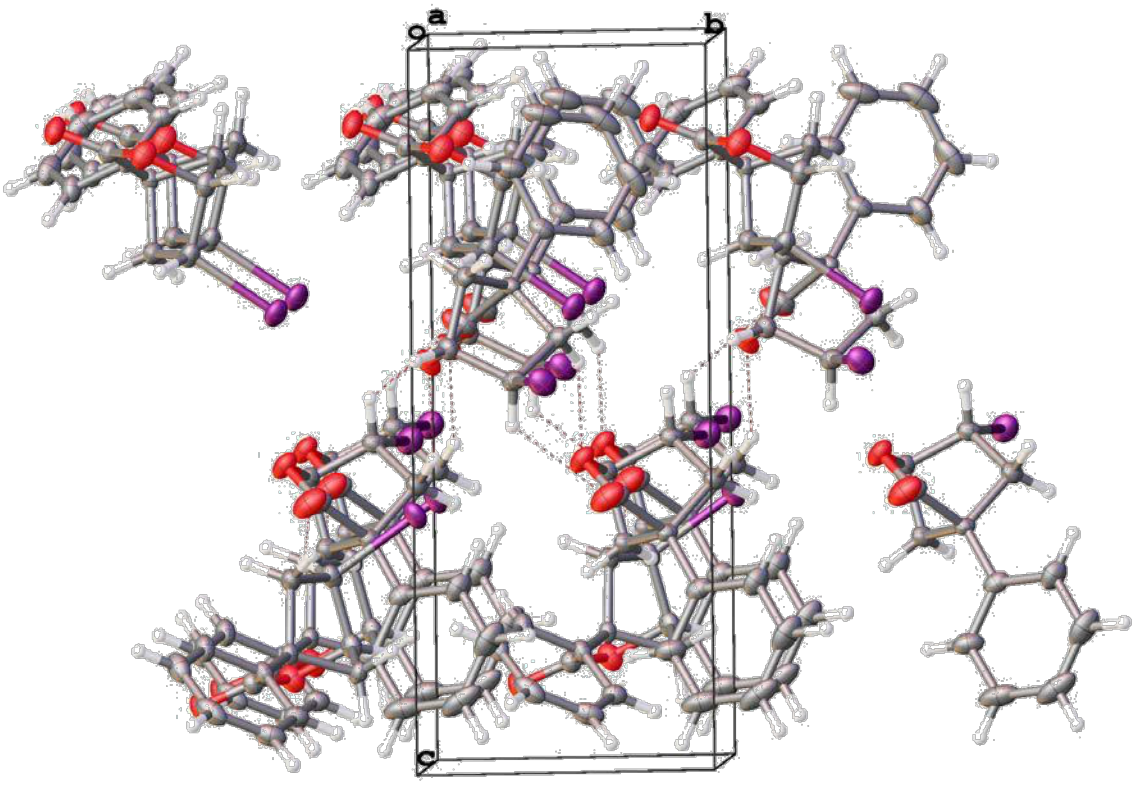

Cell plot, view along *a*.

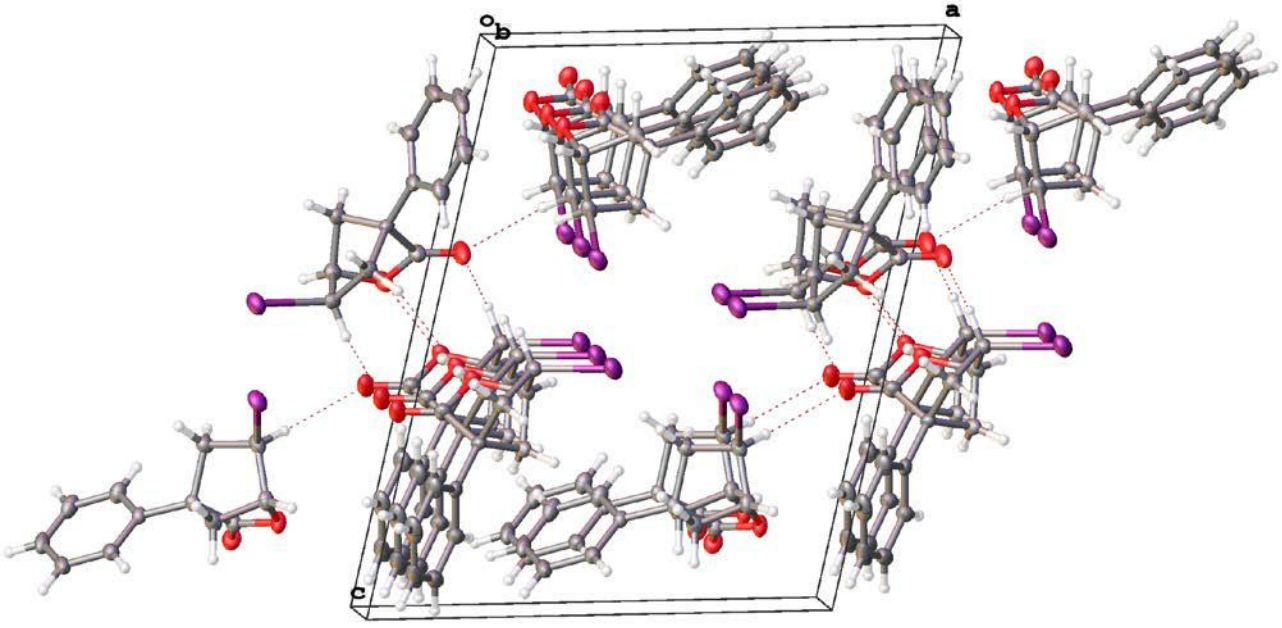

Cell plot, view along *b*.

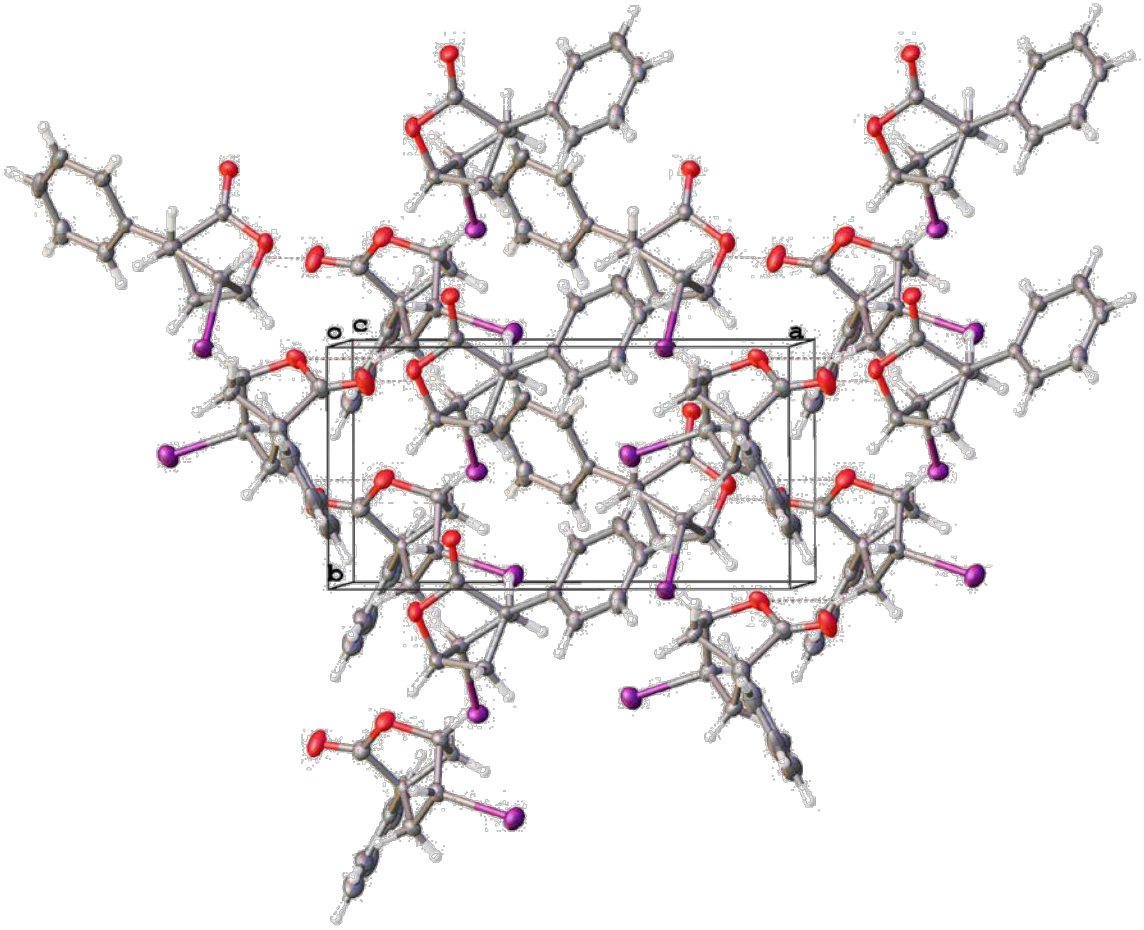

Cell plot, view along *c*.

Table 1. Crystal data and structure refinement for 16042.

Empirical formula	C12 H11 I O2	
Formula weight	314.11	
Crystal color, shape, size	colorless plate, 0.31 × 0.14 × 0.05 mm^3	
Temperature	150(2) K	
Wavelength	0.71073 Å	
Crystal system, space group	Monoclinic, $P2_1$	
Unit cell dimensions	a = 12.2856(8) Å	α= 90°.
	b = 6.1896(4) Å	β= 103.702(4)°.
	c = 15.4428(11) Å	γ = 90°.
Volume	1140.89(13) $Å^3$	
Z	4	
Density (calculated)	1.829 Mg/m^3	
Absorption coefficient	2.784 mm^{-1}	
F(000)	608	

Data collection

Diffractometer	APEX II Kappa Duo, Bruker
Theta range for data collection	1.357 to 30.130°.
Index ranges	-17<=h<=17, -8<=k<=6, -21<=l<=21
Reflections collected	26319
Independent reflections	6227 [R_{int} = 0.0256]
Observed Reflections	5978
Completeness to theta = 25.242°	100.0 %

Solution and Refinement

Absorption correction	Semi-empirical from equivalents
Max. and min. transmission	0.7460 and 0.5707
Solution	Intrinsic methods
Refinement method	Full-matrix least-squares on F^2
Weighting scheme	$w = [\sigma^2 Fo^2 + AP^2 + BP]^{-1}$, with
	$P = (Fo^2 + 2\,Fc^2)/3$, A = 0.0198, B = 0.2503
Data / restraints / parameters	6227 / 1 / 271
Goodness-of-fit on F^2	1.056
Final R indices [I>2sigma(I)]	R1 = 0.0186, wR2 = 0.0427
R indices (all data)	R1 = 0.0201, wR2 = 0.0434
Absolute structure parameter	0.002(7)
Largest diff. peak and hole	0.638 and -0.833 e.$Å^{-3}$

Goodness-of-fit = $[\Sigma[w(F_o^2 - F_c^2)^2]/N_{observns} - N_{params})]^{1/2}$, all data.

$R1 = \Sigma(|F_o| - |F_c|) / \Sigma |F_o|$. $wR2 = [\Sigma[w(F_o^2 - F_c^2)^2] / \Sigma [w(F_o^2)^2]]^{1/2}$.

Table 2. Atomic coordinates ($\times 10^4$) and equivalent isotropic displacement parameters ($Å^2 \times 10^3$) for 16042. U(eq) is defined as one third of the trace of the orthogonalized U^{ij} tensor.

	x	y	z	U(eq)
I1A	3024(1)	5258(1)	3649(1)	30(1)
O1A	1804(2)	969(4)	1410(1)	28(1)
O2A	2609(2)	-2062(4)	1065(2)	29(1)
C1A	3758(2)	1040(5)	1790(2)	18(1)
C2A	2713(2)	-281(5)	1375(2)	22(1)
C3A	2257(2)	3012(5)	1846(2)	25(1)
C4A	2701(2)	2411(5)	2823(2)	24(1)
C5A	3777(2)	1106(5)	2808(2)	24(1)
C6A	3307(2)	3302(5)	1499(2)	23(1)
C7A	4813(2)	230(5)	1562(2)	20(1)
C8A	5289(2)	1341(5)	961(2)	25(1)
C9A	6240(2)	523(6)	726(2)	31(1)
C10A	6708(2)	-1410(6)	1080(2)	34(1)
C11A	6243(2)	-2517(6)	1684(2)	33(1)
C12A	5302(2)	-1705(5)	1928(2)	27(1)
I1B	3704(1)	9641(1)	5459(1)	34(1)
O1B	902(2)	5627(4)	5708(1)	30(1)
C1B	1214(2)	8433(5)	6746(2)	19(1)
O2B	-607(2)	6556(5)	6205(2)	40(1)
C2B	359(2)	6828(5)	6221(2)	26(1)
C3B	2072(2)	6374(5)	5914(2)	24(1)
C4B	2030(2)	8560(5)	5454(2)	23(1)
C5B	1453(2)	10023(5)	6025(2)	25(1)
C6B	2258(2)	6951(5)	6898(2)	24(1)
C7B	899(2)	9487(6)	7526(2)	24(1)
C8B	340(3)	11464(6)	7427(2)	32(1)
C9B	71(3)	12473(7)	8158(3)	44(1)
C10B	350(3)	11494(8)	8988(3)	49(1)
C11B	883(2)	9524(8)	9089(2)	43(1)
C12B	1157(2)	8495(6)	8363(2)	31(1)

Table 3. Bond lengths [Å] and angles [°] for 16042.

I1A-C4A	2.156(3)	O1A-C2A	1.370(3)
O1A-C3A	1.478(4)	O2A-C2A	1.197(4)
C1A-C7A	1.507(3)	C1A-C2A	1.530(4)
C1A-C6A	1.534(4)	C1A-C5A	1.567(4)
C3A-C6A	1.520(4)	C3A-C4A	1.524(4)
C3A-H3A	1.0000	C4A-C5A	1.554(4)
C4A-H4A	1.0000	C5A-H5A	0.9900
C5A-H5B	0.9900	C6A-H6A	0.9900
C6A-H6B	0.9900	C7A-C8A	1.390(4)
C7A-C12A	1.398(4)	C8A-C9A	1.399(4)
C8A-H8A	0.9500	C9A-C10A	1.383(5)
C9A-H9A	0.9500	C10A-C11A	1.384(5)
C10A-H10A	0.9500	C11A-C12A	1.392(4)
C11A-H11A	0.9500	C12A-H12A	0.9500
I1B-C4B	2.161(3)	O1B-C2B	1.369(4)
O1B-C3B	1.472(3)	C1B-C7B	1.499(4)
C1B-C2B	1.531(4)	C1B-C6B	1.549(4)
C1B-C5B	1.565(4)	O2B-C2B	1.193(4)
C3B-C4B	1.524(4)	C3B-C6B	1.525(4)
C3B-H3B	1.0000	C4B-C5B	1.548(4)
C4B-H4B	1.0000	C5B-H5C	0.9900
C5B-H5D	0.9900	C6B-H6C	0.9900
C6B-H6D	0.9900	C7B-C8B	1.393(5)
C7B-C12B	1.398(4)	C8B-C9B	1.397(5)
C8B-H8B	0.9500	C9B-C10B	1.385(7)
C9B-H9B	0.9500	C10B-C11B	1.375(6)
C10B-H10B	0.9500	C11B-C12B	1.398(4)
C11B-H11B	0.9500	C12B-H12B	0.9500
C2A-O1A-C3A	106.2(2)	C7A-C1A-C2A	114.1(2)
C7A-C1A-C6A	120.4(2)	C2A-C1A-C6A	99.0(2)
C7A-C1A-C5A	115.7(2)	C2A-C1A-C5A	104.2(2)
C6A-C1A-C5A	100.9(2)	O2A-C2A-O1A	121.7(2)
O2A-C2A-C1A	131.2(2)	O1A-C2A-C1A	107.0(2)
O1A-C3A-C6A	101.6(2)	O1A-C3A-C4A	104.5(2)
C6A-C3A-C4A	104.1(2)	O1A-C3A-H3A	115.0
C6A-C3A-H3A	115.0	C4A-C3A-H3A	115.0
C3A-C4A-C5A	102.6(2)	C3A-C4A-I1A	111.06(19)
C5A-C4A-I1A	113.32(18)	C3A-C4A-H4A	109.9
C5A-C4A-H4A	109.9	I1A-C4A-H4A	109.9
C4A-C5A-C1A	102.6(2)	C4A-C5A-H5A	111.3

C1A-C5A-H5A	111.3	C4A-C5A-H5B	111.3
C1A-C5A-H5B	111.3	H5A-C5A-H5B	109.2
C3A-C6A-C1A	93.8(2)	C3A-C6A-H6A	113.0
C1A-C6A-H6A	113.0	C3A-C6A-H6B	113.0
C1A-C6A-H6B	113.0	H6A-C6A-H6B	110.4
C8A-C7A-C12A	119.0(2)	C8A-C7A-C1A	120.8(3)
C12A-C7A-C1A	120.1(2)	C7A-C8A-C9A	120.3(3)
C7A-C8A-H8A	119.9	C9A-C8A-H8A	119.9
C10A-C9A-C8A	120.3(3)	C10A-C9A-H9A	119.9
C8A-C9A-H9A	119.9	C9A-C10A-C11A	119.7(3)
C9A-C10A-H10A	120.1	C11A-C10A-H10A	120.1
C10A-C11A-C12A	120.4(3)	C10A-C11A-H11A	119.8
C12A-C11A-H11A	119.8	C11A-C12A-C7A	120.3(3)
C11A-C12A-H12A	119.8	C7A-C12A-H12A	119.8
C2B-O1B-C3B	106.8(2)	C7B-C1B-C2B	115.6(2)
C7B-C1B-C6B	119.9(2)	C2B-C1B-C6B	97.8(2)
C7B-C1B-C5B	115.2(2)	C2B-C1B-C5B	104.6(2)
C6B-C1B-C5B	101.1(2)	O2B-C2B-O1B	122.0(3)
O2B-C2B-C1B	131.1(3)	O1B-C2B-C1B	107.0(2)
O1B-C3B-C4B	104.7(2)	O1B-C3B-C6B	101.4(2)
C4B-C3B-C6B	103.8(2)	O1B-C3B-H3B	115.1
C4B-C3B-H3B	115.1	C6B-C3B-H3B	115.1
C3B-C4B-C5B	102.9(2)	C3B-C4B-I1B	110.21(18)
C5B-C4B-I1B	112.4(2)	C3B-C4B-H4B	110.4
C5B-C4B-H4B	110.4	I1B-C4B-H4B	110.4
C4B-C5B-C1B	103.1(2)	C4B-C5B-H5C	111.2
C1B-C5B-H5C	111.2	C4B-C5B-H5D	111.2
C1B-C5B-H5D	111.2	H5C-C5B-H5D	109.1
C3B-C6B-C1B	93.7(2)	C3B-C6B-H6C	113.0
C1B-C6B-H6C	113.0	C3B-C6B-H6D	113.0
C1B-C6B-H6D	113.0	H6C-C6B-H6D	110.4
C8B-C7B-C12B	119.0(3)	C8B-C7B-C1B	120.6(3)
C12B-C7B-C1B	120.4(3)	C7B-C8B-C9B	120.6(4)
C7B-C8B-H8B	119.7	C9B-C8B-H8B	119.7
C10B-C9B-C8B	119.9(4)	C10B-C9B-H9B	120.1
C8B-C9B-H9B	120.1	C11B-C10B-C9B	120.0(3)
C11B-C10B-H10B	120.0	C9B-C10B-H10B	120.0
C10B-C11B-C12B	120.7(4)	C10B-C11B-H11B	119.6
C12B-C11B-H11B	119.6	C11B-C12B-C7B	119.8(4)
C11B-C12B-H12B	120.1	C7B-C12B-H12B	120.1

Table 4. Anisotropic displacement parameters ($Å^2 \times 10^3$) for 16042. The anisotropic displacement factor exponent takes the form: $-2\pi^2[h^2 a^{*2} U^{11} + ... + 2 h k a^* b^* U^{12}]$

	U^{11}	U^{22}	U^{33}	U^{23}	U^{13}	U^{12}
I1A	33(1)	26(1)	35(1)	-9(1)	16(1)	0(1)
O1A	18(1)	31(1)	37(1)	-7(1)	7(1)	0(1)
O2A	27(1)	22(1)	36(1)	-7(1)	5(1)	-2(1)
C1A	18(1)	15(1)	23(1)	0(1)	7(1)	-1(1)
C2A	20(1)	22(2)	25(1)	-1(1)	6(1)	-1(1)
C3A	22(1)	22(2)	33(1)	-3(1)	10(1)	3(1)
C4A	25(1)	21(2)	30(1)	-5(1)	13(1)	-2(1)
C5A	28(1)	21(1)	24(1)	-1(1)	9(1)	3(1)
C6A	26(1)	18(1)	27(1)	4(1)	10(1)	4(1)
C7A	16(1)	19(1)	23(1)	-4(1)	4(1)	0(1)
C8A	22(1)	31(2)	22(1)	-1(1)	6(1)	0(1)
C9A	22(1)	49(2)	25(1)	-7(1)	9(1)	-2(1)
C10A	18(1)	46(2)	36(2)	-19(1)	5(1)	4(1)
C11A	23(1)	29(2)	44(2)	-10(1)	-1(1)	7(1)
C12A	22(1)	21(2)	36(2)	-1(1)	4(1)	1(1)
I1B	32(1)	38(1)	38(1)	-4(1)	17(1)	-7(1)
O1B	31(1)	30(1)	33(1)	-13(1)	15(1)	-7(1)
C1B	19(1)	22(1)	16(1)	-1(1)	2(1)	2(1)
O2B	27(1)	55(2)	42(1)	-21(1)	13(1)	-14(1)
C2B	27(1)	29(2)	24(1)	-7(1)	7(1)	-2(1)
C3B	25(1)	23(2)	25(1)	-2(1)	8(1)	3(1)
C4B	23(1)	28(2)	20(1)	2(1)	6(1)	4(1)
C5B	27(1)	24(2)	24(1)	3(1)	6(1)	6(1)
C6B	24(1)	25(2)	22(1)	3(1)	6(1)	8(1)
C7B	16(1)	32(2)	24(1)	-7(1)	5(1)	-3(1)
C8B	26(1)	32(2)	40(2)	-11(1)	13(1)	3(1)
C9B	31(2)	44(2)	63(2)	-27(2)	23(2)	-2(1)
C10B	29(2)	75(3)	48(2)	-37(2)	22(2)	-18(2)
C11B	28(1)	78(3)	25(1)	-14(2)	11(1)	-11(2)
C12B	25(1)	48(2)	22(1)	-4(1)	7(1)	-1(1)

Table 5. Hydrogen coordinates (× 10^4) and isotropic displacement parameters (Å^2 × 10^3) for 16042.

	x	y	z	U(eq)
H3A	1726	4260	1736	30
H4A	2149	1462	3024	29
H5A	3744	-368	3050	28
H5B	4456	1847	3154	28
H6A	3799	4473	1806	27
H6B	3143	3510	845	27
H8A	4966	2661	709	30
H9A	6566	1299	320	38
H10A	7345	-1976	910	41
H11A	6567	-3838	1932	40
H12A	4991	-2470	2346	32
H3B	2622	5323	5771	29
H4B	1564	8468	4829	28
H5C	749	10643	5662	30
H5D	1954	11213	6303	30
H6C	2968	7738	7133	28
H6D	2205	5686	7279	28
H8B	141	12132	6857	39
H9B	-303	13828	8086	53
H10B	174	12184	9487	58
H11B	1066	8854	9659	52
H12B	1518	7128	8439	38

Table 6. Torsion angles [°] for 16042.

C3A-O1A-C2A-O2A	179.0(3)	C3A-O1A-C2A-C1A	-0.8(3)
C7A-C1A-C2A-O2A	17.9(4)	C6A-C1A-C2A-O2A	147.1(3)
C5A-C1A-C2A-O2A	-109.2(3)	C7A-C1A-C2A-O1A	-162.3(2)
C6A-C1A-C2A-O1A	-33.1(3)	C5A-C1A-C2A-O1A	70.6(3)
C2A-O1A-C3A-C6A	35.1(3)	C2A-O1A-C3A-C4A	-73.0(3)
O1A-C3A-C4A-C5A	73.0(2)	C6A-C3A-C4A-C5A	-33.2(3)
O1A-C3A-C4A-I1A	-165.59(15)	C6A-C3A-C4A-I1A	88.2(2)
C3A-C4A-C5A-C1A	-3.0(3)	I1A-C4A-C5A-C1A	-122.80(19)
C7A-C1A-C5A-C4A	169.1(2)	C2A-C1A-C5A-C4A	-64.9(3)
C6A-C1A-C5A-C4A	37.4(3)	O1A-C3A-C6A-C1A	-52.9(2)
C4A-C3A-C6A-C1A	55.4(2)	C7A-C1A-C6A-C3A	175.5(2)
C2A-C1A-C6A-C3A	50.7(2)	C5A-C1A-C6A-C3A	-55.8(2)
C2A-C1A-C7A-C8A	106.3(3)	C6A-C1A-C7A-C8A	-11.1(4)
C5A-C1A-C7A-C8A	-132.9(3)	C2A-C1A-C7A-C12A	-71.1(3)
C6A-C1A-C7A-C12A	171.5(2)	C5A-C1A-C7A-C12A	49.7(3)
C12A-C7A-C8A-C9A	0.2(4)	C1A-C7A-C8A-C9A	-177.2(2)
C7A-C8A-C9A-C10A	0.8(4)	C8A-C9A-C10A-C11A	-1.2(4)
C9A-C10A-C11A-C12A	0.6(5)	C10A-C11A-C12A-C7A	0.4(4)
C8A-C7A-C12A-C11A	-0.8(4)	C1A-C7A-C12A-C11A	176.6(3)
C3B-O1B-C2B-O2B	-178.9(3)	C3B-O1B-C2B-C1B	1.8(3)
C7B-C1B-C2B-O2B	16.8(5)	C6B-C1B-C2B-O2B	145.4(4)
C5B-C1B-C2B-O2B	-110.9(4)	C7B-C1B-C2B-O1B	-164.0(3)
C6B-C1B-C2B-O1B	-35.4(3)	C5B-C1B-C2B-O1B	68.3(3)
C2B-O1B-C3B-C4B	-74.2(3)	C2B-O1B-C3B-C6B	33.5(3)
O1B-C3B-C4B-C5B	71.1(2)	C6B-C3B-C4B-C5B	-34.8(3)
O1B-C3B-C4B-I1B	-168.89(16)	C6B-C3B-C4B-I1B	85.2(2)
C3B-C4B-C5B-C1B	-1.0(3)	I1B-C4B-C5B-C1B	-119.56(19)
C7B-C1B-C5B-C4B	166.3(2)	C2B-C1B-C5B-C4B	-65.6(2)
C6B-C1B-C5B-C4B	35.5(2)	O1B-C3B-C6B-C1B	-52.8(2)
C4B-C3B-C6B-C1B	55.6(2)	C7B-C1B-C6B-C3B	177.4(3)
C2B-C1B-C6B-C3B	51.9(2)	C5B-C1B-C6B-C3B	-54.7(2)
C2B-C1B-C7B-C8B	-92.5(3)	C6B-C1B-C7B-C8B	150.8(3)
C5B-C1B-C7B-C8B	29.8(3)	C2B-C1B-C7B-C12B	87.3(3)
C6B-C1B-C7B-C12B	-29.4(4)	C5B-C1B-C7B-C12B	-150.4(3)
C12B-C7B-C8B-C9B	1.8(4)	C1B-C7B-C8B-C9B	-178.4(3)
C7B-C8B-C9B-C10B	-0.6(5)	C8B-C9B-C10B-C11B	-0.6(5)
C9B-C10B-C11B-C12B	0.6(5)	C10B-C11B-C12B-C7B	0.6(5)
C8B-C7B-C12B-C11B	-1.8(4)	C1B-C7B-C12B-C11B	178.4(3)

Table 7. Hydrogen bonds for 16042 [Å and °].

D-H...A	d(D-H)	d(H...A)	d(D...A)	<(DHA)
C4A-H4A...O2B#1	1.00	2.47	3.314(4)	142.2
C5A-H5A...I1A#2	0.99	3.06	4.027(3)	166.0
C5A-H5B...I1B#3	0.99	3.22	4.195(3)	167.2
C4B-H4B...O2B#4	1.00	2.59	3.307(4)	128.7
C5B-H5C...O1B#4	0.99	2.56	3.464(3)	151.8

Symmetry transformations used to generate equivalent atoms:
#1 -x,y-1/2,-z+1 #2 x,y-1,z #3 -x+1,y-1/2,-z+1 #4 -x,y+1/2,-z+1

INDIANA UNIVERSITY DEPARTMENT OF CHEMISTRY

Molecular Structure Center

Report No. 15113

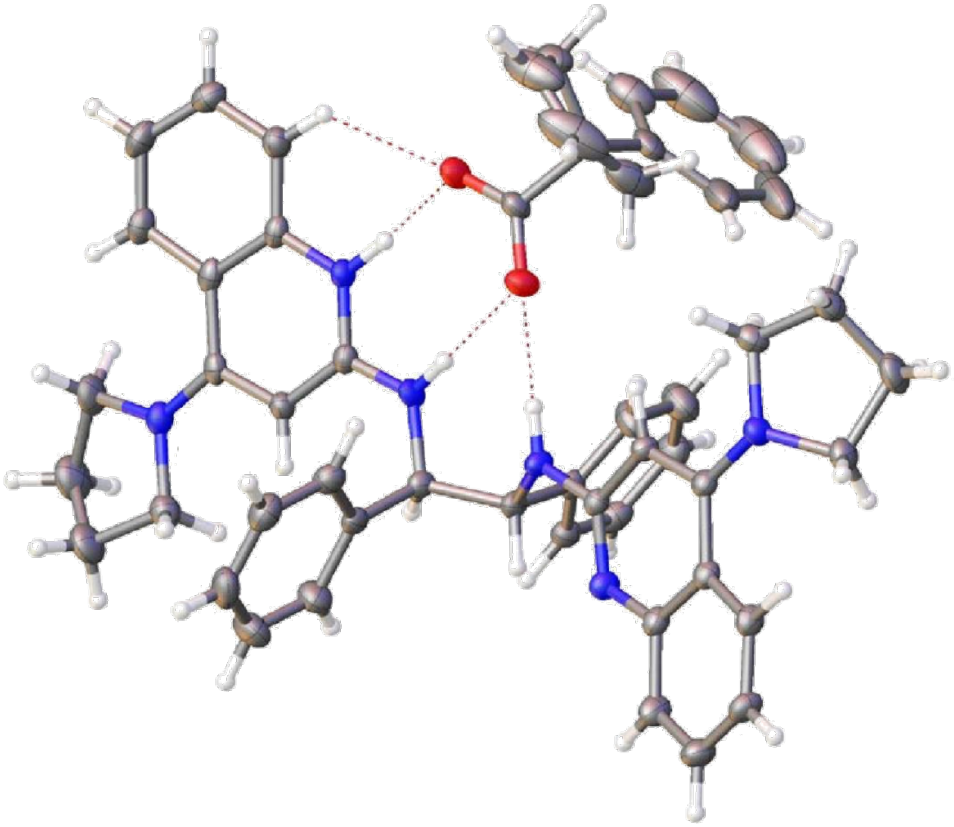

$C_{52}H_{52}N_6O_2 \cdot 0.32\ CH_2Cl_2$

Prepared for
Matthew Knowe and Professor J. Johnston

by M. Pink

November 24, 2015

IUMSC
Molecular Structure Center

E 2: X-ray cocrystal structure of 14 • 107a.

The sample was submitted by Matthew Knowe (research group of Jeffrey Johnston, Department of Chemistry, Vanderbilt University). A colorless crystal (approximate dimensions 0.24 × 0.13 × 0.05 mm^3) was placed onto the tip of a 0.05 mm diameter glass capillary and mounted on a Bruker APEX II Kappa Duo diffractometer equipped with an APEX II detector at 150(2) K.

Data collection

The data collection was carried out using Mo Kα radiation (graphite monochromator) with a frame time of 20 seconds and a detector distance of 40 mm. A collection strategy was calculated and complete data to a resolution of 0.70 Å with a redundancy of 4 were collected. Five major sections of frames were collected with 0.50º ω and φ scans.

Axis	2θ/°	ω/°	φ/°	χ/°	Frames	Time/s
Omega	-30.50	-134.05	-231.31	41.78	220	20.00
Omega	-23.00	-28.39	-73.14	-58.65	157	20.00
Phi	-30.50	182.00	-144.08	99.23	373	20.00
Phi	14.50	-31.53	24.82	30.74	130	20.00
Omega	22.00	129.45	-129.95	-99.10	113	20.00

A total of 993 frames were collected. The total exposure time was 5.52 hours. The frames were integrated with the Bruker SAINT software package[1] using a narrow-frame algorithm. The integration of the data using a monoclinic unit cell yielded a total of 20962 reflections to a maximum θ angle of 27.53° (0.77 Å resolution), of which 9504 were independent (average redundancy 2.206, completeness = 99.2%, Rint = 3.58%, Rsig = 5.71%) and 7401 (77.87%) were greater than 2σ(F2). The final cell constants of a = 11.0401(7) Å, b = 15.2838(11) Å, c = 13.7571(9) Å, β = 99.998(4)°, volume = 2286.0(3) Å3, are based upon the refinement of the XYZ-centroids of 6280 reflections above 20 σ(I) with 4.597° < 2θ < 54.07°. Data were corrected for absorption effects using the multi-scan method (SADABS[2]). The ratio of minimum to maximum apparent transmission was 0.836. The calculated minimum and maximum transmission coefficients (based on crystal size) are 0.9740 and 0.9950. Please refer to Table 1 for additional crystal and refinement information.

Structure solution and refinement

The space group $P2_1$ was determined based on intensity statistics and systematic absences. The structure was solved and refined using the SHELX suite of programs.[3] An intrinsic-methods solution was calculated, which provided most non-hydrogen atoms from the E-map. Full-matrix least squares / difference Fourier cycles were performed, which located the remaining non-hydrogen atoms. All non-hydrogen atoms were refined with anisotropic displacement parameters with exception of the partially occupied solvent molecule (DCM). The hydrogen atoms were placed in ideal positions and refined as riding atoms with relative isotropic displacement parameters. The final anisotropic full-matrix least-squares refinement on F2 with 566 variables converged at R1 = 5.57%, for the observed data and wR2 = 14.35% for all data. The goodness-of-fit was 1.043. The largest peak in the final difference electron density synthesis was 0.814 $e^-/Å^3$ and the largest hole was -0.464 $e^-/Å^3$ with an RMS deviation of 0.049 $e^-/Å^3$. On the basis of the final model, the calculated density was 1.191 g/cm^3 and F(000), 871 e^-.

4 SAINT, Bruker Analytical X-Ray Systems, Madison, WI, current version.
5 SADABS, Bruker Analytical X-Ray Systems, Madison, WI, current version.
6 A short history of *SHELX*, G. M. Sheldrick, *Acta Cryst*. A64, 112 - 122 (2008).

Bulk material.

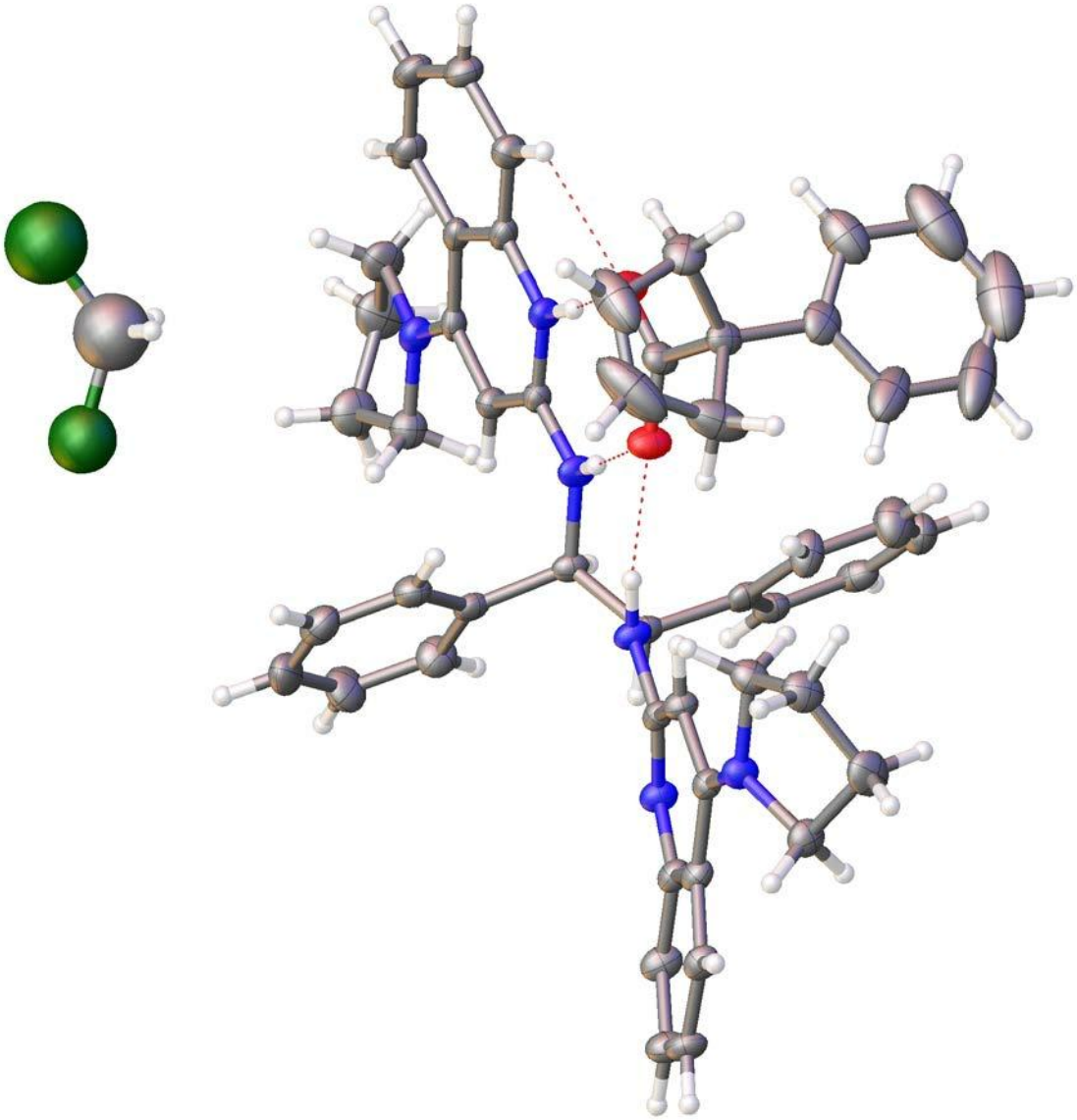

Formula unit.

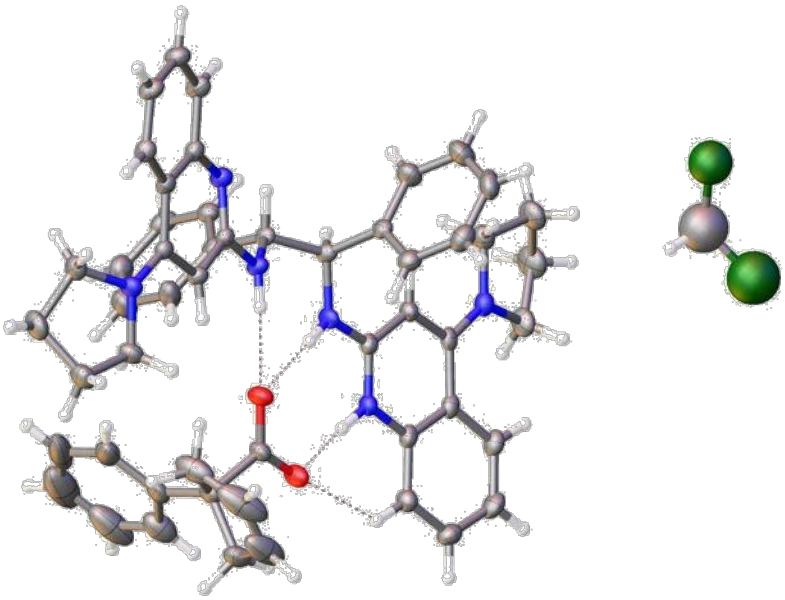

Formula unit.

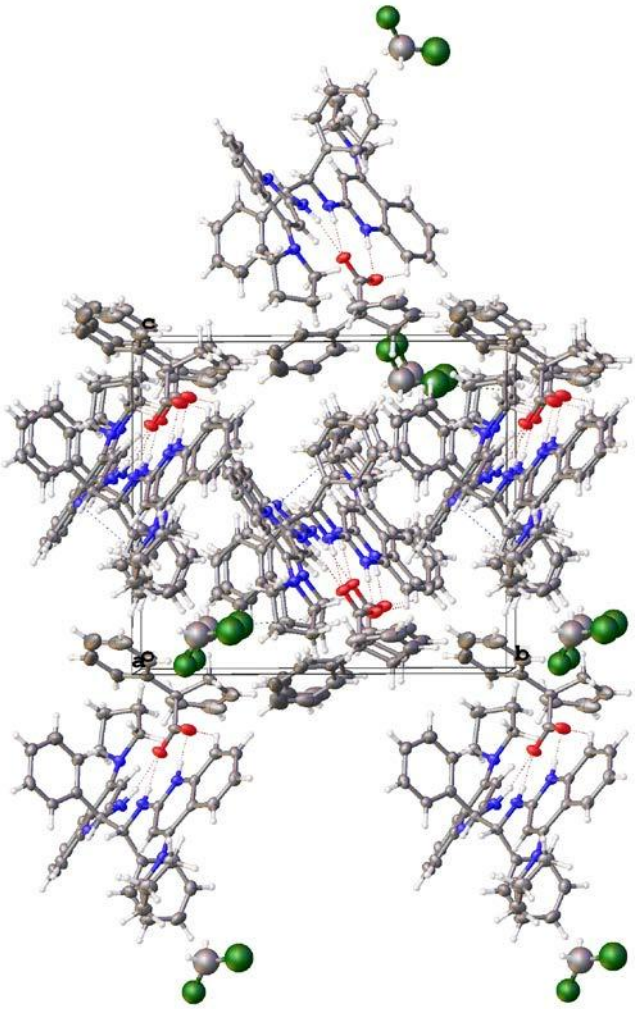

Cell plot, view along *a*.

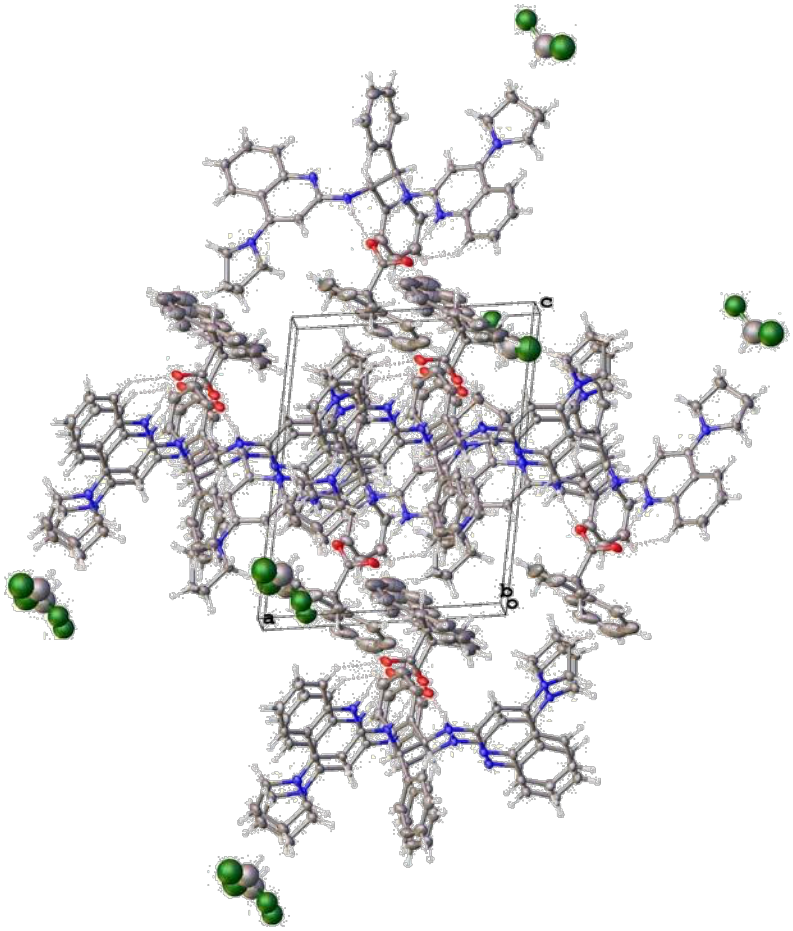

Cell plot, view along *b*.

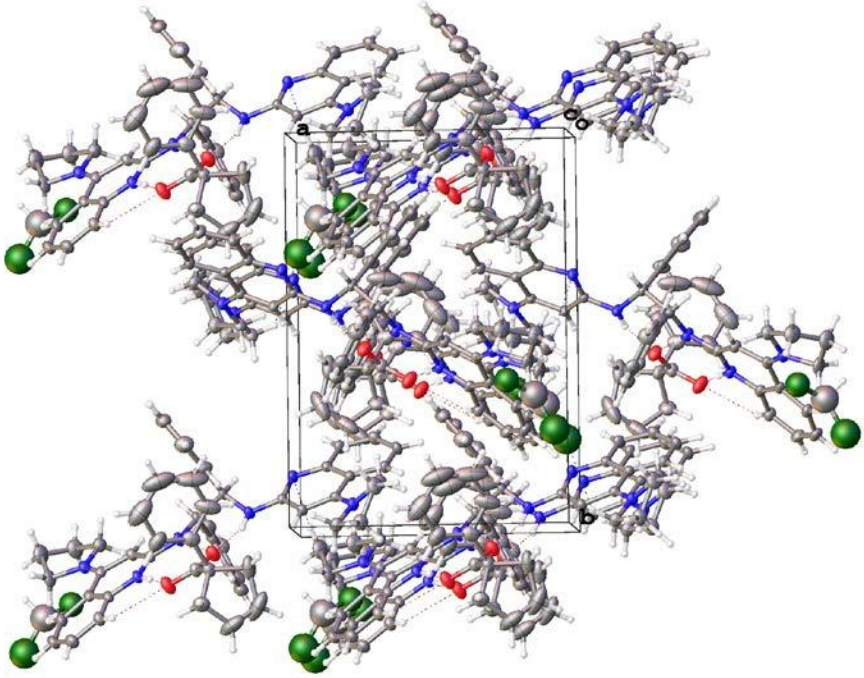

Cell plot, view along *c*.

Table 1. Crystal data and structure refinement for 15113.

Empirical formula	C52.31 H52.63 Cl0.64 N6 O2	
Formula weight	819.93	
Crystal color, shape, size	colorless plate, 0.24 × 0.13 × 0.05 mm^3	
Temperature	150(2) K	
Wavelength	0.71073 Å	
Crystal system, space group	Monoclinic, $P2_1$	
Unit cell dimensions	a = 11.0401(7) Å	α= 90°.
	b = 15.2838(11) Å	β= 99.998(4)°.
	c = 13.7571(9) Å	γ = 90°.
Volume	2286.0(3) $Å^3$	
Z	2	
Density (calculated)	1.191 Mg/m^3	
Absorption coefficient	0.109 mm^{-1}	
F(000)	871	

Data collection

Diffractometer	APEX II Kappa Duo, Bruker
Theta range for data collection	1.873 to 27.530°.
Index ranges	-14<=h<=13, -19<=k<=19, -17<=l<=15
Reflections collected	20962
Independent reflections	9504 [R_{int} = 0.0358]
Observed Reflections	7401
Completeness to theta = 25.242°	99.8 %

Solution and Refinement

Absorption correction	Semi-empirical from equivalents
Max. and min. transmission	0.7456 and 0.6236
Solution	Intrinsic methods
Refinement method	Full-matrix least-squares on F^2
Weighting scheme	$w = [\sigma^2 Fo^2 + AP^2 + BP]^{-1}$, with
	$P = (Fo^2 + 2\,Fc^2)/3$, A = 0.0707, B = 0.5367
Data / restraints / parameters	9504 / 2 / 566
Goodness-of-fit on F^2	1.043
Final R indices [I>2σ(I)]	R1 = 0.0557, wR2 = 0.1321
R indices (all data)	R1 = 0.0769, wR2 = 0.1435
Absolute structure parameter	0.06(11)
Largest diff. peak and hole	0.814 and -0.464 e.$Å^{-3}$

Goodness-of-fit = $[\Sigma[w(F_o^2 - F_c^2)^2]/N_{observns} - N_{params})]^{1/2}$, all data.

$R1 = \Sigma(|F_o| - |F_c|) / \Sigma |F_o|$. $wR2 = [\Sigma[w(F_o^2 - F_c^2)^2] / \Sigma [w(F_o^2)^2]]^{1/2}$.

Table 2. Atomic coordinates (× 10^4) and equivalent isotropic displacement parameters (Å^2 × 10^3) for 15113. U(eq) is defined as one third of the trace of the orthogonalized U^{ij} tensor.

	x	y	z	U(eq)
O1	7151(2)	5568(2)	2463(2)	33(1)
O2	5561(2)	6371(2)	1763(2)	37(1)
N1	8407(2)	4508(2)	4081(2)	23(1)
N2	9949(3)	3594(2)	4877(2)	24(1)
N3	12175(3)	4369(2)	2811(2)	24(1)
N4	5887(3)	5153(2)	4009(2)	25(1)
N5	4409(2)	6101(2)	3271(2)	23(1)
N6	2414(3)	5768(2)	5541(2)	27(1)
C1	7453(3)	4005(2)	4437(3)	22(1)
C2	9585(3)	4171(2)	4174(3)	20(1)
C3	11168(3)	3353(2)	5007(3)	23(1)
C4	11610(3)	2837(3)	5846(3)	29(1)
C5	12833(3)	2626(3)	6096(3)	31(1)
C6	13663(3)	2908(3)	5501(3)	29(1)
C7	13259(3)	3387(2)	4666(3)	25(1)
C8	12003(3)	3617(2)	4382(3)	23(1)
C9	11513(3)	4154(2)	3540(3)	21(1)
C10	10324(3)	4475(2)	3490(3)	22(1)
C11	11600(3)	4911(3)	1972(3)	28(1)
C12	12505(4)	4872(3)	1256(3)	36(1)
C13	13006(4)	3950(3)	1412(3)	40(1)
C14	13160(3)	3822(3)	2523(3)	30(1)
C15	6790(3)	3361(2)	3671(3)	24(1)
C16	6855(4)	3390(3)	2678(3)	36(1)
C17	6189(4)	2798(3)	2022(3)	47(1)
C18	5445(4)	2180(3)	2349(3)	38(1)
C19	5365(3)	2144(3)	3337(3)	31(1)
C20	6039(3)	2726(2)	3988(3)	26(1)
C21	6497(3)	4603(2)	4811(3)	22(1)
C22	4828(3)	5580(2)	4040(3)	22(1)
C23	3356(3)	6593(2)	3240(3)	24(1)
C24	3056(3)	7170(3)	2435(3)	28(1)
C25	2069(3)	7729(3)	2401(3)	33(1)
C26	1385(3)	7719(3)	3156(3)	34(1)
C27	1652(3)	7139(3)	3928(3)	29(1)
C28	2634(3)	6538(2)	3989(3)	24(1)
C29	3028(3)	5921(2)	4800(3)	22(1)
C30	4158(3)	5491(2)	4804(3)	23(1)

C31	1155(3)	6043(3)	5634(3)	37(1)
C32	827(4)	5412(4)	6416(4)	49(1)
C33	2028(4)	5262(3)	7081(3)	45(1)
C34	2935(3)	5197(3)	6370(3)	31(1)
C35	6990(3)	5111(2)	5738(3)	24(1)
C36	6811(4)	4790(3)	6654(3)	36(1)
C37	7210(4)	5262(3)	7501(3)	44(1)
C38	7779(4)	6060(3)	7474(3)	43(1)
C39	7970(4)	6383(3)	6569(3)	38(1)
C40	7571(3)	5913(3)	5707(3)	30(1)
C41	7080(3)	6013(3)	768(3)	28(1)
C42	8486(4)	5985(4)	996(3)	55(1)
C43	8787(6)	6958(5)	1136(4)	83(2)
C44	7880(6)	7443(4)	741(4)	68(2)
C45	6805(4)	6909(3)	275(3)	38(1)
C46	6561(3)	5989(3)	1753(3)	26(1)
C47	7082(6)	4442(3)	144(4)	60(2)
C48	6528(10)	3747(4)	-388(5)	89(3)
C49	5374(11)	3813(5)	-891(6)	99(3)
C50	4710(7)	4578(6)	-875(4)	87(2)
C51	5282(5)	5311(4)	-333(3)	52(1)
C52	6476(4)	5243(3)	171(3)	37(1)
Cl1S	107(9)	7857(7)	8530(7)	151(4)
C1S	820(30)	6966(18)	8650(20)	131(11)
Cl2S	1759(6)	6614(5)	9582(5)	103(3)

Table 3. Bond lengths [Å] and angles [°] for 15113.

O1-C46	1.254(4)	O2-C46	1.251(4)
N1-C2	1.383(4)	N1-C1	1.456(4)
N1-H1N	0.89(4)	N2-C2	1.320(4)
N2-C3	1.376(4)	N3-C9	1.379(4)
N3-C11	1.472(5)	N3-C14	1.479(5)
N4-C22	1.346(4)	N4-C21	1.455(4)
N4-H4N	0.85(4)	N5-C22	1.341(5)
N5-C23	1.379(4)	N5-H5N	0.94(4)
N6-C29	1.339(5)	N6-C34	1.473(5)
N6-C31	1.479(4)	C1-C15	1.532(5)
C1-C21	1.550(5)	C1-H1	1.0000
C2-C10	1.426(5)	C3-C4	1.413(5)
C3-C8	1.423(5)	C4-C5	1.373(5)
C4-H4	0.9500	C5-C6	1.399(5)
C5-H5	0.9500	C6-C7	1.370(5)
C6-H6	0.9500	C7-C8	1.418(5)
C7-H7	0.9500	C8-C9	1.446(5)
C9-C10	1.392(5)	C10-H10	0.9500
C11-C12	1.522(5)	C11-H11A	0.9900
C11-H11B	0.9900	C12-C13	1.515(6)
C12-H12A	0.9900	C12-H12B	0.9900
C13-C14	1.522(5)	C13-H13A	0.9900
C13-H13B	0.9900	C14-H14A	0.9900
C14-H14B	0.9900	C15-C16	1.382(5)
C15-C20	1.395(5)	C16-C17	1.394(6)
C16-H16	0.9500	C17-C18	1.378(6)
C17-H17	0.9500	C18-C19	1.378(6)
C18-H18	0.9500	C19-C20	1.384(5)
C19-H19	0.9500	C20-H20	0.9500
C21-C35	1.511(5)	C21-H21	1.0000
C22-C30	1.393(5)	C23-C24	1.409(5)
C23-C28	1.411(5)	C24-C25	1.379(5)
C24-H24	0.9500	C25-C26	1.387(6)
C25-H25A	0.9500	C26-C27	1.374(6)
C26-H26	0.9500	C27-C28	1.413(5)
C27-H27	0.9500	C28-C29	1.468(5)
C29-C30	1.409(5)	C30-H30	0.9500
C31-C32	1.534(6)	C31-H31A	0.9900
C31-H31B	0.9900	C32-C33	1.492(7)
C32-H32A	0.9900	C32-H32B	0.9900
C33-C34	1.520(5)	C33-H33A	0.9900

C33-H33B	0.9900	C34-H34A	0.9900
C34-H34B	0.9900	C35-C40	1.387(5)
C35-C36	1.397(5)	C36-C37	1.376(6)
C36-H36	0.9500	C37-C38	1.375(7)
C37-H37A	0.9500	C38-C39	1.389(6)
C38-H38	0.9500	C39-C40	1.391(6)
C39-H39	0.9500	C40-H40	0.9500
C41-C52	1.522(6)	C41-C42	1.531(5)
C41-C45	1.535(6)	C41-C46	1.560(5)
C42-C43	1.528(9)	C42-H42A	0.9900
C42-H42B	0.9900	C43-C44	1.287(9)
C43-H43	0.9500	C44-C45	1.491(7)
C44-H44	0.9500	C45-H45A	0.9900
C45-H45B	0.9900	C47-C48	1.372(9)
C47-C52	1.399(7)	C47-H47	0.9500
C48-C49	1.344(11)	C48-H48	0.9500
C49-C50	1.383(12)	C49-H49	0.9500
C50-C51	1.431(9)	C50-H50	0.9500
C51-C52	1.382(7)	C51-H51	0.9500
Cl1S-C1S	1.57(2)	C1S-Cl2S	1.592(19)
C1S-H1S1	0.9900	C1S-H1S2	0.9900

C2-N1-C1	119.8(3)	C2-N1-H1N	119(2)
C1-N1-H1N	117(2)	C2-N2-C3	116.1(3)
C9-N3-C11	119.6(3)	C9-N3-C14	124.5(3)
C11-N3-C14	110.2(3)	C22-N4-C21	123.1(3)
C22-N4-H4N	119(2)	C21-N4-H4N	117(2)
C22-N5-C23	121.5(3)	C22-N5-H5N	121(2)
C23-N5-H5N	118(2)	C29-N6-C34	120.8(3)
C29-N6-C31	128.7(3)	C34-N6-C31	110.3(3)
N1-C1-C15	113.3(3)	N1-C1-C21	112.1(3)
C15-C1-C21	109.6(3)	N1-C1-H1	107.2
C15-C1-H1	107.2	C21-C1-H1	107.2
N2-C2-N1	118.6(3)	N2-C2-C10	124.4(3)
N1-C2-C10	117.1(3)	N2-C3-C4	116.5(3)
N2-C3-C8	124.6(3)	C4-C3-C8	118.9(3)
C5-C4-C3	121.4(3)	C5-C4-H4	119.3
C3-C4-H4	119.3	C4-C5-C6	119.8(3)
C4-C5-H5	120.1	C6-C5-H5	120.1
C7-C6-C5	120.3(3)	C7-C6-H6	119.9
C5-C6-H6	119.9	C6-C7-C8	121.6(3)
C6-C7-H7	119.2	C8-C7-H7	119.2
C7-C8-C3	118.0(3)	C7-C8-C9	124.9(3)

C3-C8-C9	116.9(3)	N3-C9-C10	119.6(3)
N3-C9-C8	123.1(3)	C10-C9-C8	117.2(3)
C9-C10-C2	119.7(3)	C9-C10-H10	120.1
C2-C10-H10	120.1	N3-C11-C12	104.1(3)
N3-C11-H11A	110.9	C12-C11-H11A	110.9
N3-C11-H11B	110.9	C12-C11-H11B	110.9
H11A-C11-H11B	109.0	C13-C12-C11	102.1(3)
C13-C12-H12A	111.3	C11-C12-H12A	111.3
C13-C12-H12B	111.3	C11-C12-H12B	111.3
H12A-C12-H12B	109.2	C12-C13-C14	103.6(3)
C12-C13-H13A	111.0	C14-C13-H13A	111.0
C12-C13-H13B	111.0	C14-C13-H13B	111.0
H13A-C13-H13B	109.0	N3-C14-C13	103.8(3)
N3-C14-H14A	111.0	C13-C14-H14A	111.0
N3-C14-H14B	111.0	C13-C14-H14B	111.0
H14A-C14-H14B	109.0	C16-C15-C20	117.8(3)
C16-C15-C1	124.0(3)	C20-C15-C1	118.1(3)
C15-C16-C17	120.5(4)	C15-C16-H16	119.7
C17-C16-H16	119.7	C18-C17-C16	120.8(4)
C18-C17-H17	119.6	C16-C17-H17	119.6
C17-C18-C19	119.5(4)	C17-C18-H18	120.3
C19-C18-H18	120.3	C18-C19-C20	119.6(4)
C18-C19-H19	120.2	C20-C19-H19	120.2
C19-C20-C15	121.7(3)	C19-C20-H20	119.1
C15-C20-H20	119.1	N4-C21-C35	113.2(3)
N4-C21-C1	109.9(3)	C35-C21-C1	114.6(3)
N4-C21-H21	106.1	C35-C21-H21	106.1
C1-C21-H21	106.1	N5-C22-N4	116.5(3)
N5-C22-C30	119.8(3)	N4-C22-C30	123.7(3)
N5-C23-C24	116.6(3)	N5-C23-C28	121.6(3)
C24-C23-C28	121.7(3)	C25-C24-C23	119.4(4)
C25-C24-H24	120.3	C23-C24-H24	120.3
C24-C25-C26	119.9(4)	C24-C25-H25A	120.1
C26-C25-H25A	120.1	C27-C26-C25	120.9(3)
C27-C26-H26	119.5	C25-C26-H26	119.5
C26-C27-C28	121.7(4)	C26-C27-H27	119.2
C28-C27-H27	119.2	C23-C28-C27	116.3(3)
C23-C28-C29	117.6(3)	C27-C28-C29	125.9(3)
N6-C29-C30	118.7(3)	N6-C29-C28	124.6(3)
C30-C29-C28	116.6(3)	C22-C30-C29	122.5(3)
C22-C30-H30	118.8	C29-C30-H30	118.8
N6-C31-C32	102.9(3)	N6-C31-H31A	111.2
C32-C31-H31A	111.2	N6-C31-H31B	111.2

C32-C31-H31B	111.2	H31A-C31-H31B	109.1
C33-C32-C31	103.5(4)	C33-C32-H32A	111.1
C31-C32-H32A	111.1	C33-C32-H32B	111.1
C31-C32-H32B	111.1	H32A-C32-H32B	109.0
C32-C33-C34	103.3(3)	C32-C33-H33A	111.1
C34-C33-H33A	111.1	C32-C33-H33B	111.1
C34-C33-H33B	111.1	H33A-C33-H33B	109.1
N6-C34-C33	104.3(3)	N6-C34-H34A	110.9
C33-C34-H34A	110.9	N6-C34-H34B	110.9
C33-C34-H34B	110.9	H34A-C34-H34B	108.9
C40-C35-C36	118.5(4)	C40-C35-C21	121.9(3)
C36-C35-C21	119.6(3)	C37-C36-C35	120.3(4)
C37-C36-H36	119.8	C35-C36-H36	119.8
C38-C37-C36	121.5(4)	C38-C37-H37A	119.3
C36-C37-H37A	119.3	C37-C38-C39	118.7(4)
C37-C38-H38	120.6	C39-C38-H38	120.6
C38-C39-C40	120.3(4)	C38-C39-H39	119.8
C40-C39-H39	119.8	C35-C40-C39	120.6(4)
C35-C40-H40	119.7	C39-C40-H40	119.7
C52-C41-C42	115.0(4)	C52-C41-C45	114.6(3)
C42-C41-C45	103.4(3)	C52-C41-C46	105.0(3)
C42-C41-C46	109.5(3)	C45-C41-C46	109.3(3)
C43-C42-C41	100.9(4)	C43-C42-H42A	111.6
C41-C42-H42A	111.6	C43-C42-H42B	111.6
C41-C42-H42B	111.6	H42A-C42-H42B	109.4
C44-C43-C42	111.8(4)	C44-C43-H43	124.1
C42-C43-H43	124.1	C43-C44-C45	111.7(5)
C43-C44-H44	124.2	C45-C44-H44	124.2
C44-C45-C41	102.5(4)	C44-C45-H45A	111.3
C41-C45-H45A	111.3	C44-C45-H45B	111.3
C41-C45-H45B	111.3	H45A-C45-H45B	109.2
O2-C46-O1	124.9(3)	O2-C46-C41	117.2(3)
O1-C46-C41	118.0(3)	C48-C47-C52	121.4(6)
C48-C47-H47	119.3	C52-C47-H47	119.3
C49-C48-C47	120.7(7)	C49-C48-H48	119.6
C47-C48-H48	119.6	C48-C49-C50	120.9(7)
C48-C49-H49	119.6	C50-C49-H49	119.6
C49-C50-C51	118.9(7)	C49-C50-H50	120.6
C51-C50-H50	120.6	C52-C51-C50	119.9(6)
C52-C51-H51	120.0	C50-C51-H51	120.0
C51-C52-C47	118.1(5)	C51-C52-C41	120.2(4)
C47-C52-C41	121.7(4)	Cl1S-C1S-Cl2S	129(2)
Cl1S-C1S-H1S1	105.1	Cl2S-C1S-H1S1	105.1

Cl1S-C1S-H1S2	105.1	Cl2S-C1S-H1S2	105.1
H1S1-C1S-H1S2	105.9		

Table 4. Anisotropic displacement parameters ($Å^2 \times 10^3$) for 15113. The anisotropic displacement factor exponent takes the form: $-2\pi^2[h^2 a^{*2} U^{11} + ... + 2 h k a^* b^* U^{12}]$

	U^{11}	U^{22}	U^{33}	U^{23}	U^{13}	U^{12}
O1	34(1)	42(2)	25(1)	11(1)	9(1)	9(1)
O2	37(1)	52(2)	27(1)	8(1)	15(1)	18(1)
N1	20(1)	24(2)	26(2)	7(1)	9(1)	5(1)
N2	20(1)	27(2)	28(2)	5(1)	8(1)	2(1)
N3	21(1)	30(2)	24(2)	4(1)	9(1)	2(1)
N4	22(1)	34(2)	22(2)	4(1)	12(1)	7(1)
N5	21(1)	27(2)	22(2)	-1(1)	7(1)	5(1)
N6	24(1)	28(2)	29(2)	-4(1)	9(1)	2(1)
C1	17(2)	26(2)	24(2)	4(2)	8(1)	6(1)
C2	18(1)	18(2)	24(2)	-1(1)	5(1)	0(1)
C3	22(2)	20(2)	28(2)	0(2)	7(1)	1(1)
C4	25(2)	29(2)	35(2)	7(2)	13(2)	2(2)
C5	31(2)	31(2)	32(2)	9(2)	6(2)	6(2)
C6	21(2)	29(2)	37(2)	6(2)	4(2)	6(1)
C7	20(2)	25(2)	31(2)	1(2)	10(1)	0(1)
C8	22(2)	19(2)	27(2)	1(2)	6(1)	0(1)
C9	22(2)	18(2)	23(2)	0(1)	5(1)	1(1)
C10	21(2)	22(2)	24(2)	4(2)	5(1)	2(1)
C11	28(2)	35(2)	23(2)	5(2)	6(1)	-2(2)
C12	36(2)	47(3)	27(2)	3(2)	13(2)	1(2)
C13	38(2)	55(3)	32(2)	-5(2)	18(2)	5(2)
C14	30(2)	34(2)	29(2)	0(2)	13(2)	2(2)
C15	19(2)	25(2)	29(2)	2(2)	9(1)	7(1)
C16	50(2)	30(2)	34(2)	-3(2)	20(2)	-6(2)
C17	64(3)	47(3)	33(2)	-1(2)	17(2)	-2(2)
C18	42(2)	32(2)	38(2)	-6(2)	3(2)	0(2)
C19	24(2)	26(2)	42(2)	6(2)	3(2)	2(1)
C20	23(2)	28(2)	27(2)	4(2)	7(1)	6(1)
C21	18(2)	26(2)	25(2)	6(2)	8(1)	4(1)
C22	20(2)	24(2)	22(2)	-4(2)	3(1)	3(1)
C23	20(2)	24(2)	27(2)	-6(2)	4(1)	3(1)
C24	25(2)	33(2)	26(2)	0(2)	7(1)	5(1)
C25	33(2)	30(2)	34(2)	5(2)	3(2)	6(2)
C26	28(2)	30(2)	45(2)	-2(2)	5(2)	10(2)
C27	21(2)	31(2)	37(2)	-5(2)	8(2)	5(1)
C28	20(2)	24(2)	28(2)	-9(2)	2(1)	1(1)
C29	20(2)	24(2)	23(2)	-8(2)	5(1)	-1(1)

C30	23(2)	26(2)	20(2)	-1(2)	6(1)	4(1)

C31	25(2)	51(3)	38(2)	-3(2)	15(2)	8(2)
C32	38(2)	68(4)	48(3)	0(2)	24(2)	4(2)
C33	45(2)	58(3)	37(2)	3(2)	23(2)	4(2)
C34	31(2)	35(2)	29(2)	0(2)	11(2)	0(2)
C35	22(2)	27(2)	25(2)	4(2)	6(1)	9(1)
C36	44(2)	37(2)	30(2)	5(2)	15(2)	1(2)
C37	57(3)	51(3)	25(2)	1(2)	10(2)	2(2)
C38	46(2)	47(3)	35(2)	-14(2)	6(2)	12(2)
C39	37(2)	31(2)	47(3)	-2(2)	8(2)	5(2)
C40	29(2)	30(2)	31(2)	4(2)	4(2)	6(2)
C41	28(2)	37(2)	21(2)	3(2)	10(1)	5(2)
C42	30(2)	100(4)	36(2)	19(3)	10(2)	5(2)
C43	64(4)	138(7)	41(3)	14(4)	-3(3)	-55(4)
C44	99(4)	63(4)	37(3)	5(3)	2(3)	-46(3)
C45	50(2)	38(3)	27(2)	9(2)	10(2)	0(2)
C46	26(2)	34(2)	18(2)	2(2)	6(1)	2(2)
C47	114(5)	41(3)	33(3)	8(2)	33(3)	16(3)
C48	195(9)	39(4)	48(4)	-6(3)	61(5)	-5(5)
C49	184(9)	65(5)	58(4)	-11(4)	50(5)	-55(6)
C50	102(5)	121(7)	39(3)	-2(4)	13(3)	-59(5)
C51	55(3)	65(3)	36(2)	2(2)	9(2)	-22(2)
C52	54(2)	41(3)	21(2)	3(2)	18(2)	2(2)

Table 5. Hydrogen coordinates (× 10^4) and isotropic displacement parameters ($Å^2$ × 10^3) for 15113.

	x	y	z	U(eq)
H1N	8160(30)	4900(20)	3610(30)	16(9)
H4N	6300(30)	5290(20)	3570(30)	10(8)
H5N	4860(40)	6180(30)	2760(30)	30(11)
H1	7864	3653	5013	26
H4	11049	2633	6247	35
H5	13114	2289	6671	37
H6	14511	2767	5677	35
H7	13834	3569	4267	30
H10	10006	4895	3003	26
H11A	11489	5521	2184	34
H11B	10791	4671	1668	34
H12A	12085	4962	567	43
H12B	13166	5313	1422	43
H13A	13805	3894	1183	48
H13B	12422	3518	1057	48
H14A	13053	3200	2689	36
H14B	13981	4022	2856	36
H16	7357	3817	2440	43
H17	6248	2822	1342	57
H18	4990	1781	1896	45
H19	4851	1723	3569	37
H20	5988	2692	4670	31
H21	5849	4205	4986	27
H24	3530	7174	1921	33
H25A	1859	8120	1861	39
H26	723	8119	3140	41
H27	1164	7144	4432	35
H30	4475	5127	5349	27
H31A	581	5978	5000	44
H31B	1142	6658	5858	44
H32A	221	5678	6780	59
H32B	487	4858	6111	59
H33A	2012	4714	7463	54
H33B	2236	5756	7545	54
H34A	3760	5403	6685	37
H34B	3002	4586	6145	37
H36	6412	4243	6692	43
H37A	7089	5031	8118	53

H38	8036	6384	8063	51
H39	8374	6929	6538	46
H40	7699	6142	5091	36
H42A	8788	5647	1604	66
H42B	8834	5735	440	66
H43	9550	7178	1473	99
H44	7895	8064	746	81
H45A	6760	6870	-449	46
H45B	6024	7154	417	46
H47	7894	4378	501	73
H48	6965	3212	-401	107
H49	5010	3327	-1263	119
H50	3887	4617	-1219	105
H51	4842	5844	-319	62
H1S1	1277	6942	8096	157
H1S2	175	6510	8518	157

Table 6. Torsion angles [°] for 15113.

C2-N1-C1-C15	-86.9(4)	C2-N1-C1-C21	148.5(3)
C3-N2-C2-N1	-173.1(3)	C3-N2-C2-C10	7.1(5)
C1-N1-C2-N2	-25.2(5)	C1-N1-C2-C10	154.6(3)
C2-N2-C3-C4	171.0(3)	C2-N2-C3-C8	-6.3(5)
N2-C3-C4-C5	-174.1(4)	C8-C3-C4-C5	3.3(6)
C3-C4-C5-C6	-1.3(6)	C4-C5-C6-C7	-0.7(6)
C5-C6-C7-C8	0.6(6)	C6-C7-C8-C3	1.5(5)
C6-C7-C8-C9	176.9(4)	N2-C3-C8-C7	173.9(3)
C4-C3-C8-C7	-3.3(5)	N2-C3-C8-C9	-1.9(5)
C4-C3-C8-C9	-179.1(3)	C11-N3-C9-C10	-2.0(5)
C14-N3-C9-C10	-152.7(3)	C11-N3-C9-C8	179.3(3)
C14-N3-C9-C8	28.5(5)	C7-C8-C9-N3	12.6(5)
C3-C8-C9-N3	-172.0(3)	C7-C8-C9-C10	-166.2(3)
C3-C8-C9-C10	9.3(5)	N3-C9-C10-C2	172.4(3)
C8-C9-C10-C2	-8.7(5)	N2-C2-C10-C9	0.4(5)
N1-C2-C10-C9	-179.4(3)	C9-N3-C11-C12	-170.4(3)
C14-N3-C11-C12	-15.8(4)	N3-C11-C12-C13	34.4(4)
C11-C12-C13-C14	-40.3(4)	C9-N3-C14-C13	143.9(3)
C11-N3-C14-C13	-9.2(4)	C12-C13-C14-N3	30.8(4)
N1-C1-C15-C16	-15.2(5)	C21-C1-C15-C16	110.8(4)
N1-C1-C15-C20	167.3(3)	C21-C1-C15-C20	-66.8(4)
C20-C15-C16-C17	-0.2(6)	C1-C15-C16-C17	-177.7(4)
C15-C16-C17-C18	0.6(7)	C16-C17-C18-C19	-0.3(7)
C17-C18-C19-C20	-0.4(6)	C18-C19-C20-C15	0.9(5)
C16-C15-C20-C19	-0.6(5)	C1-C15-C20-C19	177.1(3)
C22-N4-C21-C35	-66.8(4)	C22-N4-C21-C1	163.6(3)
N1-C1-C21-N4	61.1(4)	C15-C1-C21-N4	-65.5(4)
N1-C1-C21-C35	-67.7(4)	C15-C1-C21-C35	165.6(3)
C23-N5-C22-N4	-177.7(3)	C23-N5-C22-C30	3.6(5)
C21-N4-C22-N5	176.4(3)	C21-N4-C22-C30	-4.9(5)
C22-N5-C23-C24	175.0(3)	C22-N5-C23-C28	-3.5(5)
N5-C23-C24-C25	-175.0(3)	C28-C23-C24-C25	3.4(5)
C23-C24-C25-C26	0.1(6)	C24-C25-C26-C27	-2.1(6)
C25-C26-C27-C28	0.5(6)	N5-C23-C28-C27	173.6(3)
C24-C23-C28-C27	-4.8(5)	N5-C23-C28-C29	-1.1(5)
C24-C23-C28-C29	-179.5(3)	C26-C27-C28-C23	2.8(5)
C26-C27-C28-C29	177.1(3)	C34-N6-C29-C30	3.0(5)
C31-N6-C29-C30	-171.1(4)	C34-N6-C29-C28	-174.5(3)
C31-N6-C29-C28	11.3(6)	C23-C28-C29-N6	-177.1(3)
C27-C28-C29-N6	8.7(5)	C23-C28-C29-C30	5.3(4)
C27-C28-C29-C30	-168.9(3)	N5-C22-C30-C29	1.0(5)

N4-C22-C30-C29	-177.6(3)	N6-C29-C30-C22	176.8(3)
C28-C29-C30-C22	-5.4(5)	C29-N6-C31-C32	160.3(4)
C34-N6-C31-C32	-14.4(4)	N6-C31-C32-C33	33.5(4)
C31-C32-C33-C34	-39.9(5)	C29-N6-C34-C33	175.0(3)
C31-N6-C34-C33	-9.9(4)	C32-C33-C34-N6	30.9(5)
N4-C21-C35-C40	-41.2(4)	C1-C21-C35-C40	85.9(4)
N4-C21-C35-C36	135.7(3)	C1-C21-C35-C36	-97.1(4)
C40-C35-C36-C37	-0.3(6)	C21-C35-C36-C37	-177.3(4)
C35-C36-C37-C38	0.7(6)	C36-C37-C38-C39	-1.1(7)
C37-C38-C39-C40	1.1(6)	C36-C35-C40-C39	0.2(5)
C21-C35-C40-C39	177.2(3)	C38-C39-C40-C35	-0.7(6)
C52-C41-C42-C43	154.9(4)	C45-C41-C42-C43	29.2(4)
C46-C41-C42-C43	-87.3(4)	C41-C42-C43-C44	-19.5(6)
C42-C43-C44-C45	0.5(7)	C43-C44-C45-C41	18.7(6)
C52-C41-C45-C44	-155.4(4)	C42-C41-C45-C44	-29.5(5)
C46-C41-C45-C44	87.1(4)	C52-C41-C46-O2	-86.3(4)
C42-C41-C46-O2	149.7(4)	C45-C41-C46-O2	37.1(5)
C52-C41-C46-O1	91.5(4)	C42-C41-C46-O1	-32.4(5)
C45-C41-C46-O1	-145.1(3)	C52-C47-C48-C49	-0.9(8)
C47-C48-C49-C50	-0.9(10)	C48-C49-C50-C51	1.6(10)
C49-C50-C51-C52	-0.6(8)	C50-C51-C52-C47	-1.1(6)
C50-C51-C52-C41	-178.6(4)	C48-C47-C52-C51	1.8(7)
C48-C47-C52-C41	179.3(4)	C42-C41-C52-C51	-160.3(4)
C45-C41-C52-C51	-40.7(5)	C46-C41-C52-C51	79.3(4)
C42-C41-C52-C47	22.3(5)	C45-C41-C52-C47	141.9(4)
C46-C41-C52-C47	-98.1(4)		

Table 7. Hydrogen bonds for 15113 [Å and °].

D-H...A	d(D-H)	d(H...A)	d(D...A)	<(DHA)
N1-H1N...O1	0.89(4)	2.04(4)	2.905(4)	163(3)
N4-H4N...O1	0.85(4)	1.97(4)	2.812(4)	175(3)
N5-H5N...O2	0.94(4)	1.71(4)	2.647(4)	174(4)
C11-H11B...Cl1S#1	0.99	2.94	3.665(11)	130.9
C12-H12A...Cl2S#2	0.99	2.86	3.523(8)	125.2
C24-H24...O2	0.95	2.60	3.298(4)	130.8
C32-H32B...N2#3	0.99	2.57	3.526(6)	161.7

Symmetry transformations used to generate equivalent atoms: #1 -x+1,y-1/2,-z+1 #2 x+1,y,z-1#3 x-1,y,z

INDIANA UNIVERSITY DEPARTMENT OF CHEMISTRY

Molecular Structure Center

Report No. 16066

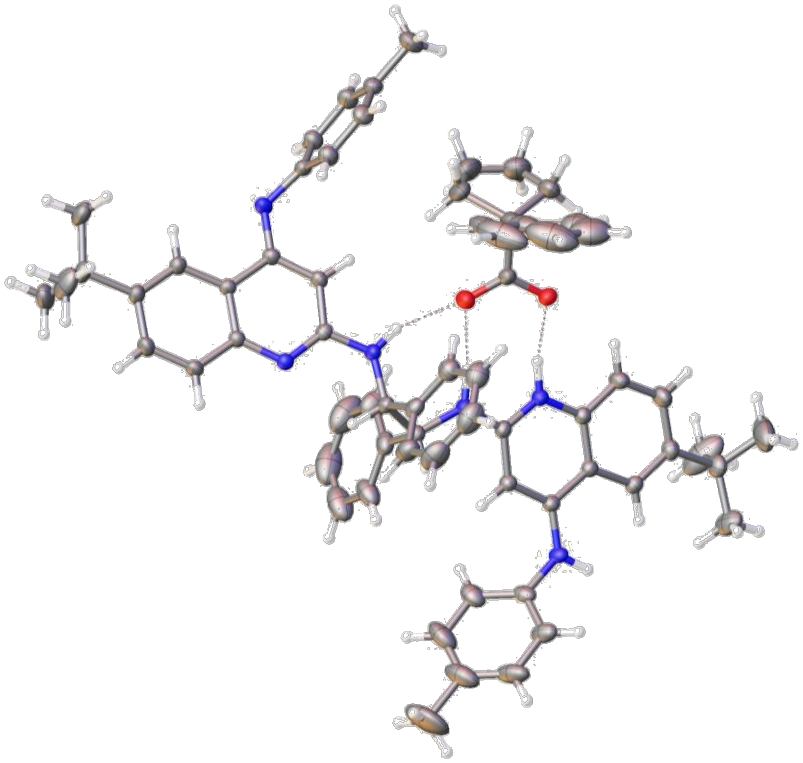

$[C_{54}H_{56}N_6][C_{12}H_{13}O_2] \cdot 2\ C_7H_{16}$

Prepared for
Matthew Knowe and Professor Jeffrey N. Johnston

by M. Pink

July 27, 2016

E 3: X-ray cocrystal structure of 126d • 107a.

The sample was submitted by Matthew Knowe (research group of J. Johnston, Department of Chemistry, Vanderbilt University). A colorless crystal (approximate dimensions 0.19 × 0.15 × 0.12 mm^3) was placed onto the tip of a 0.05 mm diameter glass capillary and mounted on a Bruker APEX II Kappa Duo diffractometer equipped with an APEX II detector at 150(2) K.

Data collection

The data collection was carried out using Mo Kα radiation (graphite monochromator) with a frame time of 20 seconds and a detector distance of 4.00 cm. A collection strategy was calculated and complete data to a resolution of 0.70 Å with a redundancy of 4 were collected. Six major sections of frames were collected with 0.50º ω and ϕ scans. The total exposure time was 11.18 hours. The frames were integrated with the Bruker SAINT software package[1] using a narrow-frame algorithm. The integration of the data using an orthorhombic unit cell yielded a total of 139860 reflections to a maximum θ angle of 30.09° (0.71 Å resolution), of which 20232 were independent (average redundancy 6.913, completeness = 99.8%, R_{int} = 4.99%, R_{sig} = 3.34%) and 16070 (79.43%) were greater than $2\sigma(F^2)$. The final cell constants of a = 18.4334(12) Å, b = 18.4544(11) Å, c = 20.2984(14) Å, volume = 6905.1(8) $Å^3$, are based upon the refinement of the XYZ-centroids of 9926 reflections above 20 σ(I) with 4.581° < 2θ < 54.54°. Data were corrected for absorption effects using the multi-scan method (SADABS).[2] The ratio of minimum to maximum apparent transmission was 0.890. The calculated minimum and maximum transmission coefficients (based on crystal size) are 0.6640 and 0.7460.

Structure solution and refinement

The space group $P2_12_12_1$ was determined based on intensity statistics and systematic absences. The structure was solved and refined using the SHELX suite of programs.[3] An intrinsic-methods solution was calculated, which provided most non-hydrogen atoms from the E-map. Full-matrix least squares / difference Fourier cycles were performed, which located the remaining non-hydrogen atoms. All non-hydrogen atoms were refined with anisotropic displacement parameters. Disorder was refined for co-crystallized solvent (heptane). The final anisotropic full-matrix least-squares refinement on F^2 with 861 variables converged at R1 = 6.01%, for the observed data and wR2 = 18.17% for all data. The goodness-of-fit was 1.020. The largest peak in the final difference electron density synthesis was 0.549 $e^-/Å^3$ and the largest hole was -0.352 $e^-/Å^3$ with an RMS deviation of 0.053 $e^-/Å^3$. On the basis of the final model, the calculated density was 1.134 g/cm^3 and F(000), 2556 e^-.

7 SAINT, Bruker Analytical X-Ray Systems, Madison, WI, current version.
8 SADABS, Bruker Analytical X-Ray Systems, Madison, WI, current version.
9 A short history of *SHELX*, G. M. Sheldrick, *Acta Cryst*. A64, 112 - 122 (2008).

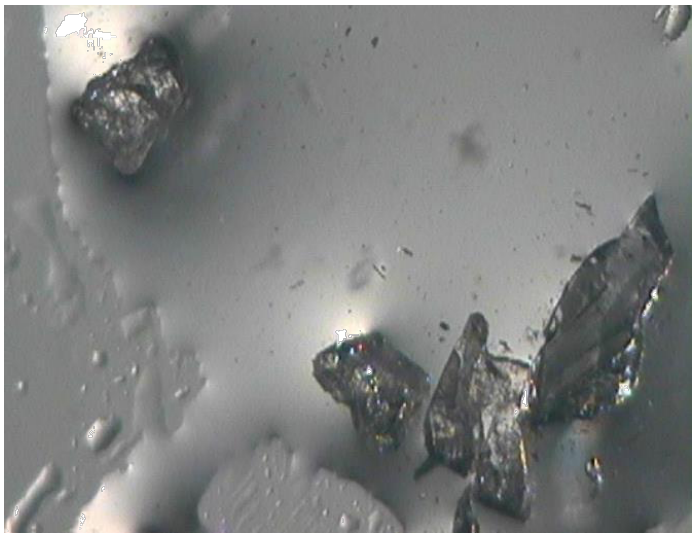

Bulk material.

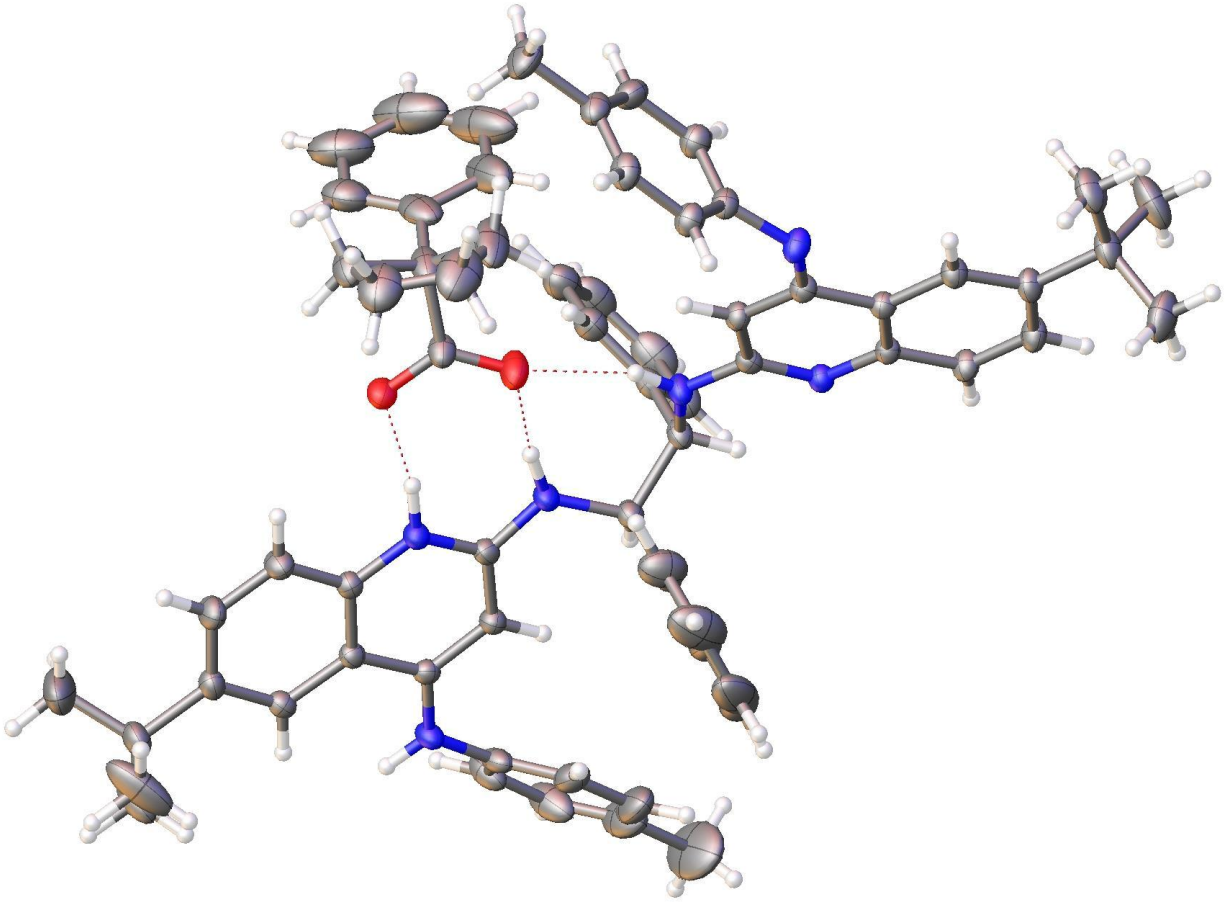

Formula unit, solvent omitted.

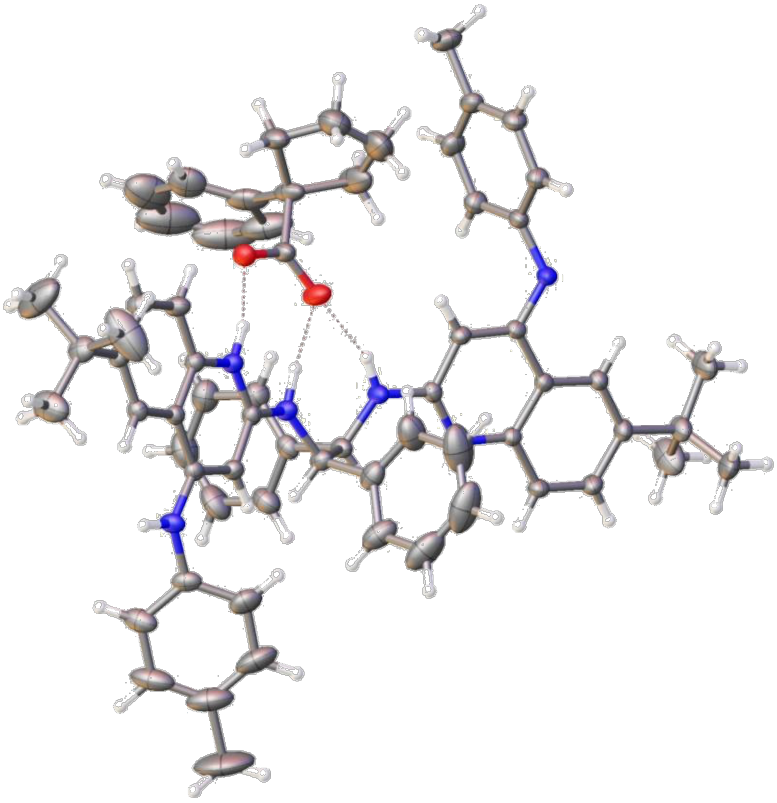

Formula unit, solvent omitted.

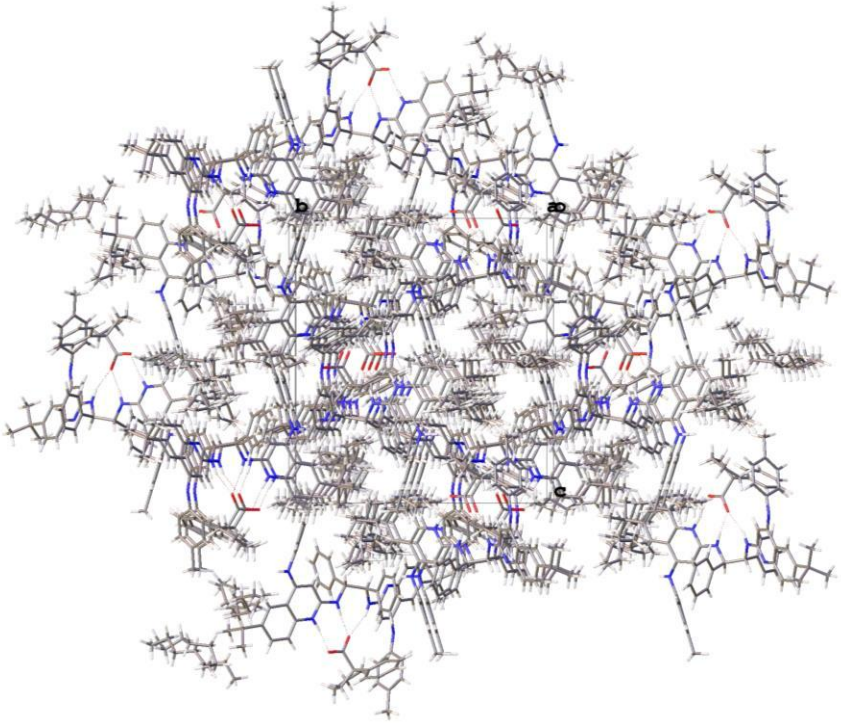

Cell plot, view along *a*.

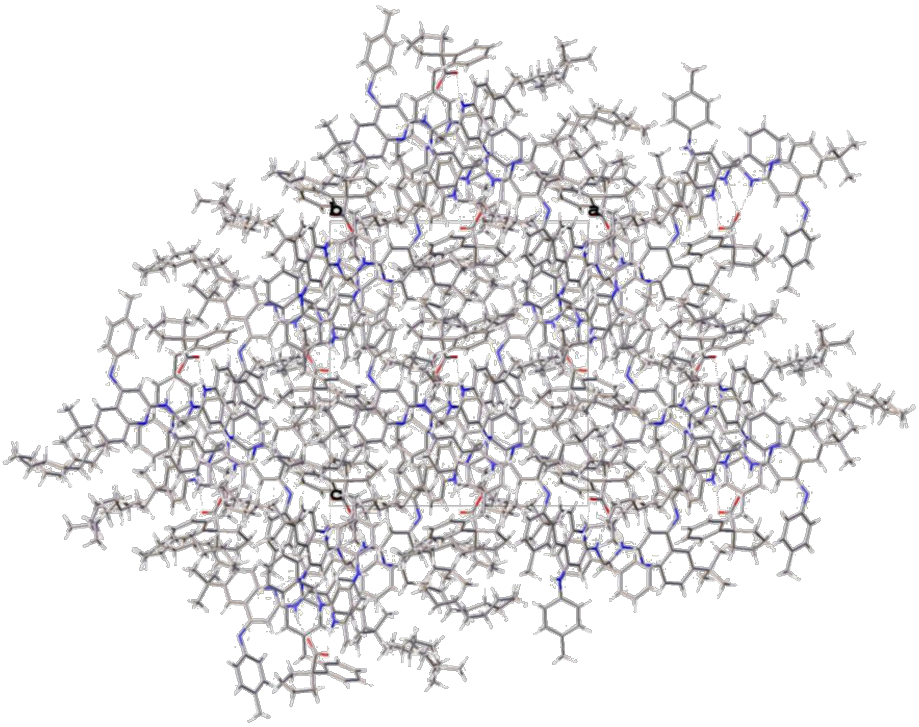

Cell plot, view along *b*.

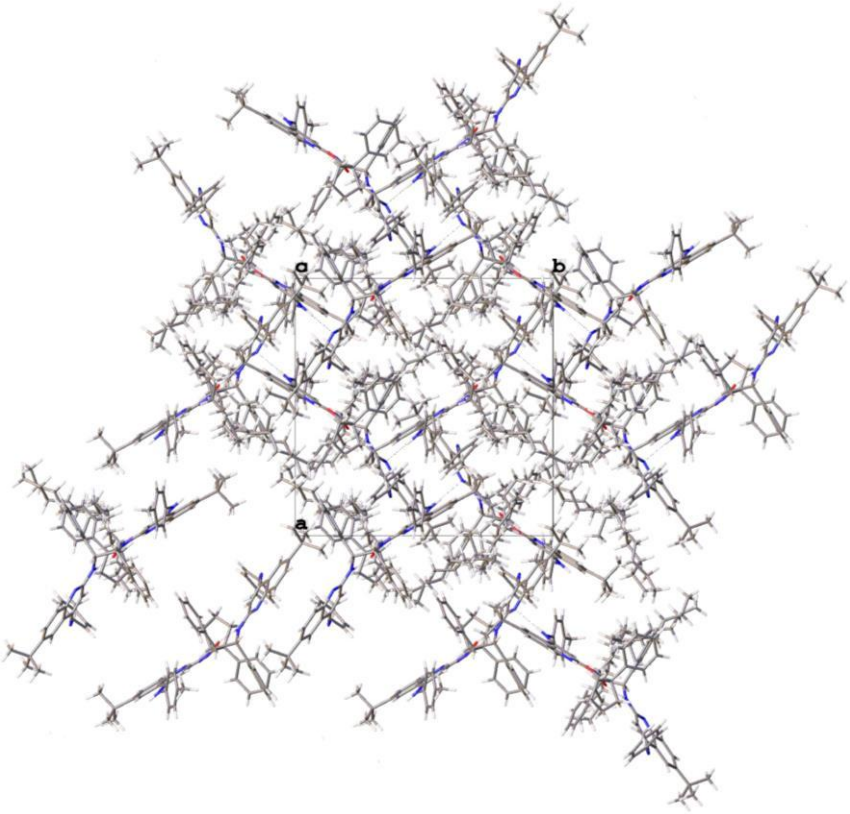

Cell plot, view along *c*.

Table 1. Crystal data and structure refinement for 16066.

Empirical formula	C80 H101 N6 O2	
Formula weight	1178.66	
Crystal color, shape, size	colorless block, 0.19 × 0.15 × 0.12 mm^3	
Temperature	150(2) K	
Wavelength	0.71073 Å	
Crystal system, space group	Orthorhombic, $P2_12_12_1$	
Unit cell dimensions	a = 18.4334(12) Å	α= 90°.
	b = 18.4544(11) Å	β= 90°.
	c = 20.2984(14) Å	γ = 90°.
Volume	6905.1(8) $Å^3$	
Z	4	
Density (calculated)	1.134 Mg/m^3	
Absorption coefficient	0.068 mm^{-1}	
F(000)	2556	

Data collection

Diffractometer	APEX II Kappa Duo, Bruker
Theta range for data collection	1.491 to 30.091°.
Index ranges	-25<=h<=25, -26<=k<=25, -28<=l<=28
Reflections collected	139860
Independent reflections	20232 [R_{int} = 0.0499]
Observed Reflections	16070
Completeness to theta = 25.242°	100.0 %

Solution and Refinement

Absorption correction	Semi-empirical from equivalents
Max. and min. transmission	0.7460 and 0.6640
Solution	Intrinsic methods
Refinement method	Full-matrix least-squares on F^2
Weighting scheme	$w = [\sigma^2 Fo^2 + AP^2 + BP]^{-1}$, with $P = (Fo^2 + 2\,Fc^2)/3$, A = 0.1128, B = 1.3497
Data / restraints / parameters	20232 / 278 / 861
Goodness-of-fit on F^2	1.020
Final R indices [I>2sigma(I)]	R1 = 0.0601, wR2 = 0.1642
R indices (all data)	R1 = 0.0808, wR2 = 0.1817
Absolute structure parameter	0.3(3)
Largest diff. peak and hole	0.549 and -0.352 e.$Å^{-3}$

Goodness-of-fit = $[\Sigma[w(F_o^2 - F_c^2)^2]/N_{observns} - N_{params})]^{1/2}$, all data.
$R1 = \Sigma(|F_o| - |F_c|) / \Sigma |F_o|$. $wR2 = [\Sigma[w(F_o^2 - F_c^2)^2] / \Sigma [w(F_o^2)^2]]^{1/2}$.

Table 2. Atomic coordinates (× 10^4) and equivalent isotropic displacement parameters (Å^2 × 10^3) for 16066. U(eq) is defined as one third of the trace of the orthogonalized U^{ij} tensor.

	x	y	z	U(eq)
N1	4693(1)	6597(1)	6510(1)	27(1)
N2	5178(1)	5653(1)	5928(1)	25(1)
N3	6095(1)	4737(1)	7595(1)	27(1)
N4	3662(1)	7818(1)	6456(1)	26(1)
N5	2865(1)	8516(1)	7086(1)	22(1)
N6	1505(1)	8702(1)	5415(1)	29(1)
C1	4380(1)	6916(1)	7104(1)	28(1)
C2	5065(1)	5969(1)	6517(1)	23(1)
C3	5574(1)	5024(1)	5866(1)	24(1)
C4	5670(2)	4728(2)	5238(1)	32(1)
C5	6050(2)	4098(2)	5159(1)	36(1)
C6	6355(1)	3728(1)	5702(1)	28(1)
C7	6259(1)	4025(1)	6323(1)	24(1)
C8	5872(1)	4678(1)	6419(1)	22(1)
C9	5770(1)	5023(1)	7055(1)	22(1)
C10	5351(1)	5648(1)	7092(1)	24(1)
C11	3751(2)	6468(2)	7359(2)	37(1)
C12	3750(2)	6247(2)	8017(2)	50(1)
C13	3188(3)	5830(2)	8269(2)	70(1)
C14	2620(3)	5631(2)	7862(3)	83(2)
C15	2619(2)	5837(3)	7209(3)	82(2)
C16	3186(2)	6254(2)	6954(2)	56(1)
C17	6736(2)	2999(2)	5589(2)	39(1)
C18	7170(4)	2993(3)	4964(3)	94(2)
C19	6127(3)	2425(2)	5512(4)	97(2)
C20	7192(2)	2761(2)	6168(2)	59(1)
C21	6046(2)	5004(1)	8249(1)	32(1)
C22	6685(2)	5121(2)	8600(2)	43(1)
C23	6655(3)	5332(2)	9257(2)	60(1)
C24	6004(3)	5445(2)	9565(2)	68(1)
C25	5365(3)	5338(2)	9209(2)	63(1)
C26	5377(2)	5105(2)	8557(2)	43(1)
C27	5962(5)	5683(4)	10284(2)	117(3)
C28	4187(1)	7729(1)	6985(1)	26(1)
C29	3040(1)	8220(1)	6511(1)	22(1)
C30	2215(1)	8887(1)	7110(1)	21(1)
C31	2012(1)	9224(1)	7706(1)	26(1)
C32	1395(1)	9644(2)	7746(1)	29(1)

C33	939(1)	9766(1)	7198(1)	28(1)
C34	1122(1)	9418(1)	6620(1)	25(1)
C35	1744(1)	8970(1)	6566(1)	22(1)
C36	1959(1)	8638(1)	5952(1)	23(1)
C37	2607(1)	8274(1)	5935(1)	23(1)
C38	4875(1)	8168(1)	6884(1)	30(1)
C39	5246(2)	8438(2)	7434(2)	42(1)
C40	5893(2)	8815(2)	7364(2)	56(1)
C41	6186(2)	8927(2)	6743(2)	55(1)
C42	5824(2)	8673(2)	6192(2)	46(1)
C43	5171(2)	8302(2)	6266(2)	36(1)
C44	285(2)	10276(2)	7265(1)	37(1)
C45	-97(2)	10400(2)	6608(2)	48(1)
C46	-262(2)	9942(3)	7746(2)	54(1)
C47	539(2)	11004(2)	7537(2)	61(1)
C48	1739(1)	8607(1)	4750(1)	26(1)
C49	2269(2)	9063(2)	4494(1)	32(1)
C50	2442(2)	9024(2)	3827(1)	35(1)
C51	2101(2)	8539(2)	3411(1)	34(1)
C52	1575(2)	8083(2)	3675(1)	34(1)
C53	1398(1)	8110(2)	4344(1)	30(1)
C54	2296(2)	8495(2)	2690(2)	51(1)
O1	4165(1)	7041(1)	5289(1)	44(1)
O2	4906(1)	6294(1)	4757(1)	32(1)
C55	4340(2)	7245(2)	4127(1)	44(1)
C56	4373(2)	6728(2)	3528(1)	46(1)
C57	3610(2)	6469(3)	3454(2)	64(1)
C58	3162(2)	6913(3)	3766(2)	77(1)
C59	3546(2)	7514(3)	4095(2)	70(1)
C60	4470(2)	6816(2)	4778(1)	32(1)
C61	4912(3)	7834(2)	4131(2)	57(1)
C62	5594(3)	7721(2)	3850(2)	59(1)
C63	6140(4)	8243(3)	3881(3)	86(2)
C64	5997(6)	8899(3)	4188(3)	114(3)
C65	5337(6)	9021(3)	4455(3)	112(3)
C66	4782(4)	8498(2)	4438(2)	82(2)
C1S	8707(16)	2209(18)	7077(13)	69(3)
C2S	9156(5)	2426(5)	6504(5)	86(2)
C3S	9855(5)	2817(6)	6638(4)	89(2)
C4S	10351(5)	2889(7)	6070(6)	108(3)
C5S	10993(5)	3375(6)	6155(4)	98(2)
C6S	11519(5)	3087(8)	6673(5)	109(3)
C7S	12169(12)	3574(13)	6758(12)	155(9)

C1D	8720(30)	2250(30)	7160(30)	69(3)
C2D	9300(9)	2758(9)	6991(8)	86(2)
C3D	9682(10)	2665(11)	6328(8)	89(2)
C4D	10284(8)	3198(11)	6321(11)	108(3)
C5D	11005(9)	3078(11)	6564(8)	98(2)
C6D	11569(9)	3640(14)	6387(9)	109(3)
C7D	12140(20)	3960(30)	6770(20)	155(9)
C8S	9027(7)	2733(6)	3805(7)	157(5)
C9S	9088(15)	2372(12)	4402(11)	278(9)
C10S	9055(11)	1580(11)	4331(11)	240(8)
C11S	8667(11)	1189(11)	4799(13)	268(10)
C12S	8628(12)	422(13)	4737(14)	294(10)
C13S	8110(20)	140(20)	5240(17)	366(15)
C14S	7798(14)	-512(15)	5006(14)	289(10)
C8D	10010(30)	1770(30)	4250(30)	157(5)
C9D	9280(40)	2040(60)	4330(50)	278(9)
C10D	8970(40)	1780(40)	4970(40)	240(8)
C11D	9010(30)	990(40)	5050(50)	268(10)
C12D	8300(40)	690(50)	5230(60)	294(10)
C13D	8100(70)	10(90)	4850(80)	366(15)
C14D	7400(50)	-240(60)	5110(60)	289(10)

Table 3. Bond lengths [Å] and angles [°] for 16066.

N1-C2	1.347(3)	N1-C1	1.459(3)
N1-H1N	0.97(3)	N2-C2	1.345(3)
N2-C3	1.377(3)	N2-H2N	0.96(4)
N3-C9	1.357(3)	N3-C21	1.418(3)
N3-H3N	0.90(3)	N4-C29	1.371(3)
N4-C28	1.456(3)	N4-H4N	0.90(3)
N5-C29	1.329(3)	N5-C30	1.381(3)
N6-C36	1.379(3)	N6-C48	1.427(3)
C1-C11	1.515(4)	C1-C28	1.561(3)
C1-H1	1.0000	C2-C10	1.411(3)
C3-C4	1.398(3)	C3-C8	1.403(3)
C4-C5	1.367(4)	C4-H4	0.9500
C5-C6	1.413(4)	C5-H5	0.9500
C6-C7	1.386(3)	C6-C17	1.534(4)
C7-C8	1.414(3)	C7-H7	0.9500
C8-C9	1.452(3)	C9-C10	1.389(3)
C10-H10	0.9500	C11-C16	1.385(5)
C11-C12	1.397(4)	C12-C13	1.388(6)
C12-H12	0.9500	C13-C14	1.383(8)
C13-H13	0.9500	C14-C15	1.380(9)
C14-H14	0.9500	C15-C16	1.397(6)
C15-H15	0.9500	C16-H16	0.9500
C17-C18	1.501(5)	C17-C20	1.510(5)
C17-C19	1.553(6)	C18-H18A	0.9800
C18-H18B	0.9800	C18-H18C	0.9800
C19-H19A	0.9800	C19-H19B	0.9800
C19-H19C	0.9800	C20-H20A	0.9800
C20-H20B	0.9800	C20-H20C	0.9800
C21-C22	1.394(4)	C21-C26	1.395(4)
C22-C23	1.390(4)	C22-H22	0.9500
C23-C24	1.367(8)	C23-H23	0.9500
C24-C25	1.397(8)	C24-C27	1.526(5)
C25-C26	1.390(5)	C25-H25	0.9500
C26-H26	0.9500	C27-H27A	0.9800
C27-H27B	0.9800	C27-H27C	0.9800
C28-C38	1.520(4)	C28-H28	1.0000
C29-C37	1.420(3)	C30-C31	1.411(3)
C30-C35	1.413(3)	C31-C32	1.378(3)
C31-H31	0.9500	C32-C33	1.412(3)
C32-H32	0.9500	C33-C34	1.379(3)
C33-C44	1.535(3)	C34-C35	1.418(3)

C34-H34	0.9500	C35-C36	1.445(3)
C36-C37	1.371(3)	C37-H37	0.9500
C38-C43	1.389(4)	C38-C39	1.401(4)
C39-C40	1.388(5)	C39-H39	0.9500
C40-C41	1.387(6)	C40-H40	0.9500
C41-C42	1.385(5)	C41-H41	0.9500
C42-C43	1.393(4)	C42-H42	0.9500
C43-H43	0.9500	C44-C45	1.526(4)
C44-C47	1.527(5)	C44-C46	1.532(5)
C45-H45A	0.9800	C45-H45B	0.9800
C45-H45C	0.9800	C46-H46A	0.9800
C46-H46B	0.9800	C46-H46C	0.9800
C47-H47A	0.9800	C47-H47B	0.9800
C47-H47C	0.9800	C48-C53	1.384(4)
C48-C49	1.391(4)	C49-C50	1.393(4)
C49-H49	0.9500	C50-C51	1.383(4)
C50-H50	0.9500	C51-C52	1.390(4)
C51-C54	1.508(4)	C52-C53	1.397(4)
C52-H52	0.9500	C53-H53	0.9500
C54-H54A	0.9800	C54-H54B	0.9800
C54-H54C	0.9800	O1-C60	1.252(3)
O2-C60	1.254(3)	C55-C61	1.514(6)
C55-C56	1.546(4)	C55-C59	1.546(5)
C55-C60	1.560(4)	C56-C57	1.494(6)
C56-H56A	0.9900	C56-H56B	0.9900
C57-C58	1.324(7)	C57-H57A	0.9900
C57-H57B	0.9900	C58-C59	1.476(8)
C58-H58A	0.9900	C58-H58B	0.9900
C59-H59A	0.9900	C59-H59B	0.9900
C61-C66	1.396(5)	C61-C62	1.396(6)
C62-C63	1.393(7)	C62-H62	0.9500
C63-C64	1.387(10)	C63-H63	0.9500
C64-C65	1.351(12)	C64-H64	0.9500
C65-C66	1.407(11)	C65-H65	0.9500
C66-H66	0.9500	C1S-C2S	1.483(16)
C1S-H1S1	0.9800	C1S-H1S2	0.9800
C1S-H1S3	0.9800	C2S-C3S	1.502(11)
C2S-H2S1	0.9900	C2S-H2S2	0.9900
C3S-C4S	1.477(12)	C3S-H3S1	0.9900
C3S-H3S2	0.9900	C4S-C5S	1.495(12)
C4S-H4S1	0.9900	C4S-H4S2	0.9900
C5S-C6S	1.527(12)	C5S-H5S1	0.9900
C5S-H5S2	0.9900	C6S-C7S	1.507(15)

C6S-H6S1	0.9900	C6S-H6S2	0.9900
C7S-H7S1	0.9800	C7S-H7S2	0.9800
C7S-H7S3	0.9800	C1D-C2D	1.46(2)
C1D-H1D1	0.9800	C1D-H1D2	0.9800
C1D-H1D3	0.9800	C2D-C3D	1.529(17)
C2D-H2D1	0.9900	C2D-H2D2	0.9900
C3D-C4D	1.483(17)	C3D-H3D1	0.9900
C3D-H3D2	0.9900	C4D-C5D	1.435(18)
C4D-H4D1	0.9900	C4D-H4D2	0.9900
C5D-C6D	1.511(18)	C5D-H5D1	0.9900
C5D-H5D2	0.9900	C6D-C7D	1.43(2)
C6D-H6D1	0.9900	C6D-H6D2	0.9900
C7D-H7D1	0.9800	C7D-H7D2	0.9800
C7D-H7D3	0.9800	C8S-C9S	1.388(18)
C8S-H8S1	0.9800	C8S-H8S2	0.9800
C8S-H8S3	0.9800	C9S-C10S	1.469(18)
C9S-H9S1	0.9900	C9S-H9S2	0.9900
C10S-C11S	1.391(17)	C10S-H10A	0.9900
C10S-H10B	0.9900	C11S-C12S	1.422(18)
C11S-H11A	0.9900	C11S-H11B	0.9900
C12S-C13S	1.488(19)	C12S-H12A	0.9900
C12S-H12B	0.9900	C13S-C14S	1.42(2)
C13S-H13A	0.9900	C13S-H13B	0.9900
C14S-H14A	0.9800	C14S-H14B	0.9800
C14S-H14C	0.9800	C8D-C9D	1.45(2)
C8D-H8D1	0.9800	C8D-H8D2	0.9800
C8D-H8D3	0.9800	C9D-C10D	1.50(2)
C9D-H9D1	0.9900	C9D-H9D2	0.9900
C10D-C11D	1.48(2)	C10D-H10C	0.9900
C10D-H10D	0.9900	C11D-C12D	1.45(2)
C11D-H11C	0.9900	C11D-H11D	0.9900
C12D-C13D	1.51(2)	C12D-H12C	0.9900
C12D-H12D	0.9900	C13D-C14D	1.46(2)
C13D-H13C	0.9900	C13D-H13D	0.9900
C14D-H14D	0.9800	C14D-H14E	0.9800
C14D-H14F	0.9800		

C2-N1-C1	122.7(2)	C2-N1-H1N	112(2)
C1-N1-H1N	123(2)	C2-N2-C3	121.9(2)
C2-N2-H2N	118(3)	C3-N2-H2N	120(3)
C9-N3-C21	126.4(2)	C9-N3-H3N	124(2)
C21-N3-H3N	109(2)	C29-N4-C28	123.8(2)
C29-N4-H4N	112(2)	C28-N4-H4N	124(2)

C29-N5-C30	116.42(19)	C36-N6-C48	123.6(2)
N1-C1-C11	111.4(2)	N1-C1-C28	110.51(19)
C11-C1-C28	113.7(2)	N1-C1-H1	107.0
C11-C1-H1	107.0	C28-C1-H1	107.0
N2-C2-N1	116.3(2)	N2-C2-C10	119.7(2)
N1-C2-C10	124.0(2)	N2-C3-C4	118.6(2)
N2-C3-C8	121.2(2)	C4-C3-C8	120.1(2)
C5-C4-C3	120.2(2)	C5-C4-H4	119.9
C3-C4-H4	119.9	C4-C5-C6	121.6(2)
C4-C5-H5	119.2	C6-C5-H5	119.2
C7-C6-C5	117.9(2)	C7-C6-C17	122.7(2)
C5-C6-C17	119.4(2)	C6-C7-C8	121.7(2)
C6-C7-H7	119.1	C8-C7-H7	119.1
C3-C8-C7	118.4(2)	C3-C8-C9	117.38(19)
C7-C8-C9	124.2(2)	N3-C9-C10	121.6(2)
N3-C9-C8	119.3(2)	C10-C9-C8	119.0(2)
C9-C10-C2	120.7(2)	C9-C10-H10	119.6
C2-C10-H10	119.6	C16-C11-C12	118.9(3)
C16-C11-C1	121.9(3)	C12-C11-C1	119.2(3)
C13-C12-C11	121.1(4)	C13-C12-H12	119.5
C11-C12-H12	119.5	C14-C13-C12	119.5(4)
C14-C13-H13	120.3	C12-C13-H13	120.3
C15-C14-C13	120.2(4)	C15-C14-H14	119.9
C13-C14-H14	119.9	C14-C15-C16	120.4(5)
C14-C15-H15	119.8	C16-C15-H15	119.8
C11-C16-C15	120.1(4)	C11-C16-H16	120.0
C15-C16-H16	120.0	C18-C17-C20	111.1(3)
C18-C17-C6	112.1(3)	C20-C17-C6	113.2(2)
C18-C17-C19	107.2(4)	C20-C17-C19	106.4(3)
C6-C17-C19	106.4(3)	C17-C18-H18A	109.5
C17-C18-H18B	109.5	H18A-C18-H18B	109.5
C17-C18-H18C	109.5	H18A-C18-H18C	109.5
H18B-C18-H18C	109.5	C17-C19-H19A	109.5
C17-C19-H19B	109.5	H19A-C19-H19B	109.5
C17-C19-H19C	109.5	H19A-C19-H19C	109.5
H19B-C19-H19C	109.5	C17-C20-H20A	109.5
C17-C20-H20B	109.5	H20A-C20-H20B	109.5
C17-C20-H20C	109.5	H20A-C20-H20C	109.5
H20B-C20-H20C	109.5	C22-C21-C26	119.7(3)
C22-C21-N3	118.6(3)	C26-C21-N3	121.5(3)
C23-C22-C21	120.1(4)	C23-C22-H22	120.0
C21-C22-H22	120.0	C24-C23-C22	121.0(4)
C24-C23-H23	119.5	C22-C23-H23	119.5

C23-C24-C25	118.8(3)	C23-C24-C27	121.7(6)
C25-C24-C27	119.5(6)	C26-C25-C24	121.5(4)
C26-C25-H25	119.3	C24-C25-H25	119.3
C25-C26-C21	118.9(4)	C25-C26-H26	120.6
C21-C26-H26	120.6	C24-C27-H27A	109.5
C24-C27-H27B	109.5	H27A-C27-H27B	109.5
C24-C27-H27C	109.5	H27A-C27-H27C	109.5
H27B-C27-H27C	109.5	N4-C28-C38	113.2(2)
N4-C28-C1	112.0(2)	C38-C28-C1	110.0(2)
N4-C28-H28	107.1	C38-C28-H28	107.1
C1-C28-H28	107.1	N5-C29-N4	119.8(2)
N5-C29-C37	124.0(2)	N4-C29-C37	116.1(2)
N5-C30-C31	118.6(2)	N5-C30-C35	124.04(19)
C31-C30-C35	117.3(2)	C32-C31-C30	121.1(2)
C32-C31-H31	119.5	C30-C31-H31	119.5
C31-C32-C33	122.3(2)	C31-C32-H32	118.8
C33-C32-H32	118.8	C34-C33-C32	116.8(2)
C34-C33-C44	123.5(2)	C32-C33-C44	119.7(2)
C33-C34-C35	122.3(2)	C33-C34-H34	118.9
C35-C34-H34	118.9	C30-C35-C34	120.0(2)
C30-C35-C36	117.4(2)	C34-C35-C36	122.4(2)
C37-C36-N6	123.4(2)	C37-C36-C35	117.9(2)
N6-C36-C35	118.7(2)	C36-C37-C29	120.2(2)
C36-C37-H37	119.9	C29-C37-H37	119.9
C43-C38-C39	117.7(3)	C43-C38-C28	123.0(2)
C39-C38-C28	119.3(3)	C40-C39-C38	121.1(3)
C40-C39-H39	119.5	C38-C39-H39	119.5
C41-C40-C39	120.2(3)	C41-C40-H40	119.9
C39-C40-H40	119.9	C42-C41-C40	119.7(3)
C42-C41-H41	120.1	C40-C41-H41	120.1
C41-C42-C43	119.7(3)	C41-C42-H42	120.1
C43-C42-H42	120.1	C38-C43-C42	121.6(3)
C38-C43-H43	119.2	C42-C43-H43	119.2
C45-C44-C47	109.0(3)	C45-C44-C46	108.3(3)
C47-C44-C46	109.0(3)	C45-C44-C33	112.1(2)
C47-C44-C33	109.3(2)	C46-C44-C33	109.1(3)
C44-C45-H45A	109.5	C44-C45-H45B	109.5
H45A-C45-H45B	109.5	C44-C45-H45C	109.5
H45A-C45-H45C	109.5	H45B-C45-H45C	109.5
C44-C46-H46A	109.5	C44-C46-H46B	109.5
H46A-C46-H46B	109.5	C44-C46-H46C	109.5
H46A-C46-H46C	109.5	H46B-C46-H46C	109.5
C44-C47-H47A	109.5	C44-C47-H47B	109.5

H47A-C47-H47B	109.5	C44-C47-H47C	109.5
H47A-C47-H47C	109.5	H47B-C47-H47C	109.5
C53-C48-C49	119.8(2)	C53-C48-N6	120.5(2)
C49-C48-N6	119.4(2)	C48-C49-C50	119.5(3)
C48-C49-H49	120.2	C50-C49-H49	120.2
C51-C50-C49	121.5(3)	C51-C50-H50	119.2
C49-C50-H50	119.2	C50-C51-C52	118.3(2)
C50-C51-C54	121.3(3)	C52-C51-C54	120.4(3)
C51-C52-C53	121.0(3)	C51-C52-H52	119.5
C53-C52-H52	119.5	C48-C53-C52	119.8(3)
C48-C53-H53	120.1	C52-C53-H53	120.1
C51-C54-H54A	109.5	C51-C54-H54B	109.5
H54A-C54-H54B	109.5	C51-C54-H54C	109.5
H54A-C54-H54C	109.5	H54B-C54-H54C	109.5
C61-C55-C56	114.8(3)	C61-C55-C59	115.4(3)
C56-C55-C59	101.7(3)	C61-C55-C60	104.6(2)
C56-C55-C60	110.3(3)	C59-C55-C60	110.1(3)
C57-C56-C55	103.8(3)	C57-C56-H56A	111.0
C55-C56-H56A	111.0	C57-C56-H56B	111.0
C55-C56-H56B	111.0	H56A-C56-H56B	109.0
C58-C57-C56	110.0(4)	C58-C57-H57A	109.7
C56-C57-H57A	109.7	C58-C57-H57B	109.7
C56-C57-H57B	109.7	H57A-C57-H57B	108.2
C57-C58-C59	112.5(4)	C57-C58-H58A	109.1
C59-C58-H58A	109.1	C57-C58-H58B	109.1
C59-C58-H58B	109.1	H58A-C58-H58B	107.8
C58-C59-C55	103.4(3)	C58-C59-H59A	111.1
C55-C59-H59A	111.1	C58-C59-H59B	111.1
C55-C59-H59B	111.1	H59A-C59-H59B	109.0
O1-C60-O2	124.8(2)	O1-C60-C55	117.7(2)
O2-C60-C55	117.4(2)	C66-C61-C62	117.8(5)
C66-C61-C55	120.9(5)	C62-C61-C55	121.3(3)
C63-C62-C61	122.0(5)	C63-C62-H62	119.0
C61-C62-H62	119.0	C64-C63-C62	119.0(7)
C64-C63-H63	120.5	C62-C63-H63	120.5
C65-C64-C63	119.8(7)	C65-C64-H64	120.1
C63-C64-H64	120.1	C64-C65-C66	122.0(6)
C64-C65-H65	119.0	C66-C65-H65	119.0
C61-C66-C65	119.3(6)	C61-C66-H66	120.4
C65-C66-H66	120.4	C2S-C1S-H1S1	109.3
C2S-C1S-H1S2	109.6	H1S1-C1S-H1S2	109.5
C2S-C1S-H1S3	109.5	H1S1-C1S-H1S3	109.5
H1S2-C1S-H1S3	109.5	C1S-C2S-C3S	117.8(13)

C1S-C2S-H2S1	107.9	C3S-C2S-H2S1	107.9
C1S-C2S-H2S2	107.9	C3S-C2S-H2S2	107.9
H2S1-C2S-H2S2	107.2	C4S-C3S-C2S	115.6(8)
C4S-C3S-H3S1	108.4	C2S-C3S-H3S1	108.4
C4S-C3S-H3S2	108.4	C2S-C3S-H3S2	108.4
H3S1-C3S-H3S2	107.4	C3S-C4S-C5S	117.0(9)
C3S-C4S-H4S1	108.0	C5S-C4S-H4S1	108.0
C3S-C4S-H4S2	108.0	C5S-C4S-H4S2	108.0
H4S1-C4S-H4S2	107.3	C4S-C5S-C6S	112.0(10)
C4S-C5S-H5S1	109.2	C6S-C5S-H5S1	109.2
C4S-C5S-H5S2	109.2	C6S-C5S-H5S2	109.2
H5S1-C5S-H5S2	107.9	C7S-C6S-C5S	112.1(12)
C7S-C6S-H6S1	109.2	C5S-C6S-H6S1	109.2
C7S-C6S-H6S2	109.2	C5S-C6S-H6S2	109.2
H6S1-C6S-H6S2	107.9	C6S-C7S-H7S1	109.4
C6S-C7S-H7S2	109.6	H7S1-C7S-H7S2	109.5
C6S-C7S-H7S3	109.5	H7S1-C7S-H7S3	109.5
H7S2-C7S-H7S3	109.5	C2D-C1D-H1D1	109.4
C2D-C1D-H1D2	109.4	H1D1-C1D-H1D2	109.5
C2D-C1D-H1D3	109.6	H1D1-C1D-H1D3	109.5
H1D2-C1D-H1D3	109.5	C1D-C2D-C3D	118(2)
C1D-C2D-H2D1	107.7	C3D-C2D-H2D1	107.7
C1D-C2D-H2D2	107.7	C3D-C2D-H2D2	107.7
H2D1-C2D-H2D2	107.1	C4D-C3D-C2D	106.2(14)
C4D-C3D-H3D1	110.5	C2D-C3D-H3D1	110.5
C4D-C3D-H3D2	110.5	C2D-C3D-H3D2	110.5
H3D1-C3D-H3D2	108.7	C5D-C4D-C3D	126.0(19)
C5D-C4D-H4D1	105.8	C3D-C4D-H4D1	105.8
C5D-C4D-H4D2	105.8	C3D-C4D-H4D2	105.8
H4D1-C4D-H4D2	106.2	C4D-C5D-C6D	116.7(17)
C4D-C5D-H5D1	108.1	C6D-C5D-H5D1	108.1
C4D-C5D-H5D2	108.1	C6D-C5D-H5D2	108.1
H5D1-C5D-H5D2	107.3	C7D-C6D-C5D	131(2)
C7D-C6D-H6D1	104.4	C5D-C6D-H6D1	104.4
C7D-C6D-H6D2	104.4	C5D-C6D-H6D2	104.4
H6D1-C6D-H6D2	105.6	C6D-C7D-H7D1	109.5
C6D-C7D-H7D2	109.5	H7D1-C7D-H7D2	109.5
C6D-C7D-H7D3	109.3	H7D1-C7D-H7D3	109.5
H7D2-C7D-H7D3	109.5	C9S-C8S-H8S1	109.9
C9S-C8S-H8S2	109.3	H8S1-C8S-H8S2	109.5
C9S-C8S-H8S3	109.2	H8S1-C8S-H8S3	109.5
H8S2-C8S-H8S3	109.5	C8S-C9S-C10S	112.8(19)
C8S-C9S-H9S1	109.0	C10S-C9S-H9S1	109.0

C8S-C9S-H9S2	109.0	C10S-C9S-H9S2	109.0
H9S1-C9S-H9S2	107.8	C11S-C10S-C9S	118.1(18)
C11S-C10S-H10A	107.8	C9S-C10S-H10A	107.8
C11S-C10S-H10B	107.8	C9S-C10S-H10B	107.8
H10A-C10S-H10B	107.1	C10S-C11S-C12S	118.9(17)
C10S-C11S-H11A	107.6	C12S-C11S-H11A	107.6
C10S-C11S-H11B	107.6	C12S-C11S-H11B	107.6
H11A-C11S-H11B	107.0	C11S-C12S-C13S	108.5(19)
C11S-C12S-H12A	110.0	C13S-C12S-H12A	110.0
C11S-C12S-H12B	110.0	C13S-C12S-H12B	110.0
H12A-C12S-H12B	108.4	C14S-C13S-C12S	109(2)
C14S-C13S-H13A	109.9	C12S-C13S-H13A	109.9
C14S-C13S-H13B	109.9	C12S-C13S-H13B	109.9
H13A-C13S-H13B	108.3	C13S-C14S-H14A	109.5
C13S-C14S-H14B	109.7	H14A-C14S-H14B	109.5
C13S-C14S-H14C	109.3	H14A-C14S-H14C	109.5
H14B-C14S-H14C	109.5	C9D-C8D-H8D1	109.1
C9D-C8D-H8D2	108.2	H8D1-C8D-H8D2	109.5
C9D-C8D-H8D3	111.1	H8D1-C8D-H8D3	109.5
H8D2-C8D-H8D3	109.5	C8D-C9D-C10D	110(3)
C8D-C9D-H9D1	109.6	C10D-C9D-H9D1	109.6
C8D-C9D-H9D2	109.6	C10D-C9D-H9D2	109.6
H9D1-C9D-H9D2	108.2	C11D-C10D-C9D	113(3)
C11D-C10D-H10C	109.0	C9D-C10D-H10C	109.0
C11D-C10D-H10D	109.0	C9D-C10D-H10D	109.0
H10C-C10D-H10D	107.8	C12D-C11D-C10D	111(3)
C12D-C11D-H11C	109.4	C10D-C11D-H11C	109.4
C12D-C11D-H11D	109.4	C10D-C11D-H11D	109.4
H11C-C11D-H11D	108.0	C11D-C12D-C13D	114(3)
C11D-C12D-H12C	108.6	C13D-C12D-H12C	108.6
C11D-C12D-H12D	108.6	C13D-C12D-H12D	108.6
H12C-C12D-H12D	107.6	C14D-C13D-C12D	108(3)
C14D-C13D-H13C	110.1	C12D-C13D-H13C	110.1
C14D-C13D-H13D	110.1	C12D-C13D-H13D	110.1
H13C-C13D-H13D	108.4	C13D-C14D-H14D	111.1
C13D-C14D-H14E	110.6	H14D-C14D-H14E	109.5
C13D-C14D-H14F	106.7	H14D-C14D-H14F	109.5
H14E-C14D-H14F	109.5		

Table 4. Anisotropic displacement parameters ($Å^2 \times 10^3$) for 16066. The anisotropic displacement factor exponent takes the form: $-2\pi^2[h^2 a^{*2} U^{11} + ... + 2 h k a^* b^* U^{12}]$

	U^{11}	U^{22}	U^{33}	U^{23}	U^{13}	U^{12}
N1	31(1)	27(1)	23(1)	2(1)	0(1)	10(1)
N2	28(1)	25(1)	22(1)	1(1)	0(1)	6(1)
N3	36(1)	23(1)	23(1)	1(1)	-4(1)	8(1)
N4	28(1)	30(1)	21(1)	-3(1)	-2(1)	10(1)
N5	22(1)	24(1)	21(1)	-2(1)	-2(1)	1(1)
N6	24(1)	42(1)	20(1)	-4(1)	-2(1)	3(1)
C1	31(1)	27(1)	24(1)	1(1)	1(1)	8(1)
C2	22(1)	23(1)	25(1)	2(1)	1(1)	3(1)
C3	24(1)	23(1)	23(1)	0(1)	1(1)	2(1)
C4	42(1)	31(1)	22(1)	1(1)	-2(1)	8(1)
C5	49(2)	33(1)	25(1)	-5(1)	3(1)	9(1)
C6	30(1)	25(1)	30(1)	-3(1)	4(1)	3(1)
C7	24(1)	21(1)	27(1)	1(1)	-1(1)	2(1)
C8	21(1)	22(1)	23(1)	1(1)	0(1)	1(1)
C9	23(1)	21(1)	22(1)	2(1)	0(1)	0(1)
C10	27(1)	23(1)	22(1)	1(1)	0(1)	3(1)
C11	39(1)	30(1)	43(2)	6(1)	12(1)	11(1)
C12	75(2)	33(2)	42(2)	4(1)	22(2)	7(2)
C13	98(3)	44(2)	70(3)	14(2)	43(3)	8(2)
C14	70(3)	47(2)	132(5)	28(3)	47(3)	6(2)
C15	48(2)	63(3)	134(5)	27(3)	2(3)	-8(2)
C16	43(2)	54(2)	72(2)	17(2)	-3(2)	-8(2)
C17	48(2)	30(1)	38(1)	-4(1)	4(1)	14(1)
C18	119(4)	87(3)	75(3)	17(3)	44(3)	62(3)
C19	88(3)	32(2)	170(6)	-8(3)	-51(4)	7(2)
C20	76(3)	42(2)	58(2)	-13(2)	-18(2)	30(2)
C21	52(2)	21(1)	22(1)	2(1)	-4(1)	6(1)
C22	63(2)	29(1)	36(1)	-7(1)	-16(1)	15(1)
C23	105(3)	39(2)	36(2)	-9(1)	-28(2)	19(2)
C24	126(4)	49(2)	29(2)	-4(1)	-1(2)	8(2)
C25	101(3)	53(2)	34(2)	2(1)	24(2)	5(2)
C26	62(2)	35(1)	32(1)	6(1)	10(1)	0(1)
C27	207(8)	110(4)	32(2)	-21(2)	-1(3)	9(5)
C28	28(1)	28(1)	24(1)	-2(1)	-3(1)	9(1)
C29	21(1)	19(1)	25(1)	1(1)	-1(1)	0(1)
C30	21(1)	22(1)	21(1)	-2(1)	-1(1)	0(1)
C31	26(1)	31(1)	20(1)	-4(1)	-3(1)	2(1)
C32	28(1)	36(1)	24(1)	-9(1)	0(1)	4(1)

C33	22(1)	33(1)	29(1)	-5(1)	0(1)	5(1)
C34	22(1)	28(1)	25(1)	-4(1)	-2(1)	2(1)
C35	21(1)	24(1)	21(1)	-1(1)	-1(1)	0(1)
C36	22(1)	24(1)	21(1)	-2(1)	-2(1)	-2(1)
C37	25(1)	25(1)	20(1)	-4(1)	0(1)	2(1)
C38	29(1)	25(1)	36(1)	-2(1)	-6(1)	7(1)
C39	42(2)	42(2)	42(2)	-7(1)	-12(1)	6(1)
C40	46(2)	47(2)	75(3)	-14(2)	-21(2)	-2(2)
C41	38(2)	40(2)	86(3)	-4(2)	-6(2)	-5(1)
C42	43(2)	38(2)	58(2)	5(1)	5(1)	1(1)
C43	37(1)	31(1)	39(1)	-1(1)	-1(1)	2(1)
C44	30(1)	43(2)	38(1)	-11(1)	-4(1)	14(1)
C45	40(2)	53(2)	50(2)	-10(1)	-8(1)	24(1)
C46	32(2)	87(3)	44(2)	-10(2)	7(1)	14(2)
C47	56(2)	45(2)	83(3)	-27(2)	-13(2)	22(2)
C48	23(1)	33(1)	21(1)	-2(1)	-3(1)	6(1)
C49	31(1)	36(1)	30(1)	-3(1)	0(1)	-2(1)
C50	35(1)	39(1)	31(1)	8(1)	5(1)	1(1)
C51	34(1)	45(2)	23(1)	4(1)	0(1)	11(1)
C52	34(1)	42(2)	26(1)	-8(1)	-4(1)	3(1)
C53	28(1)	36(1)	26(1)	-4(1)	0(1)	-1(1)
C54	56(2)	73(2)	24(1)	3(1)	6(1)	9(2)
O1	51(1)	55(1)	24(1)	-1(1)	1(1)	25(1)
O2	32(1)	37(1)	26(1)	4(1)	-1(1)	12(1)
C55	59(2)	53(2)	21(1)	1(1)	-4(1)	30(2)
C56	53(2)	59(2)	24(1)	-6(1)	-5(1)	18(2)
C57	60(2)	88(3)	45(2)	1(2)	-11(2)	13(2)
C58	52(2)	123(4)	55(2)	12(3)	-10(2)	30(3)
C59	72(3)	98(3)	39(2)	4(2)	-5(2)	59(3)
C60	33(1)	41(1)	22(1)	-1(1)	-3(1)	14(1)
C61	102(3)	40(2)	28(1)	8(1)	-13(2)	18(2)
C62	80(3)	45(2)	52(2)	16(2)	-9(2)	3(2)
C63	112(4)	71(3)	74(3)	28(3)	-20(3)	-21(3)
C64	213(9)	67(3)	63(3)	11(3)	-26(5)	-42(5)
C65	242(10)	43(2)	50(3)	0(2)	-20(4)	-16(4)
C66	161(5)	47(2)	38(2)	-2(2)	5(2)	22(3)
C1S	59(2)	67(4)	81(7)	0(5)	-17(4)	27(2)
C2S	85(4)	87(5)	86(4)	-1(3)	-13(3)	15(3)
C3S	102(5)	100(5)	65(4)	-2(4)	-13(4)	-16(4)
C4S	97(4)	112(7)	115(7)	-38(5)	15(4)	11(5)
C5S	110(5)	124(6)	60(4)	-16(4)	18(4)	5(4)
C6S	87(5)	174(9)	66(5)	2(4)	10(4)	0(5)
C7S	109(6)	250(30)	104(6)	12(13)	11(5)	-51(14)

C1D	59(2)	67(4)	81(7)	0(5)	-17(4)	27(2)
C2D	85(4)	87(5)	86(4)	-1(3)	-13(3)	15(3)
C3D	102(5)	100(5)	65(4)	-2(4)	-13(4)	-16(4)
C4D	97(4)	112(7)	115(7)	-38(5)	15(4)	11(5)
C5D	110(5)	124(6)	60(4)	-16(4)	18(4)	5(4)
C6D	87(5)	174(9)	66(5)	2(4)	10(4)	0(5)
C7D	109(6)	250(30)	104(6)	12(13)	11(5)	-51(14)
C8S	177(9)	115(7)	180(10)	-90(7)	24(8)	21(7)
C9S	238(13)	337(18)	259(14)	-37(12)	54(12)	93(13)
C10S	182(12)	321(16)	218(14)	-28(11)	32(11)	103(12)
C11S	186(14)	350(17)	268(19)	-37(12)	106(14)	114(12)
C12S	209(14)	349(18)	320(20)	27(14)	68(13)	120(13)
C13S	340(20)	440(20)	320(30)	-1(19)	95(19)	10(18)
C14S	278(19)	370(20)	219(17)	123(16)	-40(15)	71(17)
C8D	177(9)	115(7)	180(10)	-90(7)	24(8)	21(7)
C9D	238(13)	337(18)	259(14)	-37(12)	54(12)	93(13)
C10D	182(12)	321(16)	218(14)	-28(11)	32(11)	103(12)
C11D	186(14)	350(17)	268(19)	-37(12)	106(14)	114(12)
C12D	209(14)	349(18)	320(20)	27(14)	68(13)	120(13)
C13D	340(20)	440(20)	320(30)	-1(19)	95(19)	10(18)
C14D	278(19)	370(20)	219(17)	123(16)	-40(15)	71(17)

Table 5. Hydrogen coordinates (× 10^4) and isotropic displacement parameters ($Å^2$ × 10^3) for 16066.

	x	y	z	U(eq)
H1N	4532(18)	6721(18)	6070(17)	33(8)
H2N	5020(20)	5900(20)	5540(20)	55(12)
H3N	6412(18)	4368(19)	7583(16)	29(8)
H4N	3728(16)	7659(17)	6043(16)	26(7)
H1	4766	6904	7450	33
H4	5470	4966	4865	38
H5	6111	3905	4729	43
H7	6459	3783	6694	29
H10	5257	5862	7509	29
H12	4140	6385	8297	60
H13	3194	5682	8717	85
H14	2230	5352	8033	99
H15	2230	5695	6930	98
H16	3184	6391	6503	67
H18A	7559	3354	4993	140
H18B	6853	3111	4591	140
H18C	7382	2512	4898	140
H19A	6344	1949	5426	145
H19B	5811	2559	5143	145
H19C	5840	2403	5918	145
H20A	7579	3115	6244	88
H20B	7406	2286	6074	88
H20C	6886	2727	6562	88
H22	7141	5057	8391	51
H23	7093	5399	9496	72
H25	4911	5426	9416	75
H26	4938	5017	8326	52
H27A	5490	5546	10467	175
H27B	6021	6210	10311	175
H27C	6349	5446	10536	175
H28	3953	7911	7398	32
H31	2305	9161	8087	31
H32	1272	9859	8156	35
H34	820	9481	6244	30
H37	2766	8056	5536	28
H39	5051	8362	7862	50
H40	6135	8997	7742	67
H41	6633	9177	6696	66

H42	6020	8751	5765	55
H43	4921	8137	5885	43
H45A	-498	10741	6669	71
H45B	-286	9938	6442	71
H45C	249	10601	6289	71
H46A	-686	10260	7783	81
H46B	-35	9886	8179	81
H46C	-415	9466	7582	81
H47A	122	11328	7586	92
H47B	890	11220	7232	92
H47C	769	10930	7967	92
H49	2512	9399	4773	39
H50	2803	9339	3654	42
H52	1333	7748	3396	41
H53	1045	7789	4519	36
H54A	2530	8028	2600	77
H54B	2630	8890	2579	77
H54C	1855	8538	2424	77
H56A	4535	6989	3128	55
H56B	4707	6319	3613	55
H57A	3480	6449	2981	77
H57B	3565	5975	3639	77
H58A	2885	6635	4099	92
H58B	2810	7115	3446	92
H59A	3349	7600	4542	84
H59B	3508	7966	3835	84
H62	5690	7276	3632	71
H63	6603	8150	3693	103
H64	6362	9261	4211	137
H65	5244	9474	4660	134
H66	4324	8595	4633	98
H1S1	8877	1741	7245	104
H1S2	8198	2166	6941	104
H1S3	8748	2576	7424	104
H2S1	8855	2739	6217	103
H2S2	9272	1983	6249	103
H3S1	9739	3308	6803	107
H3S2	10114	2558	6994	107
H4S1	10065	3068	5690	130
H4S2	10530	2400	5954	130
H5S1	10825	3863	6286	117
H5S2	11250	3420	5728	117
H6S1	11263	3043	7100	131

H6S2	11685	2598	6543	131
H7S1	12568	3396	6483	232
H7S2	12320	3574	7221	232
H7S3	12042	4068	6624	232
H1D1	8587	1972	6770	104
H1D2	8297	2527	7316	104
H1D3	8886	1926	7509	104
H2D1	9674	2728	7341	103
H2D2	9097	3254	7006	103
H3D1	9872	2166	6282	107
H3D2	9341	2761	5961	107
H4D1	10342	3347	5855	130
H4D2	10101	3629	6559	130
H5D1	11175	2603	6397	117
H5D2	10981	3043	7050	117
H6D1	11815	3439	5994	131
H6D2	11283	4059	6226	131
H7D1	12062	4482	6801	232
H7D2	12607	3866	6552	232
H7D3	12143	3744	7209	232
H8S1	9509	2794	3608	236
H8S2	8807	3209	3879	236
H8S3	8720	2449	3507	236
H9S1	8692	2532	4698	334
H9S2	9554	2505	4612	334
H10A	8844	1472	3893	288
H10B	9559	1395	4329	288
H11A	8164	1377	4801	321
H11B	8879	1299	5235	321
H12A	9114	207	4806	353
H12B	8459	290	4290	353
H13A	8371	52	5659	439
H13B	7727	506	5323	439
H14A	7780	-502	4523	434
H14B	7306	-562	5182	434
H14C	8095	-922	5151	434
H8D1	10290	1872	4653	236
H8D2	10236	2019	3878	236
H8D3	10016	1244	4170	236
H9D1	8973	1857	3963	334
H9D2	9280	2571	4317	334
H10C	9240	2015	5337	288
H10D	8457	1939	5003	288

H11C	9175	763	4637	321
H11D	9360	865	5403	321
H12C	7926	1063	5146	353
H12D	8297	578	5703	353
H13C	8053	120	4376	439
H13D	8472	-365	4912	439
H14D	7178	-594	4806	434
H14E	7069	163	5179	434
H14F	7503	-481	5530	434

Table 6. Torsion angles [°] for 16066.

C2-N1-C1-C11	-69.1(3)	C2-N1-C1-C28	163.5(2)
C3-N2-C2-N1	177.5(2)	C3-N2-C2-C10	-0.6(3)
C1-N1-C2-N2	165.3(2)	C1-N1-C2-C10	-16.7(4)
C2-N2-C3-C4	-179.9(2)	C2-N2-C3-C8	0.7(4)
N2-C3-C4-C5	-179.0(3)	C8-C3-C4-C5	0.4(4)
C3-C4-C5-C6	0.1(5)	C4-C5-C6-C7	-0.2(4)
C4-C5-C6-C17	176.3(3)	C5-C6-C7-C8	-0.2(4)
C17-C6-C7-C8	-176.6(2)	N2-C3-C8-C7	178.6(2)
C4-C3-C8-C7	-0.8(3)	N2-C3-C8-C9	-2.2(3)
C4-C3-C8-C9	178.4(2)	C6-C7-C8-C3	0.7(3)
C6-C7-C8-C9	-178.5(2)	C21-N3-C9-C10	1.7(4)
C21-N3-C9-C8	-179.5(2)	C3-C8-C9-N3	-175.1(2)
C7-C8-C9-N3	4.0(3)	C3-C8-C9-C10	3.7(3)
C7-C8-C9-C10	-177.1(2)	N3-C9-C10-C2	175.1(2)
C8-C9-C10-C2	-3.7(3)	N2-C2-C10-C9	2.2(4)
N1-C2-C10-C9	-175.8(2)	N1-C1-C11-C16	-50.6(4)
C28-C1-C11-C16	75.0(4)	N1-C1-C11-C12	127.5(3)
C28-C1-C11-C12	-106.9(3)	C16-C11-C12-C13	-1.1(5)
C1-C11-C12-C13	-179.3(3)	C11-C12-C13-C14	-0.1(6)
C12-C13-C14-C15	1.0(7)	C13-C14-C15-C16	-0.7(7)
C12-C11-C16-C15	1.4(6)	C1-C11-C16-C15	179.6(4)
C14-C15-C16-C11	-0.6(7)	C7-C6-C17-C18	-144.8(4)
C5-C6-C17-C18	38.9(5)	C7-C6-C17-C20	-18.1(4)
C5-C6-C17-C20	165.6(3)	C7-C6-C17-C19	98.4(4)
C5-C6-C17-C19	-77.9(4)	C9-N3-C21-C22	-128.7(3)
C9-N3-C21-C26	55.5(4)	C26-C21-C22-C23	0.6(4)
N3-C21-C22-C23	-175.3(3)	C21-C22-C23-C24	-1.6(5)
C22-C23-C24-C25	0.5(6)	C22-C23-C24-C27	-179.5(4)
C23-C24-C25-C26	1.5(6)	C27-C24-C25-C26	-178.5(4)
C24-C25-C26-C21	-2.4(5)	C22-C21-C26-C25	1.4(4)
N3-C21-C26-C25	177.2(3)	C29-N4-C28-C38	-105.3(3)
C29-N4-C28-C1	129.6(2)	N1-C1-C28-N4	60.0(3)
C11-C1-C28-N4	-66.0(3)	N1-C1-C28-C38	-66.8(3)
C11-C1-C28-C38	167.1(2)	C30-N5-C29-N4	-177.3(2)
C30-N5-C29-C37	0.6(3)	C28-N4-C29-N5	-4.6(4)
C28-N4-C29-C37	177.3(2)	C29-N5-C30-C31	-178.6(2)
C29-N5-C30-C35	-0.4(3)	N5-C30-C31-C32	175.4(2)
C35-C30-C31-C32	-2.9(4)	C30-C31-C32-C33	-0.6(4)
C31-C32-C33-C34	2.8(4)	C31-C32-C33-C44	-176.4(3)
C32-C33-C34-C35	-1.3(4)	C44-C33-C34-C35	177.8(2)
N5-C30-C35-C34	-174.0(2)	C31-C30-C35-C34	4.2(3)

N5-C30-C35-C36	0.5(3)
C33-C34-C35-C30	-2.2(4)
C48-N6-C36-C37	-20.4(4)
C30-C35-C36-C37	-0.8(3)
C30-C35-C36-N6	179.2(2)
N6-C36-C37-C29	-178.9(2)
N5-C29-C37-C36	-1.0(4)
N4-C28-C38-C43	-33.6(3)
N4-C28-C38-C39	148.0(2)
C43-C38-C39-C40	-1.2(4)
C38-C39-C40-C41	-0.4(5)
C40-C41-C42-C43	-0.5(5)
C28-C38-C43-C42	-176.5(3)
C34-C33-C44-C45	-4.9(4)
C34-C33-C44-C47	-125.8(3)
C34-C33-C44-C46	115.1(3)
C36-N6-C48-C53	124.8(3)
C53-C48-C49-C50	1.1(4)
C48-C49-C50-C51	-0.2(4)
C49-C50-C51-C54	-179.4(3)
C54-C51-C52-C53	178.9(3)
N6-C48-C53-C52	172.4(2)
C61-C55-C56-C57	-153.1(3)
C60-C55-C56-C57	89.0(3)
C56-C57-C58-C59	-0.8(5)
C61-C55-C59-C58	152.1(3)
C60-C55-C59-C58	-89.7(4)
C56-C55-C60-O1	-149.2(3)
C61-C55-C60-O2	-89.2(3)
C59-C55-C60-O2	146.1(3)
C59-C55-C61-C66	33.6(4)
C56-C55-C61-C62	-31.0(4)
C60-C55-C61-C62	90.0(3)
C55-C61-C62-C63	-176.5(3)
C62-C63-C64-C65	0.3(8)
C62-C61-C66-C65	-0.2(6)

C64-C65-C66-C61 -0.7(8) C2S-C3S-C4S-C5S 170.4(9) C4S-C5S-C6S-C7S 179.8(15) C2D-C3D-C4D-C5D 88(2) C4D-C5D-C6D-C7D 139(4) C9S-C10S-C11S-C12S 180(2) C11S-C12S-C13S-C14S 152(3)

C31-C30-C35-C36	178.7(2)
C33-C34-C35-C36	-176.4(2)
C48-N6-C36-C35	159.7(2)
C34-C35-C36-C37	173.6(2)
C34-C35-C36-N6	-6.5(3)
C35-C36-C37-C29	1.0(3)
N4-C29-C37-C36	177.0(2)
C1-C28-C38-C43	92.5(3)
C1-C28-C38-C39	-85.9(3)
C28-C38-C39-C40	177.3(3)
C39-C40-C41-C42	1.2(5)
C39-C38-C43-C42	2.0(4)
C41-C42-C43-C38	-1.1(5)
C32-C33-C44-C45	174.2(3)
C32-C33-C44-C47	53.3(4)
C32-C33-C44-C46	-65.8(3)
C36-N6-C48-C49	-61.1(4)
N6-C48-C49-C50	-173.0(2)
C49-C50-C51-C52	-0.1(4)
C50-C51-C52-C53	-0.4(4)
C49-C48-C53-C52	-1.6(4)
C51-C52-C53-C48	1.2(4)
C59-C55-C56-C57	-27.8(4)
C55-C56-C57-C58	18.9(5)
C57-C58-C59-C55	-17.6(5)
C56-C55-C59-C58	27.2(4)
C61-C55-C60-O1	86.9(3)
C59-C55-C60-O1	-37.8(4)
C56-C55-C60-O2	34.7(4)
C56-C55-C61-C66	151.5(3)
C60-C55-C61-C66	-87.6(4)
C59-C55-C61-C62	-148.8(3)
C66-C61-C62-C63	1.1(5)
C61-C62-C63-C64	-1.2(7)
C63-C64-C65-C66	0.6(9)

C55-C61-C66-C65 177.4(4) C1S-C2S-C3S-C4S 168.1(19) C3S-C4S-C5S-C6S 65.2(13) C1D-C2D-C3D-C4D -175(4) C3D-C4D-C5D-C6D 168.4(18) C8S-C9S-C10S-C11S -140(2) C10S-C11S-C12S-C13S -173(3) C8D-C9D-C10D-C11D -55(10)

Table 7. Hydrogen bonds for 16066 [Å and °].

D-H...A	d(D-H)	d(H...A)	d(D...A)	<(DHA)
N1-H1N...O1	0.97(3)	1.82(4)	2.786(3)	173(3)
N2-H2N...O2	0.96(4)	1.76(5)	2.703(3)	167(4)
N3-H3N...N5#1	0.90(3)	2.17(4)	3.029(3)	160(3)
N4-H4N...O1	0.90(3)	2.07(3)	2.919(3)	157(3)

Symmetry transformations used to generate equivalent atoms: #1 -x+1,y-1/2,-z+3/2